

ISSN 1822-5934

ELECTRICAL AND CONTROL TECHNOLOGIES

PROCEEDINGS
OF THE 4TH INTERNATIONAL CONFERENCE ON
ELECTRICAL AND CONTROL TECHNOLOGIES



KAUNAS, TECHNOLOGIJA, 2009

UDK 621.3(474.5)(06); 681.5(474.5)(06)

**The 4th International Conference on Electrical and Control Technologies
ECT-2009.**

Selected papers of the International Conference, May 7-8, 2009, Kaunas, Lithuania (Kaunas University of Technology), edited: A. Navickas (general editor), A. Sauhats, A. Virbalis, M. Ažubalis, V. Galvanauskas, A. Jonaitis

The 4th International Conference on Electrical and Control Technologies ECT-2009 is the continuation of series of annual conferences on electrical, power engineering, electrical drives and control technologies held earlier in Kaunas Polytechnic Institute and from 1990 in Kaunas University of Technology.

The aim of the Conference is to create the forum for presentations and discussions to consider the newest research and application results of investigations on electrical and power engineering, electric drives, power converters, automation and control technologies.

All papers were reviewed by Conference Editorial Committee and Conference Program Advisory Committee and independent peer reviewers.

For information write to:

Kaunas University of Technology
Department of Electric Power Systems
Studentų g. 48, LT-51367 Kaunas
Lithuania

Conference organizers

Kaunas University of Technology, Lithuania
IFAC Committee of National Lithuanian Organisation
Lithuanian Electricity Association, Full Member of EURELECTRIC

Conference Chairman

Prof. **J. Daunoras**, Dean of Kaunas University of Technology,
Electrical and Control Engineering faculty, Lithuania

Honorary Chairman

Prof. **R. J. Kažys**, Vice Rector of Kaunas University of Technology, Lithuania

Conference Program Advisory Committee:

Prof. R. Deksnys, Kaunas University of Technology, Lithuania
Prof. L. Fara, Polytechnic University of Bucharest, Romania
Prof. J. Gerhards, Riga Technical University, Latvia
Prof. E. Heinemann, Schmalkalden University, Germany
Dr. B. Jaekel, Siemens AG, Germany
Prof. T. Jokinen, Helsinki Technical University, Finland
Prof. V. Kaminskas, Vytautas Magnus University, Lithuania
Prof. S. Kaušinis, Kaunas University of Technology, Lithuania
Prof. J. Laugis, Tallinn University of Technology, Estonia
Assoc. Prof. V. Mačerauskas, Kaunas University of Technology, Lithuania
Prof. L. A. Markevičius, Kaunas University of Technology, Lithuania
Prof. V. Miškinis, Lithuanian Energy Institute, Lithuania
Prof. A. Morkvėnas, Kaunas University of Technology, Lithuania
Prof. A. Nargėlas, Kaunas University of Technology, Lithuania
Prof. A. Nemura, Lithuanian Energy Institute, Lithuania
V. Paškevičius, President of Lithuanian Electricity Association, Lithuania
Prof. L. Ribickis, Riga Technical University, Latvia
Assoc. Prof. J. Sa da Costa, Technical University of Lisbon, Portugal
Prof. A. Sauhats, Riga Technical University, Latvia
Prof. R. Simutis, Kaunas University of Technology, Lithuania
Prof. A. W. Sowa, Bialystok Technical University, Poland
Prof. R. Strzelecki, Zielona Gora University, Poland
Prof. M. Valdma, Tallinn University of Technology, Estonia

Conference Editorial Committee:

General Editor: Prof. A. Navickas, Kaunas University of Technology, Lithuania
Prof. A. Sauhats, Riga Technical University, Latvia
Prof. A. Virbalis, Kaunas University of Technology, Lithuania
Assoc. Prof. V. Ažubalis, Kaunas University of Technology, Lithuania
Assoc. Prof. V. Galvanauskas, Kaunas University of Technology, Lithuania
Assoc. Prof. A. Jonaitis, Kaunas University of Technology, Lithuania

Organizing committee:

Assoc. Prof. M. Ažubalis, Kaunas University of Technology, Lithuania
Assoc. Prof. V. Galvanauskas, Kaunas University of Technology, Lithuania
Assoc. Prof. A. Jonaitis, Kaunas University of Technology, Lithuania

CONTENTS

A new approach based on support vector machine to analyse and control the REM-sleep-stage	11
<i>Maria Krautwald, Rudolf Baumgart-Schmitt, Daniel Trommer, Christian Walther University of Applied Sciences Schmalkalden, Faculty of Electrical Engineering, Germany</i>	
Adaption of fuzzy rules by different multi criteria optimization procedures to control stages of anaesthesia	15
<i>Christian Walther, Rudolf Baumgart-Schmitt, Maria Krautwald, Daniel Trommer University of Applied Sciences Schmalkalden, Faculty of Electrical Engineering, Germany</i>	
Investigation of the influence of fuzzy set structure to the color segmentation	19
<i>Toma Nakvosaitė, Vidas Raudonis, Rimvydas Simutis, Audrius Pukevičius Department of Control Technologies, Kaunas University of Technology, Lithuania, Department of Process Control, Kaunas University of Technology, Lithuania</i>	
Development and investigation of an efficient algorithm for alternative cursor control	23
<i>Audrius Pukevičius, Vidas Raudonis, Rimvydas Simutis, Toma Nakvosaitė Department of Control Technologies, Kaunas University of Technology, Lithuania Department of Process Control, Kaunas University of Technology, Lithuania</i>	
Optimal control of robots by dynamic programming	27
<i>Rudolf Baumgart-Schmitt, Stephan Liebetrau, Christian Walther, Maria Krautwald, Daniel Trommer University of Applied Sciences Schmalkalden, Faculty of Electrical Engineering, Germany</i>	
Map drawing of unknown environment using autonomous mobile robot	31
<i>Šarūnas Germanas, Gintautas Narvydas Department of Mathematics Research in System, Kaunas University of Technology, Lithuania Department of Process Control, Kaunas University of Technology, Lithuania</i>	
Influence of dimensions of a mobile robot on navigation using vector marks	36
<i>Virginijus Baranauskas, Stanislovas Bartkevičius, Kastytis Šarkauskas Kaunas University of Technology, Lithuania</i>	
Optimization of hexapod robot locomotion	40
<i>Tomas Luneckas, Dainius Udris Vilnius Gediminas Technical University, Lithuania</i>	
Faster autonomous mobile robot learning using decision correction	44
<i>Gintautas Narvydas, Petras Ražanskas Kaunas University of Technology, Lithuania</i>	
Voice controlled telephony services	48
<i>Rytis Maskeliūnas, Algimantas Rudžionis, Kastytis Ratkevičius, Vytautas Rudžionis Kaunas University of Technology; Vilnius University, Kaunas Faculty, Lithuania</i>	
Data acquisition in OPC-based industrial it systems	54
<i>Roman Kwiecień, Elżbieta Szycha, Leszek Szycha Technical University of Radom, Faculty of Transport and Electrical Engineering, Poland</i>	
Synthesis of program modules for typical boiler-house applications	58
<i>Gediminas Danilevičius, Darius Ezerskis Kaunas University of Technology, Lithuania</i>	
Distributed substation units control system in district heating network	62
<i>Julius Kaluževičius, Vytautas Deksnys, Virgilijus Pamakštis Kaunas University of Technology; AB Axis Industries</i>	
Estimation of typical safety circuits for medium power industrial boilers	66
<i>Algirdas Čebatorius, Darius Ezerskis ABB UAB, Lithuania; Kaunas University of Technology, Lithuania</i>	
Positioning of stepper motors in graphical data acquisition system	70
<i>Raimundas Liutkevičius, Andrius Davidsonas Department of Systems Analysis, Vytautas Magnus University, Lithuania</i>	

Visibility of text in multimedia presentation	75
<i>Stanislovas Masiokas, Miglė Kriuglaitė-Jarašiūnienė, Valdas Pakėnas Kaunas University of Technology, Department of Electrical Engineering, Lithuania</i>	
Automatic PLC-source-code generation of C4.5 decision trees	79
<i>Elmar Heinemann, Jolanta Repšytė, André Wenzel University of Applied Sciences Schmalkalden, Germany; Kaunas University of Technology, Lithuania</i>	
A new wireless solution to transmit and evaluate biomedical signals under low signal noise ratio to control the state of relaxation	83
<i>Daniel Trommer, Markus Greulich, Rudolf Baumgart-Schmitt, Maria Krautwald Christian Walther, Andreas Wenzel University of Applied Sciences Schmalkalden, Faculty of Electrical Engineering, Germany Fraunhofer-Institute for Information and Data Processing, Applications Center System Technology, Germany</i>	
Correction of measuring track processing errors in vibration measurements of coal wagon	87
<i>Mirosław Luft, Radosław Cioć, Daniel Pietruszczak Kazimierz Pulaski Technical University of Radom, Faculty of Transport and Electrical Engineering, Poland</i>	
Regression modelling using adaptive basis function construction	93
<i>Gints Jekabsons Institute of Applied Computer Systems, Riga Technical University, Latvia</i>	
Categorizing sequences of laryngeal data for decision support	99
<i>Adas Gelžinis, Evaldas Vaiciukynas, Edgaras Kelertas, Marija Bacauskiene, Antanas Verikas, Virgilijus Uloza, Aurelija Vegiene Kaunas University of Technology, Lithuania; Halmstad University, Sweden; Kaunas University of Medicine, Lithuania</i>	
System parameters identification in the state space	103
<i>Leonas Balaševičius, Kęstas Rimkus Department of Control Technology, Kaunas University of Technology, Lithuania</i>	
Model of current space vector control	107
<i>Robertas Janickas, Algirdas Smilgevičius Vilnius Gediminas Technical University, Lithuania</i>	
Parameter estimation of induction motor at locked rotor	111
<i>Andrius Petrovas, Roma Rinkevičienė, Saulius Lisauskas Vilnius Gediminas Technical University, Lithuania</i>	
Modelling of ammonia production process	115
<i>Giedrius Oberauskas, Vytautas Galvanauskas Process Control Department, Kaunas University of Technology, Lithuania</i>	
Mathematical model for adaptive control of dissolved oxygen concentration in biological wastewater treatment process	121
<i>Kęstutis Jonelis, Kęstutis Brazauskas, Donatas Levišauskas Process Control Department, Kaunas University of Technology, Lithuania</i>	
Adaptive control system for dissolved oxygen concentration in Kaunas wastewater treatment plant	125
<i>Jolanta Repšytė, Ieva Cebatorienė, André Wenzel Kaunas University of Technology (KTU), Lithuania University of Applied Sciences Schmalkalden (fhS), Germany</i>	
Analysis of efficiency of a pump set operating in an irrigation system	131
<i>Elżbieta Szychta, Leszek Szychta, Radosław Figura Technical University of Radom, Faculty of Transport and Electrical Engineering, Poland</i>	
Different simulation models in exemplary employment for “pump aggregate – pipeline” systems	135
<i>Anna Koziorowska, Jacek Bartman University of Rzeszów, Institute of Technology, Poland</i>	

Application of simulation tools for a fertilizer granulation circuit	139
Gediminas Valiulis, Rimvydas Simutis	
<i>Process Control Department, Kaunas University of Technology, Lithuania</i>	
<i>Electrical Engineering Department, Šiauliai University, Lithuania</i>	
Innovative moisture control method for concrete mixing systems	143
Gintautas Lengvinas, Vytautas Deksnys	
<i>Department of Electronics and Measurement Systems, Kaunas University of Technology, Lithuania</i>	
The independent fuzzy control with correction of two dimensional process	146
Gediminas Liaučius, Vytautas Kaminskas	
<i>Department of Systems Analysis, Vytautas Magnus University, Lithuania</i>	
Investigation of adaptive pH control system	152
Vytautas Galvanauskas	
<i>Process Control Department, Kaunas University of Technology, Lithuania</i>	
Building of securities valuation IT system using multi-agents approach	156
Andrius Jurgutis, Rimvydas Simutis	
<i>Department of Process Control, Kaunas University of Technology, Lithuania</i>	
<i>AB Bankas Finasta, Lithuania</i>	
Modelling of ATM cash turnover	162
Vaidas Kazlauskas, Vygasdas Vaitkus	
<i>Scientific service company "GTV", Kaunas University of Technology, Lithuania</i>	
Lithuanian energy after 2009	166
Arvydas Galinis	
<i>Lithuanian Energy Institute, Lithuania</i>	
Analysis of Latvian power system development in the Kurzeme region using multicriterion optimization	170
Anatoly Mahnitko, Alexander Gavrilo	
<i>Riga Technical University, Power Engineering Institute, Latvia</i>	
Balance management in the Baltic countries and possibilities for harmonization	176
Aušra Pažėraitė, Mindaugas Krakauskas, Giedrius Radvila, Vidmantas Baltakis	
<i>Lithuanian Energy Institute; Lietuvos Energija AB;</i>	
<i>Sprendimų erdvė, Lithuania</i>	
Integration of tracking standard into electricity markets of Baltic states	182
Inga Konstantinavičiūtė, Dalius Tarvydas	
<i>Lithuanian Energy Institute, Lithuania</i>	
Tendencies of nuclear fuel utilization modes	186
Gediminas Adlys, Alvydas Jotautis, Ramūnas Naujokaitis Pranas Kanapeckas	
<i>Kaunas University of Technology, Lithuania</i>	
Nuclear energy mix in the Baltic see region	192
Gediminas Adlys, Olegs Linkevičs, Saulius Raila, Rūta Adlytė, Helmut Alt	
<i>Kaunas University of Technology, Lithuania; Latvenergo, Latvia;</i>	
<i>FH Aachen Fachbereich Elektrotechnik, Germany</i>	
Perspectives of nuclear cogeneration technologies	196
Gediminas Petrauskas, Gediminas Adlys, Diana Adlienė, Kęstutis Gediminskas, Algimantas Valinevičius	
<i>Kaunas University of Technology, Lithuania;</i>	
<i>Ignalina nuclear power plant, Lithuania</i>	
Allocating production cost of CHP plant to heat and power	200
Viktoria Neimane, Antans Sauhats, Guntars Vempers, Inga Tereskina	
<i>Vattenfall Research & Development, Sweden;</i>	
<i>Riga Technical University, Latvia;</i>	
<i>Riga Technical University, Latvia</i>	
<i>JSC "Siltumelektroprojekts", Latvia</i>	

Cross-border capacity auctions	205
Rimantas Deksnys, Robertas Staniulis, Giedrius Radvila <i>Kaunas University of Technology, Lithuania, AB „Lietuvos energija“, Lithuania</i>	
The neural network as the inductive engines states analyser	211
Boguslaw Twarog, Zbigniew Gomolka <i>University of Rzeszow, Institute of Technology, Poland</i>	
Investigation of the induction motor start up process using star-delta start	215
Marina Konuhova, Karlis Ketners, Elena Ketnere, Svetlana Klujevskā <i>Riga Technical University, Latvia</i>	
Rational geometry of a magnetic circuit of axial inductor generator	219
Svetlana Orlova, Vladislav Pugachov, Nikolaj Levin, Edmunds Kamolins <i>Institute of Physical Energetics, Latvia; Riga Technical University, Latvia</i>	
The edge effects influence on the braking force of linear induction motor	223
Bronius Karaliūnas, Edvardas Matkevičius <i>Vilnius Gediminas Technical University, Lithuania</i>	
Modeling of two-mass system with elasticity	227
Sigitas Juraitis, Roma Rinkevičienė, Jonas Kriaučiūnas <i>Vilnius Gediminas Technical University, Lithuania</i>	
The means of electromagnetic flow meter magnetic circuit testing	231
Valdas Jonas Pakėnas, Juozapas Arvydas Virbalis <i>Kaunas University of Technology, Lithuania</i>	
The attenuation of the electric reactor magnetic field strength	235
Jevgenij Morozionkov, Juozapas Arvydas Virbalis <i>Kaunas University of Technology, Lithuania</i>	
Digitally selected speeds for a direct current (DC) motor's applications	239
Sambwa Adoko, Onyekachi Adoko <i>Asa-Lambda Technology Ltd., Nigeria; Benson Idahosa University, Nigeria</i>	
Intensification of heat exchange in refrigeration technologies by use of corona field	243
Stasys Žebrauskas, Irmantas Beniulis <i>Kaunas University of Technology; Lithuania, Lithuanian University of Agriculture, Lithuania</i>	
Using of corona fields in building material industries	247
Stasys Žebrauskas, Ričardas Barčiauskas <i>Kaunas University of Technology, Lithuania</i>	
A comparative study between small traditional induction motors and small conducting sleeve induction motors using 3D finite element transient analysis	251
Seyed Mohsen Hosseini, Javad S. Moghani, Akram Hosseini <i>Amirkabir University of Technology, Iran</i>	
Graphical method of estimating optimum values for the main dimensions of a D.C. Machine	256
C. Easwarlal, V. Palanisamy, M.Y. Sanavullah <i>Sona College of Technology, India, Principal Info Institute of Engineering, India K.S.R. College of Technology, India</i>	
The research of causes and consequences of parameters changes of grounding electrical installations	261
Marina Kizhlo, Arvids Kanbergs <i>Riga Technical University, Institute of Power Engineering, Latvia</i>	

A simple transient-based wide-area selectivity technique for earth-faults in isolated and compensated neutral medium voltage networks	266
Mohamed F. Abdel-Fattah, Matti Lehtonen <i>Helsinki University of Technology (TKK), Espoo, Finland</i>	
Sensors for on-line partial discharge detection in covered-conductor overhead distribution networks	272
G. Murtaza Hashmi, Matti Lehtonen, Mikael Nordman, Muzamir Esa <i>Power Systems and High Voltage Engineering, Helsinki University of Technology (TKK), Espoo, Finland</i> <i>Ensto Utility Networks, Porvoo, Finland</i>	
Failures and diagnostics of power transformers	278
Sandra Vitolina, Janis Dirba <i>Riga Technical University, Latvia</i>	
Influence of the distribution of the axial, radial and circumferential component of the magnetic induction vector within the space between switches on rupturing capacity of vacuum switches	282
Bogdan Kwiatkowski, Robert Pękala <i>Rzeszow University, Technology and IT Institute; Rzeszow University, Technology and IT Institute, Poland</i>	
The research of the influence of the boundary conditions of the atmospheric overvoltages on the insulation of high voltage equipment	286
Saulius Gudžius, Linas Andronis Markevičius, Alfonsas Morkvėnas <i>Kaunas University of Technology, Lithuania</i>	
Insulation limit resistance performance assessment model	290
Alfonsas Morkvėnas, Renata Stanionienė, Povilas Valatka <i>Kaunas University of Technology, Lithuania</i>	
The models of sources of electromagnetic interferences over UHV line for transient processes investigation ...	294
Linas A. Markevičius, Vytautas Šiožinys <i>Kaunas University of Technology, Lithuania</i>	
Application of actual power deficiency value on load-shedding	298
Vladimir Chuvychin, Nikolay Gurov, Santa Kiene <i>Riga Technical University, Latvia</i>	
Technical advance in the automation of distributed network control	302
Virginijus Radziukynas, Arturas Klementavičius, Sigita Kadiša, Algimantas Leonavičius, Neringa Rutkauskaitė, Antanas Nemura, Feliksas Bielinskis, Viktorija Nezvanova <i>Lithuanian Energy Institute, Lithuania</i>	
Distributed generators: definition identification	308
Dainius Slušnys <i>Kaunas University of Technology, Lithuania</i>	
New accurate fault location method for multi-terminal power lines	312
Przemysław Balcerek, Marek Fulczyk, Jan Izykowski, Eugeniusz Rosolowski, Murari Mohan Saha <i>ABB Corporate Research Center, Poland;</i> <i>Wroclaw University of Technology, Poland;</i> <i>ABB Power Technology Systems, Sweden</i>	
Transient analysis of variable speed wind turbine	318
Djilali Kairous, Bachir Belmadani, Mostapha Benghanem <i>Faculty of Science and Sciences Engineering, UHB, Chlef, Algeria, Dpt. of Electrotechnics, UST, Oran, Algeria</i>	
Selected high-frequency power supply systems	323
Elżbieta Szychta, Kamil Kiraga <i>Technical University of Radom, Poland</i>	
Identification of parameters of synchronous generators' dynamic models	327
Mindaugas Ažubalis, Vaclovas Ažubalis, Audrius Jonaitis, Ramunas Ponelis <i>Kaunas University of Technology, Lithuania;</i> <i>Lietuvos energija AB, Lithuania</i>	

Potential of non-traditional energy sources for cold recovery in absorption refrigerating machines	333
Michail G. Berengarten, Semyon I. Vainshtein, Aleksandr S. Pushnov, Vytautas Adomavičius <i>Moscow State University of Ecological Engineering, Russian Federation</i> <i>The Centre of Renewable Energy Technologies at KTU, Lithuania</i>	
Possible perspectives of cooling tower application for electric energy production	337
Aleksandr S. Pushnov, Michail G. Berengarten, Semyon I. Vainshtein, Vytautas Adomavičius <i>Moscow State University of Ecological Engineering, Russian Federation</i> <i>The Centre of Renewable Energy Technologies at KTU, Lithuania</i>	
Application of renewable energy sources for feeding of water recycling systems technological equipment	343
Michail G. Berengarten, Semyon I. Vainshtein, Aleksandr S. Pushnov, Vytautas Adomavičius <i>Moscow State University of Ecological Engineering, Russian Federation</i> <i>The Centre of Renewable Energy Technologies at Kaunas University of Technology, Lithuania</i>	
Wind power plant with redox flow battery inverter – system converter energy conversion processes research	347
Povilas Balčiūnas, Povilas Norkevičius <i>Kaunas University of Technology</i> <i>The Centre of Renewable Energy Technologies at KTU, Lithuania</i>	
Hybrid water heating system based on solar collectors and heat exchanger fed from the centralised heat supply grid	352
Vytautas Adomavičius, Gytis Petrauskas <i>The Centre for Renewable Energy at KTU, Lithuania</i> <i>Kaunas University of Technology, Lithuania</i>	
Optimisation of hybrid water heating system based on solar collectors and heat exchanger in order to maximize solar heat energy's share	356
Vytautas Adomavičius, Gytis Petrauskas <i>The Centre of Renewable Energy Technologies at KTU, Lithuania</i> <i>Kaunas University of Technology, Lithuania</i>	
Control of energy fluxes in the grid-tied domestic power system based on wind energy	362
Česlovas Ramonas, Vytautas Adomavičius, Vytautas Kepalas <i>Kaunas University of Technology, Lithuania</i> <i>The Centre of Renewable Energy Technologies at KTU, Lithuania</i>	
Research of the power conversion processes in the system of power supply from a number of wind turbines over the one grid-tied inverter	368
Česlovas Ramonas, Vytautas Adomavičius, Vytautas Kepalas <i>Kaunas University of Technology, Lithuania</i> <i>The Centre of Renewable Energy Technologies at KTU, Lithuania</i>	
Comparison of small scale wind turbines' properties	374
Vytautas Adomavičius, Thomas Watkowski, Edmundas Žilinskas, Alfonsas Adomavičius <i>The Centre for Renewable Energy Technologies at Kaunas University of Technology, Lithuania</i> <i>Lithuanian-German joint venture UAB Tometa, Germany</i> <i>Joint Stock Company UAB Saules energija, Lithuania</i> <i>Kaunas Business Machines Company, Lithuania</i>	
Peculiarities of wind power plants' work in the small power system	380
Tomas Deveikis, Enrikas Nevardauskas, Renata Stanionienė <i>Kaunas University of Technology, Lithuania</i> <i>The Centre of Renewable Energy Technologies at KTU, Lithuania</i>	

A NEW APPROACH BASED ON SUPPORT VECTOR MACHINE TO ANALYSE AND CONTROL THE REM-SLEEP-STAGE

Maria KRAUTWALD, Rudolf BAUMGART-SCHMITT, Daniel TROMMER, Christian WALTHER
University of Applied Sciences Schmalkalden, Faculty of Electrical Engineering, Germany

Abstract: The sleep stage of rapid-eye movement (REM) should be recognized in real-time to evaluate the current sleep quality. A robust recognition on the basis of only one frontal electro-encephalogram (EEG) channel is necessary to give the sleep stage researcher the opportunity to control the following sleep-stages of the patient.

A new approach based on a Support Vector Machine was developed. We classify the REM-stage with different data sets. An adapted kernel with RBF (radial basis function) topology was applied. On the base of these we try to implement the algorithm on a microcontroller-platform. By this way a mobile wireless device can diagnose the actual sleep stage and the further sleep-profile can control by medical treatments.

Keywords: nonlinear classification, EEG, REM-sleep-stage, support vector machine.

1. Introduction

The purpose of this paper is to show a solution for analyzing the sleep-stages concerning the REM or Non-REM-sleep-stages.

Besides the REM-sleep there are four other sleep-stages. From Stage I, the drowsy sleep, to Stage IV, the deep sleep, the depths of the sleep increase and in order that the relaxation of the body increase too. Coevally the threshold for awakening becomes more and more high.

The REM-sleep, the dream sleep, has a special part there. It gets this name because this stage is characterized by rapid eye movements especially in the early morning hours.

Currently there are only hypotheses concerning the meaning of REM-sleep which is the aim of many experimental studies. Searchers try to find this meaning by analyzing the REM-sleep and coevally the memory of the subject or even deprive REM-Sleep and observe the consequences [1]. But there is still further need for research.

The conventional method of analyzing the sleep-stage is to collect the EEG with a 2-channel Electro-Encephalograph at least and classify this EEG by an expert manually. To support the scientists and to disburden this procedure a mobile device with a one-channel EEG-receiver shall be developed for automatic online classification.

A Support-Vector-Machine (SVM) approach shall be used. This is a mathematic method to differ between two or more classes. The SVM is especially suitable for solving two-class-problems.

To get a mobile device it is necessary to implement the SVM on a microcontroller. Therefore this paper should give a perspective for realizing this problem.

Furthermore by knowing REM or Non-REM-stage it is possible to control externally the stage by administration of pharmaceutical or distortions of the REM-sleep.

2. Methods

The Support Vector Machine (SVM) is a mathematical method to solve classification problems. For training a SVM a set of training data are required [2]. In our cases that means the training data consists of a set of EEG-data and the associated classification which was done by an expert. With this training data it is possible to define a decision function. To valuate the SVM it has to be tested with testing data. The SVM calculates with the EEG-data and the decision function the class. A comparison of the artificial classification to the manual classification of the expert is done afterwards. At the end it is possible to estimate the performance of the SVM and the decision function which is a result of the training data. To demonstrate the functionality an easy type of classification is shown in the following.

The easiest type is the separation of two classes in a two dimensional decision space. The advantage of this example is that it can easily visualize. So it is possible to imagine the mathematical relations.

Figure 1 shows a two dimensional room with a training-dataset $\{\underline{x}_i, y_i\}$ illustrate by a set of white circles (class 1) and a set of black circles (class 2).

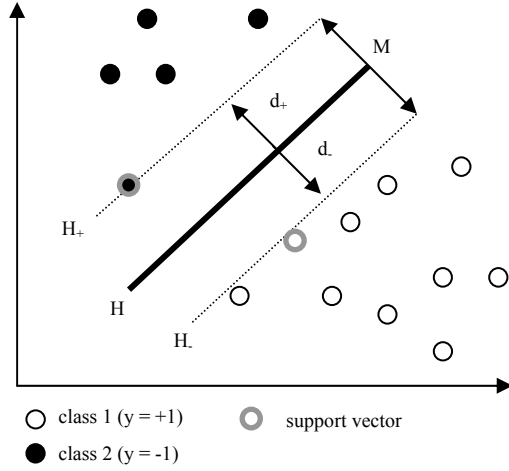


Fig. 1. Two classes in a two dimensional decision space, with class 1 as white circles, class 2 as black circles, H as the hyperplane, M as the margin, H_+ as positive shifted hyperplane, H_- as negative shifted hyperplane, d_+ as the distance from the hyperplane to a shifted hyperplane and the grey circle as the support vectors

The index $i = 1, 2, \dots, n$ and describe a consecutive numbering where n is the quantity of data pairs $\{\underline{x}, y\}$. For identifying a decision function a straight line (the so called hyperplane) has to be placed between both sets. The hyperplane is defined as:

$$H = \{\underline{x} \mid \langle \underline{w}, \underline{x} \rangle + b = 0\}, \quad (1)$$

where \underline{w} is the normal vector, which is orthogonal to the hyperplane, b the displacement and $\langle \underline{w}, \underline{x} \rangle$ describe the dot product.

It result the decision function:

$$f(\underline{x}_{new}) = \text{sign}(\langle \underline{w}, \underline{x}_{new} \rangle + b). \quad (2)$$

Of cause there exist infinite possibilities for such a hyperplane. So it is necessary to define the restriction: the margin M has to be maximized. The maximum margin depends on the vectors next to the hyperplane. These vectors are called support vectors (marked in Figure 1). That's the reason why this method is called support vector machine.

Furthermore the data were scaled so that the support vectors are in a distance of 1 to the hyperplane. That means that y_i are only +1 or -1. So the straight lines H_1 and H_2 are defined as:

$$H_1 = \{\underline{x} \mid \langle \underline{w}, \underline{x} \rangle + b = 1\} \quad (3)$$

and

$$H_2 = \{\underline{x} \mid \langle \underline{w}, \underline{x} \rangle + b = -1\}. \quad (4)$$

The distance d is defined as:

$$d(H, \underline{x}_i) = y_i \left(\left\langle \frac{\underline{w}}{\|\underline{w}\|}, \underline{x}_i \right\rangle + \frac{b}{\|\underline{w}\|} \right), \quad (5)$$

where $\|\underline{w}\|$ is the norm of the vector \underline{w} which is defined as:

$$\|\underline{w}\| = \sqrt{\langle \underline{w}, \underline{w} \rangle}. \quad (6)$$

For this reason:

$$d_+ = +1 = \langle \underline{w}, \underline{x}_+ \rangle + b \rightarrow \left\langle \frac{\underline{w}}{\|\underline{w}\|}, \underline{x}_+ \right\rangle + \frac{b}{\|\underline{w}\|} = \frac{1}{\|\underline{w}\|} \quad (7)$$

and

$$d_- = -1 = \langle \underline{w}, \underline{x}_- \rangle + b \rightarrow \left\langle \frac{\underline{w}}{\|\underline{w}\|}, \underline{x}_- \right\rangle + \frac{b}{\|\underline{w}\|} = \frac{1}{\|\underline{w}\|}, \quad (8)$$

the margin M result from:

$$M = d_+ + d_- = \left\langle \frac{\underline{w}}{\|\underline{w}\|}, (\underline{x}_+ - \underline{x}_-) \right\rangle = \frac{2}{\|\underline{w}\|}. \quad (9)$$

That means to maximize the margin requires minimizing $\|\underline{w}\|$ which is equivalent to minimize $\|\underline{w}\|^2$. So the constrains are:

$$\langle \underline{w}, \underline{x}_i \rangle + b \geq 1 \text{ if } y_i = 1 \quad (10)$$

and

$$\langle \underline{w}, \underline{x}_i \rangle + b \leq -1 \text{ if } y_i = -1. \quad (11)$$

But usually the datasets aren't completely separable like it is shown in Figure 2. For this case parameter C , the penalty factor, and ε , the slack variable, are established. C controls the trade off between errors and margin maximization. If C is too small there are too many training errors and the SVM is under fitted, if C is too large the SVM is over fitted, the hyperplane is to complex, there are many support vectors and the margin becomes small.

The slack variable ε is the distance of error vectors to their correct position. The sum of ε_i for $i = 1, 2, \dots, n$ should has it's minimal value.

Now there are two restrictions: the margin and the number of errors have to be minimized. Therefore the goal of minimizing is modified to:

$$\frac{1}{2} \|\underline{w}\|^2 + C \sum_{i=1}^n \varepsilon_i, \quad (12)$$

with the constraints:

$$\langle \underline{w}, \underline{x}_i \rangle + b \geq 1 - \varepsilon_i \text{ if } y_i = 1 \quad (13)$$

and

$$\langle \underline{w}, \underline{x}_i \rangle + b \leq -1 + \varepsilon_i \text{ if } y_i = -1. \quad (14)$$

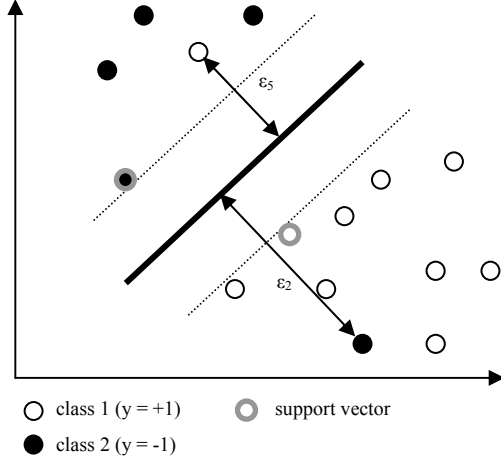


Fig. 2. Linear non-separable case of data classification, with class 1 as white circles, class 2 as black circles, grey circles as support vectors, ε_i with $i = 2, 5$ as the distance of error vectors to their correct position

An approach for solving this optimization problem is the Lagrange-function:

$$L(x, \alpha) = f(x) + \alpha h(x), \quad (15)$$

with optimization function $f(x)$, constrain in 0-form $h(x)$ and Lagrange multiplier α .

For separable case is the primal form of L:

$$L_p(\underline{w}, b, \alpha) = \frac{1}{2} \|\underline{w}\|^2 - \sum_{i=1}^n \alpha_i (y_i (\langle \underline{w}, \underline{x}_i \rangle + b - 1)), \quad (16)$$

where \underline{w} and b have to minimize and α have to maximize ($\min_{\underline{w}, b} \max_{\alpha} L(\underline{w}, b, \alpha)$). For this purpose the first derivation after \underline{w} and after b is set equal to zero. One obtains:

$$\frac{dL_p}{db} = 0 \rightarrow \sum_{i=1}^n \alpha_i y_i = 0 \quad (17)$$

and

$$\frac{dL_p}{d\underline{w}} = 0 \rightarrow \underline{w} = \sum_{i=1}^n \alpha_i y_i \underline{x}_i. \quad (18)$$

Inserted in L_p it follows the dual form:

$$L_d(\alpha) = \sum_{i=1}^n \alpha_i - \frac{1}{2} \sum_{i,j=1}^n \alpha_i \alpha_j y_i y_j \langle \underline{x}_i, \underline{x}_j \rangle, \quad (19)$$

with the constraints:

$$\alpha_i \geq 0 \text{ and } \sum_{i=1}^n \alpha_i y_i = 0. \quad (20, 21)$$

Then α_i can be calculated such that L_d is maximized. The decision function can be written as:

$$f(\underline{x}_{new}) = \text{sign} \left(\sum_{i=1}^n \alpha_i y_i \langle \underline{x}_i, \underline{x}_{new} \rangle + b \right). \quad (22)$$

That's the solution for a linear and separable problem. But most of the problems in the nature are nonlinear. To avoid the nonlinear problem there is the possibility to go in a higher dimension where the problem becomes linear. Figure 3 and 4 visualize this circumstance.

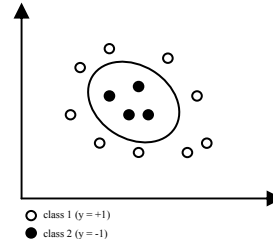


Fig. 3. Complex classification in a two dimensional decision space

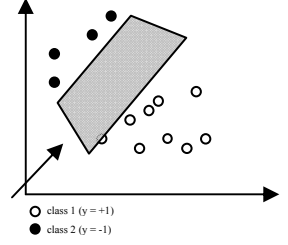


Fig. 4. Simple classification in a three dimensional decision space

In the two dimensional space the dot product are used. In a higher dimension the dot product have to be converted. That can be very complex or not possible. In this situation the so called "kernel trick" afford an answer. A kernel is a function which behave in a higher dimension like the dot product in the two dimensional space. The decision function has the form:

$$f(\underline{x}_{new}) = \text{sign} \left(\sum_{i=1}^n \alpha_i y_i K(\underline{x}_i, \underline{x}_{new}) + b \right). \quad (23)$$

For the results a Raial Basis Function(RBF)-Kernel was used.

$$K(\underline{x}_i, \underline{x}_j) = \exp(-\gamma \|\underline{x}_i - \underline{x}_j\|^2) \quad (24)$$

with the real valued parameter $\gamma > 0$.

In the following the cycle of training and testing a SVM is described for our sleep data set based on the approach of [3]. At first 53 features are calculated with a raw-EEG data and the associated classification. Then a file with the relative time of an epoch, the 53 features and a eight class classification is created. In the next step the

eight-class-file is converting to a two-class-file with the classes REM or Non-REM. Now the epochs were sorted according to the manually classified classes. This procedure is executed with the training- and the testing data.

Of cause the Non-REM class is more dominant then the REM class. Because of that the same of samples are taken from each class in a randomized mode. That's avoiding one class proffered. Next step is the scaling of the training data. After that the SVM try to optimize the parameter C and γ by testing C and γ in a specific grid. For testing the SVM the cross validation is applied. That means all training datasets except one are used for training and the remaining one for testing. This procedure (one has to leave out) will be repeated for all possible combinations of data.

If C and γ are defined the training of the SVM begins. Subsequent to this also the testing data are scaled and the SVM predict the classes of the test data and compare the result with existing classification.

3. Results

Because of the individualism of every human it is difficult to classify EEG-signals on the basis of training data from another patient.

In consideration of this the result of 83.07% correct classification is satisfying.

The results have to observe critically. Often one class was preferred. And even if the SVM can classify to 90% it is disuse because it only classified Non-REM which was present to 90%. There are two possibilities to avoid this situation. First is to test the SVM with Non-REM and REM in a data record ratio 1:1. Another is to adjust prediction of the SVM that both classes are predicted percent similar.

The results were analyzed by calculating how much percent of each class was classified correctly. Like it shown in Table 1 class Non-REM were classified by 83.84 % and REM by 79.26 %. These values are nearly similar. Then the SVM is suitable for online classification.

Table 1. Results of classification by the Support Vector Machine

testing-data	Non-REM	REM
number of epochs	10793	2175
number of epochs in %	83.23	16.77
right classify epochs	9049	1724
right classify epochs in %	83.84	79.26

For online classification at first all necessary data for classification have to save on microcontroller. That includes mainly the model file which is between 30kB and 100kB. At second the EEG-data have to sample and scale. Next 53 features need to calculate. Then the prediction-program can make a decision. For real time classification this procedure must take four milliseconds at most.

4. Conclusion

The results of the SVM have to observe critically because of a possible preference of one class.

The SVM is suitable for a two class classification. Even for classification of biological signals it can be used but it doesn't achieve excellent percent values.

The suitability of the SVM concerning two-class classification of biological signals was also shown before with anaesthetic classification between awake - not awake and stage A4 - not A4. The results were over 80% by using different datasets [4].

In multiclass-classification a SVM show similar results compared to Fuzzy-Logic and neuronal networks [5].

Every learnt SVM only need one prediction algorithm and appending upon Training-data different Input data. That is the reason why a SVM could be very efficient on a microcontroller platform.

5. References

1. Rasch B., Pommer J., Diekelmann S. & Born J. Pharmacological REM sleep suppression paradoxically improves rather than impairs skill memory Nature Neuroscience advance online publication Published online: 5 October 2008 doi:10.1038/nn.2206
2. Suykens J.A.K., Van Gestel T., De Brabanter J., De Moor B. & Vandewalle J. Least squares support vector machines World Scientific Publishing Co. Pte. Ltd: 2002 ISBN 9812381511
3. Hsu C.-W., Chang C.-C. and Lin C.-J. A Practical Guid to Support Vector Classification. Dec 20 2007. www.csie.ntu.edu.tw/~cjlin
4. Walther C., Baumgart-Schmitt R. and Backhaus K. Support Vector Machines and Optimized Neural Networks – Adaptive Tools for Monitoring and Controlling the Depth of Anaesthesia. Proceedings of International Conference “Electrical and Control Technologies – 2008”, Kaunas, 2008. p. 11-14.
5. Baumgart-Schmitt R., Walther C. and Backhaus K. Design and Assessment of Fuzzy Rules by Multi Criteria Optimization to Classify Anaesthetic Stages. 4th European Congress of the International Federation for Medical and Biological Engineering, Antwerp, Belgium, 2008.

ADAPTION OF FUZZY RULES BY DIFFERENT MULTI CRITERIA OPTIMIZATION PROCEDURES TO CONTROL STAGES OF ANAESTHESIA

Christian WALTHER, Rudolf BAUMGART-SCHMITT, Maria KRAUTWALD, Daniel TROMMER
University of Applied Sciences Schmalkalden, Faculty of Electrical Engineering, Germany

Abstract: Fuzzy rules were designed to classify four different stages of anaesthesia and the wake stage additionally. Feature sets of one frontal EEG channel measured during operations in hospitals were used to create and adapt fuzzy models. The topology and the parameters of the models were optimized by evolutionary algorithms based on three different multi criteria optimization procedures: NSGA II, SPEA II and IBEA. Typical fuzzy models were selected from the amount of trained fuzzy rules contained in the resulting Pareto set. The performance of the fuzzy models to classify and control the depth of anaesthesia was tested by independent data sets.

Keywords: Fuzzy modelling and control, multi criteria optimization, evolutionary algorithms, anaesthesia, frontal EEG.

1. Introduction

The analysis of the depth of anaesthesia is a challenge for the anaesthesiologists. Because of the difficulties to predict the exact patient's reaction to medical drugs a lot of experiences are necessary up to now. To get information about the actual patient state they use vital and breathing parameters of the patient. The whole procedure of anaesthesia is very complex. Both the consciousness and pain are gradually suppressed by different kinds of medicinal drugs. The muscles are relaxed too by this way to permit an optimal surgical access to the operation site. The information from vital parameters, breathing activity and dosages of the administered medicinal drugs are used by the anaesthesiologist to control the depth of anaesthesia of the patient. Another way to get information about the consciousness stages of the patient is to analyze the electroencephalogram (EEG). But in this case the anaesthesiologist has to be an expert in analyzing the EEG in real-time. To support the anaesthesiologist we developed algorithms to calculate the depth of anaesthesia based on the frontal one-channel EEG [1,2,3]. Different fuzzy rules are used to classify four

different stages of anaesthesia and one wake stage. During the training procedure of the fuzzy sets evolutionary operators and multi criteria optimization algorithms were used. We optimized the fuzzy models by three different multi objective evolutionary algorithms (MOEA). The final result is represented by a set of solutions in the multi criteria space called Pareto set. The first implemented algorithm was the Non-dominated Sorting Genetic Algorithm II (NSGAI) developed by Deb et al. [7]. To test the hypothesis that the results are depended on the used approach further MOEA's were employed: The Strength Pareto Evolutionary Algorithm II (SPEAII) and the Indicator-Based Evolutionary Algorithm (IBEA) were included. The last two evolutionary algorithms were developed by Zitzler et al. [8, 9].

2. Materials and Methods

The frontal one-channel electroencephalogram from different patients was recorded during the operation procedure in cooperation with our hospital partners in Schmalkalden and Zella-Mehlis (Germany). The corresponding autonomous parameters like heart rate, blood pressure or breathing information from the patients were also saved. Based on this vital information the anaesthesists were able to rate the whole data sets and to divide the EEG into different epochs of stages of anaesthesia. They distinguish between the stages "W - wake", "A1 - light sedation", "A2 - surgical tolerance", "A3 - deep anaesthesia" and "A4 - Burst-Suppression" with A4 as the deepest stage of anaesthesia. Every stage describes an EEG epoch with the length of 10 seconds within the whole EEG recording of a patient. We divided the rated EEG recordings of 20 patients into two different data sets for training and validation. Basically we used the rated EEG data sets from 10 different patients for training purposes (Table 1).

In [3] we have already presented an opportunity to classify the frontal one-channel EEG by using fuzzy models. Furthermore we used artificial neural networks

and support vector machines to solve this nonlinear classification problem [1,2]. To increase the performance of the selected fuzzy model we introduced more than one fuzzy rule for one class. The number of fuzzy rules which can be used for classification is theoretically unrestricted. Up to now one rule per class was used [3]. To improve the performance of the classifier on the one hand and to limit the computing time on the other hand the number of fuzzy rules were restricted to three per class in this case.

To optimize the structure and the parameters of the fuzzy model by the evolutionary procedure we tested three different MOEAs: the NSGAI, SPEAI and IBEA. The implemented algorithms are described in [4,6,7,8] and [9]. All three MOEAs have in common an internal elitist population of individuals which is updated throughout the optimization process. In our case one individual is represented by a certain fuzzy model, which will be optimized. A set of individuals form a population.

The multi criteria optimization procedures use four different quality values to decide if a fuzzy model is able to classify the five anaesthetic stages correctly and if it is working effectively. The first quality value q_1 evaluate the number of epochs of EEG in the training set which were correctly classified by the fuzzy model. The second goal function q_2 is defined by a mean value of correctly classified epochs for each class of anaesthesia separately. The third criterion q_3 evaluates the worst rated class by the fuzzy model. The last quality criterion q_4 is a value of effectiveness. It represents the counted activated fuzzy sets within the fuzzy model as a value in percentage. If this value is high, the fuzzy model is using a lower number of fuzzy sets for classification.

At the beginning of the optimization process a population is randomly initialized (fig. 1). In a first step, after the calculation of the criteria for every individual of the population, the population is sorted. For every individual a value of density is calculated within the MOEA. This value represents the position of the individual as an element inside the Pareto set and describes the relationship to the other individuals of the population. In a last step the best individuals are selected out of the population to create an updated elite pool, which is saved for the next iteration. Apart from this elite population a further child population is generated by the genetic operators "recombination" and "mutation". This child population forms the new population of individuals for the next iteration.

The MOEAs differs in internal sorting procedures and calculation of the density values. These algorithms were implemented to find and select the best fuzzy models for the genetic operators to generate the next generation of new fuzzy model populations. When a new fuzzy model is generated by the recombination process it could be randomly influenced by a mutation operator (fig. 1). The two genetic operators are responsible for the inclusion of single fuzzy sets, which belongs to the resulting fuzzy model.

Table 1. General information about the data sets recorded from different patients used in the training set

Data Set	Gender	Age	Epochs
0066	F	52	1180
0007	F	62	1438
0006	F	63	449
0010	F	45	1286
0011	F	66	947
0009	F	36	355
0072	F	75	1828
0012	F	37	614
0021	F	42	1068
0024	F	41	995

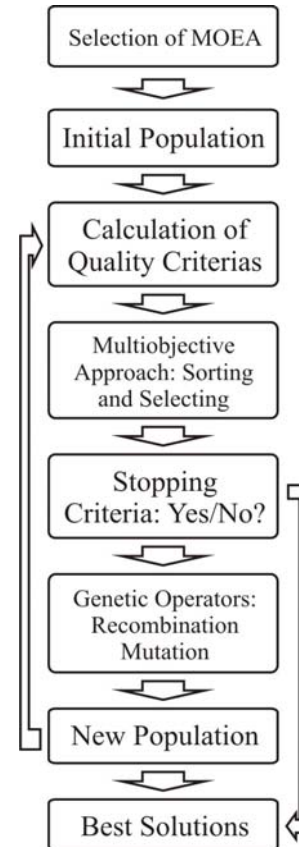


Fig. 1. General approach to generate and optimize fuzzy models, which are able to classify anaesthetic stages. Multi-objective evolutionary algorithms are used for optimization. A population consists of different individuals. One individual represents one adapted fuzzy model

Table 2. General information about the data sets recorded from different patients used in the validation set. The capital F means female and M means male

Data Set	Gender	Age	Number of Epochs
0121	F	73	1745
0118	F	77	385
0117	M	47	546
0116	M	65	371
0125	F	84	399
0127	F	24	440
0126	F	45	283
0134	F	45	299
0135	M	67	467
0128	M	55	1389

The generally used structure of membership function $\mu(x,a,b)$ for each fuzzy set is:

$$\mu(x,a,b) = e^{[-0.5((x-a)/b)]}, \quad (1)$$

with x as normalized input value and a and b as real parameters. The two parameters a and b are changed by the mutation operator in a defined range.

To end up the whole optimization procedure a stopping criterion is needed. For that purpose a subset of EEG epochs from the training set was extruded to check the performance of the actual population of fuzzy models. To calculate the stopping criteria every fuzzy model of the elitist population has to classify this EEG subset. Furthermore the median on all resulting classifications is used to represent the performance of all fuzzy models together. If the quality of the Pareto set significantly decreases in the actual population, the optimization procedure is stopped and the elitist population of one generation before is saved as the final result.

To validate the performance of the trained fuzzy models a validation set of 10 other patient EEG recordings was used (table 2). These data sets were not used to train the fuzzy models.

3. Results

To get the final results, which are represented in the tables 4, 5, 6 and 7 a sub set of fuzzy models was extracted from the Pareto-optimal front for every MOEA-Run. At the end of a multi-criteria optimization process a suitable number of solutions have to be selected from the Pareto set. In our case a general selection criterion was defined by the sum of the weighted criteria q_1 to q_4 for every individual of the Pareto-optimal front. If this selection criterion has a high value the evaluated individual implies a high performance within the search space. The used weight modes A_w and B_w with different weight vectors are presented in table 3.

After the selection of the individuals, these different optimized fuzzy models were used to classify the validation data (table 2). To explain the problem of finding the best solutions using the two different weight modes A_w and B_w the validation results of the respective individuals are presented in table 4 and 5. Both sets of individuals were trained in the optimization process using the NSGAI algorithm. The fuzzy models used to calculate the solutions presented in table 5 show a slightly better performance in comparison to the solutions of table 4. The performance is measured by the degrees of concordance between the automatic classification in each column and the given ratings of the anaesthesiologists in each row. Beside the diagonal fields there are also some grey highlighted rectangles in the tables 4, 5, 6 and 7. This means that confusions indicated by these values inside the rectangles are negligible. The fuzzy models which have performed the results of table 5 were only found by using the weight mode B_w .

Table 3. Used selection weight modes applied to the criteria of every single individual to extract a subset of individuals from the Pareto-optimal front. The criteria are multiplied by the presented weight factors. The sum of these weighted single criteria forms the applied selection criterion

Criteria	q_1	q_2	q_3	q_4	Table
Weight mode A_w	0.4	0.3	0.3	0.0	4,6,7,8
Weight mode B_w	0.2	0.4	0.4	0.0	5

Table 4. Validation results of the fuzzy models, which were optimized using the non-dominated sorting genetic algorithm II and selected from the Pareto-front using weight mode A_w . Each row represents the classification estimation given by an anaesthesiologist for all epochs of this class. Each column presents the degrees of concordance of the automatic classification done by the selected fuzzy models with the manually rated epochs

NSGAI	W	A1	A2	A3	A4
W (E)	19.8	47.8	9.9	2.7	19.8
A1 (E)	3.2	43.6	16.5	21.4	15.3
A2 (E)	0.1	4.9	32.7	60.4	1.7
A3 (E)	0.0	0.3	14.3	82.4	3.0
A4 (E)	0.0	0.8	5.7	31.3	62.1

Table 5. Validation results of the fuzzy models, which were optimized using the Non-dominated Sorting Genetic Algorithm II and selected from the Pareto-front using weight mode B_w

NSGAI	W	A1	A2	A3	A4
W (E)	21.6	44.1	8.1	1.8	24.3
A1 (E)	5.2	42.3	17.4	13.3	21.8
A2 (E)	0.1	5.4	35.4	57.7	1.5
A3 (E)	0.0	0.3	16.7	78.5	1.5
A4 (E)	0.0	1.4	4.3	27.4	66.9

Table 6. Validation results of the fuzzy models, which were optimized using the Strength Pareto Evolutionary Algorithm II and selected from the Pareto-front using weight mode A_w

SPEAI	W	A1	A2	A3	A4
W (E)	27.9	43.2	4.5	7.2	17.1
A1 (E)	5.24	44.8	18.2	16.1	15.7
A2 (E)	0.6	4.9	27.6	63.3	3.5
A3 (E)	0.1	0.9	8.4	86.6	4.0
A4 (E)	0.3	2.0	7.6	30.8	59.4

Table 7. Validation results of the fuzzy models, which were optimized using the Indicator-Based Evolutionary Algorithm and selected from the Pareto-front using weight mode A_w

IBEA	W	A1	A2	A3	A4
W (E)	63.1	10.8	0.0	2.7	23.4
A1 (E)	10.5	41.5	17.3	5.7	25.0
A2 (E)	0.0	4.4	43.1	46.5	6.0
A3 (E)	0.0	1.8	20.6	70.9	6.8
A4 (E)	0.1	6.0	11.9	17.2	64.8

The performances of the generated fuzzy models, which were optimized using the evolutionary algorithms SPEAII and IBEA are presented in the tables 6 and 7. In table 8 the degrees of concordance are additionally presented for a two class problem, based on the distinction between the deepest narcotic stage A4 to all other stages.

Table 8. Validation results of the fuzzy models, which were optimized using the Non-dominated Sorting Genetic Algorithm II and selected from the Pareto-front using weight mode A_w . The fuzzy models were trained to solve a two-class problem to distinguish between the set of the stages W, A1, A2, A3 and the stage A4

NSGAI	W,A1,A2,A3	A4
W,A1,A2,A3 (E)	89.4	10.6
A4 (E)	31.6	68.4

4. Discussion

Despite using different multi criteria procedures the results differ only slightly in classification of the validation data.

Differences in the degrees of concordance obviously only depend on the chosen individuals and the used selection criteria, which were defined by a weight mode. Mainly the three multi-objective evolutionary algorithms differ in sorting the individuals and calculating the density value for each fuzzy model. This causes a different speed of the optimization process itself for each algorithm. In every case a population of optimized individuals is generated as a result. Measurements of the optimization speed of such algorithms (NSGAI, SPEAII and IBEA) were not analyzed within this work. To estimate the efficiency of the multi criteria optimization procedures defined test functions were employed by coworker Hoffmann [4].

The tables 4, 5, 6 and 7 contain higher degrees of confusions of the stage W and A1 to the stage A4. These values are a result of the higher dimensionality of the fuzzy models in the training procedure in comparison to [3]. It is possible to distinguish correctly between Wake, A1 and A4, which was shown in [1] and [3]. This is underlined by the results shown in Table 8.

5. Conclusions

The performance of the fuzzy models measured by the validation set is mainly dependent on the selection criterion. All members of the Pareto set represent a knowledge base, which was optimized during the multi-objective evolutionary optimization process.

This knowledge base established during training is used to generalize. By means of the weight vectors the generalizing can be controlled in a final step.

6. References

1. Walther C., Baumgart-Schmitt R. and Backhaus K. Support Vector Machines and Optimized Neural Networks – Adaptive Tools for Monitoring and Controlling the Depth of Anaesthesia. Proceedings of International Conference “Electrical and Control Technologies – 2008”, Kaunas, 2008. p. 11-14.
2. Baumgart-Schmitt R., Walther C., Backhaus K., Reichenbach R., Sturm K.-P. and Jäger U. Robust Nonlinear Adaptive Network Classification of Anaesthesia. 2008 IAPR Workshop on Cognitive Information Processing, Santorini, Greece, 2008.
3. Baumgart-Schmitt R., Walther C. and Backhaus K. Design and Assessment of Fuzzy Rules by Multi Criteria Optimization to Classify Anaesthetic Stages. 4th European Congress of the International Federation for Medical and Biological Engineering, Antwerp, Belgium, 2008.
4. Hoffmann T. Erprobung von Methoden mehrkriterieller Optimierung zur nichtlinearen Klassifikation am Beispiel von simulierten Evolutionsstrategien. Diploma thesis. University of Applied Sciences Schmalkalden, Germany, 2009.
5. Kim M.-S., Kim C.-H. and Lee J.-J. Structure/Parameter Optimization of Fuzzy Models by Evolutionary Algorithm. Proceedings of the IASTED International Conference on Intelligent Systems and Control, Salzburg, Austria, 2003.
6. Laabidi K., Bouani F. and Ksouri M. Multi-criteria optimization in nonlinear predictive control. Mathematics and Computers in Simulation, Volume 76, Issue 5-6, 2008. p. 363-374.
7. Deb K., Pratap A., Agarwal S. and Meyerivan T. A Fast and Elitist Multiobjective Genetic Algorithm: NSGA-II. IEEE Transactions on Evolutionary Computation, Volume 6, Issue 2, 2002. p. 182-197.
8. Zitzler E., Laumanns, M. and Thiele L. SPEA2: Improving the Strength Pareto Evolutionary Algorithm. TIK-Report 103, Swiss Federal Institute of Technology Zurich, Switzerland, 2001.
9. Zitzler E. and Künzli S. Indicator-Based Selection in Multiobjective Search. Proceedings of the 8th International Conference on Parallel Problem Solving from Nature (PPSN VIII), Birmingham, UK, 2004. p. 832-842.

INVESTIGATION OF THE INFLUENCE OF FUZZY SET STRUCTURE TO THE COLOR SEGMENTATION

Toma NAKVOSAITĖ*, Vidas RAUDONIS**, Rimvydas SIMUTIS**, Audrius PUKEVIČIUS*

*Department of Control Technologies, Kaunas University of Technology, Lithuania,

**Department of Process Control, Kaunas University of Technology, Lithuania

Abstract: An Adaptive Neuro-Fuzzy Inference System (ANFIS) with a hybrid learning algorithm is used for color segmentation in this work. An algorithm for testing different fuzzy set structures was composed and it was used to extract the iris of a human eye in a color image. An efficiency of each tested fuzzy set structure was evaluated according to its applicability to an eye position tracking system. A desirable precision of extraction was reached with the simplest ANFIS structure possible. Image processing rate depends on the structure of the fuzzy set.

Keywords: Adaptive Neuro-Fuzzy Inference System, color segmentation, fuzzy set.

1. Introduction

Over the last decade there has been growing interest within the computer vision and pattern recognition communities in the problem of analyzing the human eye behaviour in the video. A real-time eye tracking requires a method and algorithm, which allows effective and fast determination of a human eye position in a two dimensional data space. The position of the eye pupil can be tracked using various techniques based on the measurements of the potential differences which appear between electrodes mounted around the user eye or using video cameras. One of the relatively cheapest ways to gather information for this purpose is to use a web camera, so this leaves us with analysis of color images of an eye.

Color segmentation of an image for feature extraction is researched and applied widely. Many segmentation methods and algorithms are developed and tested, such as brightness invariant segmentation using B-spline curve fitting [1], context-dependent segmentation [2], segmentation using luminance histograms [3], spatial color histograms [4]. However most of the proposed methods are suitable only for particular application.

Several approaches of color segmentation based on the fuzzy logic are proposed in [5, 6, 8] – instead of traditional CCHs, Fuzzy Color Histogram (FCH) is

proposed. FCH considers the color similarity information by spreading each pixel's total membership value to all the histogram bins. Other approaches measure fuzzy homogeneity in path of image pixels [7], where resemblance between color features is calculated on the basis of distances in the HSI color space.

In this work a potential of using fuzzy sets for color segmentation in the image is investigated. We use an Artificial Neuro-Fuzzy Inference System (ANFIS), which requires to be trained. Pixel values of an image in RGB color space was used as an input for the developed algorithm and black - white image is obtained as an output. ANFIS allows choosing different structures of fuzzy sets (quantity and shape of membership functions). Our task in this work was to find the most efficient fuzzy set structure, which can be used in real-time eye position estimation.

This paper is organized in 4 sections. Basic idea of ANFIS algorithm is presented in the second section, investigation algorithm is presented in the third, more detailed description of the experiments and their results are presented in the fourth.

2. Theoretical background

General fuzzy inference is used in systems whose rule structures are predetermined by the user and membership functions are fixed and arbitrarily chosen. ANFIS allows generating fuzzy inference system automatically, without having predetermined structure based on characteristics of variables in the system. Membership function parameters are set during learning process of the inference system. Adaptive network based fuzzy inference systems (ANFIS) is a FIS implemented in the framework of an adaptive fuzzy neural network. Neuro-adaptive learning techniques provide a method for the fuzzy modelling procedure to learn information about a data set, in order to compute the membership function parameters that best allow the associated fuzzy inference system to track the given input/output data. ANFIS constructs a fuzzy inference

system, (FIS) whose membership function parameters are adjusted using either a backpropagation algorithm alone, or in combination with a least squares type of method (used in this work). The computation of parameters associated with membership functions is facilitated by a gradient vector, which provides a measure of how well the fuzzy inference system is modelling the input/output data for a given set of parameters. Once the gradient vector is obtained, any of several optimization routines could be applied in order to reduce some error measure.

ANFIS only supports Sugeno-type systems that follow requirements:

- Be first or zeroth order Sugeno-type systems.
- Have a single output, obtained using weighted average defuzzification.
- Have no rule sharing. Different rules cannot share the same output membership function.
- Have unity weight for each rule. A typical rule in a Sugeno fuzzy model has the form

If the system with two inputs and one output is used, where first input is equal to x and second is equal to y , then output can be written as:

$$z = ax + by + c \quad (1)$$

For a zero-order Sugeno model, the output level z is a constant ($a=b=0$).

The output level z_i of each rule is weighted by the firing strength w_i of the rule. For example, for an AND rule with Input 1 = x and Input 2 = y , the firing strength is

$$w_i = \text{AndMethod}(F_1(x), F_2(y)),$$

where $F_{1,2}$ are the membership functions for Inputs 1 and 2. An AND operation of 2 triangular fuzzy sets A and B is shown in Fig. 1. The result of intersection is a fuzzy set "A and B".

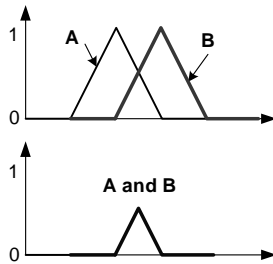


Fig. 1. The AND operation of two membership functions

The final output of the system is the weighted average of all rule outputs, computed as

$$\text{FinalOutput} = \frac{\sum_{i=1}^N w_i z_i}{\sum_{i=1}^N w_i} \quad (2)$$

3. Segmentation algorithm

An algorithm for image segmentation using different trained fuzzy set structures is presented in Fig. 2. It detects iris of a human eye. The color composition of

the iris usually differs from its surroundings. Images in RGB color space are used as ANFIS learning data. Data sample for learning all FIS structures is selected manually from one of the images.

After ANFIS trains certain FIS structures, segmentation of experimental data is performed. Output of ANFIS is an intensity image, where pixel values closest to 1 belong to the region of the iris. Areas that are not likely to belong to the identified iris are filtered.

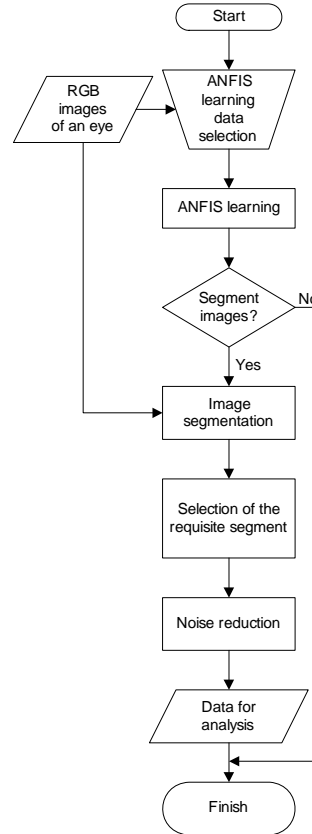


Fig. 2. Algorithm of experiments

4. Results of experiments

Experimental data consists of RGB images, gathered with ordinary web-camera. Size of the gathered and later processed frame is 320x240 pixels.

18 different fuzzy set structures trained by ANFIS algorithm were tested. Structures differ by number of membership functions for each input, their shape and number of training iterations (epochs). All inference systems are trained using the same learning data sample from random RGB image. Learning data consists of two manually selected regions: one from the iris region (1144 pixels), another from its surroundings (1666 pixels). Notifiable that effectiveness of learning FIS and segmentation depends on color composition of the selected regions. In example, the sample that represents the iris should have all its colors proportionally to the entire iris.

Experiments with each FIS were performed using 200 images of an eye that is looking straight to the camera, up, down, right and left (40 frames each).

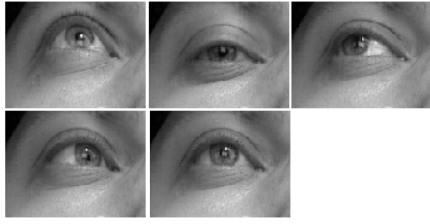


Fig. 3. The data base of the images with human eye positioned in five different positions

As an input of trained FIS are red, green and blue values of image pixels. Fuzzy inference system gives segmented intensity image of an eye (Fig. 4, upper right). The brightest region is selected according to intensity threshold equal to 0.7 (Fig. 4, lower left, colors in Fig. 4 upper right, lower left and right are inverted). Then small areas that don't belong to the iris are cleared (Fig. 4, lower right). After iris of an eye is extracted from the image, the center coordinates of it are calculated.

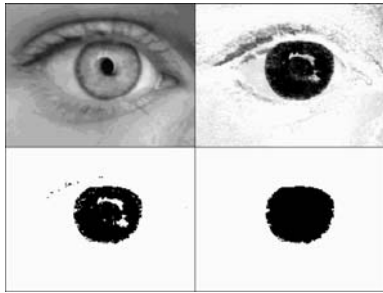


Fig. 4. Processing of an image when FIS has 8 fuzzy rules, trapezoidal-shaped MFs, trained in 20 epochs

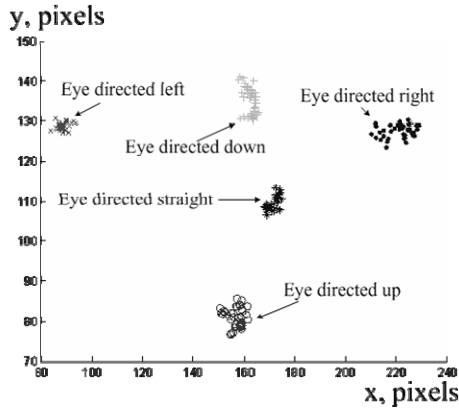


Fig. 5. Calculated centers of the iris when FIS has 2 Gaussian curve-shaped MFs for each input, trained in 20 epochs

The results of segmentation with all FIS structures are similar. An algorithm finds the iris in all of the processed images. Centers of the extracted regions are grouped into 5 apparent clusters (Fig. 5, 6), which represent 5 different eye positions. In these figures center points that represent eye position “up” are lower than centers of eye looking down, because y coordinates of image pixels starts from 1 at the top of the image (reverse y axis).

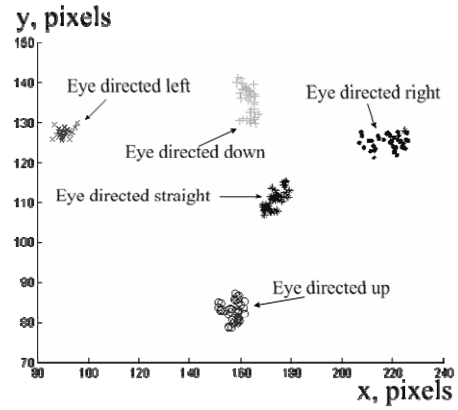


Fig. 6. Calculated centers of the iris when FIS has 3 triangular-shaped MFs for each input, trained in 100 epochs

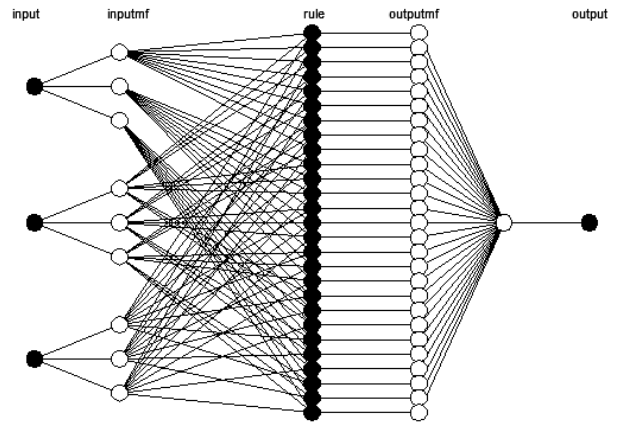


Fig. 7. FIS structure when each input has 3 membership functions

Training time increases significantly when ANFIS trains 3 MFs for each input instead of 2 (Table 1).

Table 1. Training and processing time

Structure N°	Learning epochs	Number of MFs	MF shape	Training time, s	Processing speed, fps
1	20	2	Triangular	1.49	8.14
2			Trapezoidal	1.44	8.27
3			Gaussian curve	1.53	7.28
4	50	3	Triangular	10.78	5.09
5			Trapezoidal	10.83	5.26
6			Gaussian curve	10.96	4.65
7	100	2	Triangular	3.33	8.17
8			Trapezoidal	3.51	8.26
9			Gaussian curve	3.72	7.23
10		3	Triangular	26.71	5.10
11			Trapezoidal	26.96	5.32
12			Gaussian curve	27.66	4.74
13	100	2	Triangular	6.79	8.23
14			Trapezoidal	6.71	8.35
15			Gaussian curve	7.49	7.30
16		3	Triangular	54.05	5.02
17			Trapezoidal	54.14	5.19
18			Gaussian curve	55.50	4.60

Therefore structures with 4 or more MFs per input weren't investigated. Calculated images processing speed also depends on shape of input membership functions. Using trapezoidal MFs caused a bit faster processing than using triangular shaped. Gaussian curve-shaped MFs processing is much slower, than the rest two shapes investigated. All investigated fuzzy set structures are listed in Table 1. They differ by number of training iterations (learning epochs), number of membership functions per input, and shape of membership functions. Variations of center coordinates are shown in Fig. 8 and 9. Numbering of each structure (1-18) is according to structure numbering in Table 1. Greatest variations calculated while processing images with eye directed straight and using Gaussian curve shaped membership functions.

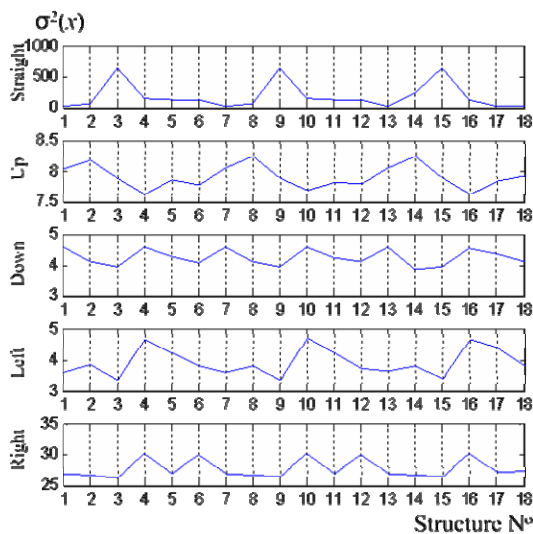


Fig. 8. Variation of x coordinates of the iris center

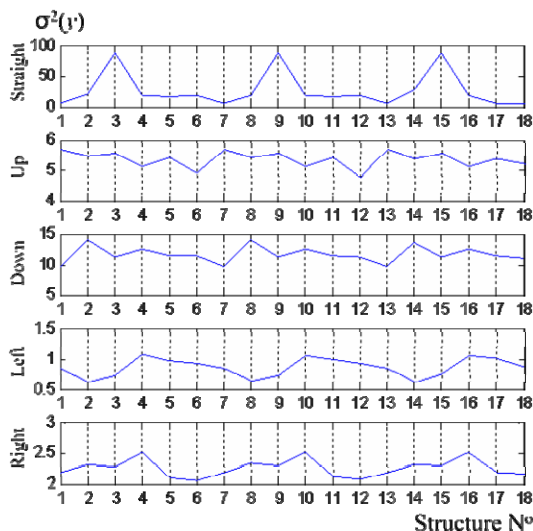


Fig. 9. Variation of y coordinates of the iris center

5. Conclusions and discussions

An algorithm for FIS structure evaluation is presented. FIS structures are trained automatically by Adaptive Neuro-Fuzzy Inference System (ANFIS), and it requires an expert to select training data. Results of experiments

showed that segmentation quality doesn't depend on FIS structure and number of training iterations. Desirable results were reached with the simplest FIS structure (with 2 triangular – shaped membership functions). Training time increases significantly when number of membership functions is increased by 1. Images processing speed is greater with triangular and trapezoidal membership functions – up to 8.35 frames per second. The results of this paper can be used for the development of efficient associative communication systems, human face tracking and systems which analyzes medical images. The future work will incorporate the development of the position classifier and applications of the external device control.

6. Acknowledgment

The authors appreciate the financial support of the Lithuanian state science and studies foundation.

7. References

1. Chi-Ho Kim, Bum-Jae You, Hagbae Kim, Color Segmentation Robust to Brightness Variations by Using B-spline Curve Modeling, Intelligent Robots and Systems, 2006 IEEE/RSJ International Conference, 2006, p. 4874 – 4879.
2. Palma-Amestoy, Rodrigo A., Guerrero, Pablo A., Vallejos P.A., Ruiz-del-Solar J., Context - dependent color segmentation for Aibo robots, Robotics Symposium, 2006. LARS '06. IEEE 3rd Latin American, 2006, p. 128 – 136.
3. Albiol A.; Torres L.; Delp E.J., An unsupervised color image segmentation algorithm for face detection applications, Image Processing, 2001. Proceedings. 2001 International Conference, Volume 2, 2001, p. 681 - 684 vol.2.
4. Aibing Rao; Srihari, R.K.; Zhongfei Zhang, Spatial color histograms for content-based image retrieval, Tools with Artificial Intelligence, 1999. Proceedings. 11th IEEE International Conference, 1999, p.183 – 186.
5. Ju Han, Kai-Kuang Ma, Fuzzy color histogram and its use in color image retrieval, Image Processing, IEEE Transactions on Volume 11, Issue 8, 2002, p. 944 – 952.
6. Yongzhong Wang, Quan Pan, Chunhui Zhao, Yongmei Cheng, Fuzzy Color Histogram Based Kernel Tracking under Varying Illumination, Fuzzy Systems and Knowledge Discovery, 2007. FSKD 2007. Fourth International Conference on Volume 4, 2007, p. 235 – 239.
7. Chamorro-Martinez J., Sanchez D., Prados-Suarez B., Galan-Perales E. Fuzzy Homogeneity Measures for Path-Based Color Image Segmentation, Fuzzy Systems, 2005. FUZZ '05. The 14th IEEE International Conference, 2005, p. 218 – 223.
8. El-Feghi I., Aboasha H., Sid-Ahmed M.A., Ahmadi M, Content-Based Image Retrieval based on efficient fuzzy color signature, Systems, Man and Cybernetics, 2007. ISIC. IEEE International Conference, 2007, p. 1118 – 1124.

DEVELOPMENT AND INVESTIGATION OF AN EFFICIENT ALGORITHM FOR ALTERNATIVE CURSOR CONTROL

Audrius PUKEVIČIUS*, Vidas RAUDONIS**, Rimvydas SIMUTIS**, Toma NAKVOSAITĖ*

*Department of Control Technologies, Kaunas University of Technology, Lithuania

**Department of Process Control, Kaunas University of Technology, Lithuania

Abstract: The development and investigation of alternative computer mouse control system is presented in this work. The system uses 2D visual information, which is acquired from ordinary web-cam, and controls cursor position in the monitor by tracking the movements of the hand. Hand tracking is achieved by using an algorithm, which combines two methods: statistical Gaussian method and artificial neural networks. This algorithm helps to avoid an expert intervention in system calibration process. Before starting to control cursor, the user has to put hand in front of web-cam and wait a few moments while system calibrates itself.

Keywords: object tracking, neural networks, vision-based human-computer interface.

1. Introduction

Nowadays cursor control in computer monitor is realized in various ways: computer mouse, touch-pad, touch-screen. An alternative algorithm is represented in this work, which uses 2D visual information from ordinary web-camera. With this algorithm it is possible to control cursor position by moving hand, placed in front of camera. In this case user has an opportunity to control cursor position without any physical contact with cursor control devices.

Cursor is realized with Neuro-Gaussian algorithm, which combines statistical Gaussian mixture model [1] with neural networks. There is known other statistical methods for background subtraction by using color segmentation, such as mean, median background models [2]. It is known that for making such models it is necessary to use more than one frame with static background picture. It is important to choose right values for pixel classification constants in order to gain accurate background extraction. Gaussian mixture model can be made from one frame with static background. Statistical Gaussian method is combined with neural networks, which nowadays are widely used

in visual information processing area. They are successfully used in road signs recognition [3], [4], human face recognition [5], [6]. It is possible to combine neural networks with other methods [7] in order to get an effective hybrid system for skin lesion detection.

In Neuro-Gaussian algorithm statistical Gaussian method is used to form a training material for neural network. With Gaussian mixture model color segmentation is applied to static background. Mahalanobis distance is calculated between the pixels of the new picture with user's hand and background's regions. The pixels of the hand region do not combine with any earlier segmented regions and are classified as object pixels, which is above background. Pixels of hand region and some of background pixels are used to form training data for neural network. This algorithm helps to avoid an expert intervention in system calibration process. In further process pixels are classified with trained neural network, because it performs faster and more accurately than Gaussian method.

The paper is organized in four main sections. In the second section is overviewed theoretical background of Neuro-Gaussian algorithm. Third section gives more information about hand tracking system, an algorithm of hand position detection and cursor control. Experimental results are represented in section 4.

2. Theoretical background

Background subtraction is widely used to detect moving object from static cameras. It is usually regarded as one of the most important steps in applications such as traffic monitoring, human motion capture, recognition and video surveillance, etc. In order to get a good performance of the whole system, the background subtraction method should not be so time and space consuming, and the accuracy is also required. Gaussian mixture model is a robust background subtraction method and is widely used ever since it is proposed.

Gaussian mixture model has parameters, which describes backgrounds color features. Static background picture is clustered in to chosen number of familiar color regions. Every region is parameterized like a Gaussian distribution and described with its pixels mean value μ_i and covariance matrix \mathbf{K}_i in three color spaces ($c = (r, g, b), v = 3$). Gaussian distribution is represented in (1) expression.

$$p_i(c) = \frac{1}{(2\pi)^{v/2} \sqrt{\det K_i}} \cdot \exp\left(-\frac{1}{2}(c-\mu_i)^T K_i^{-1}(c-\mu_i)\right) \quad (1)$$

Mahanalobis distance between new pictures pixel and i -th region is calculated as follows in (2) expression:

$$\Delta_M(c, i) = (c - \mu_i)^T K_i^{-1} (c - \mu_i) \quad (2)$$

Pixels of the new picture are classified by using Gaussian mixture model and classification is realized with (3) expression:

$$\mathbf{M}(x, y, t) = \begin{cases} 1 & \text{if } \Delta_M(x, y, t) > \theta \\ 0 & \text{otherwise} \end{cases} \quad (3)$$

Mahanalobis distance is calculated to all regions. If this distance is bigger than constant θ , then it's considered that pixel belongs to foreground object. After first classification stage, classified pixels are used to form the training data for neural network.

Neural network consists of three inputs for RGB color spaces, one hidden layer with three neurons and one output with sigmoid activation function. Neural network is trained with Levenberg – Marquardt algorithm. Neural networks structure is represented in 1 figure.

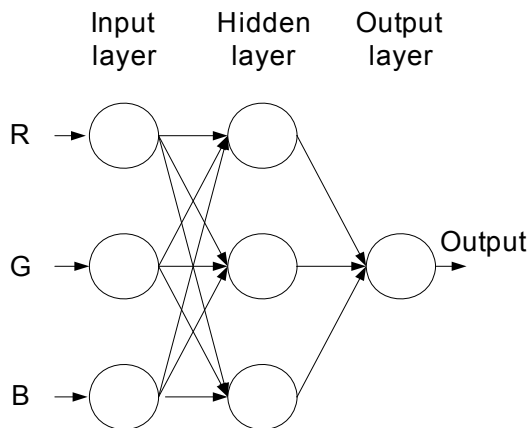


Fig. 1. Neural networks structure

As a result binary picture is generated, where background is marked with 0 and users hand region with 1.

3. Hand tracking algorithm

Alternative cursor control system visual information gathers from web-cam, fixed in front of hand and directed vertically down as it shown in 2 figure.

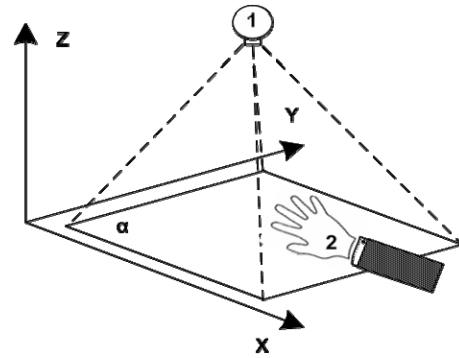


Fig. 2. Cursor control systems web-cam position: α – web-cam's capturing region horizontal to xy plane; 1 – vertically down directed web-cam; 2 – user's hand. Hand movement directions are horizontal to α plane

It is taken in account that the user's hand movements are parallel to α plane. Visual information and calculations are processed with PC. Cursor can be controlled when camera captures the hand of the user.

The Neuro-Gaussian algorithm begins from the evaluation stage of static background. After calculations represented in 2nd section, Gaussian background mixture model is formed. After model is formed, picture with hand in front of camera is captured and regarding to Gaussians background mixture model, pixels are classified in two classes: first class – background pixels, second – foreground object (user's hand region) pixels. Neural networks training data is formed from hand region pixels, extracted with statistical Gaussian method, and background pixels. This helps to avoid an expert intervention in neural network training process. Other subsequent picture pixels are classified with trained neural network. After extracting hand region, top extreme point is detected as it shown in figure 3. Usually this point is the top of the hand's middle finger. Cursors positioning in computers monitor is realized regarding to this point position in picture.

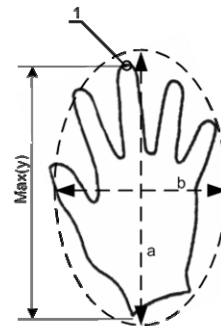


Fig. 3. Extracted hand's region handling. 1 – top extreme hand region point that controls cursor position; a, b – ellipse, that has the same second-moments as the region, axes

By measuring eccentricity of hand's region, left mouse button press is initialized. The eccentricity is the ratio of the distance between the foci of the ellipse and its major axis length. This value changes when fingers are spread or folded together. Now it is realized that left mouse

button is initialized when fingers are folded. This Neuro-Gaussian algorithm is represented in fig. 4.

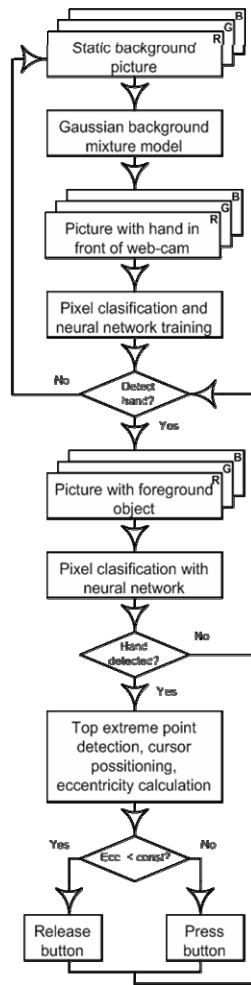


Fig. 4. Neuro-Gaussian algorithm

First four steps in Neuro-Gaussian algorithm are system calibration process and it's done automatically without expert intervention. Other steps represent normal functioning of alternative cursor control system.

4. Experiments and results

Experimental data consists of 200 frames with different hand positions. Experiments were made with three different frame sizes (160x120, 320x240, 640x480) in purpose to evaluate dependence on frame size and one iteration time, cursor positioning accuracy. First of all hand tracking system was calibrated: Gaussian background mixture model is calculated and neural network is trained. On Fig. 5 are shown hand recognition results during system calibration process.

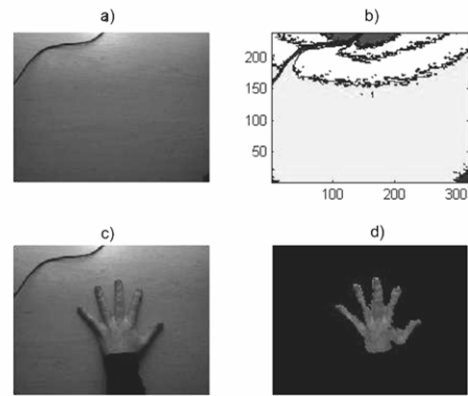


Fig. 5. Hand recognition results with statistical Gaussian method: a) – static background picture; b) – background clustered in 5 similar color regions; c) – picture with hand in front of web-cam; d) – extracted white hand region

With recognized hand region pixels and part of background pixels neural network was trained. Further pixel classification was made with neural network. During experiment hand was moved in circles in front of camera and recognized hand coordinates was logged. On the same frames expert selected real hand position coordinates they were compared with recognition results (Fig. 6).

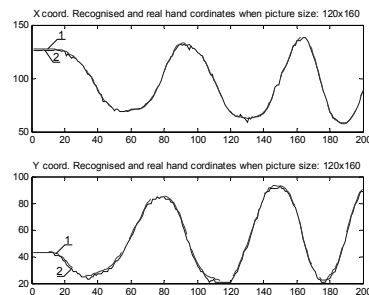


Fig. 6. Recognized and real hand coordinates : 1 – recognized, 2 – real coordinates

From comparison results in Fig. 6 it is visible that recognized and real coordinate curves are similar. Error function of x and y coordinates on Fig. 7 also shows that tracking algorithm is quite accurate: the offset between recognized and real coordinates is not bigger than five pixels.

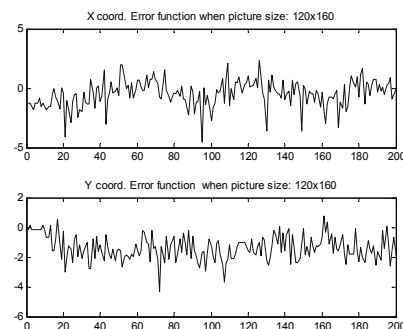


Fig. 7. Error functions between recognized and real hand coordinates

As it was mentioned above, experiments were made with three different size frames. Results displayed in Fig. 8 shows that one iteration time increases with bigger frame resolution.

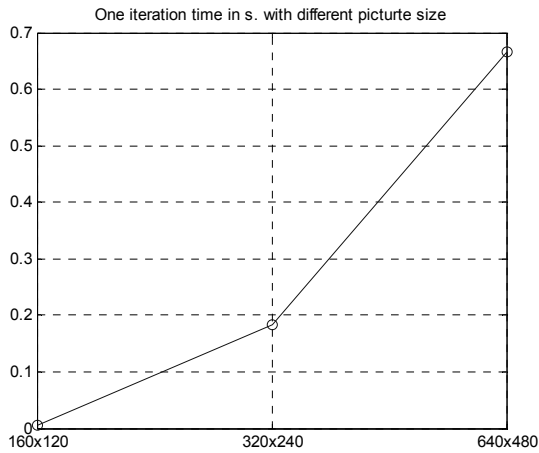


Fig. 8. One iteration time in seconds with different picture size

By increasing frame size 16 times, number of iterations per second decreased approximately from 200 to 2. Whereas cursor movement steps on monitor with 1440x900 resolution decreased, but error dispersion increased (Table 1). That invokes cursor position instability on the monitor.

Table 1. Experimental results

	t, s	$\delta^2(x)$	$\delta^2(y)$	X step	Y step
160x120	0.005	1.241	0.667	9	8
320x240	0.184	6.797	2.393	5	4
640x480	0.665	59.911	16.185	2	2

Cursor control system was tested with other applications. User used this system to draw in windows application “Paint”. Results are represented in figure 9.

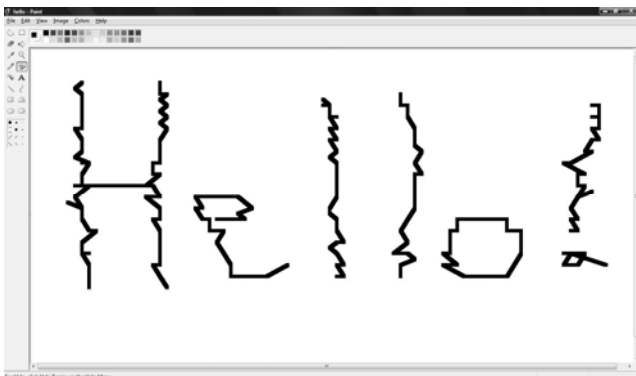


Fig. 9. Drawing results with represented cursor control system

5. Conclusions and discussions

A Neuro-Gaussian algorithm was presented. Statistical Gaussian method enables to avoid an expert intervention in system calibration process. System is calibrated automatically. Neural network usage enables to reach good performance in hand position tracking task. Experimental results showed that Neuro-Gaussian algorithm can perform an accurate and fast hand position tracking and cursor positioning on monitor. Alternative cursor control system works faster with smaller resolution frames, but cursor positioning on computer monitor is more accurate with higher resolution frames.

6. Acknowledgment

The authors appreciate the financial support of the Lithuanian state science and studies foundation.

7. References

1. Zhen Tang, Zhenjiang Miao. Fast Background Subtraction and Shadow Elimination Using Improved Gaussian Mixture Model. Haptic, Audio and Visual Environments and Games. IEEE International Workshop on 12-14 Oct. 2007. p. 38 – 41.
2. Shi Peijun, Jones E.G., Zhu Qiuming. Median model for background subtraction in intelligent transportation system. Proceedings of the SPIE, Volume 5298, 2004. p. 168-176.
3. Alberto Broggi, Pietro Cerri, Paolo Medici, Pier Paolo Porta. Real Time Road Signs Recognition. Proceedings of the 2007 IEEE Intelligent Vehicles Symposium Istanbul, Turkey, June 13-15, 2007. p. 981 – 986.
4. Shuangdong Zhu, Lanlan Liu. Traffic Sign Recognition based on Color Standardization. Proceedings of the 2006 IEEE International Conference on Information Acquisition August 20 - 23, 2006. p. 951 – 955.
5. Yang Kun, Zhu Hong, Pan Ying-jie. Human Face Detection Based on SOFM Neural Network. Proceedings of the 2006 IEEE International Conference on Information Acquisition August 20 - 23, 2006. p. 1253 – 1257.
6. Paliy I., Kurylyak Y., Kapura V., Sachenko A, Lamovsky D, Sadykhov R. Combined Approach to Face Detection for Video-Surveillance. IEEE International Workshop on Intelligent Data Acquisition and Advanced Computing Systems: Technology and Applications 6-8 September, 2007. p. 594 – 598.
7. Andy Chiem, Adel Al-Jumaily, Rami N. Khushaba. A Novel Hybrid System for Skin Lesion Detection. 1-4244-1502-0/07, 2007. p 567 – 572.

OPTIMAL CONTROL OF ROBOTS BY DYNAMIC PROGRAMMING

Rudolf BAUMGART-SCHMITT, Stephan LIEBETRAU, Christian WALTHER,
Maria KRAUTWALD, Daniel TROMMER
University of Applied Sciences Schmalkalden, Faculty of Electrical Engineering, Germany

Abstract: A swarm of robots are adapted to an unknown environment by reinforcement learning. Each of the robots is able to scan the environment and to measure the distance to the next hindrance. The information collected by the robots are transferred in a wireless mode by the serial Bluetooth protocol to the central unit. This unit performs the backward recursion of Dynamic Programming to get the optimal route from one place to another for each of the robots. The general goal consists of finding the route with the minimal number of steps from the initial to the final point of a two dimensional area. The performance of the approach can be demonstrated by both the simulation and the real robots.

Keywords: control of robots, cellular automata, dynamic programming.

1. Introduction

The autonomous navigation of mobile robots is the main topic in a growing number of papers. The different approaches in soft computing like neural networks, genetic algorithms and fuzzy rules are successfully applied to control mobile robots [1, 2, 3]. The quality of the control strategies or the fitness of the robots in the context of genetic algorithms can be evaluated in different ways and serve as feedback for the optimal adaptation. Several optimization procedures have been implemented to find the global or local optima of the optimization problem with restrictions. That task should be performed in real time. By means of Dynamic Programming invented by Bellman the global optimum can be found but at the expense of strongly increased computation time if the dimension of the state space is large. In [4] a hierarchical Dynamic Programming approach is used for path planning to reduce the effort and make the approach more efficient. Low-level and high-level maps were formalized as Markov Decision Processes. The idea of cooperation between mobile robots supported by Petri-Net communication models is presented in [5]. A new reinforcement learning

algorithms is introduced by [6] which support the collaboration of a set of robots.

In our contribution a swarm of robots navigate in a complete unknown environment and try to find an optimal path from the start to the final area. The robots are able to recognize hindrances by distance sensors and use compass modules to be able to correct turnings and courses. The relevant data are transmitted to the central data processing unit in a wireless mode by Bluetooth. The unit collects and processes the information. A two dimensional model with a pre selected spatial resolution of the three dimensional unknown world are updated. The model is adapted to the actual dimensions of the robots by rules of cellular automata. Then the unit calculates the optimal path for each robot by Discrete Dynamic Programming (DDP) and transmits the next commands to the robots wireless. Each valid transition of the robots from one position to the next is connected with a fixed effort. The accumulated effort of the complete route should be minimized. That means the reinforcement learning strategy is used. The processing of the modules

- the scanning of the environment by the sensors of the robots,
- the updating of the model by the central computing unit,
- the calculation of the optimal path by the central computing unit,
- the transmission of the further command to the robots and
- the executions of the commands by the robots,

has to be repeated until the goals are reached by all participants of the running.

2. Sensors and Microcontroller Hierarchy of the Robots

Six robots RP6 developed by the company Arexx were used as basic experimental platforms. The RP6 is an autonomous mobile robot system. The navigation is

originally supported by several sensors: bumper sensors, light and infrared sensors. The RP6 is controlled by the microcontroller ATMEGA32L with 8-Bit RISC architecture. To improve the abilities of RP6 the expansion module with a second ATMEGA32 microcontroller and further accessories were mounted on the top of the robot [7]. The distance sensor sharp GP2D12, the compass module CMPS03 and the Bluetooth module BTM222 were also included. Fig. 1 shows the side view of the modified robot. The local processing units can be seen at three layers which are connected by the IIC Bus. The distance sensor GP2D12 uses infrared to detect barriers up to 80 cm away. There is a nonlinear output voltage of the sensor in relation to the distance. After analogue digital conversion the voltages were processed by means of a look up table. The sensor was positioned on a servomotor and it can scan the distances to the next hindrances in an angle of 180 degrees with a resolution of 2 degrees. In this way the measuring tolerances of the distances because of robot moving can be minimized.

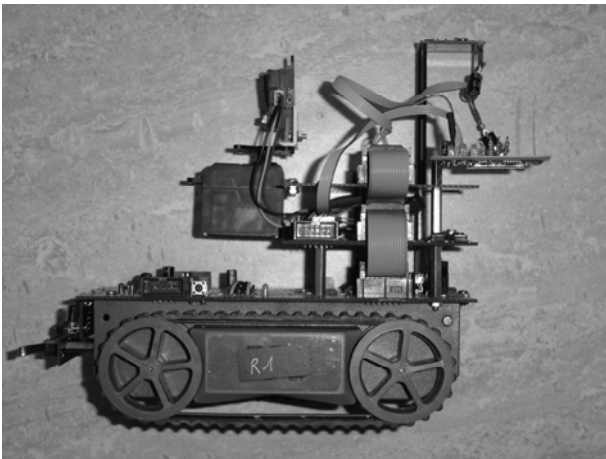


Fig. 1. Robot RP6 produced by Arexx and modified by Liebetrau (2008). The autonomous driving RP6 is controlled by the microcontroller ATMEGA32L at 8 MHz clock with an external 32KB SPI EEPROM. The expansion module with a second microcontroller (ATMEGA32 at 16 MHz), an additional distance sensor sharp GP2D12, compass module CMPS03 and the Bluetooth module BTM222 are included

3. Cellular Automata

Cellular automata were successfully applied in image processing [10]. The optimization procedure bases on a model which is created by sensor data and modified by cellular automata. We solved three different image processing problems by a cellular automat. The first problem is connected with recognized gaps between the hindrances which are too small for passing by the selected robots. The rules of the defined automat are responsible to close the gates before the optimization procedure starts. The next problem arise if the selected resolution of the two dimensional model of the world is too small compared to space which is necessary for one robot. The optimal path calculated by DDP can lead beside the hindrances too narrow for passing by. The cellular automat is used to make the walls virtually

broader in the model world to shift the optimal path calculated by the optimization procedure. The third problem which has to be solved by cellular automat before the optimization procedure starts is the correction of false edge detection by the distance sensor.

4. Discrete Dynamic Programming

To find the shortest distance from start to destination the backward recursion of discrete dynamic programming was used. That means the stages and states had to be defined at first. The destination should be the stage N with one state only. Than the places with immediate transitions to the destination are the two dimensional states x_{N-1} of stage N-1 and so on. Recognized hindrances are restrictions which interrupt the possible path. The scalar decisions d_n at stage n are limited to 4. The robots can go right, left, upward and downward. The scalar returns r_n at stage n are accumulated. The transitions $x_n = t_n(x_{n-1}, d_{n-1})$ for $n = 1, 2, \dots, N$ are defined by the two dimensional table. According to the principle of optimality developed by Bellman [8, 9] the backward recursion of the Discrete Dynamic Programming can be formulated by the following recursion equation:

$$f_{n-1}(x_{n-1}) = \min_{d_{n-1}} \{r_{n-1}(x_{n-1}, d_{n-1}) + f_n(x_n)\} \quad (1)$$

with $n = N, N-1, \dots, 2$, $f_{n-1}(x_{n-1})$ as the optimal return from the stages N, N-1, ..., n-1 and $f_n(x_n) = 0$. To find the optimal path to the final state the set of optimal decisions should be applied to the transitions starting with the values of the initial state.

5. Reinforcement Learning

Reinforcement learning can be classified as a non-super-wised method of machine learning. In our case the agent (robot) tries to minimize a long term negative reward (return) in goal directed moving through an unknown environment. The on-line learning takes place during the complete actions. The state specific decisions are the results of (1).

6. Simulation

To test the reinforcement learning and the implementation in C++ the world for path finding was simulated by software. The simulated robots were placed on one square only according the pre selected spatial resolution. Therefore there was no need to apply the rules of the cellular automat. By means of a drawing program the model can be created on the selected spatial resolution without any limitation. Up to 6 robots can be started. Because of the high speed of this simulation the different models of the world can be tested and evaluated very efficiently. Fig. 2 presents the output of the program in simulation mode. The path of

the simulated robot is drawn by gray coloured circles. The hindrances are in black colour.

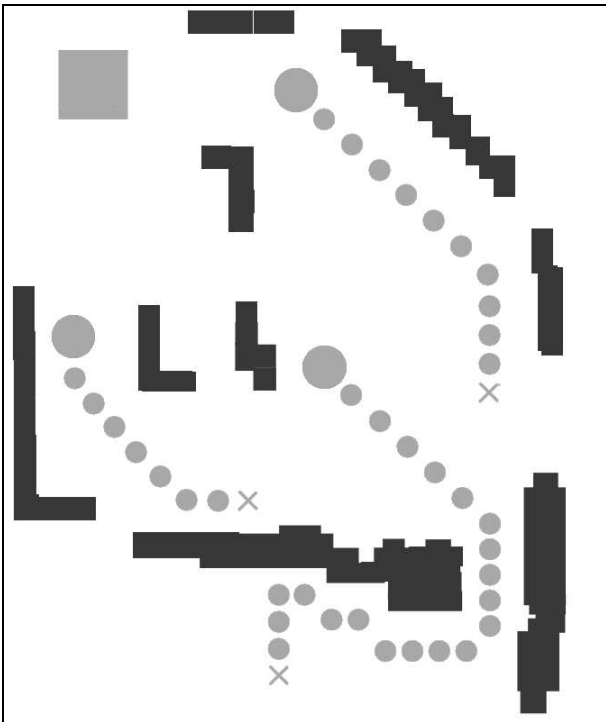


Fig. 2. Simulated path finding. The path is indicated by gray coloured circles

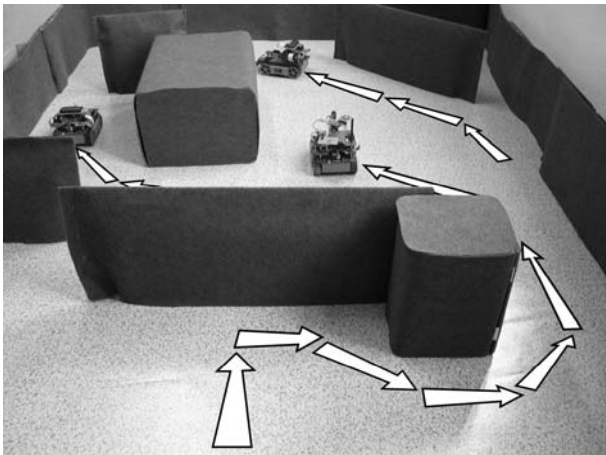


Fig. 3. Training and testing area of the robots. The movement directions are shown by arrows

7. Experiences with Mobile Robots

The firmware of the robots was written in C and was processed by bus connected microcontroller. The robots training and testing area can be seen in Fig. 3. It shows three robots which move to the destination. In contrast to the simulation processing the rules of the cellular automat had to be included. They were used to balance the deficits of the sensors in recognizing edges and to adapt the dimensions of the hindrances to the spatial resolution. The optimization procedure worked very successfully and efficiently. The command for the next step was calculated and transmitted after correcting the actual position of the robot by means of direction

measured by the compass module. The compass had to be adjusted before using. After the execution of the next step the actual position of the robot had to be corrected too if necessary. Because of the danger to end up in undefined places, the original bump and infrared sensors were switch off.

8. Summary and further research

The system works reliable. The wireless communication is efficient. The learning and controlling procedure is able to find the optimal path. Up to now the distance sensor takes to much time for scanning. Therefore it should be exchanged. During the experiences with the robot swarm we recognized the necessity for a stronger parallelizing the actions of the robots. The parallel scanning of the robots can lead to inferences of the reflected light. Furthermore the detection of the exact location by a camera system described in [12] should be included to improve the accuracy. The Discrete Dynamic Programming approach will be extended to handle multiple criteria and time varying constraints in the next working steps [10].

9. References

1. Narvydas G., Simutis R. and Raudonis V. Autonomous Mobile Robot Control Using Fuzzy Logic and Genetic Algorithm. Intelligent Data Acquisition and Advanced Computing Systems: Technology and Application, IDAACS 2007 4.th IEEE Workshop, 2007, p. 460-464.
2. Narvydas G., Simutis R. and Raudonis V. Autonomous Mobile Robot Control Using If-Then Rules Fuzzy and Genetic Algorithm. ISSN 1392-124X Information Technology and Control, 2008 Vol. 37, No 3.
3. Janglova D. Neural Networks in Mobile Robot Motion. Int. J. of Advanced Robotic Systems, Vol. 1 Nu. 1 (2004).
4. Bakker B., Zivkovic Z. and Kröse B. Hierarchical Dynamic Programming for Robot Path Planning. IEEE / RSJ International Conference on Intelligent Robots and Systems 2005 (IROS 2005).
5. Stambolov G. Development of Petri-Net Communication Model for Cooperative Mobile Robot System. The 3 rd International Conference on Electrical and Control Technologies, Kaunas, Lithuania, 2008.
6. Kartoun U., Stern H., Edan Y., Feid C., Handler J., Smith M. and Gillam M. Collaborative Q(λ) Reinforcement Learning Algorithm – A Promising Robot Learning Framework. In: Robotics and Applications (RA 2005), Gerhardt, L. A. (Editor), Cambridge MA USA.
7. Liebetau St. Entwurf von Algorithmen zur optimalen Navigation von Robotern unter Nutzung von Reinforcement Learning Strategien und ihre Erprobung mittels C/C++ Softwaremodulen. Diploma thesis. Faculty of Electrical Engineering University of Applied Sciences Schmalkalden, Germany, 2008.

8. Bellman R. Dynamic Programming. Princeton University Press, 1957.
9. Robinett III R., Wilson D., Eisler G. and Hurtato J. Applied Dynamic Programming for Optimization of Dynamic Systems, Society for Industrial and Applied Mathematics (SIAM), Philadelphia, 2005.
10. Popovici A. and Popovici D. Cellular Automata in Image Processing, Fifteenth International Symposium on Mathematical Theory of Cellular Automata, 2002.
11. Santos dos R. Steffen V. and Saramago S. Robot path planning in a constrained workspace by using optimal control techniques, Multibody Syst Dyn (2008) 19, p. 159-177.
12. Altenburg J. and Altenburg U. Mobile Roboter. Hanser, 2002.

MAP DRAWING OF UNKNOWN ENVIRONMENT USING AUTONOMOUS MOBILE ROBOT

Šarūnas GERMANAS*, Gintautas NARVYDAS**

*Department of Mathematics Research in System, Kaunas University of Technology, Lithuania

**Department of Process Control, Kaunas University of Technology, Lithuania

Abstract: This paper focuses on map drawing using autonomous mobile robot. A small robot E-puck with eight infrared proximity sensors and two wheels is programmed to detect obstacles and walls, and in this way to draw a map of unknown environment. Program in computer analyses this information and draws points which are calculated as obstacle points.

Position of the robot at any time is calculated using wheel odometry. The values of the sensors are calculated to the distance measured in metric system. Every time robot tries to detect the obstacles and when it approaches too close to the obstacle, it changes the direction of the movement.

Keywords: Map drawing, odometry, E-puck, autonomous mobile robot.

1. Introduction

Mobile robots are widely used in industry, military, research and entertainment [9, 8, 1]. Robots can help people to make works that are simple for machine and perhaps complex for human. Unfortunately robots can not do intellectual works, such as creative work, solving abstract situations. When there are very big amount of variants of decisions, it is very hard to determine the decisions in all possible situations.

Important area of robots application is drawing maps of unknown environments. There could be environments that are too dangerous or impregnable for humans. So we must use mobile programmed robots [6, 2]. One must put some instructions to the robot, which could let the robot to make some exercises, for example, searching for mines, making the map, detecting conditions of the environment. The example is the Mars project [7], where mobile robots are sent to the Mars and there they must search for life, take the pictures and do not get into dangerous situations.

There is a project which teaches the robot Zoe [3] to draw a map of the desert. It must understand if the composition

of the terrain is basalt or clay. It uses the absorption and reflection patterns of the terrain. Later this robot could be sent to Mars to make maps of this planet.

The area of map drawing could be divided to two parts – topological maps and metric approaches. Metric maps deal with geometric properties, and topological maps describe with the connectivity of different objects [10, 5].

In our work the robot E-puck is programmed to explore unknown environment and to make a clear map of that environment without any human influence. The main task is to use data of the sensors of the robot that we could see obstacles. We have initial robot position and direction. Also robot's position every moment is calculated. Together the positions of all sensors are known. The robot sends to computer the values of proximity sensors, which show the distance between the current sensor and the point of the obstacle. With this distance and the sensor coordinate we can determine the coordinate of the point of the obstacle. With the speed of information sending speed we can get the values of the coordinates of obstacles. When the program determines that the robot is very close to the obstacle it sends instruction it to go in the other direction.

2. Robot E-puck

E-puck [4] is small and elegant robot. It is comfortable to use in research because it is small, light and fast. It's view from the top is showed in Figure 1.

The diameter of it is 70mm. The structure of this robot can be defined by three parts – the body, motors and printed circuit. The body ensures other parts, including the battery. The battery is connected with printed circuit by two contacts. The battery is based on LiION technology, has 5Wh capacity and is sufficient for about 2-3 hours of intensive use.

The motor uses steppers with gear reduction. There are 20 steps per revolution, the gear reduction is 50:1. The Robot

has two wheels, which have diameter of 41mm and the distance between them of 53mm. The maximum speed of wheel spinning is 1000 steps/s. 1000 steps correspond to 12.8 cm. The wheels can spin to both directions. When spinning the wheels to special directions robot can go by any angle.

The robot has information about the count of steps driven by both wheels. These values are used to calculate other parameters, for example, the coordinates of the robot.

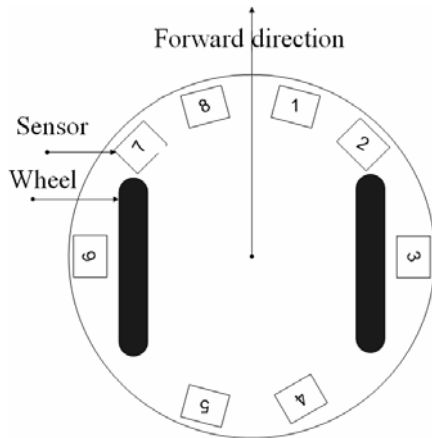


Fig. 1. The view from the top of the robot e-puck

There are eight infrared (IR) proximity sensors. They are placed around the robot. There are 4 sensors in the front of the robot, two sensors on the sides, and two sensors in the back side.

Also the robot has dsPIC family processor. The robot connects the host computer via Bluetooth interface.

3. Research

First of all we need to examine the sensors. The function which relates the value of the sensor and the distance between that sensor and the obstacle must be found. So the robot is put in different distances from the obstacle (the wall) to the examining sensor. With a different distance the sensor gives a different value. The distances varied from the initial – 0.5 cm – to the final – 6 cm – increasing the distance by 0.5 cm. At every distance the sensor was requested to give 1000 values. Then the mean, standard deviation and median were calculated. Then there were eight pairs of quantity – the distance and the mean of the sensor’s value. The diagram of the example experiment is shown in figure 2. The vertical axis represents values of the sensor and the horizontal axis represents the distance.

The values of the sensors are not linear depending on the distance. So, we need get the analytical function which relates values of the sensors and the distance. Then we always could have the distance value and work in metrical space.

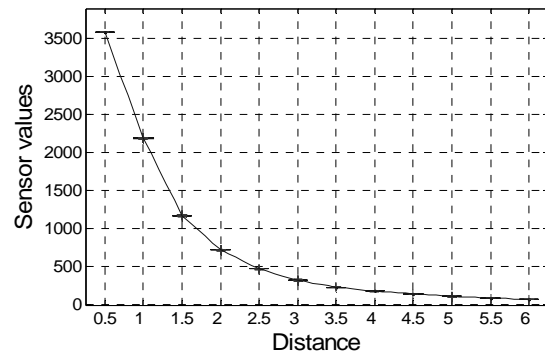


Fig. 2. Analysis of the 2nd sensor

The first task is to understand what type of function relates the distance and the sensor’s value. After several guesses the most appropriate form is

$$y = a \cdot x^b, \quad (1)$$

where y represents the distance, and x represents the value of the IR proximity sensor.

The least square method is used to find out the parameters a and b . Though sensors are the same type, but their returned values are different for the same distance. Therefore for every sensor we get different parameters. These different functions are used in the later research.

The next task is to create the algorithm with which the coordinates of the robot could be known at every moment during the wandering of the robot. In this model the coordinates (named global coordinates) contain three variables: x coordinate, y coordinate and the angle of the robot in Cartesian coordinate system. The problem is that using information sent by robot we calculate different parameters (local coordinates): x and y coordinates, and the angle of the robot. The value of the angle sent by robot is measured in different system than the angle we need in Cartesian coordinate system. To be precise the angle sent by robot could also be measured in Cartesian system, but all these angles are transformed changing the coordinate quarters. The figure 3 shows this situation more apparently.

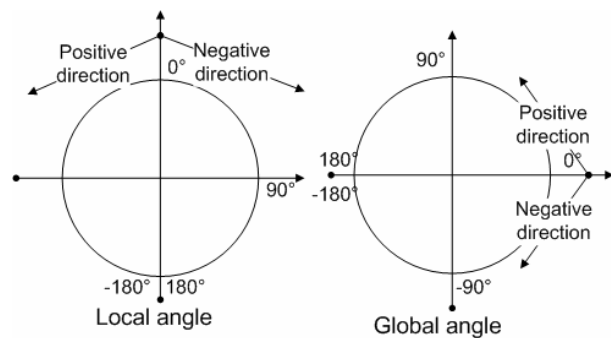


Fig. 3. Diagrams which show change of local and global angle systems

The formulas which relate the angle of the global coordinates and the angle of the local coordinates appear so:

$$\alpha_{global} = \begin{cases} 90 - \alpha_{local} & , \alpha_{local} \in [-90; 180] \\ -270 - \alpha_{local} & , \alpha_{local} \in (-180; -90] \end{cases} \quad (2)$$

α_{global} and α_{local} vary in range of $(-180; 180]$. Formula (2) is represented in figure 4:

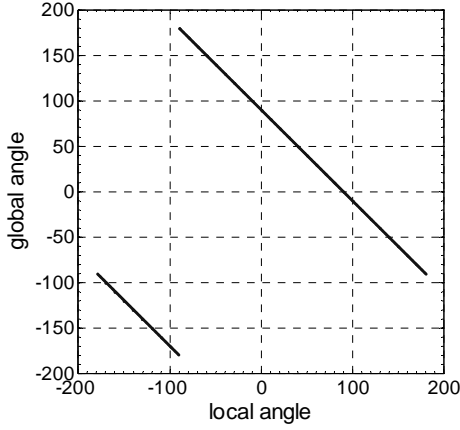


Fig. 4. Relationship of global and local coordinate systems

Analogously:

$$\alpha_{local} = \begin{cases} 90 - \alpha_{global} & , \alpha_{global} \in [-90; 180] \\ -270 - \alpha_{global} & , \alpha_{global} \in (-180; -90] \end{cases} \quad (3)$$

The x and y coordinates also must be recalculated:

$$\begin{cases} x_{global} = y_{local} \\ y_{global} = x_{local} \end{cases} \quad (4)$$

The robot does not send his coordinates in Cartesian form but it sends the amount of the steps of every wheel. There are used formulas which calculate the coordinate of the robot center point and the angle of the robot using data sent from the robot.

When the robot turns to right i.e. $d_{left} > d_{right}$,

$$\begin{cases} x = x_0 + D \cdot \sin(\alpha_{local}) - D \cdot \sin\left(\frac{d_{right} - d_{left}}{d} + \alpha_{local}\right) \\ y = y_0 - D \cdot \cos(\alpha_{local}) + D \cdot \cos\left(\frac{d_{right} - d_{left}}{d} + \alpha_{local}\right) \end{cases} \quad (5)$$

When the robot turns to left i.e. $d_{left} < d_{right}$,

$$\begin{cases} x = x_0 - D \cdot \sin(\alpha_{local}) + D \cdot \sin\left(\frac{d_{right} - d_{left}}{d} + \alpha_{local}\right) \\ y = y_0 + D \cdot \cos(\alpha_{local}) - D \cdot \cos\left(\frac{d_{right} - d_{left}}{d} + \alpha_{local}\right) \end{cases} \quad (6)$$

When the robot moves straight i.e. $d_{left} = d_{right}$,

$$\begin{cases} x = x_0 + \frac{d_{right} + d_{left}}{2} \cdot \cos(\alpha_{local}), \\ y = y_0 + \frac{d_{right} + d_{left}}{2} \cdot \sin(\alpha_{local}), \end{cases} \quad (7)$$

$$\alpha_{local_new} = \alpha_{local} + \frac{d_{left} - d_{right}}{d}, \quad (8)$$

where $D = d_{baseline} \cdot \frac{d_{right} + d_{left}}{|d_{right} - d_{left}|}$; $d_{baseline}$ is distance

between the wheels; x_0 and y_0 are old coordinates; α_{local} is old angle; x , y are new coordinates; α_{local_new} is new angle; d_{right} and d_{left} are number of steps of right and left wheels. But formulas work only in local coordinate system. The coordinates are renewed in every program cycle, so there are used two odometry values from the next moments. So only the change of the coordinates is calculated. Therefore this change must be added to the old values. Because old values are calculated in global system and the formulas work in local system, old information must be converted to local system before it is used when adding the update to it. After adding updated information must be converted back to global system.

The next task is to calculate the coordinates of the committed obstacle. To do that we must use two before calculated values – distance from the obstacle to the sensor and the coordinates of the robot. The coordinates of the sensors are calculated easily. Every angle of the sensor coordinate vector in global system is known (The initial angle of the robot in our experiment is 90°). The distance between the sensor and the center of the robot is 3.5 cm. So, as follows:

$$(Sx_k, Sy_k) = (x_{global}, y_{global}) + 3.5 \cdot (\cos(\beta_k), \sin(\beta_k)). \quad (9)$$

Here (Sx_k, Sy_k) is the coordinate of the k^{th} sensor,

β_k is the angle of the k^{th} sensors in global system.

This angle is calculated in this way:

$$\beta_k = \beta_{k0} + 90 - \alpha_{local}, \quad (10)$$

where β_{k0} is the angle of the robot in global system.

So now we have the coordinates of the sensors and the distance from the obstacles to the sensors. We must make the same thing which we made when we were calculating the coordinates of the sensors.

$$(Ox_k, Oy_k) = (Sx_k, Sy_k) + y \cdot (\cos(\beta_k), \sin(\beta_k)), \quad (11)$$

where (Ox_k, Oy_k) is the coordinate of the obstacle committed by the k^{th} sensor; y is the distance between the k^{th} sensor and the obstacle.

So, now we can calculate dynamically the coordinates of the obstacles during the wandering of the robot. The robot is asked to avoid the obstacles. When the values of the distances between the robot and the obstacle are too small, the robot must change direction.

4. Results

The result of the experiment must be a clear map of the given unknown environment. At first the map is made of the points which represent points of the obstacles. The example result is given in figure 5. The initial coordinate of the center of the robot is (0, 0). Primarily the robot starts to move when it is parallel to the Y-axis. Outer points represent detected obstacles, inner points represent the trajectory of the robot. Black line represents the real obstacles of the environment. Measure unit is centimeter.



Fig. 5. Map of unknown environment drawn by points

As seen in the picture there is some noise while detecting the points. This noise is caused by errors of the sensors values and by the slide of wheels. At the point (3, 0) wheels of the robot have slipped. After that we can see that the right part of the map is turned down. Approximately the error of point's position is not bigger than 2.5 cm. Despite this we can get enough clear map. The next task is to convert this data to the more discrete form. To achieve this, the point grouping algorithm was used. The essence of it is to divide the area of the map to the small squares (for example, the side of the square could have length of 0.5 cm). The number of the points which fall to the square is counted. The marginal number of points is defined. If the number of points is sufficient the square is painted.

Unfortunately the result is not passable. If the marginal number of the points is relatively large, then we get too less walls and the map is not correct. Then we could take smaller marginal number. But in this project we get passable results only when we take marginal number equal to 1. Then we get the same result like in the map

drawn with points. So, more research must be done and other methods must be applied.

We tried to control robot in distance not looking directly to the unknown environment but just looking to the information received from the robot sensors. Such situation could be performed when human can not enter some dangerous environment but wants get the map of that environment. So he sends the robot to the environment and controls it by control device. In this work as control device was used the joystick. With this device a person who controls robot can see dynamically drawn map. Regarding to the information in the map he controls the robot. Then if the robot appears in difficult situation the person can help it. Results of the controlled robot are shown in figure 6.

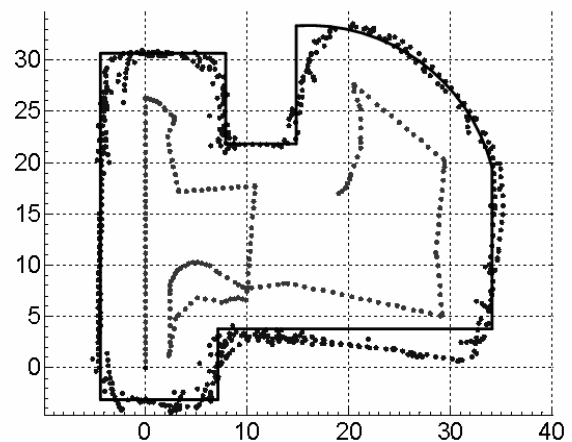


Fig. 6. The map got using joystick

We get better results but there also is some noise and the slide of the wheels. Perhaps robot must turn around slower because it has problems then.

5. Conclusions and future works

The robot can send enough information to draw fairly correct map. Approximately the error of point's position is not bigger than 2.5 cm.

The process of points of the map descreeting is not passable. Either robot must drive slower or different method must be used.

The way how the robot must behave in the environment was very simple. Robot must only avoid obstacles. In this way it theoretically must explore more and more territory. But practically sometimes the robot gets into difficult situations and struggles. Hence, the more intellectual and intended behaviour must be programmed for robot. In future works robot could be programmed to follow the wall. Also the problems caused by unexpected situations, for example, wheel slide, fast wall reaching, must be solved.

Interesting and practical solve of robot wandering problem is use of control device. It can be used when human can

not enter the territory but wants get the map of that territory

6. Acknowledgements

We would like to express our acknowledgement to Lithuanian State Science and Studies foundation for the received support.

7. References

1. Autonomous Robot Vision. <http://www.cis.udel.edu/~cer/arv>, retrieved February 25, 2009.
2. Batavia P.H., Nourbakhsh I. Path Planning for the Cyc Personal Robot. Intelligent Robots and System, 2002. IEEE/RSJ International Conference on Intelligent Robots and Systems, Takamatsu, Japan, 2000, p. 15-20 vol.1.
3. Calderon F., Thompson D.R., Wettergreen D. Autonomous Rover Reflectance Spectroscopy with Dozens of Targets. International Symposium on Artificial Intelligence, Robotics and Automation in Space (iSAIRAS), Los Angeles, USA, February, 2008.
4. E-puck official webpage. www.e-puck.org, retrieved February 9, 2009.
5. Hafner V.V. Evaluating cognitive maps for mobile robot navigation behaviour. Proceedings of the AISB'03 Symposium on "Scientific Methods for the Analysis of Agent-Environment Interaction", Aberystwyth, UK, 2003.
6. Hähnel D., Schulz D., Burgard W. Map Building with Mobile Robots in Populated Environments. Intelligent Robots and System, 2002. IEEE/RSJ International Conference on Intelligent Robots and Systems, Lausanne, Switzerland, 2002, vol.1, p. 496-501.
7. Hunstberger T.L., Baumgartner E.T., Aghazarian H., Cheng Y., Schenker P.S., Leger P.C, Iagnemma K.D., Dubowski S. Sensor-Fused Autonomous Guidance of a Mobile Robot and Applications to Mars Sample Return Operations. Proceedings of the SPIE Symposium on Sensor Fusion and Decentralized Control, 1999, Boston, USA, vol. 3839, p. 2-8.
8. Myers G.K., Julia L.E., Cheyer A.J., Gerbi S. Multimodal User Interface. Communications of the ACM, New York, USA, 2004, p. 57-59.
9. Setalaphruk Y., Uneno T., Kono Y., Kidode M. Topological Map Generation from Simplified Map for Mobile Robot Navigation. Proceedings of the Annual Conference of JSAI, 2002, p. 109-110.
10. Thrun S. Robotic Mapping: A Survey. Exploring artificial intelligence in the new millennium, San Francisco, USA, 2002, p. 1-35.

INFLUENCE OF DIMENSIONS OF A MOBILE ROBOT ON NAVIGATION USING VECTOR MARKS

Virginijus BARANAUSKAS, Stanislovas BARTKEVIČIUS, Kastytis ŠARKAUSKAS
Kaunas University of Technology, Lithuania

Abstract: Vector marks allow us to find shortest path between initial position of the robot and target point. This path is shortest, when the robot is viewed as a material point. According to the dimensions of the robot, not only the length of the path changes, but there situations, when the robot could not pass existing openings may arise. The purpose of the article is to create robot with real dimensions navigation algorithm, keeping simplicity of the usage of vector marks. Also, the aim is to find shortest path. Algorithm and modelling results of navigation are represented.

Keywords: mobile robots, path planning, navigation.

1. Introduction

The problem of robot navigation in known environment with obstacles is the purpose of the article. The simplest case is when there are no obstacles between robot and target point. This case can be solved using scanners. If the robot and the target point are not on the same straight visible line, the problem of target point search evokes. [1, 2] suggest using vector marks, i. e. virtual vector marks to target, allowing robot to orientate in the environment and to choose direction of movement to target point. A set of vector marks is attribute of the target and describes all possible paths to the target point. Dimensions of the mobile robot are not fixed, for example, the dimensions of the transport robot depend of the clearance of the consignment. Therefore not all paths, described using vector marks fits for particular robot with known dimensions, because there could be narrow places, through which robot could not pass. The simplest solution for this problem is described [3], is to enlarge artificially all obstacles (in all directions) by the half of a robot width. This solution closes all narrow openings and all passing paths are remaining. But, if the dimensions of the robot are not known a priori, early search of the path becomes impossible. Search of the path, when robot moves, slows this process, because this search is complicated.

2. Assessment of robot dimensions in model of environment

Model (map) of the environment, in which robot moves, is known to robot or to the attendant supervisor program. This model comprises from vector marks (fig. 1) and inventory of obstacles. It is easy to describe a set of marks as a tree. Then all possible paths are visible.

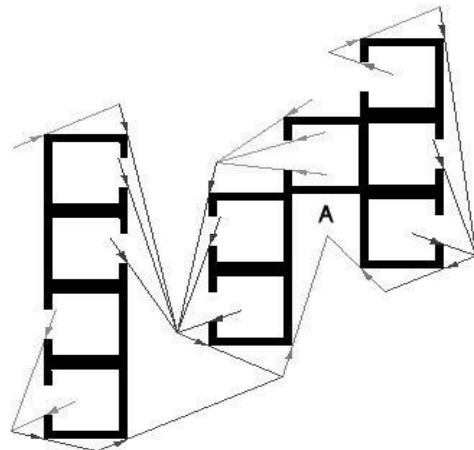


Fig. 1. Model of the environment. A – target point

Each vector mark is specified with weight coefficient, i.e. distance from tail point of the mark to the target. Robot orients according to the directly visible marks and chooses the “easiest”. So, it moves at the shortest path.

Robot, which has finite dimensions, could have various forms, which, depending on the direction of the movement, could change. For example, when robot stretches out or folds up the manipulator. It is rational, especially when you are modelling, to put robot into “cocoon”, geometrical figure, limiting dimensions of which involves not only clearance of robot, but also necessary openings between robot and obstacles, not elaborating dimensions of the robot. Such figure could be ellipse or circle. In this work, robots cocoon is circle. Conflict emerges, when cocoon intersects obstacle.

3. Solution of the conflicts

It is necessary to predict robot reaction to conflict. Robot, reacting to possible conflict, must change the direction of the movement, i.e. retire from possible path.

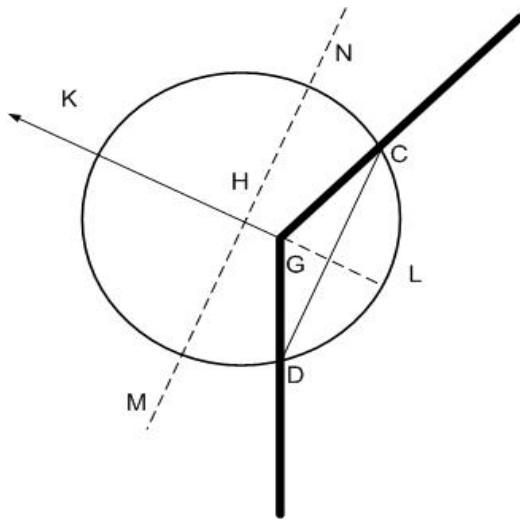


Fig. 2. Direction of the robot displacement after conflict with corner of the obstacle

If there is collision between robot cocoon and obstacle in the predictable robot position fig. 2 “thick line”, it is rational to move robot in such way, that its movement would be minimal. As we can see from fig. 2, it would be then, when the robot will be moved along the direction of vector K , i.e. athwart cocoon and obstacle intersection chord $D-C$. Movement must be such, that the distance between straight line $M-N$ passing the circle centre H , parallel to chord $D-C$ and nearest obstacle point G would be not less than the radius of the circle. Point G can be described as a farthest point from chord $D-C$ of obstacle fragment, situated in the indoor of the circle. Algorithm of conflict solution must perform such stages:

1. Verify, that robot cocoon does not cross any obstacle;
2. Determine cocoon and obstacle cross chord ($D-C$);
3. Determine direction of the movement (vector K), perpendicular to cross chord;
4. Find farthest, from chord point, which is situated in the indoor of the circle, obstacle point (G);
5. Determine distance between founded point (G) and part of the circle, overlapping with obstacle, moving perpendicularly to crossing chord (section $G-L$).
6. Move cocoon in the direction of vector K by distance $G-L$.

4. Determination of too narrow opening

There could be openings, through which robot could not pass, in the robot path. It is important to find such openings. It is evident, that in too narrow opening robot cocoon must cross obstacles in both sides. There are

cases, when there is the same obstacle in both sides fig. 3. So, the number of obstacles with which robot cocoon crosses, could not be criterion for determining narrow opening.

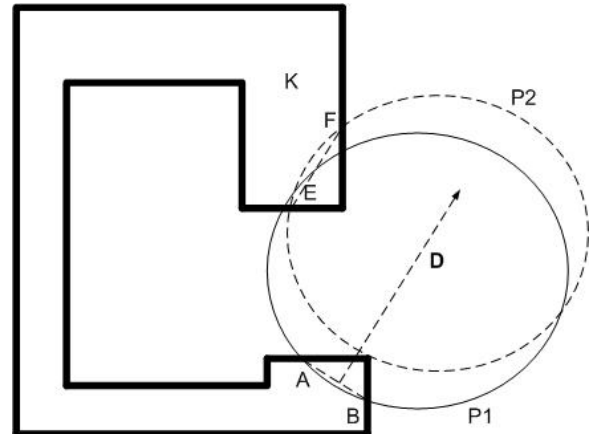


Fig. 3. Robot in narrow opening

It is rational to find too narrow opening using decision procedures of conflict with obstacle. If cocoon of the robot crosses obstacle K in several places (see fig. 3), it is necessary to solve conflict in one of the intersection places. Let's say, that we solve conflict, associated with chord $A-B$. If then, i.e. we move cocoon of the robot along the vector D , from position $P1$ to position $P2$, conflict with each of the obstacle persists – the opening is too narrow. Algorithm of determination of too narrow opening uses algorithm of solution of conflicts and its stages are:

1. Solve the conflict, if it emerges;
2. Verify if new conflict does not emerges;
3. If so – opening is too narrow.

If narrow opening is determined, we must form new reaction of the robot – it must find other path.

5. Closing of the opening, trim and supplement of the marks tree

It is possible to start new search of the path from the start position of the robot and to use usual algorithm of the path search. It is necessary to close determined too narrow openings in order to not find them again. In order to do it, the array of the pseudo obstacles are formed, these supposed obstacles are segments, closing narrow openings. The length and place of each segment are determined too narrow opening. Too narrow opening, showed in fig. 3, is closed using segment of conjunctive nearest points A and E of chords end points, which were found after initial and repeated conflict. The coordinates of these points determines place of the pseudo obstacle. Pseudo obstacles, during the search of the path, are treated as real obstacles.

Robot searches the path using the tree of vector marks, which could lead robot to closed opening. So it is necessary to modify tree of the marks. It is necessary to eliminate the branch (branches), which is cut by new pseudo obstacle. Also, all other branches, outgoing from the branch, that we cut, becomes pointless. In

other words, it is necessary to “cut” all fragment of marks branch, which was following from the branch that we “cut”. Such recast of vector marks tree is showed in fig. 4.

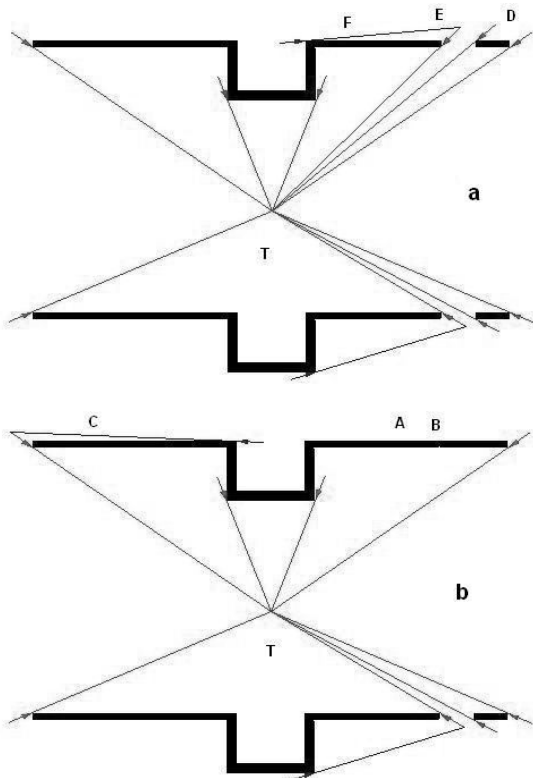


Fig. 4. Modification of vector mark tree, when to narrow opening is found; *a*– tree before alteration, *b* – tree after alteration

If opening, through which goes tree branches *E* and *D*, is too narrow, then, if we close it with pseudo obstacle *A–B*, not only the branches *E* and *D* are eliminated, but also branch *F*, emerged from point *E* is eliminated too. If we want to find all possible paths, when these branches are eliminated, it is necessary to add branch *C* into the tree. Recast of the tree do not requires finding it newly, it is enough to augment pollard. Stages of the tree modification:

1. Find branches of the tree, which intersects pseudo obstacle;
2. Eliminate it and it’s “child’s” from tree;
3. Add new tree branches, according to [1] formed conditions.

7. Robot in the maze

Generation of vector marks and the movement of a robot, according to it’s dimensions, are viewed in mazes, using different size of corridors and possible paths between initial point and the target point. Robot navigation is executed according to vector marks, which has weight coefficients, which enables robot to choose shortest path between initial position and the target point. Three examples of different size robot are selected and the functionality of created system is viewed.

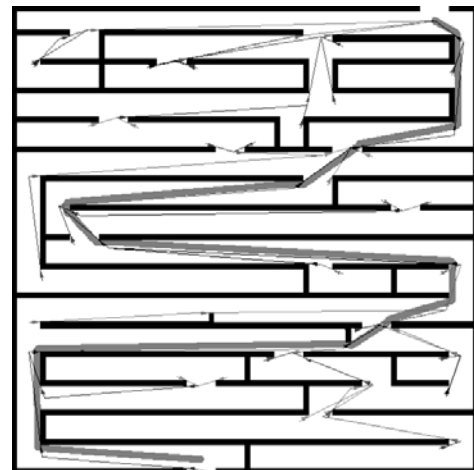


Fig. 5. Path of the first size robot in maze. Robot chooses shortest path, depending on vector marks and it’s weight coefficients



Fig. 6. Path of the second size robot in maze. Robot selects shortest path, according to vector marks, but finds contraction in the maze, which is too small. Robot, according to described methodology, searches new shortest path

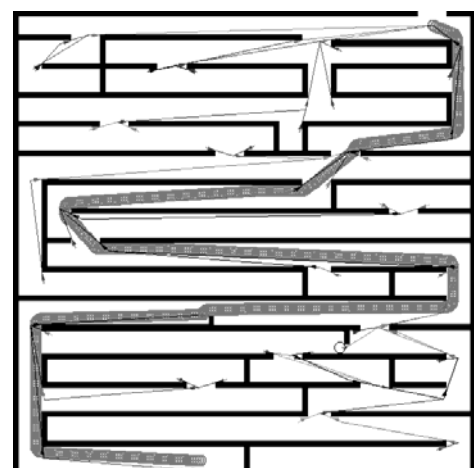


Fig. 7. Path of the second size robot in maze. Robot finds another shortest path and reaches exit of the maze. The obstacle of the shortest path, which does not let robot to pass over it, is viewed as circle, with diameter equal to robots diameter, near the obstacle

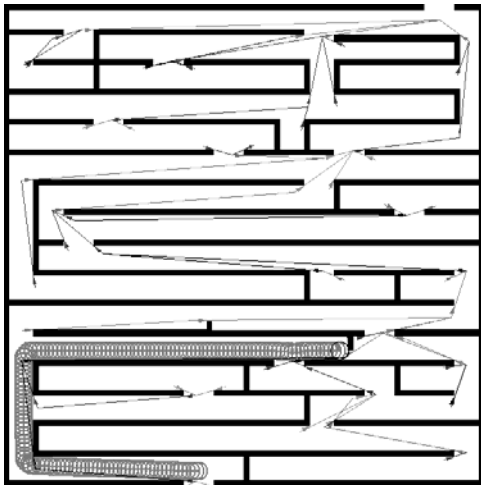


Fig. 8. Path of the third size robot in the maze. Robot finds first too narrow opening and searches for new shortest path

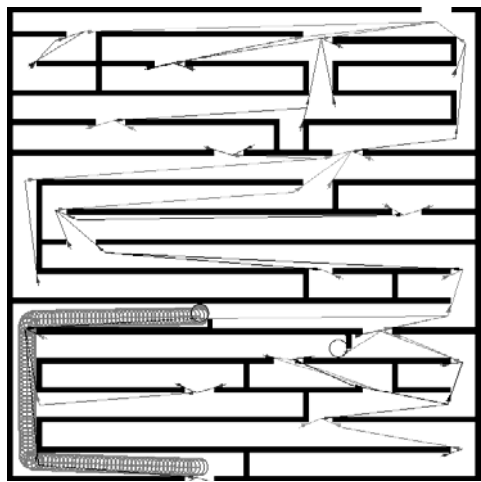


Fig. 9. Path of the third size robot in maze. Robot finds another (too narrow opening) obstacle and searches for new shortest path

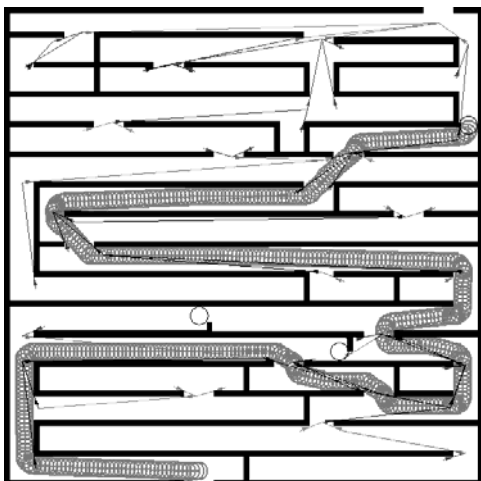


Fig. 10. Path of the third size robot in maze. Robot finds new possible shortest path, but another too narrow corridor is found and robot must find new shortest path, according to vector marks

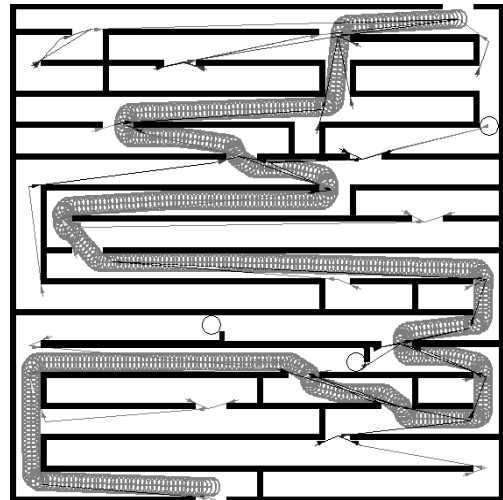


Fig. 11. Path of the third size robot in the maze. Search of the shortest path was successful. Circles in maze shows places, where robot does not pass obstacle

7. Conclusions

Suggested method allows using of vector marks to find nearly shortest path for a robot with finite dimensions as well as in the case of a robot represented by a material point. That makes the finding the path quite simple and quick.

Too narrow openings can be detected and “closed” by artificial obstacles to avoid in future. The tree of vector marks is modified cutting not useful and adding new necessary branches, when artificial obstacles added.

The algorithm finds the shortest possible way with respect to too narrow openings in quite complicated environments (mazes), as shown in examples.

8. References

1. Baranauskas V., Šarkauskas K., Bartkevičius S. Target Retrieval in Known Environment. *Electronics and Electrical Engineering*, 2008, No. 8(88). p.91-94.
2. Baranauskas V., Bartkevičius S., Šarkauskas K. Modified Algorithm of Vector Marks Formation. *Proceedings of the Conference on Electrical and Control Technologies*, 2008, Kaunas, 2008. p. 15-18.
3. Pimenta L.C.A., Fonseca A.R., Pereira G.A.S., Mesquita R.C., Silva E.J., Caminhas W.M., Campos M.F.M. Robot Navigation based on Electrostatic Field Computation. *IEEE Transactions on magnetics*, Vol. 42, No.4, April 2006. p. 1459-1462.

OPTIMIZATION OF HEXAPOD ROBOT LOCOMOTION

Tomas LUNECKAS, Dainius UDRIS
Vilnius Gediminas Technical University, Lithuania

Abstract: Hexapod robot moving through irregular terrain must adapt its locomotion in order to sustain stable and fast movement. Chosen gaits and control methods have to vouch an optimal leg positioning and coordination. An inverse kinematics method is introduced for positioning legs to a needed point. Means of leg contact with ground indications using tactile sensors are discussed and their influence to robot control is discussed. Simple obstacle detection method using IR sensors is presented. Aim is to adapt all these methods into a real-time control system.

Keywords: Hexapod robot, inverse kinematics, Denavit-Hartenberg method, IR sensors, tactile sensors, obstacle detection.

1. Introduction

For a movement of a hexapod robot (Fig. 1) on irregular terrain one of described gaits with different features can be chosen [1]:

Tripod gait – the most popular hexapod robot gait. In tripod gait case three legs are in air at given moment while other three are on the ground, positioning the body. This form of locomotion is good for navigating through relatively smooth surface giving maximum speed for the robot. The drawback of tripod gait is a difficulty to control each leg simultaneously.

Wave gait – only one leg is in the air at a time giving robot five points of contact with the surface. This gives robot the stable posture, making this gait ideal for moving over unfamiliar and particularly irregular terrain. It is easier to control each leg, but robot speed suffers greatly.

Ripple gait – this gait is very similar to wave gait as two separate waves are formed on both sides of the robot. This makes the robot body balancing easier.

Biped gait – it is a mediate variant of tripod and wave gaits as simultaneously two legs are repositioned. This gives robot mediate stability and speed than tripod or wave gaits.

Considering these gait descriptions it is important that robot would change its gait in order to maintain set speed or stability on different surfaces. The decision must be taken according to task given to a robot.

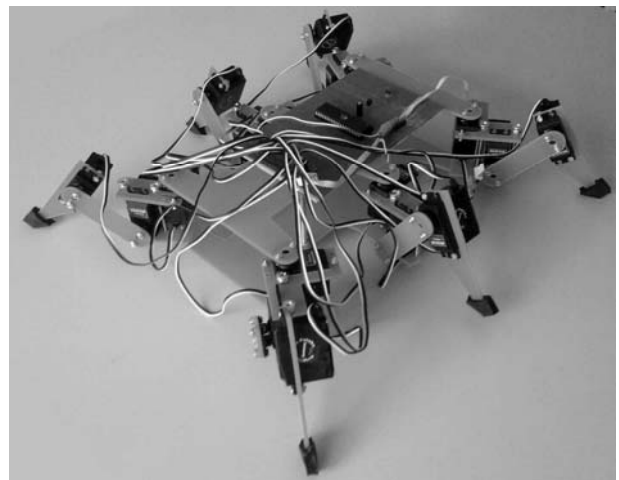


Fig. 1. Hexapod robot model

2. Robot control methods

Robot control refers to the way in which the sensing and action of a robot are coordinated. There are infinitely many possible robot programs, but they all fall along a well-defined spectrum of control. Along this spectrum, there are four basic practical approaches being used today [2]:

- *Deliberative Control*: Think hard, then act.
 - *Reactive Control*: Don't think, (re)act.
 - *Hybrid Control*: Think and act independently, in parallel.
 - *Behaviour-Based Control*: Think the way you act.
- No single approach is the best for all robots; each has its strengths and weaknesses. Control requires some unavoidable trade-offs, as follows [2]:
- Thinking is slow.
 - Reaction must be fast.
 - Thinking allows looking ahead (planning) to avoid bad actions.
 - Thinking too long can be dangerous (e. g., falling off a cliff, being run over).
 - To think, the robot needs (a lot of) accurate information.
 - The world keeps changing during thinking, so the long time for it can cause inaccurate solutions.

As a result of these trade-offs, some robots are made don't think at all, while others mostly think and act very little. It all depends on the robot's task and the environment. If the task and environment require the robot to move and react very quickly, there is usually no time for thinking, such as in automated fast-moving cars, or in soccer playing robots. On the other hand, if the environment does not change much and the robot has enough time, it can plan far ahead to find the best action, such as playing chess, monitoring a warehouse at night, or assembling a complicated object [2].

Control method of the robot depends on time it has for planning or acting. If robots task is not required to be carried out as quickly as possible, it is better to give some time for the coordination and planning ahead.

3. Gait and control method connection

The gait and control methods of a robot strongly depends on environment it woks in and time available for decision making and planning. Thus gait and control method are closely connected. This suggests such gate and control combinations:

1. *Tripod gait – reactive control*. This combination is suitable for fast moving over familiar terrain when planning and careful acting is not a priority.
2. *Wave gait – deliberative control*. This combination ensures that robot is acting deliberately, slowly moving over unfamiliar surface and planning its decisions far ahead.

Hybrid and behaviour-based control methods are separate cases because planning and locomotion are performed simultaneously. So it is not so important on what terrain robot is walking.

During robots movement some locomotion parameters must be respected. These parameters can be freely chosen by robot designers, can be given or obvious from working area.

The main purpose of a walking robot is navigation over irregular terrain, so there is a great importance of its body stability. Stability can be described as retention of body's given position and orientation independently from terrain's irregularity. In other words, robot legs have to adapt to terrain. This can be achieved by using sensors for detecting nearing obstacle (distance and height). According to this information angles for each leg's motor are calculated at which they have to turn in order to position foot to a needed point.

In most cases the robot has to move quickly and independent from a surface travelling on. The speed usually is set by the robot's task. Moving through the well known and smooth terrain a tripod gait (fastest gait) and reactive control should be chosen. In this way robot just reacts to external obstructions not thinking much about leg positioning or planning. While moving through irregular terrain two variants are possible. The first is just as for moving through a smooth terrain. However robot most likely will lose balance, run into an obstacle and etc. The second variant is to change robot's gait to biped, wave or ripple and control method to deliberative or hybrid. In this case robot will devote more time for leg positioning and body balancing.

Energy saving is one of the important criteria of autonomous robot. Energy saving could be achieved by optimizing angles and speeds at which motors have to turn ensuring their low loads. Angle optimization is done by giving the minimal angles needed to position legs into a needed point. For example, when robot is moving over smooth terrain it's not needed to lift legs very high as there is no need to step over obstacles. In other words, it is energetically inefficient for robot to lift legs higher than needed. Horizontal foot motion is always dependent from speed.

4. Indication of foot contact with a surface

Robot's body will swing when walking over irregular terrain if leg lifting and lowering angles are static. To avoid this, robot has to stop lowering the leg when it touches ground. In order to do this each foot must be fitted with tactile sensor. When leg touches ground, sensor indicates it to the controller. Controller stops the corresponding motor at a present angle, and memorizes it. In order to avoid too deep cavities, leg lowering angle limit must be set. This is the maximum angle that motor can turn down.

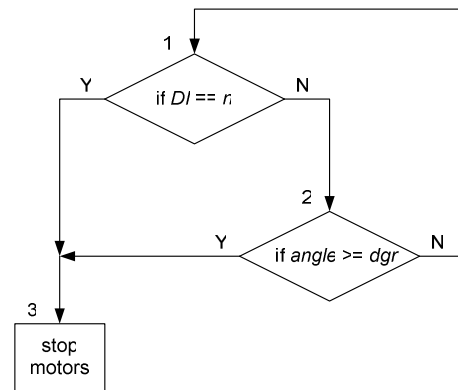


Fig. 2. Algorithm for checking is the leg on the ground or has it reached an angle limit

In the block 1 (Fig. 2) a check is performed if leg is on the ground (DI is a controller's digital input port, connected to the leg's tactile sensors; n – code of a checked leg). If DI value is equal to a code indicating that one or more legs are on the ground, program stops the motors at present angles. If not all needed legs are on the ground (Fig. 2, block 2), the program compares present leg's angles to the limits ($angle$ – present motors angle; dgr – set permissible angle limit). When motor's present angle equals to the set angle, corresponding motors are stopped. This way robot will be able to avoid too deep cavities.

5. Obstacle detection using IR sensors

Robot can adapt to terrain's irregularity, but it is needed to obtain information about surroundings. Most important information is the distance to and the height of the incoming obstacle. That is needed to avoid a collision with obstacle and make a decision: step over, lift the body higher or turn around the obstacle. The simplest way to solve this problem is to put two IR

sensors on each of the front foot, pointed to the front, and one IR sensor at the bottom of robot's body also pointed to the front. All sensors must be configured to detect obstacles at a given distance. Preferable distance is a bit longer than the step's length. In this way only obstacles interfering with recent step will be detected. While nothing is detected within defined area robot continues movement with no changes to its locomotion. If one of the foot sensors detect an obstacle robot must stop leg's horizontal motion and lift this leg until there is no signal from IR sensor, meaning that foot is higher than obstacle. Then robot can resume leg's horizontal motion. If IR sensor's signal does not disappear while robot is lifting leg, that means that obstacle is too high to step over and robot must look for way around it. When body's IR sensor detects obstacle, it means that there is an obstacle in front of the robot, and it must lift the body higher to avoid collision with the obstacle.

6. Inverse kinematics for one leg using Denavit-Hartenberg method

The hexapod leg consists of four links and three kinematic pairs (Fig. 3). Each one has given a coordinate system.

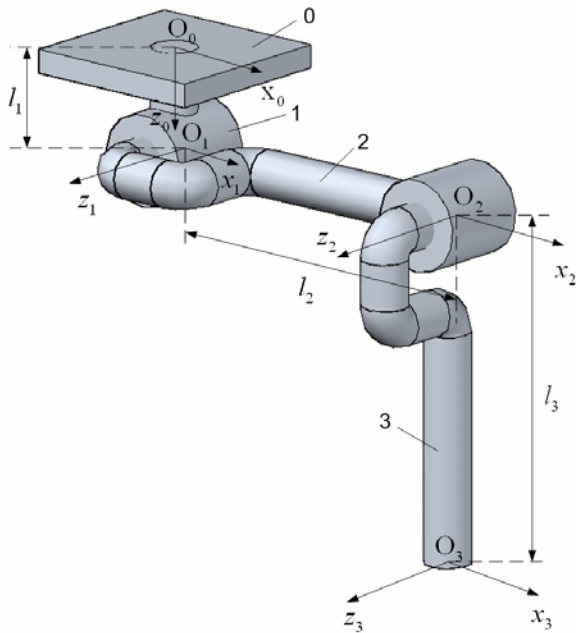


Fig. 3. Kinematic layout of robot's leg

All Denavit-Hartenberg parameters for every kinematic pair in one leg are written out into Table 1.

Table 1. Denavit-Hartenberg parameters for one leg

Kinematic pair	Kinematic pair type	Link No.	Parameters			
			θ	d	a	α
0, 1	Rotational	1	θ_1	l_1	0	-90°
1, 2	Rotational	2	θ_2	0	l_2	0
2, 3	Rotational	3	θ_3	0	l_3	0

Transformation matrices for each kinematic pair are presented in (1–3):

$$\mathbf{T}_{0,1} = \begin{bmatrix} \cos \theta_1 & 0 & -\sin \theta_1 & 0 \\ \sin \theta_1 & 0 & \cos \theta_1 & 0 \\ 0 & -1 & 0 & -l_1 \\ 0 & 0 & 0 & 1 \end{bmatrix}, \quad (1)$$

$$\mathbf{T}_{1,2} = \begin{bmatrix} \cos \theta_2 & -\sin \theta_2 & 0 & l_2 \cdot \cos \theta_2 \\ \sin \theta_2 & \cos \theta_2 & 0 & l_2 \cdot \sin \theta_2 \\ 0 & 0 & 1 & 0 \\ 0 & 0 & 0 & 1 \end{bmatrix}, \quad (2)$$

$$\mathbf{T}_{2,3} = \begin{bmatrix} \cos \theta_3 & -\sin \theta_3 & 0 & l_3 \cdot \cos \theta_3 \\ \sin \theta_3 & \cos \theta_3 & 0 & l_3 \cdot \sin \theta_3 \\ 0 & 0 & 1 & 0 \\ 0 & 0 & 0 & 1 \end{bmatrix}. \quad (3)$$

Each transformation matrix describes how one kinematic pair's coordinate system translates to previous. In order to find transformation matrix to translate foot's coordinates to bases coordinate system, transformation matrices $\mathbf{T}_{0,1}$, $\mathbf{T}_{1,2}$, $\mathbf{T}_{2,3}$ must be multiplied:

$$\mathbf{T} = \mathbf{T}_{0,1} \cdot \mathbf{T}_{1,2} \cdot \mathbf{T}_{2,3}. \quad (4)$$

This multiplication of matrices was done using package *MatLab* and in a Fig. 4 presented task.

```

syms l1 l2 l3
syms t1 t2 t3

T1=[cos(t1) 0 -sin(t1) 0; sin(t1) 0 cos(t1) 0; 0 -1 0 -l1; 0 0 0 1]

T1 =
[ cos(t1),    0, -sin(t1),    0]
[ sin(t1),    0,  cos(t1),    0]
[    0,   -1,    0,   -l1]
[    0,    0,    0,    1]

T2=[cos(t2) -sin(t2) 0 l2*cos(t2); sin(t2) cos(t2) 0 l2*sin(t2); 0 0 1 0; 0 0 0 1]

T2 =
[ cos(t2), -sin(t2), 0, l2*cos(t2)]
[ sin(t2),  cos(t2), 0, l2*sin(t2)]
[    0,    0,    1,    0]
[    0,    0,    0,    1]

T3=[cos(t3) -sin(t3) 0 l3*cos(t3); sin(t3) cos(t3) 0 l3*sin(t3); 0 0 1 0; 0 0 0 1]

T3 =
[ cos(t3), -sin(t3), 0, l3*cos(t3)]
[ sin(t3),  cos(t3), 0, l3*sin(t3)]
[    0,    0,    1,    0]
[    0,    0,    0,    1]

T=T1*T2*T3

```

Fig. 4. *MatLab* task for matrix multiplication

Result of these calculations is a homogenous transformation matrix \mathbf{T} (5).

$$\mathbf{T} = \begin{bmatrix} C\theta_1 C\theta_2 C\theta_3 - C\theta_1 S\theta_2 S\theta_3 & -C\theta_1 C\theta_2 S\theta_3 - C\theta_1 S\theta_2 C\theta_3 & -S\theta_1 & C\theta_1 C\theta_2 l_3 C\theta_3 - C\theta_1 S\theta_2 l_3 S\theta_3 + C\theta_1 l_2 C\theta_2 \\ S\theta_1 C\theta_2 C\theta_3 - S\theta_1 S\theta_2 S\theta_3 & -S\theta_1 C\theta_2 S\theta_3 - S\theta_1 S\theta_2 C\theta_3 & C\theta_1 & S\theta_1 C\theta_2 l_3 C\theta_3 - S\theta_1 S\theta_2 l_3 S\theta_3 + S\theta_1 l_2 C\theta_2 \\ -S\theta_2 C\theta_3 - C\theta_2 S\theta_3 & S\theta_2 S\theta_3 - C\theta_2 C\theta_3 & 0 & -S\theta_2 l_3 C\theta_3 - C\theta_2 l_3 S\theta_3 - l_2 S\theta_2 - l_1 \\ 0 & 0 & 0 & 1 \end{bmatrix}, \quad (5)$$

where: $S = \sin$, $C = \cos$.

Three first members of last column represent foot coordinates in base's coordinate system:

$$\begin{aligned} x &= \cos\theta_1 \cos\theta_2 l_3 \cos\theta_3 - \cos\theta_1 \sin\theta_2 l_3 \sin\theta_3 + \cos\theta_1 l_2 \cos\theta_2; \\ y &= \sin\theta_1 \cos\theta_2 l_3 \cos\theta_3 - \sin\theta_1 \sin\theta_2 l_3 \sin\theta_3 + \sin\theta_1 l_2 \cos\theta_2; \\ z &= -\sin\theta_2 l_3 \cos\theta_3 - \cos\theta_2 l_3 \sin\theta_3 - l_2 \sin\theta_2 - l_1. \end{aligned}$$

7. Step forming using derived homogenous transformation matrix

As it is necessary to position foot to a needed point, each motor's angle must be known. These angles are $\theta_1, \theta_2, \theta_3$ and must be worked out from equation system. Irrespective of chosen calculation method, a step for one leg can be represented as a three dimensional trajectory (Fig. 5).

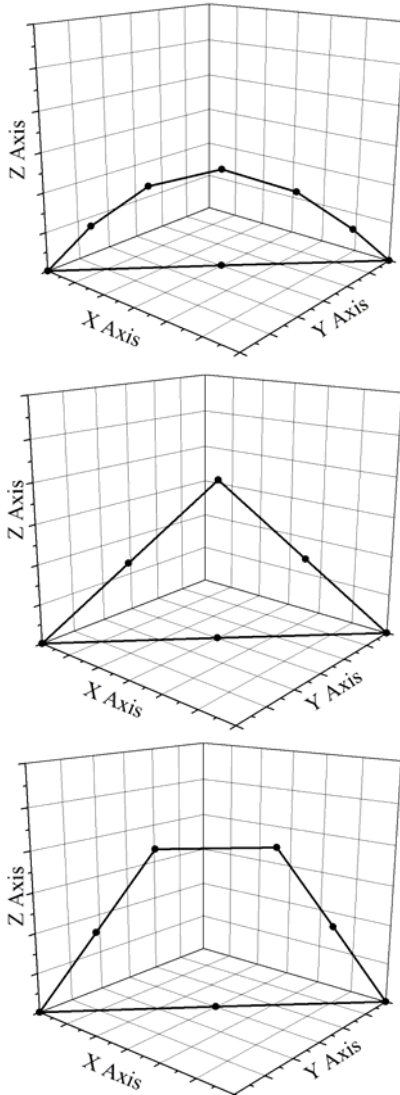


Fig. 5. Possible one step trajectories

Sometimes such calculation task can be hard to solve or even unsolvable. Other solution is to use iterations, when foot coordinates are recalculated at different motor angles and compared to the known coordinates. If result is not equal, angles are increased or decreased further. Coordinates are recalculated again and compared to known coordinates. This is repeated until set and present coordinates become equal, meaning that foot is at needed point. This method can be unsuitable if fast leg repositioning is needed. So calculation method must depend on motion requirements, and searching optimization methods like simplex search [3] can be used to reduce time and increase reliability.

Each trajectory must contain several points with coordinates x_n, y_n, z_n representing different parts of trajectory. Each leg is positioned to these points in sequence, forming a full step.

8. Conclusions

Hexapod robot movement over smooth terrain can be organized using tripod gait and reactive control method. That way controlled it only reacts to external obstructions. While navigating over irregular terrain requires more precise leg positioning, and wave gait and deliberative control method becomes very suitable for this task.

The simplest way to control robot's vertical position (feet are on the ground or in the air) is by using tactile sensors on each foot. For robot to be able to step over or avoid obstacles IR sensors can be used. To detect incoming obstacle and evaluate height the IR sensors on each of the front foot and under the robot base can be used.

An inverse kinematics calculation for each leg and robot as a whole is needed so that robot could calculate step trajectories and body position. Using this information more precise decision can be inducted, so the next task for this investigation is to describe transformation matrix for a whole robot.

For unsolvable by calculation tasks a direct search algorithm can be implemented into the main program.

9. References

1. Analysis of Multi-Legged Animal + Robot Gaits. <http://www.oricomtech.com/projects/leg-time.htm>, last accessed April 10, 2008.
2. Mataric M.J. The Basics of Robot Control. <http://www-robotics.usc.edu/~maja/robot-control.html>, last accessed February 15, 2009.
3. Dambrauskas A. Statistical Theory of Simplex Search. (In Lithuanian), Vilnius, 2007. 260 p.

FASTER AUTONOMOUS MOBILE ROBOT LEARNING USING DECISION CORRECTION

Gintautas NARVYDAS, Petras RAŽANSKAS
Kaunas University of Technology, Lithuania

Abstract: In this paper an approach to teaching artificial neural network by decision adaptation is described. Our task is to define an algorithm for an autonomous mobile robot “e-puck” to learn to follow a wall utilizing a mechanism, which would alter the already made decisions post factum toward a better solution by evaluating their outcome. The algorithm is then tested for performance and briefly compared with other known approaches for advantages and disadvantages.

Keywords: autonomous mobile robot, artificial neural network, control system, decision correction, machine learning.

1. Introduction

Robotics is a branch of science that is currently gaining importance and acclaim very fast. New uses for robots are discovered every day, including but not limited to industrial robots for car assembling, transportation of heavy machinery, welding and other tasks [1], military robots for reconnaissance, minesweeping and combat missions [2], exploration robots, which can be sent into various hazardous places of scientific interest, for example, volcanoes [3], deep ocean [4] or even outer space [5] and other planets beside Earth [6]. On other frontiers, toy robots help children learn various basic concepts of robotics and allow them to explore robots from an early age.

There are many advantages to use robots in various fields. First and foremost, robots can withstand a lot bigger tensions and loads than human beings, they are able to survive extremely acidic and caustic environment for longer periods of time and are overall more robust. Secondly, robots do not exhibit as fast degradation of their work quality as humans over time, meaning that they could work without stopping for days, weeks or even months. Also, maintaining a single robot is frequently a lot cheaper than its equivalent group of human workers. Finally, robots do not get bored, depressed or otherwise psychologically inhibited.

While it is perfectly acceptable for a robot to have a human controller who would make all of the decisions for it, usually the circumstances require the robot to have at least some degree of autonomy. This automatically raises a whole batch of control problems, how to make robot respond adequately to whatever situation it might find itself in. Many different algorithms have been proposed throughout the years for various applications.

A subset of the proposed algorithms deal with a powerful mathematical construct named an artificial neural network. The most prominent feature of artificial neural networks is their ability to learn. Given a set of data and a corresponding set of results to be obtained from these data, an artificial neural network can be adapted using one of the many known algorithms to approximate those given results and detect general relationships between various parameters, which could then be used to make appropriate decisions even for the sets of data not previously encountered. This makes an artificial neural network perfect for robot navigation purposes, since a mobile robot is usually embedded into a dynamic environment that is constantly evolving and thus accounting for each and every possible situation would be simply unfeasible or even impossible.

In this paper we will attempt to define an algorithm which would teach a mobile robot with an artificial neural network to solve a classic problem of following a wall on the right using decision correction technology.

2. Algorithm overview

The main idea of the algorithm is that the decisions are immediately evaluated for their success and a special subsystem tries to adjust them so that they would perform better in the next generation.

The robot obtains proximity sensor information and passes it to an artificial neural network, saving a copy of sensor values in an array. After this, both the sensor information and the decision of the network are forwarded to a primary IF-THEN test. The exact content of this test is unimportant for our purposes,

however, minimally it should be able to detect and appropriately override network decision in these situations:

- when the robot is about to make contact with a wall;
- when the neural network attempts to move the robot backwards;
- when the neural network attempts to move the robot exceeding its maximum speed;
- when the neural network attempts to move the robot away from the wall.

After the final decision is established, it is forwarded to engines of the robot. A little timeout is given, after which new proximity information is obtained. Here we enter a second batch of IF-THEN tests, however, this time they are not meant to override decisions but to apply corrections to them. In our experiment, the following correction rules were applied:

- if a wall is approaching in front of the robot, encourage turning left;
- if a wall on the right is getting closer, encourage turning left slightly (Fig. 1);
- if a wall on the right is getting further, encourage turning right slightly;
- if everything went well, increase the speed.

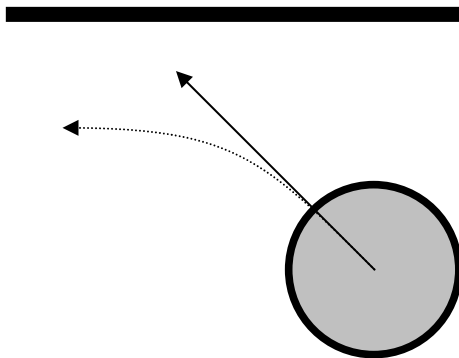


Fig. 1. An example of a made decision (solid arrow) and an adjusted decision (dashed arrow)

Encouraging certain behaviour is achieved simply by adding a certain amount of speed to one of the wheels, unless its speed is already approaching maximum, when the speed of an opposite wheel is reduced instead for turning, or nothing is changed at all for accelerating.

The old proximity data and the adjusted decision are saved into a database. After a certain predetermined amount of iterations, where the data are acquired and decisions are made and adapted, the workflow is temporarily halted, the old artificial network destroyed and a new created instead. This new network is taught all the corrected decisions that were obtained, and then the workflow resumes.

3. “e-puck” mobile robot

“e-puck” mobile robot is a low cost mobile robot, constructed specifically for various research applications with simplicity and robustness in mind. The whole structure is built around a single-part plastic

frame 70mm in diameter, which holds two engines and a battery, as well as circuitry board.

Miniature stepper motors are used, which have 20 steps per revolutions, which are further reduced with 1:50 gear reduction. Gears and the wheels are mounted directly on the axis. The wheels are made of lightweight plastic and have 41mm in diameter. The maximum speed of a single engine is 1000 steps per second, which is equivalent to a single revolution of a wheel, or 129mm.

The “e-puck” robot determines its position in space using eight infrared proximity sensors (Fig. 2), deployed around the perimeter of the body – four in front, two to the sides and two in the rear. Each of the sensors has about 40mm effective range, which further depends on the noise level of the surrounding area. The returned values fall into a range from 0 to 3000, higher numbers meaning closer object. The relationship is non-linear, but irrelevant to our further discussion.

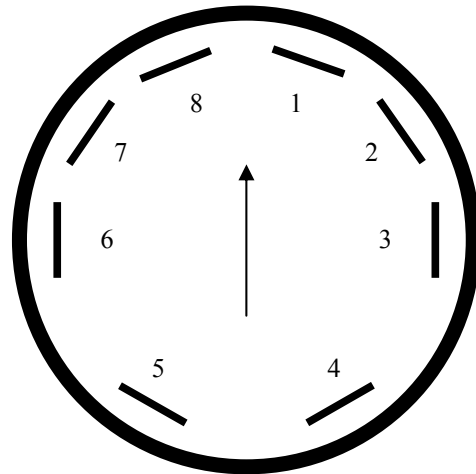


Fig. 2. The sensor layout of an “e-puck” mobile robot

“e-puck” is also equipped with three microphones, a 640x480 pixel camera, accelerometer and ground sensors which were not used in this particular experiment.

4. Experiment setup

For our experiment the “e-puck” robot was connected to MATLAB™ computing environment, which was then used to implement the algorithm and obtain various debugging information in an accessible graphical representation. The connection was achieved via Bluetooth™ technology, with all data sent to and read from an emulated COM serial port.

The robot was put into a box approximately 60 centimetres long and 40 centimetres wide, with several cardboard obstacles inside (Fig. 3). Both the inside walls of the box and obstacles were covered with sheets of white paper to enhance their reflectivity to infrared waves. Obstacles were not fixed to the box in any way to make changing the configuration of the test maze in the middle of an experiment possible.

Fluorescent lights were turned off in the surrounding area to reduce the noise picked by infrared sensors.

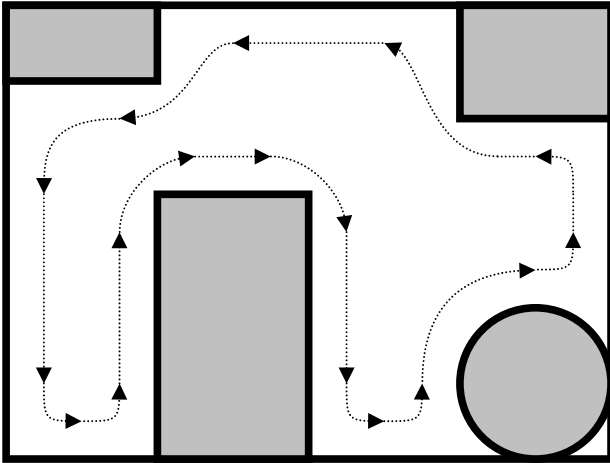


Fig. 3. An example setup of the testing box with an approximation of the best route marked

On the software side of things it was decided to use a feed-forward back propagation artificial networks with a single hidden layer, made of four tangential sigmoid neurons, and an output layer, consisting of two tangential sigmoid neurons (Fig. 4). To reduce the dependence on the exact type of robot used and increase the speed of learning, both the input (proximity sensor) and output (speed) data were normalized to the range 0.0-1.0.

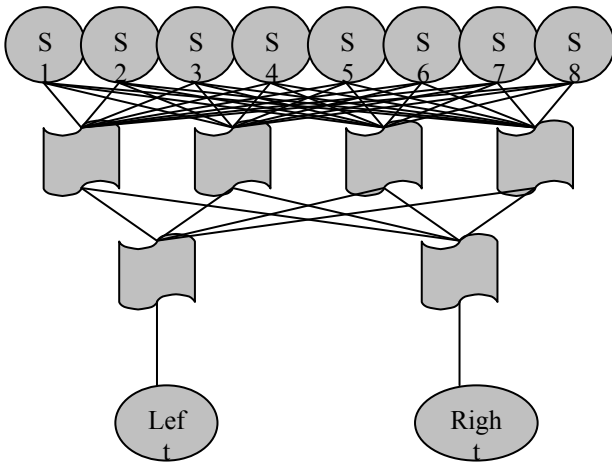


Fig. 4 The structure of the used neural network

A single artificial neural network was used for 500 work cycles, collecting proximity data and adjusted decisions. After the life cycle was over, the network would be destroyed, another one of the same structure would be created and it would be taught according to the batch of data its predecessor had collected. After this switch, the new network would proceed with collecting new, improved data for its successor.

During the experiment the robot was observed visually as well as some of its parameters, namely the value of the third proximity sensor, the sum and the difference of wheel speeds, were monitored through MATLAB™ environment. A well-behaved robot would do the following:

- keep the value of the third proximity sensor stable, which translates into keeping a stable distance to the right side wall;
- keep the sum of wheel speeds as stable and as high as possible, which means that robot would navigate the maze as fast as it can;
- keep the difference of wheel speeds as stable as possible, which means that robot would avoid changing direction of travel unnecessarily.

5. Results

For our experiments we restricted ourselves with 20 generations of the neural network and limited the speed of the robot to 500 steps (6.3 centimetres) per second. Both IF-THEN routines were absolute for the first experiment, meaning that they didn't account for the size of an error, just for its type. The first generation was a zero network, thus the robot was guided around the maze by the first IF-THEN routine. Since we elected to use a discrete control scheme, the path of the robot was noticeably rough. Also, the IF-THEN routine was designed to keep the travelling speed constant at 200 steps (2.5 centimetres) per second, which is rather slow. After the first generation finished, a new artificial neural network was taught everything the previous network collected. The smoothing of the trajectory was evident immediately, and the maximum speed of the robot rose up to 300 steps (3.8 centimetres) per second, with the average being around 230 steps (2.9 centimetres per second).

On the fifth generation the average speed was already in the 400 steps (5 centimetres) range, however, some problems became evident. Since we used constant corrections for our data, situations started to arise where the neural network started taking evidently wrong decisions which would have led into sudden spikes of speed, minor collisions with obstacles or turning more than necessary to negotiate a corner due to overcompensation, which led to IF-THEN routine becoming more active again (Fig. 5).

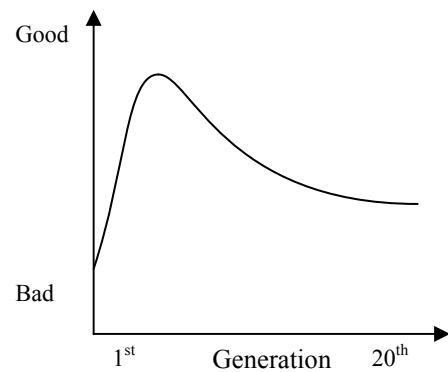


Fig. 5. The evaluation of the performance of the neural network compared to its generation

From the tenth generation onward the IF-THEN override percentage rose dramatically to the range of 40-60% because the data correction algorithm began to under-compensate the errors at an increasing rate, which led to robot going too fast for its maximum data transfer rate and sometimes even losing the wall on the right, and then driving very slow because of the override, resulting in very twitchy control and bad overall performance.

For our second experiment the corrections were made proportional to the speed the robot was travelling at the moment. This reduced the under-compensation problem significantly, allowing robot to negotiate right-hand corners a lot more effectively, however, the problems of spiking speed, colliding into the walls and turning too much in the left-hand corners still persisted somewhat, making IF-THEN override percentage rise again after several generations of staying below 10%.

6. Future work

The algorithm has shown a great potential to teach a robot to navigate a maze in a matter of minutes as opposed to hours. However, the simplest variants of the correction rule set showed convergence only for several generations and then started to diverge away. One obvious way to take care of the problem would be to reformulate the rule sets to take into account not only the speed of a robot, but the size of an error as well. Also, this dependence of a correction from the size of an error might not be linear. A further work in that direction could bring some more satisfactory results.

7. Conclusions

With well formed primary and secondary IF-THEN blocks, this algorithm is capable of converging to a good solution very quickly. In our tests it was revealed that the robot was capable of navigating the maze sufficiently fast with a minor percentage (below 10%) of overridden network decisions in very few iterations of the algorithm without any further input from a human expert. However, after a while the quality of the artificial network started degrading considerably, with increasing twitchiness of control by neural network, which led to IF-THEN overrides and thus decreased average speed. A further work on avoiding such degradation or finding a best neural network and stopping the teaching process is required.

With this algorithm the burden of the problem is transferred from actual network manipulation into finding those well formed control blocks. Here lies the main advantage and disadvantage of this method at the same time. On one hand, for sufficiently simple tasks describing a rule set for adapting behaviour could be a very easy and intuitive task, on another hand, when the difficulty rises, finding the appropriate rules may prove to be bordering impossible, and very complex rule sets may be very time consuming to parse through, which could inhibit the responsiveness of a system.

Compared to evolutionary algorithms, this method showed a potential for a lot faster convergence, measurable in minutes instead of hours or days. On the other hand, expert teaching algorithms are of comparable convergence speed; however, the input from human expert is constantly needed, which is a waste of human resources.

8. Acknowledgements

We would like to express our gratitude to Lithuanian State Science and Studies foundation for the received support and to Vidas Raudonis and Arūnas Lipnickas for their help and suggestions along the way.

9. References

1. Zavlangas P.G., Tzafestas S.G. Industrial Robot Navigation and Obstacle Avoidance Employing Fuzzy Logic, 2004.
2. McLain T., Beard R., Kelsey J. Experimental Demonstration of Multiple Robot Cooperative Target Intercept, 2002.
3. Caltabiano D., Muscato G. A Robotic System for Volcano Exploration, 2005.
4. Whitcomb L., Yoerger D., Singh H, Howland J. Advances in Underwater Robot Vehicles for Deep Ocean Exploration: Navigation, Control, and Survey Operations, 1999.
5. Brown G.M., Bernard D.E., Rasmussen R.D. Attitude and Articulation Control for the Cassini Spacecraft: A Fault Tolerance Overview, 1995.
6. Maki J.N., Litwin T., Schwochert M., Herkenhoff K. Operation and Performance of the Mars Exploration Rover Imaging System on the Martian Surface, 2005.

VOICE CONTROLLED TELEPHONY SERVICES

Rytis MASKELIŪNAS*, Algimantas RUDŽIONIS*, Kastytis RATKEVIČIUS*, Vytautas RUDŽIONIS**

*Kaunas University of Technology; **Vilnius University, Kaunas Faculty, Lithuania

Abstract: Paper deals with voice controlled telephony services. Main speech server and TAPI 3.0 telephony control activities are reviewed. Microsoft speech server based voice control prototype telephony application – interactive voice controlled phonebook is described. Experiments on Lithuanian names and surnames recognition are offered.

Keywords: telephony control, Lithuanian voice commands recognition.

1. Introduction

Speech based interfaces for the control of various home appliances and as a basic modality for the control of telephony based services has enormous potential and advantages. In recent years we saw significant number of new such type services and prototypes presented and developed in various countries and in various fields. There were two important factors that influenced development and caused growing number of applications: appearance of well established and easily available telephony application program interface (TAPI) and tools for development of such type interfaces and even more importantly appearance of speech application programming interfaces (SAPI) with appropriate speech engines. Such speech recognition engines or engines integrated into Microsoft Speech Server (OCS-SS) enables to achieve highly accurate speaker independent recognition of speech commands necessary for the control of various speech based telephony services.

Speech recognition engines have one very important factor: they are not language independent and depend on the language spoken by the users of the system [1]. Microsoft and other major speech technologies providers develop and market speech engines for popular languages having many native speakers (English, Spanish, French, etc.). Many other less widely used languages remains out of the scope of interest for the major speech recognition solution providers.

In such situation businesses and state institutions, in countries where such less popular languages are used as a

main source of spoken language communication, faces a challenge of development of own speech recognition tools. Two major ways for solution are as follows [2]:

- to develop own speech recognition engine from scratch;
- to adapt the foreign language based engine for the recognition of the native language.

The first approach has potentially higher capabilities to exploit peculiarities of selected language and hence to achieve higher recognition accuracy. But the drawback of such approach is the same why the providers of major speech technologies avoid the implementation of such languages in their products – high costs in the general sense of this word.

The second approach [3-5] has the potential to achieve some practically acceptable results faster than developing entirely new speech recognition engine [6]. Another advantage of this approach is potential to achieve faster compatibility with the existing technological platforms. Such advantage is often important for business customers, since they need to follow various technical specifications in order to guarantee consistent functioning of the enterprise. This approach also requires careful investigation of the ways of adapting and optimizing adaptation algorithms [7].

This paper deals with the attempts to evaluate possibilities to adapt some foreign language oriented speech engines for the development of Lithuanian spoken language based telephony services. Chapters 2 and 3 briefly introduces with the modern call control technologies used in our applications. Chapter 4 presents the results of experiments carried out to optimize performance of some Lithuanian speech recognition using telephony services.

2. Call control technologies for Windows

This chapter introduces with the telephony application programming interfaces (TAPI) that were used in our experiments and for the development of Lithuanian speech programming interfaces.

Telephony Application Programming Interface (TAPI) 3.0 is an evolutionary API providing convergence of

both traditional PSTN telephony and VoIP telephony. TAPI 3.0 supports standards-based H.323 conferencing and VoIP multicast conferencing.

Similar to TAPI 3.0, Speech Server supports VoIP for telephone calls over the Internet, using Session Initiation Protocol (SIP).

There are four major call control components to TAPI 3.0:

- TAPI 3.0 COM API - this API is implemented as a suite of COM objects. Moving TAPI to the COM model allows component upgrades of TAPI features. It also allows developers to write TAPI-enabled applications in any language.
- TAPI Server - this process abstracts the TSPI (TAPI Service Provider Interface) from TAPI 3.0 and TAPI 2.1, allowing TAPI 2.1 Telephony Service Providers to be used with TAPI 3.0, maintaining the internal state of TAPI.
- Telephony Service Providers - (TSPs) are responsible for resolving the protocol-independent call model of TAPI into protocol-specific call-control mechanisms. TAPI 3.0 provides backward compatibility with TAPI 2.1 TSPs.
- Media Stream Providers - TAPI 3.0 provides a uniform way to access the media streams in a call, supporting the DirectShow™ API as the primary media-stream handler.

In the OCS-SS case the following activities allow the developer to control call connectivity:

- AnswerCall - Answers a call from a telephony device using the Computer Supported Telecommunications Applications (CSTA) AnswerCall service.
- DisconnectCall - Disconnects a call using the Computer Supported Telecommunications Applications (CSTA) ClearConnection service. When the DisconnectCall control completes its operation successfully, the Speech Platform terminates the dialog.
- MakeCall - Initiates a telephone call using the Computer Supported Telecommunications Applications (CSTA) MakeCall service. The MakeCall control initiates an outbound call to the specific number on the telephony device when activated by RunSpeech.
- BlindTransfer – used to initiate a blind call transfer.
- DetectAnsweringMachine – allows detecting answering machines.
- DeclineCall – refuses the incoming call.

3. Call control in speech processing system

In order to place a call in TAPI 3.0 the client has to create and initialize a TAPI object, then use the TAPI object to enumerate all available Address objects on a computer (for example, network cards, modems, and

ISDN lines. Then it must enumerate the supported address types of each Address object (for example, a phone number, IP address), choose an Address object, based on queries for support for appropriate media (audio, video, etc.) and address types, use the CreateCall method of the Address object to create a Call object associated with a particular address. Then it must select the appropriate Terminals on the Call object and finally call the Connect method of the Call object to place the call.

In order to answer a call the client similarly must create and initialize a TAPI object, to use the TAPI object to enumerate all available Address objects on a computer, to enumerate the supported address types of each Address object, to choose an Address object, based on queries for support of appropriate media and address types, to register an interest in the specific media types with the appropriate Address object, to register a call event handler with the Address object. TAPI notifies the application of a new call through ITCallNotification and creation of a Call object, to select the appropriate Terminals on the Call object and finally to process incoming call using the Answer method of the Call object to answer the call.

In the case if Speech Server registers client application with an SIP server then SIP server is giving certain data, such as its location, IP address, and the protocol it supports. When a user wants to place a call to another registered user, an INVITE message is sent to the registered user, based on the data that client gave the SIP server when it registered. Once the client accepts the INVITE, the two clients can communicate. The reason for the INVITE is that a client can be registered at multiple locations, such as a mobile device and a computer. The first location which accepted the INVITE will receive subsequent messages. If a network does not currently support VoIP protocols, the traditional telephony setup may be used: a telephony card and the associated Telephone Interface Manager (TIM) software. Speech Server provides backward compatibility via the Telephony Interface Service (TIS), which serves as an interface between TIM and the telephony application proxy (TAP). The TAP acts very much like a SIP redirect server, as it interprets requests to and from the TIS and other SIP peers, and routes them to the appropriate server.

Speech server allows direct combining of call controls with proprietary voice input and output processing activities. For TAPI 3.0 speech controls (i.e. system.speech namespace) from .NET framework 3.0 must be used.

The usage scenario of the interactive voice controlled phonebook (Fig. 1) application was developed to imitate phone book directory service by most popular information access ways – telephony calls using regular GSM phone.

After the user calls the application on speech server, the telephony answerCall activity is started and the dialog workflow is initiated. At this stage the telephone user needs to ask a person to give by voice some information (to tell the last and/or first name of the person he is

looking for) or to enter the last name by letters using phone keypad (letters abc=2, def=3 and so on, i.e. “maskeliunas”=6275354627)).

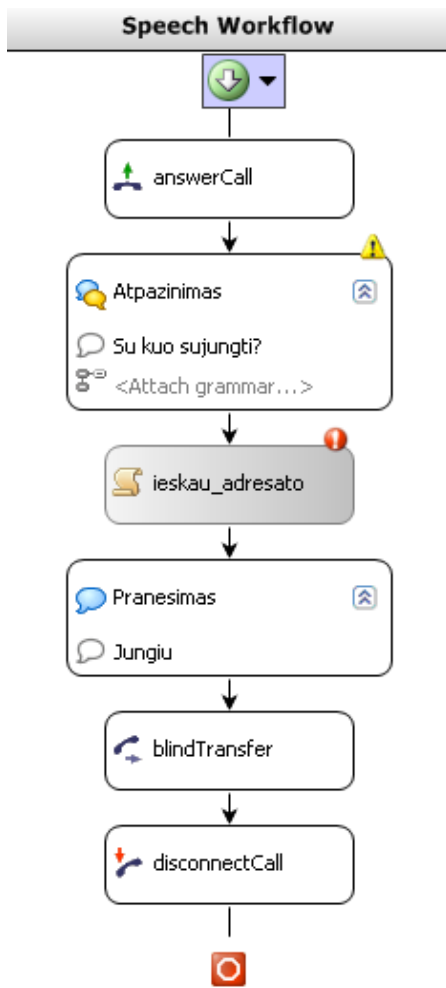


Fig. 1. Interactive voice controlled phonebook – visual studio workflow window

Both voice and DTMF recognition grammars are controlled using speech QuestionAnswer activity, utilizing W3C standard based grammars. Lithuanian language recognition is possible using cross lingual language models [8]. If the user said only the last name, and there were found more than one alternatives, n-best search algorithm is fired, system offers the best possible choices and asks to choose the correct one at any time (i.e. user may say “this is the one I’m looking for”, “this one”, “stop”, etc. or press # key). Once the person searched has been determined, workflow initiates code activity “ieskau_adresato” and searches for the details of that person (phone number in this case) in the SQL database. Once the required data is fetched, the direct transfer can be initiated (in this case the Speech Server issues a command to a telephony gateway to dial the associated number and transfer the call (using a telephony blindTransfer activity). After a successful transfer, telephony disconnectCall activity starts and dialog is stopped and switched to the ready state for another caller.

4. Experiments

The prototype of Lithuanian speech recognition system for telephony services aims to recognize a set of Lithuanian names and family names. The examples of such services could be the phone directory of small or medium enterprise or information service aimed to the company’s personnel. Since the variety of names and particularly family names is very big we’ve limited the number to 100 names and surnames.

4.1. Speech corpora

For the Lithuanian first and family names speech database 40 different speakers uttered each name and surname once. The total number of combinations first name + family name was equal to 100 in this case (4000 utterances total). Two speech databases were applied in the experiments: the initial corpora and the corrected corpora. Corrected database was freed from various inadequacies and mistakes that were present in the initial database. Between inadequacies and mistakes were the pronunciation errors. Most of such pronunciation errors were situations when speaker used other phoneme than the phoneme present in the original family name, but still getting grammatically correct and often really existing name (in example, speaker said *Pojarskaite* instead of *Bojarskaite* or *Laimis* instead of *Laimius*). Other errors were related with such problems as a stammer near family name or some technical spoilage such as a truncated part of the word (most often at the end of the name – the error of automatic segmentation system).

4.2. Lithuanian proper names recognition experiments

The experiments were carried out using the 100 Lithuanian names data. In these experiments we used the transcription formation methodology proposed in [3]. Microsoft SAPI 5.3 based English speech recognition engines were used as a basis for the adaptation.

The experiments were performed for the male and female speakers separately and also for all speakers together.

Before going to the deeper analysis of experimental evidence let us introduce several definitions used further. The following abbreviations are used in tables of results:

- C – Correctly recognized voice commands;
- U – Unintelligible voice commands;
- S – Substitution;
- O – Omission;
- I – Initial speech corpora version;
- V – Verified speech corpora version.

Table 1 show the results obtained in the experiments. Last row in the table presents results obtained using corrected speech corpora.

Based on the results the male speaker’s recognition accuracy was slightly higher than females’ speakers.

One of the most interesting observations was that the recognition accuracy for the initial and corrected databases was almost equal which show, that a quite robust recognition system for the small pronunciation errors may be developed (rather probable in applications, where we need to recognize people names). The biggest number of errors was the unintelligible voice commands. The omissions were the least often observed type of errors. Substitution errors are the worst type of errors, because the system accepts wrongly recognized word as the correct one.

Table 1. Experiment results using verified and initial speech corpora

Corpora Version	Speakers	Recognition results			
		C, %	U, %	S, %	O, %
I	20 males	89.2	6.8	3.8	0.2
I	20 females	91.2	4.5	3.9	0.4
I	all 40 speakers	90.1	5.7	3.8	0.4
V	all 40 speakers	90.8	5.4	3.6	0.2

Detailed error analysis (Table 2, 3) showed, that speaker RYTMİK made as much as 19 errors (he mixed (pronounced wrongly) at least one phoneme in name or surname while reading names), but all words were recognized correctly.

Table 2. The error list that speaker RYTMİK made in the initial corpora

speaker RYTMİK				
	Initial corpora		Verified corpora	
U	Aleksandravičiūtė Ramutė Biaigo Sandra Drungilienė Gintarė		Aleksandravičiūtė Ramutė Ančerevičiūtė Giedrė Andziulytė Loreta Bartuškaitė Aušra Biaigo Sandra Bojarskaitė Eglė Bulaxienė Danguolė Domarkienė Inga Drungilienė Gintarė	
S	Recognized as	Should be	Recognized as	Should be
	Gedutis Eugenijus	Giedra Nerijus	Gedutis Eugenijus	Giedra Nerijus
	Butkus Valdas	Gudas Audrius	Butkus Valdas	Gudas Audrius
	Dutkevičiūtė Ieva	Ivancevičiūtė Erika		

This wasn't a clear result, as the names list has a lot of phonetically correct names.

In the original corpora the recognition accuracy for speaker RYTMİK was 94 % (C = 94), ASR unrecognized 3 phrases (U = 3), and substituted 3 phrases (S = 3).

There were 20 various mistakes in the RYTMİK corpora. Using the verified corpora the 89 % (C = 89) recognition accuracy was achieved (much lower than for unverified corpora), ASR system unrecognized 9 phrases (U = 9), substituted 2 phrases (S = 2).

Table 3. Examples of errors that speaker RYTMİK made in the initial corpora

speaker RYTMİK	
Should be	Corpora error
Adamonytė Asta	Adomonytė Asta
Ališauskienė Jadvyga	Ališausstienė Jadvyga
Ančerevičiūtė Giedrė	Reading in syllables
Andziulytė Loreta	Andžiulytė Loreta
Averjanovienė Violeta	Averjovienė Violeta
Bartuškaitė Aušra	Bartu.škaitė Aušra
Bilat Eugenius	Bilat Audenius
Binkevičius Ramūnas	Binnkevičius Ramūnas
Bojarskaitė Eglė	Pojarskaitė Eglė
Brūzga Juozas	Background noise, pant
Bučinskas Artūras	Bučinskas Arūnas
Bulachienė Danguolė	Buloctienė Danguolė, background noise
Butkus Valdas	background noise
Daugėla Andrius	Daudėla Andrius
Domarkienė Inga	Domartienė Inga
Džiaugys Audrius	Džiaugys Andrius
Giedraitis Laimius	Giedraitis Laimis
Gudas Audrius	background noise
Ignatavičius Gintaras	First letter cut
Ivancevičiūtė Erika	...ančerevičiūtė Erika

4.3. Analysis of errors

In order to improve the recognizer performance and to find the ways to optimize the adaptation procedure, the detailed error analysis was done.

There were 300 substitution and insertion errors (126 substitutions and 174 insertions) for 40 speakers (4000 phrases) and it was natural to expect that not all names will produce the equal number of errors. Table 4 shows the 5 names that produced the largest number of errors in the experiments.

The 5 most confusing names produced almost 40% of all substitution errors and slightly more than 35% of all insertion errors. So the "concentration" of errors is big and more attention to the names that resulted in larger amounts of errors is necessary.

Table 4. Five names that result in the largest number of the recognition errors in the 100 Lithuanian names recognition experiment

Substitution errors (S)		Unintelligible errors (U)	
Name	Rec. errors	Name	Rec. errors
Gudas Audrius	17	Biaigo Sandra	16
Baublys Algis	12	Dolgiy Andrej	16
Biaigo Sandra	6	Grigonis Audrius	11
Balcius Ernestas	6	Baublys Algis	10
Gailiunas Rytis	6	Giedra Nerijus	8

Detailed view to the most confusing names in these experiments showed that most of those names don't have particularly difficult phonetic structure (the family name *Biaigo* may be treated as the more difficult case).

The bigger number of errors obtained by the name *Gailiunas Rytis* may be explained by the presence of the name *Gailiunas Vytautas* in the same list. But most of those errors can't be explained straightforwardly.

For example, the name *Gudas* often was confused with the name *Butkus*. Such situation shows, that there's still plenty of room for the optimization and further investigation and the better recognition accuracy is obtainable.

4.4. Experiments using multiple transcriptions for the same word

In order to improve recognition accuracy we tried to use multiple transcriptions instead of single transcription for the same Lithuanian word. The idea here was that for different speakers, different transcriptions will be better suited and will allow achievement of higher overall recognition accuracy. This assumption is based on the belief that there is no single mapping from a phonemic units space in one language to the phonemic units space in another language, that'll be equally efficient for all speakers.

In this experiment the two family names from the list of 100 Lithuanian names – *Beliukeviciute* and *Varanauskas* – were selected. These family names are longer and have more phonemes in their phonemic structure and allow generating more phonetic transcriptions that will be sensible and may produce valuable result during the recognition. In the case of family name *Beliukeviciute* 1152 transcriptions were generated for this experiment and for the family name *Varanauskas* 188 transcriptions were obtained. Then the two speakers pronounced each of the family names 100 times and the recognition system was coded to select which of the transcription is the most likely for that speaker and that name. Table 6 shows the four most popular transcriptions for each of the speakers investigated and could serve as a good basis for a further development of the Lithuanian foreign language based speech recognizer adaptation system. One of the observations that could be seen from the data in the Table 5 is that a big number of transcription variations were recognized as the most similar ones for each of the speaker.

For the name *Beliukeviciute* 27 transcription variations were recognized for the first speaker and 21 transcription variations were recognized for the second speaker. It is worth noting that in both cases the first speaker tended to activate more different transcriptions than the second.

Even more important observation is that the most often recognized (as the most similar) transcriptions aren't the same for the different speakers. For example, for the first speaker the most often used transcriptions for the word *Beliukeviciute* were transcription variations 111th, 99th, 15th and 3^d. At the same time for second speaker the most often used transcriptions were the transcription variations 505th, 121st, 504th and 507th. Similar situation has been observed for the name *Varanauskas*.

These results allowed drawing conclusion that the usage of multiple transcriptions in the adaptation of the foreign language speech recognition engine to the Lithuanian language is a reasonable step and it is worth further investigation and implementation in the practical applications.

4.5. Experiments using noisy and clipped speech

The following experiments were carried out using clean and noisy or clipped speech. The aim was to evaluate the robustness of recognizer for the speech signal distortions. 10 speakers participated in this experiment and several SNR levels were selected and clipping coefficients were used (using the algorithms below). Signal to Noise Ratio (SNR) has been measured using formula "(1)":

$$SNR = 20 \lg \frac{S_{\max}}{n_{\max}}, \quad (1)$$

Clipping level has been obtained using formula "(2)":

$$s_c = \alpha \cdot s_{\max}; \quad (2)$$

where:

$$s_{\max} = \max_{i \in \{1, N\}} (abs(s_i)), \quad (3)$$

Clipped signal s_i^c itself has been determined using equations "(4)":

$$s_i^c = \begin{cases} s_c, & \text{if } s_i > s_c \\ -s_c, & \text{if } s_i < -s_c \end{cases}. \quad (4)$$

Table 5. The four most frequently recognized transcription for the two speaker uttering 2 Lithuanian names

Name							
Beliukeviciute				Varanauskas			
speaker				speaker			
ALGRUD		RYTMAS		ALGRUD		RYTMAS	
transcr.	occur.	transcr.	occur.	transcr.	occur.	transcr.	occur.
111	23	505	18	67	24	19	10
99	20	121	12	130	11	166	8
15	13	504	11	4	8	144	8
3	10	507	11	70	8	6	8

Table 6 shows the results obtained in those experiments.

Table 6. Recognition accuracy (10 speakers) of 100 Lithuanian names using different quality of speech corpora

Corpora	Recognition results			
	C, %	U, %	S, %	O, %
unmodified	96.2	1.3	2.3	0.2
SNR 40 dB	95.8	1.8	2.3	0.1
SNR 30 dB	91.1	1.9	6.9	0.1
SNR 20 dB	43.0	12.0	30.4	14.6
Clipping 0,3	92.5	5	2.5	0.0
Clipping 0,1	81.0	13.2	4.8	1.0

The performance of the recognizer began to deteriorate significantly when the SNR level dropped below 30 dB and was in principle unacceptable at the SNR levels below 20 dB. So the performance can't be treated as robust one looking from the SNR variations point of view. Using the clipping coefficient $\alpha = 0.3$ the recognizer performance dropped relatively insignificantly while the clipping coefficient $\alpha = 0.1$ resulted in the much bigger loss in accuracy.

5. Conclusions

Speech recognition engines are not language independent and depend on the language spoken by the users of the system. Two major ways for Lithuanian speech recognition solution are: a) developing own speech recognition engine from scratch; b) adapting the foreign language based engine for the recognition of the native language.

The application of the English based engine for the 100 Lithuanian names recognition allowed achieving recognition accuracy of more than 90 %. These results show that the implementation of longer commands and transcription generation method proposed by [3] were confirmed.

The 5 most confusing names produced almost 40 % of all substitution errors and slightly more than 35 % of all insertion errors. Most of those names don't have particularly difficult phonetic structure (the family name *Biaigo* may be treated as the more difficult case). The bigger number of errors obtained by the name *Gailiunas Rytis* may be explained by the presence of the name *Gailiunas Vytautas* in the same list. But most of those errors can't be explained straightforwardly. For example, the name *Gudas* often was confused with the name *Butkus*. Such situation shows, that there's still plenty of room for the optimization and further investigation and the better recognition accuracy is obtainable.

The most often recognized (as the most similar) transcriptions aren't the same for the different speakers. A big number of transcriptions were recognized as the most similar ones for each of the speaker (27 transcription variations of the name *Beliukeviciute* 27 for the first speaker and 21 for the second speaker). Each speaker tended to activate more different transcriptions than the second.

The usage of multiple transcriptions in the adaptation of the foreign language speech recognition engine to the Lithuanian language is a reasonable step and it is worth further investigation and implementation in the practical applications.

The robustness of the speech recognizer used the robustness was verified using the distorted speech corpora. The performance of the recognizer began to deteriorate significantly when the SNR level dropped below 30 dB and was in principle unacceptable at the SNR levels below 20 dB. Using the high clipping coefficient ($\alpha = 0.1$) resulted the significant drop in recognition accuracy.

6. References

1. Fung, P., Schultz, T. Multilingual spoken language processing. In: IEEE Signal Processing Magazine, Vol. 25, Issue 3, pp. 89-97 (2008).
2. Zgank A., et al. The COST278 MASPER initiative – crosslingual speech recognition with large telephone databases. In: Proc. of 4th International Conference on Language Resources and Evaluation LREC'04, pp. 2107 – 2110, Lisbon (2004).
3. Kasparaitis P. Lithuanian Speech Recognition Using the English Recognizer. In: INFORMATICA 2008, Vol. 19, No 4, pp. 505–516, Institute of Mathematics and Informatics, Vilnius (2008).
4. Beyerlein, P., et al. Towards Language Independent Acoustic Modeling, In: Proc. of IEEE ICASSP'00, Vol. 2, pp. II1029-II1032, Istanbul (2000).
5. Lindberg B., et al. Noise Robust Multilingual Reference recognizer Based on Speech Dat. In: Proc. Of ICSLP 2000, vol. 3, pp. 370–373, Beijing (2000).
6. Villaseñor-Pineda L., et. al. Toward Acoustic Models for Languages with Limited Linguistic Resources, In: CICLing-2005, Lecture Notes in Computer Science, Vol. 3406/2005, pp. 433-436, Springer-Verlag (2005).
7. Schultz T. and Kirchhoff, K. (Eds.), Multilingual Speech Processing, Academic Press, 2006.
8. Maskeliunas R. Modeling Aspects of Multimodal Lithuanian Human - Machine Interface. A. Esposito et al. (Eds.): Multimodal Signals, LNAI 5398, pp. 75–82, Springer-Verlag Berlin, Heidelberg (2009).

DATA ACQUISITION IN OPC-BASED INDUSTRIAL IT SYSTEMS

Roman KWIECIEN, Elzbieta SZYCHTA, Leszek SZYCHTA
Technical University of Radom, Faculty of Transport and Electrical Engineering, Poland

Abstract: This article illustrates utility of data transmission as part of the manufacturing process when OPC technology is used. It presents results of research of loading of Ethernet for the purpose of verification of manner of transmission of process data in this technology. The results also verify that current standard of OPC technology is a good solution.

Keywords: OPC technology, OPC Foundation, OPC specification, COM, DCOM, OPC UA, SOAP, XML

1. Introduction

Data acquisition in industrial IT systems is the key link in management of a manufacturing company [1, 7]. Data obtained from the lowest strata of the engineering process lead to appropriate decision making in higher strata, which should enhance effectiveness of manufacturing and improve product quality. However, development of the information technologies increases information flows across the entire IT system of an enterprise.

2. Model of IT system infrastructure which represents the engineering process

A growing trend can be observed in industrial automatics towards building real-time systems [8]. These become increasingly important in the process of information sharing. Production process management systems are implemented with a view to information sharing systems, for instance (Fig. 1):

- ERP (Enterprise Resource Planning),
- MES (Manufacturing Execution Systems),
- SCADA (Supervisory Control and Data Acquisition).

At lower echelons of the engineering process, higher-level control and data acquisition SCADA, industrial CNC (Computer Numerical Control), PLC (Programmable Logic Controller), IPC (Industrial PC), systems, sensors, actuators, and other industrial automatic equipment are employed. This equipment and its software build a real-time IT system. The

fundamental purpose of this system is to control equipment to implement production objectives and to collect information which will serve to utilize an appropriately managed IT system in the decision-making process.

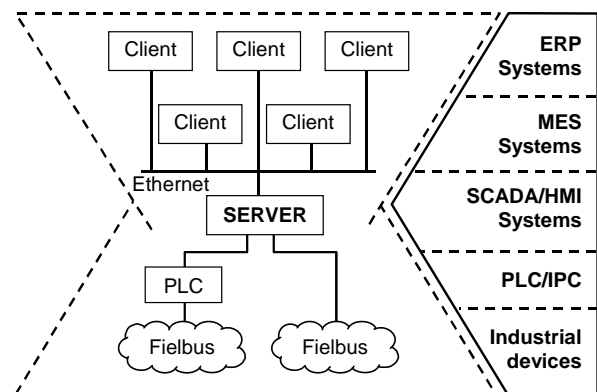


Fig. 1. Model of IT system infrastructure representing the engineering process

Industrial automatics IT systems can be divided into two subsystems [1], creating a model that consists of two pyramids (Fig. 1):

- manufacturing subsystem (bottom pyramid), where the supervisory unit (server) reads processing data (from industrial automatics equipment [4]) and gathers them in an industrial database. The data become a component of the information describing functionality of an enterprise.
- management subsystem (top pyramid, oriented towards the bottom one), where the supervisory units of the highest production management strata play the main role. Using the data in the industrial database and their engineering and economic analysis, decisions are made to adequately represent functioning of the engineering process control systems.

Servers, linking two subsystems in the information sharing process, are key elements of the IT system. They supply process data to clients in accordance with a clearly defined communication Ethernet protocol. OPC

(OLE for Process Control) technology is the current information sharing standard in the client-server scheme of industrial automatics equipment [6].

3. Technique of OPC information transmission

Work on a standard of communication among industrial equipment led OPC Task Force to develop, in 1996, the first OPC specification, which defined access to process data. Since then, activities have been coordinated to maintain and publish new OPC specifications. In effect, the following specifications are currently available [3]:

- OPC Data Access (OPC DA) – provides real-time access to current process data.
- OPC Historical Data Access (OPC HDA) – provides for reviewing and analysis of collected historical data, e.g. to assess system efficiency or anticipate errors. A client gains access to archive data (readings of a device, etc.) by filing enquiries with the OPC HDA server.
- OPC Alarms & Events (OPC A&E) – informs of events and alarms in the system. An alarm is defined as an abnormal condition of an object which requires special attention. An event may be related to a condition, e.g. a transition of a given value to an alarm condition, or not related to a condition, like configuration changes or system errors.
- OPC Security – provides security of access to data offered by OPC servers. It enables correct verification of a client wishing to gain access and of correct transmission (whether data have not been altered).
- OPC Batch – required in batch management.
- OPC and XML – integrating OPC and XML (eXtensible Markup Language) to build Internet applications.
- OPC Unified Architecture – enables communication between different operating systems via SOAP (Simple Object Access Protocol – a protocol for calling remote access to objects using XML).

OPC DA specification provides access to a single process datum with reading or recording capability, each having a value, timestamp, and quality (Fig. 2).

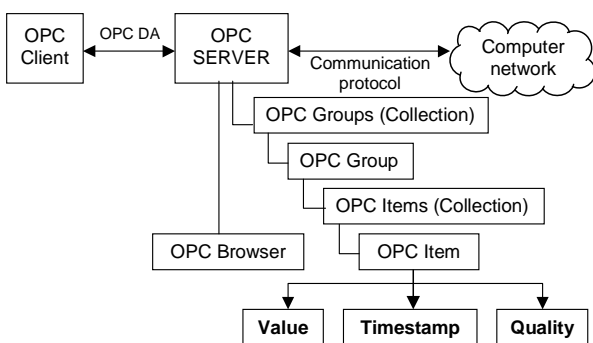


Fig. 2. Architecture of access to process variables via OPC DA

A device or OPC server can generate the timestamp (if the device does not have this capability). Using this

specification, only current process data can be viewed or changed.

Due to complexity of processes executed by OPC server, process data are logically divided into groups (Fig. 2). The process data in these groups are characterized by various scan times, reading modes, etc. Depending on OPC DA version, two data readout modes are possible:

- synchronous – readout always occurs at identical time intervals,
- asynchronous – readout occurs when certain data change – levels can be defined for the readout to occur when they have been exceeded.

Access to data by means of OPC DA can be gained in three ways:

- using COM/DCOM [2],
- using XML (eXtensible Markup Language) and SOAP (Simple Object Access Protocol),
- via .NET Remoting technology, offering broader capability than DCOM (supporting different formats and communication protocols, easy communication by the Internet).

OPC DA comes in a number of versions, with 3.0. being the latest (each version provides another range of interfaces, though reverse compatibility should be maintained).

OPC specifications define communication in the client-server scheme as vertical communication. On the basis of defined OPC DA specification, horizontal communication can be executed between the OPC servers (Fig. 3). This is implemented by an intermediary application called DX (Data eXchange).

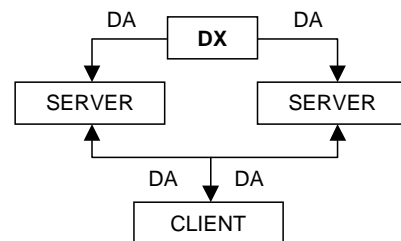


Fig. 3. Communication in the server-server scheme of OPC technology

4. Testing of network's load-carrying capacity

The system shown in Fig. 4 is employed to test load-carrying capacity of a computer network using OPC. PC1 and PC2 computers are connected to Access Point AP TP-LINK, TL-WR543G. Access Point acts as a link in the process of information sharing among computers in a LAN following TCP/IP protocol.

OPC server: "Matrikon Simulation Server" – process data simulator - is installed on PC1. Readout of one type of process datum – 4-bite integer – is assumed, as shown in Fig. 5. Software of OPC client, created by Delphi compiler of Borland, educational version, is installed on PC2. OPC "Sentrol" components are used to create the application, accelerating its construction at the stage of design and sending orders to OPC server in the

executive mode. The author's own application provides for automated creation of any quantities of process data.

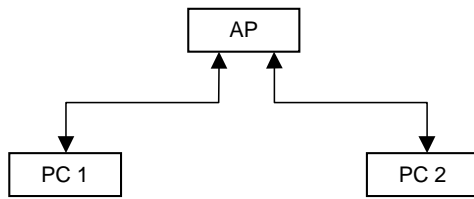


Fig. 4. Diagram for testing load-carrying capacity of a computer network using OPC

AP – Access Point AP TP-LINK, TL-WR543G; PC1 – Notebook HP compaq nx9020 (1,30GHz, 736MB RAM, card Realtek RTL8139 Family PCI Fast Ethernet NIC 100Mbps); PC2 – Notebook Toshiba 1410 (1,80GHz, 256MB RAM, card Intel(R) PRO/100 VE Network Connection 100Mbps)

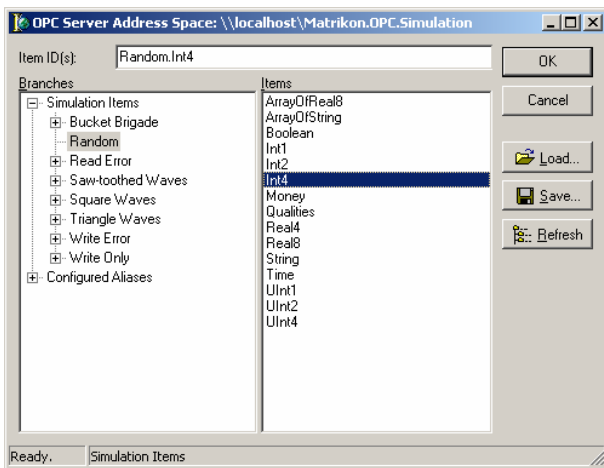


Fig. 5. Selection of process datum – type of 4-bit integer Int4

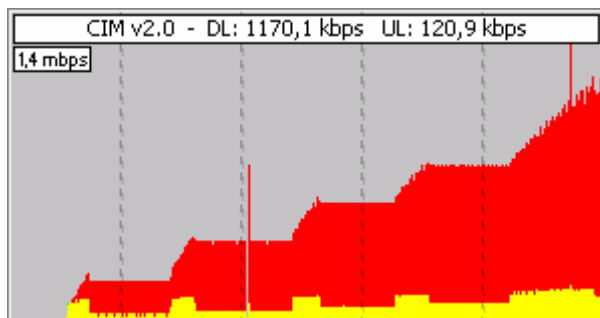


Fig. 6. LAN load-carrying capacity when +500, +500, +500, and +1000 of process data are initiated, respectively

CIM (Crystal Internet Meter) is used to measure load-carrying capacity of the network. This software enables to measure quantities of UL (Upload) and DL (Download). The measurement is possible in KB/s (kilobyte per second) and kbps (kilobit per second). A process of LAN load-carrying capacity is shown in Fig. 6.

The measurements are carried out for several different loads of process data read out. The measurement results are presented in Fig. 7.

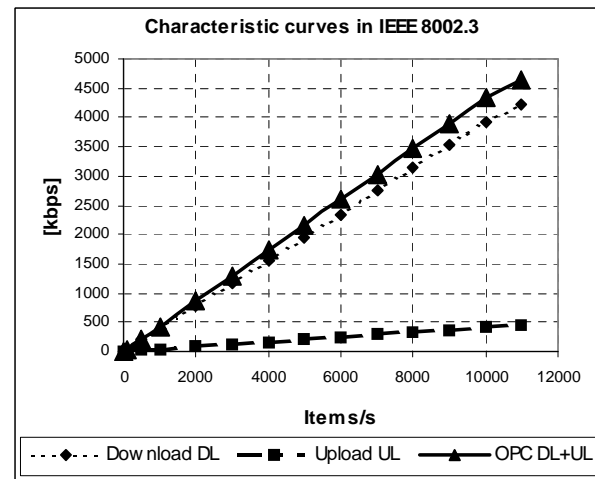


Fig. 7. Characteristic curves of IEEE 8002.3 load-carrying capacity using OPC

5. Analysis of LAN load-carrying capacity when data are transmitted by means of database server protocol

Cyclical loading of process data can be affected by means of a communication protocol, which is currently utilised between a client and database server. Data are tabulated in this protocol. In respect of a process datum, three fields (Fig. 2) can be distinguished, similar to those found in OPC:

- Value, depending on the data type – it is 4 bytes for Int4,
- Timestamp – 8 bytes,
- Quality – 1 byte.

Each table must have a unique name of maximum 16 bites. In consideration of the 8-bytes protocol header, the size of 4-bytes data can be formulated:

$$N = 24 + 13 \cdot n, \quad (1)$$

where:

- N – the size of 4-bytes communication protocol data,
- n – quantity of process data,
- 24 – protocol header including the table name = 8 + 16 = 24 bytes,
- 13 – value + quality + timestamp = 4 + 1 + 8 = 13 bytes.

Theoretical loading of Ethernet can be determined according to the formula. Given this value as dependent on the quantity of process data, the network's load-carrying capacity is tested when data are loaded as tabularic datasets. The characteristic curve in comparison to OPC technology is shown in Fig. 8.

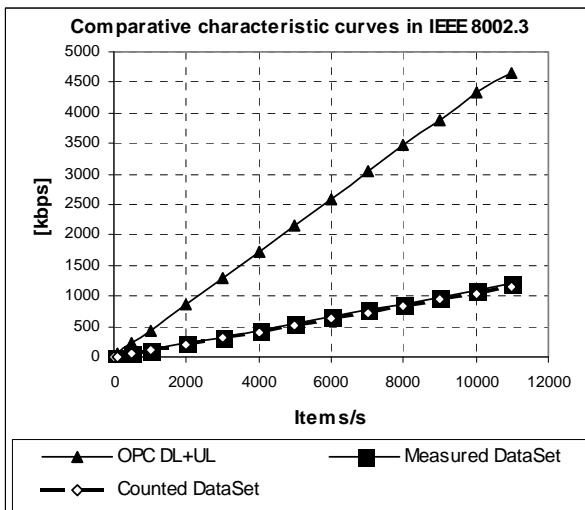


Fig. 8. Comparative characteristic curves of LAN load-carrying capacity for OPC and information transmission by means of DataSet technology

6. Conclusion

OPC standard is based on Microsoft-developed COM (Component Object Model) and DCOM (Distributed Component Object Model) technologies. These technologies are a kind of communication platforms which define the way OPC applications communicate with one another and share process data. Unfortunately, when OPC applications are configured in network operating conditions, certain drawbacks of COM/DCOM based communication become apparent, namely:

- difficulties with configuring the connection,
- problems with establishing the connection,
- problems with maintaining the client – server connection.

In extreme cases, sharing of process data may be interrupted and the manufacturing process may be stopped.

In addition, according to the objective of this paper, it has been established that the method of process data transmission using OPC technology is not the optimum solution. Primarily, it overloads a computer network approximately four times over and above the actual quantity of loaded data (when the protocol of tabularic data transmission is utilised). This is due to the fact that, for purposes of client – OPC server communication, DCOM servers are employed, which additionally include data needed only for DCOM technology in their communication protocol structure. Globally, it increases electricity consumption, which is in direct proportion to the continually increasing quantity of data loaded in Ethernet [5].

7. References

1. Chrupek R. Data Acquisition in Industrial Systems. (In Polish), Napędy i sterowanie, issue 4, April 2008.
2. DCOM: <http://www.microsoft.com/com/>
3. Iwanitz F., Lange J. OPC: Fundamentals, Implementation and Application. Huthig Verlag, Heidelberg, Germany, 2002.
4. Luft M., Cioć R. Increase of Accuracy of Measurement Signals Reading From Analog Measuring Transducers. Silesian University of Technology Scientific Publications 2005, Transport vol. 59 (1691), Gliwice, 2005.
5. Moore G. Energy-Efficient Ethernet, IEEE Spectrum, Int 9, May 2008.
6. OPC: <http://www.opcfoundation.org>
7. Skura K. Issues of IT System Integration in Automation of Manufacturing Processes Based on OPC Technology. (In Polish), Napędy i sterowanie, issue 10, October 2007.
8. Ułasiewicz J. Real Time systems QNX6 Neutrino. (In Polish), BTC, Warsaw, 2007, ISBN 978-83-60233-27-6.

SYNTHESIS OF PROGRAM MODULES FOR TYPICAL BOILER-HOUSE APPLICATIONS

Gediminas DANILEVIČIUS, Darius EZERSKIS
 Kaunas University of Technology, Lithuania

Abstract: A Paper suggests automated control program synthesis for typical boiler-house of small to medium power. Due to typical boiler-house architecture even part of control algorithms for the equipment or overall program structure can be ready made. This paper presents the way to build those control algorithms and automated generation of the control program for programmable logic controller. Process signal coding, special PLC templates and meta-program for the boiler-house control program is also presented.

Keywords: Boiler-house, meta-program, PLC programming.

1. Introduction

A significant part of control problems are similar for small to medium boiler-house applications. For instance, control solutions for boiler control and protection, heating network pressure and temperature control, supplement water supply into network are general for any boiler-house. Therefore those typical control algorithms can be well documented and like framework used for program building in such applications.

Similarly a structure of control program, especially using programming systems conform to programming standard IEC 61131-3 [4], do not depend on a specific boiler-house. Moreover due to local regulations for the boiler-houses they have similar architecture of the technological equipment. This makes it possible to build a program structure, which can be used as core structure.

In the following chapter typical algorithms are discussed and the implementation of a network pump algorithm is presented. Those algorithms will be used as basic algorithms for the automated generation of the PLC program for the boiler-house control.

Essential steps for automated program synthesis as process signal coding in order to order them for right algorithms to meta-program, which builds PLC program code, are presented in following chapters.

2. Finding of typical control algorithms

2.1. Decomposition of a process

Boiler-house is a complex of equipment, where are the boiler for heat generating, and auxiliary technological equipment for the heat supply [1]. Small and medium power water heating boiler-houses can be defined as a *technological unit*.

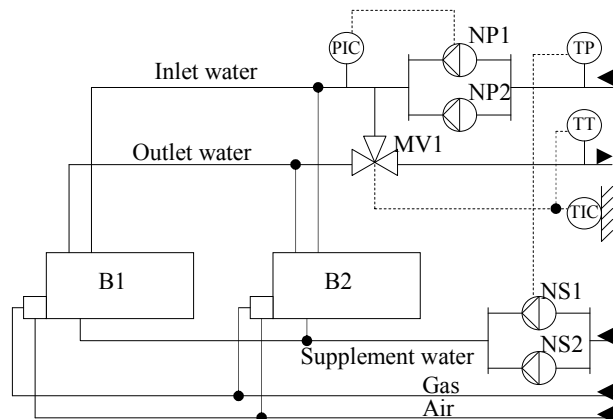


Fig. 1. Typical boiler-house technological scheme

To better understand the system, it is convenient to expand a technological unit into components - *technological branches* [2]. Technological unit is decomposed into technological branches according to technological or energy transfer operations.

There are several typical technological branches in a boiler-house from Fig.1:

- Fuel tract that consists of gas, air supply equipment.
- Heat generation tract that consists of boilers B1 and B2.
- Heated agent tract that consists of water network equipment e.g. network pumps NP1 and NP2, temperature control valve MV1.
- Network supplementation tract, that consists of supplementation pumps NS1 and NS2.

Every technological branch consists of a group of devices which are typical in control terms. It's best to

group *technological devices* according to their design purpose, for example:

- Valves: positional, discontinuous and continuous control.
- Motors (pumps, fans); discontinuous and continuous control.
- Control loops.

Typical control algorithms as function blocks for those technological devices can be designed. Water heating boiler [1] builds normally an isolated control system with well specified algorithm, interfaces for status supervision and mode control.

2.2. Specific requirements for a boiler-house control

Lithuanian requirements for boiler-house equipment installation [3] regulates the automation requirements of the boiler-house, which can be regarded as typical control task for all small and medium power water heating boiler-houses.

Power control task - ensuring the maintenance of the basic operational boiler-house parameters, for example, a supply water temperature to the district heating network.

Device reservation task - ensuring the installed performance of the boiler-house, for example, additional network pump activation in case of faults.

Security task - the boiler-house technological scheme and control equipment that guarantees secure and automated processes operation.

User interface task - boiler operating parameters for monitoring information system must show the values of parameters and alarms deviations.

According to these control tasks, following control algorithms are common for boiler-houses:

- Boiler cascade control
- Network pump control
- Water pressure in a network control
- Water temperature to network

In a following chapter one of these algorithms and its implementation is presented in details.

2.3. Network pump control algorithm example

Two as presented in Fig. 1 or more network pumps are normally installed in a boiler-house to ensure water circulation reliability. Therefore set-point for network pump operation is water pressure to boilers. In a general case capacity of one pump is not enough for normal boiler-house operation. Thus, the typical algorithm should be designed for the control of at least two pumps with easy formal extension capabilities for more pumps. Pressure control algorithm depends on the pump control equipment, signals and their type. If the pumps are operated by circuit breakers, control system action to the system can be only discrete signals to switch-on one of the pumps according to the water pressure in the heating network. System feedback is measured water pressure to the network and status of each pump. In this case the control algorithm should switch-on the pump if water pressure less than min and switch-off the pump if

the water pressure is higher as the max specified pressure, as presented in Fig. 2.

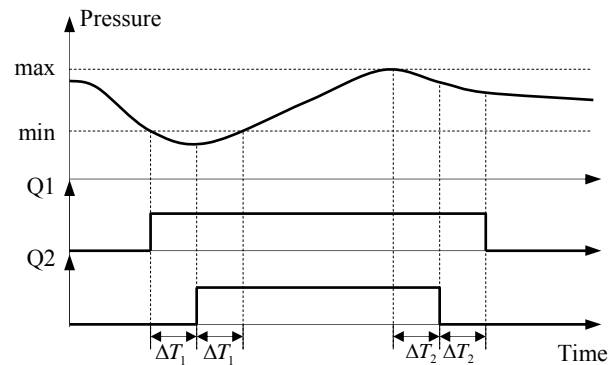


Fig. 2. The network pumps pressure control diagram

In this control diagram Q1 and Q2 are representing the pump contactors status, ΔT_1 and ΔT_2 are the pumps start-up and braking times. Start and stop times are required to record the measured parameter changes during this time.

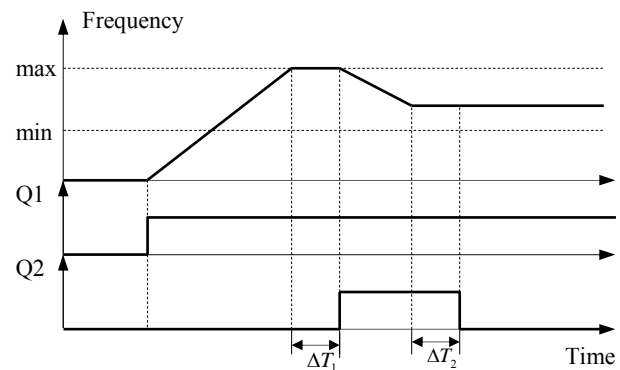


Fig. 3. The network pumps frequency control diagram

If one of the pumps is controlled by frequency converter and the pumping capacity can be controlled by analogue signals, an algorithm should implement a closed loop pressure control algorithm. Then the feedback for the starting and stopping of other pumps is the first pump rotational speed as presented in Fig. 3. Q1 and Q2 are the pump contactors, ΔT_1 and ΔT_2 are the pumps start-up and braking times that should be considered in the algorithm.

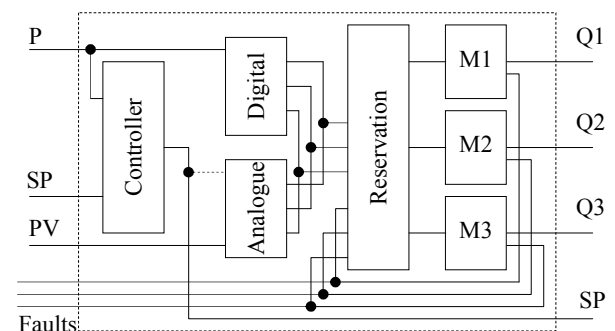


Fig. 4. Pressure control algorithm block diagram

Both algorithms are similar and can be combined into a single control block as presented in Fig. 4. The control block designed in object-oriented design manner [4]. Algorithm consists of a set of mutually cooperated object each of them represents clearly declared and isolated control task like closed loop controller, digital signal evaluation, analogue signal evaluation, basic motor control, reservation algorithms. These objects have all possible connections and operations between objects.

On the left side of the block diagram are control loop inputs: measured pressure (P), the pump with a frequency converter frequency (PV), set point parameter (SP) and the external fault signals. The control block combines the two previously described cases in which the network pumps are controlled by the pump pressure, or under the speed of rotation. Depending on what are the input and output signal types, control block uses the „Digital“ or the „Analogue“ and the „Controller“ control objects. The object named „Reservation“ controls pumps „M1“, „M2“ and „M3“ and ensure to the election in case of fault. On the right side of the block are control loop outputs: pump switching contactors and frequency converters control signal - the rotation speed or frequency (SP).

3. Meta-program of the control algorithm

Main idea of program synthesis algorithms is to identify signals at detailed design phase to which technological branch they belong and order them to corresponding function block inputs and outputs.

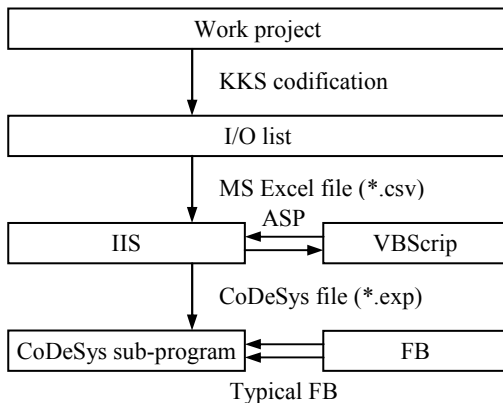


Fig. 5. Automated control algorithm functional scheme

Automated program synthesis process is presented in Fig. 5. From work project at basic design stage, the information will be exported into comma separated value format to analysis program that generates instances of typical function blocks and assigns corresponding O/I channels to them. As the result a program code for industrial PLC programming package CoDeSys is generated.

Input-output data from the detailed design project are uploaded in to the meta-program using project I/O list export. In order to identify I/O signal exported data must have the certain restrictive conditions to provide complete information on the work project Fig. 5. The main restrictive condition is a formal technical

description of the equipment. This means that the design of equipment must be described according to certain rules. The issue: the real object signals must be unambiguous encoded because of the meta-program could respectively attribute them to the objects groups. Such a decision should be known to the power industry. The energy industry is often subject to KKS codification system [5]. Based on this system all of the low average power and water heating equipment may be specified as presented in Table 1.

Table 1. KKS codification system

0	1			2			3			
G	F0	F1	F2	F3	Fn	A1A2	An	A3	B1B2	Bn
A~N	N	A	A	A	NN	AA	NNN	A	AA	NN

It is worthwhile to note that the level „0“ and the level „1“ first column „F0“ indicates the technological unit of code, which during the event is not important. Level „1“ second column „F1F2F3“ refers to the pipeline, but during the event is important only in the last sub-scheme of „F3“, but the general case, the pipeline must be used to describe the entire column, „F1F2F3“ code. This code is quite accurately refers to the device function, such as the pipeline network pumps boilers always labelled as „NDC“ code.

Level „2“ is by far the most important in the present proceeding, as describing the device type. For example, using the „VBScript“ text in the identification of all the tools are selected, all records mentioning the column „F1F2F3“ code, and then from the list drawn up by the election of the engine or valve describing the level of „2“ code.

Design software „EPLAN“ has the possibility to export of the work project KKS signal list, which contains the information elements are separated by semicolons. Useful information is deemed to be that which will require automation of the sub-creation. Without this information the next automated creation are impossible. It is noted that each signal functional text also has a strict form, where must be the signal KKS code and signal function as a commentary.

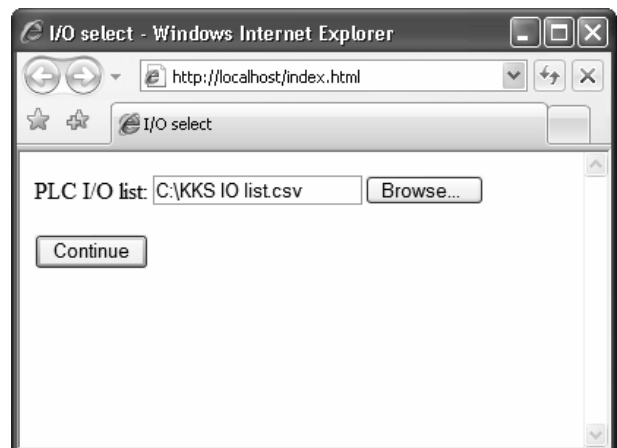


Fig. 6. Data input form

Continuing the development of an automated sub-program exported KKS signal list must be examined. For this purpose a prototype program using visual Basic

programming language is created. User interface and file reading functions are implemented by using Internet Information Service (IIS) platform based scripting forms. Example is presented in the „index.html“ file form Fig. 6. In this form the user can specify the file and then by clicking „Continue“ button to carry out its analysis.

Uploaded data analysis is performed in another file, entitled „submit.asp“. There is all of the analysis scripts called as a meta-program Fig. 7 in this file.

Meta-program analyses data file and split them into the array. One column array consists of rows of data file lines. Data array is filtered by removing the elements that will not be used for further analysis.

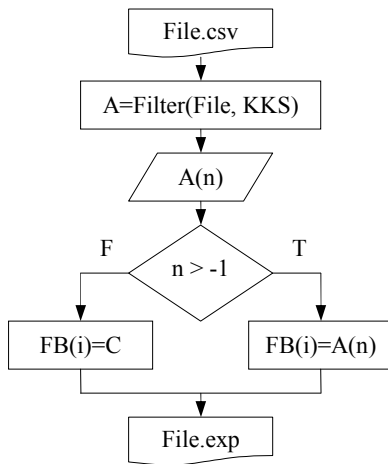


Fig. 7. Meta-program algorithm block scheme

Array is analyzed for KKS codes the global inputs and outputs list. The latter list should be indicated in the sub-logic of the variables used as unique names [5]. Each variable corresponding to the physical address, KKS code, inputs and outputs addresses and commentary.

Global input-output list is designed using the following rules:

- type (DI, DO, AI, AO);
- number (01, 02, ..., 10, 11, ...);
- name (KKS functional text);
- physical address (for example: „AT% IX62.0“);
- type of variable (BOOL, INT, WORD, ...);
- comments (functional text).

After the signals are described with unique names and addresses, sub-programmes can be designed. Sub-programmes consist of blocks of typical control algorithms, such as a network pumps control block which is described in the user library. This block was made on the basis of a representative pressure control equipment control algorithm.

In this case, in process of automation of control sub-programmes are possible to conclude the block inputs and outputs to options, and assign them to the block input and output.

The result as presented in Fig. 8 last line is formed in the export file (which has extension *.exp). Otherwise if export file can not be created because of bad input file format the meta-program returns explanations of error.



Fig. 8. Data output form

Exported file has file format for CoDeSys programming package and can be imported into this package. After this import a program and basic functions for boiler-house control are generated.

6. Conclusions

Analysis of boiler-house control algorithms offers possibility to make them typical and implement as function blocks. This analysis leads to typical program for the boiler-house control too.

In order to assign input and output channels to corresponding technological functions, widely used in energetic KKS coding is used. The meta-program analyses KKS code of the signal and orders them to corresponding technological branch and unit. Finally the instances for program modules and function blocks are created and import file for industrial PLC programming package is generated.

7. References

1. Gimbutis G. Thermo-technology. (In Lithuanian), Vilnius, 1993. 333 p.
2. Ezerskis D. Development and Application of Programming Methodology for Automation Control Systems, Based on Design Patterns. Dissertation, Kaunas, 2006. 128 p.
3. LRS. Requirements for boiler-house equipment installation. (In Lithuanian), Vilnius, 2006. <http://www3.lrs.lt/>.
4. IEC. IEC 61131-3 Programmable controllers – Part 3: Programming languages, Second edition 2003. <http://www.plcopen.org/>.
5. VGB. Identification System for Power Stations (KKS). <http://www.vgb.org/>.

DISTRIBUTED SUBSTATION UNITS CONTROL SYSTEM IN DISTRICT HEATING NETWORK

Julius KALUŽEVIČIUS*, Vytautas DEKSNYS*, Virgilijus PAMAKŠTIS**
*Kaunas University of Technology; **AB Axis Industries

Abstract: Drastically rising energy production costs, continuously increasing demand for environment-friendly and reliable technologies require rational and economic usage of energy resources. This creates objectives to develop an advanced metering and energy control system.

Rising energy consumption could be reduced by optimizing the energy supply chain. This can be done in many ways: using real time control of building environment (heating, air conditioning and ventilation), increasing measurement accuracy, distributing heating consumption network and optimizing substation units control algorithms.

There is a list of automated building environment and substation unit control devices that optimizes plant energy consumption and ensures maximum comfort level. While these devices are saving energy used for single house heating they are misbalancing energy transportation system. This effect can be easily seen during peak period failures.

Misbalance of district heating network leads to tangible energy losses and increased damage warning level. To solve this problem, it is needed to control peak period failures that could be avoided or their impact minimized by using efficient and intelligent distributed control system. It covers all substation units on the district heating network.

Such distributed system equipped with intelligent load management algorithms is able to minimize peak load influence to the network.

Keywords: district heating, distributed control, substation unit control.

1. Introduction

District heating and heat transportation network characteristic to former Eastern block countries. The bigger majority of these plants were built before several decades and at the moment are being renovated or planned to be renovated. It is expected that all morally and technically worn out network parts will be changed into new ones meeting requirements formed by new

data communication capabilities. Growing requirements for safety and security, form new tasks for maintenance and support personnel.

Growing energy prices and rising customers' requirements for quality of service, forces heat energy and hot water suppliers to look for new ways of lowering production costs while increasing quality of service and reliability.

There has been inherited district heating network from former Soviet times. All these energy supply networks have their pros and cons that require constant investments into renovation. Part of these plants are already modernized and insulated, equipped with automated control units responsible for heating substation control and maintenance. Heating substation control units are mainly equipped with powerful controllers that realize building heating models and places heating control in much higher comfort level.



Fig. 1. Automated district heating substation module

The majority of automated substation controllers are regulating building heating depending on air temperature. All the devices in the district heating network react simultaneously to any weather change.

This is the reason why peak load balancing and weather anomalies became much more important than several years ago.

Substation units' automation has solved lots of problems but there has emerged new ones that have to be coped with in much more sophisticated way.

2. Heating regulation model of the building

Heating mode or regime of the building depends on various climatic factors (such as air temperature, wind speed and direction, solar radiation and similar), also heat sources (heating system, people, home appliances and other devices radiating heat). All these influences (except heating systems) change randomly and have different effect for diversity of living quarters [2].

According to the previous statement, heating system should adjust feeding line energy separately for every room, taking into account factors influencing heating mode and ensuring stable temperature in controlled area. In the majority of the houses it is not possible while heating infrastructure is not suited for such precise control. In these plants there are used heating substations that control heat stream for the whole building. The problem of room temperature stabilization is solved by centralizing heating supply for the whole building.

Using qualitative regulation model feeding line temperature is controlled according to air temperature. Heat carrier temperature fed to heating system dependency upon air temperature expressed in the following equation [2]:

$$t_3 = t_{in} + t_A + t_B, \quad (1)$$

$$t_A = \left(\frac{t_{3n} + t_{2n} - t_{in}}{2} \right) \cdot \left(\frac{t_{in} - t_e}{t_{in} - t_{en}} \right)^{0.75}, \quad (2)$$

$$t_B = \left(\frac{t_{3n} - t_{2n}}{2} \right) \cdot \left(\frac{t_{in} - t_e}{t_{in} - t_{en}} \right), \quad (3)$$

where t_3 – heat carrier temperature, t_{3n} – heat carrier temperature under standard conditions, t_{2n} – return heat carrier temperature under standard conditions, t_{in} – room temperature, t_e – air temperature, t_{en} – air temperature under normal conditions [2].

Returned heat carrier temperature is calculated in analogues way as t_3 (heat carrier in feeding line) (1).

Heat quantity which is given by the heating device can be calculated [2]:

$$Q = c \cdot g \cdot (t_3 - t_2) = \alpha_{sp} \cdot F_{sp} \cdot \left(\frac{t_3 + t_2}{2} - t_i \right), \quad (4)$$

where c – heat carrier specific heat, g – heat quantity, α_{sp} – heat supply coefficient of heating device; F_{sp} – heating device area.

Using this model automated heating regulator has to control temperature according to equation (1). When there is a change of air temperature during regulation

process it (feeding heat carrier temperature) has to be recalculated using following dependency [2]:

$$T_3' = \frac{dt_3(\tau)}{d\tau} + t_3(\tau) = K \cdot (1 - \sigma) \cdot t_e(\tau), \quad (5)$$

$$T_3'' = \frac{dt_3(\tau)}{d\tau} + t_3(\tau) = K \cdot \sigma \cdot t_e(\tau)$$

where σ – windows and infiltration areas ratio with outer thermal insulation area.

Coefficient K is calculated taking heat carrier temperature change and air temperature change ratio:

$$K = \frac{\Delta t_3}{\Delta t_e}, \quad (6)$$

where Δt_3 – heat carrier temperature change in feeding line, Δt_e – air temperature change.

Coefficients T_3' and T_3'' describes inertia of thermal insulation. It is calculated using equation [2]:

$$T_3 = \frac{C}{2 \cdot \alpha_e + \alpha_i + \alpha_j \cdot R}, \quad (7)$$

where α_e – return coefficient of outer thermal insulation, R – thermal resistance of outer insulation, C – outer thermal insulation heat receptivity coefficient.

Described mathematical model for heating regulation of the building is suited for automated substation unit control. It evaluates changing air temperature and describes feeding as well as return line heat carrier temperature recalculation and control modes.

Using this model there will be saved energy recourses in the scope of one building but they can be wasted viewing to the whole district heating network.

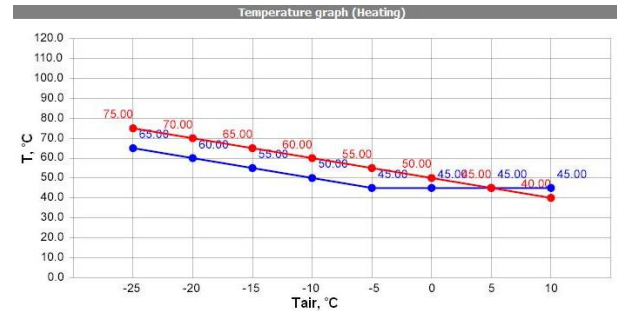


Fig. 2. Heat carrier temperatures in feeding and return lines dependencies on RS3 device

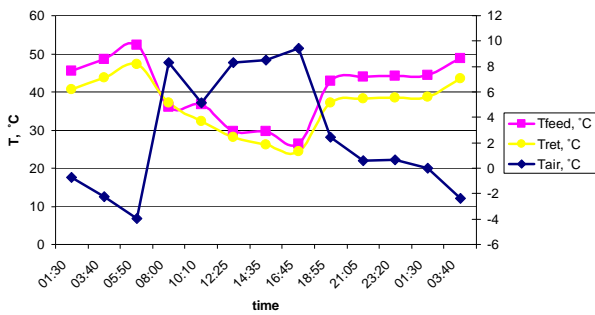


Fig. 3. Weather anomaly when air temperature increases 10 °C in less than two hours

3. Automated substation unit control

Automated substation unit controllers (Fig. 4) are the most important part of building heating system. The whole comfort of the house (heating, air conditioning and ventilation, hot water preparation) depends on this relatively small but full of intelligence electronic device. Automated substation unit saves not only maintenance costs but also energy recourses. Both sides, heat energy provider and energy user, are interested to install automated substation units.

These devices have control algorithms that can ensure comfortable living conditions for rational usage of energy recourses. So today, it is hard to imagine a new building or renovation that would not have had automated control of its heating system.

Almost every automated substation control unit that is on the market fulfils heating regulation model described above or similar.

In most cases heat carrier temperature function of air temperature is given in the graphic form (Fig. 2). Depending on thermal insulation of the building, regulation curve steepness can be readjusted.



Fig. 4. Automated substation unit controller

Regulation of all these devices depends on air temperature. If it drops, heat carrier temperature is increased and if it grows up – heat carrier temperature is decreased. This is a feature which lowers energy consumption that is needed for building heating and

increases comfort. Looking from customers' point of view it is a very beneficiary function but for energy providers it brings a complicated energy distribution network management problem.

Peak loads is another huge problem that automated district heating regulators has to cope with. Normally during critical situations standard regulators can even worsen the situation. If heat carrier is not capable to deliver enough energy, usual heating regulator will try to take as much energy as it needs. This process can become exponentiation if there hasn't been taken any precautions. In such cases, only prioritized task control can offer a quick solution. Heat water preparation and heating control are two separate processes that are controlled depending on heat carrier status and circuit priority.

Water cycle in distributed heating network is about 24 hours. So heating energy preparation must be started at least 24 hours before expected air temperature changes. Because of this district heating network is very sensitive to weather forecasts accuracy and weather anomalies such as sudden temperature changes (more than 10°C in one or two hours) that are unpredictable. Automated heating regulation might even worsen such situation while it does not have feedback from the distributed heating network and its current capabilities. During sudden air temperatures all heating all controllers in the same area start or stop energy usage affecting water pressure in their pipe branch.

There are existing ways how soften this situation by implementing self adaptable air temperature filters, monitoring pressure in feeding and return lines, setting up heating and hot water preparation priorities.

The most efficient way to solve or at least minimize effect of this problem is to create a distributed network of all district heating substation units. This way every control device will have a possibility to receive remote information about network capabilities.

4. Distributed control network

New communication technologies and their provided possibilities can easily add remote access functionalities to almost every control or monitoring device. In today's world it is very hard to imagine automation unit which is responsible for precise and complex processes control that would not have remote access.

Automated substation unit controllers equipped with Ethernet or GSM/GPRS modems become more and more attractive to the market due to their simple remote access and configuration possibilities. When there is an electronic automation device in every district heating substation module there has evolved an idea to centralize such devices management. Connecting all automated district control units into one common information network opens new ways for district heating network maintenance.

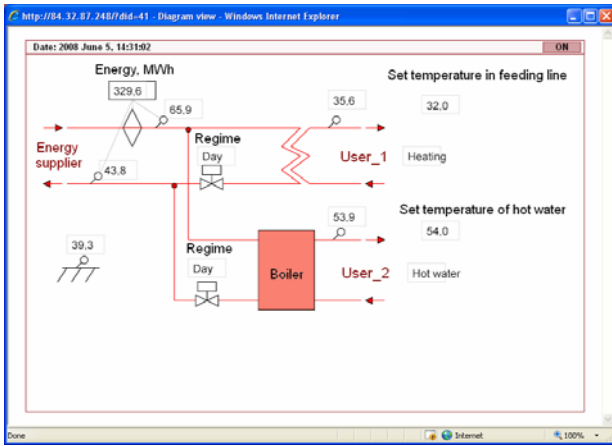


Fig. 5. Remote substation unit control interface

Monitoring actual power capacity at the most vulnerable district heating network points, it is possible to detect dangerous situations that can lead to degradation of working parameters (decrease of heat carrier temperature, pressure losses, and similar). Getting warning events about parameters degradation there will be sent an adjusted set of control parameters to the group of district heating substation units. This way every device will have a feedback about global network situation.

Automated regulation units might misbalance heat distribution network during peak loads or temperature anomalies. The impact to the pipes network is minimized or abolished by adjusting control parameters for a large scale of substation modules installed on the same pipe network branch.

Using distributed network monitoring and remote control functions, heat energy providers acquire new and exceptional tools for network maintenance. These tools can be used as a prevention of accidents and simplified global distributed network remote control.

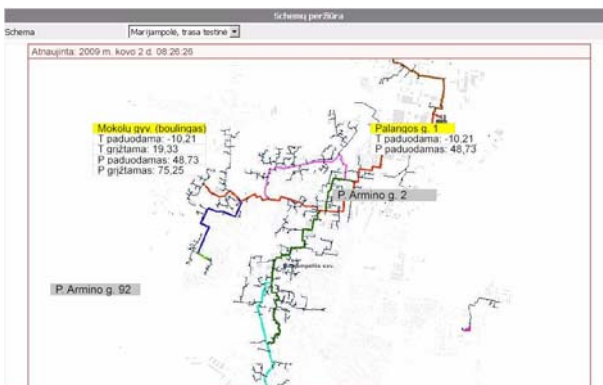


Fig. 6. Monitored distributed substation units network

5. Conclusions

Rising energy prices as well as maintenance and support costs made perfect situation for district heating network as well substation units' renovation. Benefits could have been seen by customers (higher comfort level, lower heating and hot water preparation costs), maintenance and support companies (easier remote maintenance capabilities, lower requirements for support personnel), and heat producing companies (more rational usage of supplied energy, capabilities to adapt and more exactly fulfill mathematical network modeling). Nevertheless peak load balancing and temperature fluctuations became more important problems. Also due to automated regulation there has emerged new risk of hydraulic network misbalancing. Right here should come new ideas of connecting whole district heating network into distributed substation units' network. Where will be possibilities to control groups of substations paying attention to global network situation.

6. References

1. Pamakštis V., Ragauskas A., Kaluževičius J., Petkus V., Bagdonas A., Borodičas P. Advanced energy metering and control system, ISSN 1392 – 1215, Elektronika ir elektrotechnika. N 7 (87), 2008.
2. Morkvėnas R. Šilumos tiekimo pastatų šildymo reguliavimo matematinis modelis. Delta T, 2008 gegužė, p. 27-31.

ESTIMATION OF TYPICAL SAFETY CIRCUITS FOR MEDIUM POWER INDUSTRIAL BOILERS

Algirdas ČEBATORIUS*, Darius EZERSKIS**

*ABB UAB, Lithuania; ** Kaunas University of Technology, Lithuania

Abstract: A safety level evaluation of medium power industrial boiler safety circuits according to international standard EN61508 is presented in this paper. According to safety level estimation requirements for the components and overall circuit is made. Also there is made an analysis of technological boilers safety system and found out typical decisions. After that the calculation of average probability of failure for typical safety systems is made to estimate the safe integrity level. After calculation the possible safety problems and safety improvement suggestions are made.

Keywords: Functional safety, safety integrity level, control system analysis and design, fail safe programming, IEC 61508.

1. Introduction

Medium power industrial steam boiler produce from 10 t/h to 50 t/h of steam. Typical life time of an industrial medium power steam boiler is more than 25 years. International safety standards are obtaining importance during the last 10 years [2]. Boilers can be classified as potentially dangerous equipment therefore much of boiler protection systems to actual safety standards is very important.

Historically three types of protection system solutions are used for boiler protection: relay based, relay based with programmable logic controller (PLC) guided start up system and fail safe PLC based. In the chapter 3 a average probability of failure on demand, PFD_{avg} for the components and overall circuits are presented. According to calculations fulfilment of international standard IEC 61508 [5] is evaluated. The most critical components of protections circuits and safety improvements of existing protection circuits are presented.

In order to evaluate estimated safety integrity level of typical boiler protection systems first required level for industrial boilers should be determined. This is presented in following chapter.

2. Determining the SIL of boiler protection circuits

Safety integrity level of middle power steam boiler protection system is estimating using reliability analysis based on risk evaluation graph presented in next chapter.

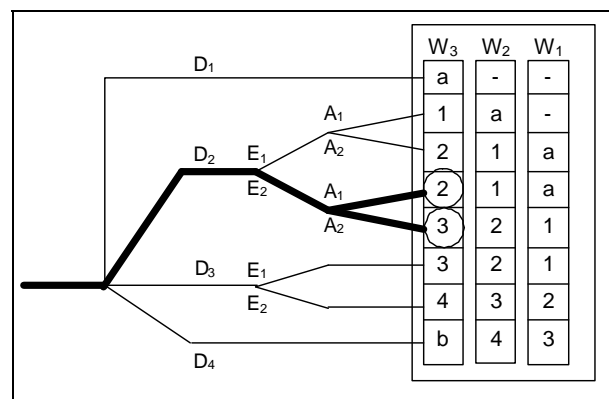


Fig. 1. Risk graph of boiler protection system

2.1. Risk graph

Risk evaluation graph according to IEC 61508-5 appendix D [6] of boiler protection system is presented in Fig. 1. Typically a boiler is driven by one man therefore is assumed that damage due to boiler malfunction is restricted to one person (D₂). Furthermore it is assumed that boiler is permanently observed by authorized personal in the vicinity of boiler and thus in the danger zone (E₂). Danger avoidance is depending on the boiler construction. If explosion flaps are installed then (A₁) and (A₂) when not. Finally the probability that and explosion can occur by protection system malfunction is very high (W₃) due to explosive gas supply into burner furnace.

Required reliability analysis shows that required safety integrity level for boiler without explosion flaps protections system must meet SIL3 and for the boiler with explosion flaps protection system must meet SIL2.

3. Determining SIL of a safety circuit

Typically standard automation equipment has no reliability data from supplier. In this case an average probability of failure on demand (PFD_{avg}) for 1ool systems can be calculated according to (1) [2, 4].

$$PFD_{avg} = \lambda T / 2, \quad (1)$$

where λ - failure rate, T – system usage time. Some automation products manufacturers gives mean time between failure parameter (MTBF) instead of PFD and its proportional to failure rate as shown in (2) [2, 4].

$$\lambda = 1 / MTBF, \quad (2)$$

where MTBF – mean time between failure; [2, 3]. For older equipment that has no reliability data from manufacturer typical failure rates from special reliability databases in chemistry and offshore can be taken as shown in Table 1 [1, 7].

Table 1. Example data from reliability databases [1, 7]

No.	Device	failure rate, $\lambda \text{ h}^{-1}$
1	Differential pressure transmitter	$2,18 \cdot 10^{-4}$
2	Pressure relay	$4,96 \cdot 10^{-5}$
3	Relay	$1,91 \cdot 10^{-6}$
4	Flame scanner	$4,23 \cdot 10^{-4}$
5	Natural gas shut-off valve	$4,564 \cdot 10^{-5}$
6	Boiler PLC	$3,211 \cdot 10^{-6}$

After calculation of PFD_{avg} for every component continue to system PFD_{avg}. System PFD_{avg} depends from circuit connection. If components are connected in series PFD_{avg} is sum of each component's PFD as shown in following formula [2, 3]

$$PFD_{sys} = \sum_i PFD_i \quad (3)$$

where PFD_{sys} – system probability of failure on demand, PFD_i – component's probability of failure on demand.

Safety integration level evaluation according to PFD_{avg} is presented in following Table 2 [2, 4].

Table 2. SIL equivalents to PFD_{avg}

SIL	PFD _{avg}
SIL1	$10^{-2} < PFD_{avg} < 10^{-1}$
SIL2	$10^{-3} < PFD_{avg} < 10^{-2}$
SIL3	$10^{-4} < PFD_{avg} < 10^{-3}$
SIL4	$10^{-5} < PFD_{avg} < 10^{-4}$

4. Evaluation of safety circuits

Typical medium power steam boiler pipe and instrumentation diagram is shown in Fig. 2 [3]. Typical sop conditions for steam boiler are:

1. Operator command

2. Water level in boiler drum LIC1LH over limits
3. Too low traction in furnace PIC4H
4. Air pressure PIC2 over limits
5. Gas pressure PIC3 over limits
6. No flame at any burner

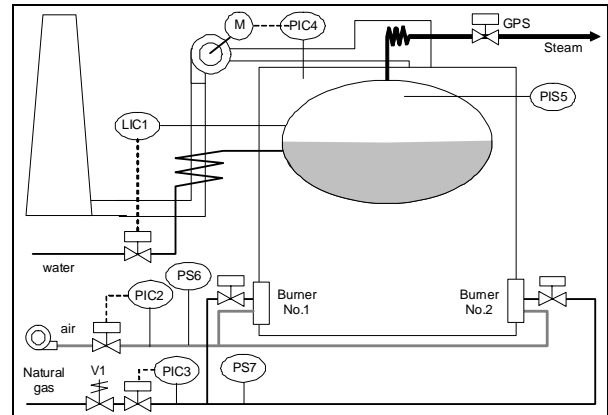


Fig. 2. Medium power steam boiler diagram

Boilers start-up and shut-down typical algorithm is a strictly sequence of operations [3]:

1. No fire in furnace, then next step
2. Furnace ventilation, after set time next step allowed
3. Fuel system leakage test
4. Fuel pressure to main valve check
5. Air pressure to burner check
6. Traction in furnace check
7. Igniters start-up
8. Igniters flame check
9. Natural gas shut-off valve opening
10. Burner start up
11. Burner flame check

If there is any fault condition at any step boiler is shutting down by closing gas shut-off valve V1. Control problem in that algorithm is to start boiler, because flame control unit doesn't let to open fuel shut-off valve if there is no burner flame. Main problem is how safely to disable flame control condition during boiler start-up. When such function is in control algorithm there is additional risk possibility that it will start when burner is working and on such case flame control will be lost. That can initiate explosion in the furnace. Three typical safety system solutions are discussed in following chapters.

4.1. Relay based protection system

This type medium power steam boiler safety system is controlled by standard relays and flame control unit disabling is initiated by operator command. In Fig. 3 there is shown scheme of such system.

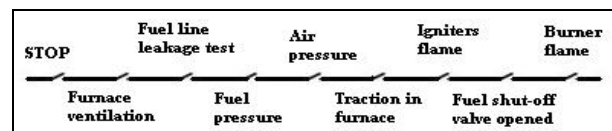


Fig. 3. Relay based protection system

Control algorithm in such type protection system is realized by simple standard components: relays (pressure, level, temperature and interface). Such type of systems is without diagnostic function. According to Table 2 and (1) system probability of failure on demand is calculated for 10 years [2].

$$T = T_p \cdot n_1 \cdot n = 24 \cdot 365 \cdot 10 = 87600h \quad (4)$$

Where T – life time, T_p – day hours, n_1 – day amount in year, n – year amount;

$$PFD_p = 4.96 \cdot 10^{-5} h^{-1} \cdot 87600h / 2 = 2.1725, \quad (5)$$

where PFD_p – pressure relay probability of failure on demand, λ_p – pressure relay failure rate;

$$PFD_{LD} = 4.23 \cdot 10^{-4} h^{-1} \cdot 87600h / 2 = 18.5274, \quad (6)$$

where PFD_{LD} – flame scanner probability of failure on demand, λ_{LD} – flame scanner failure rate;

$$PFD_R = 1.91 \cdot 10^{-6} h^{-1} \cdot 87600h / 2 = 0.083658, \quad (7)$$

where PFD_R – relay probability of failure on demand, λ_R – relay failure rate;

$$PFD_{ATK} = 4.564 \cdot 10^{-5} h^{-1} \cdot 87600h / 2 = 1.99903, \quad (8)$$

where PFD_{ATK} – fuel shut-off valve probability failure of demand, λ_{ATK} – fuel shut-off valve failure rate
Overall probability of failure on demand is calculated using (3).

$$PFD_{SISR} = PFD_R + PFD_R + PFD_p + PFD_p + PFD_p + PFD_p + PFD_{LD} + PFD_{LD} + PFD_{ATK} + PFD_{LD} = 47.91115, \quad (9)$$

where PFD_{SISR} – medium power steam boiler relay based protection system probability of failure on demand;

The result doesn't satisfy reliability requirements for any SIL as presented in Table 3. This is mainly due to using non fail safe sensors and actuators in a system. Relay protection circuit itself could satisfy SIL2 and could be used for boiler protection with integrated explosion flaps.

4.2. Relay based with PLC

Such type medium power steam boiler safety system is controlled by standard relays, but it has differences from relay based protection systems, because flame scanner signal in boiler start-up cycle is simulated by programmable logic controller and there are diagnostic functions. In Fig. 4 is shown scheme of such system.

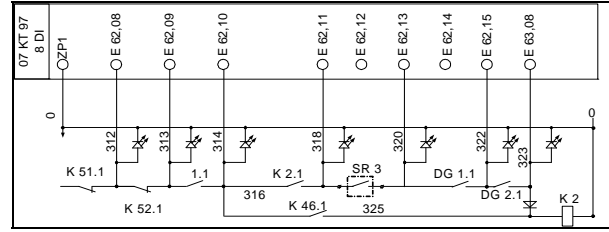


Fig. 4. Relay based with PLC protection system

Control algorithm in such type protection system is realized by simple standard relays and programmable logic controlled, which also realize diagnostic functions. From schematic view system has only series connections, so for calculations will be used in chapter 3 given formulas.

Protection system life time for the system is the same like in chapter 4.1 analyzed system.

$T=87600$ h, where T – system life time;

Probability of failure on demand for every system components is the same as (5), (6), (7), (8), so calculation will be made only for programmable logic controller using (1).

$$PFD_{PLC} = 4.695 \cdot 10^{-6} h^{-1} \cdot 87600h / 2 = 0.20564, \quad (10)$$

where PFD_{PLC} – programmable logic controller probability of failure on demand, λ_{PLV} – programmable logic controller failure rate.

Overall probability of failure on demand for relay based with PLC protection system is calculated using (3).

$$PFD_{RPLC} = PFD_R + PFD_R + PFD_p + PFD_p + PFD_p + PFD_p + PFD_{LD} + PFD_{LD} + PFD_{ATK} + PFD_{LD} + PFD_{PLC} = 48.11679, \quad (11)$$

where PFD_{RPLC} - medium power steam boiler relay based with PLC protection system probability of failure on demand;

The result doesn't meet any reliability requirements. This type of system is even worse that system in chapter 4.1, because standard PLC rises up probability of failure on demand. This is also due to standard system equipment and it doesn't satisfy even SIL2 requirements for boiler with explosion flaps.

4.3. Fail safe PLC based

Control algorithm in such type system is fully realized by fail safe PLC. According to chapter 2.1 it is clear that all devices in system must meet SIL3 requirements. But there is left third probability to make fail safe system standard. There is human mistake probability in such systems, because control algorithm for PLC is written by programmer. To lower this probability it is better to use standard manufacturers programming methods, for example standard data and function blocks. Such type of programming solutions meets all required safety requirements.

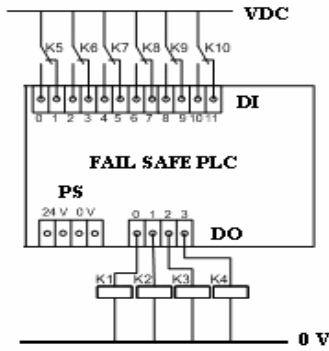


Fig. 5. Fail safe PLC based protection system

There is shown system structure in Fig. 5, but system works like relays connected in series.

Data for system probability off failure on demand is taken from fail safe devices database. [8]. All fail safe devices failure rate is listed in Table 3.

Table 3. Fail safe devices probability of failure on demand [8]

No.	Device	failure rate, $\lambda \text{ h}^{-1}$
1	Differential pressure relay	$8.7 \cdot 10^{-9}$
2	Pressure relay	$6.1 \cdot 10^{-9}$
3	Flame scanner	$1.27 \cdot 10^{-8}$
4	Natural gas shut-off valve	$4.28 \cdot 10^{-8}$
5	Boiler fail safe PLC	$7.69 \cdot 10^{-9}$

According to Table 3 and (1) system probability of failure on demand is calculated for 10 years [2]. System life time is the same as (4), $T=87600 \text{ h}$

$$PFD_p = 6.1 \cdot 10^{-9} \text{ h}^{-1} \cdot 87600 \text{ h} / 2 = 0.00026718, \quad (12)$$

where PFD_p – pressure relay probability of failure on demand, λ_p – pressure relay failure rate;

$$PFD_{LD} = 1.27 \cdot 10^{-8} \text{ h}^{-1} \cdot 87600 \text{ h} / 2 = 0.00055626, \quad (13)$$

where PFD_{LD} – flame scanner probability of failure on demand, λ_{LD} – flame scanner failure rate;

$$PFD_{DP} = 8.7 \cdot 10^{-9} \text{ h}^{-1} \cdot 87600 \text{ h} / 2 = 0.00038106, \quad (14)$$

where PFD_{DP} – differential pressure relay probability of failure on demand, λ_R – differential pressure relay failure rate;

$$PFD_{ATK} = 4.28 \cdot 10^{-8} \text{ h}^{-1} \cdot 87600 \text{ h} / 2 = 0.00186, \quad (15)$$

where PFD_{ATK} – fuel shut-off valve probability of failure on demand, λ_{ATK} – fuel shut-off valve failure rate;

$$PFD_{FSPLC} = 7.69 \cdot 10^{-9} \text{ h}^{-1} \cdot 87600 \text{ h} / 2 = 0.0003368, \quad (16)$$

where PFD_{FSPLC} – fail safe PLC probability of failure on

demand ; λ_{FSPLC} – fail safe PLC failure rate;

Overall probability of failure on demand is calculated using (3).

$$PFD_{SISSIL} = PFD_{PR} + PFD_{PR} + PFD_p + PFD_p + PFD_p + PFD_{DP} + PFD_{LD} + PFD_{PR} + PFD_{ATK} + PFD_{LD} = 5.18 \cdot 10^{-3}, \quad (17)$$

where PFD_{SISSIL} - medium power steam boiler fail safe PLC based protection system probability of failure on demand;

The result fully satisfies the requirements for the boiler with explosion flaps but it is still not enough for boiler without explosion flaps. This is mainly due to using only fail safe devices and fail safe software solutions, but there are not used reservation methods. That is why system meets only SIL2 safety requirements.

5. Conclusions

The risk analysis of middle power steam boiler shows that protections system of such boiler should fulfil SIL3 according to EN 61508. Analysis of a typical existing protection system shows demand for improving existing protection systems.

Relay based systems should be used only for boilers those require SIL2 protection equipment. In this case only certified SIL sensors and actuators could be used.

Using standard PLC in a start-up sequence of a boiler for flame sensor bypass improves overall system PFD and makes system unsafe.

Only fail safe PLC's should be used for protection systems and boiler start-up system.

6. References

1. American Institute of Chemicals Engineers „Guidelines for process equipment reliability data with data tables“, New-York, 1989. 312 p.
2. Boercoek J. Functional Safety. Basic Principles of Safety-related Systems Heidelberg, 2007. 538 p.
3. Ezerskis D. Development and Application of Programming Methodology for Automation Control Systems, Based on Design Patterns. Dissertation, Kaunas, 2006. 128 p.
4. Exida „Safety engineering“ Exida, 2005. 275 p.
5. IEC 61508-1. Functional safety of electrical/electronic/programmable electronic safety-related systems. General requirements. Geneva, 1998. 115 p.
6. IEC 61508-5. Functional safety of electrical/electronic/programmable electronic safety-related systems. Examples of methods for the determination of safety integrity levels. Geneva, 1998. 57 p.
7. OREDA „Offshore reliability data book“, 4th edition, Trodheim, 2002. 835 p.6.
8. <http://www.exida.com/applications/sael/index2.asp> - fail safe equipment database

POSITIONING OF STEPPER MOTORS IN GRAPHICAL DATA ACQUISITION SYSTEM

Raimundas LIUTKEVIČIUS, Andrius DAVIDSONAS
Department of Systems Analysis, Vytautas Magnus University, Lithuania

Abstract: This paper analyses stepper motors position tracing problems, found in 3D scanner application. Attention is paid to the position track methods of the stepper motors in a PC-based application and the use of position data along with the data from optical sensor for the construction of 3D model of the scanned objects. The methods were implemented into the real time 3D data scanning and visualization application and were analyzed in several aspects: the execution time and the positioning precision.

Keywords: PLC application, stepper motor control, stepper motor positioning, 3D data modelling, 3D scanning.

1. Introduction

PLC controlled stepper motors are one of the most versatile forms of positioning systems. They are frequently used in different precision positioning equipment such as 3D scanners, image/flatbed scanners, computer printers, plotters, floppy disk drives, CNC machines, fluid control systems, packaging machinery and many other devices and systems. To compare with competitive closed loop servo motors, they are simpler, cheaper and more rugged. Both motor types can be easily digitally controlled using different PLC systems. Despite this fact, accurate position tracking of stepper motors may become a challenging task. That's why it is main object of this paper.

In this paper the use of stepper motors for the 3D scanner is described. The tasks of stepper motors are: 1) to rotate an object; 2) and to move vertically optical sensor that reads distance to the scanned object. Position tracking of each stepper motor is very important to accurately acquire object's surface coordinates and to create a sufficient 3D model. Even small position tracking errors can cause considerable deflections in a 3D model and the result can become unrecognizable. So, stepper motors positioning and position tracking techniques must be taken into account when programming 3D scanning or similar applications.

Another important factor in such graphical applications is a huge amount of the process data and complex process tasks. Stand-alone PLC system is not suitable for whole object scanning and reconstruction process, which consist of: control of the 3D scanner, acquisition of the data, pre-processing it, forming a 3D model from scanned data and displaying it. The acquisition of data, processing of this data and graphical representation of 3D model is transferred to non real time PC-based application to deal with a problem. Non-real time means that it is impossible to acquire data from 3D scanner at equally spaced intervals and to calculate the position of a scanned object based on motor rotation time or other characteristics. There are many stepper motors positioning and position tracking techniques, but they all differ in quality, speed, etc. and not all of them are appropriate for 3D scanning and other similar tasks. In this paper stepper motor positioning and position tracking solutions, which help to produce sufficient quality for 3D object reconstruction is presented and analyzed.

2. Graphical data acquisition system

3D scanning systems, analyzed in this paper, consists of a scanner, a PLC and a PC. For the control of stepper motors and the acquisition of data, Beckhoff PLC controller CX1020 is used (Fig. 1).

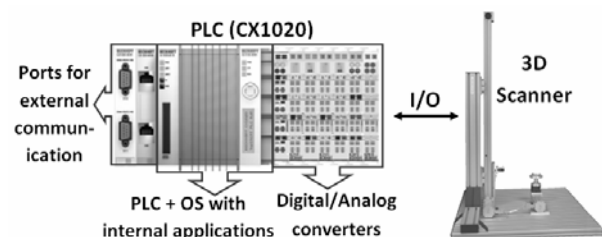


Fig. 1. PLC controlled graphical data acquisition system

CX1020 is an embedded PC with Intel Celeron M 1.0 GHz processor, 1GB RAM, hard drive, Windows XP Embedded OS and ability to attach selected I/O

modules/converters. Three modules/converters for the entire control of 3D scanner are used: 2xKL2541 (step motor controllers) and KL3052 (analogue data input module). All modules are integrated into one 3D scanning system and are programmed using TwinCAT software.

The 3D scanner consists of two stepper motors, the optical distance sensor and additional proximity sensors. During the scanning process the scanner rotates an object about its centre and constantly measures distance to its surface. Another stepper motor is used to move the optical sensor up or down (Fig. 2).

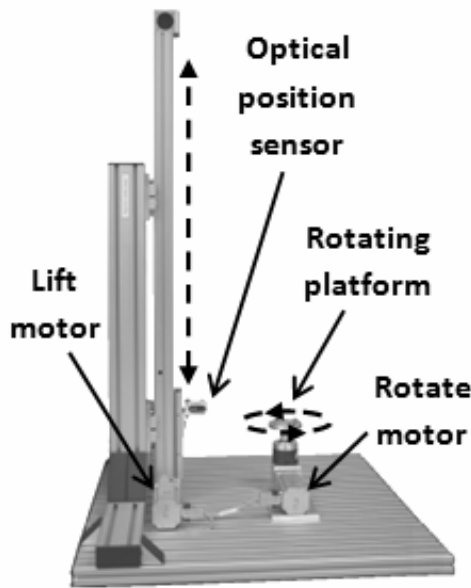


Fig. 2. 3D scanner. Dashed lines show movement directions, straight lines – scanner components

Both stepper motors are controlled with separate KL2541 modules – stepper motor controllers. Each module has two types of internal memory: temporary (RAM) and persistent (EEPROM) and can be programmed using internal registers or manually controlled through TwinCat System Manager application [1].

Object surface coordinates are measured with optical position sensor, which measures distance to particular point of scanned object. KL3052 module is used to digitize analogue data and transfer it to PLC.

3. Acquisition of 3D coordinates

In order to construct 3D model of a scanned object, the precise acquisition of surface point's coordinates are required. This can be achieved by tracking the positions of both - object rotating and sensor lift up stepper motors and acquiring the data from optical sensor. The motor, that rotates an object, produces angle θ , the lift motor – height H and the optical position sensor – radius R . As a result object surface points in cylindrical coordinate system are acquired. At this point, they can be transferred and visualized with the real time visualization system as described in [2], or easily converted to Cartesian coordinates using formulas:

$$X = R \cdot \cos(\theta), \quad (1)$$

$$Y = R \cdot \sin(\theta), \quad (2)$$

$$Z = H. \quad (3)$$

Converted data can be saved in internal data storage for later visualization using other 3D reconstruction methods such as point based rendering [3], power crust or cocone methods described in [3, 4, 5].

It is obvious that quality of the 3D model of a scanned object depends on three main factors: 1) the precision of the stepper motors' position tracking; 2) the quality of the distance measurements; and 3) the quality of the algorithms used for the construction of the 3D model. It was experimentally shown that only small inaccuracies of 3D scanning system can be digitally corrected by 3D modelling algorithms and different filters [2]. So, big attention should be paid to the accuracy of the calculation of the scanned object's points coordinates. Careless control of 3D scanning system usually leads to digitally un-correctable errors and incorrect 3D model. In the next sections the aspects, that cause such errors and how to avoid them by selecting right way to control 3D scanning system are analyzed in more details.

4. Control of stepper motors

The rotation angle and the height of the scanned object are evaluated depending on stepper motors position. So, the calculation of the exact rotation angle and optical sensor lift up position is mandatory in order to get the correct coordinates of the scanned object. Inaccurate calculations result in the deformation of 3D object model - the twists and bends of the model are inevitable (Fig. 7-8). The stepper motor is an open loop system. This means that stepper motor's rotation is controlled without any feedback mechanism. This is the main reason of the positioning problem, because angular position of the motor shaft cannot be estimated. It doesn't mean stepper motors are inaccurate. On the contrary, stepper motors can be positioned as precise, as closed loop based systems, however they can't return the feedback about the current position reached [6].

Depending on the stepper motor type the rotation angle of its shaft can be calculated in several different ways: a) evaluating the rotation time, b) rotating a motor a specified number of micro steps and c) if a motor is equipped with the encoder – reading its data. These methods are analyzed in the next paragraphs.

4.1. Positioning, based on the evaluation of time

Rotation speed of the stepper motor is expressed in terms of steps and micro-steps per second. Every step can be translated into rotation angle θ_s (degrees) or lift-up height H_s (mm). Stepper motor is a precise system and can rotate the exact number of steps during the same period of time. So, the particular position of the motor's shaft can be easily calculated from its operation time using the following formulas:

$$\theta = V \cdot \theta_s \cdot \Delta t, \quad (4)$$

$$H = V \cdot H_s \cdot \Delta t. \quad (5)$$

Where V is the rotation/lift speed (steps/ms); θ_s/H_s – one step angle/distance; and Δt – time difference. In this case motor's control algorithm of 3D scanner can be:

1. Make the shaft of the motor to rotate the specified number of micro seconds, necessary to rotate the object 360° around its centre. Every t_2 seconds:
 - Read object's surface coordinate R from optical distance sensor;
 - Calculate rotation angle θ using (4);
 - Write object's surface point coordinate $p_i(R, \theta, H)$ to memory or disk;
2. Stop rotating the motor;
3. Move the optical sensor up for the specified number of micro seconds;
4. Calculate new optical sensor position value H using (5).
5. Repeat 1-5 steps while entire object is scanned.

The main problem with this method is how to resolve the exact motor rotation time. In order to use this method a real time PLC system should be used. A PC based control systems are built on top of other non-real time operating systems, cannot guaranty equal cycle execution periods (Fig. 3) and causes wrong evaluation of object's surface coordinates.

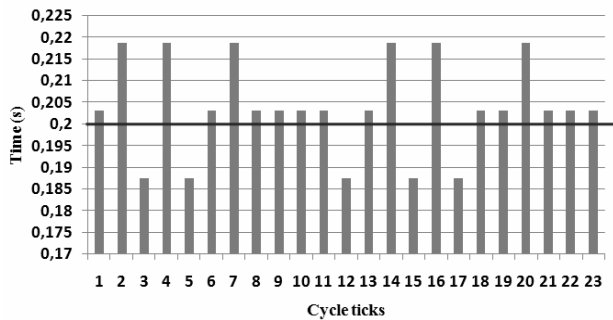


Fig. 3. Execution of commands in real and non-real time control systems. In real time systems all commands is executed in e.g. exact 0.2s intervals, but non-real time system cannot guaranty that

These small time skews, displayed in Fig. 3, appears because of the fact that in non-real time systems execution time is not controlled by PLC application, but by the operating system's tasks supervisor. The task supervisor executes the commands in the order they arrive and depending on their priority, but not at the exact time. As a result, coordinate measurement errors grow depending on the command's execution frequency (motor speed) and the overall system load. In addition to that, coordinate displacement errors continuously grow (Fig. 4).

These problems can be reduced in two ways: 1) by decreasing the velocity of stepper motors, or 2) by decreasing the time intervals between different

revolutions and resetting the timer at the beginning of each turn. Both methods apparently prolong the overall scanning process, but are capable to only slightly reduce displacement errors. Using the first method it is possible to decrease the time skews and using the second one – to decrease the displacement error. Exact position of the turn should be determined in order to completely avoid the growth of the errors. The position, indicating the beginning of a new turn can be determined by using an additional proximity switch and a special mark on the shaft of the motor.

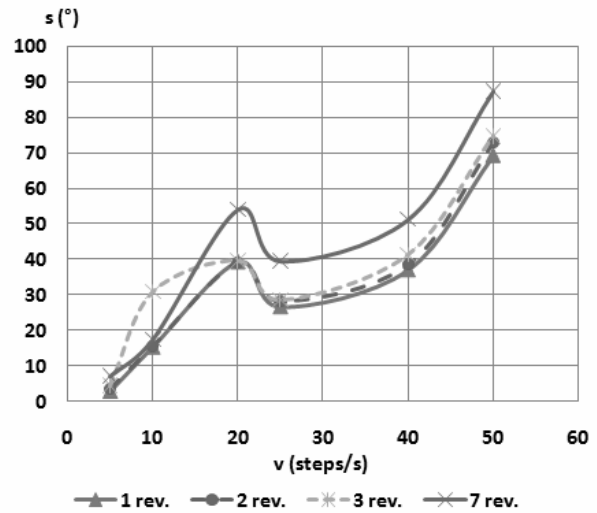


Fig. 4. Motor position error growth depending on stepper motor speed (v) and revolutions (rev.). s – standard deviation

4.2. Positioning based on the motor control

The rotation angle of the stepper motor can also be tracked by programming a PLC to rotate the stepper motor for the exact number of steps. Most PLC systems support this directly if digital encoder is present or through referencing (homing) mode [1]. In both cases rotation angle can be determined using this algorithm:

1. Rotate the motor shaft a specified number of steps x ;
 - Read surface coordinate R from optical distance sensor;
 - Calculate rotation angle: $\theta = \theta + x \cdot \theta_s$;
 - Write object surface point coordinate $p_i(R, \theta, H)$ to memory or disk;
2. Repeat 1 step until the full revolution (360° degrees) is completed;
3. Move the optical sensor the specified number of steps y .
4. Calculate optical sensor's new position value $H = H + y \times H_s$.
5. Repeat 1- 4 steps until the entire object is scanned.

This approach is one of the slowest and suffers from the limited precision. Even if the digital encoder is present, a motor can rotate for at least one step and most micro-stepping advantages are lost. In the used system one step is equivalent to 1.8° . This means that if radius of the

object increases, the quality of the reconstructed object decreases and this fact cannot be avoided (Fig. 5). Another disadvantage of this method for the calculation of the motor shaft rotation angle is that the motor's positioning commands usually are much slower than the direct commands, because communication with PLC modules and data exchange at register level is required. This leads to additional slow down of scanning process. Speed up of the scanning process can be achieved if the motor, that controls the optical sensor's position, can be rotated $x>1$, $y>1$ steps and timer controlled angular positioning is used. In this case the desired trade-off between speed, precision and error rate can be achieved.

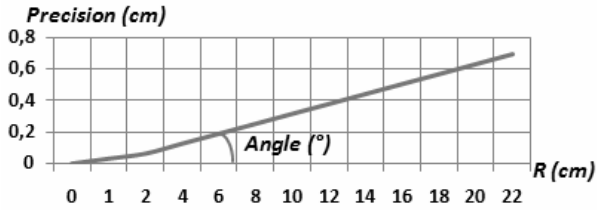


Fig. 5. The dependency of the precision of the coordinate measurements on the rotation angle and the object's size (R – radius of an object)

4.3. Positioning based on the motor encoder

In case stepper motors are equipped with internal encoders, sufficient positioning accuracy can be achieved by using method similar to time controlled positioning. In this case the time tracking algorithm should be substituted with tracking of the encoder increments. An internal encoder cannot show the exact position of the stepper motor's shaft position, because it along with the stepper motor remains an open loop system. Nevertheless, encoders can provide the information about the change in the shaft position angle. The quality of acquired object surface points then will depend on 1) the number of increments, supported by the internal encoder, 2) the ratio of the motor speed and data acquisition frequency. Because of an encoder, position tracking errors are avoided even at higher shaft rotation speeds (Fig. 7).

5. Operation of optical position sensor

Last thing to be mentioned is the acquisition of the radius R (the distance to the scanned surface). The optical position sensor measures distance from the imaginary origin to the particular point of object surface R_{abs} only. Actual radius R_t can be calculated using the characteristics of the optical sensor (6):

$$R_t = \frac{R_{abs} \cdot R_{t_max}}{R_{abs_max}} - \Delta l, \quad (6)$$

where R_{t_max} is the measurement range, R_{abs_max} – max resolution of the PLC channel, Δl – shift between real and imaginary origin [2].

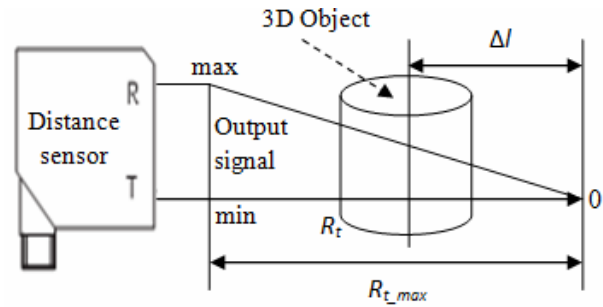


Fig. 6. Operation of distance sensor. T – light transmitter, R – receiver [2]

Operation of optical position sensor is based on the properties of light. Optical sensor have transmitter T, which project red laser beam on to the object. Object surface reflects part of the light back to the receiver R with different radius, depending on its distance from sensor. Position of object surface point using this angle is calculated.

6. The experiments

The methods for the evaluation of the motor's shaft rotation angle were experimentally analyzed. The difference between methods is graphically demonstrated in the Fig. 7-9. The cube was taken as the test object and its models were constructed using different coordinates calculation methods. Fig. 7 shows the layers of the models. First two models, Fig. 7 a) and b) are constructed using timer based shaft angle calculation and the third one – using encoder's data. Experiment proves that the increase of the scan speed decreases the accuracy of the model, Fig. 7 b). Because timers are reset every 360° , positioning lines are coincident. Otherwise twists of object surface would be noticeable as shown in Fig. 8. The decrease of the scanning speed can solve the problem, but still the model is not accurate enough - the model of the object does not maintain the exact proportions (Fig. 7 a). Best results are achieved when encoder's data are used (Fig. 7 c).

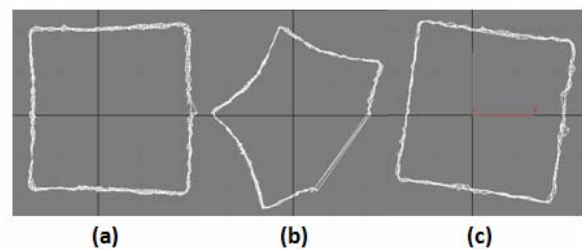


Fig. 7. The layers of the cube's 3D models, that are created using different object's position calculation methods and scan speeds:
a) 5 steps/s, time based evaluation,
b) 20 steps/s, time based evaluation, and
c) 50 steps/s, encoder based evaluation

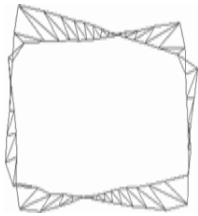


Fig. 8. Evaluation of the angular position of the motor shaft using time based approach, errors are not reset after complete turn

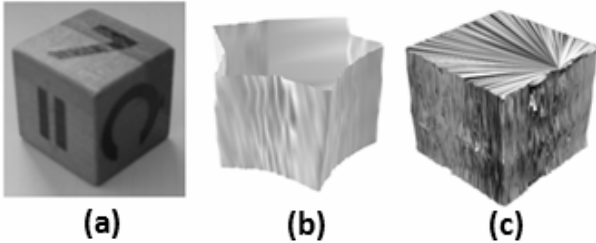


Fig. 9. a) Real object, b) model of the real object, acquired using time based approach, rotation speed – 5 steps/s. c) model of the real object, acquired using encoder based approach, rotation speed – 50 steps/s

7. Conclusions

In the paper, stepper motor positioning and position tracking problems, typical in the programming of 3D scanning systems are presented and the solutions to the problems are suggested.

It was experimentally shown that, motors, used in the 3D scanner should have encoders in order to increase scanning speed and quality. It was also demonstrated, that even if it is possible to precisely control the rotation of the stepper motor, it is impossible to precisely calculate its shaft rotation position evaluating the time in PC-based systems without the encoders.

In case stepper motors are not equipped with encoders, the modelling errors can be reduced by installing external proximity switches that indicate some positions of the motor shaft. An intermediate solution can also be used where the motor control based positioning is applied. This method is slow; nevertheless rate of the positioning errors can be reduced to the desirable level at the expense of the scanning speed. It should be noticed that not all PLC systems supports this method also called referencing or homing.

Time controlled positioning should be avoided in non-real time systems but can be used in PLC systems where equal cycle execution periods are ensured.

8. References

1. TwinCat Information System. Documentation for KL2531 and KL2541, One Channel Stepper Motor Terminals, Version 1.5, 2006.
2. Davidsonas A., Liutkevičius R. A PLC Application for Data Scanning and Visualization. Proceedings of International Conference “Electrical and Control Technologies – 2008”, Kaunas, 2008. p. 144-149.

3. Pajarola R. Stream-Processing Points. Proceedings of 16th International Conference “IEEE Visualization – 2005 (VIS 2005)”, 2005. p. 31.
4. Matukas V., Paulinas M., Ušinskas A., Adaškevičius R., Meškauskas R., Valinčius D. A Survey of Point Cloud Reconstruction Methods. Proceedings of International Conference “Electrical and Control Technologies – 2008”, Kaunas, 2008. p. 150-153.
5. Dey T.K. Curve and Surface Reconstruction. Algorithms with Mathematical Analysis. Cambridge University Press, New York, 2007. p. 59 – 112.
6. Jones D.W. Control of Stepping Motors. A Tutorial, The University of Iowa Department of Computer Science, 1995. Internet source: <http://www.cs.uiowa.edu/~jones/step>.

VISIBILITY OF TEXT IN MULTIMEDIA PRESENTATION

Stanislovas MASIOKAS, Miglė KRIUGLAITĖ-JARAŠIŪNIENĖ, Valdas PAKĖNAS
 Kaunas University of Technology, Department of Electrical Engineering, Lithuania

Abstract: Digital projection on screen is the main way of information visualization in science, teaching and business. The main drawback of presentations is deficient text visibility, which depends on text parameters and its contrast with background. Visibility determines identifying speed. With reference to published results of experimentation accomplished with a view to establish relation between luminance, contrast and visual angle, in this paper identifying speed reliance on abovementioned factors confidence probability being different was analysed. Results bespeak, that identifying speed depends on angular dimension most of all. In accordance with results practical recommendations were formulated.

Keywords: visualization, presentation, visibility, visual angle, contrast, identifying speed, text.

1. Introduction

Digital projection on screen is the main way of information visualization today. Science, teaching and business areas can not manage without it. Though lots of presentations are made, only negligible part of them accomplish their purpose – are well seen for the observer. Poor text visibility is the main problem of mostly all presentations. Text on the screen must be clearly seen and easily read. That depends on basic parameters of text (font and its characteristics) and its contrast with background. Visibility determines identifying (and reading) speed.

High visibility not only accelerates identifying speed, but also tires vision less. The aim is to ascertain a relation between identifying speed and deciding factors: visual angle, background luminance and contrast between task and background. By analysing graphical data we can ascertain which factors influence increment of identifying speed most of all. Furthermore, an optimal value of visual angle which would give a proper identifying speed and information output will be set. Also we will determine practicable boundaries of background luminance and contrast values.

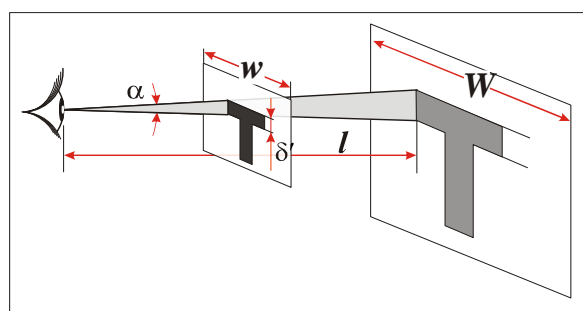


Fig. 1. Visual angle in slide and its projection on screen

Generally, visibility depends on physiological characteristics of the eye and physical factors. There are four top ones: physical size of an object, its contrast with background, observation time and luminance [1]. Increasing all these factors increases visibility. In case of text visibility in slide observation time is not restricted. Luminance of a task entirely is not so important if there's a high contrast with background. While creating a presentation we are free to choose high contrast task and background combinations. Therein lies that there are two main determinants deciding text visibility in a slide – visual angle and contrast. In this case we can manage both of them.

2. Main factors, determining visibility in a slide

Visual angle α is relevant size, which characterizes visual size of an object and depends on physical dimension of an object, the angle of inclination of the target from normal to the line of sight and the distance from the viewer [2]. It is angle which object subtends at the eye (Fig. 1). Visual angle helps to determine how well an object can be seen.

$$\alpha = 2 \arctan \frac{d \times \cos \theta}{2l}, \quad (1)$$

where d – dimension of an object; θ – angle of inclination of the target from normal to the line of sight; l – distance from the viewer to an object. $\theta = 0$ in case of projection on screen.

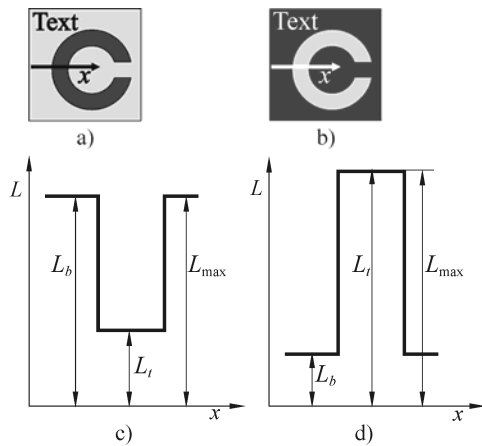


Fig. 2. Diagram of negative (a, c) and positive (b, d) luminance contrast

A target can only be seen if it differs in luminance from background. On this understanding luminance contrast which defines visibility may be calculated. There are several ways of defining luminance contrast, though here is traditional one:

$$C = (L_t - L_b) / L_b, \quad (2)$$

where L_t – task luminance; L_b – background luminance. Agreeably to luminance values of task and background there may be positive or negative contrast. Dark task in lighter background gives negative contrast ($C < 0$), which ranges from 0 to minus 1 (Fig. 2a). Light task on dark background is frequent in presentations and gives positive contrast ($C > 0$), which ranges from 0 to infinity (Fig. 2b). Such wide variation of contrast range aggravates comparison of image visibility. It's essential to say that in both cases lighting of the room remains the same, so greater part of adaptational field maintains the same luminance value. For more convenient comparison of different contrasts classic formula may be modified by changing L_b value to higher luminance value in denominator.

$$C = (L_t - L_b) / L_{\max}, \quad (3)$$

where L_{\max} – highest luminance value in slide which may be both – luminance of target or background.

This interpretation with regard to negative contrast (positive image) L_b is replaced with L_{\max} (Fig. 2c). In case of positive contrast (negative image) $L_b = L_{\max}$ (Fig. 2d).

After changes made positive contrast (black text on white paper) ranges from minus 1 to 0, negative contrast (white text on dark background) ranges from 0 to 1. Either way, adaptational luminance L_a , which depends on lighting of the room, remains the same. Such changes make comparison of experiment results easier.

Contrast and visual size are closely interdependent. For objects smaller than $1.5'$, a small change in visual size requires a big change in contrast, so that the same visibility level would be reached. As we talk about

bigger targets in slide, visibility is more sensitive function of contrast than it is of size [1].

3. Literature analysis

There are no many researches related to visibility of text in slide. Visibility in chromatic regard is better explored – interaction between task and background colours and influence of luminance contrast over visibility was analysed [3]. It is none the less important to explore influence of text parameters over visibility.

Quite comprehensive study of four visibility determining factors was taken by H. Richard Bleckwell. Light discs of different luminance and visual angle values in the center of darker background were used. Observer's task was to identify the time interval which was needed to notice the disk. However, results of this experiment are not most suitable for visibility of text research as it was performed in too wide visual angle range ($1'-64'$) with not practiceable values for a slide ($1' - 4'$) [1].

Especially significant in this area are results of researches made by A. S. Shaikevic (*A. C. Шайкевич*) [4]. A research was made with a view to explore, how identifying speed depends on visual angle (α), contrast between task and background (C) and background luminance (L_b).

Observers with normal vision were watching light Landolt's rings in dark background. The task was to identify position of a cutout. In Shaikevic's research Visual angle varied from $0.7'$ to $10'$. Values of contrast between task and background and background luminance were also transcriptive data.

In accordance with collected data, diagrams were plotted, which show identifying speed reliance on visual angle and contrast for different background luminance values and confidence probability 0.7 [4]. Therefore we can evaluate identifying speed, i. e. efficiency of a visual task.

It can be seen that increment of identifying speed is not linear function of contrast between task and background. It's especially noticeable in range of sizeable visual angle. Magnification of background luminance positively influences identifying speed, especially in low luminance values.

Using these diagrams necessary value of contrast or background luminance may be determined so that required identifying speed would be obtained under certain conditions.

In this paper redrawn, modified and press-fitted diagrams are given (Fig. 3, 4, and 5). Narrowed research area will be further analysed, which is relevant for the visibility of text case.

4. Selecting practiceable values of visual angle and background luminance

Research area must be narrowed so that only practiceable conditions would be analysed. A new diagram for ascertaining identifying speed reliance over contrast, background luminance and visual angle needs to be plotted (Fig. 6). Contrast range from 0.5 to 0.8 is under

consideration. Values under 0.5 are not practicable, because it is range of poor visibility. Realistically contrast 0.8 can be achieved today. Fig. 6 shows that there is linear dependence between logarithm of visibility and contrast. We talk only about contrast of slide here, which corresponds to absolutely dark room. It can be apparently seen that identifying speed grows most rapidly when visual angle does not exceed 2'. Growth above 2' is not so speedy. When background luminance L_b varies from 42 to 205 cd/m^2 increment of identifying speed is not sizeable. Contrast and visual angle influence increment of identifying speed most of all, especially up to 2'.

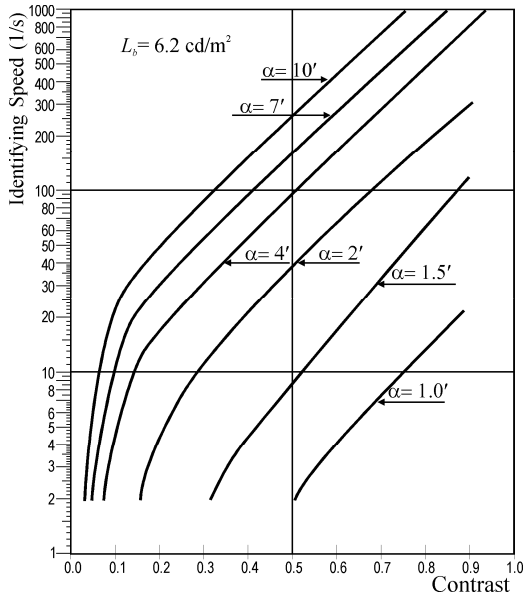


Fig. 3. Identifying speed reliance on contrast and visual angle, when $L_b = 6.2 \text{ cd/m}^2$

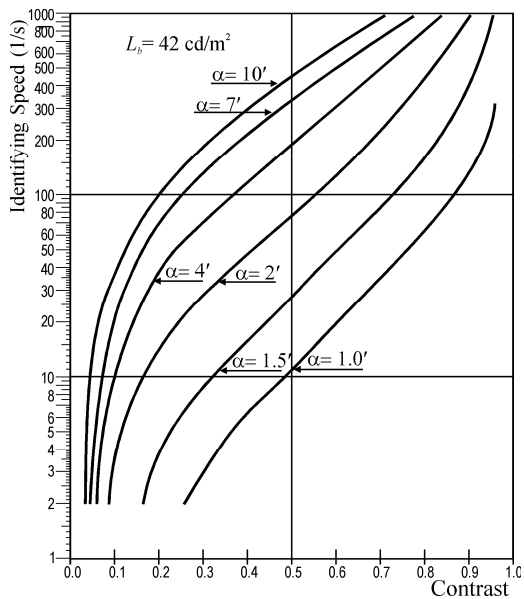


Fig. 4. Identifying speed reliance on contrast and visual angle, when $L_b = 42 \text{ cd/m}^2$

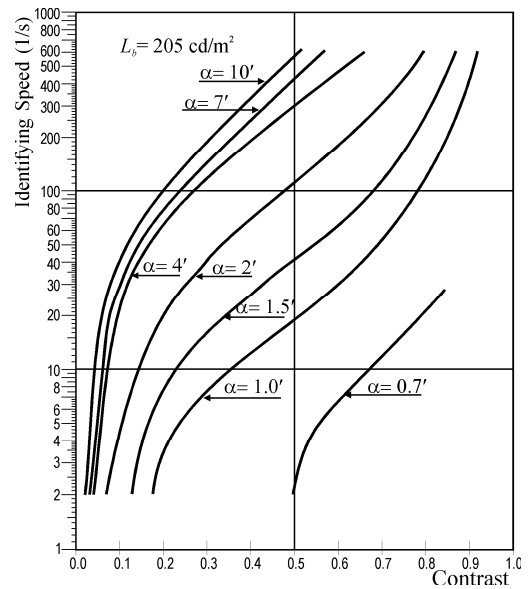


Fig. 5. Identifying speed reliance on contrast and visual angle, when $L_b = 205 \text{ cd/m}^2$

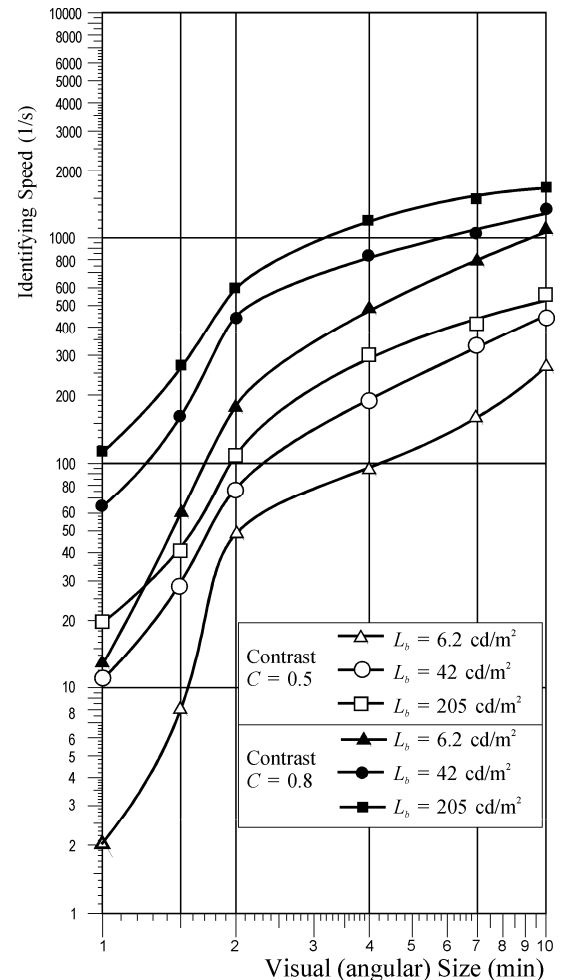


Fig. 6. Influence of contrast and background luminance over identifying speed

To perform a visual task we need to determine visual angle of the smallest detail that needs to be seen. If the thinnest text line – subscripts and superscripts – is attributed to 2', then according to publishing

requirements main text should be 1½ time bigger, i. e. 3'. When optimal visual angle is stated, necessary line thickness on display may be calculated:

$$\delta' = \frac{\alpha \times l \times w}{3.44 \times W}, \quad (4)$$

where l – distance from viewer to screen; w – width of slide in computer display; W – width of slide in projection screen.

If there is enough space in a slide and it is aesthetic, large font, corresponding to more than 3', may be used. However, capacity of a slide approximately commensurates with square height of a letter, therefore large fonts restrict information output of a slide.

For further analysis $L_b = 6.2 \text{ cd/m}^2$ value is eliminated as it corresponds to 30–40 lx (when reflectance of walls is about 0.50–0.65) and that is too dark room. Screening presentations in such dark rooms is unacceptable today. Value $L_b = 205 \text{ cd/m}^2$ corresponds to 1000–1300 lx. Till these levels of illuminance become standard in major part of scholastic institutions and other close purpose rooms, it is believable hardware of displaying presentations may change essentially.

Value $L_b = 42 \text{ cd/m}^2$ corresponds to 200–260 lx and may be held as today's norm (when reflectance of walls is about 0.50–0.65).

Though major part of illuminance norms for communal and especially educational rooms in most of EU countries is 300–500 lx, however these results are closest to real situation.

5. Influence of confidence probability and proper identifying speed

So far all analysed data corresponded to confidence probability 0.7. Later derived data of the same research was offered for other confidence probability values [5]. New diagram for ascertaining confidence probability influence over identifying speed was plotted (Fig. 7). It emerged that the highest identifying speed is for lowest confidence probability value 0.5. The lowest speed is for confidence probability 0.99. The identifying speed between these two cases differs more than 7 times.

After sifting results of this experiment quite reliable and easy read footing of text presentation may be defined. In proper visual situation reading rate of english text is about 15–20 print symbols per second and faintly depends on visibility level (VL ranges from 2 to 10) [2]. Considering that we may state that in case of visual angle $\alpha \geq 2'$, contrast $C \geq 0.5$ and confidence probability 0.99, identifying speed is higher than regular (28 s^{-1}) identifying speed.

In case of higher contrast or lower confidence probability, identifying speed (i. e. reserve of identifying speed) signally exceeds practiceable value. Under these circumstances we can create high-grade slides wherein displayed text is clearly seen and does not tire vision even in a long run. It is especially talking-point to educational process (at schools,

universities), where is a risk to ruin vision of lots of young people.

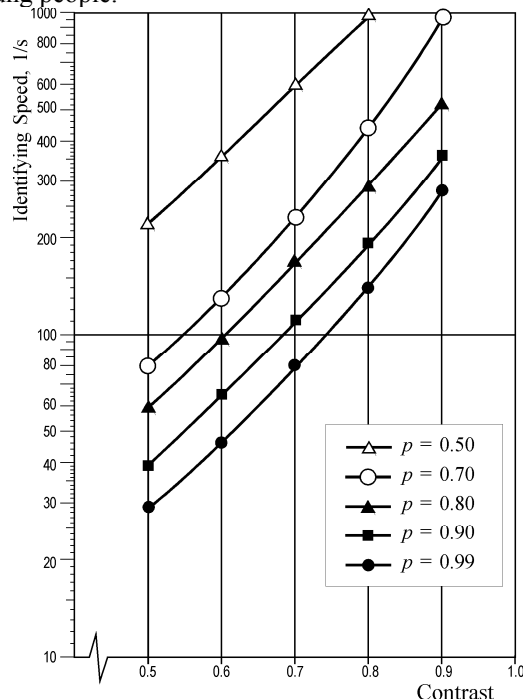


Fig. 7. Influence of confidence probability over identifying speed, when $L_b = 42 \text{ cd/m}^2$, $\alpha = 2'$

6. Conclusion

1. Optimal value of visual angle in slide is 2' for subscripts and superscripts and 3' for main text. If it's aesthetic and there is free space in slide larger fonts can be used.
2. In case of good lighting (300–500 lx) contrast between text and background must be no less than 0.5, i. e. screen illuminance created by projector must be no less than twice bigger than illuminance created by surroundings.
3. If visual angle is greater than 3' and contrast is higher than 0.5, identifying speed with confidence probability 0.99 exceeds practiceable average reading rate of english text.

7. References

1. Murdoch J. B. Illumination Engineering from Edison's Lamp to the Laser. New York, 1985. p. 542.
2. The IESNA lighting handbook. New York, 2000. p. 800.
3. Masiokas S., Kriuglaitė M., Otas K. Colour luminance contrast of digital projection image. Electronics and Electrical Engineering, no. 7(79). Kaunas, 2007. p. 19–22.
4. Shaikevic A. S. About classifying visual performances. Lighting engineering, no 5. Moscow, 1958. p. 13–20 (in Russian).
5. Shaikevic A. S. Nomogram for assessing identifying speed and confidence probability. Lighting engineering, no 1. Moscow, 1964. p. 19–22 (in Russian).

AUTOMATIC PLC-SOURCE-CODE GENERATION OF C4.5 DECISION TREES

Elmar HEINEMANN*, Jolanta REPŠYTĖ **, André WENZEL*

* University of Applied Sciences Schmalkalden, Germany; ** Kaunas University of Technology, Lithuania

Abstract: Decision trees are widely-applied for classification problems. One of the most common methods to create a decision tree is Quinlan's C4.5. Beside the decision tree development is the implementation of a decision tree on a PLC very extensive especially if a tree is changing during the development and test phase. In this case a manual tree implementation is not economically justifiable. Therefore a method and tool are shown which automatically generates a C4.5 decision tree and the associated PLC source-code out of feature data.

Keywords: decision tree, PLC, automatic source code generation.

1. Introduction

Decision trees are widely used for classification problems. Their advantages compared with other classification techniques are:

- Decision trees can be effectively applied to any data structure, in particular to discrete, continuous or mixed data. [3]
- Decision trees are very robust against outliers. [3]
- Prediction rules are easy to interpret. [3]
- Decision trees perform a stepwise variable selection and complexity reduction. [3]

A decision tree is generated out of evaluated feature data. The most common methods to create a decision tree are C4.5 [7], CART¹ [3] and CHAID² [2]. The generated tree is often very complex and overfits the classification problem. Hence to improve the classification ability is a tree pruning necessary. Pruned trees are the base for a real word classification application. Therefore is a decision tree implementation on a target environment required, for example on a microcontroller or a PLC³.

A manual conversion of the develop decision tree into a target source code is often not expedient. Automatic

source code generation is useful if it is often necessary to develop new decision trees for various applications, if application tests make the chance of a decision tree necessary, to avoid mistakes by the implementation of complex decision trees, to be independent from a personal programmer style and to have an identical interface of the decision tree unit in every application. To achieve an automatic source-code generation out of feature data is an integrated design draft needed.

This paper describes the entire process of C4.5 tree generation, pruning and conversion into IEC 61131-3 [1] conform PLC source-code.

2. Decision Trees

Goal of the classification is the assignment of a target variable attribute to an unknown object. The classification is done by a classifier which learns the classification based on classified training data. To build a classifier can be several methods like neuronal networks [9], support vector machines [4], fuzzy systems [8,6] or trees [2,3,5,7] used. The classifier in this work based on trees.

Trees parting a feature space into a subset of rectangles. An attribute of a target variable, a label, is assigned to every rectangle. There exist two different types of tree based models; regression trees and classification trees. Regression trees work with continuous target variables and try to minimize the distance between the label and the target variable values in the feature space subset. Classification trees work with discrete target variables. They try to achieve that a subset only contains attribute for the target variable which are identical with the subset label. [5]

This work uses classification trees and as learning method Quinlan's C4.5 algorithm.

The C4.5 algorithm is an improved version of the ID3⁴ algorithm.[7] The learning algorithm searches for a hierarchical split structure to divide the data set T into subsets T_i with the goal that a subset at the lowest split layer only contains objects with the same class C_k.

¹ Classification and Regression Trees

² Chi-square Automatic Interaction Detectors

³ Programmable Logical Controller

⁴ Iterative Dichotomiser 3

Every split point in the hierarchical structure depends on the attributes of one feature variable and is called a node. Final sub sets which contain only data with the same label are called leaf. For the selection of the splitting variable at a certain hierarchical layer uses C4.5 the normalized information gain. The normalized information gain of a variable is calculated by the following schema.

In the first step is the information content, the entropy, of the variable for the classes in the dataset with (1) calculated. This is the information content before the split.

$$info(T) = - \sum_{m=1}^n p_m \log_2(p_m) \quad (1)$$

info – information content
p_m – probability distribution of the classes

The second step, displayed in (2), calculates the weighted information content of the probability distribution for each possible subsets generated by the splitting attributes of the variable. This can be interpreted as the information content after the split.

$$infox(T) = - \sum_{i=1}^o \frac{|T_i|}{T} info(T_i) \quad (2)$$

infox – information content after split
T_i – data subset
T – data set

The information gain, shown in (3), is the difference between the information contents before and after the split.

$$gain(X) = info(T) - infox(T) \quad (3)$$

gain – information gain of the split

To achieve a good comparability a normalization of the information gain is necessary. Thereto is the information content of the variable class distribution calculated with (4) and the information gain divided with it (5).

$$split\ info(X) = - \sum_{i=1}^o \frac{|T_i|}{T} \log_2\left(\frac{|T_i|}{T}\right) \quad (4)$$

split info – information content of class distribution

$$gain\ ratio(X) = \frac{gain(X)}{split\ info(X)} \quad (5)$$

gain ratio – normalized information gain

The C4.5 chooses the variable with the maximum gain ratio as split variable on the hierarchical layer. The procedure continues for each out coming subset until a subset contains only one class.

The accrued decision tree has a complex structure with long path through the tree to a leaf. The tree achieves very good classification quality for the learning data but mostly a very worse classification quality for unseen data because the tree is overfitted to the learning data. To improve the classification quality is a pruning process are whole sub trees, nodes, replaced by a leaf or another sub node. There exist several pruning methods. It is possible to define a maximum depth of the tree, a frequency threshold or to minimize the error rate of a

test data set. But every pruning indicates a loss of information. To measure the information loss by the pruning is it feasible to associate confidence information with the assigned leaf or node. As confidence measure can be the misclassification or error probability of the pruned tree used.

As test and comparison environment for decision tree classifier is the in [6] and Fig. 1 displayed system used.

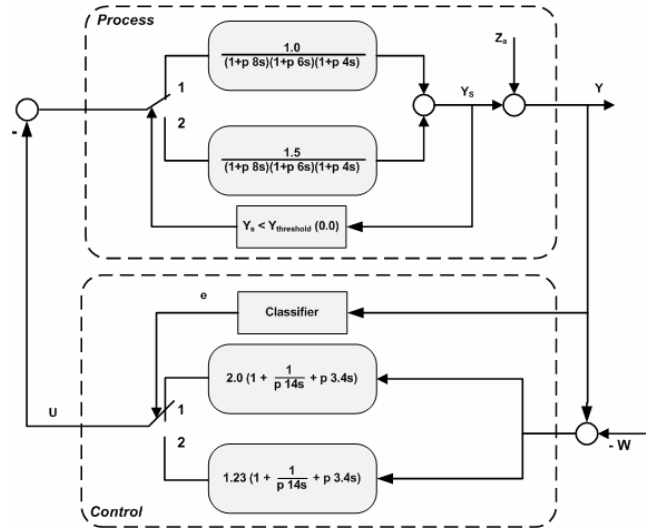


Fig. 1. Testing system

The test environment contains a process with two operating points described as PT₃-systems and a PID controller for each operating point. The system switches between the operating points when the system output Y_s is below zero. The function of the classifier is to detect the change of the operating point and select the correct controller. Reference [6] uses the system for the analysis of bayes and fuzzy classifier.

The learning base contains the feature vector and the according operating point for a rectangle set value W. The feature vector o_k consists of the last three values for Y at the time k; o_k = (y_k y_{k-1} y_{k-2}). The quality of the learned classification is tested with rectangle and sinus function for the set value W with and without disturbance on the output Y. Fig. 2 shows the generated tree and Tab. 1 a comparison of the results with [6].

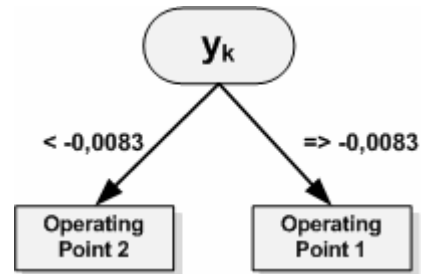


Fig. 2. Decision tree

Table 1. Simulation results

Set value function	Fuzzy classifier	Relative Error (n_{wrong} / n) [%]		Tree
		Bayes classifier direct regression	Bayes classifier crestline regression	
Rectangle $Z_a = 0$	2.0	2.0	2.0	0.0
Sinus $Z_a = 0$	2.0	2.0	2.0	2.0
Sinus $Z_a = N(0,0.04)^5$	4.5	38.5	3.5	4.0

The generated tree reduces the feature space from three to one dimension and classifies the non-disturbed set value function with no error because the tree detects the correct operating threshold. The error for the disturbed sinus set value function is smaller as by the fuzzy classifier and bayes classifier with direct regression. Only the bayes classifier with crestline regression is better as the tree classifier.

If the learning data consists of the disturbed sinus set value data then a more complex tree outcomes that has to be pruned. The resulting tree is shown in Fig. 3 and is the base for the automatic source code generation.

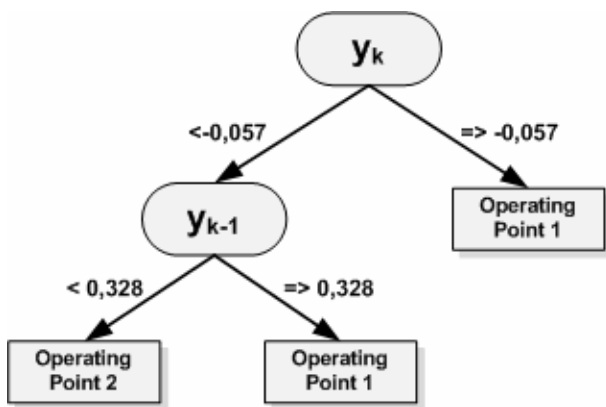


Fig. 3. Complex decision tree

3. Automatic Source-Code Generation

As decision tree implementation environment are PLCs selected because they are widely used for process control. The PLC programming languages and program organization units (POE) are defined in the IEC 61311-3 norm. [1][10]

The whole PLC control program is parted by POEs into several encapsulated duties. A decision tree is one of these duties and accordingly it is the goal to generate a corresponding POE. The decision tree POE is based on the POE-types function or function block. As programming language is structured text selected.

To achieve automatic POE generation is the definition of a standardized POE layout necessary. Many parts of the layout are defined by the IEC 61131-3. The definition of the POE interface and the implementation of the decision tree itself are left to define.

The first step is the definition of the POE interface. The input of the decision tree contains categorical and/or

continuous features which differ for every decision tree. The output of a decision tree consists of the resulting class and error probability. To achieve a small and always equal interface are structures used. With the use of structures is the POE head for every decision tree implementation identical except the different output handling by the implementation as function or function block. Fig. 4 shows the structures for the example tree and Fig. 5 the head of the example tree implemented as function POE. On the input side is an “object” structure defined that comprise the itemized features. In a loop along the whole decision tree is the structure filled with all occurring features. For categorical features is the data type “string” and for continuous feature the data type “real” used. As POE output is a “solution” structure developed which contains the classification result in the data type “string” and the probability error in a “real” data type.

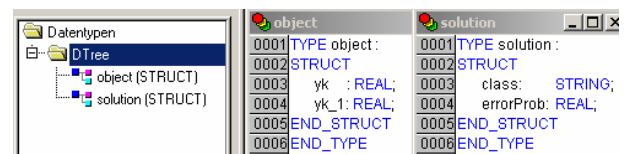


Fig. 4. Interface structures

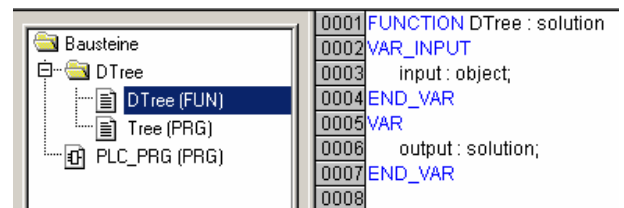


Fig. 5. Head of a decision tree implementation as function

The second step is the decision tree implementation. The realization of the decision tree is carried out as nested “if-elseif-end_if” statements. Every hierarchical layer of the decision tree is a nesting level. For the nesting generation is the decision tree first of all pass from the top node through to the first leaf on the left hand side. In every hierarchical layer is an “if” statement opened with the comparison of the assigned variable on the node and the branch value to the next layer. The access to the value of the variable is done by the variable name and their association in the “object” structure. On the last layer, the leaf, are the associated class and error probability stored on the “solution” structure. As second of all is a retrace from the leaf too the node one level above done. In this node is an “elseif” statement for the next branch generated and the source generation for all nodes and leaf among this branch done. As third of all is after the last branch of a node the closing of a nesting level with an “end_if” statement done and a retrace too the node above performed. The result of this recursive algorithm for the example is shown in Fig. 6.

At the end of the automatic source code generation are the global variables “feature” as object and “classification” as solution created. In the “feature” variable stores the end user the actual feature values and receives in the “classification” variable the decision tree result. Therefore is a program POE created that calls the

⁵ Gaussian distribution $\mu=0$; $\sigma^2=0.04$

decision tree POE and stores the output on the “classification” variable. The end user binds the program POE in a suitable position in the control program. The global variables and the program POE are displayed in Fig. 7.

```

0001 IF input.yk<=-0.0574899945 THEN
0002     IF input.yk_1<=0.327950752 THEN
0003         output.class := 'OP2';
0004         output.errorProb := 0;
0005     ELSIF input.yk_1>=0.327950752 THEN
0006         output.class := 'OP1';
0007         output.errorProb:=0;
0008     END_IF
0009 ELSIF input.yk>=-0.0574899945 THEN
0010     output.class := 'OP1';
0011     output.errorProb:=0.34;
0012 END_IF
0013 DTree:=output;

```

Fig. 6. Implemented decision tree as function

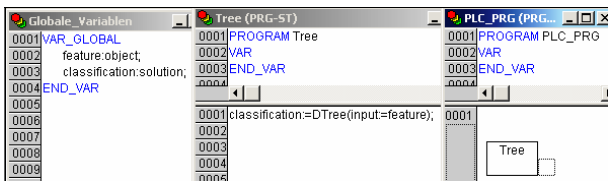


Fig. 7. Global variables and program POE

5. Decision Tree Tool

For the realization is a software tool developed that supports the user by the decision tree building and implementation process.

The decision tree tool contains the following components:

1. import of the feature data,
2. creating training and validation data set,
3. decision tree generation,
4. decision tree pruning,
5. PLC decision tree source code generation and
6. PLC source code export for CoDeSys⁶ V2.3

The tool is programmed in Microsoft[®] Visual Studio.net with C# and the generated PLC source code is tested with CoDeSys V2.3.9.3. and executed on a Wago[®] 750-841 controller.

6. Conclusions

In times of decreasing innovation cycles becomes the area of automatic source code generation more imported. This challenge is also valid for automation engineering. Hence is essential to develop methods for automatic source code generation in the field of PLC applications. The paper shows a small introduction into this area on the example of decision trees and can be seen as motivation for further research activities.

7. References

1. Norm. IEC 61131-3:2003. Speicherprogrammierbare Steuerungen Teil 3: Programmiersprachen
2. Bankhofer U. Datenanalyse und Statistik: Eine Einführung für Ökonomen im Bachelor. Gabler. Wiesbaden, 2008.
3. Breiman L. Classification and regression trees. Chapman & Hall. New York, 1993.
4. Cristianini N. An introduction to support vector machines and other kernel-based learning methods. Cambridge Univ. Press. Cambridge, 2002.
5. Hastie T. The elements of statistical learning: Data mining, inference, and prediction. Springer. New York, 2001.
6. Koch M. Klassifikator-konzepte zur Steuerung dynamischer Prozesse. Ilmenau, 1995.
7. Quinlan J. C4.5 programs for machine learning. Kaufmann. San Mateo, 1993.
8. Russo M., Jain C. Fuzzy learning and applications. CRC Press. Boca Raton, 2001.
9. Seiffert U. Self-organizing neural networks: Recent advances and applications. Physica-Verl. Heidelberg, 2002.
10. Seitz M. Speicherprogrammierbare Steuerungen: Von den Grundlagen der Prozessautomatisierung bis zur vertikalen Integration. Fachbuchverl. Leipzig im Hanser-Verl. München, 2003.

⁶ A common PLC programming tool developed by 3S

A NEW WIRELESS SOLUTION TO TRANSMIT AND EVALUATE BIOMEDICAL SIGNALS UNDER LOW SIGNAL NOISE RATIO TO CONTROL THE STATE OF RELAXATION

Daniel TROMMER*, Markus GREULICH*, Rudolf BAUMGART-SCHMITT*, Maria KRAUTWALD*
Christian WALTHER*, Andreas WENZEL**

*University of Applied Sciences Schmalkalden, Faculty of Electrical Engineering, Germany

**Fraunhofer-Institute for Information and Data Processing, Applications Center System Technology, Germany

Abstract: A handheld data recording system originally developed in our laboratory to extract EEG features was extended in two ways: to transmit the data wireless and to evaluate ECG.

By means of these features it is possible to control the state of relaxation and the general status of cardiovascular system e.g. before the operation.

Especially in medical environments it is necessary to take the low signal noise ratio into consideration. According to this the serial protocol of Bluetooth and the Sigma-Delta-Analog Digital converter were applied.

The prototype of the developed system is able to pre-process the data in real time mode and to store the raw data and the extracted features for classification, forecasting and controlling purposes.

Keywords: Bluetooth, ECG, EEG, microcontroller, relaxation, SD, wireless transmission.

1. Introduction

In some environments, such as medical and industrial, it is necessary to integrate components for data acquisition close to the subjects to be controlled so there is no place for the processing unit.

Different measurement and control tasks are requiring real time processing, storing data, to be robust against low signal noise ratio and small mobile devices.

The solution presented in this paper was developed and configured to fulfill these requirements.

The purpose of the device called „Quilax” presented in this paper is to control the states of relaxation of a subject. The device was originally developed to control the states of relaxation by measuring the electrical activity produced by the brain, the Electroencephalography (EEG).

The EEG was originally measured by electrodes wired with the processing system. A low-pass filter and a sigma delta analog-digital converter were used to get a digital EEG signal for processing.

There are 10 light emitting diodes (LED) with red, yellow and green color which are showing the states of relaxation.

The idea of the device is to measure and display the states of relaxation of a subject. The subjects control their own state of relaxation with techniques like breath-control, defocusing a.e., they get the feedback of the success of their techniques by looking at the LEDs. They should continuously improve their skills in obtaining the state of relaxation. Depending on the level of their skills it could be possible to relax later without the support by this device.

To measure the EEG we used wired bipolar one channel frontal site EEG electrodes as shown in Fig.1 up to now.

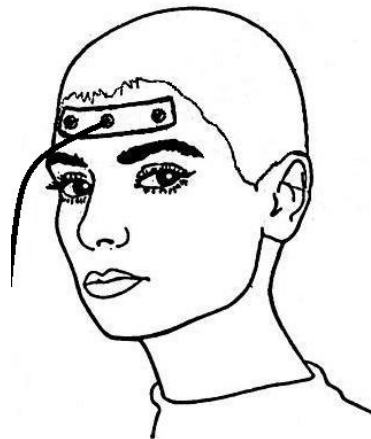


Fig. 1. Draft of a wired bipolar one channel frontal site EEG electrode

We suppose that the state of relaxation is related with the relative power of the alpha- band.

The alpha-band of the EEG Signal is placed between 8 and 13 Hz. The relative power of the alpha- band $relP_{alpha}$ is calculated by

$$relP_{alpha} = \frac{P_{alpha}}{P_{total}} * 100\%, \quad (1)$$

with P_{total} as the accumulated power of the EEG between 0 – 64 Hz, P_{alpha} as the accumulated power of the EEG between 8 and 13Hz.

We measured the EEG with a sampling rate of 250 samples per second.

The Nyquist–Shannon sampling theorem

$$f_{sample} \geq 2 * f_{max}, \quad (2)$$

with f_{sample} as the sampling rate restricts f_{max} as the maximum frequency of the evaluable EEG band.

That means it is possible to analyse signals up to 125 Hz. To avoid the aliasing effect it was necessary to integrate a low pass (anti-aliasing) filter with a -3dB frequency of 110 Hz. The 16 bit AD7715 from Analog Devices, a sigma delta analog digital converter ($\Sigma\Delta$ -ADC), was applied to have the useful feature according to over sampling of the analog signal. The signal noise ratio was dramatically improved in the interested signal range.

To process the spectrum of the EEG signal we are using a simplified fast real time sliding DFT algorithm (RFT) [1, 2]. In contrast to the original versions of discrete Fourier transformation (DFT) algorithms the processing time of our recursive version of the DFT do not depend on the number of elements of the input vector. Furthermore the algorithm used a Look- Up Table (LUT) to store the values of the periodic trigonometric functions which have been processed at the initialization of the algorithm. To save further processing time it is possible to process only frequencies we are interested in. Therefore the complete processing time could be minimized.

The extracting of the EEG feature and the classification is performed by the microcontroller MSP430F1611.

We proposed to extend the described device in several ways. At first we integrate a Secure Digital (SD) Card slot to store raw and extracted data for a further processing. Secondly we implemented a wireless one channel EEG electrode. It is now possible to collect data of the subject in a wireless mode. Third we implemented an electro cardiogram processing (ECG) in the handheld device.

2. Methods

2.1. Integration of the SD Card device

For integrating a SD card slot into a microcontroller driven device it is necessary to implement an algorithm to manage the file system. After this the SD card can be easily read by a personal computer (PC) as well as in other handheld devices with SD card support.

For implementing the file allocation table (FAT) management on the microcontroller device we use the Portable FAT Library for MCU Applications [3].

There are two different ways to communicate with a SD card. On the one hand in the fast 4- bit communication mode and on the other hand in the simple serial peripheral interfaces (SPI) mode. We decided to use the SPI mode. This modus turned out to be as fast enough to transmit the data during one sampling period. This mode is efficient enough to implement it on a microcontroller with small program memory.

The device with integrated SD- card data storing is shown in Fig.2.



Fig. 2. Picture of the Quilax in revision with integrated SD- card device

The microcontroller MSP430F1611 has two integrated SPI ports. The original device uses one SPI port for the communication with the $\Sigma\Delta$ - ADC. Therefore the second SPI port can be used for communication with the SD Card.

Our intention was that the microcontroller stores the raw data values in real time. That means the raw data value should be stored in one sample period. In fact of the use of a FAT management by the microcontroller the transmission of one data value only is not efficient, because the FAT has to be updated too. The updating time of the FAT is not linearly dependent on the number of bytes stored before. Therefore we try to store the raw data values in blocks by using of two memory buffers.

The memory space for both buffers is allocated with 512 bytes. With 512 bytes for each buffer 128 ADC values with 16 Bit and 128 extracted features with 16 Bit can be stored in each buffer.

If there is a new analog value completely converted an interrupt occurs. With the new raw value the features will be extracted and displayed. After this there is time to perform the data storing.

Over the period of time the first buffer will be filled with the data the other buffer is ready for storing.

Because of this buffer management the data can be stored without delaying the acquisition and extraction process.

2.2. Implementation of a wireless electrode

The electrode band as shown in Fig.3 uses a cable to realize the connection to the microcontroller driven device of Fig. 2. Our aim was to make the connection more comfortable to the relaxing subject by a wireless data transmission.



Fig. 3 Picture of a wired one channel EEG electrode

We consider to use a method that has a safe transmission and which could be easily implemented.

The safe transmission refers to the protection of personal rights. That means no one should get the data without the agreement of the owner and the electrode should be able to communicate with almost every handheld device or PC. Therefore we decided that Bluetooth is the right transmission method for this application. Up to now we developed and tested the first prototype successfully.

The wireless one channel electrode adapter consists of four main parts:

- the power supply,
- the amplifier and data acquisition,
- the Bluetooth module and
- the msp430F2013 microcontroller.

As a power supply we use a 500mAh lithium-ionic-accumulator. With an overall power consumption of 40mA (in transmission mode) and the 500mAh accumulator the electrode has an operation time of more than 10 hours approximately. With a deep discharge protection, by using a mirror comparator, the use of regular accumulators from mobile devices with higher capacities is possible. Operation times with more than 40 hours are supposable.

The amplifier and data acquisition part as shown in Fig.4 is necessary for being robust against low signal noise ratio. Only with an efficient amplifier the extraction and classification of the EEG signal can be performed.

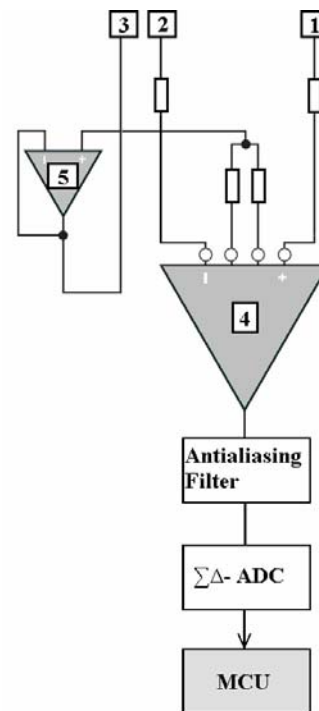


Fig. 4 The block diagram of the amplifier and data acquisition consists of the V_{IN+} input of the EEG electrode (1), the V_{IN-} input of the EEG electrode (2), the common input of the EEG electrode (3), the instrumental amplifier (4) and the impedance converter (5).

The instrumental amplifier increases the values of the inputs V_{IN+} V_{IN-} with a factor of 5 referred to a voltage based on the common input of the electrode. After this

an active anti-aliasing filter and a $\Sigma\Delta$ - ADC follows in Fig. 4. The sampling rate of the $\Sigma\Delta$ - ADC is 512 samples per second.

For the management and control between the Bluetooth module and the $\Sigma\Delta$ - ADC we use a MSP430F2013 microcontroller. The firmware of the microcontroller only has the task to fetch the data from the $\Sigma\Delta$ - ADC and send it to the Bluetooth module on its internal serial port.

The btm-112 from RAYSON was selected as Bluetooth module. This module is able to send data by the serial protocol of Bluetooth. The module has a self management for the frequency hopping and the connection process.

2.3. Implementing of ECG processing

The implemented processing for EEG is one method to measure the state of relaxation. Another method is to process ECG features. There are several ECG features which are representing the state of relaxation of a subject.

One feature which reflects the state of relaxation is the power density at 0.1Hz [4]. We implemented the extraction of the spectrum, in the same way like the power- spectrum extraction of the EEG signal, with the RFT. Therefore we calculate the relative power $relP_{0.1Hz}$ of the 0.1Hz band with the equation

$$relP_{0.1Hz} = \frac{P_{0.1Hz}}{P_{total}} * 100\%, \quad (3)$$

with P_{total} as the accumulated power of the ECG between 0 – 64 Hz, $P_{0.1Hz}$ as the power of the ECG at 0.1Hz. The state of relaxation is also shown by the LEDs.

Furthermore we implemented the Percentage Index (PI) of heart period duration and its probability [3]. The Percentage Index $PI(n)$ of heart period variation is calculated by

$$PI(n) = \frac{[H(n) - H(n+1)] \times 100}{H(n)}, \quad (4)$$

for

$$1 < n < N - 1, \quad (5)$$

with n as the serial number of beats, $H(n)$ as the time series of the heartbeats, N is the total number of heartbeats in the range.

The PI becomes positive when the heart rate accelerates and it becomes negative when the heart rate inhibits.

Oida et.al. supposes that the probability of the PI represents the autonomous nerve activity which reflects the state of relaxation [5, 6].

We implemented and tested these two methods of measuring the state of relaxation on our device. To analyse in future if it is possible to connect these

methods for multi feature processing of the state of relaxation.

3. Conclusion

We extended the Quilax device in several ways.

By implementing a wireless one channel EEG electrode we afford the possibility to become in relaxation in a more comfortable way for the subject. Furthermore we offer a small mobile alternative to measure and control units of the market. The device we developed has the potential to fulfill several measurement tasks with signals up to 250Hz.

The implementation of the ECG processing methods allows us to assist our EEG analysis to predict the state of relaxation. Only with the multi feature processing with EEG and both ECG methods a measurement and control of the state of relaxation is accurate enough.

By the integration of the SD- card device we are able to collect data for post- processing, analysis and to archive training results of the relaxation techniques.

4. References

1. Baumann, C. RFT: a simplified fast real time sliding DFT algorithm, Convict Episcopal de Luxembourg-http://www.restena.lu/convict/Jeunes/ultimate_stuff_RFT.pdf, 2005.
2. Baumgart-Schmitt, R. systemanalytische Ansätze in der kognitiven Psychophysiologie unter besonderer Berücksichtigung stationärer visueller Strukturbildungsprozesse, Humboldt Universität Berlin, 1986.
3. Sham I., Hue W., Rizun P. Portable FAT Library for MCU Applications <http://www.circuitcellar.com/magazine/#176>, March 2005.
4. Peng, C.-K. Heart rate dynamics during three forms of meditation, International Journal of Cardiology, February 2003.
5. Oida E., Moritani T., Yamori Y. Tone-entropy analysis on cardiac recovery after dynamic exercise Proceeding of 4th eMBEC 2008
6. Kamiya N., Yokoyama K., Niwa S. Evaluation of Parasympathetic Nerve Activity Level Monitoring System, IEIC Technical Report, VOL.102, NO.727, 2003.

CORRECTION OF MEASURING TRACK PROCESSING ERRORS IN VIBRATION MEASUREMENTS OF COAL WAGON

Mirosław LUFT, Radosław CIOĆ, Daniel PIETRUSZCZAK

Kazimierz Pułaski Technical University of Radom, Faculty of Transport and Electrical Engineering, Poland

Abstract: The paper outlines investigation outcomes of decreasing the dynamic errors resulting from non-ideal transformation of the vibration measuring track of a coal wagon's, Faals type, vibrations. Obtained measuring errors with correction were compared to errors without correction. Requirements of the UIC 518 norm are given.

SIMULINK, a MATLAB-based interactive software package turned out to be an irreplaceable tool here. It offers a possibility of an analysis and synthesis of continuous and discrete dynamic systems.

Keywords: railway car vibration, UIC 518 norm, software correction, error of measurement, measurement transducers.

1. Introduction

Before being referred for use as well as during their operation, means of transport undergo different examinations that are to confirm their safety and parameters determining their usefulness for specific applications in transport. One of such types of examinations is vibration measurements during a vehicle movement. Depending on the type of means of transport different norms are binding which specify the way of their manufacture. In Europe rail vehicles must meet requirements included in the document of the International Union of Railways – UIC 518. Ref.: [3, 5, 13].

The focus of this paper is how the input value is influenced by measurement errors resulting from the use of non-ideal devices transforming this input value. They concentrate on dynamic vibration measurements of a coal wagon and examine errors caused by the transformation properties of measuring transducers and the errors resulting from the filtering methodology (enforced by the necessity to apply the UIC-518 norm). The paper shows the software method of correction of transformation characteristics which diminishes values

of these errors during the on-line dynamic measurements. Ref.: [6, 9, 13].

During vibration measurements of coal wagons which aim at defining the vehicle safety criteria, problems with accuracy and speed of measurements occur, especially in on-line measurements. They are a result of properties of the transducer input signal reproduction which are non-ideal, and the requirements imposed by norms.

The UIC-518 norm specifies the measuring operating frequency range as being between 0.4 Hz and 10 Hz as well as the band-pass filter used to this end and located in the measuring chain after the analogue-digital transducer. The tolerance of the filter is ± 0.5 dB in the operating frequency range and ± 1 dB outside it. The filter transfer function is written as:

$$A(s) = \frac{4\pi^2 f_2^2 s^2}{\left(s^2 + \frac{2\pi f_1}{Q_1} s + 4\pi^2 f_1^2\right) \left(s^2 + \frac{2\pi f_2}{Q_1} s + 4\pi^2 f_2^2\right)} \quad (1)$$

where $f_1 = 0.4$ Hz, $f_2 = 10$ Hz, $Q_1 = 0.71$.

For measuring the signal frequency from 0.4 Hz and 10 Hz, the signal delay after filtration compared to the signal before filtration can be between 625 ms to 25.5 ms, respectively. Measurement errors result from non-ideal reproduction of the measurement signal by measuring transducers, amplifiers and other elements of the measuring track. The measurement of the relative error depends mostly on the type and accuracy of the applied measuring transducers. For example, for measuring transducers revealing sensitivity of 10 mV/m·s⁻² (used in a coal wagon vibration research), in dynamic measurements the relative value stands at about 30 %. A decrease in the measurement errors and the measurement signal delay can be achieved with the help of a method of software correction.

2. Vibration examinations of railway wagons according to UIC 518 norm

Vibration examinations of rail vehicles are a type of examinations which are to confirm safety of vehicles and vibration parameters determining their usefulness for specific transport applications. The UIC-518 norm specifies:

- conditions of test performance,
- measured magnitudes referring to dynamic behaviour of a vehicle,
- conditions allowing for automatic and statistical measurements.

Rail vehicles are passed as fit for use on the basis of the test-determined parameters:

- the movement of a vehicle on the track of specific geometry and with a specified velocity,
- wheel-track contact geometry,
- vehicle condition,
- measurement of a magnitude referring to dynamic performance of a vehicle,
- fulfilling requirements of automatic measurements and statistical data processing,
- assessment of measured magnitudes,
- determining border values of measured magnitudes.

Apart from the above said, the norm defines:

- the way of conducting the full measurement procedure (type of a tested zone of track geometry, vehicle load),
- the way of conducting partial tests,
- measuring methods:
 - correct method (of measuring interaction of forces affecting the wheel set and/or measurements of the wheel set acceleration, vehicle frame and body).
 - Simplified method (measurements of side forces affecting the wheel set and/or wagon frame and body).

The results obtained can be presented in the form of characteristics of:

- forces of wheel-rail contact pressure in a crosswise and longitudinal direction on the two smallest external axes of a wagon or carriage, depending on whether the wagon/carriage is equipped with separate axes,
- horizontal and vertical acceleration at the wagon body ends above the carriage or above the axis inside the carriage box. Measurements must be carried out on the carriage floor surface or, when the carriage has no floor – on the top part of the frame at the point indicated in the test report. Ref.: [5, 13].

Figure 1 shows the response of the band pass-filter to the sinusoidal input signal at the frequency of 5 Hz. The signal after filtration is delayed by 175 ms in relation to the input signal.

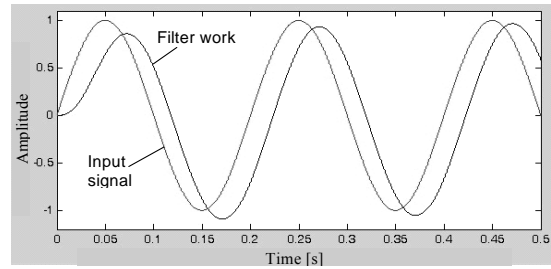


Fig. 1. Response of the band-pass filter

Figure 2 shows filter response to the same signal with addition of the Gauss noise.

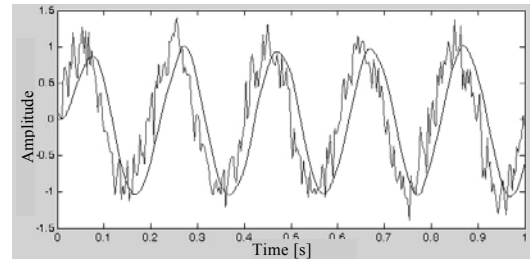


Fig. 2. Response of the band-pass filter to the disturbed sinusoidal signal

Figure 3 depicts theoretical characteristics of filter amplification and tolerance assumed in the UIC-518 norm.

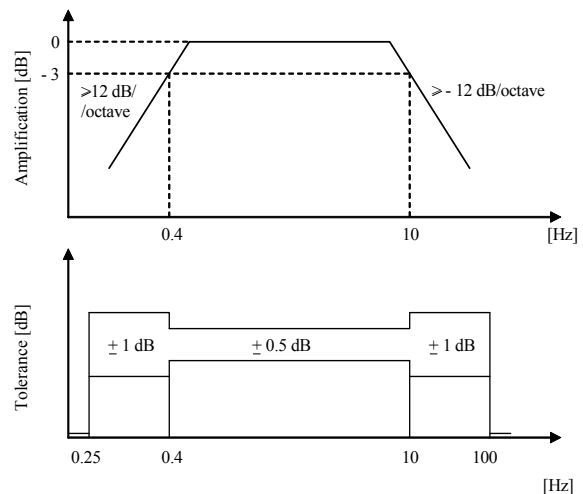


Fig. 3. Characteristics of correction and tolerance of the filter specified in the UIC-518 norm.

The UIC-518 norm does not specify what type of sensors is to be used and what measuring class they should represent. Freedom in applied equipment causes that correctness and accuracy of the signal depend on the designer of the measuring track. Due to signal processing properties depending on the applied equipment and their great number it is necessary to draw particular attention to errors made by them (often reproduced by the following elements of the measuring track). Ref.: [13].

In conformity with the UIC-518 norm requirements, vibration diagnostics tests are carried out in two stages:

1. Taking and registering data from measuring sensors
2. Filtration and developing results obtained from measurements in laboratory conditions according to the methodology included in the UIC-518 norm.

The main reasons for errors in the measurement process are:

- Reproduction of measured quantities by the measuring system,
- Performance properties of the band-pass filter

In order to reduce the filter response delay to the input signal, software correction was applied. Figure 4 shows a block diagram of the correction system. Measurements were taken in the MATLAB environment.

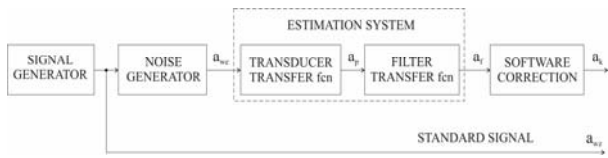


Fig. 4. Block diagram of system correction, a_{wz} – transducer input acceleration, a_{wz} – standard acceleration, a_p – transducer output acceleration, a_f – acceleration after filtration, a_k – acceleration after correction

Transducer transfer fcn (represents transfer function of real accelerometer) is written down as follows:

$$G(s) = \frac{0.03215s^2 + 1319.6s + 1.338 \cdot 10^6}{s^2 + 4.678 \cdot 10^4 s + 2.309 \cdot 10^7} \quad (2)$$

Figure 5 presents the magnitude and phase characteristics of the system whose transmittance is (2). High amplification visible in the magnitude characteristics results from the application of sensors of different sensitivities for examining voltage signals.

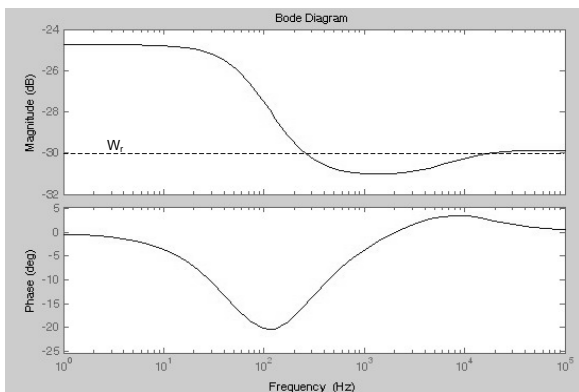


Fig. 5. Frequency characteristics of the measuring track with accelerometer

The referential level of amplification is determined as a ratio of a measuring transducer's sensitivity to a model one in the logarithmic scale $W_r = -29.87$ dB. For the above value, the ratio of acceleration determined on the basis of the measuring sensor voltage signal to the

acceleration determined by means of the model sensor is $a_{A1} / a_{A2} = 1$. Magnitude characteristics for the adopted border value of amplification 2dB W_r is within the frequency range above 117 Hz. Ref.: [1, 9]

Transfer function (2) has been determined experimentally by identification method ARX on the basis of measurements made on electro-dynamics shaker with high-class standard accelerometer. Ref.: [2, 7]

The transfer function (2) has been determined experimentally with the use of the ARX identification method on the basis of measurements taken on an electro-dynamic shaker with a high-class accelerometer.

Filter transfer function describes dynamic properties of the band-pass filter (1). The *software correction* block represents the correction algorithm. Figure 6 shows the block diagram of this algorithm. Equations of the algorithm of correction look as follows:

$$\begin{aligned} \hat{x}_{(k)} &= \frac{1}{b_2} [y_{(k)} - \hat{u}_{1(k)}] \\ \hat{u}_{1(k+1)} &= \varphi_{11} \hat{u}_{1(k)} + \varphi_{12} \hat{u}_{2(k)} + \psi_1 \hat{x}_{(k)} \\ \hat{u}_{2(k+1)} &= \varphi_{21} \hat{u}_{1(k)} + \varphi_{22} \hat{u}_{2(k)} + \psi_2 \hat{x}_{(k)} \end{aligned} \quad (3)$$

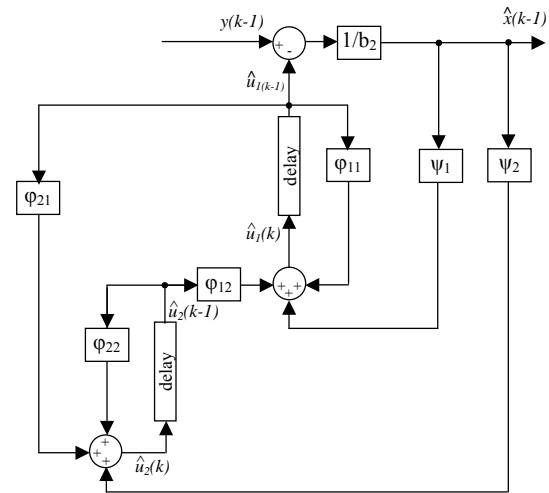


Fig. 6. Block diagram of correction algorithm: $\hat{x}_{(k-1)}$ - the estimate of input quantity at moment $k-1$ calculated on the basis of measurement result $y_{(k-1)}$ and estimation of variable \hat{u}_1 from the previous step; $\varphi_{11} \dots \varphi_{22}$, $\psi_1 \dots \psi_2$ – factors of discrete model

Figure 7 presents characteristics of acceleration after filtration, standard acceleration and acceleration after use of the correction algorithm. Negative effects of the filter operation in the form of amplitude of acceleration change and delays of response were reduced by the correction algorithm.

The values of 20-25 ms representing a delay of signal characteristics after filtration in relation to the standard signal were reduced after correction to 0.1-1 ms.

The results given are for the transducer operation time of over 0.1 s from the start of the input signal. Table 1 shows average values of maximum acceleration amplitudes (a series of 2000 measurement samples).

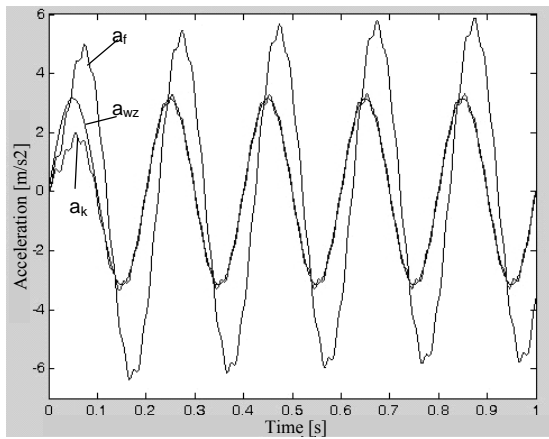


Fig. 7. Characteristics of standard acceleration, acceleration after filtration and acceleration after correction

Table 1. Acceleration amplitudes of the measuring-track simulation with correction

Acceleration [m/s ²]			
A_{wz}	A_p	A_f	A_k
3.15	16.66	5.89	3.31

Estimator response to the signal without noise which is a component of sinus run with frequency: regarding to a) 5 Hz, 8 Hz, 50 Hz, 200 Hz and 500 Hz and regarding to b) 1 Hz, 5 Hz, 50 Hz, 200 Hz and 500 Hz are shown in figure 8.

The filter (1) is responsible for elimination of components that are outside the frequency range 0.4 Hz – 10 Hz. In both cases correction algorithm operation improves the transducer replay characteristic, bringing it closer to the standard characteristic.

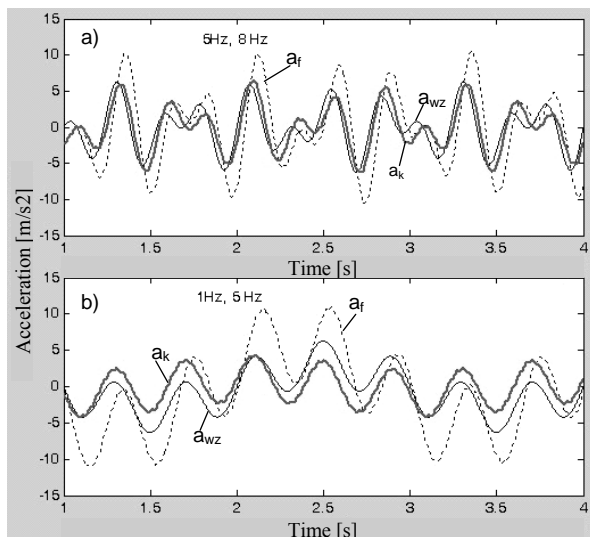


Fig. 8. Correction of the complex sinusoidal signal

3. Correction of processing errors in vibration investigations of the coal wagon, Faals type

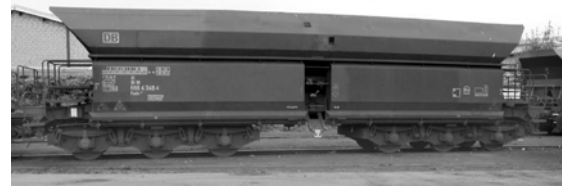


Fig. 9. Coal wagon, Faals type

Examination of a coal wagon, Faals type was conducted on the basis of a measuring system applied in CNTK Warsaw for determining parameters of railway wagon vibrations. On the basis of the data obtained in the measurements, a decision is made about accepting the vehicle for operation, which is conformable with the guidelines included in the UIC-518 norm binding in Europe. These parameters are determined on the basis of sensor readings. Sensors are located in carefully specified places of the vehicle moving on the track of specific geometry and with the set velocity. The basic elements on which sensors are located include: wagon frame, wagon body and axle-boxes. The values of crosswise and vertical acceleration and forces are read out from them.

The following magnitudes have been selected for the examination of the impact of reproducing transducer properties on the measurement result and possibilities of eliminating errors resulting from this:

1. Crosswise acceleration on the frame of the first car moving along the straight-line.
2. Crosswise acceleration on the frame of the first car moving along an arch
3. Vertical acceleration of an axle-box in the first wagon-set on the right in its movement along the straight line
4. Vertical acceleration of an axle-box in the first wagon-set on the right moving along an arch
5. Vertical acceleration of the car-frame above the first pin of the turn
6. Crosswise acceleration of the car-frame over the first pin of the turn

The magnitudes describing and at the same time affecting the behaviour of the wagon on the track are its velocity and geometry of the track. Examinations used measurement results obtained at the wagon velocity of 120 km/h on the straight line track and along arches of the turn radius being 600 m and 90 km/h along the arch of turn having the radius from 400 m to 600 m.

Effects of the method of software correction of measuring system transformation errors have been checked in vibration research of a coal wagon, Faals type. It is a six-axle self-discharging coal wagon of special construction and is allowed to move with the maximum speed of 100 km/h. Figure 10 shows the research measuring system. The *Data from wagon Faals type* block contains measurement results of velocity, acceleration and coal wagon deflection.

The *Transducer model and filtration* block represents laboratory determined dynamic equation of real accelerometer and dynamic equation of band pass-filter described by the UIC-518 norm. The *algorithm of correction* block includes equations of transformation error correction.

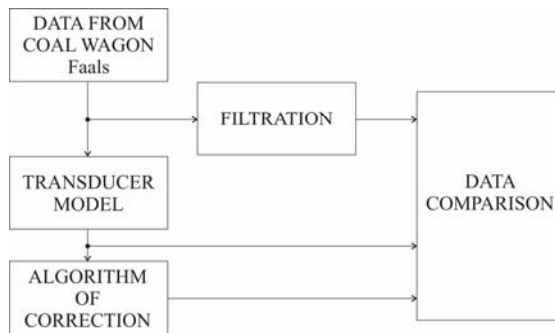


Fig. 10. Block diagram of the researched measuring system

Figure 11 presents the measurement results for velocity, deflection and lateral acceleration at wagon body ends. A standard accelerometer whose sensitivity was approximately 30 times higher than that normally used in railway car vibration practice was used for reading the standard acceleration value.

The characteristic of measured acceleration after correction is nearly the same as standard acceleration characteristics. Relative error values *1 and *2 were reduced to the values of 217 % and 51 %, respectively. The mean square error is a measure that indicates high values of measurement errors and is used in the practice of dynamic measurements. Characteristics of mean square errors for a measurement with and without correction are depicted in Figure 11. A comparison of the two characteristics reveals a significant decrease in the error in the case of a measurement with correction (by about 10,000 times). It is possible to conclude that after correction a capability of the measuring system to reproduce the input quantity was improved and sensitivity of the system which accounts for gross errors – was decreased.

The characteristics of the dynamic absolute error with and without correction are illustrated in Fig. 12. The difference between the measurements is grade 10^3 in favour of the correction. The absolute error in the case of dynamic measurements without correction is between -7.143 and 6.674 m/s. The values of the absolute error stand at 0.0026 m/s^2 and 0.0035 m/s^2 for measurements with correction. Ref.: [5, 6, 10, 13].

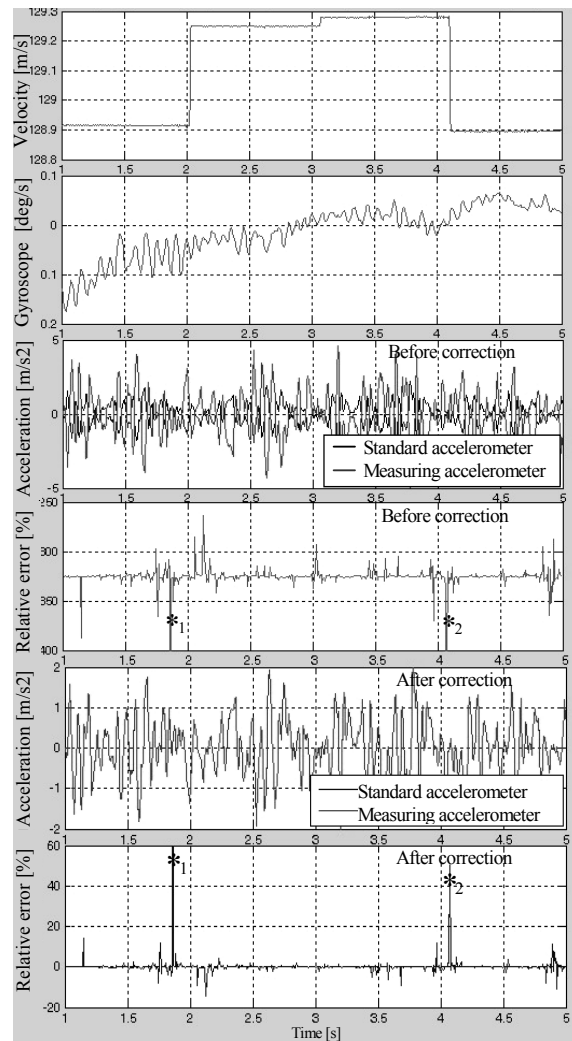


Fig. 11. Crosswise vibration of coal wagon body ends

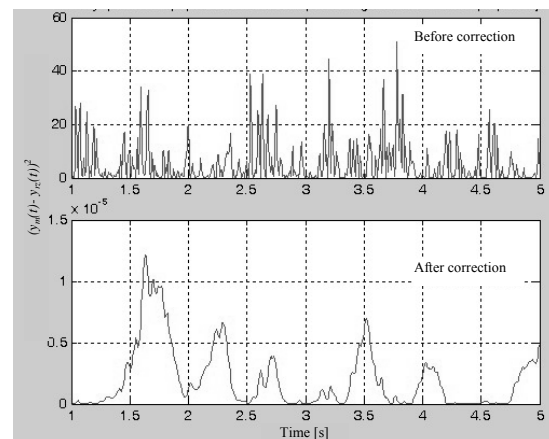


Fig. 12. Mean square error measurement

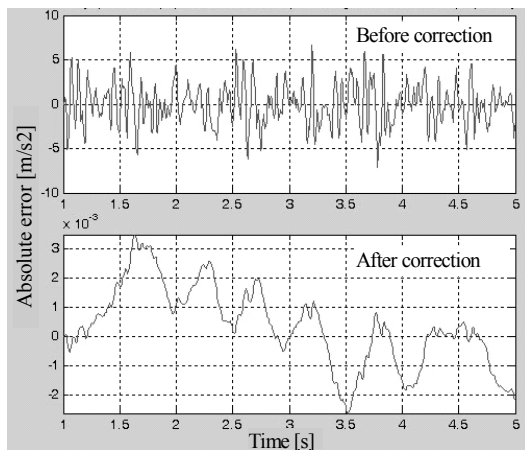


Fig. 13. Absolute error measurement

The Table below shows the values of measured quantities in vibration research of coal wagon Faals type.

Table 2. The values of measuring quantities

	Before correction	After correction
Measuring time range t [s]	1 ÷ 5	
Velocity range [m/s]	128.89 ÷ 129.28	
Railway car deflection range α [deg/s]	-0.17 ÷ 0.06	
Relative error range δ_w [%]	-1102 ÷ -263	-14.5 ÷ 217.7
Median of relative error range M_δ [%]	-325.2	0.01
Standard acceleration range a_w [m/s ²]	-2.054 ÷ 2.196	
Value of absolute error range Δ [m/s ²]	-7.143 ÷ 6.674	-0.0026 ÷ 0.0035

4. Conclusion

Absolute errors in vibration measurements of a coal wagon Faals type as well as the median of relative error were considerably decreased when the algorithm of correction was applied.

Owing to the said algorithm the problems with accuracy of the measuring signal reproduction are significantly reduced. As a result the requirements of the UIC 518 norm are fulfilled.

5. References

1. Analog devices technical references books: Practical design techniques for sensor signal conditioning, Analog Devices, Inc., USA 1999
2. Andrae J., Hons C., Sawla A.: High precision force transducer with new method for online

- compensation of parasitic effects, Measurement Vol.33, Elsevier, Ltd., 2003
3. Beards C. F.: Engineering vibration analysis with application to control systems, Edward Arnold, London 1995
4. Cakar O., Sanliturk K.Y.: Elimination of transducer mass loading effects from frequency response functions, Mechanical Systems and Signal Processing Vol. 19, Elsevier, Ltd. 2005
5. Cioć R.: Correction of measuring transducers dynamic characteristics in vibration of railway car, Doctoral dissertation, Biblioteka Główna Politechniki Radomskiej, Radom 2007, (in Polish)
6. Cioć R.: ARX method in the context of identification of dynamic correction parameters of vibration measuring system, Prace naukowe PRad, Elektryka 1(9), Radom 2005, (in Polish)
7. Cioć R., Luft M.: Valuation of software method of increase of accuracy measurement data on example of accelerometer, Advances in Transport Systems Telematics, Monograph, Faculty of Transport, Silesian University of Technology, Katowice, 2006.
8. Cioć R., Luft M.: Correction of transducers dynamic characteristics in vibration research of means of transport – part 1 – simulations and laboratory research, 10th International Conference “Computer Systems Aided Science, Industry and Transport”, Transcomp 2006, vol.1, Zakopane, 2006.
9. Jakubiec J.: Real-time numerical reconstruction of instantaneous values of dynamic input quantities of nonlinear transducers, Politechnika Śląska, Zeszyty Naukowe nr 964, Gliwice 1988, (in Polish)
10. Luft M., Cioć R.: Increase of accuracy of measurement signals reading from analog measuring transducers, Zeszyty Naukowe Politechniki Śląskiej 2005, Transport z. 59, nr kol. 1691, Gliwice 2005.
11. Luft M., Cioć R., Pietruszczak D.: Increasing the accuracy of non-linear measuring transducers processing, Advances in Transport Systems Telematics, p. 189-196, (ISBN 978-83-206-1715-3), WKŁ, Warszawa 2008.
12. Szychta E.: Zero voltage switched multiresonant converters – analysis and design, Monograph University of Žilina, 2008
13. Testing and approval of railway vehicles from the point of view of their dynamic behaviour – Safety – Track fatigue – Ride quality, 3rd edition, Leaflet UIC 518, International Union of Railways, October 2005.

REGRESSION MODELLING USING ADAPTIVE BASIS FUNCTION CONSTRUCTION

Gints JEKABSONS

Institute of Applied Computer Systems, Riga Technical University, Latvia

Abstract: The task of estimating “good” predictive models from available finite (training) data acquired through, e.g., experiments or simulations is common in virtually all fields of science and engineering. The most commonly used predictive models in the case of continuous dependent variable are polynomial regression models acceptable predictive performance of which are usually attempted to achieve by adjusting a maximal degree and using subset selection techniques requiring non-trivial exponential runtime. The paper outlines a different approach not requiring manual degree adjustments and running in a polynomial time and demonstrates its efficiency in a number of applications in the field electrical and control technologies.

Keywords: Regression modelling, approximation, Adaptive Basis Function Construction, polynomial regression, sparse polynomials.

1. Introduction

The task of estimating “good” predictive models from available data is common in virtually all fields of science and engineering. The goal of the task is to estimate unknown (input, output) dependency (or model) from training data (consisting of a finite number of samples acquired through, e.g., experiments or simulations) with good prediction (generalization) capabilities [2,6].

One of the specific model estimation tasks is regression – estimation of an unknown real-valued function in the relationship

$$y = G(x) + \varepsilon, \quad (1)$$

where ε is independent and identically distributed random noise with zero mean, $x = (x_1, x_2, \dots, x_d)$ is d -dimensional input, and y is scalar output. The estimation is made based on a finite number of samples (training data) provided in form of matrix \mathbf{x} of input values for each sample and vector \mathbf{y} of output values for each

corresponding sample. Using the finite number n of training samples $(\mathbf{x}_i, \mathbf{y}_i)$, ($i = 1, 2, \dots, n$) one wants to build a model F that allows predicting the output values for yet unseen input values as closely as possible. In practical applications of regression most commonly low-degree polynomial models are used. Generally, a linear regression model may be defined as a linear expansion of basis functions

$$F(x) = \sum_{i=1}^k a_i f_i(x), \quad (2)$$

where $\mathbf{a} = (a_1, a_2, \dots, a_k)$ are model’s parameters, k is the number of basis functions included in the model (equal to the number of model’s parameters), and $f_i(x)$ ($i = 1, 2, \dots, k$) are basis functions of the input x . As such models are linear in the parameters, the estimation of their parameters is typically done using the Ordinary Least-Squares (OLS) method [6,22] minimizing the squared-error:

$$\mathbf{a} = \arg \min_{\mathbf{a}} \sum_{i=1}^n (\mathbf{y}_i - F(\mathbf{x}_i))^2. \quad (3)$$

The basis function representation enables moving beyond pure linearity, by defining nonlinear transformations of x (e.g., products of input variables in polynomials) while still working with linear models (and employing OLS).

For example, for $d = 1$ a polynomial model of fixed degree p can be expressed as follows

$$F(x) = \sum_{i=0}^p a_i x^i. \quad (4)$$

A low-degree polynomial has low number of unknown parameters and tends to smooth out noise in the data. However, it may exhibit too little flexibility for modelling highly nonlinear behaviours (causing underfitting). Higher-degree polynomials can be used,

but they may contain too many parameters and therefore either overfit the data or prohibit parameter estimation because the number of parameters exceeds the number of training data samples.

The most popular approach to controlling model's complexity is subset selection [6,22,23]. The goal of subset selection is from a fixed full predetermined dictionary of basis functions to find a subset that corresponds to a model (a sparse polynomial) of the best predictive performance.

Before performing the actual subset selection the user must first predefine the dictionary basis functions of which will be used for model generation. This is usually done by setting the maximal degree of a full polynomial and taking the set of its basis functions.

In polynomial regression, increase in the full model's degree leads to exponential growth of the number of basis functions in the dictionary [2,6] leading to double-exponential growth of the number all possible subsets of basis functions. Efficient heuristic subset selection methods such as Sequential Forward Selection, SFS (also known as Forward Selection or Stepwise Forward Selection [6,22]) and many others (see, e.g., [23]) considerably reduce the time. However, it is still exponential in the degree and the number of input variables [10].

The problem is that the approach of subset selection assumes that the chosen fixed finite dictionary of the predefined basis functions contains a subset that is sufficient to describe the target relation sufficiently well. However, generally the required maximal degree is not known beforehand and needs to be guessed (or found by additional search over the whole subset selection process) since it will differ from one regression task to another. In many cases (especially when the studied data dependencies are complex and not well studied) this means either a non-trivial and long trial and error process or acceptance of a possibly inadequate model.

In [11,12] we proposed an alternative approach to that of typical subset selection – Adaptive Basis Function Construction (ABFC). The goal of this procedure is to overcome some of the limitations associated with the subset selection approach outlined above. ABFC is developed for sparse polynomial regression model building without restrictions on model's degree and enables model building in polynomial time instead of exponential. The required basis functions are automatically adaptively constructed specifically for the data set at hand without using a restricted fixed finite user-defined dictionary. The dictionary of ABFC is infinite and polynomials of arbitrary complexity can be generated.

In this paper we will shortly review the ABFC approach (Section 2), briefly characterize two of its special cases (Section 3), and demonstrate the efficiency of the ABFC methods in a number of applications in the field electrical and control technologies (Section 4).

2. Adaptive basis function construction

The basis functions in a polynomial regression model generally can be defined as a product of original input variables each with an individual exponent:

$$f_i(x) = \prod_{j=1}^d x_j^{r_{ij}}, \quad (5)$$

where \mathbf{r} is a $k \times d$ matrix of nonnegative integer exponents such that r_{ij} is the exponent of the j -th variable in the i -th basis function. Note that when for a particular i -th basis function $\forall j: r_{ij} = 0$, the basis function is the intercept term.

Given a number of input variables d , matrix \mathbf{r} with a specified number of rows k and with specified values of each of its elements completely defines the structure of a polynomial model with all its basis functions.

Moreover, as neither the upper bounds of \mathbf{r} elements' values nor the upper bound of k are defined, it is possible to generate polynomials of arbitrary complexity, i.e., of arbitrary number of basis functions each with arbitrary exponent for each input variable.

In order to efficiently build a sufficiently good regression model for a particular dataset an efficient search mechanism is required enabling searching in an infinite space of polynomial models. The search mechanism of ABFC is organized as follows (see [11,12] for details).

The search is started from the simplest model – the model with one basis function which corresponds to the intercept term. New models are generated using so-called model refinement operators which enable adding, copying, modifying, and deleting the rows of \mathbf{r} , i.e., adding, copying, modifying, and deleting the basis functions of the model (not only adding and deleting, like in the subset selection methods). Next an efficient search strategy and a model evaluation measure are required. In the special case of ABFC termed Floating ABFC (F-ABFC) the search strategy of Sequential Floating Forward Selection [20,21] is adapted and the corrected Akaike's Information Criterion (AICC) [8] is employed. The termination condition of the search process is met when the algorithm has generated a model which cannot be further refined using any of the refinement operators.

Additionally, in order to lower the general model building issues of selection bias and selection instability [1,9,16,19,23], a technique of model averaging (also called ensembling or combining) is carried out. This leads to the second special case of ABFC termed Ensemble of F-ABFC (EF-ABFC) [9].

The ABFC methods attempt to model arbitrary dependencies in data with little or no knowledge of the system under study. The user is normally not required to tune any hyperparameters. However, if there is sufficient additional domain knowledge outside the specific data at hand it may be appropriate to place some constraints on the final model. If the knowledge is

fairly accurate, such constraints can improve the accuracy while saving computational resources.

For example the constraints might be one or more of the following: 1) limiting the maximal degree of all the basis functions (similar to the subset selection), i.e.,

$$\forall i: 0 \leq \sum_{j=1}^d r_{ij} \leq p; 2) \text{ limiting the maximal value of}$$

the exponent for each particular input variable in all the basis functions, i.e., $\forall i: 0 \leq r_{ij} \leq p_j$, where p_j is

maximal exponent of the j -th variable; 3) restricting contributions of specific input variables that are not likely to interact with others so that those variables can enter the model in basis functions only solely – with exponents of all other variables fixed to zero.

These constraints, as well as far more sophisticated ones, can be easily incorporated in the ABFC. However, note that in all the experiments described in this paper we did not use any kind of constraints.

Finally it must be noted that in special cases when the data is of low dimensionality (e.g., $d \leq 4$) and/or the existing structure in the data is very complex (so a very complex model is required) the search algorithm may get stuck in a local minimum too early in the search returning a too simple and underfitted model [10,11]. As a remedy for this problem some of the refinement operators are applied recursively [10,11]. In this way the probability of getting stuck in too early local minima is considerably decreased (though not removed).

A more detailed description of F-ABFC, and EF-ABFC, as well as detailed empirical comparisons to subset selection methods and other popular regression modelling methods is given in our previous studies [9,10,12]. The biggest disadvantage of the EF-ABFC compared to F-ABFC is that it requires larger computational resources. However, the fact that before the model combining the models are built completely separately allows for an easy parallelization of the process.

In [13,14] we applied the ABFC methods in metamodelling for optimum design of laser welded sandwich structures and glass fibre composite structures. However, the methods of ABFC are really a general-purpose regression modelling tools.

The next section will demonstrate the efficiency of the ABFC methods in a number of applications in the field electrical and control technologies.

3. Applications

This section describes a number of regression modelling applications where the ABFC methods were used as well as demonstrates results of empirical comparisons of the ABFC methods to other well known and widely used regression modelling methods.

The methods compared are the following: 1) “full” polynomials (FP) of different degree; 2) sparse polynomials of different degree built using one of the most popular subset selection methods SFS utilizing AICC as the evaluation criterion; 3) F-ABFC; 4) EF-ABFC; 5) Locally Weighted Polynomials (LWP) of different degree utilizing cross-validated Gaussian

weight function [3,14]; 6) Multivariate Adaptive Regression Splines (MARS) with and without cross-validated degrees of freedom [4]; 7) multiquadric Radial Basis Function (RBF) interpolation [5]; 8) Kriging interpolation [17]. Note that for FP the maximal degree p is varied in such interval that the number of basis functions m is always lower than or equal to the size of the training set n . This is because with higher values of p the number of full model’s parameters exceeds the number of training data samples.

All the methods are implemented in the VariReg software tool version 0.9.13 freely available at <http://www.cs.rtu.lv/jekabsons/>. For all the methods all the parameters had default values except were stated otherwise.

The modelling methods are compared in terms predictive performance of the built models estimated using resampling techniques [15]. The specific resampling technique used in an application depends on the amount of the available data. The errors were measured using the Relative Root Mean Squared Error (RRMSE) criterion

$$RRMSE = 100\% \frac{RMSE}{SD} = 100\% \frac{\sum_i (\mathbf{y}_i - F(\mathbf{x}_i))^2}{\sum_i (\mathbf{y}_i - \bar{y})^2}, \quad (6)$$

where RMSE is Root Mean Squared Error calculated in the test data, SD is standard deviation either in the test data or in all the data (depending on the specific application), and \bar{y} is the mean of the \mathbf{y} values. The closer the value of RRMSE is to zero the more accurate is the model.

Additionally, note that for the problems in which the dataset had only two input variables (the first and the last) the refinement operators of F-ABFC and EF-ABFC were applied recursively four times in each iteration.

3.1. Ball thrower simulation

The problem considered here (P1) is prediction of the accuracy of a robotic arm throwing a ball to the target. The aim is to predict the distance from the ball to the target as closely as possible when the ball is hitting the ground while taking different other parameters into account. Accurate prediction of the distance enables optimization of arm’s control parameters for high throwing accuracy.

Fig. 1 depicts some of the ball thrower simulation parameters. The simulations are performed using free software available at <http://www.cs.rtu.lv/jekabsons/>.

The following parameters are tuneable: 1) initial velocity of the ball in the moment of its release (x_1); 2) the angle of the arm when the ball is released (x_2); 3) the distance from the arm’s base to the target (x_3); 4) the length of the robot’s arm (x_4); 5) air resistance (x_5); 6) the weight of the thrown ball (x_6); 7) gravity (x_7); 8) the distance from the arm’s base to the wall (x_8).

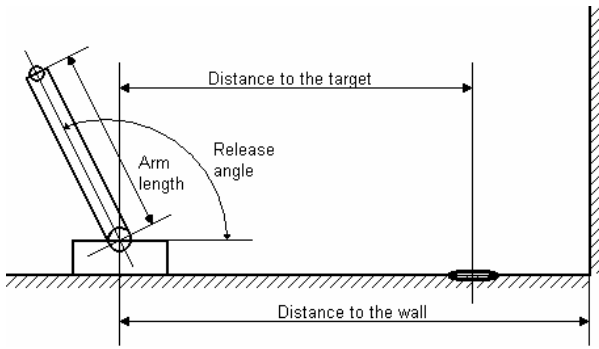


Fig. 1. Ball thrower parameters (see text for details)

The problem pursued here is the prediction of the distance from the ball to the target when the ball is hitting the ground while varying the ball release angle (from 45 to 135 degrees) and the distance from the arm's base to the target (from 120 to 400). All the other variables are held fixed $x_1 = 85$, $x_4 = 100$, $x_5 = 0.08$, $x_6 = 1$, $x_7 = 9.81$, $x_8 = 490$ (here the ball is never hitting the wall).

The properties of the dataset are the following: $d = 2$ and $n = 100$ (a regular 10×10 grid). For predictive performance estimation of the regression modelling methods 10-fold Cross-Validation [15] was used. The SD was calculated using test data sets.

Fig. 2 shows the surface of the model built by EF-ABFC predicting the distance. When the distance from the arm to the target (x_3) is known, ball's distance to the target (i.e., throwing accuracy) can be minimized by changing ball release angle (x_2).

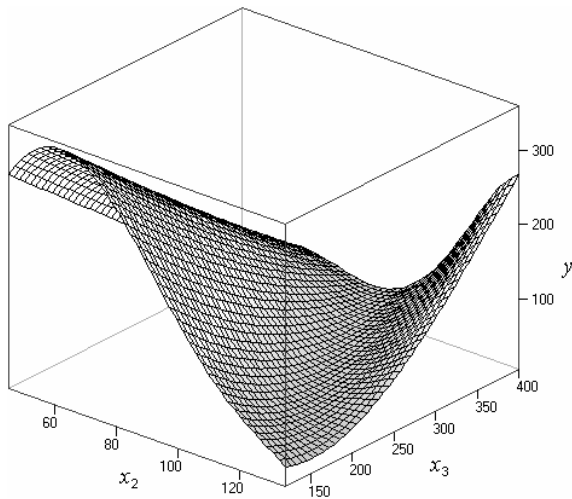


Fig. 2. Surface of the model built by EF-ABFC

3.2. Robot arm forward kinematics

The problem considered here (P2) is prediction of the distance of the end-effector of an 8 link all-revolute robot arm from a target. The aim is to predict the distance, given the angular positions of the joints. The datasets from the simulations as well as a more detailed description of the problem are available at the Delve repository (<http://www.cs.toronto.edu/~delve/>).

The properties of the dataset are the following: $d = 8$ and $n = 64$ (from available 8192). For predictive

performance estimation of the regression modelling methods the 64 samples were randomly selected from the available data while the remaining 8128 samples were used as a test set. The process was repeated 10 times and the results were averaged. The SD was calculated using test data sets.

3.3. Servomechanism rise time

The problem considered here (P3) is prediction of the rise time of a servomechanism (the time required for the system to respond to a step change in a position set point) in terms of two gain settings and two choices of mechanical linkages. The dataset as well as a more detailed description of the problem are available at the UCI repository (<http://archive.ics.uci.edu/ml/>).

The properties of the dataset are the following: $d = 4$ and $n = 167$. For predictive performance estimation of the regression modelling methods 10-fold Cross-Validation was used. The SD was calculated using test data sets.

3.4. Robot vision

The problem considered here (P4) is prediction of the shoulder-joint angle of a six-joint robot arm learning to grasp an object (a small brick) presented visually on a table surface. The dataset is taken from a study described in [7]. Each data sample in the dataset combines the visual information of the brick with the grasping arm posture of the robot. To collect a data sample, the robot put the object on the table, recorded the corresponding arm posture, removed the arm, and took a picture of the brick. The visual information consists of a 4×4 -pixels grid providing a coarse-grained view of the table surface and a histogram showing the edge distribution over four orientations within the camera image.

The properties of the dataset are the following: $d = 20$ and $n = 100$ (from available 3368). For predictive performance estimation of the regression modelling methods the 100 samples were randomly selected from the available data while the remaining 3268 samples were used as a test set. The process was repeated 10 times and the results were averaged. The SD was calculated using test data sets.

3.5. Electromagnetic processes in Switched Reluctance Drives

The problem considered here (P5) is prediction of flux linkages between the poles of the rotor and the stator in a Switched Reluctance Drive [11,18]. The problem has two input variables, phase current and rotor position, and an output variable, flux linkage. The data is generated using finite element simulations. A more detailed description of the problem is given in [18].

The properties of the dataset are the following: $d = 2$ and $n = 24$. As the number of samples is very small, for predictive performance estimation of the regression modelling methods Leave-One-Out Cross-Validation

[15] was used. The SD was calculated using all the available data.

3.6. Analysis of the results

Table 1 presents the results of the performed regression modelling experiments. In the first four problems (P1, P2, P3, and P4), where a larger amount of data is available, EF-ABFC gives better or similar results than those of F-ABFC. In the fifth problem (P5) however F-ABFC outperforms EF-ABFC. This is because if there is too little data, the gains achieved via an ensemble may not compensate for the decrease in accuracy of individual models, each of which now sees an even smaller training set.

In P1, P2, and P5 the subset selection method SFS either outperforms full polynomials only a little or behaves worse. In all the three problems LWP succeeded to outperform SFS. However, with P5 the best results are reached using full polynomials while apparently both SFS and LWP are just too complex modelling methods for such a little amount of data. In P3 and P4 the SFS outperforms FP as well as LWP.

Table 1. Average predictive performance of the modelling methods in terms of RRMSE

Method	P1	P2	P3	P4	P5
FP, $p = 1$	91.88	29.94	79.29	12.33	36.19
FP, $p = 2$	57.79	35.37	52.30	-	29.83
FP, $p = 3$	31.48	-	44.44	-	13.20
FP, $p = 4$	27.65	-	61.85	-	12.76
FP, $p = 5$	18.06	-	382.65	-	7.80
SFS, $p = 1$	91.88	29.94	79.29	13.04	36.19
SFS, $p = 2$	56.83	28.58	54.31	12.02	28.79
SFS, $p = 3$	35.65	49.67	49.36	16.04	13.21
SFS, $p = 4$	29.66	53.91	41.06	-	9.49
SFS, $p = 5$	27.12	72.73	39.59	-	10.09
LWP, $p = 1$	28.70	25.75	48.84	12.32	12.89
LWP, $p = 2$	20.35	35.68	45.90	-	15.51
LWP, $p = 3$	23.01	-	48.81	-	9.43
LWP, $p = 4$	16.17	-	127.84	-	10.05
LWP, $p = 5$	16.38	-	305.94	-	12.41
F-ABFC	17.60	41.15	41.66	15.98	8.00
EF-ABFC	12.77	26.25	42.04	9.36	14.58
MARS	14.69	35.54	38.63	17.77	36.31
MARS, CV	15.60	34.88	38.24	15.13	28.72
RBF	11.74	27.19	39.67	16.60	12.60
Kriging	14.45	28.02	34.02	9.38	4.66

In all the problems the ABFC methods either outperformed FP, SFS, and LWP or at least gave comparable results. Additionally it must be noted that in practice with FP, SFS, and LWP very commonly the modelling task is done in a one-shot manner choosing the degree p only once, which makes it difficult to obtain good results (for instance in the experiments performed here the best value for p was almost each time a different one). An alternative is to check results for all the values of p in some interval but this takes a much larger amount of computational resources and demands for an additional cross-validation loop over the

whole modelling process in order to evaluate the methods reliably.

The ABFC methods on the other hand do not require the user to choose the degree. Instead they automatically adapt to the data at hand.

Additionally, in the performed experiments the ABFC methods also compare rather well to the state-of-the-art “non-polynomial” methods MARS, RBF, and Kriging.

4. Conclusions

In this paper we shortly reviewed the ABFC approach, briefly characterized two of its special cases – F-ABFC and EF-ABFC, and demonstrated the efficiency of the methods in a number of applications in the field electrical and control technologies while comparing them to other widely used methods.

The ABFC methods, in contrast to the methods of subset selection, do not require the user to predefine the maximal degree or the dictionary of the basis functions. Instead they automatically adapt to the particular data at hand.

Overall, in the performed empirical experiments it is concluded that in the considered problems the adaptive model building methods of ABFC can outperform the other polynomial regression modelling methods and compare rather well to the other state-of-the-art methods – MARS, RBF, and Kriging. The ABFC methods can be viewed as competitive tools for regression modelling.

Directions of future research include employment of ABFC or derivations of it in different real-world applications, further theoretical studies concerning the efficiency of ABFC, as well as adaptation of ABFC for other types of tasks, e.g., classification.

F-ABFC and EF-ABFC together with many other regression modelling methods are implemented in VariReg software tool freely available for non-commercial research and educational purposes at <http://www.cs.rtu.lv/jekabsons/>.

5. References

1. Breiman L. Heuristics of instability and stabilization in model selection. *Annals of Statistics*, vol. 24, 1996. p. 2350-2383.
2. Cherkassky V., Mulier F.M. *Learning from Data: Concepts, Theory, and Methods*, 2nd ed. Wiley-IEEE Press, 2007. 538 p.
3. Cleveland W.S., Devlin S.J. Locally weighted regression: An approach to regression analysis by local fitting, *Journal of the American Statistical Association*, vol. 83, 1988. p. 596-610.
4. Friedman J.H. Multivariate Adaptive Regression Splines (with discussion), *The Annals of Statistics*, vol. 19, no. 1, 1991. p. 141.
5. Gutmann H.-M. A Radial Basis Function Method for Global Optimization, *Journal of Global Optimization*, vol. 19, 2001. p. 201-227.
6. Hastie T., Tibshirani R., Friedman J. *The Elements of Statistical Learning*. Springer, 2003. 552 p.

7. Hoffmann H., Schenck W., Moeller R. Learning visuomotor transformations for gaze-control and grasping. *Biological Cybernetics*, vol. 93, 2005. p. 119-130.
8. Hurvich C.M., Tsai C-L. Regression and Time Series Model Selection in Small Samples. *Biometrika*, 76, 1989. p. 297-307.
9. Jekabsons G. Ensembling Adaptively Constructed Polynomial Regression Models, *International Journal of Intelligent Systems and Technologies (IJIST)*. vol. 3, no. 2, 2008. p. 56-61. (<http://www.waset.org/ijist/v3/v3-2-11.pdf>)
10. Jekabsons G., Lavendels J. A Heuristic Approach for Surrogate Modelling. *Proceedings of Conference "Applied Information and Communication Technologies"*, Jelgava, Latvia, 2008. p. 11-20.
11. Jekabsons G., Lavendels J. A Heuristic Approach for Surrogate Modelling of Electro-technical Systems. *Proceedings of International Conference "Electrical and Control Technologies – 2008"*, Kaunas, 2008. p. 62-67.
12. Jekabsons G., Lavendels J. Polynomial Regression Modelling using Adaptive Construction of Basis Functions. *Proceedings of IADIS International Conference, Applied Computing 2008*, Algarve, Portugal, 2008. p. 269-276.
13. Kalnins K., Eglitis E., Jekabsons G., Rikards R. Metamodels for Optimum Design of Laser Welded Sandwich Structures. *Scientific Proceedings of International Conference on Welded Structures, Design, Fabrication, and Economy 2008*, Miskolc, Hungary, 2008. p. 119-126.
14. Kalnins K., Ozolins O., Jekabsons G., Metamodels in Design of GFRP Composite Stiffened Deck Structure. *Proceedings of 7th ASMO-UK/ISSMO International Conference on Engineering Design Optimization, Association for Structural and Multidisciplinary Optimization in the UK*, Bath, UK, 2008, 11 p. (in press).
15. Kohavi R. A Study of Cross-Validation and Bootstrap for Accuracy Estimation and Model Selection. *Proceedings of the Fourteenth International Joint Conference on Artificial Intelligence*, Morgan Kaufmann, San Mateo, CA, 1995. p.1137-1145.
16. Loughrey J., Cunningham P. Overfitting in Wrapper-based Feature Subset Selection: the Harder You Try the Worse It Gets. *24th SGAI International Conference on Innovative Techniques and Applications of Artificial Intelligence*, 2004. p. 33-43.
17. Martin J.D., Simpson T.W., Use of Kriging Models to Approximate Deterministic Computer Models. *AIAA Journal*, vol. 43, no. 4, 2005. p. 853-863.
18. Matveev A. Development of Methods, Algorithms and Software for Optimal Design of Switched Reluctance Drives, PhD thesis. Eindhoven University of Technology, Eindhoven, The Netherlands, 2006.
19. Opitz D., Maclin R. Popular Ensemble Methods: An Empirical Study. *Journal of Artificial Intelligence Research*, vol. 11, 1999. p. 169-198.
20. Pudil P., Ferri F.J., Novovicova J., Kittler J. Floating search methods for feature selection with nonmonotonic criterion functions. *Proceedings of the International Conference on Pattern Recognition*, vol. 2, IEEE, Los Alamitos, CA, 1994. p. 279-283.
21. Pudil P., Novovicova J., Kittler J. Floating Search Methods in Feature Selection. *Pattern Recognition Letters*, 15, 1994. p. 1119-1125.
22. Rawlings J.O. *Applied Regression Analysis: A Research Tool*, 2nd ed. Wadsworth & Brooks/Cole, Pacific Grove, CA, 1998.
23. Reunanen J. Search Strategies. *Feature Extraction: Foundations and Applications*, Guyon I., Gunn S., Nikravesh M., Zadeh L.A. (eds.), Springer, 2006. p. 119-137.

CATEGORIZING SEQUENCES OF LARYNGEAL DATA FOR DECISION SUPPORT

Adas GELŽINIS *, Evaldas VAIČIUKYNAS *, Edgaras KELERTAS *, Marija BAČAUSKIENĖ *,
Antanas VERIKAS **, Virgilijus ŪLOZA ***, Aurelija VEGIENĖ ***

* Kaunas University of Technology, Lithuania; ** Halmstad University, Sweden; *** Kaunas University of
Medicine, Lithuania

Abstract: This paper is concerned with kernel-based techniques for categorizing laryngeal disorders based on information extracted from sequences of laryngeal colour images. The features used to characterize a laryngeal image are given by the kernel principal components computed using the N -vector of the 3-D colour histogram. The least squares support vector machine (LS-SVM) is designed for categorizing an image sequence into the *healthy*, *nodular* and *diffuse* classes. The kernel function employed by the SVM classifier is defined over a pair of matrices, rather than over a pair of vectors. An encouraging classification performance was obtained when testing the developed tools on data recorded during routine laryngeal videostroboscopy.

Keywords: Larynx pathology, Image sequence, Classification, Support vector machine.

1. Introduction

Laryngeal still images, image sequences, voice signal, and patient's questionnaire data can be considered as the main information sources to characterize human larynx. Nowadays, automated analysis of voice is increasingly used for detecting and screening laryngeal pathologies [1–3]. It was demonstrated that even telephone-based voice may lend itself for screening laryngeal disorders [1].

There were very few attempts to create systems for automated analysis of still colour laryngeal images. In [4], a technique for automated categorization of manually marked suspect lesions into *healthy* and *diseased* classes was presented. The categorization is based on textural features extracted from co-occurrence matrices [5, 6] computed from manually marked areas of vocal fold images, taken by a CCD camera. The classification accuracy of 81.4% was reported when testing the technique on a very small set of 35 images. A set of 785 colour laryngeal images has been used in studies presented in [7–9]. The classifi-

cation accuracy of over 95% was achieved when categorizing the images into one healthy and two pathological (nodular and diffuse) classes. Fig. 1 presents characteristic examples from the three decision classes considered, namely, *nodular*, *diffuse*, and *healthy*. As can be seen from Fig. 1, examples representing the different classes are rather different. However, it is worth noting that due to the large variety of appearance of vocal fold mass lesions, the classification task can sometimes be difficult to solve even for a trained physician [10].



Fig. 1. Images from the *nodular* (left), *diffuse* (middle), and *healthy* (right) classes

When categorizing the same set of images into seven classes (one healthy and six pathological), the classification accuracy of over 80% was reported [11]. Image texture, distribution of colour, and geometry of edges of vocal folds are the types of features used for the categorization. It was found that colour is amongst the most discriminative types of features.

1.1. Videostroboscopy

Laryngeal videostroboscopy is used extensively for analysis of vocal folds and in the clinical practice for diagnosing voice disorders [12]. For example, videostroboscopy is a well-established technique for measuring the glottal gap or examining the glottic closure [13]. Videostroboscopy is one of the standard methods used to examine moving objects. Flashing light is used to illuminate an object in stroboscopy. When the flashes are synchronized with the vocal fold vibrations, a stationary view of the vocal folds is obtained.

However, the single-flash-timing laryngeal videostroboscopy has a limitation that it is effective only when

This study was supported by COST Action 2103 Advanced Voice Function Assessment.

vocal fold vibrations exhibit only one single fundamental frequency. Multiple tones (fundamental frequencies) may be recorded in the case of some diseases, such as polyps, nodules, and cysts [14]. In such cases, a clear view of the vibrating vocal folds can not be obtained with the single-flash-timing laryngeal videostroboscopy. A multiple-flash-timing laryngeal videostroboscopy technique was proposed by Deguchi et al. [14], to deal with such cases. Multiple light emitting diodes are used as illumination sources.

In [15] image sequences recorded with the stroboscopy system have been used to measure the glottic angle and the angular velocities of vocal fold abduction and adduction. The authors point out that semi-automated edge tracking would be an important improvement of the technique.

It is worth mentioning that not only edge tracking but also other tasks usually carried out when analyzing video data need automated or semi-automated procedures. Decision making is one of such tasks. In clinical practice, decision making is quite often based on subjective evaluation of video data. Quantitative measures of motion, colour distribution and geometry of vocal folds can provide objective information and be useful in medical treatment planning and greatly facilitate tracing progress over time.

The long-term goal of this work is a decision support system for diagnostics of laryngeal diseases. A voice signal, sequences of colour vocal folds images obtained from videostroboscopy, and questionnaire data [16] are the information sources to be used in the analysis. This paper is concerned with automated characterization of image sequences obtained from laryngeal videostroboscopy into a healthy class and two classes of disorders.

2. The data

The medical task considered in this paper concerns laryngeal colour image sequences, based automated categorization of laryngeal disorders into three decision classes: *healthy* and two *pathological* classes, namely *diffuse* and *nodular* mass lesions of vocal folds [7]. Mass lesions of vocal folds could be categorized into six classes namely, *polypus*, *papillomata*, *carcinoma*, *cysts*, *keratosis*, and *nodules*. This categorization is based on clinical signs and histological structure of the mass lesions of vocal folds. We distinguished two groups of mass lesions of vocal folds i.e. *nodular* lesions (localized thickenings)—*nodules*, *polyps*, and *cysts*—and *diffuse* lesions—*papillomata*, hyperplastic laryngitis with *keratosis*, and *carcinoma*.

The data have been recorded at the Department of Otolaryngology, Kaunas University of Medicine, Lithuania. The image sequences were acquired during routine videostroboscopy. The duration of one image sequence was equal to 4s. The resolution of 720×576 pixels was used to record the image sequences.

3. Features

Various types of features characterizing colour, texture, and geometry of biological structures seen in

colour images of vocal folds can be extracted [8,17,18]. Features characterizing distribution of image colour is used in this study.

The approximately uniform $L^*a^*b^*$ colour space [19] was employed to represent colours. We characterize the colour content of an image by the probability distribution of the colour represented by the 3-D colour histogram of $N = 4096$ ($16 \times 16 \times 16$) bins and consider the histogram as an N -vector. Most of bins of the histograms were empty or almost empty. Therefore, to reduce the number of components of the N -vector, the histograms built from a set of training images were summed up and the N -vector components corresponding to the bins containing less than N_α hits in the summed histogram were left aside. Hereby, when using $N_\alpha = 10$ we were left with 733 bins — a ψ vector of measurements with 733 components.

Having a vector of measurements ψ , the feature vector \mathbf{x} is computed in the following way. We assume that κ is a kernel [20] and Φ is a mapping of ψ onto the feature space F , such that $\kappa(\psi_i, \psi_j) = \langle \Phi(\psi_i), \Phi(\psi_j) \rangle$, where $\langle \cdot, \cdot \rangle$ stands for the inner product. Let $\tilde{\Phi}(\psi_i)$ denote the centered data point in the feature space F

$$\tilde{\Phi}(\psi_i) := \Phi(\psi_i) - \frac{1}{M} \sum_{i=1}^M \Phi(\psi_i) \quad (1)$$

with M being the number of data points. The features x are then given by the kernel principal components (kPC) computed as projections of the centered Φ -pattern $\tilde{\Phi}(\psi)$ onto the eigenvectors

$$\mathbf{v} = \sum_{i=1}^M \alpha_i \tilde{\Phi}(\psi_i) \quad (2)$$

of the covariance matrix $K_{ij} = \langle \tilde{\Phi}(\psi_i), \tilde{\Phi}(\psi_j) \rangle$ of the centered data points, where the expansion coefficients α_i of the eigenvector are found from the eigenvalue problem

$$\lambda \boldsymbol{\alpha} = \mathbf{K} \boldsymbol{\alpha}, \quad (3)$$

where the solutions $\boldsymbol{\alpha}$ are normalized by requiring $\lambda \langle \boldsymbol{\alpha}, \boldsymbol{\alpha} \rangle = 1$. Thus, the feature x is given by

$$x = \langle \mathbf{v}, \tilde{\Phi}(\psi) \rangle = \sum_{i=1}^M \alpha_i \langle \tilde{\Phi}(\psi_i), \tilde{\Phi}(\psi) \rangle. \quad (4)$$

The optimal number of components (features) used is determined experimentally.

4. The classifier

Depending on the definition of the optimization problem, several forms of support vector machine (SVM) can be distinguished, for example, 1-norm or 2-norm SVM. Assuming that $\Phi(\mathbf{x})$ is the non-linear mapping of the data point \mathbf{x} into the new space, the 1-norm soft margin SVM can be constructed by solving the following minimization problem:

$$\min_{\mathbf{w}, b, \xi} \frac{1}{2} \mathbf{w}^T \mathbf{w} + \gamma \sum_{i=1}^M \xi_i \quad (5)$$

subject to

$$y_i (\langle \mathbf{w}, \Phi(\mathbf{x}_i) \rangle + b) \geq 1 - \xi_i, \\ \xi_i \geq 0, \quad i = 1, \dots, M, \quad (6)$$

where \mathbf{w} is the weight vector, $y_i = \pm 1$ is the desired output (± 1), M is the number of training data points, $\langle \cdot \rangle$ stands for the inner product, ξ_i are the slack variables, b is the threshold, and γ is the regularization constant controlling the trade-off between the margin and the slack variables. The discriminant function for a new data point \mathbf{x} is given by:

$$f(\mathbf{x}) = \mathcal{H} \left[\sum_{i=1}^M \alpha_i^* y_j k(\mathbf{x}, \mathbf{x}_i) + b^* \right], \quad (7)$$

where $k(\mathbf{x}, \mathbf{x}_i)$ stands for the kernel and the Heaviside function $\mathcal{H}[y(\mathbf{x})] = -1$, if $y(\mathbf{x}) \leq 0$ and $\mathcal{H}[y(\mathbf{x})] = 1$ otherwise. The optimal values α_i^*, b^* of the parameters α_i and b are found during training.

4.1. Least squares SVM

Suykens and Vandewalle [21] have introduced a least squares version of the SVM classifier (LS-SVM). We use this type of SVM in this work. Parameters of the LS-SVM are estimated by solving the following optimization problem:

$$\min_{\mathbf{w}, b, \mathbf{e}} \frac{1}{2} \mathbf{w}^T \mathbf{w} + \gamma \frac{1}{2} \sum_{i=1}^M e_i^2 \quad (8)$$

subject to

$$y_i (\langle \mathbf{w}, \Phi(\mathbf{x}_i) \rangle + b) = 1 - e_i, \quad i = 1, \dots, M. \quad (9)$$

The main difference between the LS-SVM and SVM is the equality constraints (Eq.(9)) used in LS-SVM instead of unequally constraints defined by Eq.(6). Due to the equality constraints, the optimal parameter values can be found by solving a set of linear equations, instead of quadratic programming applied in the case of SVM. The solution is given by [21]

$$\left[\begin{array}{c|c} 0 & -\mathbf{y}^T \\ \hline \mathbf{y} & \mathbf{Z} + \gamma^{-1} \mathbf{I} \end{array} \right] \left[\begin{array}{c} b \\ \boldsymbol{\alpha} \end{array} \right] = \left[\begin{array}{c} 0 \\ \mathbf{1} \end{array} \right], \quad (10)$$

where $Z_{ij} = y_i y_j \kappa(\mathbf{x}_i, \mathbf{x}_j)$, \mathbf{I} is the identity matrix, $\mathbf{1} = [1_1, \dots, 1_M]$, $\mathbf{y} = [y_1, \dots, y_M]$, and $\boldsymbol{\alpha} = [\alpha_1, \dots, \alpha_M]$. Since an SVM is a binary classifier while the task is to distinguish between three classes, the one-against-one scheme is used to make the categorization in this work.

4.2. Kernel function

For $\kappa(\mathbf{x}_i, \mathbf{x}_j)$, one usually uses the linear: $\mathbf{x}_i^T \mathbf{x}_j$, Gaussian: $\exp\{-\|\mathbf{x}_i - \mathbf{x}_j\|^2 / \sigma\}$ or polynomial: $(\mathbf{x}_i^T \mathbf{x}_j + 1)^d$ kernel. The kernel is defined over a pair of vectors.

In this work, classification is based on a set of vectors rather than on a single vector. For example, a sequence of images is recorded from a patient. Each image is represented by a feature vector. Feature vectors are then collected into a matrix (each vector constitutes a matrix column) and used to make a decision. Therefore, a kernel function utilized by the LS-SVM classifier is defined over a pair of matrices (\mathbf{A}, \mathbf{B}) rather than over a pair of vectors. A positive definite kernel of such type has been recently proposed by Wolf and Shashua [22]. The authors use the principal angles between the two column spaces defined by the matrices (\mathbf{A}, \mathbf{B}) to assess the matching

between the spaces and derive a positive definite kernel based on that concept. The "QR" factorization of the matrices (\mathbf{A}, \mathbf{B}) and the kernel Gram-Schmidt orthogonalization process are used to derive the kernel. Applying the "QR" factorization the matrices (\mathbf{A}, \mathbf{B}) can be written as $\mathbf{A} = \mathbf{Q}_A \mathbf{R}_A$ and $\mathbf{B} = \mathbf{Q}_B \mathbf{R}_B$, where \mathbf{Q} is an orthonormal basis and \mathbf{R} is an upper-diagonal matrix of size $M \times M$ of the Gram-Schmidt coefficients representing the columns of the original matrix in the new basis. The principal angles $\cos(\theta_i)$ are given by the singular values σ_i of the matrix $\mathbf{Q}_A^T \mathbf{Q}_B$, $\cos(\theta_i) = \sigma_i, i = 1, \dots, M$. It was shown that

$$\kappa(\mathbf{A}, \mathbf{B}) = \det(\mathbf{Q}_A^T \mathbf{Q}_B)^2 = \prod_{i=1}^M \cos(\theta_i)^2 \quad (11)$$

is a positive definite kernel [22]. We use this kernel in our work. The algorithm for evaluating the kernel without explicit computation of \mathbf{Q}_A and \mathbf{Q}_B can be found in [22]. Only inner-products between the columns of \mathbf{A} and the columns of \mathbf{B} are used.

5. Experimental investigations

5.1. Experimental setup

Data were available from 30 patients. Amongst those, 10 patients belong to the nodular class, 12 to the diffuse class and 8 to the healthy class. There were 100 of image frames in one image sequence. However, only 10 image frames were used to estimate the kernel defined over a pair of matrices. Due to the small number of data points available for the experiments, the leave-one-out test [23] has been used to estimate the classification accuracy. The data used were normalized to zero mean and variance one. The polynomial kernel of degree $q = 1, 2$ and 3 has been used to extract the kernel principal components. The Gaussian kernel has been used to estimate the kernel defined over a pair of matrices.

5.2. Results

Table 1, Fig. 2, and Fig. 3 summarize results of the tests. In Table 1, shown is the number of kernel principal components used to characterize colour of one image frame along with the test data set classification accuracy.

Table 1. The test set data classification accuracy

# of kPC	5	7	8	9	10	11	13
Accuracy, %	33.0	44.9	69.8	85.7	78.3	72.1	63.3

The graph presented in Fig. 2 plots the correct classification rate of the test set data as a function of the percentage of the data variance accounted for by the number of the kernel principal directions used. As can be seen from Fig. 2, the percentage of the data variance accounted for by the optimal number of the components is close to 90. The graph presented in Fig. 3 relates classification accuracy the regularization constant γ , and the number of the kernel principal components used.

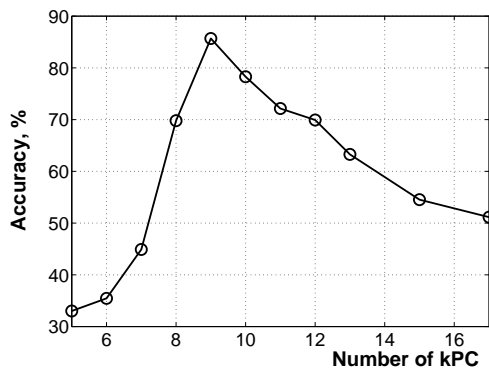


Fig. 2. The correct classification rate of the test set data as a function of the percentage of the data variance accounted for by the number of the kernel principal components used

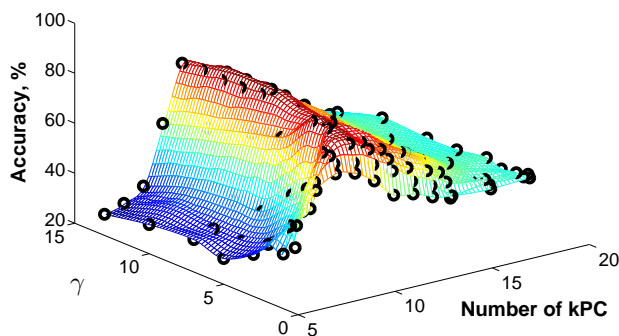


Fig. 3. The classification accuracy as a function of the regularization constant γ and the number of the kernel principal components used

6. Conclusions

Sequences of colour laryngeal images were categorized into the *healthy*, *nodular* and *diffuse* classes using an LS-SVM with a kernel defined over a pair of matrices. The relatively high classification accuracy obtained in the experimental tests encourages further studies in this area.

References

1. R. J. Moran, R. B. Reilly, P. de Chazal, P. D. Lacy, Telephony-based voice pathology assessment using automated speech analysis, *IEEE Trans Biomedical Engineering* 53 (3) (2006) 468–477.
2. J. I. Godino-Llorente, P. Gomez-Vilda, Automatic detection of voice impairments by means of short-term cepstral parameters and neural network based detectors, *IEEE Trans Biomedical Engineering* 51 (2) (2004) 380–384.
3. A. Gelzinis, A. Verikas, M. Bacauskiene, Automated speech analysis applied to laryngeal disease categorization, *Computer Methods and Programs in Biomedicine* 91 (1) (2008) 36–47.
4. J. F. R. Ilgner, C. Palm, A. G. Schutz, K. Spitzer, M. Westhofen, T. M. Lehmann, Colour texture analysis for quantitative laryngoscopy, *Acta Otolaryngologica* 123 (6) (2003) 730–734.
5. R. M. Haralick, K. Shanmugam, I. Dinstein, Textural features for image classification, *IEEE Trans System, Man and Cybernetics* 3 (6) (1973) 610–621.
6. A. Gelzinis, A. Verikas, M. Bacauskiene, Increasing the discrimination power of the co-occurrence matrix-

- based features, *Pattern Recognition* 40 (9) (2007) 2367–2372.
7. A. Verikas, A. Gelzinis, M. Bacauskiene, V. Uloza, Towards a computer-aided diagnosis system for vocal cord diseases, *Artificial Intelligence in Medicine* 36 (1) (2006) 71–84.
8. A. Verikas, A. Gelzinis, D. Valincius, M. Bacauskiene, V. Uloza, Multiple feature sets based categorization of laryngeal images, *Computer Methods and Programs in Biomedicine* 85 (3) (2007) 257–266.
9. M. Bacauskiene, A. Verikas, A. Gelzinis, D. Valincius, A feature selection technique for generation of classification committees and its application to categorization of laryngeal images, *Pattern Recognition* 42 (5) (2009) 645–654.
10. P. J. P. Poels, F. I. C. R. S. de Jong, H. K. Schutte, Consistency of the preoperative and intraoperative diagnosis of benign vocal fold lesions, *Journal of Voice* 17 (3) (2003) 425–433.
11. A. Verikas, A. Gelzinis, M. Bacauskiene, V. Uloza, Integrating global and local analysis of colour, texture and geometrical information for categorizing laryngeal images, *International Journal of Pattern Recognition and Artificial Intelligence* 20 (8) (2006) 1187–1205.
12. P. S. Popolo, I. R. Titze, Qualification of a quantitative laryngeal imaging system using videostroboscopy and videokymography, *Annals of Otolaryngology and Laryngology* 117 (6) (2008) 404–412.
13. H. Rihkanen, P. Reijonen, S. Lehtikainen-Soderlund, E. R. Lauri, Videostroboscopic assessment of unilateral vocal fold paralysis after augmentation with autologous fascia, *European Archives of Oto-Rhino-Laryngology* 261 (2004) 177–183.
14. S. Deguchi, Y. Ishimaru, S. Washio, Preliminary evaluation of stroboscopy system using multiple light sources for observation of pathological vocal fold oscillatory pattern, *Annals of Otolaryngology and Laryngology* 116 (9) (2007) 687–694.
15. S. H. Dailey, J. Kobler, R. E. Hillman, K. Tangrom, E. Thananart, M. Mauri, S. M. Zeitels, Endoscopic measurement of vocal fold movement during adduction and abduction, *Laryngoscope* 115 (1) (2005) 178–183.
16. A. Verikas, A. Gelzinis, M. Bacauskiene, V. Uloza, M. Kaseta, Using the patient’s questionnaire data to screen laryngeal disorders, *Computers in Biology and Medicine* 39 (2) (2009) doi:10.1016/j.compbiomed.2008.11.008.
17. A. Verikas, A. Gelzinis, M. Bacauskiene, D. Valincius, V. Uloza, A kernel-based approach to categorizing laryngeal images, *Computerized Medical Imaging and Graphics* 31 (8) (2007) 587–594.
18. A. Verikas, A. Gelzinis, M. Bacauskiene, V. Uloza, Intelligent vocal cord image analysis for categorizing laryngeal diseases, in: M. Ali, F. Esposito (Eds.), *Lecture Notes in Artificial Intelligence*, Vol. 3533, Springer-Verlag Heidelberg, 2005, pp. 69–78.
19. A. Verikas, K. Malmqvist, M. Bacauskiene, L. Bergman, Monitoring the de-inking process through neural network-based colour image analysis, *Neural Computing & Applications* 9 (2) (2000) 142–151.
20. J. Shawe-Taylor, N. Cristianini, *Kernel Methods for Pattern Analysis*, Cambridge University Press, Cambridge, UK, 2004.
21. J. A. K. Suykens, J. Vandewalle, Least squares support vector machine classifiers, *Neural Processing Letters* 9 (1999) 293–300.
22. L. Wolf, A. Shashua, Learning over sets using kernel principal angles, *Journal of Machine Learning Research* 4 (2003) 913–931.
23. A. Verikas, M. Bacauskiene, Using artificial neural networks for process and system modeling, *Chemometrics and Intelligent Laboratory Systems* 67 (2003) 187–191.

SYSTEM PARAMETERS IDENTIFICATION IN THE STATE SPACE

Leonas BALAŠEVIČIUS, Kęstas RIMKUS
 Department of Control Technology, Kaunas University of Technology, Lithuania

Abstract: This article presents the identification of the system parameters in the state space, by using an interface between Matlab/Simulink and the programmable logic controller (PLC). The effectiveness of the estimation of the parameters was tested by calculating the arithmetic mean of the response error between the responses of the real system and the system model with an observer into the input in the real time. It is shown that the Matlab/Simulink software could be used for identifying the system parameters in real time and setting the model parameters in the PLC.

Keywords: Programmable logic controllers, Matlab, Simulink, identification.

1. Introduction

One of the main problems of control is the identification of the parameters of the control object. The control designer must have the most exact possible mathematical description of the object. The evaluation of the precision of the control system becomes relevant only when the system works under unforeseen conditions. This way, the initial conditions may differ from the calculated ones, whereas the control and measurement signals may be distorted by noises that were not evaluated during the design of the system. That is why it is important to have as much information on the controlled object as possible while designing the control. In this article, the problem of the identification of the parameters of the object in the state space is researched. For this, a link between Matlab/Simulink and the PLC is used. The PLC processes the control and measurement signals and the design of the object model is executed by Matlab and is based on received parameters. The adequacy of the object model with an observer for a real object is tested in Matlab in real time.

2. State observer

The real system can be described in the state space:

$$\begin{aligned} \dot{x} &= Ax + Bu, \quad x(0) = x_0 \\ y &= Cx \end{aligned} \quad (1)$$

Here x is an n -dimensional state vector, u is an r -dimensional control vector, y is an m -dimensional output vector, A is an $m \times n$ system matrix, B is an $n \times r$ control matrix and C is an $m \times n$ output matrix, $x(0)$ is the state of a system at time $t_0=0$. Assuming that u is a continuous time function and according to the eigenvalues of matrix A , the system is stable. Also let us assume that the object is thoroughly observed and completely under control.

The problem is that the parameters of the object - A , B , C along with the state vector x , have to be evaluated by using only the input and output data of the real system. This can be done with the help of the observer [1]

$$\begin{aligned} \hat{\dot{x}} &= \hat{A}(t)\hat{x} + \hat{B}(t)u + K(t)(y - \hat{y}) \\ \hat{y} &= [0 \dots 1]\hat{x} \end{aligned} \quad (2)$$

Here \hat{x} is the estimated state vector, \hat{y} is the estimated output vector, \hat{A} is the estimated system matrix, \hat{B} is the estimated control matrix, K is the gain matrix of the state observer. The overall system structure of the estimation of the object parameters is shown in Fig. 1.

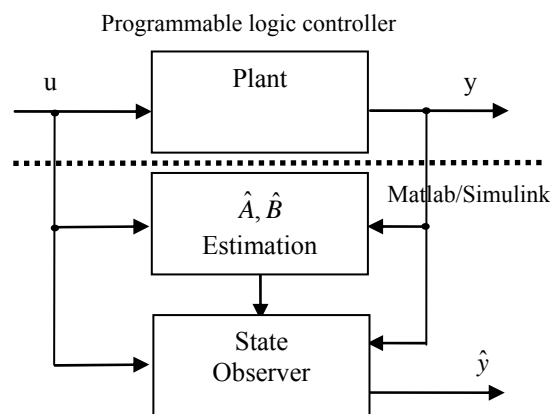


Fig. 1. System structure of the estimation of the object parameters

The response error e (hereinafter response error) between the responses of the real system and the system model with an observer into the input is calculated

$$e = y - \hat{y} \quad (3)$$

The object is connected to the PLC Modicon 140 CPU 113 03, which measures the input and output signals of the object. A Wonderware Modbus I/O server and Matlab/Simulink software are installed on a PC. The Wonderware Modbus I/O server is configured as written in [2]. The s – function blocks are used for the exchange of data between Matlab/Simulink and the Wonderware Modbus I/O server. These blocks are responsible for the plant model simulation in real time.

The program created in Matlab estimates the system parameters \hat{A} and \hat{B} .

The estimation of the object parameters is conducted in such order:

1. The order of the object is chosen and the initial values of matrixes \hat{A} , \hat{B} and \hat{C} are indicated. The initial values of matrix \hat{A} are chosen so that the system would be stable.
2. The unknown (to be estimated) elements of matrixes \hat{A} and/or \hat{B} are indicated.
3. The interval of data reading from the PLC is indicated – 100 ms.
4. Based on the values of the input and output signals the values of the elements of matrixes \hat{A} and \hat{B} are calculated [1].
5. Based on the evaluated description of the system in the state space, adaptive observer's gains are chosen by the trial and error method using simulations in order to achieve a good rate of convergence. Small gains may result in slow convergent rate, whereas large gains may make the differential equations "stiff" and difficult to solve numerically on a digital computer [1].
6. The adequacy of the system model response to the real object response to the same input signal is verified by calculating the arithmetic mean of the response error.

$$AME = \frac{1}{n} \sum_{i=1}^n |e(i)| \quad (4)$$

Here AME is arithmetic mean of the response error, n is the number of points of the calculated response error.

3. Second-order object parameters estimation

The created Matlab program will be verified by evaluating the parameters of the second-order object (see Fig. 2), connected to the PLC, in state space.

A second-order state space model with an observer will evaluate the parameters of the object. The following values for the initial values of matrixes \hat{A} , \hat{B} and \hat{C} are chosen:

$$\hat{A} = \begin{bmatrix} -2 & 0 \\ 0.154 & -0.154 \end{bmatrix}, \hat{B} = \begin{bmatrix} 2 \\ 0 \end{bmatrix}, \hat{C} = [0 \ 1]$$

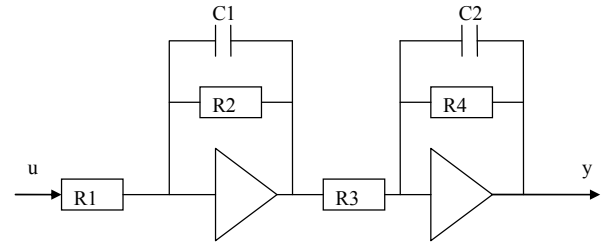


Fig. 2. The scheme of the second-order object ($R1 = 50 \text{ k}\Omega$; $R2 = 100 \text{ k}\Omega$; $R3 = 100 \text{ k}\Omega$; $R4 = 100 \text{ k}\Omega$; $C1 = 5 \mu\text{F}$; $C2 = 65 \mu\text{F}$)

It is indicated that the elements of matrixes \hat{A} and \hat{B} are evaluated. By using the values of the input and output signals of the object the evaluated values of matrixes \hat{A} and \hat{B} are acquired.

$$\hat{A} = \begin{bmatrix} -4.1032 & 0 \\ -0.0291 & -0.0194 \end{bmatrix}, \hat{B} = \begin{bmatrix} 1.9681 \\ 0.0498 \end{bmatrix}$$

The values of the gain matrix of the observer are:

$$K = [4956.6 \quad -0.01943]^T$$

These values continue to remain unchanged.

The responses of the object and the second-order state space model with an observer to the input signal of the object are presented in Fig. 3.

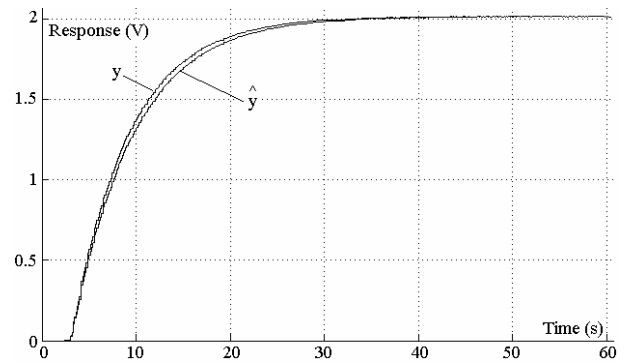


Fig. 3. The responses of the object and the second-order state space model with an observer to the input signal u of the object

The variation of the response error e is presented in Fig. 4.

The AME value is 1.62×10^{-2} .

There has been a research on what influence the selection and evaluation of the initial values of matrix \hat{A} , when the matrixes \hat{B} and \hat{C} are unchanged, have on the arithmetic mean of the response error (see Table 1).

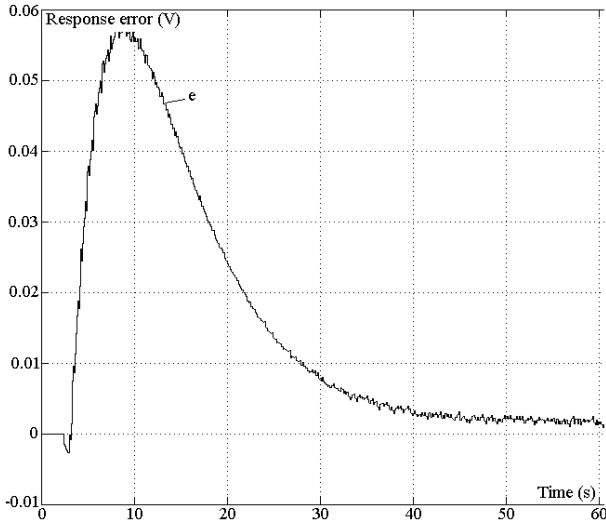


Fig. 4. Response error to the input signal of the object

Table 1. The influence of the selection of the initial values of matrix \hat{A} to the AME

$\hat{a}_{ii}, i=1,2$	AME
-20; -1	3.0254×10^{-4}
-200; -10	3.5039×10^{-4}
-0.2; -0.01	1.6916×10^{-4}
-0.2; -0.2	2.538×10^{-4}
-20; -20	4.6×10^{-4}
-36; -36 – after additionally selecting the remaining elements from matrix \hat{A}	3.9136×10^{-4}

After that a research has been conducted on what influence the selection of the initial values of matrix \hat{B} has on the value of arithmetic mean of the response error, when matrix

$$\hat{A} = \begin{bmatrix} -36.204 & 0 \\ 0 & -3 \end{bmatrix}$$

And the elements of matrix \hat{B} and the eigenvalues of matrix \hat{A} are evaluated (see Table 2).

Table 2. The influence of the selection of the initial values of matrix \hat{B} to the AME

$b_i, i=1,2$	AME
5; 2	3.3043×10^{-5}
0.1; 5	2.8067×10^{-5}
0.2; 0.2	3.0379×10^{-5}
20; 20	4.0738×10^{-5}

Initial values of the system poles and the control matrix influence the accuracy of the system.

4. Third-order object parameters estimation

The parameters of the third order object (see Fig. 5), connected to the PLC, will be evaluated in the state space.

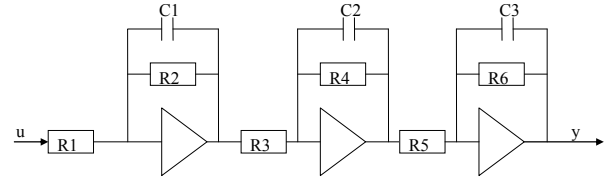


Fig. 5. The scheme of the third-order object ($R1 = 1\text{M}\Omega$; $R2 = 1\text{M}\Omega$; $R3 = 1\text{M}\Omega$; $R4 = 1\text{M}\Omega$; $R5 = 1\text{M}\Omega$; $R6 = 1\text{M}\Omega$; $C1 = 5\text{ }\mu\text{F}$; $C2 = 1\text{ }\mu\text{F}$; $C3 = 5\text{ }\mu\text{F}$)

A third-order state space model with an observer will evaluate the parameters of the object. The following values are the initial values for matrixes \hat{A} , \hat{B} and \hat{C} :

$$\hat{A} = \begin{bmatrix} -0.3 & 0 & 0 \\ 0 & -0.2 & 0 \\ 0 & 0 & -0.5 \end{bmatrix}, \hat{B} = \begin{bmatrix} 1 \\ 0 \\ 0 \end{bmatrix}, \hat{C} = [0 \ 0 \ 1]$$

It is indicated that only the elements in the diagonals of the matrix \hat{A} are evaluated. By using the values of the input and output signals of the object the evaluated matrix \hat{A} is acquired.

$$\hat{A} = \begin{bmatrix} -0.19547 & 0 & 0.2 \\ 0 & -0.2 & 0 \\ 0.145 & 0 & -0.898 \end{bmatrix}$$

The values of the gain matrix of the observer are:

$$K = [910.6911 \ 181.8901 \ 181.8901]^T$$

These values continue to remain unchanged.

The responses of the object and the third-order state space model with an observer to the input signal of the object are obtained. The variation of the response error e is presented in Fig. 6.

The AME value is 1.3555×10^{-4} .

There has been a research on what influence the selection and evaluation of the initial values of matrix \hat{A} , when matrixes \hat{B} and \hat{C} are unchanged, have on arithmetic mean of the response error (see Table 3), when the object is approximated by a third order state space model with an observer.

There will be an evaluation on the parameters of the object with a second-order state space model with an observer.

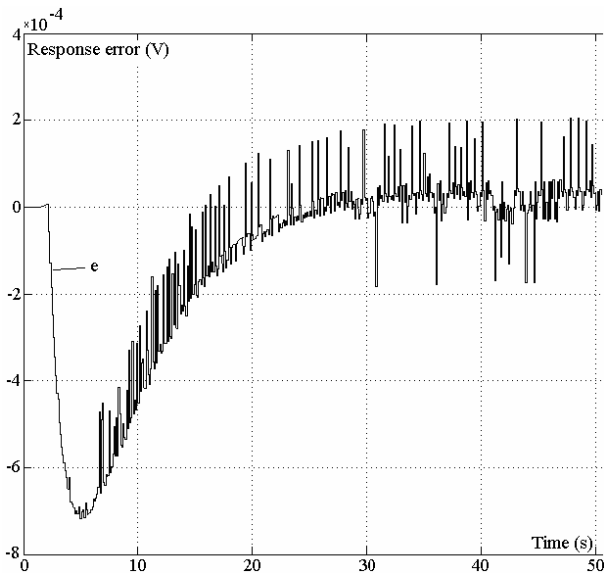


Fig. 6. Response error the input signal of the object

Table 3. The influence of the selection of the initial values of matrix \hat{A} to the AME

$\hat{a}_{ii}, i = 1,2,3$	AME
-3; -0.2; -4	4.252×10^{-4}
-0.3; -0.2; -0.5	1.3555×10^{-4}
-10; -5; -20	2.2967×10^{-4}
-10; -5; -20 – after additionally selecting the remaining elements from matrix \hat{A}	1.0642×10^{-4}

The following values are the initial values for matrixes \hat{A} , \hat{B} and \hat{C} :

$$\hat{A} = \begin{bmatrix} -10 & 0 \\ 0 & -5 \end{bmatrix}, \hat{B} = \begin{bmatrix} 1 \\ 0 \end{bmatrix}, \hat{C} = [0 \ 1]$$

It is indicated that only the elements of matrix \hat{A} are evaluated. By using the values of the input and output signals of the object the evaluated matrix \hat{A} is obtained.

$$\hat{A} = \begin{bmatrix} -14.739 & 3.1817 \\ 31.343 & -8.9445 \end{bmatrix}$$

The values of the gain matrix of the observer are:

$$K = [910.9611 \ 181.8901]^T$$

These values continue to remain unchanged. The variation of the response error e is presented in Fig. 7. The AME value is 1.9856×10^{-4} . There has been a research on what influence the selection and evaluation of the initial values of matrix \hat{A} , when matrixes \hat{B} and \hat{C} are unchanged, have on arithmetic mean of the response error (see

Table 4), when the object is approximated by a second order state space model with an observer.

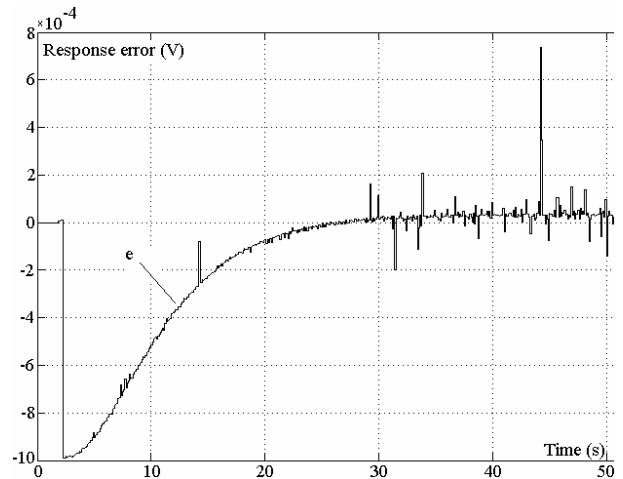


Fig. 7. Response error to the input signal of the object

Table 4. The influence of the selection of the initial values of matrix \hat{A} to the AME

$\hat{a}_{ii}, i = 1,2$	AME
-10; -5	1.9856×10^{-4}
-1; -0.5	9.6398×10^{-5}
-1; -0.5 – after additionally selecting the remaining elements from matrix \hat{A}	1.33×10^{-4}

6. Conclusions

It can be stated that the initial values of matrix \hat{A} should be chosen in a canonical form to make the system stable. The accuracy of the system model is mostly influenced by the initial values of the system poles and the control matrix.

There was no significant increase in the AME value after approximating a real object with a lower-order state space model with an observer.

Such observed behaviour is valid in the analyzed case, and the AME could be higher in the case of a high-order object if its parameters are different from the ones chosen in this article.

Unknown-order real object approximation could be started from a lower-order state space model with an observer and the order of the model should be increased until the desired AME value is obtained.

7. References

- Ioannou P. and Sun J. Robust Adaptive Control. Prentice-Hall, Inc., Upper Saddle River, NJ, 1995. 825 p.
- Balaševičius L., Dervinis G. and Šiožinys M. Communications between programmable logical controllers and Matlab/Simulink. Proceedings of International Conference “Electrical and Control Technologies – 2008”, Kaunas, 2008. p. 5-8.

MODEL OF CURRENT SPACE VECTOR CONTROL

Robertas JANICKAS, Algirdas SMILGEVIČIUS
 Vilnius Gediminas Technical University, Lithuania

Abstract: space vector control Simulink model is developed and investigated. Physical phenomena occurring in AC motor during mentioned control usage and results are discussed.

Keywords: vector control, space vector control, motor investigation, indirect vector control.

1. Introduction

Induction motor rotation speed depends on three phase grid frequency and motor pole number. If motor is powered from standard grid, its synchronous speed is constant. However, very often motor rotation speed shall be controlled in accordance with the process requirements and for energy saving purpose.

Yet, a single ability to control speed only is not enough. For precision measurements and specific process requirements it is necessary to maintain precision rotation speed when the load changes or the system is influenced by disturbances.

Europe market investigations show that frequency converters market is constantly growing. This is conditioned by competitive prices, in the long term such devices development expand their application areas for the best process control and energy saving. Implementing one popular contemporary science idea as self-diagnostic ability without usage additional sensors by using „soft sensor” technique may be implemented both in frequency converter and in motor control system. Due to this, more investigations and studies has been carried out [1, 2, 3]. Simulation is safe and not an expensive investigation alternative that is applicable for investigation of extreme conditions and for developing “soft sensor” models creating. This paper deals with elaborated Simulink model and simulation results at different inertia of the system and speed reverse as well as tracking the reference signal.

2. Vector control principle

In a three-phase induction motor, the currents are controlled in each of the phase windings in such a way

as to establish a magnetic field in the rotor and cause the rotor to align with the field flux. Then, by properly controlling the currents producing stator field the torque, developed by motor and the speed are controlled. Such technique, described above is called field-oriented control. Two reference frames shown in Fig. 1, Park’s and Clarke’s are used to simplify mathematical model of induction motor.

For required greater torque, greater i_q value is needed. For greater rotor flux, greater i_d is regarded. Knowing these two values, it is possible to solve for the vector that represents developed torque of a motor. By feeding i_d , i_q , by command values from controller, result values are generated that may be used to correct the motion of position, velocity, or torque in the device.

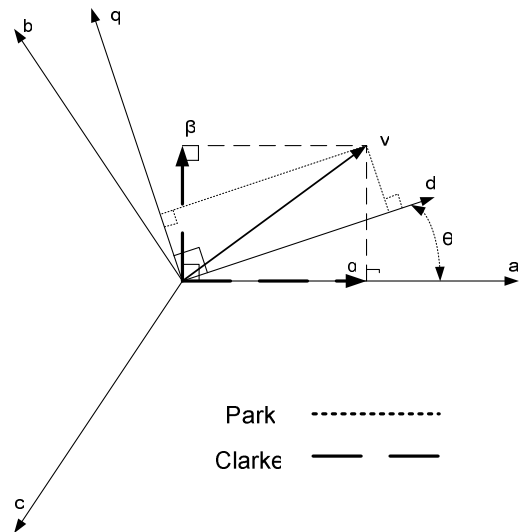


Fig. 1. Currents vectors

3. Indirect field orientation control

For very low-speed operations and for positioning control, the use of flux sensing that relies on integration which has a tendency to drift may not be acceptable. A commonly-used alternative is indirect field orientation, which does not rely on the measurement of the air gap

flux. Torque can be controlled by regulating, i_{qs}^e and slip speed, $\omega_e - \omega_r$. Rotor flux can be controlled by maintaining i_{ds}^e . Subscript denotes reference frame, rotating with synchronous speed. Given some desired level of rotor flux, λ_r^* , the desired value of necessary i_{ds}^{e*} may be obtained from [4, 5]:

$$\lambda_r^* = \frac{r_r L_m}{r_r + L_r p} i_{ds}^{e*}. \quad (1)$$

The desired torque of T_{em}^{e*} at the given value of rotor flux is calculated as:

$$T_{em}^{e*} = \frac{3}{2} \frac{P}{2} \frac{L_m}{L_r} \lambda_r^* i_{ds}^{e*}. \quad (2)$$

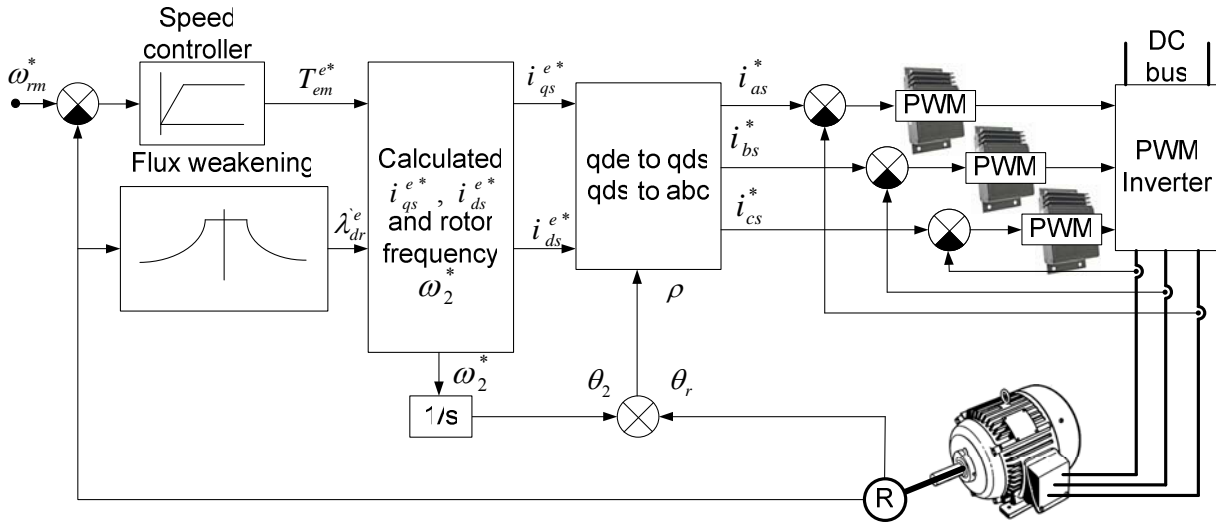


Fig. 2. Indirect field-oriented control of a current regulated PWM inverter induction motor drive

If orthogonal outputs of the form $\cos\theta_r$ and $\sin\theta_r$ are available from the shaft encoder, the values of $\cos\rho$ and $\sin\rho$ can be generated from the following trigonometric identities [4]:

$$\begin{aligned} \cos\rho &= \cos(\theta_r + \theta_2) = \cos\theta_r \cos\theta_2 - \sin\theta_r \sin\theta_2; \\ \sin\rho &= \sin(\theta_r + \theta_2) = \sin\theta_r \cos\theta_2 + \cos\theta_r \sin\theta_2. \end{aligned} \quad (4)$$

Simulation model is created by using one of MATLAB program package SIMULINK. In this program space vector controlled induction motor model is developed by using standard function blocks (Fig. 3) [5].

It has been shown that when properly oriented i_{dr}^e is equal to zero and $\lambda_{dr}^e = L_m i_{ds}^{e*}$ thus, the slip speed relation can also be written as:

$$\omega_2^* = \omega_e - \omega_r = \frac{r_r}{L_r p} \frac{i_{qs}^{e*}}{i_{ds}^{e*}}. \quad (3)$$

The above conditions, if satisfied, ensure the decoupling of the rotor voltage equations to what extent this decoupling is actually achieved will depend on the accuracy of motor parameters used.

Developed indirect field-oriented control scheme for a current controlled PWM induction motor drive is presented in Fig. 2. The field orientation, ρ , is the sum of the rotor angle given by position sensor, θ_r , and the angle, θ_2 , obtained by integrating the slip speed [6, 7, 8, 9, 10].

4. Simulation of transients

Simulation results which were got from Fig. 3 are shown in Fig 4. The greatest current value at starting reaches 110 A, but after motor starting, steady state currents amplitudes are approximately 25 A at motor starting without load. The torque change low is – from 0.5 s suddenly grows to nominal, from 1 s its goes down to half of nominal torque of machine, next from 1.25 s it grows to nominal and after 1.5 s its drop to zero. Response to that function can be seen in the second graph. During the load torque changing, motor windings currents change also. They repeat load changing behaviour.

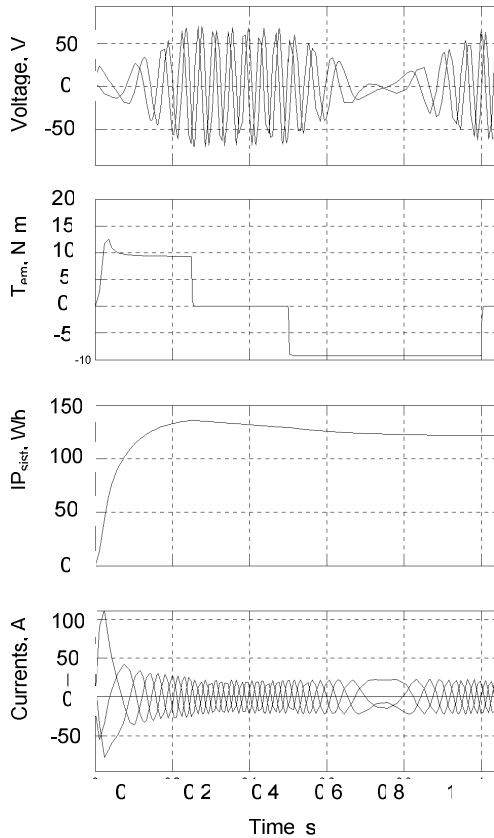


Fig. 6. Curves with changed speed reference function and reversing

From Fig. 8 and 7 rotation speed lag from set point signal is monitored. Speed lag from set point determined by motor inertia and control system existing disturbances as load torque changes.

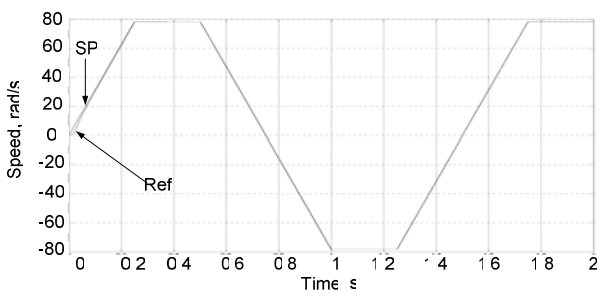


Fig. 7. Speed reference and speed response in current space vector control system

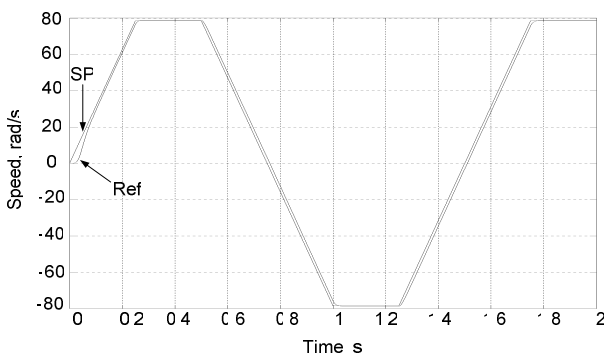


Fig. 8. Motor speed curves at ten times increased inertia

6. Conclusions

Simulink model of current space vector control is created.

Acquired simulation results allow making these conclusions:

1. Developed motor torque shows that during the start-up a slight overshoot exists. After the system start-up, the applied torque is changed by proper low for investigation of changes of motor.
2. The current composes constant part conditioned by motor resistances and variable part conditioned by motor load.
3. The speed error at motor starting due to static friction is insignificant.
4. PWM space vector control way allows using by order slower microprocessors practically without loss converter output signal quality.

7. References

1. Bierke S. Enhanced control of an alternating current motor using fuzzy logic and a TMS320 digital signal processor, Texas Instruments, 1996. 524 p.
2. Valentine R., Motor control electronics handbook [CD-ROM] 1998.
3. Kliuchev I.V. Theory of electrical drives. (In Russian) Moscow: Energoatomizdat, 1985. 253 p.
4. Holts J. Pulsewidth modulation - a survey, IEEE, 1992, 13 p.
5. Caron J.P., Hautier J.P. Modelling and Control of Induction Machine. Technip Edition, France, 1995, 312 p.
6. Field Orientated Control of 3-Phase AC-Motors. Application report, Texas Instruments, USA, 1998, 473 p.
7. Hazzab A., Bousserhane I.K., Kamli M., Rahli M. New Adaptive fuzzy PI-Sliding Mode Controller for Induction Machine Speed Control. Third IEEE International Conference on Systems, Signals & Devices SSD'05, Tunisia, 2005. 125 p.
8. Hazzab A., Bousserhane I.K., Kamli M., Rahli M. Design of fuzzy sliding mode controller by genetic algorithms for induction machine speed control. Third IEEE International Conference on Systems, Signals & Devices SSD'05, Tunisia, 2005. 56 p.
9. Lorenz R.D., Lawson D.B. Simplified A Approach to Continuous On-Line Tuning of Field-Oriented Induction Machine Drives. IEEE Trans. On Industry application, Vol.26, Issue 3, May/June 1990. 425 p.
10. Geleževičius V., Kriščiūnas K., Kubilius V. Control systems of electrical drives. (In Lithuanian) Vilnius: Mokslas, 190. 360 p.

PARAMETER ESTIMATION OF INDUCTION MOTOR AT LOCKED ROTOR

Andrius PETROVAS, Roma RINKEVIČIENĖ, Saulius LISAUSKAS
 Vilnius Gediminas Technical University, Lithuania

Abstract: Design of control systems of electrical drives deals with motor parameters whose assessment is important and complex problem. Proposed method allows estimating induction motor parameters on the base of transients of motor with locked rotor.

Keywords: induction motor, transients, parameter estimation.

1. Introduction

Advanced sensorless control of electric drives deals with computer models of motors. Mathematical model of direct current motor is simpler than induction motor, therefore problems of their parameters estimation are solved also simpler [1, 2].

Development and investigation of modern induction drives requires using models of induction motors. Just more or less exact parameters give sufficient operation of a model. Some of parameters, such as resistances of stator windings, can be measured quite easy. Nevertheless some of them require a lot of preparations. Therefore estimation of induction motor parameters is state of the art in modern electric drives.

For estimation of induction motor parameters usually two conventional experiments should be made: i. e. no load and locked rotor experiments. The first one allows calculating stator parameters, the second one – rotor parameters. The stator resistance may be measured through a d.c. voltage test with two phases in series. Calculation of other equivalent circuit parameters using motor catalogue data is presented in [3]. All these parameters are calculated from steady-state currents and voltages [4, 5].

The paper deals with estimation of motor parameters just from results of locked rotor experiments. The method differs from conventional one, using steady-state values of parameters by exploring all information for estimation from transient process.

2. Mathematical model of induction motor

Induction motor with locked rotor can be assumed as three-phase transformer with short circuit, placed across

the secondary winding. Symmetrical induction motor can be replaced by equivalent two-phase transformer. Magnetic coupling does not exist between equivalent two-phase machine orthogonal windings; therefore each of them can be analyzed separately. System of similar windings is shown in Fig. 1.

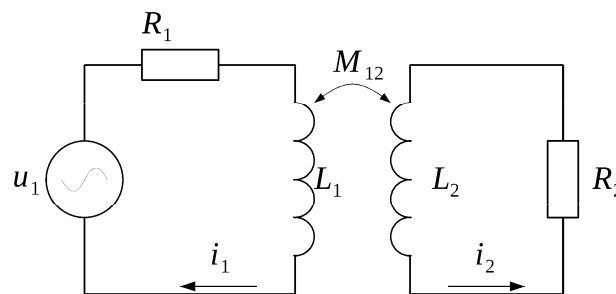


Fig. 1. Equivalent circuit of induction motor with locked rotor

The circuit, presented in Fig. 1 is described by set of differential equations in this way:

$$\begin{cases} L_1 \frac{di_1}{dt} + M_{12} \frac{di_2}{dt} = u_1 - i_1 R_1, \\ M_{12} \frac{di_1}{dt} + L_2 \frac{di_2}{dt} = -i_2 R_2, \end{cases} \quad (1)$$

where u_1 is stator supply voltage, L_1 and L_2 are inductances of stator and rotor windings, R_1 and R_2 are resistances of stator and rotor windings, i_1 and i_2 currents in the stator and rotor windings.

Set of equations (1) is the set of first order linear differential equations; therefore its solution can be obtained by analytical way. Canceling current of rotor winding i_2 , the equation, relating stator current i_1 and voltage u_2 looks like this:

$$\begin{aligned} \frac{d^2 i_1}{dt^2} + \frac{R_1 L_2 + R_2 L_1}{L_1 L_2 - M_{12}^2} \frac{di_1}{dt} + \frac{R_1 R_2}{L_1 L_2 - M_{12}^2} i_1 &= \\ = \frac{L_2}{L_1 L_2 - M_{12}^2} \frac{du_1}{dt} + \frac{R_2}{L_1 L_2 - M_{12}^2} u_1. \end{aligned} \quad (2)$$

Solution of differential equation (2) consists of natural and forced solutions. Homogeneous equation is:

$$\frac{d^2 i_1}{dt^2} + \frac{R_1 L_2 + R_2 L_1}{L_1 L_2 - M_{12}^2} \frac{di_1}{dt} + \frac{R_1 R_2}{L_1 L_2 - M_{12}^2} i_1 = 0. \quad (3)$$

The roots of characteristic equation have the form:

$$\lambda_{1,2} = \frac{1}{2} \left[\frac{-\frac{R_1 L_2 + R_2 L_1}{L_1 L_2 - M_{12}^2} \pm \sqrt{\left(\frac{R_1 L_2 + R_2 L_1}{L_1 L_2 - M_{12}^2}\right)^2 - \frac{4R_1 R_2}{L_1 L_2 - M_{12}^2}}}{2} \right], \quad (4)$$

where $\lambda_{1,2}$ are roots of characteristic equation.

Analysis of square root (4) shows, that discriminant sign is always positive, therefore $\lambda_{1,2} \in R$ and solution of (3) has the form:

$$i_{1h} = C_1 \exp(\lambda_1 t) + C_2 \exp(\lambda_2 t), \quad (5)$$

where i_{1h} is general solution of homogeneous differential equation (3), C_1 and C_2 constants defined from initial conditions.

Solution of differential equation (3) is found as sum of general solution i_{1h} of homogeneous differential equation (3) and particular solution i_{1n} of non-homogeneous differential equation (2) which depends on input voltage u_1 . At $u_1 = U_{max} \sin(\omega t)$ the particular solution is found as:

$$i_{1n} = A \cos(\omega t) + B \sin(\omega t), \quad (6)$$

where A and B are constants found from initial conditions. i_{1n} is particular solution of non-homogeneous equation.

The general solution of (2) has the form:

$$i_1 = i_{1h} + i_{1n} = C_1 \exp(\lambda_1 t) + C_2 \exp(\lambda_2 t) + A \cos(\omega t) + B \sin(\omega t). \quad (7)$$

Free constants A and B , entering (7), are obtained by solution of system, presented below:

$$\begin{bmatrix} R_1 R_2 - \omega^2 (L_1 L_2 - M_{12}^2) & (R_1 L_2 + L_1 R_2) \omega \\ -(R_1 L_2 + L_1 R_2) \omega & R_1 R_2 - \omega^2 (L_1 L_2 - M_{12}^2) \end{bmatrix} \times \begin{bmatrix} A \\ B \end{bmatrix} = \begin{bmatrix} U_{max} \omega L_2 \\ U_{max} R_2 \end{bmatrix}. \quad (8)$$

Constants C_1 and C_2 , entering (7), are calculated from initial conditions. According to the first commutation law $i_1(0) = 0$, the set of equations gets a form:

$$\begin{bmatrix} 1 & 1 \\ \lambda_1 & \lambda_2 \end{bmatrix} \cdot \begin{bmatrix} C_1 \\ C_2 \end{bmatrix} = \begin{bmatrix} -A \\ -B \omega \end{bmatrix}. \quad (9)$$

Expressions (8) and (9) relate coefficients A , B , C_1 and C_2 of solution (7) with coefficients of differential equation. By experimental measurement values of i_1 and determining of coefficients A , B , C_1 and C_2 according to that, the inverse task can be solved, i. e., according to expressions (8) and (9) both coefficients of differential equation (2) and parameters of the circuit, shown in Fig. 1 can be found. This is the base of proposed and elaborated method.

3. Identification of the system

Estimation of induction motor parameter from transients' results at locked rotor corresponds to identification of parameters of the system presented in Fig. 1. At transients experimentally are recorded values of voltage u_{1n} and current i_{1m} , where $m = 1, 2, 3, \dots, N$. N is number of measured values. Task of identification should be solved successfully, if the proper values of parameters A , B , C_1 , C_2 , λ_1 and λ_2 of expression (7) could be found, matching with minimal error experimentally obtained expression i_{1m} with analytical expression i_1 . Therefore objective function can be determined by such Euclidean norm:

$$\|\Delta i\| = \sqrt{i_{1m}^2 - i_1^2(t_m)}; \quad m = 1, 2, \dots, N, \quad (10)$$

where $i_1(t_m)$ according to (7) at the moment of time t_m analytically calculated value of current i_1 .

Parameters A , B , C_1 , C_2 , λ_1 and λ_2 are related by (8) and (9) expressions. Expression (9) shows that C_1 and C_2 can be found from coefficients A , B , λ_1 and λ_2 . Therefore parameters A , B , λ_1 and λ_2 are independent, and they can be varied by optimizing algorithm.

Coefficients of characteristic equation are denoted as:

$$\begin{aligned} b &= (R_1 L_2 + R_2 L_1) / (L_1 L_2 - M_{12}^2), \\ c &= R_1 R_2 / (L_1 L_2 - M_{12}^2). \end{aligned}$$

At known λ_1 and λ_2 coefficients b and c can be obtained by Viète's formulas.

Additional notations are introduced:

$$\begin{aligned} d &= L_2 / (L_1 L_2 - M_{12}^2), \\ e &= R_2 / (L_1 L_2 - M_{12}^2). \end{aligned}$$

Unknown variables d , e , C_1 and C_2 are found by solving set of equations at any iteration:

$$\begin{bmatrix} U_m \omega & 0 & 0 & 0 \\ 0 & U_m & 0 & 0 \\ 0 & 0 & 1 & 1 \\ 0 & 0 & \lambda_1 & \lambda_2 \end{bmatrix} \begin{bmatrix} d \\ e \\ C_1 \\ C_2 \end{bmatrix} = \begin{bmatrix} A(c - \omega^2) + Bb\omega \\ -Ab\omega + B(c - \omega^2) \\ -A \\ -B\omega \end{bmatrix}. \quad (11)$$

The equation (7) is non-linear; therefore numerical methods of optimization should be used. For this purpose Nelder-Mead optimization algorithm is chosen. This method does not require any derivative information and is widely used to solve parameter estimation, where the function values are uncertain or subject to noise [6]. Because simplicity and popularity, it is implemented in many mathematical programs like Matlab and others. However other optimization methods could be used also.

During the search of minimal value of objective function vector $\mathbf{x} = [A, B, \lambda_1, \lambda_2]$ is being varied. Any iteration begins with calculation of coefficients b and c of characteristic equation. For this purpose the Viète's formulas are applied.

$$\lambda_1 + \lambda_2 = -b, \quad \lambda_1 \lambda_2 = c. \quad (12)$$

After that the values C_1, C_2 are obtained from set of equations (11). All coefficients $A, B, C_1, C_2, \lambda_1$ and λ_2 are used to calculate the values of i_1 . At the end of iteration the calculated values of i_1 is compared with experimentally obtained values i_{1n} . For comparison of both values the Euclidean norm (10) is used.

The input parameter \mathbf{X} of the program is matrix of five vertices $\mathbf{X} = [\mathbf{x}_1; \mathbf{x}_2; \dots; \mathbf{x}_5]$, where $\mathbf{x} \in \mathbb{R}^4$. Other input parameters α, β and γ are related to transformation of simplex: α – to reflection, β – to contraction, γ – to expansion. The standard values, used in most implementations, are $\alpha=1, \beta=0,5$ and $\gamma=2$.

Conventional Nelder-Mead algorithm is committed for search of termless extreme. In this case two of used variable parameters are roots of characteristic polynomial; they should be negative. Therefore conventional Nelder-Mead algorithm is supplemented by instructions, forbidding simplex vertices with $\lambda_1 > 0$ or $\lambda_2 > 0$. These actions are important just at simplex reflection and expansion operations. Obtained simplex vertices are checked for constraints, and if they do not meet those, i. e. if $\lambda_1 > 0$ or $\lambda_2 > 0$, simplex is reduced for giving new vertices to meet constraints.

4. Comparison experimental and approximated results

All equations were derived with assumption, that sine wave voltage was applied to the windings with initial phase, equal to zero. The equipment allowing switching voltage to windings at the instant when it crosses zero, was constructed and implemented for experiment. Proposed method cancels requirement to measure instantaneous value of voltage. Solution of this type allows refusing expensive voltage sensors.

Fig. 2 indicates the good matching between experimental and approximating current curves just in the end of transient time.

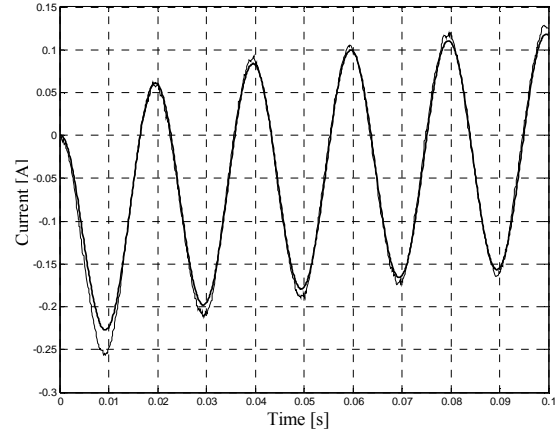


Fig. 2. Transients of current i_2 (1000 points)

The thicker line in the figure represents analytically obtained curve, approximating the experimental one. Dependence of error against time is presented in Fig. 3. Error reaches its maximum value at the beginning of transient and begins to reduce.

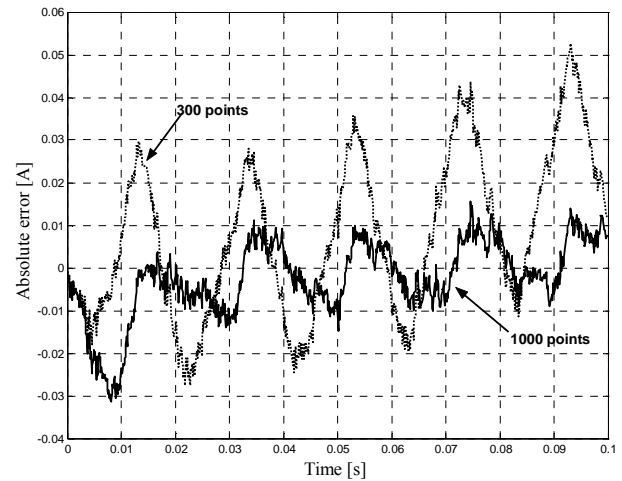


Fig. 3. Error of approximation

In the Table 1 experimentally determined and real parameter values are presented.

Table 1. Real and experimentally determined values

Parameter	1000 pt.	300 pt.	Real value
λ_1 [1/s]	-18.1	-18.95	-15.2
λ_2 [1/s]	-290	-45.8	-31.7
A [A]	0.133	0.151	0.116
B [A]	0.022	0.01	0.02
C_1 [A]	0.028	0.025	0.028
C_2 [A]	0.1	0.045	0.05

Results show the greatest error at determinations of decaying component and it occurs for the fastest decaying term $C_2 \exp(\lambda_2 t)$. Thus can be concluded, that proposed method is suitable to find harmonic

components of expression (7), and just coefficients A and B are estimated with the greater accuracy. Relative errors of estimation are:

$$\delta_A \approx \frac{|0.133 - 0.116|}{0.116} 100\% \approx 14.6\%,$$

$$\delta_B \approx \frac{|0.022 - 0.02|}{0.02} 100\% \approx 10\%.$$

Accuracy can be increased by cancelling of transients' points in the end of the process and in the same way reducing influence of harmonic components. Suppose the time interval $0 < t < 0.3$ s is chosen (300 points of measurement), then determined roots of characteristic equation get values $\lambda_1 = -18.2 \text{ s}^{-1}$ and $\lambda_2 = -45.8 \text{ s}^{-1}$. In this case the relative error of roots estimation is:

$$\delta_{\lambda_1} \approx \frac{|-18.96 + 15.2|}{-15.2} 100\% \approx -24.7\%,$$

$$\delta_{\lambda_2} \approx \frac{|-45.8 + 31.7|}{-31.7} 100\% \approx -44.5\%.$$

Nevertheless the accuracy of determining parameters A and B is reduced by reducing number of measured points. Current transient is shown in Fig. 4. The experiment was performed by taking 300 points of measurement.

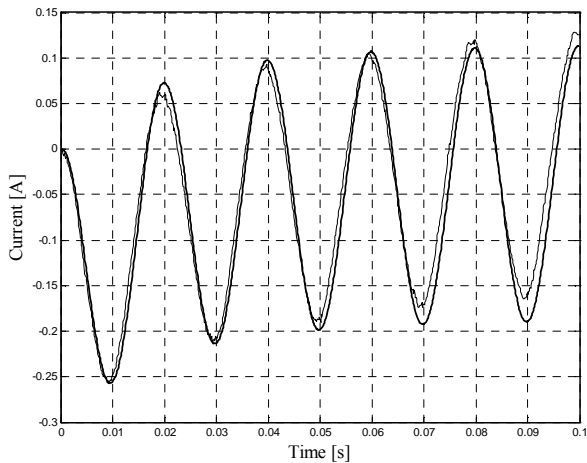


Fig. 4. Transients of current i_2 (300 points)

Approximation of current transient in the beginning of the process has evident great accuracy, but the error increases in the end of process. It can be seen from transient curve, shown in Fig. 5, where experiment includes 300 points.

6. Conclusions

1. Proposed method allows determining roots of characteristic equation and coefficients of general solution from experimental data.
2. Approximation of experimental measurement results is nonlinear problem requiring using discrete optimization methods.
3. Proposed method on the base of Euclidean norm as objective function allows approximating of solution of harmonic components with error not exceeding 15 % and is suitable for the system. It is not suitable for fast decaying exponential components due to great error.
4. Roots of characteristic equation, describing fast decaying components can be estimated with error, not exceeding 50 %, but accuracy of determining of harmonic coefficients reduces and general approximation error increases.

7. References

1. Rinkevičienė R., Petrovas A. Direct current drive with observer. *Elektronika ir Elektrotechnika. Electronics and Electrical Engineering*. 2008 Nr.5 (85). p. 53-56.
2. Rinkevičienė R., Petrovas A. Model of direct current drive with reduced order observer. 2nd International Conference on Electrical and control technologies, May 08-09, 2008. ECT-2008: proceedings of the 3rd international conference on electrical and control technologies. p. 150-153.
3. Boldea I., Nasar S.A. *The induction machine handbook*, CRC press, 2001. 950 p.
4. Chiasson J. *Modelling and high performance of electric machines*. Wiley – Interscience, 2005. 736 p.
5. Schröder D. *Elektrische Antriebe – Regelung von Antriebssystemen*. Springer – Verlag, 2001. 1172 p.
6. Singiresu S. Rao. *Engineering Optimization: Theory and Practice*, 3rd Edition. Wiley-Interscience, 1996. 920 p.

MODELLING OF AMMONIA PRODUCTION PROCESS

Giedrius OBERAUSKAS, Vytautas GALVANAUSKAS
Process Control Department, Kaunas University of Technology, Lithuania

Abstract: In this paper the detailed first principles mathematical model of industrial ammonia production process is elaborated. Mass balance equations and chemical reaction rate equations of the process are presented and analyzed. Computer simulation tests were performed using software tools created in Matlab program environment. The modelling results were compared with the experimental data and discussed.

Keywords: Mass balance, reaction rates, modelling, ammonia production process.

1. Introduction

In the context of this paper modelling of ammonia production process are representations of chemical process incorporating mass balance systems for key components, and mechanistic sub-models for modelling of absolute reaction rates.

Due to complex reaction systems in this process, like in all biotechnological and chemical processes [1, 2, 3], it is not possible to describe the process in details using only mechanistic models. Thus it is necessary to use methods that are able to fill some gaps in special chemical or engineering knowledge. Further expansions of the data and knowledge driven approaches used in chemistry engineering are mass balances systems. In the recently published literature, some interesting examples show, that hybrid combination of artificial neural networks, mechanistic kinetics and mass balance equations can lead to considerable advantages [1, 2, 3, 4]. Though, in chemistry one must work with many data of off-line or quasi-off-line types, and for this reason the above mentioned data must be generated using interpolation techniques. Regrettably, it may be challenged not only by some artificial disturbances, but also by accuracy of such interpolation methods. Moreover, in chemical technology one is most often interested in reaction rates, because they define the behaviour of the conversions in chemical processes. Rates have to be determined from the measured or estimated concentrations by differentiation. In this respect noisy

signals lead to even more distorted estimates of the specific reaction rates.

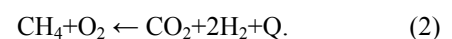
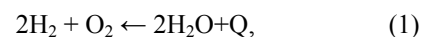
Thus, one needs a robust and effective process technique for models in chemical engineering while dealing with complex chemical processes that cannot be modelled with the necessary precision using only simple engineering correlations and mechanistic models.

2. Ammonia production process description

Modelling of ammonia production process will be performed using mass balances of the four distinct phases, i. e. secondary reforming, shift conversion, CO₂ removal, and methanation. The technological scheme of the process is presented in Fig. 1.

2.1 Secondary reforming

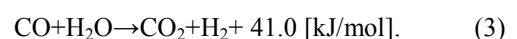
In the secondary reformer an internal combustion of the part of the gas and the process air takes place which also provides the nitrogen for the final synthesis gas.



In the conventional reforming process the degree of primary reforming is adjusted so that the air supplied to the secondary reformer meets both the heat balance and the stoichiometric synthesis gas requirement. The process gas is mixed with the air in a burner and then passed over a secondary reformer catalyst [6].

2.2 Shift conversion

Shift conversion consists of two levels. First level is average CO conversion and the second level is low CO conversion. At both levels CO parts are removed from process gas based on chemical equilibrium (3). The process gas from the secondary reformer is converted in the shift section according to the reaction:



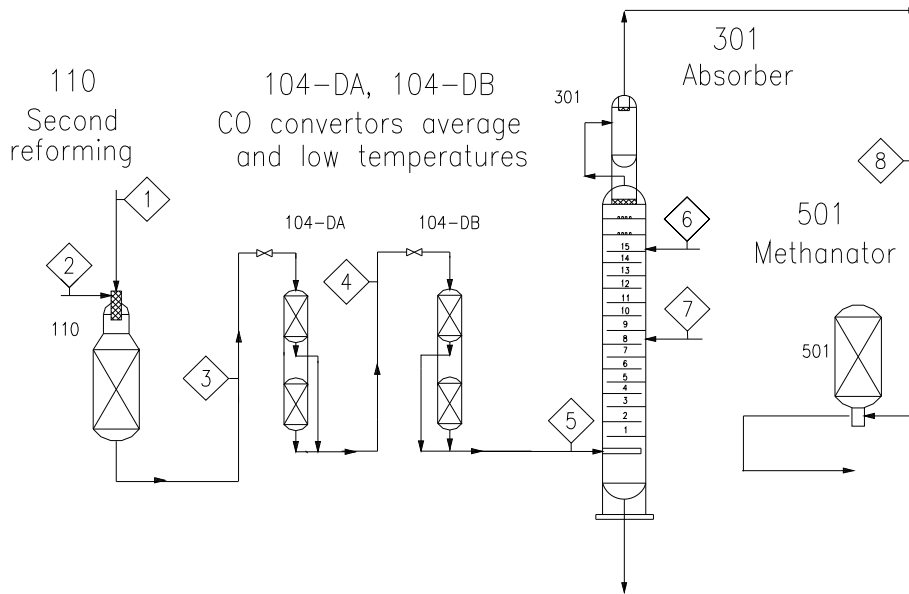
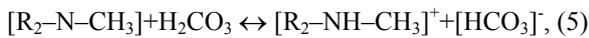


Fig. 1. Technological scheme of ammonia production process [7]

2.3 CO₂ removal

CO₂ removal process consists of absorber and stripper. Process gas from shift conversion is transferred to the absorber according to the chemical equilibriums (4–5):

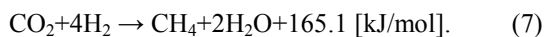
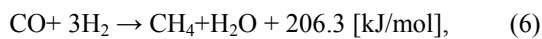


where R – HOCH₂CH₂ group.

The CO₂ is removed in a chemical or physical absorption process. The solvents used in chemical absorption processes are aqueous amine solutions. The solvent is regenerated using by stripping.

2.4 Methanation

The small amounts of CO and CO₂, remaining in the synthesis gas, are poisonous for the ammonia synthesis catalyst and must be removed by conversion to CH₄ in the methanator. The composition of the gas leaving the methanator follows the chemical equilibriums (6) and (7):



3. Mass balance equations of ammonia production process

Mass balance equations of the substances are based on mass preservation law, which means that part of particular concentration variation can be caused by chemical reactions, during which the elements of chemical reaction combine with each other to form a more complex product or decomposed into smaller compounds or elements. Additionally, the amount of

the component can change due to the feeding of the corresponding component into the reactor and due to the dilution effect. Differential equation of the mass balance for component C_{iout} is

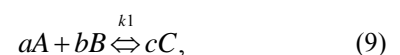
$$\frac{d(C_{iout})}{dt} = q_i C_i + C_{iin} \frac{F_{in}}{V} - C_{iout} \frac{F_{in}}{V}, \quad (8)$$

where C_{iout} – concentration of i -th component, [mol/l]; C_{iin} – concentration of i -th component in the flow, [mol/l]; $q_i C_i$ – i -th absolute reaction rate, [mol/(ls)]; V – volume, [l]; F_{in} – mass flow into the reaction volume, [l/s].

According to (1–7) chemical equilibriums and data from ammonia technological rules of procedure [7] the mass balances equations were elaborated.

Argon and nitrogen are inert gases, and for this reason they do not play a significant role in mass balances of the described chemical process.

The amounts of all participating components in a group of reactions can be expressed in terms of a number of key components equal to the number of independent stoichiometric relations. The independent rate equations will then involve only those key components. For multiple reactions, the procedure for finding the concentrations of all participating components starts by assuming that the reactions proceed consecutively. Intermediate concentrations are identified by subscripts. The resulting concentration from a particular reaction is the starting concentration for the next reaction in the series. The final value carries no subscript [6]. The compositions of the excess components will be expressible in terms of the key components. The absolute reaction rate equations for key components can be found as follows:



$$aA + cC \overset{k_2}{\rightleftharpoons} dD + bB, \quad (10)$$

where a, b, c , and d are empirical coefficients of chemical equilibriums; A, B, C , and D – components of chemical equilibriums; k_1 and k_2 – constants of reaction rates.

The absolute reaction rate for components in (9) and (10) are:

$$r_A = -ak_1A^aB^b - ak_2A^aC^c, \quad (11)$$

$$r_B = -bk_1A^aB^b + bk_2A^aC^c, \quad (12)$$

$$r_C = ck_1A^aC^c - ck_2A^aC^c, \quad (13)$$

$$r_D = dk_2A^aC^c, \quad (14)$$

where k_1 and k_2 – constants of reaction rates for (9) and (10) chemical equilibriums.

The equations (11-14) have to be solved numerically for A, B, C , and D as time functions. Alternatively, differential equations can be written and solved directly for the participating components as functions of time, thus avoiding the use of stoichiometric balances, although these are really involved in the formulation of the differential equations [6].

The constant of reaction rates taking into account the temperature effect on the process has an influence on the specific rate. The Arrhenius equation relates the absolute rate to the absolute temperature for chemical equilibrium (9):

$$k = k_0 \exp\left(-\frac{E}{RT}\right) = K \exp\left(a - \frac{b}{T}\right), \quad (15)$$

where a and b – empirical coefficients of chemical equilibriums; K and k_0 – coefficients of proportionality; E – activation energy, [J]; R – universal gas constant, [J/(K mol)].

When presumably accurate data deviate from linearity as stated by the last equation, the reaction is believed to have a complex mechanism [6].

Usually, absolute reaction rate of chemical process is not constant and depends on various factors, like process temperature, pressure, activation of catalyst, etc.

Coefficient of proportionality is necessary in order to taking into account not only the process temperature but also the process pressure, activation of catalyst and other important process parameters, which have influence on absolute reaction rate.

During the modelling mass balances of ammonia production process, the data from the ammonia technological rules of procedure [7] was used as reference. The data dimensions, like concentrations, flows and volumes, that do not agree with dimensions used in modelling of mass balances, are given in the text. E. g., in mass balances dimension of concentration is [mol/l], although in ammonia technological rules of procedure it is expressed in volumetric percents – the same as the values measured in the technological process. Concentration values were converted to the necessary dimension of concentration taking into account the process temperature and pressure (see Table 1):

$$V = \frac{nRT}{p}, \quad (16)$$

where n – amount of substance, [mol]; T – process temperature, [K]; p – absolute pressure, [Pa].

Table 1. Data of the ammonia production process

Parameters	Second reforming		Shift conversion		CO ₂ conversion			Methanation
	1(in)	2(in)	3(in)	4(in)	5(in)	6(in)	7(in)	8(in)
Temperature, [°C]	492.00	830.00	350.45	199.63	65.01	50.00	50.00	295.00
Pressure, [kPa]	3115.6	3066.5	2970.4	2868.4	2711.5	2611.5	2611.5	2518.3
Flow F_i , [l/s]	17242	60676	82376	84032	60199	77.92	151.25	49120
C_{CO_2i} , [mol/l]	4.99e-5	0.0281	0.0241	0.0715	0.1684	0.2273	0.2273	1.59e-4
C_{CO_2b} , [mol/l]	-	0.027	0.0416	0.0133	1.93e-3	-	-	1.27e-3
C_{H_2b} , [mol/l]	-	0.196	0.1845	0.279	0.5819	-	-	0.3901
C_{CH_4i} , [mol/l]	-	0.0321	8.264e-4	1.067e-3	2.31e-3	-	-	1.43e-3
$C_{H_2O_i}$, [mol/l]	0.0521	0.2042	0.1804	0.2055	0.0108	-	-	2.97e-3
C_{O_2i} , [mol/l]	0.0917	-	-	-	-	-	-	-

Mass balance and reaction rate equations of ammonia production process for several chemical elements were created in accordance with the approaches described above. According to chemical equilibriums (1–2), mass balances equations for the second reforming of ammonia production process (see structural scheme in Fig. 2) for the following components are:

$$\frac{d(C_{CO_2})}{dt} = r_{CO_2} + (C_{CO_2m1} - C_{CO_2})\frac{F_1}{V_1} + (C_{CO_2m2} - C_{CO_2})\frac{F_2}{V_1}, \quad (17)$$

$$\frac{d(C_{H_2})}{dt} = r_{H_2} + (C_{H_2m2} - C_{H_2})\frac{F_2}{V_1}, \quad (18)$$

$$\frac{d(C_{CH_4})}{dt} = r_{CH_4} + (C_{CH_4m2} - C_{CH_4})\frac{F_2}{V_1}, \quad (19)$$

$$\frac{d(C_{H_2O})}{dt} = r_{H_2O} + (C_{H_2Om1} - C_{H_2O})\frac{F_1}{V_1} + (C_{H_2Om2} - C_{H_2O})\frac{F_2}{V_1}, \quad (20)$$

$$\frac{d(C_{O_2})}{dt} = r_{O_2} + (C_{O_2m1} - C_{O_2})\frac{F_1}{V_1}, \quad (21)$$

where F_1 – process air flow to the second reforming, [l/s]; F_2 – gas/steam flow to the second reforming, [l/s]; C_{CO_2in1} , C_{H_2Oin1} , and C_{O_2in1} – component concentrations in the process air flow (F_1) to the second reforming, [mol/l]; C_{CO_2in2} , C_{H_2in2} , C_{CH_4in2} , and C_{H_2Oin2} – component concentrations in gas/steam flow (F_2) to the second reforming, [mol/l];

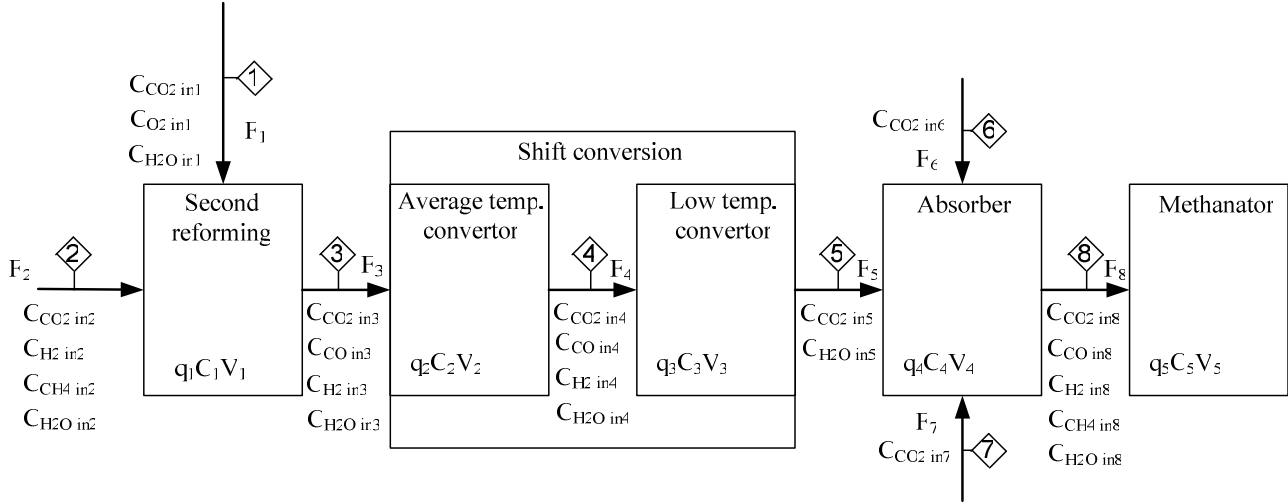


Fig. 2. Structural scheme of ammonia production process model

The absolute reaction rates of the modelled components are:

$$r_{CO_2} = k_1 C_{CH_4} C_{O_2}, \quad (22)$$

$$r_{H_2} = 2k_1 C_{CH_4} C_{O_2} - k_2 C_{H_2} C_{O_2}^{0.5}, \quad (23)$$

$$r_{CH_4} = -k_1 C_{CH_4} C_{O_2}, \quad (24)$$

$$r_{H_2O} = k_2 C_{H_2} C_{O_2}^{0.5}, \quad (25)$$

$$r_{O_2} = -k_1 C_{CH_4} C_{O_2} - 0.5k_2 C_{H_2} C_{O_2}^{0.5}, \quad (26)$$

where r_{CO_2} , r_{H_2} , r_{CH_4} , r_{H_2O} , and r_{O_2} – absolute reaction rates of component concentrations in the second reforming, [mol/(ls)]; k_1 – reaction constant of chemical equilibrium (2); k_2 – reaction constant of chemical equilibrium (1); C_{CO_2} , C_{H_2} , C_{CH_4} , C_{H_2O} , and C_{O_2} – concentrations of the modelled component in gas/steam flow after chemical reaction in the second reforming, [mol/l].

The reactor has incoming two flows (see structural scheme in Fig. 2): process air and steam/gas mixture. The mass balances equations of the reacting chemical components are (17–21), and the absolute reaction rates are (22–26).

Mass balance equations of shift conversion for the components (see structural scheme in Fig. 2) and chemical equilibrium (3) for average temperature conversion of CO are:

C_{CO_2} , C_{H_2} , C_{CH_4} , C_{H_2O} , and C_{O_2} – modelled component concentrations in gas/steam flow after chemical reaction in the second reforming, [mol/l]; V_1 – volume of the reactor, [l].

In the equations (17–21) instead of $q_i C_i$ one uses absolute reaction rate r_i , because formally they are equal to each other but the latter is more convenient to use in the process model analyzed.

$$\frac{d(C_{CO_2})}{dt} = r_{CO_2} + (C_{CO_2in3} - C_{CO_2}) \frac{F_3}{V_2}, \quad (27)$$

$$\frac{d(C_{CO})}{dt} = r_{CO} + (C_{COin3} - C_{CO}) \frac{F_3}{V_2}, \quad (28)$$

$$\frac{d(C_{H_2})}{dt} = r_{H_2} + (C_{H_2in3} - C_{H_2}) \frac{F_3}{V_2}, \quad (29)$$

$$\frac{d(C_{H_2O})}{dt} = r_{H_2O} + (C_{H_2Oin3} - C_{H_2O}) \frac{F_3}{V_2}, \quad (30)$$

where F_3 – gas/steam flow to the average temperature converter, [l/s]; V_2 – volume of the average temperature CO converter, [l]; C_{CO_2in3} , C_{COin3} , C_{H_2in3} , and C_{H_2Oin3} – component concentrations in gas/steam flow (F_3) to the average temperature converter, [mol/l]. The other parameters of the mass balances equations are the same as in the second reforming process described above.

Absolute reaction rates for the components are:

$$r_{CO_2} = -k C_{CO} C_{H_2O}, \quad (31)$$

$$r_{CO} = -k C_{CO} C_{H_2O}, \quad (32)$$

$$r_{H_2} = k C_{CO} C_{H_2O}, \quad (33)$$

$$r_{H_2O} = -k C_{CO} C_{H_2O}, \quad (34)$$

where k – reaction constant of chemical equilibrium (3).

According to Fig. 1, there are two types of CO converters, i.e. average and low temperature

convertors. Mass balance equations (27–30) are valid for the average temperature convertor. The chemical reaction (3) is the same in both convertors, except of process conditions, such as process temperature and pressure.

Mass balances of the shift conversion for the components (see structural scheme in Fig. 2) based on the chemical equilibrium (3) for low temperature conversion of CO are:

$$\frac{d(C_{CO_2})}{dt} = r_{CO_2} + (C_{CO_2in4} - C_{CO_2}) \frac{F_4}{V_3}, \quad (35)$$

$$\frac{d(C_{CO})}{dt} = r_{CO} + (C_{COin4} - C_{CO}) \frac{F_4}{V_3}, \quad (36)$$

$$\frac{d(C_{H_2})}{dt} = r_{H_2} + (C_{H_2in4} - C_{H_2}) \frac{F_4}{V_3}, \quad (37)$$

$$\frac{d(C_{H_2O})}{dt} = r_{H_2O} + (C_{H_2Oin4} - C_{H_2O}) \frac{F_4}{V_3}, \quad (38)$$

where F_4 – gas/steam flow to the low temperature convertor, [l/s], V_3 – volume of the low temperature CO convertor, [l]; C_{CO_2in4} , C_{COin4} , C_{H_2in4} , C_{H_2Oin4} – component concentrations in gas/steam flow (F_4) to the low temperature convertor, [mol/l]. The other parameters of the mass balances equations are the same as in the second reforming process described above. Absolute reaction rates for the components are:

$$r_{CO_2} = -kC_{CO}C_{H_2O}, \quad (39)$$

$$r_{CO} = -kC_{CO}C_{H_2O}, \quad (40)$$

$$r_{H_2} = kC_{CO}C_{H_2O}, \quad (41)$$

$$r_{H_2O} = -kC_{CO}C_{H_2O}, \quad (42)$$

where k – reaction constant of chemical equilibrium (3).

Mass balance equations of CO₂ conversion process for the components (see structural scheme in Fig. 2) based on the chemical equilibrium (4) are:

$$\frac{d(C_{CO_2})}{dt} = r_{CO_2} + (C_{CO_2in5} - C_{CO_2}) \frac{F_5}{V_4} + (C_{CO_2in6} - C_{CO_2}) \frac{F_6}{V_4} + (C_{CO_2in7} - C_{CO_2}) \frac{F_7}{V_4}, \quad (43)$$

$$\frac{d(C_{H_2O})}{dt} = r_{H_2O} + (C_{H_2Oin5} - C_{H_2O}) \frac{F_5}{V_4}, \quad (44)$$

where F_5 – gas/steam flow to the absorber, [l/s]; F_6 – solvent flow to the absorber, [l/s]; F_7 – solvent flow to the absorber, [l/s]; C_{CO_2in5} , C_{H_2Oin5} – component concentrations in gas/steam flow (F_5) to the absorber, [mol/l]; C_{CO_2in6} – component concentrations in solvent flow (F_6) to the absorber, [mol/l]; C_{CO_2in7} – component concentrations in solvent flow (F_7) to the absorber, [mol/l]; V_4 – volume of absorber, [l]. The other

parameters of the mass balances equations are the same as in the second reforming process described above.

Absolute reaction rates for the components are:

$$r_{CO_2} = -k_1C_{CO_2}C_{H_2O}, \quad (45)$$

$$r_{H_2O} = -k_1C_{CO_2}C_{H_2O}, \quad (46)$$

where k_1 – reaction constant of chemical equilibrium (4).

Mass balances equations of methanation process for the components (see structural scheme in Fig. 2) based on chemical equilibriums (6–7) are:

$$\frac{d(C_{CO_2})}{dt} = r_{CO_2} + (C_{CO_2in8} - C_{CO_2}) \frac{F_8}{V_5}, \quad (47)$$

$$\frac{d(C_{CO})}{dt} = r_{CO} + (C_{COin8} - C_{CO}) \frac{F_8}{V_5}, \quad (48)$$

$$\frac{d(C_{H_2})}{dt} = r_{H_2} + (C_{H_2in8} - C_{H_2}) \frac{F_8}{V_5}, \quad (49)$$

$$\frac{d(C_{CH_4})}{dt} = r_{CH_4} + (C_{CH_4in8} - C_{CH_4}) \frac{F_8}{V_5}, \quad (50)$$

$$\frac{d(C_{H_2O})}{dt} = r_{H_2O} + (C_{H_2Oin8} - C_{H_2O}) \frac{F_8}{V_5}, \quad (51)$$

where F_8 – gas/steam flow to the methanator, [l/s]; V_5 – volume of the methanator, [l]; C_{CO_2in8} , C_{COin8} , C_{H_2in8} , C_{CH_4in8} , and C_{H_2Oin8} – component concentrations in gas/steam flow (F_8) to the methanation process, [mol/l]. The other parameters of the mass balances equations are the same as in the second reforming process described above.

Absolute reaction rates for the components:

$$r_{CO_2} = -k_2C_{CO}C_{H_2}^4, \quad (52)$$

$$r_{CO} = -k_1C_{CO}C_{H_2}^3, \quad (53)$$

$$r_{H_2} = -3k_1C_{CO}C_{H_2}^3 - 4k_2C_{CO}C_{H_2}^4, \quad (54)$$

$$r_{CH_4} = k_1C_{CO}C_{H_2}^3 + k_2C_{CO}C_{H_2}^4, \quad (55)$$

$$r_{H_2O} = k_1C_{CO}C_{H_2}^3 + 2k_2C_{CO}C_{H_2}^4, \quad (56)$$

where k_1 – reaction constant of chemical equilibrium (6); k_2 – reaction constant of chemical equilibrium (7).

4. Software implementation of the model

The process model was implemented using the elements from the standard user-defined libraries for *Matlab/Simulink* environment together with the embedded *Matlab* functions. The created user-defined libraries consist of the expressions for absolute reactions rates, mass balance equation systems. Additionally, part of the software tool was programmed using *m* files.

5. Modelling results

The most important concentration components of ammonia production process are shown in Fig. 3. Concentrations of the components were chosen for illustration based on the importance to the ammonia production process and available measurement points in the plant. The model was created taking into account the data provided by ammonia technological rules of procedure (see Table 1) and the modelling results were compared with the reference values. The results, i. e.

the measured values are influenced by the disturbances and errors in the control systems and instruments, also by the procedures of measurement unit conversion (from [v/v %] to [mol/l]). Generally, concentrations are modelled with good accuracy as compared with values from ammonia technological rules of procedure. Modelling results also depend on the model parameters – coefficients of proportionality. The optimal values of the model parameters in sense of the minimal modelling error were calculated using Nelder-Mead optimization algorithm.

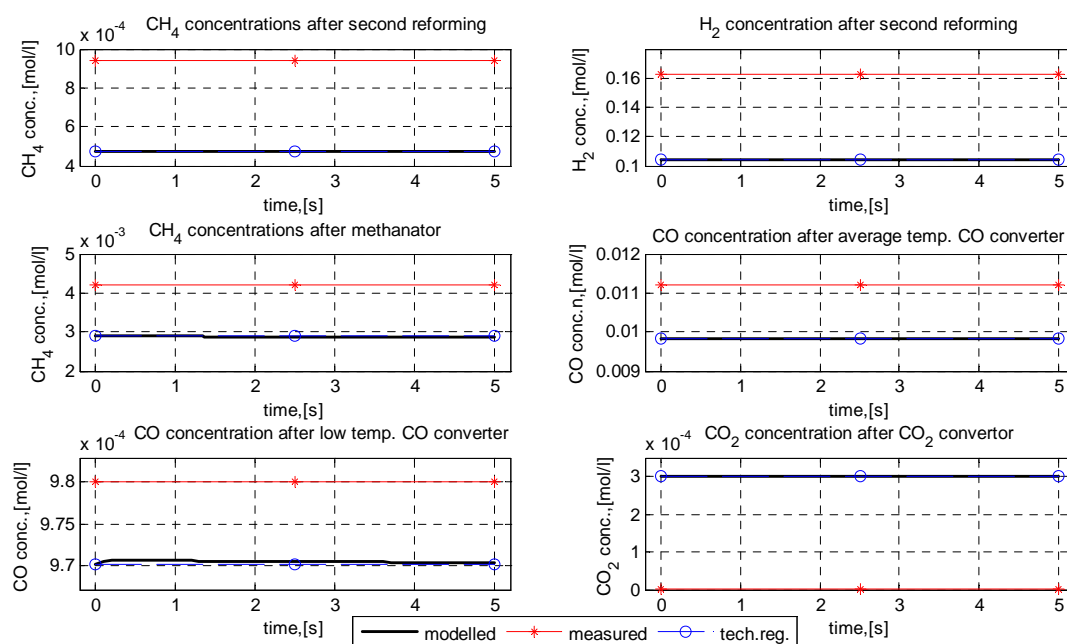


Fig. 3. Concentrations in the ammonia production process

6. Conclusions and further work

Mass balances of ammonia production process were presented. The mass balance and absolute chemical reaction rate equations of ammonia production process are analyzed and presented. The computer simulation tests were performed using software tools created in Matlab program environment. The modelling results were compared with the experimental data and discussed.

Further the extensive sensitivity analysis should be performed in order to determine the most important influencing parameters. Then the ANNs for the modelling of the reaction rates should be created, trained and validated. Depending on the identification results the appropriate model-based control strategy should be elaborated.

7. References

- Galvanauskas V., Georgieva P. and Feyo de Azevedo S. Dynamic Optimisation of Industrial Sugar Crystallization Process based on a Hybrid (Mechanistic+ANN) Model. Proceedings of IEEE World Congress on Computational Intelligence, IJCNN 2006, July 16-21, 2006, Vancouver, Canada, Vol. 6. p. 5035-5042.
- Galvanauskas V., Simutis R. and Lübbert A. Hybrid process models for process optimisation, monitoring and control. Bioprocess and Biosystems Engineering, 2004, 26(6). p. 393-400.
- Schubert J., Simutis R., Dors M., Havlik I. and Lübbert A. Bioprocess optimization and control: Application of hybrid modelling, J. Biotechn., 1994, 35. p. 51-68.
- Galvanauskas V., Simutis R. and Levišauskas D. Application of evolutionary computing for hybrid model based optimization of biochemical processes. WSEAS Transactions on Information Science and Applications, Issue 5, Vol. 2, May 2005. p. 507-511.
- European Fertilizer Manufacturers' Association, Best Available Techniques for Pollution Prevention and Control in the European Fertilizer Industry, Production of Ammonia, 2000. p. 7-21.
- Perry R.H., Green D.W. and Moloney J.O. Chemical Engineers' Handbook. 7th edition, McGraw-Hill Professional, 1997. 2640 p.
- Ammonia technological rules of procedure (AB "Achema")

MATHEMATICAL MODEL FOR ADAPTIVE CONTROL OF DISSOLVED OXYGEN CONCENTRATION IN BIOLOGICAL WASTEWATER TREATMENT PROCESS

Kęstutis JONELIS, Kęstutis BRAZAUSKAS, Donatas LEVIŠAUSKAS
 Process Control Department, Kaunas University of Technology, Lithuania

Abstract: Mathematical model has been developed for modelling dynamical behaviour of the dissolved oxygen concentration in an industrial scale biological wastewater treatment process. Parameters of the process model are identified using monitoring data from wastewater treatment plant. The model identification and validation results are presented.

Keywords: mathematical model, identification, dissolved oxygen concentration, biological wastewater treatment process.

1. Introduction

An accurate control of dissolved oxygen concentration (DOC) at optimal level during the biological wastewater treatment process is a relevant technological problem due significant energy expenses for aeration. However, automatic control of DOC is complicated by nonlinearity and time-varying dynamical characteristics of the controlled process. The traditional linear controllers (PI, PID) with constant parameters are not adequate to ensure an accurate control under process state variations [1].

Currently, various control methods are developed to cope with process nonlinearity and state variations that are based on using process state models to predict the process dynamics [2-4].

The DOC control problem is live in the Kaunas wastewater treatment plant, as the ordinary automatic DOC set-point control system demonstrates poor performance under varying technological conditions (Figure 1).

In this work, the state model is developed for modelling dynamical behaviour of DOC in the biological wastewater treatment process. The mathematical model is identified using monitoring data from wastewater treatment plant. The model is intended for design of the DOC adaptive control system.

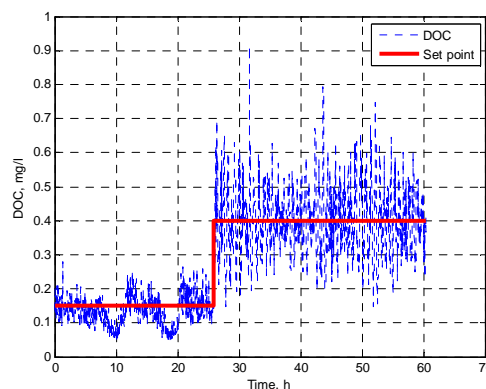


Fig. 1. Performance of the DOC control system with ordinary PI controller under varying technological conditions (data from industrial wastewater treatment plant)

2. Technological process

Technological scheme of the wastewater treatment process is shown in Figure 2. Incoming wastewater flow F_{in} with substrate concentration S_{in} through the screens, comminutor and grit chamber falls into the distribution chambers. Subject to the position of bypass gate, the flow is proportioned in two directions: one portion goes through primary sedimentation (F_{sed}) tank, the other - straight to the distribution chamber and the biological treatment tanks (F_{bypass}). The flow distribution proportion is evaluated by coefficient k_{sed} that shows the percentage of the flow through the primary sedimentation, depending on the motorized bypass gate position g (0% - closed, 100% - fully opened). This relationship is estimated by interpolation of three points given in the documentation of the distribution chamber construction (Table 1).

Table 1. Bypass gate position and k_{sed} points

Bypass gate position g , %	k_{sed} , %
0	100
28.8	50
100	0

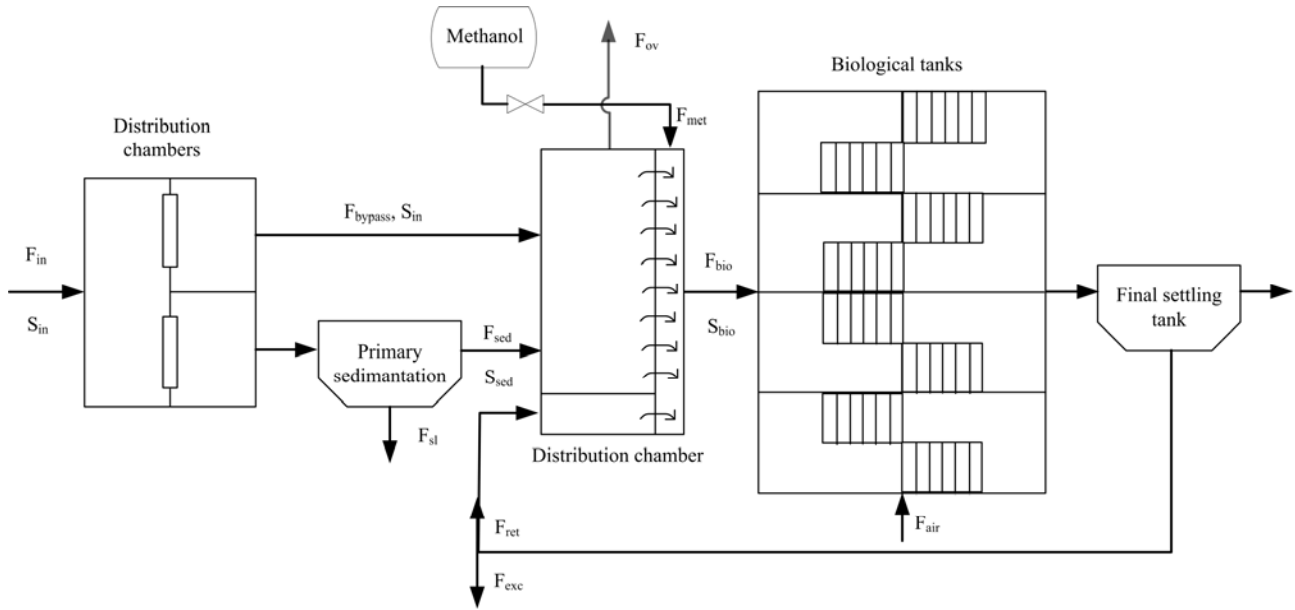


Fig. 2. Technological scheme of wastewater treatment process

The relationship is approximated by quadratic polynomial:

$$k_{sed} = 0.01034 \cdot g^2 - 2.034 \cdot g + 10. \quad (1)$$

The wastewater flow through primary sedimentation tank is

$$F_{sed} = \frac{k_{sed}}{100} F_{in}. \quad (2)$$

The sludge flow F_{sl} from primary sedimentation tank is very low, compared to the wastewater flow (~1%), so it is not taken into account in the following calculations. Depending on the wastewater flow through primary sedimentation tank, substrate concentration in the outflow decreases from 15% (at high flow rates) to 40% (at low flow rates). The percentage of the substrate concentration decrease in the outflow of sedimentation tank is evaluated by the linear relationship

$$k_{dec} = -0.0043 \cdot F_{sed} + 40, \quad (3)$$

where k_{dec} is the percentage of substrate concentration decrease in the wastewater outflow, %; F_{sed} is the flow rate through sedimentation tank, m^3/h .

With the estimated value of k_{dec} , the substrate concentration in the outflow of sedimentation tank is estimated using formula:

$$S_{sed} = S_{in} - \frac{k_{dec}}{100} S_{in}. \quad (4)$$

The two wastewater flows are mixed in the distribution chamber. If the total flow outreaches $5855 m^3/h$, the overflow F_{ov} is directed straight to the outlet passing the biological tanks and the final settling tank. Some methanol is added (F_{met}) if necessary for better biological treatment. The mixed wastewater flow F_{bio} with the substrate concentration S_{bio} falls into four

biological treatment tanks. As the methanol was not added during the process investigation period, the substrate concentration S_{bio} in the biological treatment tanks inflowing wastewater was estimated using the following formula:

$$S_{bio} = \frac{s_{in} \left(F_{in} - \frac{k_{sed}}{100} F_{in} \right) + S_{sed} \frac{k_{sed}}{100} F_{in} + s_{ret} F_{ret}}{F_{in} + F_{ret}}, \quad (5)$$

where F_{ret} is flow rate of returned sludge from the final settling tank with substrate concentration S_{ret} . The excessive sludge with the flow rate F_{exc} is removed for digestion.

The airflow F_{air} , comes from the blower station to four biological tanks and the air flow rate is evaluated by measuring power consumption P of compressors. Referring to technical documentation of the plant the air flow rate is estimated by the following linear relationship:

$$F_{air} = 0.05455 \cdot P - 1200, \quad (6)$$

where P is the power consumed by compressors.

In the presented investigation, monitoring data from one of biological treatments tanks was used. Airflow to the selected tank is estimated taking into account position of airflow valves to each tank:

$$F_{air4} = F_{air} \frac{v_4}{v_1 + v_2 + v_3 + v_4}, \quad (7)$$

where F_{air4} is airflow to the selected tank (4th), m^3/h ; v_1, v_2, v_3, v_4 are valve positions to corresponding tanks, %

3. Mathematical model of DOC in biological wastewater treatment process

The state model of the waste water biological treatment process is based on the mass balances for dissolved oxygen and substrate [1, 5]:

$$\frac{dc}{dt} = k_L a (c_{satur} - c) + (c_{in} - c) \frac{F_{bio}}{V} - OUR, \quad (8)$$

$$\frac{ds}{dt} = -\frac{\mu_{max}}{Y_{x/s}} \frac{s}{K+s} X + \frac{S_{bio} - s}{V} F_{bio}, \quad (9)$$

$$OUR = \frac{\mu_{max}}{Y_{x/o}} \frac{s}{K+s} X, \quad (10)$$

$$k_L a = \alpha N^\beta Q^\gamma, \quad (11)$$

where c is the dissolved oxygen concentration, $k_L a$ is coefficient of mass transfer from gas to liquid phase, c_{satur} is saturated value of DOC, c_{in} is DOC in the inlet wastewater, F_{bio} is the inlet flow rate of wastewater, V is volume of aeration tank, OUR is oxygen uptake rate, s is resultant substrate concentration, μ_{max} is maximum specific growth rate of biomass, K is half saturation coefficient, $Y_{x/s}$ is biomass/substrate yield coefficient, $Y_{x/o}$ is biomass/oxygen yield coefficient, X is biomass concentration, particular amount of substrate to keep biomass alive, S_{bio} is substrate concentration in inlet wastewater, N is stirring speed, Q is air flow rate, α, β, γ are parameters.

4. Model parameters identification

As the only state variable c is directly measured (the state variable s is estimated by the mathematical model), an objective of the model parameters identification procedure is to minimize the squared error

$$S = \int_0^T (c_{model} - c_{data})^2 dt \rightarrow min, \quad (12)$$

where c_{model} are model predictions of DOC, c_{data} are the DOC observation data of real process, T is time interval of observation.

For integration of the model equations (8), (9) along the observation time interval, the discrete observation data of technological parameters F_{in} , F_{ret} , Q and c were interpolated using the Matlab tools (the liner Lagrangian interpolation). Initial value of directly unmeasured state variable $s_{t=0}$ is estimated by the process expert, the inflowing substrate concentration s_{bio} is estimated by formula (5). Biomass concentration X was estimated by linear relationship

$$X = X_0 + F_{ret} \cdot k, \quad (13)$$

where X_0 and k are parameters to be identified.

Model parameter c_{in} is directly measured, c_{satur} is physical constant, V is constructive parameter. As the stirring speed in the investigated process is kept up

stable, the term αN^β is identified as parameter α^* . Preliminary values of parameters $\alpha^*, \gamma, \mu_{max}, K, Y_{x/s}, Y_{x/o}$ are taken from [6-9]. The parameters values minimizing the objective function (12) are identified using stochastic search algorithm (evolutionary programming, [10]). The computation program is realized using the Matlab tools.

The initial values of state variables and the identified values of the model (8)-(11) parameters are presented in Table 2.

Table 2. Initial values of state variables and identified values of the model

Initial values of state variables		
Variable	Unit	Value
c	mg/l	0.16
s	mg/l	32.28
Identified values of the model		
α^*	-	5.09
γ	-	0.138
μ_{max}	h^{-1}	0.10
K	mg/l	35.36
$Y_{x/s}$	mg/mg	2.80
$Y_{x/o}$	mg/mg	0.052
X_0	mg/l	140
k	-	-0.0006

The observation data for model identification and model prediction of DOC are presented in Figures 3-6.

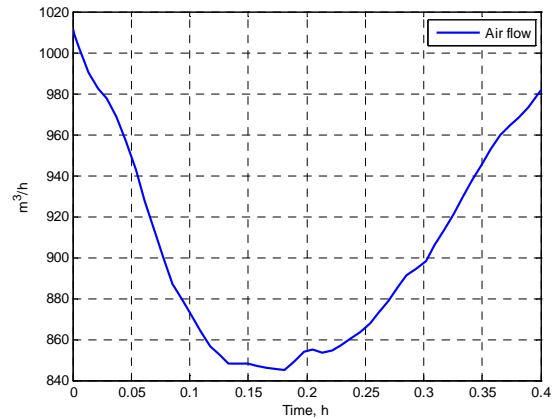


Fig. 3 Inlet air flow rate

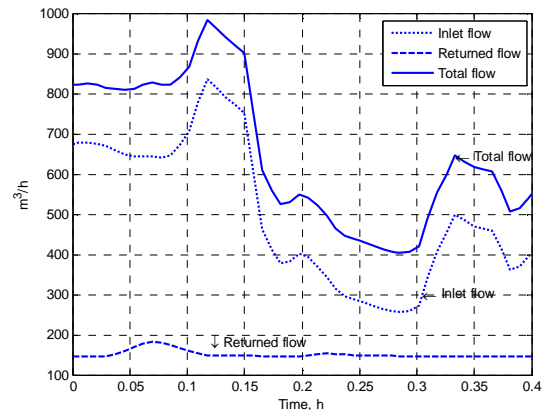


Fig. 4. Inlet, returned and total wastewater flow rates

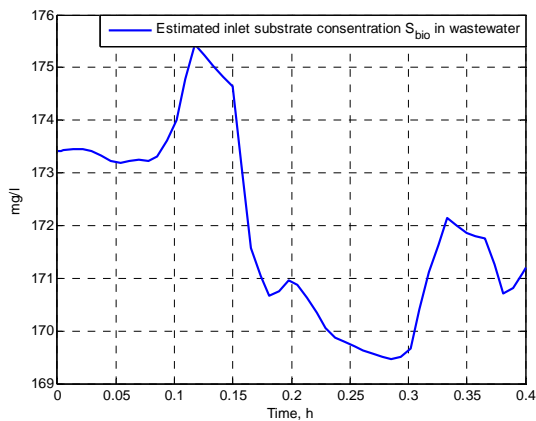


Fig. 5. Estimated substrate concentration in the biological treatment tank inflowing wastewater

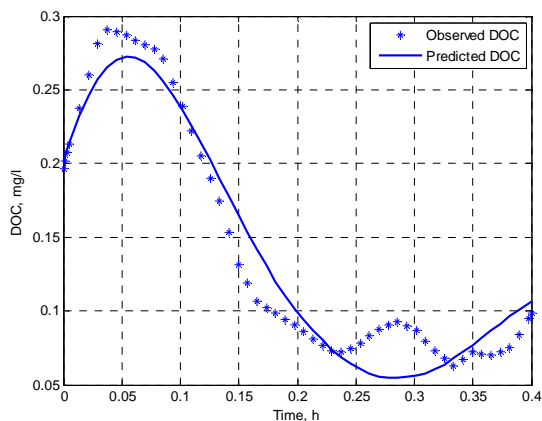


Fig. 6. Observed and model predicted DOC

In Figure 7 a-b the model validation results are presented for prediction the DOC from the process monitoring data that were not used for model identification.

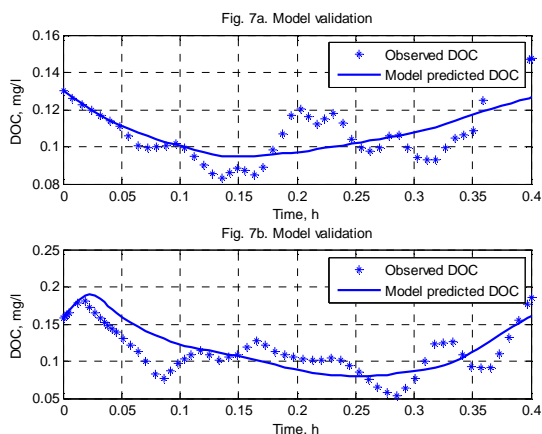


Fig. 7. Model validation results

The results presented in Fig. 6, 7 a-b demonstrate that the identified model satisfactory predicts the DOC variation under varying technological conditions of the biological wastewater treatment process.

5. Conclusions

In this work, the mathematical model is developed for modelling alternation of the dissolved oxygen

concentration in the wastewater biological treatment process under varying operating conditions. The model identification and validation results prove suitability of the model to describe and predict dynamical features of the process. The model is further intended for on-line adaptation of controller parameters in the dissolved oxygen automatic control system in order to increase performance of the system.

6. References

1. Levišauskas D. An Algorithm for Adaptive Control of Dissolved Oxygen Concentration in Batch Culture. *Biotechnology Techniques*, 1995, Vol. 9, n.2, p. 85-90.
2. Bastin, G., Dochain, D. *On-Line Estimation and Adaptive Control of Bioreactor*. Elsevier, New York, 1990.
3. Lindberg, C. F. Multivariable Modeling and Control of an Activated Sludge Process. *Wat. Sci. Tech.*, 37, 149, 1998.
4. Yoo C.K., Cho J.H., Kwak H. J., Choi S. K., Chun H.D., Lee I. Closed-Loop Identification and Control for Dissolved Oxygen Concentration in the Full-Scale Coke Wastewater Treatment Plant. *Wat. Sci. Tech.*, 2001.
5. Staniskis J., Levisauskas D., Simutis R., Viesturs U., Kristapsons M. *Automation of Biotechnological Processes: Automatic Monitoring, Optimization and Control*. (In Russian), Riga, Zinatne, 1992. 348 p.
6. Eswaramoorthi S., Dhanapal K., Chauhan D.D. *Application of membrane bioreactor for textile wastewater treatment: Pilot plant process modeling and scale-up*. New Delhi, India, 2003.
7. Daigger G.T., Buttz J.A. *Upgrading wastewater treatment plants*. Second edition. Lancaster, Pennsylvania, 1998.
8. Repšytė J., Simutis R. *Mathematical model of biological wastewater treatment process*. *Informacinės technologijos ir valdymas*. 2001, No. 4(21), p. 21-30.
9. <http://www.ensic.inpl-nancy.fr/COSTWWTP>
10. Porto V.W., Fogel D.B., Fogel L.J.. *Alternative neural networks training methods*. *IEEE Expert*, 1995, p. 16-22.

ADAPTIVE CONTROL SYSTEM FOR DISSOLVED OXYGEN CONCENTRATION IN KAUNAS WASTEWATER TREATMENT PLANT

Jolanta REPŠYTĖ*, Ieva ČEBATORIENĖ*, André WENZEL**

* Kaunas University of Technology (KTU), Lithuania

** University of Applied Sciences Schmalkalden (fhS), Germany

Abstract: The APROMOCS project researchers developed Kaunas waste water treatment plant biological wastewater treatment process mathematical model, with the goal to develop control system for strict dissolved oxygen concentration requirements. In the next stage was developed adaptive control system for dissolved oxygen concentration. This article describes the implementation of the biological wastewater treatment process model and control system into software SIMULINK (MATLAB). The adaptive control system for dissolved oxygen concentration is a part of the EUREKA-Research-Project E!3692- APROMOCS.

Keywords: Biological wastewater treatment mathematical modeling; adaptive control system.

1. Introduction

SYMBIO technology is implemented in new Kaunas wastewater treatment plant. Danish firm "BioBalance" has been patented this technology in the United States Patent Office on 1996 [1]. This is one of the modern nitrogen and phosphorus removal technologies [2].

Biological nitrogen removal from wastewater based on nitrification and denitrification processes are taking place in biological treatment plants. The aim of this technology is to assess the nitrification and denitrification rates and aeration regimes effect to the biological nitrogen removal [4].

Typically, the nitrogen removal scheme combined with the phosphorus removal schemes. One of them is the SYMBIO technology in which the nitrogen is removed. Nitrification and denitrification area is not specifically excluded in the bioreactor, and the biological removal of phosphorous against nitrification and (or) denitrification areas are equipped with anaerobic zone. The technology is based on the fact that the new technique allows the monitoring of the biological control of the process directly. The control objective is to supply a minimum quantity of air to ensure a continuous supply of oxygen

in a quantity that requires the biological processes [1, 3, 7].

Under this scheme aerobic and anoxic tanks combined. Nitrification and denitrification is achieved in alternating aeration intensity.

Aeration intensity varies cyclically recurring set of two periods, etc. and creating the conditions for full nitrification take place in aeration intensity increased by 0,5-1 mgO₂/l, the oxygen concentration to maintain. Then reduce the intensity of aeration, and maintaining 0,1-0,5 mgO₂/l, the oxygen concentration, allowing for the full denitrification occur [1].

Organic matter, phosphorus and nitrogen compounds are disposed from the sewage in Kaunas waste water treatment plant. Activated sludge, separated by secondary settler, is returned to the anaerobic chambers of the bioreactor. Technological process in the bioreactor is controlled by dissolved oxygen, temperature, pH, and the active sludge concentration sensors. The excess sludge is drained and used for biogas producing [3].

2. Object Description

Two new settlers, methanol dosing station, blower room, 4 bioreactors, and distribution chamber with the pump station were built in Kaunas waste water treatment plant in 2008 [8].

Wastewater from the primary settlers is transported to the distribution chamber. Here, wastewater is mixed with the circulated sludge and dosed methanol. Sewage and sludge mixture circulation is divided into 4 channels for sewage and sludge mixture circulation of the biological treatment tanks (bioreactors).

Kaunas waste water treatment plant has 4 biological treatment tanks, where the mixture stirred 24 mixers ensuring adequate mixing of sewage. Each mixer is equipped in the bottom of the tanks. Effluent at the origin of organic material will be removed biologically active sediment phase, seeks to phosphorus, nitrogen and carbon degradation.

The main control parameter at this stage is the dissolved oxygen concentration. Currently disposed control system does not ensure the necessary quality parameters. It is necessary to maintain the oxygen concentration is 0.15 mg/l, but it is much higher or lower. Oxygen and air valve position is shown in Figure 1.

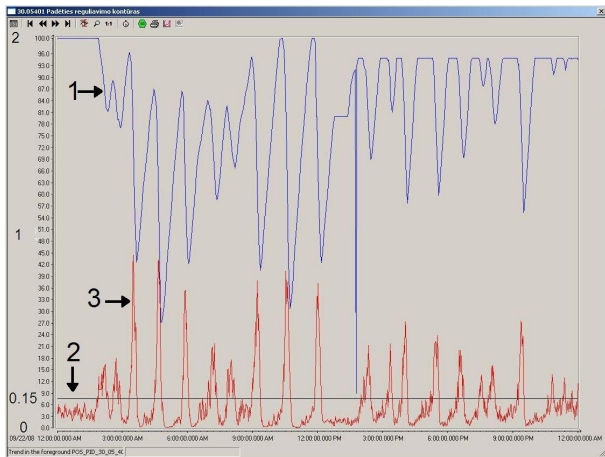


Fig. 1. Example of the dissolved oxygen concentration control in Kaunas waste water treatment plant. (1 – air valve position (0-100 %), 2 – set point (0.15 mg/l), 3 – measured dissolved oxygen concentration (0-2 mg/l))

There is a modern process control system with technological process visualization (SCADA) WinCC v6.2 (Siemens) and controllers SIMATIC S7-400 (Siemens) in Kaunas waste water treatment plant. WinCC is used to visualize the process. WinCC allows to the operator to monitor the process. The process is graphically displaying on the screen. The image is updated, a change in time. This program also allows you to control the process. This program show in details all the process and put in place control, data collection and storage functions. Experiments data of the technological process were recorded in the archiving system every 15 seconds.

Experimental data for dissolved oxygen concentration mathematical model identification were collected during two months. Experimental data was selected only when the controller was turned off and the valve was opened or closed in step manually. Total experiment time, the dissolved oxygen concentration measurement and the adjustment has been used by one meter.

All the experimental data were selected in the three experimental space (Fig. 2 – Fig. 4), of which the object was made up of mathematical models and identification of them parameters.

Before approximation, experimental data was filtered by moving average filter. Area method was selected for approximation of experimental data [9].

Object reaction curve approximation was carried out in the area method with software MATLAB. Object was described by the first row transfer function with transport delay.

The object transfer function (I model) from the first experiment:

$$W_0(s) = \frac{0.0018}{3.5962 \cdot 10^3 s + 1} \cdot e^{-12600s}, \text{ mg/l/\%} \quad (1)$$

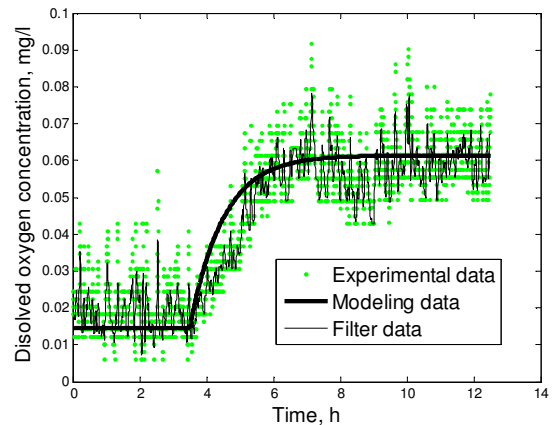


Fig. 2. Object reaction curve from the first experiment

The object transfer function (II model) from the second experiment:

$$W_0(s) = \frac{0.0029}{4.9796 \cdot 10^3 s + 1} \cdot e^{-12000s}, \text{ mg/l/\%} \quad (2)$$

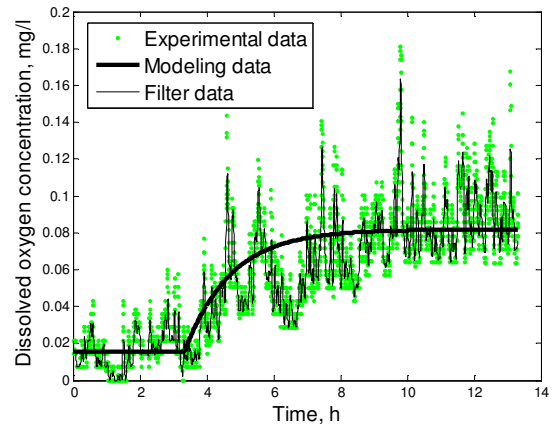


Fig. 3. Object reaction curve from the second experiment

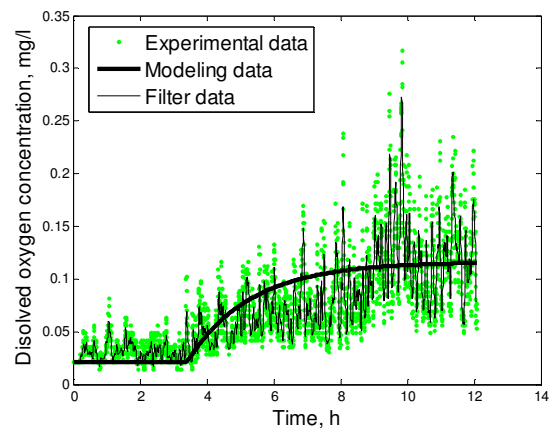


Fig. 4. Object reaction curve from the third experiment

The object transfer function (III model) from the third experiment:

$$W_0(s) = \frac{0.0039}{6.9547 \cdot 10^3 s + 1} \cdot e^{-12240s}, \text{ mg/l/\%} \quad (3)$$

3. Dissolved Oxygen Concentration Control System

Were selected PI and PID controllers for process controlling. Regulator parameters were calculated by direct quality criterion of the minimum integrated absolute error with the time weighted (ITAE) method [5]. The object transfer function with biggest gain coefficient (III mathematical model) was used for regulators parameters estimation on the basis of classic control theory.

PI regulator parameters were calculated by these equations [9]:

$$P = \frac{0.586}{K_{pr}} \cdot \left(\frac{T_{pr}}{\tau_{pr}}\right)^{0.916} = 89.53 \quad (4)$$

$$I = \frac{\frac{0.586}{K_{pr}} \cdot \left(\frac{T_{pr}}{\tau_{pr}}\right)^{0.916}}{T_{pr}} = 0.01179 \quad (5)$$

$$\left[1.03 - 0.165 \cdot \left(\frac{\tau_{pr}}{T_{pr}}\right) \right]$$

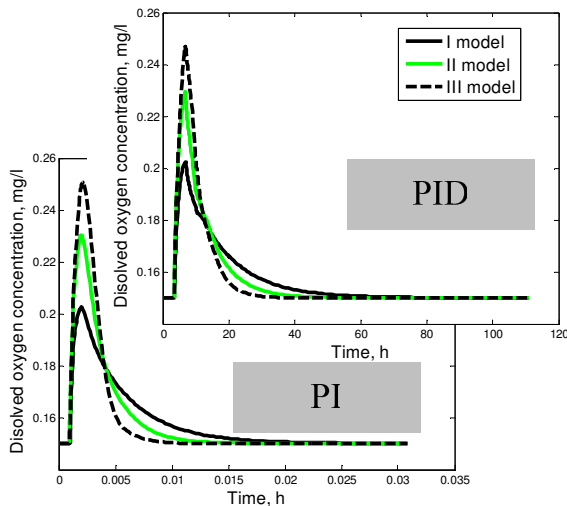


Fig. 5. Control systems reactions to process interference

PID regulator parameters were calculated by these equations [9]:

$$P = \frac{0.965}{K_{pr}} \cdot \left(\frac{T_{pr}}{\tau_{pr}}\right)^{0.855} = 152.6 \quad (6)$$

$$I = \frac{\frac{0.965}{K_{pr}} \cdot \left(\frac{T_{pr}}{\tau_{pr}}\right)^{0.855}}{T_{pr}} = 0.01179 \quad (7)$$

$$\left[0.796 - 0.147 \cdot \left(\frac{\tau_{pr}}{T_{pr}}\right) \right]$$

$$D = \frac{0.965}{K_{pr}} \cdot \left(\frac{T_{pr}}{\tau_{pr}}\right)^{0.855} \cdot 0.308 \cdot T_{pr} \cdot \left(\frac{\tau_{pr}}{T_{pr}}\right)^{0.929} = 5.527 \cdot 10^5 \quad (8)$$

The dissolved oxygen control system was realized in the software SIMULINK (MATLAB).

The control systems with different regulators (PI and PID) reaction to process interference (Fig. 5) and set – point change (Fig. 6) were presented and analyzed.

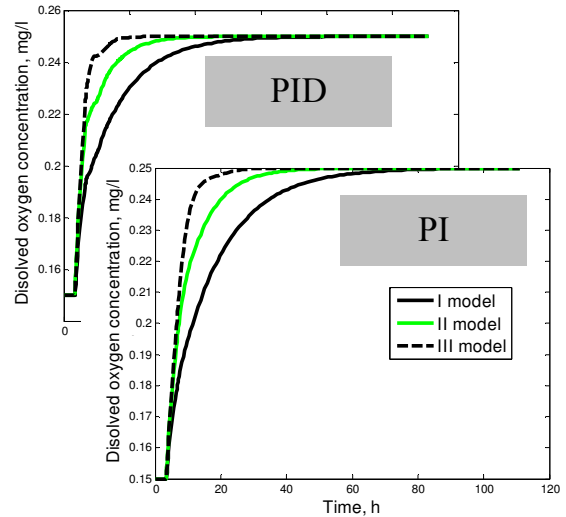


Fig. 5. Control systems reactions to set – point change

The PI controller and the PID controller works well enough, when the object is described by the third mathematical model, but not enough to ensure quality control, when object is described by the first or the second mathematical model. Therefore, it is appropriate to use adaptive dissolved oxygen concentration regulator.

Classic automatic control system is designed on the assumption that the process is linear in working point environment. From experiment data (Fig. 2 – Fig. 4) we see, that our object is not linear.

One way to solve control problems associated with the linearization is to use the design procedure, known as gain scheduling [6, 10]. Gain scheduling control system parameters are replaced, depending on the assessed real-time operation conditions.

Controller design procedure is divided into two phases. The first stage establishes local coordination parameters of the linear regulator, which are optimal in the individual points of stationary states environment.

In the next stage, localized controller parameters are interpolated and the result is obtained the global

regulator. The global regulator parameters are adjusted automatically, depending on the status of the process. One of the variables easily measured in real time and used to determine the point of stationary states. This variable may be the regulator output signal, the status of the process variable or external variable, if it unambiguously reflects the dynamic changes in controlled process parameters [6].

To determine the object mathematical model parameters dependencies, were analyzed all the measured parameters, such as flow, temperature, air pressure, etc. It was found that the object mathematical model parameters depend on the solids concentration T_{ss} .

Table 1. Transfer function parameters dependence on the T_{ss}

Transfer function, mg/l/%	T_{ss} , g/l
$W_0(s) = \frac{0.0018}{3.5962 \cdot 10^3 s + 1} \cdot e^{-12600s}$	7.99
$W_0(s) = \frac{0.0029}{4.9796 \cdot 10^3 s + 1} \cdot e^{-12000s}$	8.44
$W_0(s) = \frac{0.0039}{6.9547 \cdot 10^3 s + 1} \cdot e^{-12240s}$	8.72

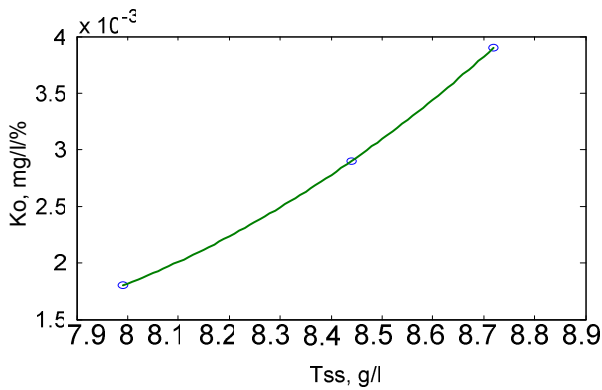


Fig. 6. Object gain coefficient dependence on the total solids materials concentration T_{ss}

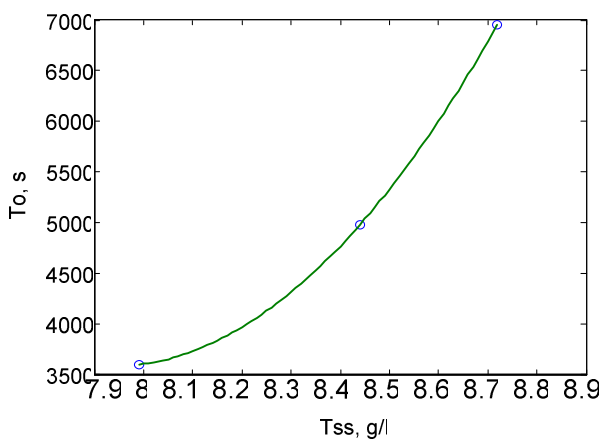


Fig. 7. Object time constant dependence on the total solids materials concentration T_{ss}

Object gain coefficient dependence on the total solids materials concentration T_{ss} :

$$K_o = 0.0015 \cdot T_{ss}^2 - 0.0229 \cdot T_{ss} + 0.0864 \quad (9)$$

Object time constant dependence on the total solids materials concentration T_{ss} :

$$T_o = 5451.65 \cdot T_{ss}^2 - 86496.43 \cdot T_{ss} + 346668.62 \quad (10)$$

Table 2. PI regulator parameters dependence on the T_{ss}

T_{ss} , g/l	P	I
7.99	106.00	0.0138
8.44	88.66	0.0111
8.72	89.53	0.0095

Table 3. PID regulator parameters dependence on the T_{ss}

T_{ss} , g/l	P	I	D
7.99	188.1	0.01547	$6.501 \cdot 10^5$
8.44	154.2	0.01346	$5.455 \cdot 10^5$
8.72	152.6	0.01179	$5.527 \cdot 10^5$

3. Adaptive Dissolved Oxygen Concentration Control System in the software SIMULINK (MATLAB)

Simulator of the adaptive dissolved oxygen control system is presented in Figure 8.

The simulator functional block "Object Parameters" is calculating object transfer function parameters in accordance with 9 – 10 equation. Next, the functional block, "Regulator Parameters" is calculating the new regulator parameters according to the recalculated object transfer function values.

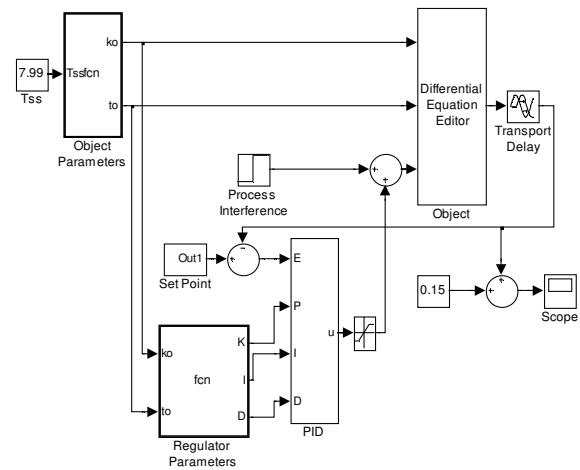


Fig. 8. Adaptive dissolved oxygen control system realized in the software SIMULINK (MATLAB)

The analysis of the dissolved oxygen control systems reactions to process interference and set – point change (Fig. 9 and Fig. 10), it was found that the control system

with the adaptive PI controller control faster the process than the control system with classic PI controller.

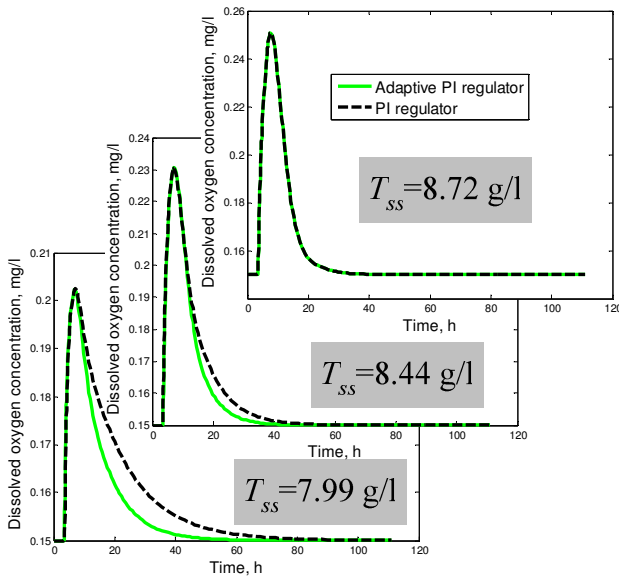


Fig. 9. Control systems (adaptive PI regulator and classic PI regulator) reactions to process interference

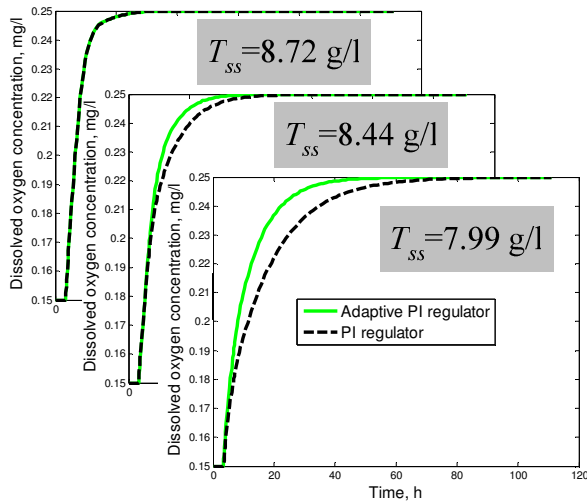


Fig. 10. Control systems (adaptive PI regulator and classic PI regulator) reactions to set – point change

The analysis of the dissolved oxygen control systems reactions to process interference and set – point change (Fig. 11 and Fig. 12), it was found that the control system with the adaptive PID controller control faster the process than the control system with classic PID controller.

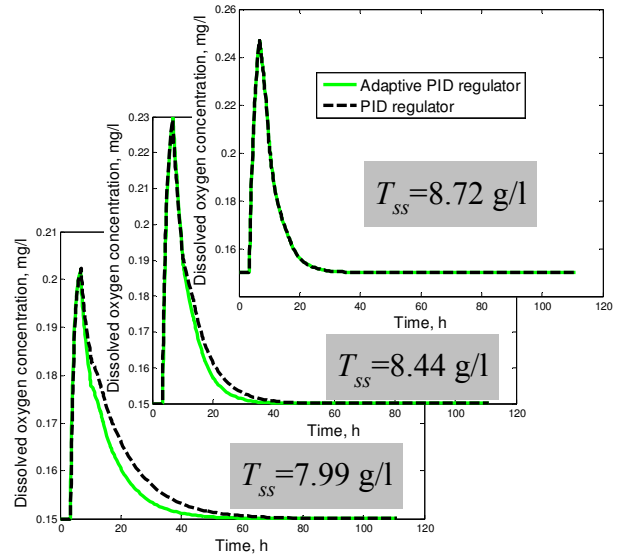


Fig. 11. Control systems (adaptive PID regulator and classic PID regulator) reactions to process interference

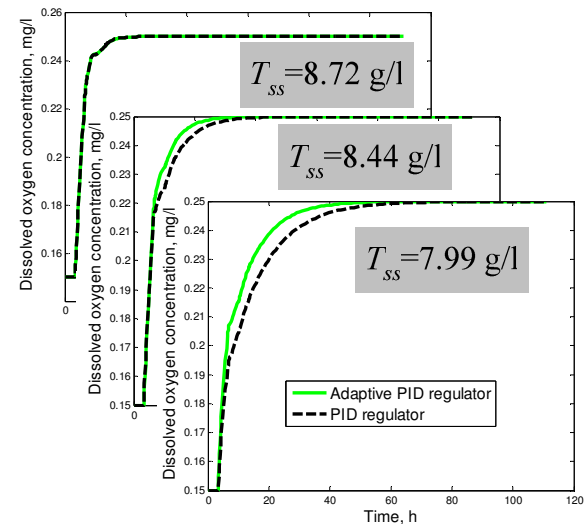


Fig. 12. Control systems (adaptive PID regulator and classic PID regulator) reactions to set – point change

The analysis of the dissolved oxygen control systems reactions to process interference and set – point change (Fig. 13 and Fig. 14), it was found that the control system with the adaptive PID controller control faster the process than the control system with adaptive PI controller.

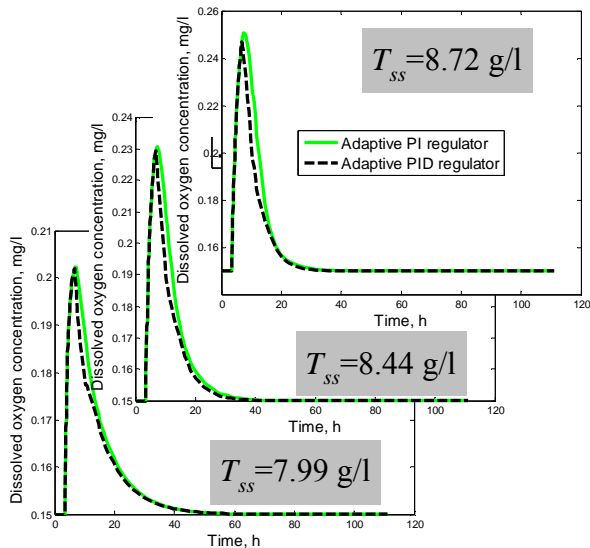


Fig. 13. Control systems (adaptive PI regulator and adaptive PID regulator) reactions to process interference

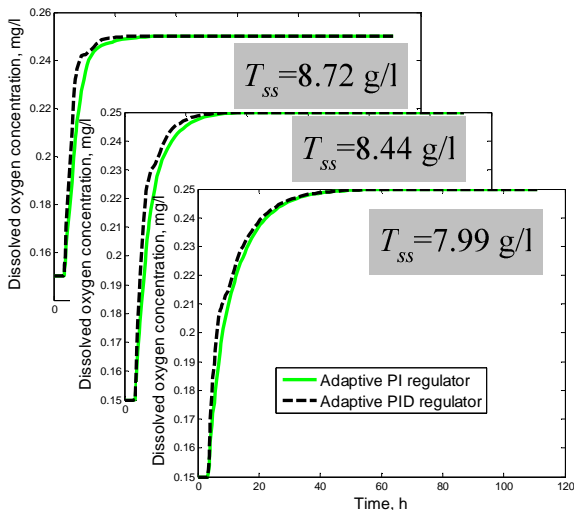


Fig. 14. Control systems (adaptive PI regulator and adaptive PID regulator) reactions to set – point change

4. Conclusions

1. To determine the object mathematical model parameters dependencies, was analyzed all the measured parameters, such as flow, temperature, air pressure, etc. It was found that the object mathematical model parameters depend on the solids concentration T_{ss} .
2. The classic PI controller and the PID controller works well enough, when the object describes the III-rd

mathematical model, but not enough to ensure quality control, when object is described by first or second mathematical model. Therefore, it is appropriate to use adaptive dissolved oxygen concentration regulator.

3. The analysis of the dissolved oxygen control systems reactions to process interference and set – point change (Fig. 9 – Fig. 14), it was found that the control system with the adaptive PID controller control faster the process than the control system with adaptive PI controller.

4. This dissolved oxygen control system with adaptive PID regulator could be installed in Kaunas waste water treatment plant control system.

5. Acknowledgment

This research is related to the Eureka project E!3692 APROMOCS supported by Agency for International Science and Technology Development Programmes in Lithuania.

6. References

1. Sewage Treatment Process. SymBio process of U. S. Pat. No. 6743362 B1., Jun.1, 2004
2. Methods and apparatus for biological treatment of aqueous waste. U. S. Pat. No. 2002/0148779 A1., Oct. 17, 2002
3. Carlsson B., Lindberg C.F. Some control strategies for the activated sludge process, Systems and Control Group, Uppsala University, Oct 96, Rev Oct 97, Aug 98, 21p.
4. http://www.enviroquip.com/tech_transfer_db//Symbio/technical_resources/technical_papers/Industrial_Wastwater_2002_SymBio_Paper.pdf.
5. Ogunnaike B.A., Ray W.H. Process Dynamics, Modeling and Control. Oxford University Press, 1994, 1260 p.
6. Hautala J., Yli-Kotila H. Parameter adaptive control: predictive control. Oulu, 1993.
7. <http://www.kaunovandenys.lt/lt/?id=178>
8. <http://www.kaunovandenys.lt/lt/aplinksauga/es/>
9. Aleksa V., Galvanauskas V. Technological processes automation and control. (In Lithuanian), Kaunas, Technologija, 2008. 284 p.
10. Levišauskas D. Adjustment of automatic control systems. Vilnius, 2008, (in Lithuanian).

ANALYSIS OF EFFICIENCY OF A PUMP SET OPERATING IN AN IRRIGATION SYSTEM

Elzbieta SZYCHTA, Leszek SZYCHTA, Radosław FIGURA
Technical University of Radom, Faculty of Transport and Electrical Engineering, Poland

Abstract: The paper presents selected properties of irrigation system and the influence of pump set control system on pumping efficiency for its system. The method of calculating pumping efficiency was shown. The variation of pump set efficiency as function of pumps flow rate was analyzed. The method of calculating pumps rate of flow for the most energy-saving control system was presented.

Keywords: irrigation system, pump set, pumping efficiency, energy-saving control system.

1. Introduction

Countereffective utilization of energy adversely affects the natural environment. Energy efficiency of operational processes, increased by developments in power electronics and emergence of modern control systems [5,7], reduces demand for energy of end users and has beneficial effects on climate phenomena, mitigates noxious emissions, improves health condition, and reduces energy consumption of the gross national product.

Water pump stations in Poland, consuming approximately 2,000 GWh per annum, constitute a group of electricity users [7]. They comprise pump stations for irrigation systems. Irrigation systems in intensive farming and sports and leisure facilities are necessary elements, while minimized operating costs boost profits and return on investment. Operating costs of irrigation systems are related to such factors as repairs, maintenance, and electricity consumption and dependent on a control system of a pump set, among other things. Selection of an appropriate control system for a pump station is a major element which should be based on a preliminary analysis of a client's requirements.

2. Selected properties of irrigation systems

Irrigation systems in Poland must supply several hundred thousand m³ of water a year [10]. The quantities of water may vary and depend on the crops,

weather conditions, and soil type. In order to distribute water to rotors, a pipeline system of several dozen kilometres is constructed all over an irrigated area [9]. Uniform water supply to the entire irrigated area is ensured by hundreds of rotors, divided into k sections. One to several pieces of rotors, depending on their flow rate, are situated in each section [9]. Sum total of flow rates Q_i of the equipment located in one section may not exceed the maximum flow rate of the pumping station at nominal head of the rotor, in consideration of the head differences in the field and of the hydraulic losses on the path from the pumping station to a working section. Combining rotors of various operating characteristics results in sections of differing flow rates Q_i , with those of maximum Q_{\max} and minimum flow rate Q_{\min} . It is assumed that i^{th} section can operate correctly if the head in the station's suction branch is H_{ti} . The value of H_{ti} is the sum total of static head H_{sti} , considering land topologies and nominal operating pressure of the equipment in i^{th} section and hydraulic losses ΔH_i resulting from hydraulic resistance of the pipeline [3], and is calculated as follows:

$$H_{ti} = H_{sti} + \Delta H_i, \quad (1)$$

$$H_{sti} = H_{ni} + \Delta H_{sti}, \quad (2)$$

where: H_{ni} – nominal head for i^{th} section at Q_i ,
 ΔH_{sti} – static losses.

The equations (1) and (2) define the required head at the station's suction branch. Depending on the value of head at the suction branch, the head of the pump set H_{di} is expressed:

$$H_{di} = H_{ti} - H_s, \quad (3)$$

where: H_s – inlet water head.

In most extensive irrigation systems, water collected by a pump station comes from open reservoirs, it is therefore assumed that $H_s=0$, and the pump set's head H_{di} equals H_{ti} . The varied static H_{sti} for the individual

sections and diverse ΔH_i cause that the head at the station's suction branch, H_{ti} , should range between H_{tmin} and H_{tmax} (1). Systems controlling pump stations in most rotors maintain a constant head of H_{tmax} at the suction branch. Those sections for which pipeline hydraulic losses, ΔH_i , and static head H_{sti} , are the greatest operate correctly. In such cases, head H_{zi} supplied to i^{th} section is expressed:

$$H_{zi} = H_{tmax} - \Delta H_{sti} - \Delta H_i. \quad (4)$$

The control system mentioned above makes it necessary to install, upstream of sections, elements that provide for choking the head from H_{zi} down to H_{ni} , which ensures correct operation of a section. Properties of an irrigation system may be illustrated as a family of pump $H=f(Q)$ -curves of a pumping system e.g. Fig.1 described with the equation (1). The maximum number of such curves depends on the number of sections k in an irrigation system.

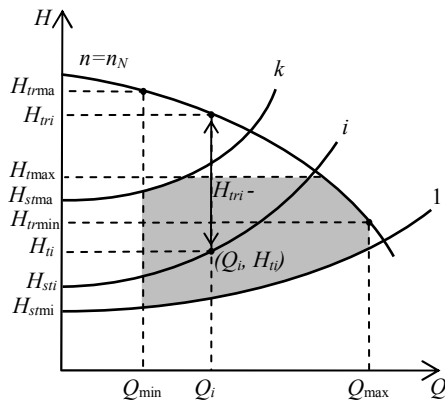


Fig.1. Pump $H=f(Q)$ -curves of irrigation system and pump's $H=f(Q)$ -curve at rotational speed $n=n_N$.

To simplify the graphic representation of a pump $H=f(Q)$ -curve, the set is assumed to comprise a single pump. Fig.1 plots the pump's $H=f(Q)$ -curve at rotational speed $n=n_N$ and pumping system's curves for selected sections. The pumping system's curves for the initial ($i=1$) and final ($i=k$) section are presented, where static heads become lowest (H_{smin}) and greatest (H_{smax}), respectively. The pumping system's curve for a selected i^{th} section is plotted as well. A point located in the pumping system's curve for i^{th} section, coordinates (Q_i, H_{ti}) , is assumed to graphically represent the operation of a single section. Heads at the pump station's collector H_{ti} , water requirement Q_i , and operating times for the particular sections t_i enable an accurate determination of distribution characteristics of an irrigation system. This helps to calculate variations of water pumping efficiency coefficient in irrigation systems and to develop a control system that minimizes energy consumption of a pump station.

3. Effect of pump set control system on pumping efficiency

Cascade and converter control are most commonly employed in irrigation systems. Results of analysis and research prove that application of converter control is

more effective than cascade control. There are cases of pump set control with smooth regulation of pump rotational speeds, however, where water pumping efficiency falls below 20%. To minimize energy consumption of pump sets, pumping efficiency should be maintained at the maximum level possible. Measures have been taken to find a control system for a pump set that would maintain its efficiency at the highest level. To establish the maximum efficiency of a pump set, variability of the efficiency function needs to be tested as dependent on such parameters as pump set's head and flow rate. This article analyses variations of the pump set's efficiency as a function of flow rate of pumps in an irrigation system's pump station.

3.1. Control of a pump set using one frequency converter

Systems controlling a pump set using one frequency converter effect shifts of the working point of only one pump unit (guiding pump). The working points of the remaining pump units in a pump set adjust to set heads at a station's suction branch H_{ti} and the current water distribution Q_i . A unit of regulated rotational speed maintains a set H_{ti} . By smoothly varying rotations of a pump unit, the guiding pump's flow rate Q_1 changes.

3.2. Control of a pump set using multiple frequency converters

Systems controlling a pump set using multiple frequency converters (Multi Motor Drive - MMD) require frequency converters to supply power to each pump unit included in a pump set. This control system provides for random variation of working points of the individual pump units (Q_{zi}, H_{ti}), while adapting heads at the station's suction branch to variable distribution of the pumping system.

The converter selects working points of the particular pump units on the basis of numerical calculations as per the instructions in the converter's internal program to maximize total efficiency of the pump set.

4. Efficiency of a pump set during operation in irrigation systems

The ultimate purpose of a system control operation of a pump set is to maintain a rated head at the pump station's collector with variable distribution of the pumping system. The controller should select rotational speeds of pump units in such a way that the overall efficiency of a pump set η_c is the greatest possible while maintaining the parameters set by the user.

4.1. Analyzing variability of the pump set's efficiency

The overall efficiency of a pump set η_c depends on efficiencies and flow rates of working pump units. The efficiency of a pump unit η_{zi} depends on the efficiency of the frequency converter η_{fi} , motor η_{si} , and pump employed η_{pi} [3,4,7].

$$\eta_{zi} = \eta_{fi} \eta_{si} \eta_{pi}. \quad (5)$$

Assuming that the rotational speed n of the asynchronous squirrel-cage motor in the pump unit is within the range from $0.5n_N$ to n_N (where n_N is the motor's rated speed), the efficiencies of both the motor and the frequency converter are constant. Therefore, the overall efficiency of the pump unit η_{zi} can be formulated as:

$$\eta_{zi} = C_\eta \eta_{pi} \quad (6)$$

$$C_\eta = \eta_{fi} \eta_{si} \quad (7)$$

The efficiency of the pump unit η_c is expressed in [7]:

$$\eta_c = \frac{Q_m}{\sum_{i=1}^m \frac{Q_{zi}}{\eta_{zi}}} \quad (8)$$

where: m – number of pump units operating in a pump set.

To determine the efficiency of i^{th} pump η_{pi} the method described in [7] has been employed. The efficiency of the pump varies as the flow rate Q_{zi} , head H_{ii} and the pump's rotational speed n_{zi} change. The efficiency $\eta = f(Q)$ for nominal rotational speed n_N is characterized by quadratic equations of varying factors depending on the pump's flow rate:

$$\begin{aligned} \eta_1 &= a_1 Q^2 + b_1 Q + c_1 & \text{for } Q \geq 0.5 Q_N \\ \eta_2 &= a_2 Q^2 + b_2 Q & \text{for } Q < 0.5 Q_N \end{aligned} \quad (9)$$

where: a_1, b_1, c_1, a_2, b_2 – factors of the quadratic equations
 Q_N – nominal flow rate of pump unit

The pump $H=f(Q)$ -curve for the nominal rotational speed n_N is also described by means of a quadratic equation [7]:

$$H_{ii} = H_0 - AQ - BQ^2 \quad (10)$$

where: H_0 – static head at the station's suction branch
 A, B – factors of the quadratic equations

The pump's operation at variable rotational speed changes its flow rate and head. According to the theory of probability, Q_{zi} is assumed to vary in accordance with [3,7]:

$$\frac{Q_{zi}}{Q_1} = \frac{n_{zi}}{n_N} \quad (11)$$

The pump's head depends on the rotational speed squared:

$$\frac{H_{ii}}{H_1} = \left(\frac{n_{zi}}{n_N} \right)^2 \quad (12)$$

A relation between the pump's head and flow rate at variable rotational speed is derived from (11) and (12):

$$\frac{H_{ii}}{H_1} = \left(\frac{Q_{zi}}{Q_1} \right)^2 \quad (13)$$

To define the pump's efficiency for the working point (Q_{zi}, H_{ii}) at a rotational speed lower than the rated

speed, it is necessary to find a flow rate Q_1 corresponding to Q_{zi} [7]. On the basis of (10) and (13), a flow rate Q_1 dependence is obtained [7]:

$$Q_1 = \frac{\sqrt{A_2 + 4H_0 \left(B + \frac{H_{zad}}{Q_{zi}^2} \right)} - A}{2 \left(B + \frac{H_{zad}}{Q_{zi}^2} \right)} \quad (14)$$

The dependence $\eta_1(Q_1)$ is determined according to (9). Employing the value of η_1 and the original power function of the pump [3,4], the pump's efficiency η_{pi} is calculated:

$$\eta_{pi} = \eta_1 \left(\frac{n_{zi}}{n_N} \right)^{0.09} = \eta_1 \left(\frac{Q_{zi}}{Q_1} \right)^{0.09} \quad (15)$$

Based on (5), (8), (14) and (15), a dependence of the overall efficiency η_c of a pump set on efficiencies of the individual pumps Q_{zi} in the set is obtained:

$$\eta_c = f(Q_{z1}, Q_{z2} \dots Q_{zm}) \quad (16)$$

Equation (16) is an implicit function of multiple variables and determination of its maximum value is complicated. It is possible, though, to analyze variability of η_c for an assumed pump set and set heads at the station's suction branch H_{zad} and a momentary distribution Q_m .

4.2. Analyzing variability of a pump set's efficiency as a function of its flow rate

Operation of a set is simulated which comprises three CR-32-6 pumps with characteristics of a pumping station distribution corresponding to distributions in irrigation systems e.g. Table 1.

Table 1. The system flow rate table

H_{ii} [m]	70	70	70	70	70	70	70	70	70	70
Q_m [m ³ /h]	90	85	80	75	70	65	60	50	40	30
H_{ii} [m]	65	65	65	65	65	65	65	65	65	65
Q_m [m ³ /h]	90	85	80	75	70	65	60	50	40	30
H_{ii} [m]	60	60	60	60	60	60	60	60	60	60
Q_m [m ³ /h]	90	85	80	75	70	65	60	50	40	30

Analysis of variability of the pump set's efficiency is based on the following assumptions:

- pumping station's flow rate ranges from 30 to 90 m³/h [1,2,9],
- the analysis is conducted in respect of three heads at the station's suction branch: 60, 65 and 70 m
- pumps flow rate ranges from 0 to 38 m³/h [8],
- variation of the pumps' flow rate $\Delta Q_m = 0.1$ m³/h,

Calculations for these cases are executed in an MS Excel spreadsheet. Fig.2 and Fig.3 illustrates variability of a pump set's efficiency η_c as dependent on the flow rates of three pumps at constant overall flow rate of the pump set $Q_m = 80$ m³/h and constant head $H_{ii} = 65$ m. Variations of the pump set's efficiency were of a similar nature in all the three cases introduced in the Table 1. The results represent an area including the maximum.

The most outlying point corresponds to the maximum efficiency of the pump set η_{cmax} . Based on flow rates of pump units read from the diagram, Q_{z1} and Q_{z2} , and a known overall flow rate of the pump set Q_m , flow rate of a third pump set can be determined:

$$Q_{z3} = Q_m - (Q_{z1} + Q_{z2}). \quad (17)$$

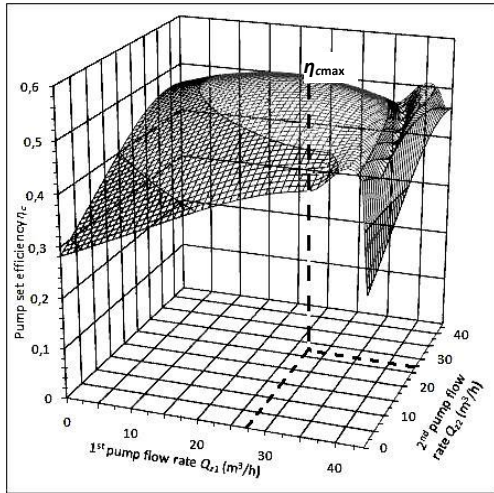


Fig.2. Variability of a pump set's efficiency η_c - 3-D view

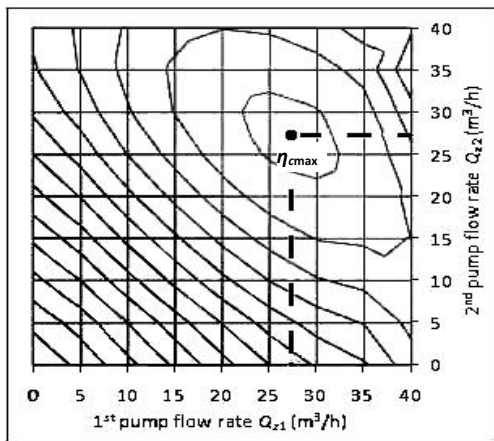


Fig.3. Variability of a pump set's efficiency η_c - top view

A careful analysis of the results leads to the conclusion that a maximum efficiency of the pump set η_{cmax} obtains for only one combination of pumps' flow rates. The calculations show that the maximum efficiency of the pump set η_{cmax} can be obtained when the pumps operate with identical flow rate Q_{zi} . Flow rates of the pumps can be calculated:

$$Q_{zi} = Q_{z1} = Q_{z2} = \dots = Q_{zm} = \frac{Q_m}{m}. \quad (18)$$

If the overall flow rate of the set diminishes, the number of working pumps is reduced. This enables to maintain the pump set's operation at an efficiency reaching its maximum for set input parameters of the pumping station. As a result, an extreme regulation system [5] can be applied, maintaining efficiency of the pump set at a maximum.

According to the theory of probability (11), it is established that pumps operating at identical flow rate Q_{zi} and at the same head at the suction branch H_{ti} have identical rotational speeds:

$$n_{zi} = n_{z1} = n_{z2} = n_{z3}. \quad (19)$$

5. Conclusion

Increased coefficient of a pump set's efficiency η_c translates into more cost effective pumping. By applying the proposed method of selecting pump rotational speeds, a maximum efficiency of a pump set can be achieved at set output parameters of a pump station. It is therefore possible to apply extreme control of a water pump station for irrigation systems. Continuous operation at maximum practicable efficiency of a pump set reduces electricity consumption, operating costs, and greenhouse gas emissions resulting from generation of electricity. Fitting all pump units in a set with frequency converters and PLC programmable controllers helps to select a rotational speed for each individual pump unit, provides for smooth startup and turn-off of the particular pump units. This solution helps eliminate water hammers that arise when pump sets are turned on directly at the mains voltage. This significantly reduces fault rates of pumping systems, minimizes repair and maintenance costs of the system equipment.

6. References

- Figura R., Szychta L. Energy Consumption of Water Pumping in Irrigation of Golf Courses. XI International Conference TRANSCOMP 2007, Zakopane.
- Figura R., Szychta L. Cost Effective Water Pumping in Extensive Sprinkling Plants. Pumps, Set Pumps 8/2008.
- Jędrał W. Impeller Pumps. PWN, Warszawa 2001.
- Jędrał W. Impeller Centrifugal Pumps. Publications of the Technical University of Warsaw, 1996.
- Luft M., Cioć R.: Increase of Accuracy of Measurement Signals Reading From Analog Measuring Transducers, Silesian University of Technology Scientific Publications 2005, Transport vol. 59 (1691), Gliwice 2005.
- Polish Standard PN-EN 127-03. PKN, 2004.
- Szychta L. Principles of Selecting Control Systems for Water Pumping Stations. Publications of the Technical University of Radom 2006,
- Technical documentation of CR/CRE Grundfos pump, July 2006.
- Rain Bird Deutschland GmbH – System Analysis & Documentation of Golf Course – Gaufelden-Nebringen 2003.
- Archive records of rainfall in central Poland <http://www.imgw.pl/wl/internet/zz/pogoda/tempsred.html>, 30.07.2007.

DIFFERENT SIMULATION MODELS IN EXEMPLARY EMPLOYMENT FOR “PUMP AGGREGATE – PIPELINE” SYSTEMS

Anna KOZIOROWSKA, Jacek BARTMAN
 University of Rzeszów, Institute of Technology, Poland

Abstract: The paper presents the application of differential equations in modelling and simulation tests of water-supply network pumps drive system together with the powered water-supply pipelines. Mathematical models of PWM converter, squirrel-cage induction motor, and pump together with a pipeline, allow to carry out computer simulations of the whole drive system consisting of the above-listed elements. Simulations of the system of such complexity pose definitely more difficult problem than simulation of each of the elements performed separately. In the following, mathematical models of individual elements and selected, simulation tests of the system are presented.

Keywords: modelling, simulation, pumps drive system.

1. Types of simulation models

Modern science uses research for pulling down cost of project design and exploitation of real system. Simulations allow to get image of system behaviour in different situations - often extreme - however, adequacy of gotten results is for reality derivative accuracy of accepted model.

So, modelling has creation of object for task, which owns chosen attributes of originals. The basic purpose is to present most important devoted – from the point of view of led analysis - attribute of original object and omitting the less important feature. Determination of its purpose is an important element of modelling - negligible features can be very important from the point of view of another analysis in a different context. It is possible to attempt building model taking into consideration all features of the original - then we would get universal model. Unfortunately, that is not always possible, but most often completely purposeless. The recent development of the information technology has caused a situation where a major group of models undergo computer simulations (so-called simulation models). They allow to simulate in an easy way extreme, sometimes unacceptable conditions of work of systems.

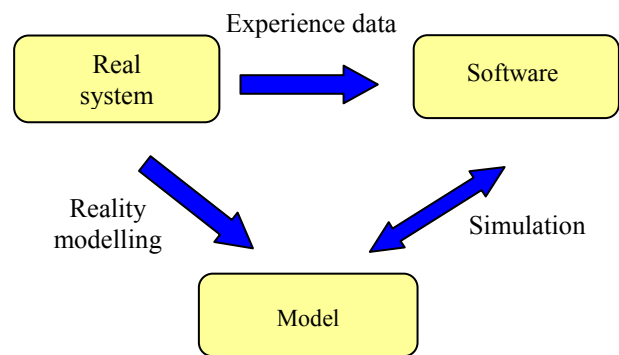


Fig. 1. Modelling and simulation scheme [1]

Simulation models can have different form and it is possible to present them as:

- algebraic and function equations;
- characteristic package;
- neuron models;
- fuzzy models;
- etc.

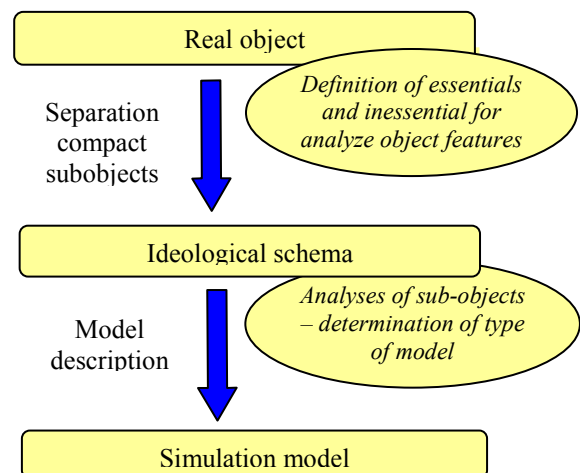


Fig. 2. Periods of development of simulation model

Selection of model’s form to employ it for definite description of system or phenomenon is the

consequence of our knowledge about the object. Models written down in the form of algebraic and function equations are characterised by grate accuracy and they are universal, unfortunately, they require acquaintance of parameter of object, but accuracy of gotten solution depends not only on description but from equation solving manner. Packages of characteristics describe concrete object, they are not universal and they are gotten most often as an experiment.

Neuron models are built as a result of artificial teaching of neuron network and they take advantage them for generalizing gotten knowledge ability. There important advantage is lack of parameters, however, they are not universal – they describe concrete object (phenomenon).

Fuzzy models have character descriptively–expert. They do not require acquaintance of parameter of object directly but experimental acquaintance of its behaviour is indispensable.

It is possible to divide process of modelling into several periods (Fig. 2).

Firstly, the ideological scheme of modelled object should be constructed, provided that all the particles have been previously distinguished. It will be necessary to carry analysis of the problem what kind of simulation model will be proper for description of chosen element. In final period it is necessary to describe simulation models of individual elements and define manner of exchange of data among them.

2. Idea of water-supply system model

Components of classical water-supply systems, in view of fulfilled functions, have differentiated technological structure, proper technical parameters and hydraulic characteristics with their local conditionality of modes of work subsequent. All of water-supply system elements match different behaviour, dependent on fulfil function and moment extortions in the form of fate conscription of water.

It is possible to differ in construction of mathematical model of water-supply system match from the point of view of its different hydraulic character, two parts of warehouse elements: static and dynamic. Static part of model includes structure of network with valves and pumps. Dynamic part of model presents reaction of system on variable conscription of water in time.

The paper presents the model of multipump system with one pump adjusted and affixed pumps unadjusted [2]. The system consists of pump system includes induction motor and pump, frequency converter with control system and pipeline (Fig. 3). Complexity of system and miscellaneous character of its individual component determines utilization of different method of modelling of different components of system:

- induction motor has been described with the aid of match of differential equations,
- frequency convertor with the aid of algebraic equations,
- pumps are described by characteristics
- pipeline by neuron model.

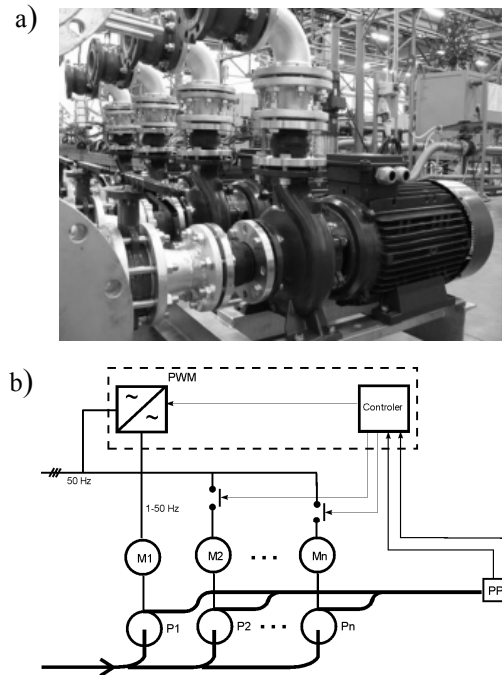


Fig. 3. Water-supply system: a) part of real water-supply system, b) scheme of ideological system

3. Mathematical model of PWM rectifier

The rectifier consists of power circuit, three-phase diode rectifier, DC circuit and three-phase voltage inverter. [4, 7]. There are accepted simplified assumption in the model:

- transistor starts up immediately;
- transistor is replaced by connector which resistance during operation corresponds to resistance of conductive transistor;
- switched off transistor does not carry electric current.

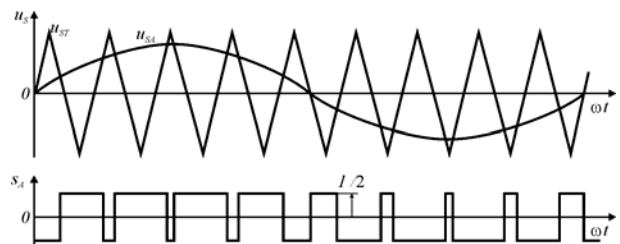


Fig. 4. Waveforms of switching functions $s_A(t)$ for sinusoidal modulating wave SPWM

Receiver phase-to-phase voltage equations have a form:

$$\begin{bmatrix} u_{AB}(t) \\ u_{BC}(t) \\ u_{CA}(t) \end{bmatrix} = U_d \begin{bmatrix} 1 & -1 & 0 \\ 0 & 1 & -1 \\ -1 & 0 & 1 \end{bmatrix} \begin{bmatrix} s_A(t) \\ s_B(t) \\ s_C(t) \end{bmatrix}, \quad (1)$$

where $U_d = \sqrt{2}U_{ac}$.

These switching functions were used to control transistors in simulation model of PWM rectifier.

4. Induction motor model

Application of A-models to description of induction motor is used in water-supply network pumps drive system. Finally, the following system of equations was adopted for simulation tests of pumps drive system. Fundamental equations of the motor:

$$\frac{d\mathbf{I}}{dt} = \frac{1}{K} \mathbf{A}(\mathbf{U} - \mathbf{R}\mathbf{I} + \boldsymbol{\Omega}\boldsymbol{\Psi}), \quad (2)$$

where:

$$K = \alpha_r + \alpha_s + \alpha_m;$$

α_m – inverse of magnetising inductance;

α_s, α_r – inverse of stator and rotor inductances;

$$\mathbf{A} = \begin{bmatrix} \alpha_s(\alpha_r + \alpha_m) & 0 & -\alpha_s\alpha_r & 0 \\ 0 & \alpha_s(\alpha_r + \alpha_m) & 0 & -\alpha_s\alpha_r \\ -\alpha_s\alpha_r & 0 & \alpha_r(\alpha_s + \alpha_m) & 0 \\ 0 & -\alpha_s\alpha_r & 0 & \alpha_r(\alpha_s + \alpha_m) \end{bmatrix};$$

$$\mathbf{U} = [u_{sa} \quad u_{sb} \quad 0 \quad 0]^T;$$

$$u_{sa} = U_m \sin(2\pi ft + \varphi);$$

$$u_{sb} = U_m \sin(2\pi ft + \varphi + 120^\circ);$$

$$\mathbf{I} = [i_{sa} \quad i_{sb} \quad i_{ra} \quad i_{rb}]^T;$$

$$\mathbf{R} = \begin{bmatrix} \frac{1}{3}(2r_{sa} + r_{sb}) & \frac{1}{3}(r_{sc} - r_{sb}) & 0 & 0 \\ \frac{1}{3}(r_{sc} - r_{sa}) & \frac{1}{3}(2r_{sb} + r_{sc}) & 0 & 0 \\ 0 & 0 & r_r & 0 \\ 0 & 0 & 0 & r_r \end{bmatrix};$$

r_{sa}, r_{sb}, r_{sc} – resistance values of stator phases;

r_r – rotor resistance value;

$$\boldsymbol{\Psi} = \begin{bmatrix} \frac{i_{sa} + i_{ra}}{\alpha_m} + \frac{i_{ra}}{\alpha_r} \\ \frac{i_{sb} + i_{rb}}{\alpha_m} + \frac{i_{rb}}{\alpha_r} \end{bmatrix}; \quad \boldsymbol{\Omega} = \begin{bmatrix} 0 & 0 \\ -\frac{\omega}{\sqrt{3}} & -\frac{2\omega}{\sqrt{3}} \\ \frac{\omega}{\sqrt{3}} & \frac{2\omega}{\sqrt{3}} \end{bmatrix}.$$

The equation of motion can be written down as:

$$\frac{d\omega}{dt} = \frac{P}{J} (T_e - T(\omega)), \quad (3)$$

$$T_e = \frac{\sqrt{3}p(i_{ra}i_{sb} - i_{rb}i_{sa})}{\tau}, \quad (4)$$

where:

$T(\omega)$ – mechanical moment;

p – number of pole pairs;

J – moment of inertia;

T_e – electromagnetic moment.

5. Pump characteristic

Pump operation basis on differential pressure generation. The characteristics of pump are shown at Fig. 5. The diagram shows set of curves for constant speed of motor-pump unit. Speed of pump is changing during the operation and pump pass from one curve to the other, keeping the forcing pressure constant (in assumed limits of pressure changes).

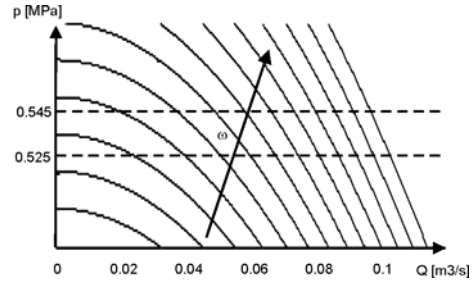


Fig. 5. An example set of pressure p vs. flow Q characteristics of a pump

There is assumed reduced model of pipeline to load the unit induction motor – pump. There are disregard effects of cavitations and water propagation in pipeline.

6. The pipeline model

A neuron model of pipeline is presented in the paper. It was indispensable to make measurements in real object and using them as teaching data for neuron network [6]. The multilayered neural network learned with back propagation rule has been used in the modelling process. Neural network was built from 3 neurons in input layer, 4 neurons in implicit layer and 1 neuron in output layer (Fig. 6).

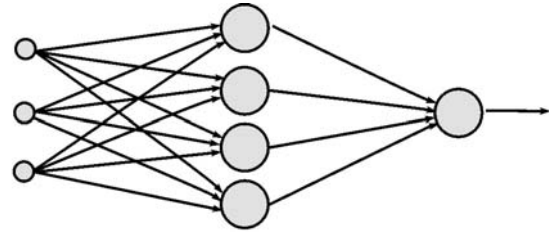


Fig. 6. Scheme of neuron network taken advantage as a model of pipeline

7. Algorithm of calculations

There is necessary to formulate a mathematical model of system and to make computer simulations for interesting dynamical states of system to make an analysis of water pump drive system and pipeline system operation.

The system consists of few elements and there is necessary to formulate an algorithm of calculations. The algorithm establishes sequence of carrying out individual operations and decides about connecting and disconnecting an additional motor, fed from power network [1, 7].

8. Simulation results

The models presented before were used to simulate work of water-supply system. There were observed parameters important from the point of view of whole exploitation system:

- water pressure - important parameter for water receivers (pressure stabilization is required and such task is required from system);
- rotary speed of pump system;
- electric current taken by asynchronous motor with adjusted speed - parameter important from the point of view of exploitation of energy system.

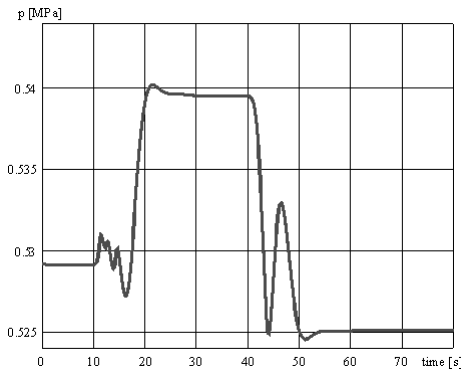


Fig. 7. Results of simulation test concerning - pressure

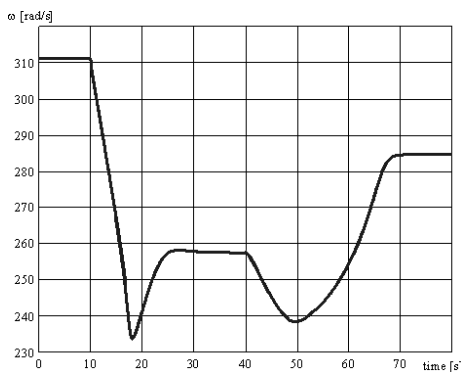


Fig. 8. Results of simulation test – motor speed

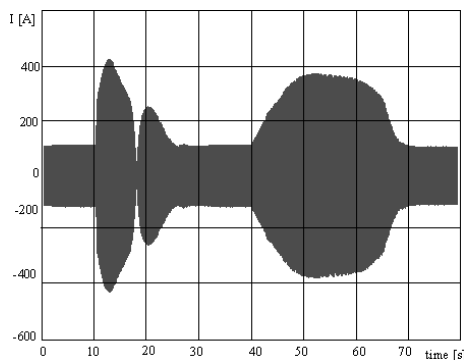


Fig. 9. Results of simulation test – motor current

Received results show, that model behaves in researched state of work according to expectations and to adequate manner for behaviour of real system. From the operational point of view it is important to keep quasi-constant delivery pressure and to limit

instantaneous current values to values admissible in given power supply system.

9. Conclusions

There are generally used the circuit models in mathematical description of drive systems, which consist of induction motor, frequency converter and control system.

They enable description with assistance of operational transmittance (linear systems) or differential equation. It makes the time of simulation shorter giving grate accuracy in engineer practice [3, 5].

Mathematical models of frequency converter, induction motor, pump and pipeline let us carry simulation tests of all drive systems consisting of the aforementioned elements [2, 3, 7]. Simulation of such complicated system presents harder problem than running the simulation of each element separately.

The differential equations representing the whole system are those of the stiff type, therefore equations describing individual elements were solved using different integration steps in order to accelerate the calculation process. The obtained results confirm that such approach is acceptable. Computer simulations are modern tool which let us analyse varied systems operation. There is important that there is possible to make lots of tests without system damage. There can be analysed critical states of system and system work with damaged elements. It is grate importance in power electronic control system and it lets decrease the tests costs.

10. References

- Gutenbaun J. Mathematical modeling of systems (in Polish). Exit, Warsaw, 2003.
- www.hydro-vacuum.com.pl, February 2009.
- Kulesza A., Kołodziej H. Systems of pumps control (in Polish). Pumps and pump stations 2/2001. p. 47–51.
- Sobczyński D. Highspeed drive system with induction motor fed from PWM rectifier (in Polish). Rzeszow, 2004.
- Tunia H., Barlik R. Theory of converters (in Polish). Warsaw, 2003.
- Duch W., Korbicz J., Rutkowski L., Tadeusiewicz R. Neural Networks, vol. 6. Exit, Warsaw, 2000.
- Koziorowska A, Bartman J., Buczek K. Forcing pressure simulations in water supply system during water requirement changing. Proceedings of 2nd Conference on Intelligent Knowledge Systems, Istanbul, Turkey, 2005. p. 97-101.
- Kulbik M. Computer Simulation and On-Site Examination of Municipal Water Supply System: a Monograph (in Polish). Gdansk, 2004.

APPLICATION OF SIMULATION TOOLS FOR A FERTILIZER GRANULATION CIRCUIT

Gediminas VALIULIS^{*,**}, Rimvydas SIMUTIS^{*}

^{*}Process Control Department, Kaunas University of Technology, Lithuania

^{**}Electrical Engineering Department, Šiauliai University, Lithuania

Abstract: The paper presents the extended modelling and simulation approach to granulation in a continuous drum granulator-dryer circuit for fertilizer production. The model is based on granule coating phenomena and involves the basic process parameters, features and equipment. For a better model performance, information from the process sensors and the experience of process experts has been applied as the extension to the main model. GrowSim simulation tool has been used to simulate some processes frequent in the real plant and test the granulation model. The simulator proposed is intended to ensure a better process understanding, staff training, and evaluation of control strategies.

Keywords: granulation, modelling, simulation, control.

1. Introduction

Many continuous granulation plants operate well below design capacity, suffering from high recycle rates and even periodic instabilities [8]. The main reasons are related to raw material properties, process equipment and control problems. The process control still depends on the experience and skills of process operators, namely experts.

Diagnostic systems show the potential to apply systems engineering approaches to complex operational problems such that operators are well informed, are able to quickly diagnose abnormal conditions, test quickly possible solutions via detailed simulations and then proceed to apply corrective actions [5]. Mathematical modelling and simulation can improve dealing with materials, energy and information through better understanding of underlying mechanisms in the system. The trade-off between the necessary accuracy and resulting complexity becomes increasingly important when the nonlinear and multivariable behaviour must be taken into account [3].

A number of scientific works deal with the modelling of granulation mechanisms. However, only a few are focused on practical implementation with a user friendly

simulator available. The increasing capabilities of computer hardware and software ensure the incorporation of complex knowledge (models) represented by differential and algebraic equations, measured process data, process experts' information, etc. But to be of use for the day-to-day work of the engineer these models have to become more user friendly, than the one that the scientist is dealing with [2]. The simulator developed according to the extended modelling approach aims at giving a better insight in granulation process features and can therefore be useful in control and staff training.

2. Main process details and model development

2.1. Brief circuit description

Drum granulation is a particle size enlargement process often obtained by spraying a liquid binder or slurry onto fine particles as they are agitated in a rotary drum [8]. A commercial continuous granulation circuit for granulated diammonium phosphate fertilizer (formed by the reaction of phosphoric acid and ammonia) production consists of: a pipe reactor, spray nozzle system, drum granulator-dryer, granule classifier (screens), crusher and nuclei feed system (Fig. 1).

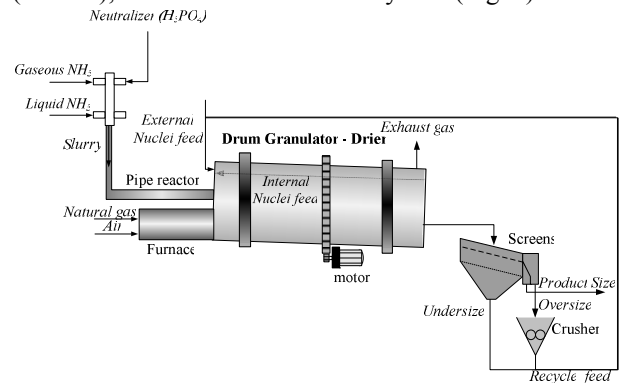


Fig. 1. Typical drum granulation-drying circuit utilized in the diammonium phosphate (DAP) production industry

Particle circulation is achieved by the action of the rotating drum and lifters. Granules are cycled many times through the spray zone and the liquid layer attached is pre-dried before the particles return to the spray zone again. After some residence time granules leave the drum and the classification procedure is performed. They are split into three fractions: small, marketable and large. Small, crushed large and even marketable granules are fed back to the drum as external nuclei.

A more detailed description of granulation circuit and granulation mechanisms can be found in [6].

2.2. Modelling Basis

The main requirements for granulated fertilizer are related to granule size, shape and chemical composition, moisture content, mechanical strength, etc. A number of different process parameters and material properties, as well as control actions, influence the granulation process (Fig. 2). This creates a strong nonlinear system exposed on different time scales that is difficult to predict just by intuition. Detailed modelling is needed in order to describe the coexisting processes and the transients of the process state variables correctly [2].

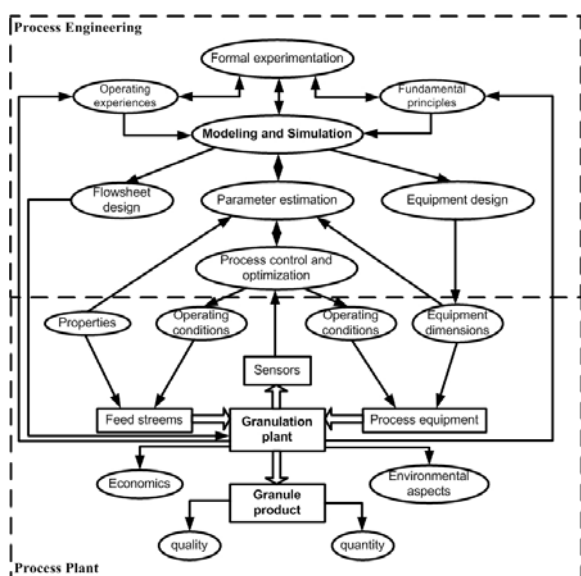


Fig. 2. Representative interfaces between process engineering and a typical granulation plant [1]

The model presented is essentially based on fundamental conservation principles and it partially takes into account equipment properties and the stochastic nature of the process. The mechanistic part incorporates the understanding of physics and underlying mechanisms (e.g. mass and energy balances, growth kinetics). The empirical part uses raw and/or filtered process sensors' data, their storage, retrieval and parameter identification techniques in addition to the mechanistic (white box) model.

The expert component involves the process experts' recommendations, which are of great value due to the lack of other knowledge mentioned above. The survey of

the granulation process model development can be found in [7].

2.3. Modelling assumptions

Obviously an extremely rigorous model that includes every phenomenon down to microscopic detail would be so complex that it would take a long time to develop and might be impractical to solve, even on the latest supercomputers [4]. An engineering compromise between a rigorous description and getting an answer that is good enough is always required [8].

Basic modelling assumptions:

- granule shape is spherical;
- each granule in the granulation circuit is analyzed;
- stochastic nature of the process is estimated;
- preferred growth is by layering;
- granule agglomeration is an unacceptable mode of operation;
- growth rate is a function of initial granule size, slurry flow rate, temperature inside the granulator, granule position in the drum, number of particles in the granule bed;
- granule moisture evaporation inside granulator-dryer;
- mechanical attrition of granules inside the granulator-drier, defined by attrition function;
- presumable nucleation (formation of new seeds) during slurry spraying;
- external classification of granules into three fractions (undersize, marketable and oversize), defined by classification function;
- external crushing of oversize granules, defined by grinding function;
- residence and transportation delays in the plant;
- internal and external feed of seeds (nuclei for new granules).

2.4. Main process variables

Table 1 presents the main input (manipulative) and output variable set available to the operator for process state prediction and control.

Table 1. Main process input and output variables

Input variables	Output variables
Slurry flow rate	Granule mass throughput from granulator
Slurry viscosity, density and moisture content	Granule size distribution parameters
Recycle feed flow rate	Granule moisture content
Natural gas flow rate	Granule mechanical properties
Slurry N:P ratio	Granule N:P ratio
$\text{NH}_{3(\text{gas})}:\text{NH}_{3(\text{liquid})}$ ratio	

However, some process variables related to unique material and equipment properties can not be evaluated and controlled directly and instantly. In such a situation, the process model can provide information about

important process states, such as recycle size flow rate and distribution, drum system jamming factor, granule moisture content, size evolution of single granule inside the granulator-dryer. This information can help to predict future process states and prevent abnormal situations, which can initiate process stoppage and loss of productivity.

3. Simulator

A new “GrowSim” simulation tool for drum granulation-drying process is under development. The simulator is based on the extended process model and is intended to be used for advanced process control and knowledge acquisition. Using powerful MATLAB software the tool simulates the physical process combining mass and heat transfer, including major units such as a drum-granulator dryer, classifier, crusher, transportation system. The graphical user interface (Fig. 3) has been built to mimic the process control environment available to the process operator in the real plant, with important additional information provided.

The simulation environment is composed of sections where the operator can change process parameters, observe the current or past states, get some advice on how the process should be controlled by the skilled operator. The simulator allows to introduce common

disturbances, faults, malfunctions. The manual or automatic process control modes are available. The operator can take a challenge to manage the process manually or leave all or part of the job to PI or Fuzzy controller. The simulation time can be easily adjusted if the computing resources are sufficient. Simulation can be paused at any moment, to make it possible to weigh one’s decisions. The main process parameters are logged and can be observed during the simulation or even later. The simulator is provided with routine to compare the simulated and real measured process data. Some experiments have been carried out for model and simulator validation purposes.

4. Results

The most common description of particles in means of their size is given by particle size distribution (PSD). Strong evidence of normal granule size distribution can be observed in Fig. 6, where the measured initial nuclei and granules out of granulator distribution data is fitted to the cumulative normal distribution curve with parameters defined.

Some simulation scenarios have been carried out to check the model and simulator using the same data as in Fig. 4. The results obtained are in fair accordance.

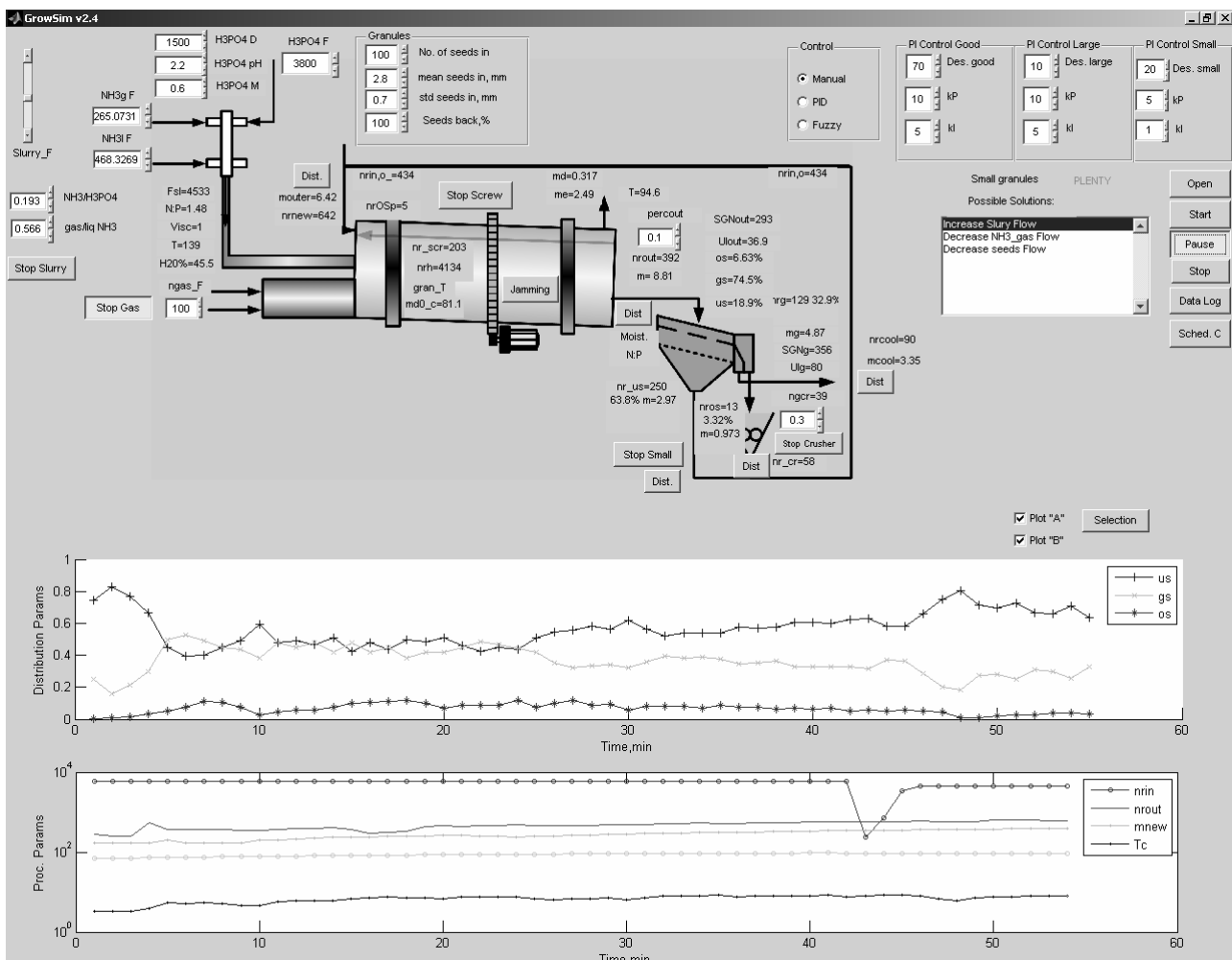


Fig. 3. Graphical user interface of “GrowSim” simulator

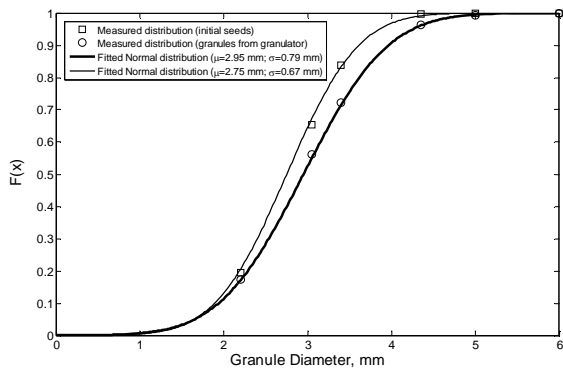


Fig. 4. Normal cumulative size distributions of initial seed flow and granule flow out of granulator

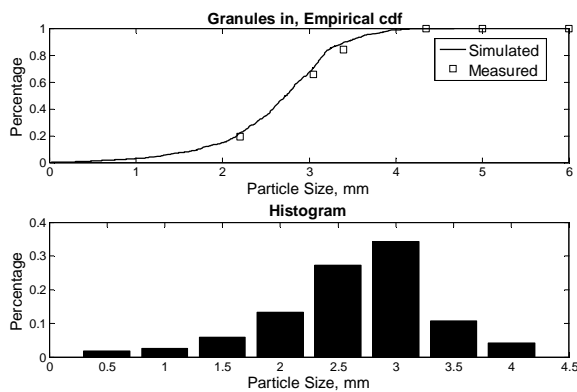


Fig. 5. Initial seed cumulative size distribution and histogram

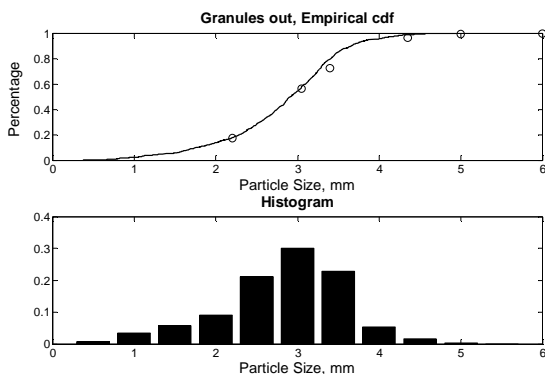


Fig. 6. Granules out of granulator cumulative size distribution and histogram

Another simulation experiment has been performed on decreasing slurry flow rate by 2/3 (Fig. 7).

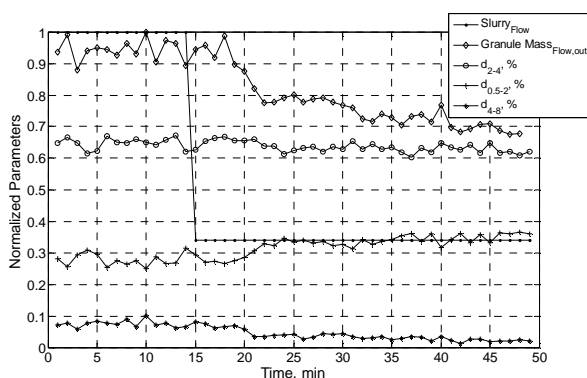


Fig. 7. Impact of the change of slurry flow rate (simulation)

The decrease of slurry flow (the recycle flow rate was kept constant) initiates the reduction of granule mass flow from the granulator as well as the decrease of median granule size. The latter is proved by the decrease of oversize and increase of undersize granule fraction. In this situation the number of marketable granules is almost the same. Compared to the measured data, these results are similar.

6. Conclusions

A DAP fertilizer granulation circuit has been modelled using basic physical principles such as growth, mass and heat transfer. The model has been implemented and simulation executed using “GrowSim” simulator in the MATLAB environment.

Some model validation procedures have been carried out and the results obtained are in fair accordance with the plant measured data.

The proposed model shows good potential for representing the behaviour of the granulation plant and hence can be advised for dynamic simulation leading to improved granulation circuit control and operator training.

7. Acknowledgment

This study is supported by the doctoral grant from the Lithuanian State Science and Studies Foundation.

8. References

- Ennis B.J. Agglomeration and Size Enlargement: Session summary paper, Powder Technology, vol. 88, 1996. p. 203-225.
- Ihlow M., Drechsler J., Peglow M., et al. A New Comprehensive Model and Simulation Package for Fluidized Bed Spray Granulation Processes. Chemical Engineering and Technology, vol. 27, 2004. p. 1139-1143.
- Juso E.K. Modelling and Simulation with Intelligent Methods. Sim-Serv, 2004, 17 p.
- Luyben W.L. Process Modeling, Simulation, and Control For Chemical Engineers. Mc Graw-Hill, 1999. 724 p.
- Salmon A.D., Hounslow M.J., Seville J.P.K. Handbook of Powder Technology, vol. 11. Granulation. Elsevier, 2007. 1390 p.
- Valiulis G., Simutis R. Analysis of Control Methods for Granulation Process. Proceedings of the 1st International Conference on Electrical and Control Technologies (ECT-2006), Kaunas, 2006. p. 496-600.
- Valiulis G., Simutis R. An Extended Modelling Approach to the Drum Granulation Processes. Proceedings of the 3rd International Conference on Electrical and Control Technologies (ECT-2008), Kaunas, 2008. p. 122-127.
- Wang F.Y., Cameron I.T. Review and future directions in the modelling and control of continuous drum granulation. Powder Technology vol. 124, 2002. p. 238-253.

INNOVATIVE MOISTURE CONTROL METHOD FOR CONCRETE MIXING SYSTEMS

Gintautas LENGVINAS, Vytautas DEKSNYS

Department of Electronics and Measurement Systems, Kaunas University of Technology, Lithuania

Abstract: Moisture control in concrete mixing systems is usually done using microwave moisture sensors. These sensors must be adapted for every type of mixture separately. We propose a new material type adaptive real-time moisture control method, which is based on transfer function time-domain analysis, used in conjunction with artificial neural network (ANN).

Keywords: ANN, time domain, transfer function, real time, moisture control, aggregates, concrete, hollow core slabs.

1. Introduction

Concrete is a construction material composed of cement (usually Portland cement) as well as other cementitious materials such as fly ash and slag cement, aggregate (generally a coarse aggregate such as gravel, limestone, or granite, and a fine-grained aggregate such as sand), water, and chemical admixtures. Concrete solidifies and hardens after mixing with water due to a chemical process known as hydration. Water reacts with cement, bonding the other components together, eventually creating a stone-like material. Concrete is being used to make pavements, foundations, motorways and bridges, parking structures, brick walls and footings for gates, fences and poles.

Aggregates, cement and water must be mixed to get a uniform mixture, suitable for moulding.

Workability is the ability to fill the form properly with a fresh concrete mix, with the desired work and without reducing the concrete's quality. Workability depends on water, aggregates (shape and size distribution), cementitious ratio and age. The quality of the product depends heavily on concrete workability. Product made of too wet concrete collapses immediately during the moulding process. On the other hand, if concrete is too dry, the resulting product will be porous and difficult to mould. The main factor contributing to poor workability of concrete is unstable water/cement ratio. If the amount of cement and aggregates in the mix is stable, the only influence on final concrete workability is water content.

There are two sources of water in concrete: wet aggregates and water added directly to the mix.

Today, the moisture of the mix is often controlled using microwave moisture sensors [1]. These sensors include an HF signal generator and resonator. Resonant frequency and resonator quality depends on dielectric permittivity and loss tangent of the surrounding substance. Water ratio changes these parameters for the given mixture. However, dielectric properties of different materials change in different ways. Consequently, the sensor parameter sets have to be calibrated for each type of material, in order to reliably monitor the dielectric properties of that material. Furthermore, this calibration is a very complicated and time consuming operation, that must be performed for every type of material or mix used in the manufacturing process. This is the main disadvantage of microwave moisture meters.

2. Moisture measurement and control in automatic concrete mixing systems

In practice, moisture sensors are not calibrated for the particular recipe of concrete. This recipe indicates the relative moisture of the mixture and the target value must also be set to a relative value. When using a moisture sensor, the concrete mixing algorithm consists of five phases. During the first phase (Fig 1.), aggregates, cement and a coarse amount of water (nearly 90% of the amount required) are added to the mix. During the second phase, the first mixing operation is performed. Depending on the mixer type, it takes 10-30 seconds. The goal of the first phase is to get a homogenous concrete mix. The third phase is the water/cement ratio correction phase. Water is added according to the moisture sensor readings. When target moisture value is reached, final mixing phase starts. It can take 15 – 150 seconds. This time depends on mixer type and water cement (w/c) ratio in the mix. If it is low, mixing time is long, and if w/c ratio is high, final mix time goes shorter. The fifth phase, is the mixer-emptying phase.

Typically, relative moisture of the mix in the mixer changes as shown in Fig. 1.

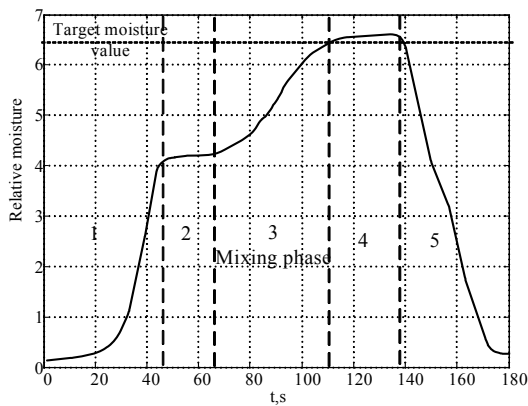


Fig. 1. Moisture changes during mixing process

Fig. 2 represents real data collected in the local facility producing hollow core slabs.

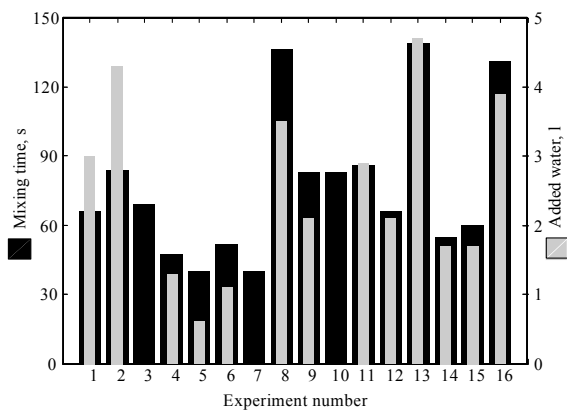


Fig. 2. Mixing times and water amount, added to the mixer

As shown in Fig. 2, the mixing time depends on the water amount, which is added to reach the target moisture. Fig. 1 and Fig. 2 show that most of the mixing time is spent on water/cement ratio correction. So, in order to reduce the mixing time and get the best workability of concrete, a new, material and mixture independent moisture measurement and control method is required.

3. Material type independent moisture control method

We present a new, material type independent moisture measurement method. The structure of our moisture measurement system with artificial neural network for material type detection is shown in Fig. 3.

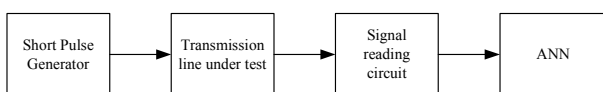


Fig. 3. Structure of the moisture sensor with ANN

A coplanar strip-line was used as a sensor. It was tuned to dielectric permittivity of $\epsilon = 6$ and electric line length of $l = \frac{1}{4} \lambda$, when the operating frequency is 1 GHz. As

dielectric in our transmission line was used testing material. The gap between ground plane and signal electrodes was filled with it [2].

Two popular materials (stone 5-11 and sand 0-2) were used for the experiments. Crushed stone is the roughest material it is useful for moisture content control, because in coarse- grained materials maximum available moisture is too small to influence the overall mix moisture. Maximum available moisture of crushed stone is 1-2 %. Sand 0-2mm is the most fine-grained material used in concrete mixtures. It can accumulate up to 15-18 % of water.

Table 1 represents mixed materials and their proportions used for our experiments. The first and the last materials are the compounds of pure sand and pure crushed stone respectively. The other materials are mixes of these two using different ratios.

Table 1. Materials used in experiments

Material number	Sand 0-2 mm, %	Crushed stone 5-11 mm, %
1	100	0
2	75	25
3	50	50
4	25	75
5	0	100

Water was added to the materials, in order to get seven different moisture ratios (0%, 1.8%, 3.7%, 5.4%, 7.1%, 8.6% and 10.2%) for measurements.

Having 5 material types and 7 moisture values for each type, 35 measurements were made in one experiment session. To get more reliable data we repeated experiment a second time. So, a total of 70 curves were collected. The power spectrum was taken as an informative parameter [3].

To find the relationship between material type and power spectrum curve the artificial neural network technology was used.

An artificial neural network (ANN) is a collection of simple interconnected analogue signal processors. The purpose of an ANN is to provide a mathematical structure that can be trained to map a set of inputs to a corresponding set of outputs. Fig. 4 illustrates an ANN used in this.

This ANN has three layers: the input, hidden and output layers. Each layer consists of nodes or neurons. Each node has sigmoid activation function, associated with it. Each interconnection between the nodes has a weight associated with it. The nodes in the hidden layers and the sum of output layers are the weighted inputs from sending nodes and applying this net input to the activation function. Applying the inputs and computing the output from the various nodes, activations and interconnection weights determine the output of the network.

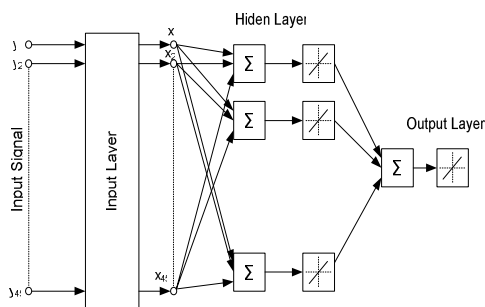


Fig. 4. Artificial Neural Network

Ten power spectrum values of different frequencies were taken as input data. The type of material was the learning target (Table 2). Target constants in the ANN output value range of -1 to +1 were acquired for different materials.

Neuron number was chosen accordingly to input layer size.

Table 2. Output values for ANN

Input data	Learning result
Material No. 1 (7 different moisture values)	-1
Material No. 2 (7 different moisture values)	-0.5
Material No. 3 (7 different moisture values)	0
Material No. 4 (7 different moisture values)	0.5
Material N. 5 (7 different moisture values)	1

4. Results

We have learned network using a collection of data with 7 different moisture points for every material. The generated network was tested using the same data used in the learning process, and the data collected during independent experiment with the same materials. Number of sample is set on x-axis. 1-7 – material No. 1, 8-14 material No. 2, 15-21 material No. 3, 22-28 material No. 4, 29-35 material No. 5. On y-axis we have set type of material (M1 – M5).

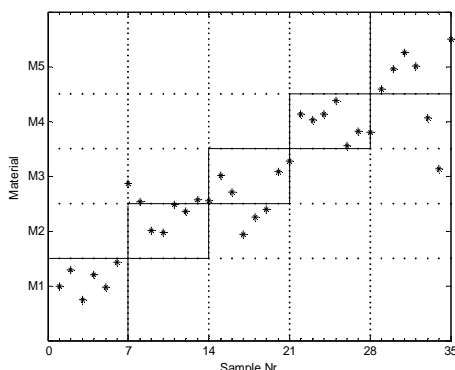


Fig. 5. ANN Tested with independent data

As it is shown in

Fig. 5, the possibility to identify the type of material was found. Most of the samples were recognized. Only a few samples were assigned to wrong material type. It shows the possibility to use this method in real time moisture control systems.

5. Conclusions

Using transfer function analysis and artificial neural network technology for material type detection makes possible material and mixture independent moisture measurement.

Single sensor, material independent technology for real time moisture control systems enables fast integration of moisture meters without individual calibration for every material or mixture used in technological process of concrete. It enables to reduce the mixing time and enhance a quality compare to classical moisture control systems.

6. References

1. Okumava S. Microwave Technology for moisture measurement. Subsurface Sensing Technologies and Applications, Vol. 1., Springer Netherlands, 2000, No. 2. p. 208-210.
2. Deksnys V., Lengvinas G.. Humidity Evaluation Method in Building Materials Using Time Domain Reflectometry. (In Lithuanian), Matavimai.– Kaunas, Technologija, 2004, Nr.2(30). p. 38-40.
3. Lengvinas G., Deksnys V., Ragauskas A. Technology For Aggregates Classification in Concrete Compounds. Electronics and Electrical Engineering, Kaunas, Technologija, 2006, No. 2(90). p. 61-65.
4. Daschner F., Knochel R. Microwave moisture sensor with nonlinear processing using artificial neural networks. Silicon 01 sensors for industry. Conference Rosemont. - Illinois, USA, 5-7 November, 2001.

THE INDEPENDENT FUZZY CONTROL WITH CORRECTION OF TWO DIMENSIONAL PROCESS

Gediminas LIAUČIUS, Vytautas KAMINSKAS
Department of Systems Analysis, Vytautas Magnus University, Lithuania

Abstract: In this paper is analyzed the independent fuzzy control of two input and two output process with additional control signals' correction. The control signal is additionally corrected by estimating other channel's control error.

The experimental analysis was performed to air pressure plant which is a nonlinear and dynamic process. The results of fuzzy control with correction are compared with PID control results.

Keywords: Fuzzy control, PID control, two input two output process, air pressure plant, nonlinear, dynamic.

1. Introduction

Lots of operational control systems in industry are multidimensional processes. Such control systems are more complex comparing with single dimensional processes. The multidimensional processes commonly are dynamic, nonlinear systems with dominance of interactions between input and output variables. The routine of multidimensional processes is that there is not enough information for designing the appropriate preciseness mathematical models.

One of the most powerful techniques for non-mathematical model based, dynamic and nonlinear system control is fuzzy control. The synthesis and tuning process of fuzzy controllers are mostly time consuming, but commonly guarantee desirable control results.

The experimental analysis was performed to the multidimensional process called an air pressure plant, which is a nonlinear and dynamic system.

2. The structure of control system

The scheme of physical control components of the plant is shown in Fig. 1. The plant consists of four main elements: the combined air channel (1), three air tanks (2), three air channels (3) and the combined air outlet channel (4). The combined air channel is connected with three air tanks which are connected with air channels, respectively. The air channels are coupled with the

combined air outlet channel at the end. A fan (7) is at the bottom of each air tank, which pumps the air from the combined air channel and makes an air pressure in the channel. The special corks of channels are forced to move depending on the sizes of generated air pressures.

The air tanks at each channel's bottom are necessary for the stabilization of air pressure oscillation. Additionally, air tanks connection with its designated fan provides a nonlinearity feature to control system. There are four special air feeding vents in the combined air channel by which may be adjusted the size of air inlet to air channels. The air channels dependence of each other is decided by the number of opened air feeding vents since fans are pumping the air from the combined air channel. The more air feeding vents are closed the greater dependence between air channels exist since the lack of air necessary for both fans. Each air channel also has an ultrasound distance sensor (5) which is operating on the ultrasound echo principle. They operate as the distance between the sensors and the air channel corks measuring equipments. The control target of the process is the maintenance of corks in desirable heights of air channels.

The input signals of the plant are the air fans voltage values, where 0V means that the fan is switched off, 10V - the fan is running at the maximum. They are controlled by direct current signals. The intermediate values of voltage effects the power of fans disproportionately.

The output signals of ultrasound distance sensors are also in 0-10V range where 0V corresponds to 0.2 metres range between the sensor and the cork, 10V - the distance of 1.2 metres. Since the moment the fan is switched off, the cork is about 1.1 metres far from its designated sensor, but the sensor measures that the distance is about 0.9 metres.

The input/output controller BK9000 is used to read the data from ultrasound distance sensors and to send the fans data to the plant. The BK9000 controller is configured and controlled by TwinCat software. The communication between the input/output controller and the software is reached via computers network and is

used the TCP/IP protocol to interchange data. The components module communicates with the BK9000 controller to directly control the air pressure plant. In this module are implemented the fans controllers which control the plant with analogue signals.

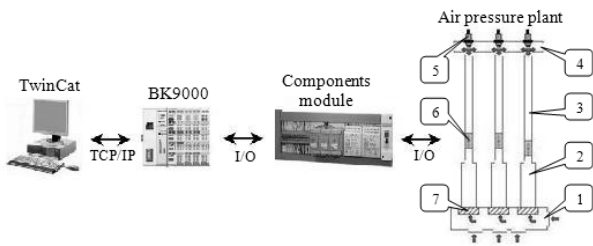


Fig. 1. The scheme of physical control components of air pressure plant

Since the experimental analysis was performed to two air channels of the plant, therefore the process was reduced to a two dimensional system. The control scheme of air pressure plant as a two dimensional process is demonstrated in Fig. 2, where $x_i(t)$, $u_i(t)$, $y_i(t)$ when $i = 1, 2$ are reference, control and output signals at t time moment of the system, respectively, W_{11} , W_{22} , W_{12} , W_{21} - transfer functions of the two dimensional process.

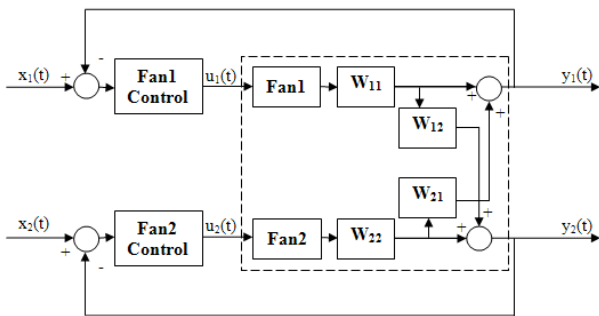


Fig. 2. The control scheme of air pressure plant as a two dimensional process

The air pressure plant was controlled with two different control types: PID and fuzzy. The principles of the synthesis of both control types are analyzed in next sections.

3. PID control

PID control is a useful as an initial control technique to almost everyone control system since the synthesis and the tuning process of it is commonly straightforward. When the studied control system is a complex one, this methodology gives an ideal opportunity to reveal the main control challenges to researcher. The above-mentioned principle of control systems analysis was used to identify the main control problems of air pressure plant.

The scheme of the synthesis of PID control of two dimensional process is demonstrated in Fig. 3.

PID controllers commonly are tuned using Ziegler-Nichols, Kappa-Tau and Takahashi methods. In order to

tune the controller gains by them are necessary to possess the information (characteristics) about the transient process which is ambiguous in air pressure plant. Accordingly, the gains were tuned by using a random search when the standard deviation of channel's control error (4) was as tuning criterion. The same tuned PID controllers were synthesized to both air channels of air pressure plant. The PID controllers were designed to control just the running intensity of appropriate fan not considering to the possible interactions between different air channels. This type of implementation was called as an independent PID control to the plant.

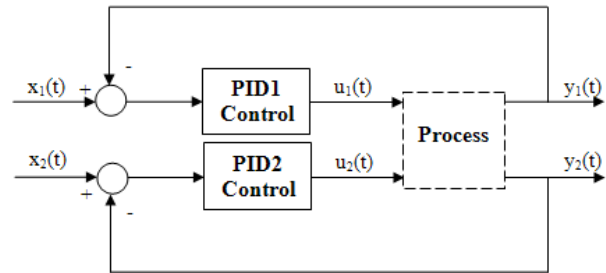


Fig. 3. The scheme of independent PID control of two dimensional process

The results of PID control (Fig. 8 and Fig. 10) acknowledged that the process was a nonlinear, dynamic system where existed interactions between different air channels.

As control results showed, the process dynamics had depended on the corks moving direction and moving proportion (the change size of reference signal). The greater corks moving proportion the greater dynamics in channels acted. A similar situation with the moving direction but the dynamics was more significant than the cork was moving down. Especially, there is a huge dynamical features difference between two situations: the cork was moving up by more than 15 centimetres and the cork was moving down by more than 15 centimetres. The results of PID control were suitable when the corks were moving up, but were not when moving down, especially when the corks were moving down by more than 15 centimetres. At this situation, the results were extremely unsatisfying since first of all the corks were moving down till reached the channels bottoms and after that achieved its reference signals.

Such a poor PID control results with static tuned PID controllers for all sets of reference signals meant the necessity of the synthesis of adaptive PID control or applying another control methods to air pressure plant. The detailed control results of PID are demonstrated in the section of experimental results.

4. Fuzzy control

The results of static tuned PID control of two dimensional process showed that this control method was not suitable for the plant. Consequently, we needed another control method which could control the plant in suitable manner. One of possible control techniques to air pressure plant is a fuzzy control.

Fuzzy control provides a formal methodology for representing, manipulation and implementing a human's heuristic knowledge about how to control a system [2]. The general scheme of fuzzy control architecture is demonstrated in Fig. 4 where the fuzzy controller is embedded in a closed-loop control system. The fuzzy controller consists of four main components: the fuzzification and defuzzification interfaces, the rule-base and the inference mechanism. The rule-base holds the knowledge, in the form of a set of rules of how best to control the system [2]. The inference mechanism evaluates which control rules are relevant (active) at the current time and then decides what the control signal to the plant should be. The fuzzification interface simply modifies the inputs so that they can be interpreted and compared to the rules in the rule-base and the defuzzification interface converts the conclusions reached by the interface mechanism into the control signal to the plant [2].

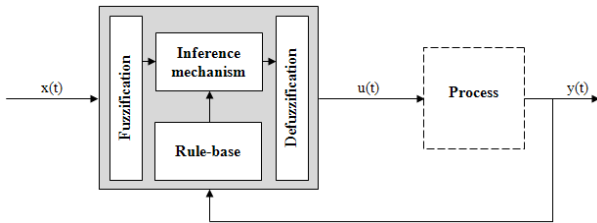


Fig. 4. The scheme of fuzzy control architecture [2]

The fuzzy controller may be interpreted as an artificial decision maker that operates in a real time closed-loop system [2]. First of all, the fuzzy controller aggregates the process output data $y(t)$, then compares it with the reference signal $x(t)$ and by that information decides what the control signal $u(t)$ of the process should be in order to ensure that the performance objectives will be met.

Considering to revealed problems of PID control and the existence of interactions between different air channels there was constructed the control scheme of independent fuzzy control with correction of the plant (Fig. 5). The main objective of independent fuzzy control with correction of two dimensional process was to improve the control results of PID. Additionally, fuzzy control had to consider to interactions between the air channels. In Fig. 5 Fuzzy1 and Fuzzy2 controls were generating the independent primal control signals of fans as in PID control scheme (Fig. 3) but additionally to them was implemented a special fuzzy control module that corrected both (Fuzzy1 and Fuzzy2 generated) control signals by estimating the interactions between channels. The interactions were estimated by calculating a moving average of the last 50 values of an appropriate channel's control error. The control error $e(t)$ of the channel is calculated by equation:

$$e(t) = y(t) - x(t). \quad (1)$$

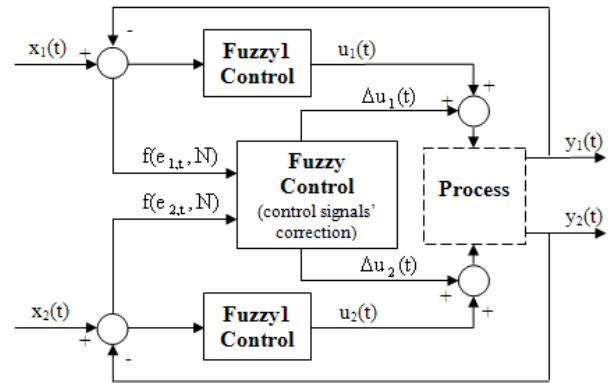


Fig. 5. The scheme of independent fuzzy control with correction of two dimensional process

The formula of moving average is:

$$f(e_{i,t}, N) = \bar{e}_{i,t} = \frac{1}{N} \sum_{j=t-N+1}^t e_{i,j}, \quad (2)$$

where: N - a sample size of moving average, $e_{i,t}$ - an N sized vector of control errors of i th air channel until time moment t , $i = 1, 2$ - an appropriate air channel.

If the cork was below its reference signal depending on the control error of another channel's cork position the primarily generated control signal must be strengthened, otherwise if the cork was above – weaken. This control signals correction module having information about the control error of each air channel produced two control signals correction values for both air channels.

4.1. The synthesis of independent fuzzy controllers

Having a general idea about the independent fuzzy control with correction of two dimensional process its time to look at the synthesis of those fuzzy controllers. Fuzzy control fuzzification interface operates linguistic variables, fuzzy sets and membership functions in order to transfer the fuzzy controller inputs to suitable data format that is necessary for comparing with the rules in the rule-base. Linguistic variables simply are the inputs of fuzzy controller. Each linguistic variable is characterized by fuzzy sets which in order are characterized by membership functions.

Each of independent fuzzy controllers used reference signal and control error as linguistic variables. Each linguistic variable was characterized by 9 fuzzy sets. There were used the triangular form of membership functions of fuzzy sets. The detailed scheme of linguistic variables, fuzzy sets and membership functions of independent fuzzy controllers is demonstrated in Fig. 6. The fuzzy sets of linguistic variable called "Reference signal" were selected without considerable constraints, lots of fuzzy sets concentrating in the middle heights of the channel in order to accurately control them. The two fuzzy sets named "15" and "75" were chosen a bit far from the main fuzzy sets concentration to ensure desirable control results when the corks were at the bottom or at the top, otherwise if the concentration of all fuzzy sets were in the middle heights area the control

results could be unsuitable since the dynamical features were different where the corks were situated at the bottom or at the top. The fuzzy sets of another linguistic variable named “Error” were selected more precisely since the control results of it depended significantly. Three fuzzy sets (with negative values) were set to control when the corks were moving up and five fuzzy sets when moving down. Five fuzzy sets were sacred to moving down in order to control such situations when PID controllers were not able to control or the control results were not desirable (the corks were moving down till reached the channels bottoms and after that achieved its reference signals). In these situations control signals had to be changed very slightly since the corks were moving down with additional power – free fall acceleration. Especially two positive fuzzy sets “10” and “30” drastically slowed down the effect of free fall acceleration when the reference signals of corks were changed more than 10 centimetres. The positive fuzzy sets values corresponded to the corks moving down direction since the corks positions in the channels were calculated not from the ultrasound distance sensors but from the bottom of each channel. Such an inverse distance calculations simplified visual estimation of actual corks positions in the channels.

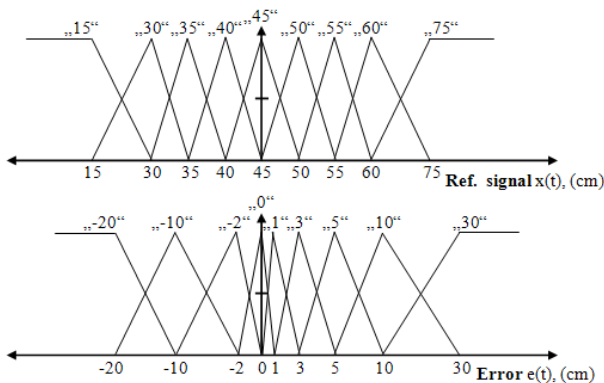


Fig. 6. Input linguistic variables, fuzzy sets and membership functions of Fuzzy1 and Fuzzy2 controls

The rule-base of each independent fuzzy controller was designed separately since the dynamics of air channels after detailed analysis were different. The rules in rule-base of independent fuzzy controllers were described by “IF Reference signal AND Error THEN Fans voltage” clauses. Each rule-base was composed of 81 rules since there were 2 input linguistic variables with 9 fuzzy sets in each.

The solution’s linguistic variable was produced by “min-max” algorithm and the final solution (control signal of the plant) was extracted by centre-average method. The “min-max” algorithm works as follows: for each rule is discovered the least (minimum) fuzzy sets truth weight of IF part which is provided to the appropriate (THEN part’s assigned) solution fuzzy set. If there was assigned a weight to the appropriate fuzzy set earlier, then has to be taken the bigger one (maximum). The final solution of fuzzy controller may be extracted, after the synthesis of solution linguistic variable with fuzzy sets weights assigned to it.

The formula of centre-average is:

$$y = \frac{\sum_{i=1}^R b_i \cdot \mu(y)}{\sum_{i=1}^R \mu(y)}, \quad (3)$$

where: b_i - the centre of the i th fuzzy set, R - the number of rules in rule-base, $\mu(y)$ - the membership function’s value (the appropriate fuzzy sets weight to the final fuzzy control solution), y - the output of fuzzy controller.

4.2. The synthesis of control signals correction module

The synthesis of fuzzy control module that corrected primarily produced control signals was similar to the synthesis of independent fuzzy controllers. The main differences were in designing the fuzzification interface, the rule-base and that the module produced two output values (control signals corrections) instead of one. The fuzzification interface was designed by two linguistic variables “Control error $\bar{e}_1(t)$ ” and “Control error $\bar{e}_2(t)$ ”. These variables were the appropriate air channels control errors average of the last 50 values. A moving average was used to calculate them since it helped to estimate the actual control error of the channel more precisely. Each input linguistic variable was characterized by five fuzzy sets “-15”, “-5”, “0”, “3” and “10” as demonstrated in Fig. 7. The fuzzy sets of each linguistic variable were chosen asymmetrically since the dynamics when the corks were moving down or up were different. Five fuzzy sets of each linguistic variable was the sufficient number in order to estimate the interactions between air channels.

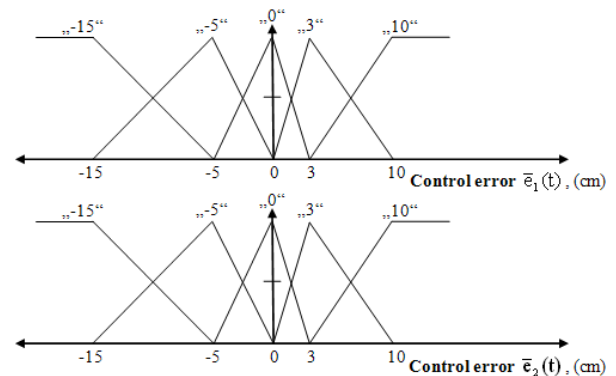


Fig. 7. Input linguistic variables, fuzzy sets and membership functions of the module of control signals correction (Fuzzy control)

Since the dynamics of air channels were a bit different, two separate rule-bases were designed in order to produce two output signals corrections. The rules of the first rule-base were described by “IF Control error $\bar{e}_1(t)$ AND Control error $\bar{e}_2(t)$ THEN Fans1 voltage correction” clauses. The rules of the second one: “IF Control error $\bar{e}_2(t)$ AND Control error $\bar{e}_1(t)$ THEN

Fans2 voltage correction” clauses. Each rule-base was composed of 25 rules.

There was used the same methodology to produce the solutions linguistic variables and the final controllers outputs as in independent fuzzy controllers but the correction module were generated two output signals instead of one.

5. Experimental results

The experiment was performed with different sets of reference signals, but the main control challenges existed when the reference signals were changed significantly, especially when they were reduced. Therefore the experiment was concentrated to those problems. In the section about the structure of control system was mentioned that the air channels dependence of each other was decided by the number of opened air feeding vents. The experiment was performed with such a fixed number of opened air feeding vents that ensured the necessary amount of air to channels fans since this configuration of opened air feeding vents guaranteed a certain amount of interactions between air channels and the corks were able to reach the reference signal values physically.

In Fig. 8 and Fig. 9 are demonstrated the results of PID and fuzzy controls, respectively, when the reference signals for both air channels are 0, then changes to 75 and later to 60, the abbreviation of such a reference signal configuration is marked as “0->75->60”.

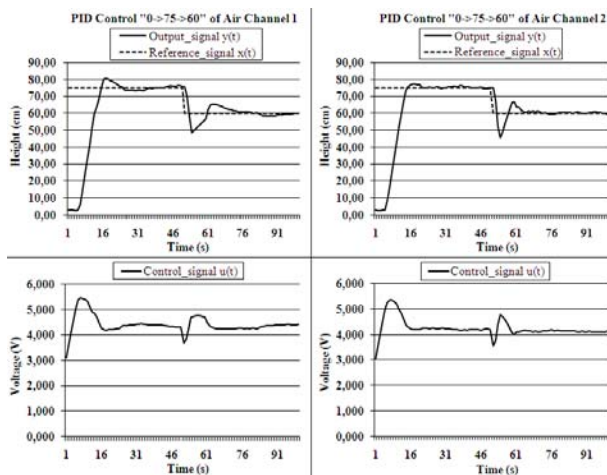


Fig. 8. PID control results, reference signal “0->75->60”

The parameters of PID controllers were static for all reference signals. This implied that the control signals of channels were produced symmetrically not depending on the corks moving direction that was a crucial factor why the PID control results were not desirable. Since the fuzzy control additionally considered the corks moving direction the control results were significantly improved. The statistical control results of PID and fuzzy when the reference signals were “0->75->60” are shown in Table 1 and Table 2, respectively.

The analysis of statistical control results was accomplished to each task mode separately. A task mode in statistical analysis was called the “75->60” notation, which meant that the reference signal was

changed from 75 to 60. The length of each task mode was 50 seconds. The statistical control results also were analyzed by two lettered modes: A – analyzing the entire task mode, B – analyzing just the portion of task mode when the output signal of air channel got steady. The control error (\mathcal{E}) was calculated by formula:

$$\mathcal{E} = \sqrt{\frac{1}{N} \sum_{t=1}^N (y(t) - x(t))^2}, \quad (4)$$

where N - the sample size.

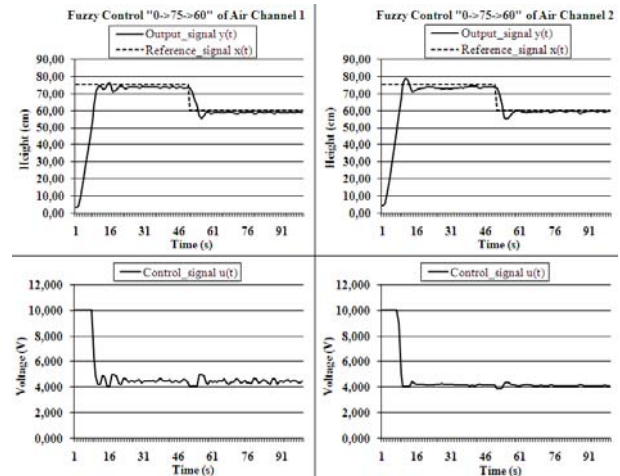


Fig. 9. Fuzzy control results, reference signal “0->75->60”

Table 1. The statistical results of PID control, reference signal 0->75->60

Control <air channel>	PID <1>		PID <2>	
	A	B	A	B
Analysis mode:	A			
Reference signal:	0 -> 75			
Sample size (N):	50	26	50	30
Control error (\mathcal{E}):	28.771	1.095	28.263	0.549
Reference signal:	75 -> 60			
Sample size (N):	50	31	50	38
Control error (\mathcal{E}):	4.48	1.13	4.11	0.44

Table 2. The statistical results of fuzzy control, reference signal “0->75->60”

Control <air channel>	Fuzzy <1>		Fuzzy <2>	
	A	B	A	B
Analysis mode:	A			
Reference signal:	0 -> 75			
Sample size (N):	50	32	50	33
Control error (\mathcal{E}):	21.535	1.084	20.938	1.589
Reference signal:	75 -> 60			
Sample size (N):	50	43	50	43
Control error (\mathcal{E}):	3.025	0.991	2.731	0.782

The output signals of air channels using fuzzy control get in steady-state faster than PID control. The statistical results of control errors when analyzing the A mode are also better in fuzzy control, but the B mode results are ambiguous.

The control results that are demonstrated in Fig. 10 and Fig. 11 when the configuration is “0->75->40” reveal

the plant's control strength of fuzzy control comparing with PID.

The tuning parameters of PID control (Fig. 10) were selected for each task mode separately since the usage of fixed parameters as in Fig. 8 produced the insufficient output signals (the mentions situation when the corks were moving down till reached the channels bottoms and after that reached its reference signals). These control results shows the necessity of the synthesis of adaptive PID control instead of static parameters to all task modes. Conversely, fuzzy control (Fig. 11) results are more desirable even if the time necessary to achieve the steady-states of output signals takes more time.

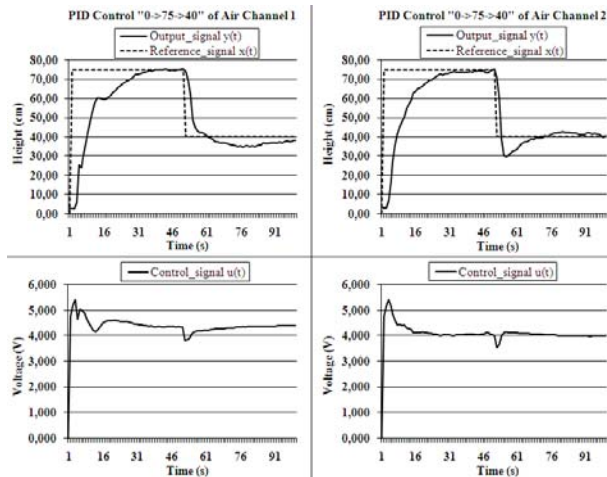


Fig. 10. PID control results, reference signal “0->75->40”

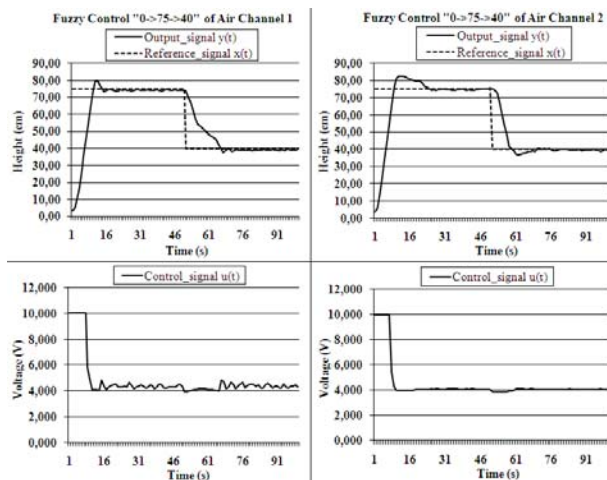


Fig. 11. Fuzzy control results, reference signal “0->75->40”

The statistical control results of PID and fuzzy control when the configuration is “0->75->40” are shown in Table 3 and Table 4, respectively. The output signals of PID control not achieve or achieve later its steady-states when the appropriate fuzzy control outputs signals. The control errors of fuzzy are better in all task modes even in the first channel's task mode “0->75” when the output signal is in its steady-state since the interval of the output steady-state values is longer in fuzzy control than PID - 35 opposite to 16.

Table 3. The statistical results of PID control, reference signal “0->75->40”

Control <air channel>	PID <1>		PID <2>	
	A	B	A	B
Analysis mode:	A			
Reference signal:	0 -> 75			
Sample size (N):	50	16	50	21
Control error (E):	23.975	0.299	23.401	1.041
Reference signal:	75 -> 40			
Sample size (N):	50	-	50	28
Control error (E):	8.056	-	6.435	1.652

Table 4. The statistical results of fuzzy control, reference signal “0->75->40”

Control <air channel>	Fuzzy <1>		Fuzzy <2>	
	A	B	A	B
Analysis mode:	A			
Reference signal:	0 -> 75			
Sample size (N):	50	35	50	28
Control error (E):	21.395	0.72	19.91	0.438
Reference signal:	75 -> 40			
Sample size (N):	50	32	50	35
Control error (E):	9.527	0.954	10.044	0.636

6. Conclusions

The analysis of experimental results proves that fuzzy control is more effective control method to air pressure plant than PID. The implementation of human's heuristic information about how to control a system, enables to estimate the critical system control problems (the dynamic and nonlinearities of system, interactions between the channels) better than PID which directly guides to better system control. The crucial factors of successful plant's control are the estimation of corks moving directions and proportions. The synthesis of adaptive PID control could be one of possible replacements to static tuned PID in order to control the plant with PID-based control.

7. References

1. Ålström K.J., Hägglund T.H. PID controllers: Theory, Design and Tuning. North Carolina, 1995. 343 p.
2. Passino K., Yurkovich S. Fuzzy Control. California, 1998. p. 9-10.
3. Kovačič Z., Bogdan S. Fuzzy Controller Design Theory and Applications. Portland, 2005. 416 p.
4. Abonyi J. Fuzzy Model Identification for Control. Boston, 2003. 273 p..
5. Albertos P., Sala A. Multivariable Control Systems. London, 2004. p. 35-38.

INVESTIGATION OF ADAPTIVE pH CONTROL SYSTEM

Vytautas GALVANAUSKAS

Process Control Department, Kaunas University of Technology, Lithuania

Abstract: The paper deals with pH control quality issues in fed-batch biochemical processes. First principles mathematical model of the process was elaborated. An adaptive pH control system based on gain scheduling approach was proposed. Simulation tests were carried out. Significant increase in control quality as compared to a standard PI control system was shown.

Keywords: adaptive control system, gain scheduling, pH control, fed-batch biochemical process.

1. Introduction

The main application fields of the pH control systems are the production processes in chemical and biochemical industry. The typical processes in this field become more and more complex, and the control quality requirements are relatively high. Modern biochemical processes are very complex and difficult to control [1]. The dynamics of such processes is nonlinear and time-varying. The problem is even more difficult since there are few reliable online measurement methods for such important biotechnological quantities like biomass concentration [1]. Therefore, often application of complex and time consuming mathematical models for off-line optimization, indirect state estimation and/or optimal online control are required. On the other hand, control systems should use mathematical models as simple as possible in order to avoid high computational load and numerical problems. This makes the task of high quality control even more complicated.

High quality control of pH level is difficult because of many reasons, some of which are: very strong nonlinearity of biotechnological processes, titration curves and pH measurement itself, high sensitivity of the microorganisms even to small temporary deviations of pH level of the cultivation media, and signal drift of the pH sensors [2, 3].

There are various approaches for high quality pH control shown in the literature. Nevertheless, most of them suffer from the already described drawbacks [3]. Therefore, it is important to elaborate simple, robust and easy to implement methods for pH control.

2. Mathematical model of the process

As an example of a control object, a laboratory scale fed-batch biochemical process was investigated. The control of pH level of cultivation medium is implemented using closed loop control with a PID controller. The pH signal is measured by means of an *in-situ* probe that returns standard electrical signal to the controller. The latter calculates the value of deviation signal and defines appropriate control action. The output of the controller is set to pulse mode and is connected to peristaltic pumps which feed alkali or acid solution into the bioreactor depending on the polarity and value of the deviation signal. The controller allows implementing either standard or adaptive PID control algorithm.

The concentration of hydrogen-ions (which is straightforwardly related to pH, [2]) in a fed-batch cultivation process can be modelled by taking into account influence of bacterial growth, addition of acid and alkali solutions during pH control and dilution effects:

$$\frac{dC_{H^+}}{dt} = (\alpha_1 \mu x + \alpha_2 x) + \frac{F_{pH}(C_{H^+}^0 - C_{H^+})}{V} - \frac{F_s C_{H^+}}{V}, \quad (1)$$

where:

C_{H^+} and $C_{H^+}^0$ – concentration of hydrogen-ions in the cultivation medium and in the feeding solution, respectively, [mol/l]; the latter concentration can differ from the theoretically calculated and is subjected to model based identification;

x – biomass concentration in the cultivation medium, [g/l];

μ – specific biomass growth rate, [1/h];

F_{pH} – flow of the alkali solution for pH control, [l/h];

F_s – flow of the feeding solution, [l/h];

V – cultivation medium volume, [l];

α_1, α_2 – model parameters to be identified.

The first summand in parenthesis on the right hand side of the differential equation (1) is related to biomass growth and maintenance, respectively. During the metabolic reactions in the microbial culture excessive production of H^+ ions takes places, and the addition of alkali solution is necessary in order to maintain constant pH level which is optimal for the growth of bacteria and/or production of the target product.

The second summand takes into account the influence of the flow of the alkali solution for pH control. The last summand accounts for the dilution effect of the feeding solution.

The initial value $C_{H^+}(0)$ is equal to 10^{-7} [mol/l], and this level corresponds to pH 7.

The biomass growth in the fed-batch process can be modelled by means of the differential equation

$$\frac{dx}{dt} = \mu x - \frac{F_s + F_{pH}}{V} x. \quad (2)$$

The initial value $x(0)$ is determined after inoculation, and is known at the beginning of each cultivation process.

Another key quantity of the process is the oxygen uptake rate, OUR . It can be evaluated from the equation taking into account oxygen demand for the biomass growth and maintenance:

$$OUR = \beta_1 \mu x V + \beta_2 x V, \quad (3)$$

where β_1, β_2 – model parameters to be identified.

The cultivation process under consideration consists of two distinct phases (biomass growth and product formation phase), in which these coefficients have different values that should be identified separately.

All the variables except of x can be measured online during the process. Each time moment the biomass concentration x is obtained applying numerical integration of (2) in real time. In a real system the value of OUR can be calculated instantly from the off-gas composition and other measurement data obtained online, and μ is derived and calculated from (3) using the most recent value of x . Then the calculated value of μ is applied in the next integration step solving (2), i. e. calculating next value of x .

3. Mathematical model of the adaptive control system

After the creation of the process model (1-3), and the identification of the unknown model parameters, a mathematical model of the adaptive pH control system can be elaborated. The general structure of the adaptive pH control system investigated is shown in the Fig. 1.

In the controller's input the deviation between the set point and the actual value is recalculated from pH to C_{H^+} .

In order to investigate, which of the controllers parameters should be adapted online, the equation (1) is

linearised around the working point. Under the equilibrium conditions around the working point the following equations are valid:

$$\frac{dC_{H^+}}{dt} = 0, \quad (4)$$

$$F_{pH}^* = \frac{(\alpha_1 \mu + \alpha_2) x V^*}{(C_{H^+}^0 - C_{H^+}^*)}. \quad (5)$$

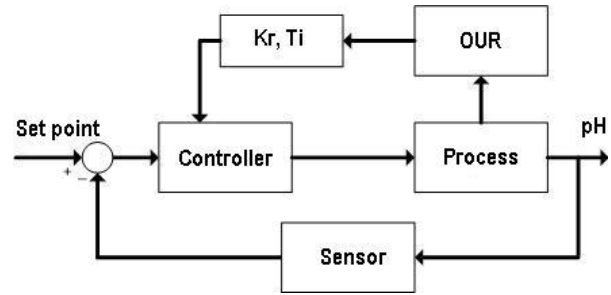


Fig. 1. General structure of the adaptive pH control system

After the linearization of the dynamic equation for C_{H^+} around the working point one gets the following equation:

$$\frac{d(\Delta C_{H^+})}{dt} = -\frac{F_{pH}^*}{V^*} (\Delta C_{H^+}) + \frac{C_{H^+}^0 - C_{H^+}^*}{V^*} \Delta F_{pH}. \quad (6)$$

Multiplication of both sides of (6) by $\frac{V^*}{F_{pH}^*}$ leads to:

$$\frac{V^*}{F_{pH}^*} \frac{d(\Delta C_{H^+})}{dt} + (\Delta C_{H^+}) = \frac{C_{H^+}^0 - C_{H^+}^*}{F_{pH}^*} \Delta F_{pH}. \quad (7)$$

Equation (7) is a first order differential equation, where the object input is change of alkali feeding rate ΔF_{pH} , and the object output is change of concentration ΔC_{H^+} .

The structure of the corresponding process transfer function (in Laplace transform) around the working point is

$$W(s) = \frac{\Delta C_{H^+}(s)}{\Delta F_{pH}(s)} = \frac{K_0}{T_0 s + 1}, \quad (8)$$

and the coefficients of the transfer function (8) are as follows:

$$K_0 = \frac{C_{H^+}^0 - C_{H^+}^*}{F_{pH}^*} = \frac{(C_{H^+}^0 - C_{H^+}^*)^2}{(\alpha_1 \mu + \alpha_2) x V^*}, \quad (9)$$

$$T_0 = \frac{V^*}{F_{pH}^*} = \frac{(C_{H^+}^0 - C_{H^+}^*)}{(\alpha_1 \mu + \alpha_2) x}. \quad (10)$$

Unfortunately, the process model has no clearly defined delay. Hence, while tuning the controller parameters it

due to exponentially growing biomass concentration that has acted as a disturbance. The simulation results (see Fig. 3) show that the tracking error of the adaptive PI controller was significantly lower than the one in the case of a PI controller with constant tuning parameters.

At the end of the process the adaptive controller still was able to keep pH value of 6.999 as compared to 6.96 in the case of the control system based on the standard PI controller.

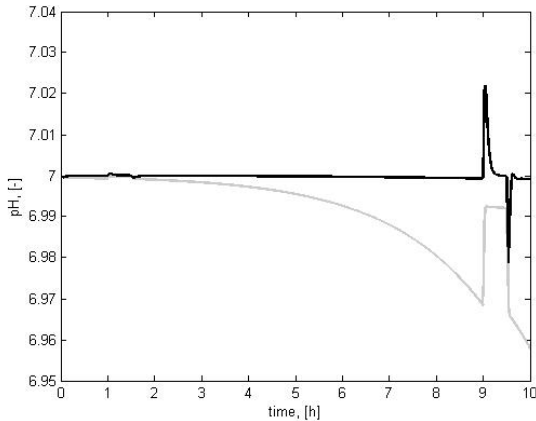


Fig. 3. Tracking quality of the adaptive (black line) and standard (grey line) control systems

The tuning parameters of the latter were chosen taking into account the dynamics of the control object at the beginning of the process. If trying to reduce the tracking error at the end of the process one tunes the controller parameters on the basis of the dynamics at the end of the process and uses these values during the whole process it can lead to instability of the control system. Hence, the only solution is to gradually adapt the value of T_i . The evolution of the T_i according to (11) during the adaptive pH control process is shown in the Fig. 4. During the 1–1.5 [h] and 9–9.5 [h] of the process the disturbance in form of stepwise reduced biomass specific growth rate (both times from 0.5 to 0.1 [1/h], and vice versa) was introduced. This is a typical case in practice when substrate or oxygen supply is disrupted due to malfunction of the equipment. In order to keep the desired pH level a rapid action of the pH controller is required.

The simulation results (see Fig. 3) show that in the case of adaptive control the overshoot was about 30 % smaller, and the tracking error during the

introduced disturbance was of the magnitude lower. This proves once more the effectiveness of the proposed control approach.

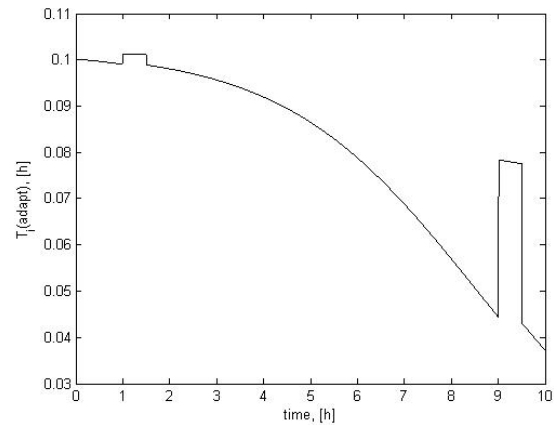


Fig. 4. The evolution of T_i value during the process control using the adaptive control system

5. Conclusions

The proposed adaptive control algorithm proved to be a robust and stable solution ensuring high quality pH control in the analyzed biotechnological fed-batch process. It can become a real alternative for standard PID control. Further practical investigations should be carried out in order to identify model parameters from the experimental data and to practically implement the proposed adaptive approach into a real control system.

6. References

1. Sonnleitner B. Instrumentation of Biotechnological Processes. *Advances in Biochemical Engineering/ Biotechnology*, 2000, 66. p. 1-64.
2. Carr-Brion K.G. (Ed.) *Measurement and Control in Bioprocessing*. Elsevier Science Publishers, London, 1991. 262 p.
3. McMillan G.K., Cameron R.A. *Advanced pH Measurement and Control*. ISA, 2005. 294 p.
4. Ljung L. *System Identification: Theory for the User*, 2nd Edition. Prentice Hall, New Jersey, 1999. 672 p.
5. Levine W.S. (Ed.) *The Control Handbook*. IEEE/CRC Press, 1996. 1566 p.

BUILDING OF SECURITIES VALUATION IT SYSTEM USING MULTI-AGENTS APPROACH

Andrius JURGUTIS^{*,**}, Rimvydas SIMUTIS^{*}

^{*} Department of Process Control, Kaunas University of Technology, Lithuania

^{**} AB Bankas Finasta, Lithuania

Abstract: Application of software agents and multi-agents systems for decision making are the new approach to the capital markets. The flow of information is increasing rapidly and is extremely important to evaluate the news on time and make the right decisions. The papers propose the basic structure of the multi-agent system that will function in real time dynamic environment in capital markets. This IT system will be able to suggest investment solutions taking into consideration variable characteristics of individual investors. IT system will acquire information from and monitor changes to stock reporting databases, interpret stock information, and predict the near future of an investment. Broad spectrum of securities valuation methods will be employed and profile of the user will be incorporated in the decision making process. A multi-agent system approach is ideal in cases that require the coordination of several component tasks across distributed and flexible networks of information sources and expertise. The paper will present the basic structure of Securities valuation IT system using multi-agents approach.

Keywords: software agents, multi-agents systems, securities valuation.

1. Introduction

Deep knowledge of fundamental, technical or other securities valuation methodology is not enough for successful trading in financial markets. Since trading moved to electronic space, new challenges have emerged. First, financial markets have become global. On one hand, the investing in any region of the world has become very simply. On the other hand, there is a need to know the specifics of the region adapt to them and learn to work with. Second, the financial markets have become dynamic. The abundance of information could quickly change the direction of the markets. Therefore, there is a need to continuously track and interpret the information and make decisions based on

it. Speed of decision-making process gains a huge significance.

The investment management is sufficiently complicated and complex task. It requires a high competence of financial assessment, quick orientation in continuous stream of information and 24 hours work a day. It is unlikely that it is reasonable for one person. The efficiency of investment management team is questionable, too. There is therefore a great need to develop intelligent information systems that could help the investor. The traditional investment advisory or investment management companies employ teams of various professionals: economists, statistics, financial brokers, IT professionals and ect. Some of them are gathering the information, the others are analysing it and making the conclusions, the third group is making the future predictions. The last group is summarizing and making the final decisions. We believe that such model of companies operations is not appropriate in the twenty-first century. It doesn't meet the investors' needs and company owners' interests. Tremendous competition between the investment management companies promotes the optimisation of operating costs. As one of the possible solutions we offer to automate a part of the functions performed by professionals: to create and develop an intelligent information system or robot consultant. Such IT system would be useful to the investors and investment management companies. First, it would allow increasing the profitability of the company. Secondly, it would provide services to investors at lower costs (such as lower commission for stock trading) and enable reduce the management fee of various investment funds. The cost reduction has a direct positive impact on the ultimate profitability of the customer portfolio. Third, the automated system accelerates the decision-making process, which is very important in dynamic market. Based on practice, we could say that the high investment returns reaches those who are first to receive, detect and correctly evaluate the information, and first to make the investments decisions. Abundance of information sources and

formats complicates and prolongs the perception of information and its processing time. Information sources vary, some of them occur, while others disappear, therefore is always desirable to know about these changes. The proposed investment robot-consultant would be able to interpret the information, compare and update it. Fourth, the automated advisory system would ensure greater confidentiality of investors. The investor would interact with IT advisory system instead of human-consultant, which autonomously and anonymously will seek his client's objectives. The human consultant may unacceptable distribute the client's ideas to other investors. Accordingly, such IT system could carry out preventive work in market manipulation and detect misleading information. The system would prevent the spread of false information. Fifth, the intelligent advisory system would be able to adapt to changing objectives of investor. In this way, the customer should be always surrounded with attention and customised individual proposals. At the same time, this will be a leap in quality of customer service standards and new approach to sales of investment ideas and products. Sixth, the robot-consultant will possess the best experience of various fields professionals thus avoiding possible human errors (such as emotions, fear, etc.). Seventhly, IT system containing all the listed properties is likely to increase the number of correct decisions as compared to traditional consulting firm. We could assume that company offering such instruments to investors will gain a significant popularity. Eight, if robot-consultant would be constructed it will possibly increase a number of people interested in investing. At the same time, it enables investors to learn about the investment world quickly. We believe that robot-consultant possessing all the listed properties would become one of the main investor tools.

The problem is how to construct the IT system capable to evaluate various financial parameters and securities. Portfolio management and investment decision-making process is complicated and complex task. The complication is found in searching data, choosing the financial instruments or assessment methods and ultimately, drawing the conclusions. The complexity means that there is a need to coordinate a number of related processes such as information collection, performance assessment, market surveillance, etc. Therefore, the recommendation to investor includes resolving of several tasks, the control and management of individual tasks [19, 20]. We like others believe that it is beneficial to create such system using the software agents and, more precisely, to develop the multi-agent systems [1, 2, 3, 4, 5, 6]. Already there are some examples of such systems, as Warren, MASST [12]. These IT systems are more focused on information collection and processing. The adaptation to user needs and investment decision-making is less important. Software agents are the new tools of artificial intelligence and software engineering. An autonomous software agent is the system (a computer program) which existing in surrounding environment (for example internet) or being a part of it executes the prepared plan at the same time monitoring these

surroundings and implements the task. In our case we will use the software agents in following order: the primary task to make a recommendation to investor to buy or sell the security will decompose into smaller tasks like information gathering or applying a certain securities evaluation approach. Independently acting software agent will execute each task in separate manner. In order to achieve the different task we will use various types of software agents. In part 2 of the article, we will review the properties of software agents. In part 3 we will analyze the types of agents used in resolving the tasks. In part 4 we'll propose the structure of securities evaluation IT system. At the end of the article we will present how the IT system should function.

2. Agents' properties

The software agents in our IT system will possess the following basic properties [7, 8]:

- **Autonomy:** the ability of the agent to act without any external interference. The agent must be able to make its own choices and make its own decisions.
- **Communication skills:** the agent must be able to establish relation with environment. The most important is the interaction between similar agents and the user.
- **Reactivity:** surrounding environment is typically dynamic and requires the adaptation ability from the agent.
- **Mental notions:** during his life cycle, the agent is learning from different situations. Thus, through the memories and through the interaction with others agents, the agent is able to gain its own knowledge.
- **Persistence:** the mobile agents life is usually longer than the length of his basic tasks. Thus, it is created to satisfy one of the following criteria:
 1. To finish after having done the basic task;
 2. To finish after having exhausted the assigned internal resources.
- **Social ability:** the agent exists among the other agents, thus it must be able to exchange the information in order to achieve its assigned goals or help the other agents.
- **Mobility:** a mobile agent has the inner attitude to vary its communication partners. It is able to interact with both a similar agent and a user.
- **Vitality:** in order to achieve its goal, the agent must cope with anomalous situation that could create a state of instability that could damage it irreparably. An agent who has a strong vitality is able to solve the most adverse situations it meets.
- **Pro-activity:** a mobile agent is able to start new interactions with other agents and coordinate various agents' activities stimulating their certain responses.
- **Truthfulness:** the agents use the information received during the exchange and not viewed

under direct control inspection entities, so they are expected to respect truthfulness.

- Benevolence: the agent must act in good will and must not perform any acts contrary to the users will or to the other agents' interests.

3. Types of agents

The securities evaluation IT system will consist of 3 types of agents:

- Interface agent,
- Information agent,
- Co-operating agent (due the functional clarity it will be named the Task agent in the further article.)

The system could have more agents, too [10, 11].

The Interface agent is the mediator between the user (investor) and the securities evaluation IT system [17, 18]. Interface agent receives the information from the user and accepts its target, then transmits it to other system elements. On the contrary, it presents the systems generated answers to the user in an understandable form.

The main functions of the Interface agent would be the following: to collect and analyze the information about the user and share it with other IT system agents, to submit the system generated responses to the user, to request for additional information and if it is necessary to inform the user. Therefore, the IT system's user interacts with interface agent only, no other agents are involved.

The main function of the Information agent is to provide the information to the Task agents [10, 15]. For example, in order to learn the fundamental value of securities, the information agent needs to gather the financial data about the issuer using the Internet data search. Then the Information agent transmits the information to the Task agent, which is responsible for fundamental analysis. The Information agents could vary and perform different information gathering strategies, use different sources of information. Information agents distinguish their selves with pro-activity feature. They are able to generate events in the surrounding environment and to start new interactions with other agents instead of waiting for assignment of the data search.

Task agents perform a lot of work in shaping the recommendation to the user. Each Task agent has certain knowledge about certain security evaluation approach. Depending on user's request, which is expressed through the interface agent, IT system may take different methods and their combinations. When performing the tasks, the agents are cooperating with others thus communication skills and social ability is the main property. Task agents are more complex than the interface and information agents.

The security evaluation IT system obtains more possibilities when agents are able to use the mental notions. It is likely to have a more efficient IT system when it is able to accumulate the history of recommendations and to select the best decisions [18].

4. Information system architecture

In the process of information system design for assessment of securities, we shall take a deeper look at development of better investment proposition generation process in consideration of individual needs, goals and suspense of investor. In other words, the structure of information system, namely the part of system responsible for investment proposition design, must safeguard the safety of system itself and proposals should correspond to the needs and goals of investor as well as coincide with natural behaviour of investor. From the point of view of us as investors, the system architecture could be double. With reference to investment solutions, investors could be divided into two groups. First would be conservative investors avoiding risk and requiring more time for final decision making. The named group appeals on several securities assessment methods before decision making, namely – use of both the technical and fundamental analysis, consultations with experts (brokers, analysts) and insert some other methods. Second group is considered as aggressive, risk unfearful and spontaneous decision makers or in other words – profiteers. Usually, such investors make use of securities assessment methods they are most fond of, for example: only technical analysis or only fundamental analysis. If they have time in their hands, than such investors verify investment solutions with other methods too, in other words – check if other method satisfies their solution. Therefore, information system must firstly determine investor's type – a job performed by Interface agent.

Interface agent determines investor's type and later revises decision through an interactive questionnaire for the investor. Questionnaire consists of two parts: general and special. General part consists of some common information about the investor: age, education, income, expenditure, investment experience, risk perception, tolerance for risk, etc. Special part introduces investor to securities assessment methods realized in the system, investor receives control questions for ascertaining methods mostly trust-worthy for him/her or investor indicates which methods system must use to perform securities evaluation and finally present proposal. Suppose every method is evaluated by investor by giving points. If investor gives approximate number of points to several methods, in this case information system generates the proposal by appealing on those methods. Influence of methods could be equal for the final decision or respectively the authority of method for final investment proposal making could be evaluated by the number of points given to that method. Information system structure of this type is presented in "Fig. 1". Interface agent informs solution agent about the methods (together with method parameters, e.g. beta ratio, Sharpe ratio, etc.) to be used by the latter in modelling the investment proposal. Solution agent launches agents of appropriate methods through coordinating agent

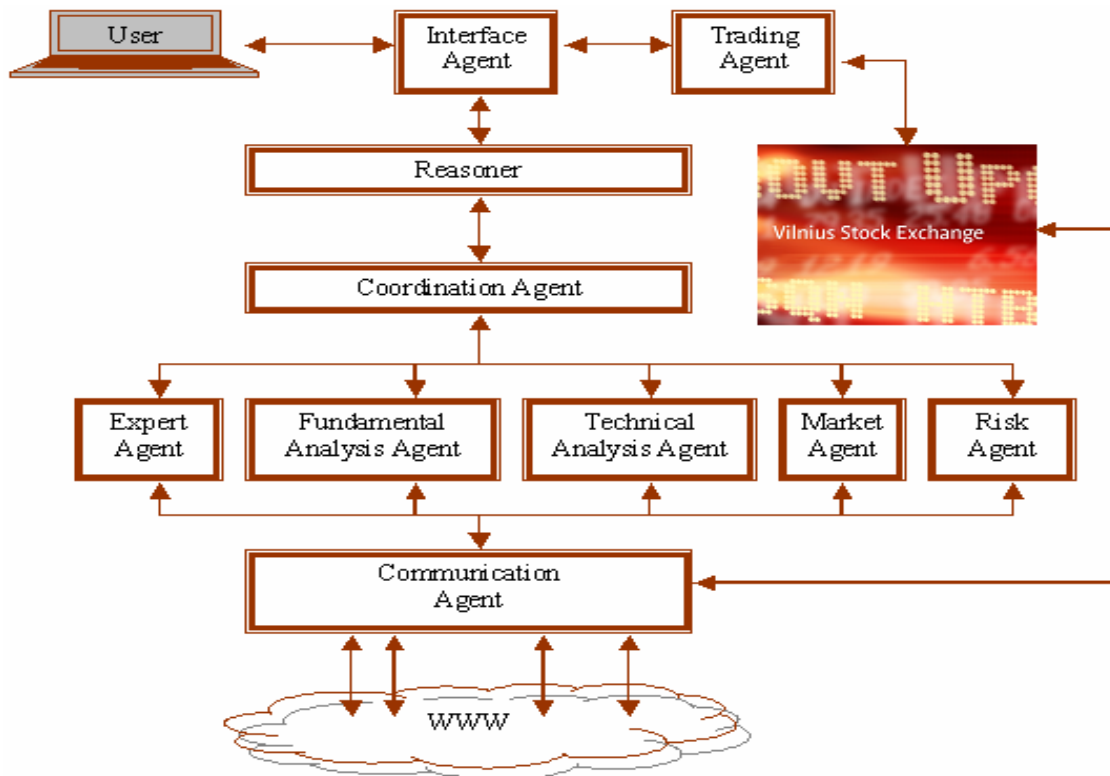


Fig. 1. Horizontal Structure of Information System

method agents do their work in an asynchronous and independent way. Expert agent searches for securities corresponding investor's needs at other expert agents or expert people. Fundamental analysis agent hunts for and evaluates securities with fundamental analysis methods, while respectively technical analysis agent makes assessment of securities through fundamental analysis tools. Market agent evaluates securities through market news [13, 14, 15]. Risk agent seeks for and selects securities through risk level (according to Sharpe ratio, beta ration, etc.). In case of finding appropriate securities by appropriate method, every method agent informs coordinating agent and the latter checks if that security was earlier evaluated by other methods and in case not – other method agents are called in additionally. In this way, system can have several agents of the same method and accelerate presentation of investment proposal. Method agents collect information with information agents' help. Finally, coordinating agent collects assessment of all methods required by the investor and presents them to solution agent eventually delivering solution to investor. Our title for this system architecture is "Horizontal Structure of Information System".

If one of securities assessment methods got extremely larger number of points than any other method, then we may call investor a profiteer with one securities assessment method he/she is most fond of and which must be referred to by the system in proposal presentation. Then, Interface agent informs solution agent about the major method and the sequence of importance for the remaining methods is determined by

the declining sequence of points scored. In this way a vertical top-down method architecture is determined for every individual investor reflecting his/her behaviour on the market. "Fig. 2" pictures vertical structure of information system. Solution (Reasoner) agent calls major method agent through a coordinating agent. Major method agent presents the selected securities through coordinating agent to solution agent. Solution agent evaluates if there's enough data to safe solution making and if not – calls next method agent by the list of importance through coordinating agent and the process repeats. Finally, solution agent provides proposal to investor.

Such type of information system structure should safeguard a kick-start of securities selection and repeat actualization of natural investor's behaviour. We may presume that with knowledge of investor's statistics, i.e. by assumption that all investors can be described by finite number, multi-agent of vertical structure, prognosis of the market reaction to speculative (future) events could be made and with this knowledge investment solutions could be formed.

From time to time Interface agent must renew investor's data, namely record changes of investor's suspenses, goals, etc. It could be done by provoking investor with securities proposal uncomfortable to him/her and observe the reaction. Another way could be to offer an overfilled questionnaire. Interface agent must also secure feedback about proposals provided by information system. Problem is – the feedback receipt is most purposeful after investment

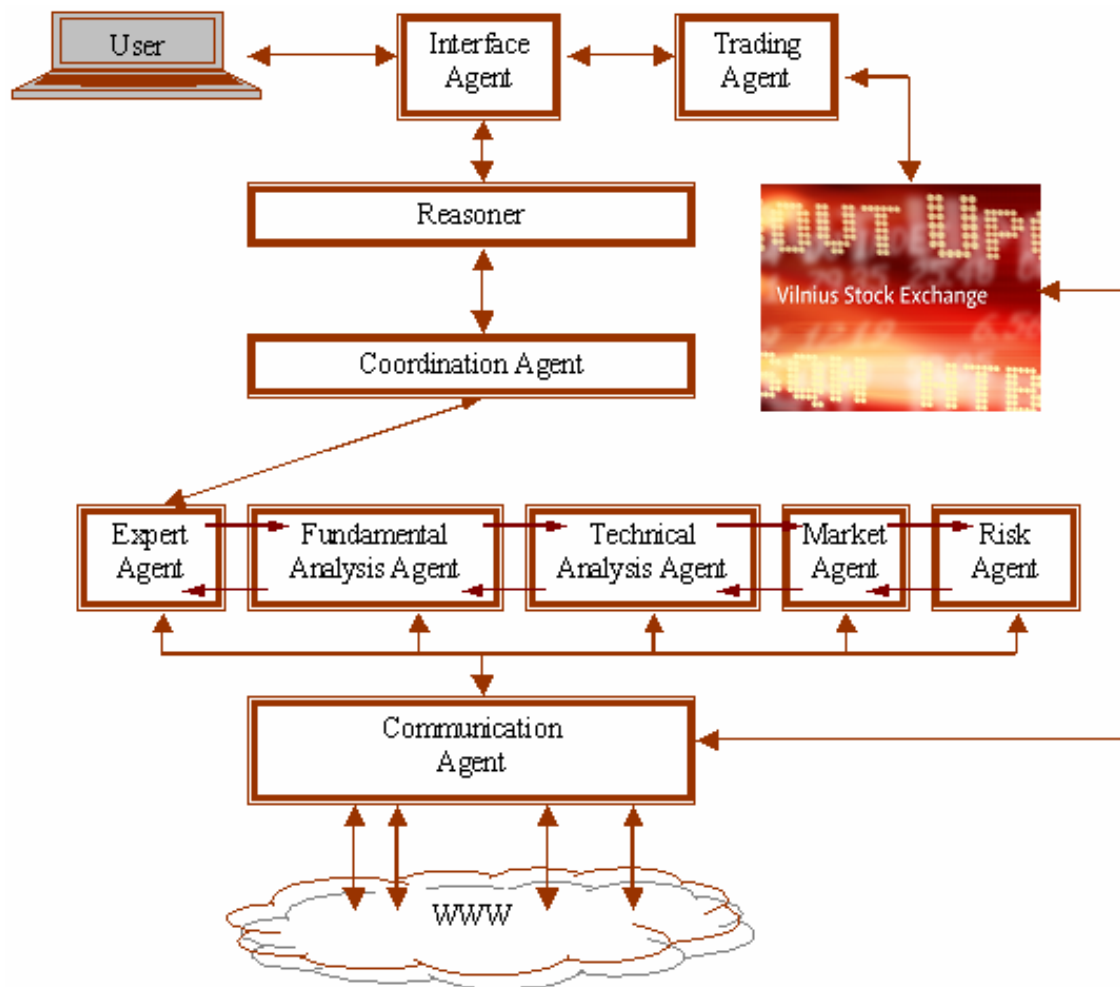


Fig. 2. Vertical Structure of Information System

proposal presentation when it is possible to say if investment proposal served the purpose or would have served the purpose even if not accepted by investor. The problem could be solved by adding a virtual portfolio formed according to all information system proposals alongside the investor's portfolio. Virtual portfolio would be automatically supplemented or reduced with financial means according to information system's proposals. Investor himself could observe the virtual portfolio beside his/her own.

The generated securities assessment information system would constantly watch the situation, composition of investor's portfolio and in case of vital events on the market possibly strongly influencing the change of investor's portfolio, would inform investor at once by e-mail or SMS when he/she is disconnected from the system. After some time, information system learns decision making satisfying investor's goals and corresponding his/her behaviour, and investor can allow the system to make deals through use of sales agent.

Securities assessment information system shall be built in JADE platform base [16]. Agents perform tasks by communicating in ACL (agent communication language) protocol, in our opinion a more functional agent protocol than KQML. ACL communication protocol conforms to the up-to-date FIPA standard.

5. Conclusions

Programming agents and multi-agent systems they design are a perfect tool for building financial means' assessment information system. Securities evaluation and their portfolio management are a complicated and integrated task requiring combination of independent and different methods of securities assessment and disperse information resources they need. Programming agents are able to unite all the necessary elements into one and complicated multi-agent system. Research with already working systems such as WARREN, MASST testify it and our hope is that our system orientated to investor's behaviour shall also answer the purpose. With possession of securities assessment information system structure we shall continue our work by gradually realizing separate system parts with JADE platform's help.

6. References

1. Cohen P. R. and Levesque H. J. Intention=choice + commitment. In Proceedings of AAAI-87, Seattle, WA., 1987. p. 410-415.
2. Kan Lang. Newsweeper: Learning to filter netnews. Proceedings of the Twelfth International Conference

- on Machine Learning, Tahoe City, California, USA 1995. p. 331-339.
3. Rao A. S. and Georgeff M. P. A model-theoretic approach to the verification of situated reasoning systems. In Proceedings of IJCAI-93, Chambéry, France, 1993. p. 318-324.
 4. Shoham Y. Agent-oriented programming. Artificial Intelligence, 1993. p. 51-92.
 5. Sycara K. and Zeng D. Towards an intelligent electronic secretary. In Proceedings of the CIKM-94, Gaithersburg, Maryland, 1994. p. 239-260.
 6. Wooldridge M. and Jennings N. R. Intelligent agents: Theory and practice. The Knowledge Engineering Review, 10(2), 1995. p. 115-152.
 7. Editor Genco A. Mobile Agents: principles of operation and application. UK, WIT Press, 2008. 271 p.
 8. Wooldridge M. An introduction to multiagent systems. UK, 2006. 348 p.
 9. Franklin S. and Greasser. It is an agent, or just a program? : a taxonomy for autonomous agents. Third international workshop on agent theories, architecture, and languages. Springer-Verlag, 1996. 12 p.
 10. Nwana H. S. Software agents: an overview. Knowledge Engineering Review, Cambridge University Press, 1996. p. 1-40.
 11. Wooldridge M., Sycara K. and Jennings N. R. A roadmap of agent research and development. Autonomous agents and multi-agent systems, Boston, 1998. p. 7-38.
 12. Sycara K., Decker K., Williamson M., Zeng D. and Pannu A. Distributed intelligent agents. The robotics institute, Carnegie Mellon University, 1996. 32 p.
 13. Sycara K., Giampapa J. and Seo Young-Woo. Financial news analysis for intelligent portfolio management. The robotics institute, Carnegie Mellon University, 2004. 17 p.
 14. Sycara K., Giampapa J. and Seo Young-Woo. Text classification for intelligent portfolio management. The robotics institute, Carnegie Mellon University, 2002. 14 p.
 15. Sycara K., Giampapa J. and Seo Young-Woo. Designing behaviors for information agents. The robotics institute, Carnegie Mellon University, 1996. 15 p.
 16. Bellifemine F., Caire G. and Greenwood D. Developing multi-agent systems with JADE. UK, 2008. 286 p.
 17. Maes P. Agents that reduce work and information overload. Communications of the ACM, 37(7), 1994. p. 30-40.
 18. Mitchell T., Caruana R., Freitag D., McDermott J. and Zabowski D. Experience with a learning personal assistant. Communications of the ACM, 37(7), 1994. p. 81-91.
 19. Oates T., Nagendra Prasad M. V. and Lesser V. R. Cooperative information gathering: A distributed problem solving approach. Technical Report, Department of Computer Science, University of Massachusetts, 1994. p. 94-66.
 20. Sycara K. and Zeng D. Coordination of multiple intelligent software agents. The robotics institute, Carnegie Mellon University, 1996. 31 p.

MODELLING OF ATM CASH TURNOVER

Vaidas KAZLAUSKAS*, Vygandas VAITKUS**

*Scientific service company "GTV", **Kaunas University of Technology, Lithuania

Abstract: This paper presents a model for money turnover prediction in automatic teller machine (ATM). This approach is based on an artificial neural network to forecast a daily money demand for ATM. At first the investigation of model variables was preceded. Then multilayer perceptron was used for prediction of money turnover. The prediction accuracy was tested on real historical money demand data by comparing ANN model prediction with Naïve prediction hypothesis.

Keywords: ATM forecast of money demand, multilayer perceptron, Naïve prediction hypothesis.

1. Introduction

Automatic taller machines (ATM) are equipment for money supply for consumers. More than one thousand ATM's are in Lithuania and over one billion in whole of the world. So it is not a difficult to imagine what amount of cash flow is needed for loading and ensuring of ATM's correct action. At present the analysis and forecast of money demand is made by human expert. He is analyzing money flow with his own empirical model witch estimate input parameters like money demand few days ago, how much days till holidays and others. Depending on strategies the ATM loading is executed daily or weekly by fixed size of money load.

The main objective is to make load of ATM exactly what it needs to be because money has a cost depending on interest rate.

Studies of ATM turnover simulation and prediction made in recent years were stimulated by private companies and were unpublished. The main attention in current publications in ATM field is concentrated to transaction security. Recently investigation in ATM turnover modelling field was performed in Kaunas University of Technology [1, 2]. The main goal of the research was to optimize ATM cash upload. It was formed and identified an artificial neural network model for each ATM and forecasted demand of cash for specified period of time. These articles focus on an optimization routine and wasn't briefly discussed significant variables, ANN model structure and parameters identification. This article tries to eliminate these deficiencies.

The paper consists of 7 sections. In section 2 data analysis is presented. In section 3 model identification procedure is defined. Modelling results are discussed in section 4. Comparison of ANN model prediction and Naïve prediction hypothesis is presented and discussed in section 5. Finally future works and conclusions are presented in sections 6 and 7.

2. Data analysis

For the project purpose a daily cash turnover from 2139 automated taller machines were received. First step was to analyze these data. For further investigation it was selected only 1213 machines which have the data accumulated in at least one year period. After discussion with human experts potential inputs were identified:

- Week day number,
- Month number of the year,
- Number of the month day,
- the average of money turnover within a few previous days,
- Number of days before the holidays and after,
- And others.

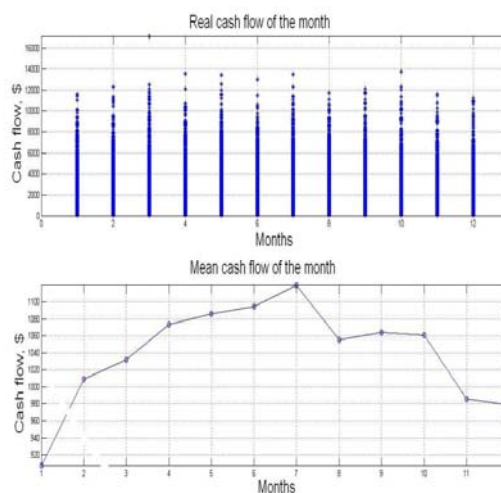


Fig. 1. Real and mean cash flow of the all ATM's dependence on week day number

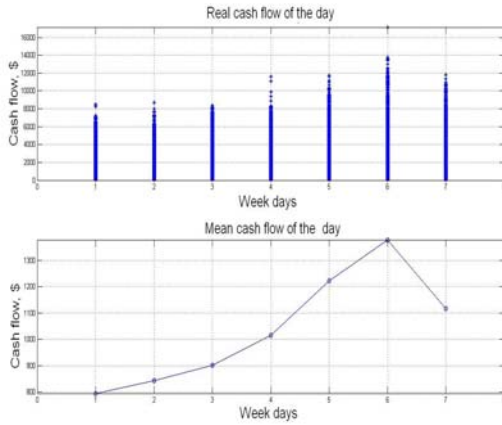


Fig. 2. Real and mean cash flow of the all ATM's dependence on month

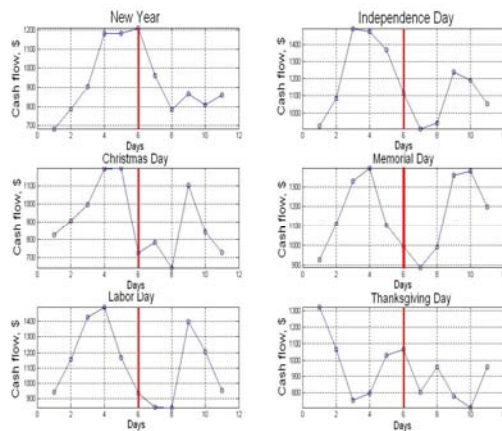


Fig. 3. Mean cash flow of the all ATM's dependence on holiday day. Red line and day number 6 mark a holiday

After data pre-processing some figures was made in order to ensure that inputs identified by human experts really have an influence to cash turnover. The cash turnover, depending on few selected features is presented above in the figures 1, 2, and 3. In columns of figures 1 and 2 is presented a daily turnover of all ATMs for one day of the week or month. Figures showed a certain dependencies between the features and money turnover, and it would be rational to use them for model identification.

3. Model identification

Artificial neural networks were selected as proper technique for nonlinear modelling. Neural networks were successfully used in many areas such as pattern recognition, classification, nonlinear modelling and others [3-7]. It is also convenient to use ANN when necessary to adapt the model settings or select an appropriate model structure. Requirements for model:

- To give best possible cash forecasting accuracy,
- To be as small structures as possible for fast learning, or adaptation to new data procedure.

MATLAB software was used for this research. Feedforward backpropagation neural network structure used for modelling is presented in figure 4.

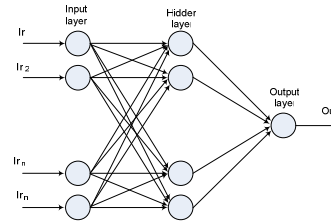


Fig. 4. Neural network structure used

The network has input layer, one hidden layer, with a different number of neurons and one output neuron. Hidden layer neurons have hyperbolic tangent sigmoid transfer function, and output – linear transfer function.

$$TF_{out} = \frac{2}{1 + e^{-2in}} - 1. \quad (1)$$

ANN training was produced by Levenberg-Marquardt training algorithm. Training on the training data set continues as long the training reduces the network's error on the validation vectors. After the network increase error on validation data, training is stopped. This technique automatically avoids the problem of over-fitting.

Before training procedure data for modelling was normalized by the rule that the standard deviation equal to 1, and average to 0.

4. Analysis of modelling results

Investigation of modelling accuracy depending on input vector is presented in table 1. Neural network model has ten neurons in hidden layer.

Table 1. Modelling results

Inputs	Mean prediction error of 5 learning restarts, MSE	Best of 5 learning restarts, MSE
[D M MD M7D]	2.1671*10 ⁵	1.8137*10 ⁵
[D M MD M5D]	2.7676*10 ⁵	1.8214*10 ⁵
[D M MD C1]	6.7330*10 ⁵	1.8473*10 ⁵
[D M MD C1 C2]	3.5555*10 ⁵	1.9098*10 ⁵
[D M MD]	2.3275*10 ⁵	1.7813*10 ⁵
[D M MD H]	2.6056*10 ⁵	2.1436*10 ⁵
[D M MD M5D C1]	2.3444*10 ⁵	1.8689*10 ⁵
[D M MD M5D C1 C2]	2.6756*10 ⁵	1.9264*10 ⁵
[D M MD C1 C2 C3]	2.4678*10 ⁵	1.9393*10 ⁵

For each ATM 5 network learning restarts were executed and mean squared error performance value calculated on testing data set.

Input variables were labelled:

- D – Day of the week number,
- M – Month's number,

- MD – Month’s day number,
- C1 – Cash turnover day ago,
- C2 – Cash turnover two days ago,
- C3 – Cash turnover three days ago,
- H – Number of days till holiday,
- M7D – mean of cash turnover during last 7 days,
- M5D – mean of cash turnover during last 5 days.

As it is seen from table 1 it was tested different input sets for cash turnover modelling. The best result was received by a model with three inputs – day of the week number, month number and day of the month number. Looking at the network outputs and real cash turnover data, it could be seen that the model can’t predict the sudden changes in the money circulation. Model’s behaviour is like a human expert’s. It is trying to predict the potential demand, but random changes are unpredictable (Fig.5).

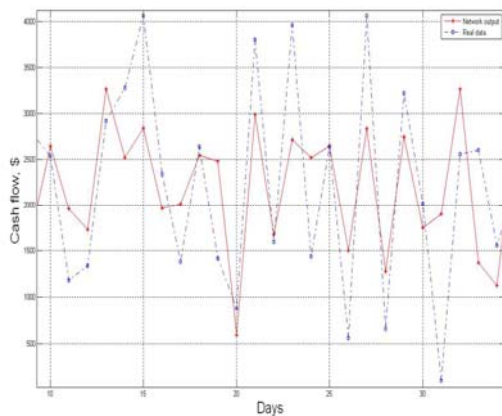


Fig. 5. Randomness in cash flow data

This indicates that the data is very noisy. We have tried to reduce the impact of random shocks to the turnover data by moving average filter with different moving window widths. Filtering of the input data didn’t make a significant influence to model prediction result.

5. ANN prediction comparison with Naïve prediction hypothesis

The question arises whether effective model is established and identified? Whether it can compete with a human expert who is predicting ATM network cash circulation? We have not had the opportunity to compare the human-expert and ANN accuracy. To ensure the efficiency of the ANN model it was compared with Naïve prediction hypothesis. The naïve prediction hypothesis took today’s cash flow as the best estimate of tomorrow’s cash flow. It can be expressed as follows:

$$\hat{y}_{t+1} = y_t, \quad (2)$$

where \hat{y}_{t+1} is the predicted value of the next period; y_t is the actual value of current period.

The prediction performance was estimated by sum absolute error of each ATM on testing data. It was computed for all 1213 ATM’s. The result is presented in table 2 and figure 6.

Table 2. Comparison of two cash flow prediction strategies

	Naïve prediction hypothesis	ANN model prediction
Prediction error	$9.5504 \cdot 10^4$	$5.8679 \cdot 10^4$

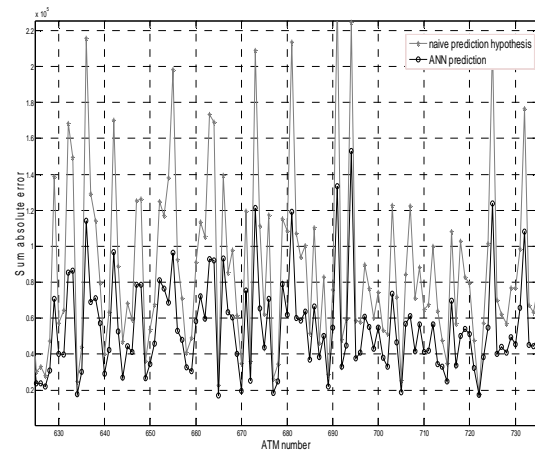


Fig. 6. Comparison of Naïve prediction hypothesis and ANN prediction error

Experimental results have proved the efficiency of ANN model proposed. The prediction error of the ANN model was significantly smaller.

6. Future works

Made abundant experimental studies showed that the model can accurately predict cash turnover in certain time intervals (Fig. 7). In other apparently an error increases. It was also investigated that model is very accurate for some of ATM, and for some of them – inaccurate. The results of this study let us to make conclusion that a strong correlation between the input variables with the turnover of money is only in certain moments.

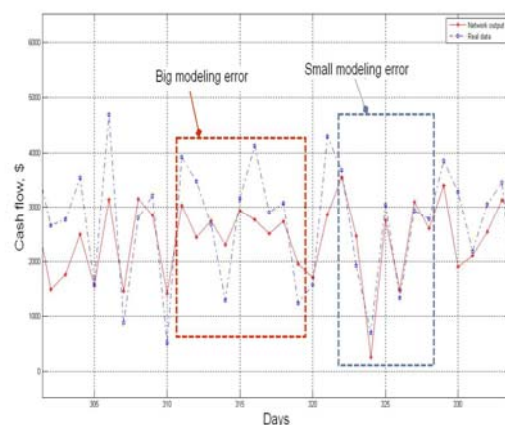


Fig. 7. Identified periods of small and big prediction error

This may be because the input variables magnitude varies over time and sometimes the model with other input variables could be significantly more accurate. If there is a big randomness in cash turnover, there is no ways to increase model accuracy. If not a random disturbance is guilty, it is necessary for further research what set of inputs for model in one or other period is more appropriate.

There will be a question of when the model needs to go to the next set of inputs? One way is to identify the error threshold of the model and if it is above the limit move to the next set. Another way could be to calculate the model by several sets of inputs and to use this one which gives the best result.

Of course some questions about the calculation resources and the time required performing them, especially if the calculations are carried out in real time will arise. All these questions will be analyzed in the next phase of our research.

7. Conclusions

Computational method for ATM cash flow forecasting using artificial neural network was proposed. Influence of various input sets to model accuracy was investigated. The best input set was used for model identification. ANN model prediction efficiency was estimated by comparison with Naïve prediction hypothesis. The error of ANN model was about 39% smaller. The result is hopeful, but further experimental investigation about practical implementation and more accurate cash turnover prediction is necessary.

Acknowledgments

This research work has been supported by means of EU structural funds (Project No. BPD2004-ERPF-3.17-06-06/0045).

8. References

1. Simutis R., Dilijonas D., Bastina L. Cash demand forecasting for ATM using neural networks and support vector regression algorithms. In: Selected papers of EurOPT-2008: the 20th International Conference "Euro Mini Conference on Continuous Optimization and Knowledge-Based Technologies", Vilnius, Technika, 2008. p. 416–421.
2. Simutis R., Dilijonas D., Bastina L., Friman J., Drobinov P. Optimization of cash management for ATM network. *Information technology and control*, 2007, vol. 36, p. 117-121.
3. Gupta M.M., Jin L., Homma N. *Static and dynamic neural networks: from fundamentals to advanced theory*. John Wiley & Sons, 2003. 700 p.
4. Gnoth S., Jenzsch M., Simutis R., Lübbert A., Control of cultivation processes for recombinant protein production: a review. *Bioprocess and Biosystems Engineering*, 2008, vol. 31, no. 1. p. 21-39.
5. Simutis R. Exploratory analysis of biochemical processes using hybrid modeling methods, *Proceedings of the First European Symposium Principles of Data Mining and Knowledge Discovery Trondheim, Norway, June 24-27, 1997*. p. 200-210.
6. Wei H., Shouyang W., Lean Y., Yukun B., Lin W. A new computational method of input selection for stock market forecasting with neural networks. *Proceedings of International Conference ICCS 2006, Part IV, 2006*. p. 308-315.
7. Huang W., Lai K.K., Nakamori Y., Wang S.Y. Forecasting foreign exchange rates with artificial neural networks: a review. *International Journal of Information Technology & Decision Making*, 3(1), 2004. p.145-165.

LITHUANIAN ENERGY AFTER 2009

Arvydas GALINIS
Lithuanian Energy Institute, Lithuania

Abstract: Government of the Lithuanian Republic committed to close the second unit of the Ignalina NP plant at the end of 2009. As a consequence Lithuanian Thermal Power Plant (Lithuanian TPP) will become the main electricity energy source. Although the provision of installed capacity at power plants is sufficient until 2014-2015, however a moderate probability exist, that under the particular circumstances a capacity deficit will be evident in 2010 and therefore part of consumers might be switched off. Nevertheless the main problem would still be economical and the scale of it would depend on the prices of fossil fuel.

Keywords: electricity, capacity, balance, production, costs, price.

1. Introduction

Lithuanian Government by signing the Treaty of the Accession to European Union committed to close the first unit of the Ignalina NPP at the end of 2004 and the second one at the end of this year. However these decisions were accepted with reference both to technical and economical analysis that was performed until 2002, and to information about global energy evolution trends, energy sector development tendencies, and main provisions in EU member states at that time. Nevertheless the situation in this field had essentially changed during the several recent years. Therefore it is advisable to examine, what situation will emerge in Lithuanian power sector after 2009, whether Lithuania itself, without the assistance of other countries could generate all required quantity of electricity. Other very important questions are the following: are there enough capacities and how this will respond both to operational cost and to the price of energy supplied?

2. Electricity generation and capacity balances

Even after the closure of the first unit, Ignalina NPP remained the main source for electricity generation in the country. There weren't significant changes because this power plant produces electricity cheaper than

thermal power plants, that use fossil fuel, do. The fraction of electricity produced at Ignalina NPP made more than 71% in electricity energy balance in 2005-2008. It is worth noting that electricity production from renewable energy sources increased from 460 GWh to 593 GWh during 2005-2007, however their share in Lithuanian electricity balance increased only slightly – from 3.9% in 2005 to 4.7% in 2007. Until 2015 the expected capacities of the renewable power plants will satisfy only approximately 10-12% of all electricity energy demanded. New large electricity generators at Lithuanian TPP or at other power plants will not appear in the market earlier than in 2012-2013. Until this time small-scale electricity generators (mainly gas based) can emerge only either in industrial or central district heating companies, but their impact on electricity and capacity balances will remain small. Considering to this, it is expedient to examine the worst case, when the increasing electricity demand is met only with at the moment existing power plants and electricity import for several reasons is not possible. Here some explicitness should be carried: in many cases the produced electricity depends on capacity installed. Electricity production at hydro power plants is an exception, because water flow of Lithuanian rivers limits the electricity production. Thus it is more relevant to analyse capacity balance than energy balance. The 1 table presents the worst case's capacity balance under basic demand scenario.

The presented data show that after closure of the second unit of the Ignalina NPP, the generating capacity of power plants will reduce from 4599 MW till 3466 MW, meanwhile demanded capacity of consumers will increase from 1917 MW in 2008 to 2471 MW in 2015. It means that capacity supplied to the transmission network is approximately 1000 MW larger than the demand; therefore there shouldn't be any problems. However, 2x150 MW units of the Lithuanian TPP are of low technical state and can't reliable work. It is considered, that this 287 MW capacity is mothballed. In addition, it is required to keep a reserve capacity in the system that is equal to capacity of the largest unit. In the case of breakdown of any unit at any power plant this reserve capacity should start operation. Thus emergency

reserve of the system would reach 289 MW. For a normal operation of the system, balancing reserve is also required. The purpose of this reserve is to compensate short-run electricity demand fluctuations. Its quantity depends on system load and increases from 102 MW in 2008 to 131 MW in 2015. Wind power plants are also not reliable power resource, because there aren't any guarantees that at the moment of maximum demand the wind will blow and rotate generators. Consequently wind power plants can't be involved into the capacity balance of system's peak load. Kruonis hydro pump storage plant (Kruonis HPSP) in some rare cases cannot also be used for system maximum demand satisfaction. Suppose, before the moment of system maximum load, accident occurred in the system and turbines of Kruonis HPSP were used as fast reserve. The turbines could consume water from the upper reservoir and therefore at the moment of system maximum demand there wouldn't be water, therefore Kruonis HPSP would not produce electricity. Thus, data presented in table 1 show that in the case electricity is not imported, 176 MW capacity deficit shall appear in 2010. If no generating units are built until 2015, the deficit will increase till 525 MW. Under conditions of high demand growth scenario, capacity deficit in 2010 and 2015 correspondingly will be 227 MW and 675 MW.

1 table. Capacity balance of Lithuanian power system under basic demand scenario, MW

	2008	2010	2015
Demand. Basic scenario	1917	2144	2471
Generating capacity (without own needs)	4599	3466	3466
Thermal power plants total	1183	2425	2425
Lithuanian TPP	2425	1722	1722
Vilnius CHP-3	1722	344	344
Kaunas CHP	344	161	161
Petrasiunai CHP	161	7	7
Mazeikiai CHP	7	148	148
Klaipeda CHP	148	9	9
Panevezys CHP	9	34	34
Industrial PP total	34	73	73
Hydro power plants and hydro pump storage plant	73	887	887
Biofuel PP total	837	29	29
Wind PP	29	52	52
Not used capacity	52	1498	1519
Mothballed capacity	2384	287	287
Emergency reserve	287	289	289
Balancing reserve	1183	110	131
Wind PP	102	52	52
Kruonis HPSP	52	760	760
Capacity used for demand satisfaction	760	1968	1947
Capacity surplus(+)/shortage(-)	2214	-176	-525

As it was mentioned, Kruonis HPSP cannot participate in covering system's maximum demand only in rare accidental cases. In normal operating regime, a part of its capacities can be used. Let's analyse which part of it's capacity can be used. Capacity of plant with limited output is utilised more efficiently, if it operates during system peak load. Kaunas HPP and Kruonis (HPSP) are limited energy output power plants. A part of Kaunas HPP capacities work in basic regime, because it is necessary to keep sanitarian flow of water below the power plant. Usually one unit of power plant works in basic regime. Thus 75.6 MW of Kaunas HPP is assigned to the peak load. Below Kaunas HPP there is a zone for Kruonis HPSP. Assuming that Kruonis HPSP is used for optimal weekly operating regime we can estimate that to the system's peak load in 2010 it can contribute by 440 MW and by 540 MW in 2015.

The results showed that in the case when new power plants are not built, but technical features of all existing power plants are maximally exploited, the demand of Lithuanian consumers with a considerable probability can be satisfied till the end of 2015 under the basic demand scenario. Under the high demand growth scenario it is expected that capacity deficit will start to emerge in 2014 and in 2015 capacity deficit can reach 135 MW. Although small, however there is a probability that because of Kruonis HPSP inability to work, there could be some capacity shortages even in 2010. In this case some consumers should be switched off. If new electricity generating units were built at Lithuanian TPP or somewhere else, the problem of capacity deficit would be postponed several years forward.

The information presented above took into account only technical aspects of functioning of Lithuanian electricity energy system. However economical questions are even more important. Perspective fuel prices have the major impact on economical aspects of power system operation.

3. Long-run fuel prices

Oil prices in global market have a significant impact on the prices of other fuel types. For this reason it is important to take a look at tendencies of oil prices. Approximately from 1986 to 2004 oil prices fluctuated in a range of 20-30 \$/barrel. Later oil price started to grow and in July 2008 it reached 145 \$/barrel. Thereafter oil prices suddenly fell down and they were less than 40 \$/barrel in the beginning of February 2009. The survey of literature shows that at the moment there is an absolute uncertainty about future oil price and therefore price of other fuels. This was excellently illustrated by data of USA Department of Energy that were presented in December 2008. The boundaries of future oil prices are very wide. Prices fluctuate from 50 \$/barrel to 170-200 \$/barrel. According to the main scenario the oil price will be near 90 \$/barrel during the period 2010 - 2015. This 90 \$/barrel oil price level was chosen for further analysis of consequences of the closure of the second unit of Ignalina NPP. With

reference to this, prices for other fuels that can be used in Lithuanian power plants are evaluated and presented in 2 table.

2 table. Prices of the main energy sources since 2010

Fuel	Unit	Price of import, production	Price at Lithuanian power plants
Fuel oil S-2,5% produced AB „Mazeikiu nafta“	Lt/t	1130	1191
	Lt/ toe	1183	1247
Diesel 0,2	Lt/t	2105	2145
	Lt/ toe	2151	2099
Natural gas	Lt/th.m ³	1000	1080
	Lt/ toe	1250	1350
Wood	Lt/m ³	140	
	Lt/toe	837	
Imported fuel oil S-3,5%	Lt/t	1100	1161
	Lt/ toe	1152	1216
Imported fuel oil S-1,0%	Lt/t	1200	1261
	Lt/ toe	1256	1320

If oil prices were high, oil refineries would be oriented towards oil deep processing, the opportunities to purchase fuel oil at reasonable price would decrease and price of natural gas for Lithuanian power plants (including transportation costs) would reach 1065-1080 Lt per 1000 m³. During winter price of natural gas can be 78 Lt per m³ higher if they are supplied to Lithuanian power plants not directly but from Latvian underground gas storage. The price of fuel oil depends on both fuel price and sulphur content. Thus when oil price is about 90 \$ per barrel, the price of low sulphur (<1%) fuel oil will be about 1260 Lt per ton in 2010. The price of high sulphur fuel oil (till 3.5%) will be about 100 Lt per ton lower than the price of low sulphur fuel oil.

4. Analysed scenarios

In order to estimate consequences of the closure of the second unit of the Ignalina NPP, six main scenarios were analysed. The assumptions made are as follows:

1 scenario. There are no limits for natural gas supply through the pipeline Minsk-Vilnius, e.g. natural gas is received when it is needed and as much, as it is needed. The guaranteed quantity of electricity imported is about 300 MW (approximately 2 TWh) from Russia and Finland at any time; since 2014 300 MW will be available from Poland at any time in summer and 300 MW at night in winter; 500 MW in summer and in off peak load in winter, but only 100 MW during peak load in winter will be available from 2016. Since 2016 500 MW will be also available from Sweden at any time.

2 scenario. There are no quantity limits on natural gas supply from Russia but supply regime is base load (constant). Assumptions regarding electricity import are the same as for scenario 1.

3 scenario. Conditions of scenario 2 are valid, however during two months in winter natural gas from Russia is not supplied with exception of Kaunas CHP.

4 scenario. Natural gas is supplied without any limits on quantity and regime; however since 2010 there are no any opportunity to import electricity.

5 scenario. Natural gas is supplied according conditions described in 2 scenario, however since 2010 there are no opportunity to import electricity.

6 scenario. Conditions of natural gas supply are the same as in scenario 3, however since 2010 there are no opportunity to import electricity.

Additionally the following assumptions have been taken into consideration: modern 400 MW combined cycle gas turbine unit at Lithuanian TPP and 320 MW combined cycle gas turbine unit at Kaunas CHP will start operation in 2012; the first unit of new nuclear power plant will come into the market since 2018. Operation of all power plants correspond to the least cost criteria.

5. The main results of the analysis

The performed analysis of power sector development confirmed the hypothesis that Lithuanian TPP will become the main source of electricity generation in Lithuania after the closure of the second unit of the Ignalina NPP. In the case when there are no additional limits on electricity and gas import (1 scenario), the existing units of the Lithuanian TPP will produce approximately 50% of electricity in 2010-2011. About 26% of all electricity will be produced at CHP's, 7% will be produced from renewable energy sources and 17% of all electricity will be imported. The role of existing units of the Lithuanian TPP in 2010-2011 would increase even more if there were no opportunity to import electricity from neighbouring countries. In this case these units would have to produce 57-59% of all electricity needed. Combined heat and power plants, that also use imported fuel, would produce 35-37% of all electricity and power plants running on renewable energy sources would generate about 7% of electricity. The most difficult period for Lithuanian electricity consumers will be 2010-2011, when existing units of Lithuanian TPP will produce the greatest part (59%) of electricity. It is worth noting that the efficiency of these units is about 38%. Therefore it is very important not later than in 2012 to start operation of new modern units both at Lithuanian TPP (400 MW) and at Kaunas CHP (320 MW). These units could produce about 5 TWh of electricity. This will make 40% of electricity needed. In addition, these units, in comparison with existing ones of the Lithuanian TPP, for the same quantity of electricity generated would require about 30% less natural gas. Therefore a share of existing units (300 MW) in electricity production balance would not exceed 20% in 2012-2015. However, their role will remain important for reserve capacity of the Lithuanian power system, especially in the case when there are some interruptions in supply of natural gas from Russia. In the first scenario it is calculated that in 2010-2011 the existing units of Lithuania TPP will consume about

1400 ktoe of natural gas and 320 ktoe of fuel oil. Since 2012 a great role will fall on new combined cycle gas turbines at Lithuanian and Kaunas power plants. Therefore natural gas demand at Lithuanian TPP will decrease till 760-860 ktoe in 2015, from which 430 ktoe will fall on the new unit of the Lithuanian TPP that will produce 2.8 TWh of electricity.

If natural gas supply through pipeline Minsk-Vilnius will be lost, lack of natural gas could be displaced by supply from Latvian underground gas storage. In extreme case when electricity import is not possible and gas supply Minsk-Vilnius is interrupted for two winter months Lithuanian power plants from Latvian gas storage will require 300 ktoe in 2010 and 380 ktoe in 2015. One third of this gas (130 ktoe in 2010 and 112 ktoe in 2015) will be consumed by units of Lithuanian TPP, that have no flue gas desulphurisation equipments. In this case electricity to Lithuanian consumers could be provided without any limits and there were no environmental violations on SO₂ emissions. If natural gas supply from Latvian gas storage to Lithuanian power plants weren't higher than 120 million m³ (about 100 ktoe), then fuel oil and other liquid fuel would be fired and this would lead to environmental violations on SO₂ emissions or to limitation of electricity consumption.

In 2010 nuclear fuel in Lithuania will be changed to expensive fossil fuel. Mainly because of increased expenditures for fuel procurement, the costs of power plant's operation will greatly increased 2.6-3.1 times and will make about 3.0-3.7 billion Lt. This would have an impact on electricity price, which will increase. Average annual electricity production price in Lithuanian power system in 2010-2011 will increase till 31 Lct/kWh (or 89.8 Euro/MWh). When new combined cycle gas turbine power units start operation, the average annual electricity production price would decrease till 26-27 Lct/kWh (or 75.3-78.2 Euro/MWh). However this price would be 3 times higher than the price of Ignalina NPP. This electricity production price will be much higher than electricity price in neighbouring countries. For example, it is forecasted that electricity production price in Scandinavian market will range from 30-45 Euro/MWh in 2010-2015, e.g. it would be 2 times lower than in Lithuania. In the beginning of February 2009 the average daily electricity production price in Scandinavian market was approximately 40.8 Euro MWh, in Poland and Germany correspondingly 44 Euro MWh and 50.7 Euro/MWh. Contrary to these prices the production price of electricity in "Europe-Ural" price zone in Russia was equal to only 12.6 Euro/MWh in January 2009.

The presented information about electricity prices in neighbouring markets illustrates the importance of connection of Lithuanian power system with Poland and Sweden systems. After connection of these systems, Lithuania will have ability to choose electricity suppliers and therefore will avoid price intrusion, which is substantial if there is the only link with one country.

It is worth to note that electricity price to final consumers is not equal to the price of electricity production. Electricity transmission, distribution, supply

prices, value added tax should be also taken into account. Thus the average electricity tariff for consumers that receive electricity from high voltage (transmission) network could reach 36.67 Lct/kWh. The costumers connected to medium voltage network should pay a price of 43.96 Lct/kWh and 55.05 Lct/kWh if electricity is supplied from low voltage network. Electricity price for households can increase till 56.55 Lct/kWh if the value added tax is included. These electricity prices are calculated assuming upper price cap values for different services approved by National Price and Energy Control Commission for 2009. If electricity transmission, distribution and other companies for their services will apply lower prices than foreseen upper cap, electricity price for consumers will be correspondingly lower. Final electricity consumers can also expect to pay lower prices, if oil price in global market will be lower than prices employed in this analysis, e.g. if oil price is lower than 90 \$/barrel. However if oil price is higher, correspondingly electricity price will be higher too.

6. Conclusions

1. If 1500 MW of Lithuanian PP could reliably operate, Lithuania after the closure of the second unit of the Ignalina NPP would not meet with considerable technical capacity shortage problems till 2014-2015 even in the case if new generating units were not built and there weren't any electricity import during peak load time.
2. If oil price in global market will approximately be 90-100 \$ barrel, then electricity generation costs would increase more than 3 times.
3. Electricity tariff for final consumers that receive electricity from transmission and distribution networks will correspondingly be 36.7 Lct/kWh and 55 Lct/kWh. Electricity tariff for household consumers will reach 56.6 Lct per kWh.

7. References

1. Annual Energy Outlook 2009. Early Release. Energy Information Administration, December 17, 2008. http://www.eia.doe.gov/oiaf/aeo/pdf/aeo2009_presentati on.pdf

ANALYSIS OF LATVIAN POWER SYSTEM DEVELOPMENT IN THE KURZEME REGION USING MULTICRITERION OPTIMIZATION

Anatoly MAHNITKO, Alexander GAVRILOV
Riga Technical University, Power Engineering Institute, Latvia

Abstract: Latvian power system is in deficit. According to prognoses of the “Latvenergo” for 2015 the most important question will be where and from whom to buy electric power. What power and what type of energy resources power plants we need to build and where should they be located – all of this is widely discussed in different articles.

The energy department of Latvian ministry of economy has examined some scenarios of power system development. In the 2010 the deficit will be already doubled, and to the 2020 the deficit is assumed to be 2.5 times more than produced power.

In the work it is attempted to analyze development of Latvian power system in the Kurzeme region. Some variants of high voltage network development are considered.

Keywords: power system, high voltage line, annual expenses, environment protection, criterions of evaluation.

1. Introduction

It is practically difficult to accumulate electric power, therefore power production, distribution and demand balance is a very important question in the economy of any state. Without required adequate networks and guidance of the system’s infrastructure it is important to provide necessary power generation, to meet requirements in primary energy and its delivery systems. Currently power industry development should be analyzed in a close context with economy and environment aspects, because still growing demand of energy resources, available fossil energy resources decrease and necessity to take care on quality of environment have pulled out notices of long-term development principles. Those principles consideration and implementation provides stable, long-term development of economic, business competitiveness increase and employment encouragement, simultaneously saving quality of environment [1-3].

2. Actuality of Latvian power system development

In our days power of Latvia power plants is not enough to cover demand in any moment, because the mode of large hydroelectric power plants depends on river Daugava water level. A state power supply lies with a base mode of Latvian and neighboring countries’ power plants. After Ignalina AES closing in the year 2009, to prevent continued overload modes in neighboring countries’ transmission networks it will be necessary substantially limit power transfers from Russia. It is possible that after the year 2010 the accessible generated power in the Baltic region strongly reduces.

As in Latvian power system is real base power deficit it is necessary to reconstruct or to build power plants. We should increase the general set power above 800MW and ability to operate in the base mode, reconstructing Riga TEC-2 (400MW) and building power plant in Kurzeme (400MW) [2, 3].

While analyzing the possible coal power plant placing variants in Kurzeme as the most perspective are selected locations in Liepaja or Ventspils (Fig. 1). Each of the examined variants has advantages and disadvantages.

Liepaja is a larger power demand center and in the future it will grow up. In the Liepaja variant power delivery in transmission network will be provided by building new 330 kV substation in Liepaja and 330 kV overhead line to substation "Grobina" (about 15 km). On the other hand in the Ventspils variant it is necessary to construct new 330 kV substation and 330 kV overhead line (119 km) to substation "Grobina".

Ventspils, by the side of Liepaja, has a number of advantages. Ventspils port can provide enter of noice class ships whole year round. There are 9 deepwater piers in the port district of the liquid shiploads with depth between 11.5 and 17.5 m. Necessary coal amounts for power plant the port can provide already. To decrease ships unloading time and expensis of conveyers it is foreseen to build temporary towertype coal storages [3].

In Liepaja port there are essentially additional means for coal terminal building and so it can provide service of ships with a less carrying capacity. In Ventspils, in contradistinction to Liepaja, is also better developed

junction that can provide coal delivery by railway. Coal transport to power plant is planned using closed conveyer gallery.

Electric power market in Baltic region is opened for all commercial consumers, but, at that moment, only formally, because there is no concluded a treaty for supply direct from sources of generation to end consumers. Relatively small market of Baltic states is isolated from other European Union (ES) markets. Physically the only possibility of trading for each of Baltic states is with one market participant in Russia (IterRAO) [1].

One of the most important question company "Latvenergo" gets busy at the present moment is Latvia – Sweden connection development. For the Baltic states connection with Sweden is very important to promote electric power market development and to provide region with missing powers. Although, due to the 350 MW cable line (CL) between Estonia and Finland Baltic states now can buy electric power in the Scandinavian electric power exchange „Nord Pool Spot”, cable power is too small to form valuable market with Western Europe. For Sweden connection building in Kurzeme the most decent place is Ventspils region, where cable line will be shorter and that will promote 330kV network development in Kurzeme instead of Liepaja [4].

According to the mentioned reasons there are examined such Latvian power system in region Kurzeme development strategies:

- φ_1 – 330 kV OL Ventspils – Grobina (119 km) building and port improvement in Ventspils (coal power plant building in Ventspils);
- φ_2 – 330 kV OL Liepaja – Grobina (15 km) building and port reconstruction in Liepaja (coal power plant building in Liepaja);
- φ_3 – CL Stockholm – Ventspils (300 km) building.

The geographical reflection of variants is shown in Fig. 1.

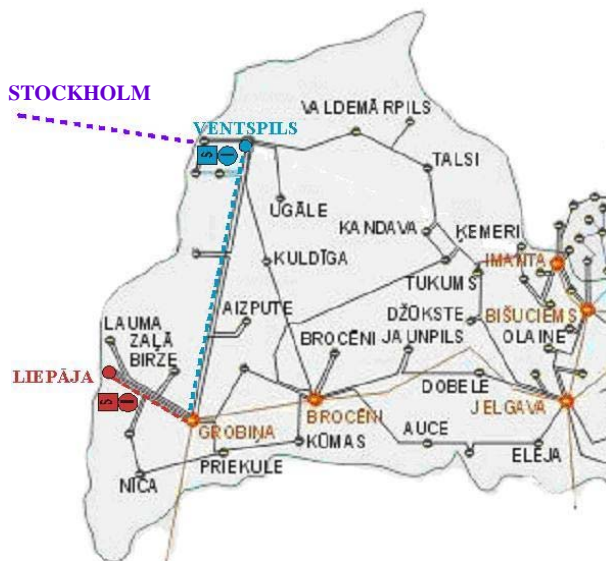


Fig.1. Latvian power system development variants in the region Kurzeme

Power system development primary purposes are: to provide qualitative and safety power supply at low expenses, and also minimally affect environment. Therefore choosing optimal development strategy there were pulled out such criterions:

C_{Σ} – total annual expenses;

A_R – undelivered amount of electric power in the year due to emergency failures;

C_{ek} – annual expenses to prevent harmful influence on the environment.

3. Annual expenses of development strategies

Let us examine the annual expenses of transmission lines. Specific capital investments in 330 kV overhead lines are $K_0 = 3.5 \cdot 10^5$ €/km, but sea cable expenses are $K_{0kab} = 1 \cdot 10^6$ €/km [4]. Then capital investments in line sections are, €:

$$K_{\Sigma j} = K_0 \cdot l_j, \quad (1)$$

Capital expenditures could be defined accepting interest rate $i = 10\%$, € [5]:

$$C_{K_j} = \frac{i}{100} \cdot K_{\Sigma j}. \quad (2)$$

In constant operational costs calculations it was accepted that:

for OL ($U_{nom} \geq 35 kV$) $p_a = 2.5\%$ and $p = 1.5\%$;

for sea CL ($U_{nom} = 110 \div 330 kV$) $p_a = 3\%$ and $p = 2\%$.

Then constant operational costs are, €/year:

$$C_{Ek1} = \frac{1}{100} \cdot \sum_{j=1}^l K_{\Sigma j} \cdot (p_a + p). \quad (3)$$

330 kV OL will be constructed using 2xAC-300/39 mark wires. Wire specific resistance is $R_0 = 0.049 \Omega$.

Active power losses due to corona are:

$$\Delta P_{k_j} = \frac{\Delta P_{k0max} + \Delta P_{k0min}}{2} \cdot l_j, \quad (4)$$

where ΔP_{k0max} – active power losses due to corona in bad whether, kW/km;

ΔP_{k0min} – active power losses due to corona in good whether, kW/km.

Total active power losses in overhead lines at maximum demand mode:

$$\Delta P_{L_j} = 3 \cdot I^2 \cdot R_0 \cdot l_j + \Delta P_{k_j}, \quad (5)$$

where $I = \frac{P}{\sqrt{3} \cdot U_n \cdot \cos \varphi}$ – demand current, A.

For CL Stockholm – Ventspils will be used XLPE cable with cross-section 2000 mm².

Power losses in wire conductor [6]:

$$\Delta P_{vad} = I^2 \cdot R''; \quad (6)$$

$$R'' = R' \cdot [1 + 1.7 \cdot (y_s + y_t)], \quad (7)$$

where R'' – conductor resistance to alternating current at 90°C, Ω/m ;

y_s – surface effect factor;

y_t – closeness effect factor;

R' – conductor resistance to direct current at 90°C, Ω/m :

$$R' = R_0 \cdot [1 + \alpha_{20} \cdot (v_p - 20)], \quad (8)$$

where $R_0 = \frac{1000}{\gamma \cdot F}$ – conductor resistance at 20°C;

γ – conductor specific conductivity

$$\gamma_{Cu} = 32 \text{ m}/\Omega \cdot \text{mm}^2;$$

$\alpha_{20} = 0.00393 \text{ 1}/^\circ\text{C}$ – temperature coefficient for copper;

$v_p = 90^\circ\text{C}$ – maximum allowed temperature for cables with plastic insulation.

Surface effect factor:

$$y_s = \frac{x_s^4}{192 + 0.8x_s^4}; \quad (9)$$

$$x_s^2 = \frac{8\pi \cdot f \cdot k_s}{R'} \cdot 10^{-7}, \quad (10)$$

where k_s – surface effect coefficient;

$$f = 50 \text{ Hz} \text{ – frequency.}$$

Closeness effect factor:

$$y_t = \frac{x_t^4}{192 + 0.8x_t^4} \cdot \left[0.312 \cdot \left(\frac{d_{dz}}{s} \right)^2 + \frac{1.18}{\left(\frac{x_t^4}{192 + 0.8x_t^4 + 0.27} \right)} \right]; \quad (11)$$

$$x_t^2 = \frac{8\pi \cdot f \cdot k_t}{R'} \cdot 10^{-7}, \quad (12)$$

where k_t – closeness effect coefficient;

s – distance between wire axes ($s = 204 \text{ mm}$);

d_{dz} – wire diameter with screen ($d_{dz} = 102 \text{ mm}$).

Active power losses in cable insulation, kW:

$$\Delta P_{iz} = U_{nom}^2 \cdot \omega \cdot C_0 \cdot tg \delta \cdot l_j, \quad (13)$$

where C_0 – cable specific capacity ($C_0 = 0.23 \mu\text{F}/\text{km}$);

ω – angular frequency;

$tg \delta$ – insulation dielectrical losses angel tangent.

For 330 kV cables with XLPE insulation $tg \delta = 0.0001 \div 0.0002$.

Power losses in cable outside metal screen, kW:

$$\Delta P_{3f} = I^2 \cdot R_0 \cdot l \cdot (3 + \lambda_{11} + \lambda_{12} + \lambda_{1V}) + 3 \cdot \Delta P_{iz}, \quad (14)$$

where λ_{11} – first outside phase metal screen losses coefficient that observe metal screen active resistance and proximal cables reactive resistance ($\lambda_{11} = 0.53 \div 0.68$);

λ_{12} – second outside phase metal screen losses coefficient ($\lambda_{12} = 0.35 \div 0.44$);

λ_{1V} – central phase metal screen losses coefficient ($\lambda_{1V} = 0.22 \div 0.36$).

Total active power losses in CL:

$$\Delta P_{KL} = \Delta P_{vad} + \Delta P_{3f}. \quad (15)$$

Transmission network parameters are taken from “Latvenergo” homepage [7]: $\beta' = 0.043 \cdot 10^3 \text{ €/MW}\cdot\text{h}$; $\beta'' = 5.27 \cdot 10^3 \text{ €/MW}$.

Maximum losses hours count, h:

$$\tau = (0.124 + T_{max} \cdot 10^{-4})^2 \cdot 8760, \quad (16)$$

where T_{max} – maximum time of usage ($T_{max} = 5000 \text{ h}$).

Variable operational costs for lines, €:

$$C_{EmLj} = \Delta P_{Lj} \cdot (\tau \cdot \beta' + \beta''). \quad (17)$$

Total operational expenses, €:

$$C_{Ej} = C_{Ekj} + C_{EmLj}. \quad (18)$$

Total annual expenses for lines, €:

$$C_j = C_{Kj} + C_{Ej}. \quad (19)$$

Total strategies φ_1 and φ_2 annual expenses taking into account capital expenditures for port improvement:

$$C_{\Sigma j} = C_j + \frac{i}{100} \cdot K_{Pj}, \quad (20)$$

where K_{Pj} – port reconstruction capital investments in Ventspils and Liepaja. As it was told above Ventspils port reconstruction include temporary towertype coal storages building ($K_{P1} = 1.5 \cdot 10^6 \text{ €}$). It is necessary to build coal terminal in Liepaja ($K_{P2} = 25 \cdot 10^6 \text{ €}$).

It was assumed that every year demand increases by 1.5%. Thereby there were gotten annual expenses for every strategy φ_1 , φ_2 and φ_3 (Table 1 – 3), where K_d – demand increase coefficient.

Table 1. Annual expenses for strategy φ_1

K_d	$C_{EmL1},$ €	$C_{EI},$ €	$C_I,$ €	$C_{\Sigma 1},$ €
1	962715	2628715	6793715	6943715
1.015	990036	2656036	6821036	6971036
1.03	1017765	2683765	6848765	6998765
1.045	1045901	2711901	6876901	7026901
1.06	1074443	2740443	6905443	7055443

Table 2. Annual expenses for strategy φ_2

K_d	$C_{EmL2},$ €	$C_{E2},$ €	$C_2,$ €	$C_{\Sigma 2},$ €
1	121351	331351	856351	3356351
1.015	124795	334795	859795	3359795
1.03	128290	338290	863290	3363290
1.045	131836	341836	866836	3366836
1.06	135434	345434	870434	3370434

Table 3. Annual expenses for strategy φ_3

K_d	$C_{EmL3},$ €	$C_{E3},$ €	$C_{\Sigma 3},$ €
1	356249	15356249	45356249
1.015	360516	15360516	45360516
1.03	364845	15364845	45364845
1.045	369239	15369239	45369239
1.06	373696	15373696	45373696

4. Loses for national economy if line breaks off

Emergency switching off load flow parameter in the year [5] for the singlecircuit 330 kV OL is $\lambda_{d,sp} = 0.005$ discon./year-count, but for CL - $\lambda_{d,sp kab} = 0.00072$ discon./year-count. Then for every strategy transmission line's emergency switching off parameter in the year:

$$\lambda_{d j} = \lambda_{d,sp} \cdot l_j. \quad (21)$$

OL emergency disconnection duration (330 kV OL emergency switching off average duration $1.3 \cdot 10^{-3}$ year/discon.) is, h:

$$T_{d,L} = 1.3 \cdot 10^{-3} \cdot 8760 = 11.4 \text{ h}. \quad (22)$$

Emergency disconnection outage probability in the year:

$$\chi_{d j} = \frac{\lambda_{d j} \cdot T_{d,L}}{T}. \quad (23)$$

Undelivered by customers energy during the year ($P_{max} = 300$ MW; $T_{max} = 5000$ h), MW·h:

$$A_{R j} = \chi_{d j} \cdot P_{max} \cdot T_{max}. \quad (24)$$

Using the accepted demand increase coefficient (1.5% per year) there were gotten results about undelivered power for each strategy if line is disconnected (table 4), where $A_{R \varphi 1}, A_{R \varphi 2}, A_{R \varphi 3}$ – undelivered power, accordingly, for strategy $\varphi_1, \varphi_2, \varphi_3$.

Table 4. Undelivered power for strategies φ_1, φ_2 and φ_3 if line disconnects

K_d	$A_{R \varphi 1},$ MW·h	$A_{R \varphi 2},$ MW·h	$A_{R \varphi 3},$ MW·h
1	1500000	1160.25	146.25
1.015	1522500	1177.65	148.89
1.03	1545338	1195.32	151.27
1.045	1568518	1213.25	153.70
1.06	1592045	1231.45	156.16

5. Damage to the environment

Alienated territory area [6], m²:

$$S_j = a \cdot l_j, \quad (25)$$

where l_j – transmission line terrestrial length, m. For CL Stockholm – Ventspils terrestrial section length is 20 km;

a – trace width, m. 330 kV OL trace width is 68 m; CL tunnel width $a_c = 6$ m.

Damage to the environment for the alienated areas, €:

$$Y_j = S_j \cdot c_Y, \quad (26)$$

where c_Y – damage to the environment specific price, €/m² (in this work it was accepted $c_Y = 10$ €/m²).

Capital expenditure for damage to the environment if interest rate is $i = 10\%$, €:

$$C_{KY j} = \frac{i}{100} \cdot Y_j. \quad (27)$$

Annual installment for the damaged nature renovation, €:

$$C_{Y j} = S_j \cdot y, \quad (28)$$

where y – region annual specific costs for ecology (in this work it was accepted $y = 0.5$ €/m²).

Total annual costs for the damage to the environment and it's renovation, €:

$$C_{ec j} = C_{KY j} + C_{Y j}. \quad (29)$$

Assuming that annual cost increases by 5% due to inflation there were gotten annual damage expenses for strategies φ_1, φ_2 and φ_3 , accordingly, $C_{ec \varphi 1}, C_{ec \varphi 2}$ and $C_{ec \varphi 3}$ (table 5).

Table 5. Damage to the environment for strategies φ_1 , φ_2 and φ_3

Year	K_d	$C_{ec \varphi_1}$, €	$C_{ec \varphi_2}$, €	$C_{ec \varphi_3}$, €
1	1	12316500	1552500	180000
2	1.015	12519722	1578375	183000
3	1.03	12712681	1604250	186000
4	1.045	12911798	1630125	189000
5	1.06	13106809	1656000	192000

6. Summarization of results and optimal strategy detection

Perspective demand possessive function was gotten using expert judgement method (table 6), where $\mu_{\tilde{S}}$ – expert judgement rationed possessive function; K_p – demand increase coefficients.

Table 6. Perspective demand possessive function

$\mu_{\tilde{S}}$	0	0.28	0.51	0.15	0.06
K_p	1	1.015	1.03	1.045	1.06

There are summarized selected strategies φ_1 , φ_2 and φ_3 partial criterions in the tables 1-7, where C_{Σ} – total annual expenses; A_R – undelivered amount of electric power in the year due to emergency failures; C_{ec} – annual expenses to prevent harmful influence on the environment.

Total annual expenses \tilde{C}_{Σ} , undelivered amount of electric power \tilde{A}_R and annual expenses to prevent harmful influence on the environment \tilde{C}_{ek} indirect groups are demand power \tilde{S} indirect function groups, that form indirect relations $\tilde{R}_1, \tilde{R}_2, \tilde{R}_3$ with possessive functions $\mu_{\tilde{R}_1}, \mu_{\tilde{R}_2}, \mu_{\tilde{R}_3}$. There are shown functions' normalized values using the expression $\mu_R(K, S) = K(S)_i / K(S)_{\max}$ in the table 7, where K – corresponding partial criterion denomination [8]. Indirect target possessive functions (table 8) were gotten using expressions:

$$\mu_{C_{\Sigma}} = \max[\min(\mu_{\tilde{R}_1}, \mu_{\tilde{S}})];$$

$$\mu_{A_R} = \max[\min(\mu_{\tilde{R}_2}, \mu_{\tilde{S}})];$$

$$\mu_{C_{ec}} = \max[\min(\mu_{\tilde{R}_3}, \mu_{\tilde{S}})].$$

Table 7. Imprecise relations possession function

	K_d	φ_1	φ_2	φ_3
$\mu_{R_1}(C_{\Sigma}, \tilde{S})$	1	0.15309	0.07400	1
	1.015	0.15368	0.07407	1
	1.03	0.15428	0.07414	1
	1.045	0.15488	0.07421	1
	1.06	0.15550	0.07428	1
$\mu_{R_2}(A_R, \tilde{S})$	1	1	0.12605	0.27925
	1.015	1	0.12643	0.28009
	1.03	1	0.12655	0.28037
	1.045	1	0.12668	0.28065
	1.06	1	0.12681	0.28093
$\mu_{R_3}(C_{ec}, \tilde{S})$	1	1	0.12605	0.01461
	1.015	1	0.12607	0.01462
	1.03	1	0.12619	0.01463
	1.045	1	0.12625	0.01464
	1.06	1	0.12635	0.01465

Table 8. Target function values

$\mu_i \backslash \varphi_j$	φ_1	φ_2	φ_3
$\mu_{C_{\Sigma}}$	0.15428	0.07414	0.51
μ_{A_R}	0.51	0.12655	0.28037
$\mu_{C_{ec}}$	0.51	0.12619	0.01463

Table 8 cells form matrix

$$A = [a_{ij}], \quad i = 1, 2, 3; \quad j = 1, 2, 3.$$

As it is known from [9], matrix A saddle point a_{ij}^* is defined using the condition $\max_i \min_j a_{ij}$. Saddle point is appropriate row minimum element and appropriate column maximal element. In this case matrix A row minimum elements are:

$$0.07414; 0.12655; 0.01463.$$

Matrix A columns' maximum elements are:

$$0.51; 0.12655; 0.51.$$

It could be concluded that

$$\max_i \min_j a_{ij} = 0.12655.$$

Element a_{22} is saddle point, that corresponds with strategy φ_2 – 330 kV OL Liepaja – Grobina (15 km) building and port reconstruction in Liepaja.

7. Conclusions

The result of proposed algorithm of Latvian power system development in region Kurzeme allow to get practical justification from the point of exercise solution multicriterion analysis.

8. References

1. <http://www.em.gov.lv> // Enerģētikas attīstības pamatnostādnes 2007.-2016.gadam
2. Maņģitko A., Gavrilovs A., Gerhards J. Проблемы развития электроэнергетики Латвии // Энергосистема: управление, конкуренция, образование. Сборник докладов III международной научно-практической конференции 13-16 октября 2008. Том 2, III Международная научно-практическая конференция, Кривяжа, Екатеринбург, 13. –16. октябрь, 2008. – 274–277. lpp.
3. <http://www.em.gov.lv> // Elektroenerģijas ražošanas jaunu bāzes jaudu ieviešanas scenārijs. Informatīvais ziņojums.
4. Zviedris I. PSO redzes lokā – gan bāzes jaudas, gan jauni starpsavienojumi un drošība // Energoforums. Enerģētikas nozares jaunumu apskats, diskusijas, analīze. – 2008. – Nr. 4 (14) – 8. – 9. lpp.
5. Krišāns Z., Oļeinikova I. Elektroenerģētisko uzņēmumu vadības pamati. – R.: RTU izdevniecība, 2007. – 160 lpp.
6. Справочник по проектированию электрических сетей / Под ред. Д.А.Файбисовича. – М.: НЦ ЭМАС, 2005. – 320 с.
7. www.latvenergo.lv
8. Лещинская Т.Б. Применение методов многокритериального выбора при оптимизации систем электроснабжения сельских районов // Электричество. – 2003. – №3 – 14 – 22 стр.
9. Зайченко Ю.П. Исследование операций. – Киев, Вища школа, 1975. – 320 с.

BALANCE MANAGEMENT IN THE BALTIC COUNTRIES AND POSSIBILITIES FOR HARMONIZATION

Aušra PAŽĖRAITĖ*, Mindaugas KRAKAUSKAS *, Giedrius RADVILA**, Vidmantas BALTAKIS***
*Lithuanian Energy Institute, Lithuania; **Lietuvos Energija AB, Lithuania; ***Sprendimų erdvė, Lithuania

Abstract: An overview of the balancing mechanisms in Baltic countries and the ways of harmonization is given in the paper. The role of Russia in the balancing process is presented as well. Lithuania has created the balancing mechanism based on the hourly regulating power market. It would be worth Latvia and Estonia to join this market and to develop it into common reserve market. The common market would lead to better usage and lower costs of the reserves. And the most important outcome could be the first step to the common Baltic electricity market. As it is shown in the paper, this balancing mechanism is very close to the Nordic system.

Keywords: transmission system operator, reserve, balance regulation, regulating power market, balancing power market.

1. Introduction

Each power system is always in balance; generation is always equal to demand, including technological losses. On an AC system, this rule is maintained in real time by the frequency, deviation of which from nominal (50 or 60 Hz) represents the difference between the 'required demand' and 'delivered demand'. The frequency has to be kept within strict limits to avoid system degradation; usually +/- 1% for normal operation. If the frequency deviates beyond 2%, automatic disconnection and measures are necessary to arrest the slide and avoid collapse [1]. Imbalances in the physical trade on the spot market must be levelled out in order to maintain the balance between production and consumption, and to maintain power grid stability. Totalling the deviations from bid volumes at the spot market yields a net imbalance for that hour in the system as a whole. The transmission system operator (TSO) is the body responsible for securing the system functioning in a region. Within its region, the TSO controls and manages the grid. The TSO is in need of a mechanism for balancing the amount of power fed into and taken out of the system at all times. This mechanism is called

balance management and contains two different functions:

- Balance regulation,
- Imbalance settlement.

Providing balance regulation the TSO in each country activates regulation for keeping the frequency stable and within the required range in the network. Regulation is based on a number of different reserves, such as:

- Automatic
 - Frequency controlled normal operation reserve,
 - Frequency controlled disturbance reserve,
 - Voltage controlled disturbance reserve.
- Manual
 - Fast active forecast reserve,
 - Fast active disturbance reserve,
 - Slow active disturbance reserve.

Most of these reserves are activated automatically, whereas others are activated manually according to the TSO commands. These reserves can be provided by special power plants which are not in ownership of the TSO, particularly, after unbundling. Therefore, appropriate procurement schemes are needed to activate these reserves. In other words, activation of reserves under such schemes means power generated or not generated according to the TSO's requirement, and it is called regulated power. The EU directive on internal electricity market in article 11 states that balancing should be organized transparently, non-discriminatory and on market based principles [2].

Regulating power market (RPM). The regulating power market is a tool for TSO's to keep balance between total generation and consumption of power in real time. The participants in the RPM are producers and consumers who can regulate their generation or consumption on request from TSO's. RPM is real-time market covering operation within the specific hour. The main function of the RPM is to provide power regulation to counteract imbalances related to day-ahead operation planned. The TSO alone makes up the demand side of this market and approved participants on the supply side, including both electricity producers and consumers. If the vendors'

offers or buyers' bids on the spot market are not fulfilled physically, the regulating market comes into force to keep system in balance.

Balancing power market (BPM). Participants in this market, in many cases, are passive, they are consumers or generators, and they are not enabled to adjust their consumption or generation in real time during delivery period according the TSO instructions. They are the main reason why imbalances occur. The basic principle for settling imbalances is that participants causing or contributing to the imbalance will pay their share of the costs for re-establishing the balance in the system. Imbalances in other words mean power deviation from generation or consumptions plans and it is named as balance power. Balance power is always automatically purchased or sold by the TSO. Balancing power market is linked to the RPM and handles participants' imbalances recorded during the previous 24-hour period of operation. The TSO alone acts on the supply side to settle imbalances. Participants with the imbalances on the spot market are price takers on the balance market.

The Regulating power market and the Balancing power market may be regarded as one entity, where the TSO acts as an important intermediary or facilitator between the supply and demand of regulating power. Regulating Power and Balancing Market is an important tool for managing the balance and stability of the system. If the grid is congested, the market breaks up into different price area markets, and equilibrium must be established in the each area.

The problem in the future to be sold is related to the fact that electricity markets under globalization process tend to integrate in the single market when system operation will remain under national TSO's control, so harmonization issues in the balance management process across countries have an important role to guarantee competitive and secure global electricity markets.

Therefore it is important to discuss about balancing problems not only in advanced market countries, but also about possibilities to adopt their experience in such emerging electricity markets as Check, Croatia, Estonia, Latvia, Lithuania, and a.c.t. [3,4,5]. These opportunities are discussed in more detail for Baltic countries, particularly, Lithuania. Additional requirement for harmonization of electricity market between Nordic and Baltic countries is related with the new interconnection between Estonia and Finland [6], and planed interconnection between Lithuania and Sweden [7]. Nordpool Spot AS has already made significant efforts to expand its market towards the Baltic countries as the separate price area, called Estlink [9,10]. The establishment of Estlink price area will facilitate the creation of common Baltic electricity market. The creation of viable and credible common Baltic States power market would secure the conditions for free trade in electricity as well as higher level of energy security. Viable and transparent market regulations based on Nordic experience should create conditions for the establishment of the transparent common Baltic electricity market.

2. Regulating and Balancing Power Trading In Lithuania

Only TSO of Lithuania has right to trade regulating and balancing power with other power systems TSOs or open balance electricity suppliers in Baltic. The internal market of Lithuania is determined by the physical territory of the country. The main players of regulating and balancing powers are TSO, balance providers, generators and open balance supplier. The main activities of TSO for managing the system balance are represented by the following actions, as show in Table 1.

Table 1. TSO actions

Time line	Actions
Before the delivery day	Calculates transmission capacity limits, losses and forecasts consumption
Before operating hour	Receives information on the volumes of fixed transactions. Receives regulation power bids
During operating hour	Monitors national balance, regulates if needed and registers regulating energy transactions
After operating hour	Collects measurement data and balance information Calculates the imbalance for each hour

According the law, all market players has mandatory to provide the bids for regulation power. The regulation power auction is organized by TSO and is done according "Trading rules at auction". The auction of regulating power is part of common trading system in Lithuanian power market governed by Market operator and TSO. Legal framework of Lithuanian power market defines the rules of electricity trading. After gate closure of spot market, each producer must submit available capacity for reserves and regulation power auction. The available capacity for RPM is defined as the difference between maximum available generation capacity and used capacity for commercial commitments defined by spot market transactions. Firstly, the TSO uses available capacity for ensuring emergence and stand-by reserves. The remaining capacity is submitted to the regulation power auction which is organized by TSO.

Each market participant submits the following information:

- Available maximum and minimum generating capacity - possible technical minimum and maximum of power station's operation.
- Capacity price for 1 MW.
- Energy price for 1 MWh of used capacities by TSO.

Only after signing the regulation-balancing contract, a market participant may submit proposals for system services i.e. sell reserved capacity and participate in regulating power auction.

TSO must ensure the required amount of reserve capacity for the internal system. Reserve capacities are used in lower price priority order from those production sources, which meet technical requirements for

providing the ancillary services.. However TSO has right to, select reserved capacity sources without taking into account the electricity price priority principle. For example, Lithuanian power plant, being strategic in respect to capacity security, has a priority for maintaining operative and stand-by reserve since it has a sufficient capacity potential after 12 hours to change the capacities of Kruonis hydro pumped storage power plant in case of emergency disconnection of Ignalina nuclear power plant.

Regulating power auction is single-sided, i.e. auction participants submit bids or offers for regulation and TSO acts as the single buyer or seller of regulation power. Ensuring that regulation in the system will be carried out under most optimal prices, TSO groups the proposals according the low price priority principle Performing system regulation by compensating the deficit which occurs during the operation hour, TSO purchases power from the producer, who suggested the lower regulating power price, and when there is a surplus in the system, he sells power with the highest price, which being submitted by the producer. It means, that TSO may reduce his own price, and when there is a surplus in the system – sells power at the highest price, proposed by the producer, which means that he may reduce his own production volume. When there are congestions or bottlenecks in transmission grid, regulation may be performed without following the price priority principle, however activate regulation proposals, taking into account technical possibilities and reliability of the system. This alternative provides more opportunities for TSO. It can operatively and technically coordinate and control system in emergency cases, when regulation resources must be forecasted for several hours or a day forward. Activating several proposals, a common regulating power price in a certain hour is calculated as weighted average price of all regulation power transactions prices.

The maximum regulating power price is restricted by the open balance supply price, defined, according to the TSO balancing agreement with the open balance provider from Russia. If the regulating power price is higher than open balance provider price, the regulation is not performed in the Lithuanian power system, and the open balance supply ensures the needed electricity which is purchased from the Russia. Only due to congestions and restrictions of system reliability margin the regulation must be performed internally and regulation power bids or offers may be activated, whenever the price is higher. The average regulation power price is basis for the setting the system balancing electricity price.

There are two options of maintaining the system balance in Lithuania. In the first case, TSO activates regulation “up” bids and buys electricity from regulation power auction or open balance supplier. The aggregated transactions allow to set the balancing power price for producers and market participants, who participate in the hourly trading and are under balance. The balancing power price defined as the weighted average price of all transactions made by TSO

multiplied by the coefficient which is determined by the regulator, i.e. 1.2.

In the case of ‘surplus’, regulation “down” is done by TSO and purchasing price of balancing power is formed analogically, however the price is reduced by multiplying the regulation “down” and open balance supplier weighted average price by coefficient 0.8.

If regulation was not performed in the system, price of balancing power is calculated by multiplying the price of open balance supplier electricity price by mentioned coefficient appropriately.

A unique method of balance settlement for consumers or suppliers who have the consumers is adopted in Lithuania. The regulation costs are included into supplementary power price, which is settled and defined by Market operator to the costumers after the month. All consumers share costs of imbalances. The applied method would have to stimulate balance responsible parties to become balance provider or choose balance provider and, therefore, participate in hourly trading. But for the time being the situation does not changes very much and the implemented method sends the week signals of balance responsibility for consumers.. The TSO has cheap regulating power sources in his own hydro pumped storage power plant and hydro power plant and rather cheap balancing power from Russia. The avoidance of additional costs for administration of hourly trading and balancing responsibility, leads the situation, when suppliers agree to share costs by ignoring their own contribution. The public supplier or the last resort supplier gains the biggest benefit from such situation. Lithuanian balancing mechanism, particularly, the regulation power auction is open for Latvian and Estonian players such as:

- Generators,
- Suppliers,
- Eligible customers,
- TSOs.

The regulation power auction is open for all market players across the Baltic States. The participants should fulfil the following requirements:

- Regulation power agreement with Lithuanian TSO,
- Information providing - bidding and offering hour by hour,
- The bids must be submitted electronically no later than 120 minutes before the beginning of the operational hour,
- Minimum power requirement for bidding or offering- 5MW,
- The bid or offer must state the power (+/- MW), price (euro/MWh),
- It must be possible to carry out the regulation, which has been bid, to its full power in 30 minutes,
- Balancing responsibility.

Lithuania has made attempt toward single Baltic market for reserves and regulating power.

3. Differences in Balance Management across Baltic States

Baltic countries are in progress on creation of common electricity market in the region. The integration of Baltic region in to the European electricity system will require the implementation of adequate organized market principles and harmonization of existing mechanisms, particularly related to the capacity allocation, congestion and balance management. TSO's have published the common approaches and differences of balance management in the Baltic countries.

Latvian and Estonian TSO's are responsible for national balance settlement. In both systems, Market participants must have an open balance agreement with an "open supplier" to provide balancing in their responsibility area. The TSO performs a balance settlement for the market participants connected directly to the grid. In Estonia, the TSO settles the balance power between TSO and balance providers. Estonian TSO has responsibility to provide the system services for TSO's of neighbouring countries. Similarly, in Lithuania, the TSO settles the balancing energy between TSO and other neighbouring countries, but in addition, the regulation energy as well.

Then, in Latvia, the TSO is responsible for performing the balance settlement for the traders who have been delegated by the generators/consumers.. Latvian TSO also performs a balance settlement for the DSO, which in their respective area provides a balance service. Lithuanian TSO is responsible of handling the national balancing function for all market players as the sole open balance supplier for internal market participants and neighbouring countries TSO'. The TSO's provide uniform, non-discriminatory and competitive conditions for all market participants.

Lithuanian TSO has implemented organized RPM principles based on Nordic experience within the own control area. The mandatory regulation power auction is organized for market participants as the tool for TSO to provide the regulation and balancing services for the power system.

The number of final balance settlements in the Estonian system is 1, as generation and consumption are viewed together. In the Latvian system, if the generator and consumer is under one trader, they are also viewed as 1 in the settlement. In Lithuania, the volumes and prices of balancing energy are estimated by the Market Operator separately for consumption and generation. At the moment, there are 4 Balance Providers in Estonia and 1 in Latvia. All market participants of regulating power market are balance providers in Lithuania. The sole open balance provider sets the price for balancing electricity in Estonia and Latvia. In Lithuanian power system – the reference RPM price is defined by combining the regulation power auction price and open supplier price. Here is where the systems differ quite a lot. In Estonia, the price of balance energy in the system has to cover the justified expenses of TSO (the justified expenses incurring in the purchase of regulating capacity, in connection with balance determination and in connection with the purchase and sale of balancing

energy and also to ensure the TSO's justified profitability), but in the Latvian system, the coefficients for the balance energy purchase and delivery for market participants are fixed and published quarterly on the Latvenergo's website. On the other hand, in the Lithuanian system, the balancing energy price is a market-based price.

In the Estonian system, the grid tariff includes costs of withholding the emergency reserve capacity on annually basis and the price of balancing electricity includes costs of activating the aforementioned emergency capacity and keeping/activating the regulating capacity [13]. The grid tariff covers emergency reserves capacity and energy and regulating capacity in the Latvian system [14]. Lithuanian grid tariffs includes costs for providing the emergency reserve for Ignalina nuclear power plant, but there is no additional costs related to the regulation or other kind of capacity withholding as in other Baltic countries. There are differences of the balance management system in each Baltic States. Significant differences exist on legal basis for promoting common electricity market. Lithuanian market is fully opened, according the EU directive, by issuing the following legal acts, as shown in the Table 2.

Table 2. Legal steps to improve electricity market in Lithuania [15]

Legal steps for markets' development	Date
Law on the reorganization of vertical integrated electricity company JSC "Lietuvos energija"	May 18, 2000
The 1st edition of Law on electricity	July 19, 2000
Trading Rules of Electricity	December 18, 2001
Beginning of the electricity trading under market conditions in wholesale electricity market	January 1, 2002
Auction Trading Rules	April 18, 2003
The 2nd edition of Law on electricity	June 1, 2004

Existing aspects of Estonian electricity market opening, mentioned in [16], could be summarized as follows. Customers with consumption over 40 GWh per year become eligible customers. Only eligible customers have the right to choose a supplier. They have also the right to apply for an import license, which is issued by the Electricity Market Regulator. At present we have in our system 13 eligible costumers who consume about 16.5 % of energy in Estonia. Starting from January 2009, 35% of market must be opened, but the decision is not made at the moment. The opening of market is planned to be completed to the full extent by the year 2013. Non-eligible customers can purchase their electricity from the grid company they are physically connected to or from the seller named by that grid company.

The regulation tariffs applied in the Estonian power system are main obstacle to facilitate the real market opening and implement Nordpool Estelink price area project [8]. Main consumers are not allowed to buy electricity from the market and they are not uses the

eligibility rights to change the suppliers until the regulated tariffs are lower the market price in Estonia or external markets.

4. Russia's Role in the Balancing Baltic Power System

Lithuanian power system, as well as power systems of others Baltic States, is a part of UPS/IPS synchronous area. The Russian UPS/IPS system has significant influence and plays the main role for balancing the Baltic region power system. Physically all imbalances in Baltic region are handled by Russian UPS/IPS system. Practically the open balance supply service is provided by one Russian balance provider. Estonian TSO differently from the Lithuanian one signed this open balance agreement not with Russia, but with the Latvian TSO [17]. But finally both these countries are balanced by Russian open balance provider due to Latvian open supply agreement.. Frequency is maintained centrally in Russia, i.e. only a few large generators perform primary frequency regulation in the whole system. The insensibility zone of other generators is determined to be rather big so that small frequency deviations from the determined 50 Hz would not impact the planned operating regime of generators. Time deviation of such system is usually higher and such strict requirements are not applied to it as in decentralized frequency control interconnected systems: UCTE or Nordel.

No unified system and balancing services market, which would enable on equal and non-discrimination principles to participate producers in regulating and balancing power markets or provide others system services is developed in Russia. Russia has huge resources, which enable to ensure the quality of power in allowable limits, without involving small parallel power systems.

But they are themselves financially responsible (according bilateral contracts) for the balancing service, provided by Russia. Since Lithuanian power system is part of Russian power system and operates under parallel operation agreement coordinated by Russia TSO, it is not participating in the primary balance maintenance.

Though all generators installed in Lithuania have technical possibilities to ensure frequency standards in accordance with the requirements, they cannot be used in the primary frequency regulation due to particularly small impact on Russian power system. But, on another hand, Russia itself may strongly affect Baltic power systems. Lack or surplus of generation in Russia may influence frequency changes, it cause the changes in Lithuanian or other Baltic states generating capacities in that direction to compensate these frequency changes. But these changes are destroying the Lithuanian balance between planned production and consumption. Thus production and consumption balance is maintained by keeping defined power flow level on the interconnected lines between defined limits. These limits are determined by TSO after evaluating Lithuanian impact's value to the Russian and Baltic systems. For

this purpose Lithuanian TSO has signed the balancing power supply agreement with the representative of Russia. According this agreement Lithuanian deviation from planned balance could not exceed 50 MW in both directions. The limits are determined taking into account system's reliability and capacities of interconnected lines. Lithuania with other Baltic countries attempt to minimize the imbalance flows with Russia by implementing and improving internal balancing principles, but unfortunately with lack of cooperation. Another reason for hindrance of aggregate balance responsibility, that separate imbalances in different Baltic state are important for Russia from technical view of point.

5. What is the most important in harmonization process?

In the year 2001 there was an attempt to harmonize a system services market by implementing the common Baltic reserve and regulation power market. The common project was not successful and experienced total failure due to different legal environment in different Baltic States.

The Nordic BPM shows a practical example of such cooperation with different approaches across Nordic countries. They established single market only for regulating power; it means a single market of all kind reserves. At the same time, trading schemes of balance power remain according national rules in each country. Several years experience shows that such reforms fully respect responsibilities of the Nordic TSO's. Thinking about new harmonization attempts in the Baltic region, the Nordic experience should be taken in to account more than only regulating power market was harmonized after 2002. Changes in operation of reserves related with legal basis of power systems, when changes in balance power trading usually relates with more wide legal base included consumers right and protection or even constitutions issues. Furthermore single balance responsibility of Baltic States to the Russia is not acceptable from Russia side. From this point of view, Lithuanian role is important, because only Lithuania has developed a regulating power market in the Baltic region under unique principles of organized market and based on Nordic experience.

5. Conclusions

After unbundling power system, balance management process becomes not only technical but commercial problem as well. Regulating power market and Balance power market shall be established.

Trading mechanism of regulating power in Lithuania is close to the Nordic model. The main difference is that price averaging procedure is included in Lithuania to minimise balancing cost.

Trading by regulating power and balancing power has significant differences across Baltic States, but differences related with regulating power could be easy harmonized.

It is not acceptable for Russia to treat Baltic States as a single balance unit.

There is no big obstacle to harmonize reserves operation and trading of regulating power between three Baltic States using Lithuanian experience.

Furthermore, it is no need to start to harmonise total balance management system; it is enough to establish integrated regulating power market.

It is very important to assure balance responsibility in Baltic's power markets in a way to enable the functioning of the common Baltic market while keeping technical integrity of the system in a decentralized way.

The harmonised balance management mechanism would be beneficial for all market players who are currently active and the ones yet preparing to become active in the Baltic region.

The common Baltic balancing mechanism is important precondition for creating the common day-ahead market in Baltic States.

6. References

1. Future Power Systems 1 - the Balance principle, Frequency and the Grid Submitted by Stephen Browning on Wed, 2007-11-28 12:48. <http://www.leonardo-energy.org/drupal/node/2422>
2. Directive 2003/54/EC of the European Parliament and of the council concerning common rules for the internal market in electricity and repealing Directive 96/92/EC.
3. Rules on balancing the electric power system in Croatian. www.hep.hr/ops/en/documents/RulesOnBalancing.pdf
4. Agreement on the access to the balancing market with regulating energy in Check Republic. http://www.ote-cr.cz/the-participants/registration-procedure/files-registration-procedure/W_Agreement_bez_revizi_080118.pdf
5. Official internet site of Lithuanian power company. www.lpc.lt
6. Baltic-Finish submarine cable. <http://www.nordicenergylink.com/index.php?id=29>
7. Baltrel annual report 2007. http://www.baltrel.org/annual_report_2007.pdf
8. Nord Pool Spot Baltic project No.97/2008. http://www.nordpoolspot.com/en/Market_Information/Exchange-information/No972008-Nord-Pool-Spot-Baltic-project-ends-31-December-2008/
9. No.55/2008 Introduction of implicit auction via the Estlink cable by 1 July 2009 at the earliest. http://www.nordpoolspot.com/en/Market_Information/Exchange-information/No522008-Introduction-of-implicit-auction-via-the-Estlink-cable-by-1-July-2009-at-the-earliest/
10. No.27/2007 Joint Baltic-Nordic project launched. http://www.nordpoolspot.com/en/Market_Information/Press-releases-list/No272007-Joint-Baltic-Nordic-project-launched/
11. The Nordic Power Exchange and the Nordic Model for a Liberalised Power Market <http://www.nordpoolspot.com/upload/Nordic%20power%20market/Nordic%20power%20market.pdf>
12. Sweden grid company official internet site. www.svk.se
13. Electrical Power System Code. The Act of the Government of Estonian Republic No.184,June. http://www.mkm.ee/failid/The_Grid_Code.doc
14. Latvian grid code.
15. Legal acts about electricity market in Lithuanian. http://www.ukmin.lt/lt/veiklos_kryptys/energetika/elektra/
Official internet site of Estonian Power system. <http://www.pohivork.ee/index.php?id=311&L=1>
16. Balancing principles for Latvia and Estonia, Arnis Staltmanis November 2006. Vilnius, Mini forum. http://www.energy-regulators.eu/portal/page/portal/EER_HOME/EER_INITIATIVES/ERI/Baltic/Meetings1/SG_meetings/3rd_Baltic%20SG/DD/A._Staltmanis_Balancing.ppt#330,1,Slide 1

INTEGRATION OF TRACKING STANDARD INTO ELECTRICITY MARKETS OF BALTIC STATES

Inga KONSTANTINAVIČIŪTĖ, Dalius TARVYDAS
Lithuanian Energy Institute, Lithuania

Abstract: Electricity supply usually is characterized in physical terms, such as voltage, frequency and etc. However, in relation to energy policy and consumer interest there is a lot of additional information, which currently becomes very interesting for electricity market stakeholders and for the final consumer. This additional information is related to generation of electricity (primary fuel sources, the related emissions, the technology used, etc.). The E-TRACK project has successfully developed a blueprint for a European electricity tracking standard. Principles of this standard have been already taken over by several countries. However, tracking systems used in Europe are still far from being coordinated. This article provides an overview of proposed tracking standard for electricity and analysis of its integration into electricity markets of Baltic States.

Keywords: electricity tracking, attributes, schemes, domains, certificates.

1. Introduction

The purpose of tracking scheme is to establish an independent, comprehensive accounting mechanism for generation attributes and to assign these characteristics to the electricity consumed by final customers [1]. Systems for the allocation of generation attributes to electricity suppliers and consumers respectively are required in order to facilitate a variety of policies on the European level. Taking into account these requirements three major uses of tracking can be distinguished:

- Electricity disclosure (labeling) of information to final consumers;
- Verification of compliance with quantitative targets, e.g. indicative targets for green electricity for 2010 or 2020;
- Management of public support to certain types of electricity generation, e.g. green electricity or electricity produced at high efficiency CHP.

The E-TRACK project, partially supported by the European Commission through the “Intelligent Energy

– Europe” Programme, has investigated the feasibility of a harmonized standard for tracking electricity in Europe [2]. The major benefit of such tracking standard is that electricity generation attributes can easily be accounted, problems of multiple counting of attributes can be avoided and cross-border trade of attributes can be facilitated. The E-TRACK standard has been designed in such way as to support implementation of European and national policies.

The term “standard” is used in an informal way. It indicates the set of rules, which can be applied by EU countries in order to implement coordinated electricity tracking system.

2. European standard for electricity tracking

The main principle of E-TRACK standard is that information should be separated from physical energy at the point of generation. Therefore the tracking system should exist separately from electricity flows.

Electricity tracking system must:

- provide meaningful information to the users, e.g. enabling consumer choice based on disclosure or facilitating support;
- provide accurate results;
- be robust against errors and fraud by the actors involved in the system;
- be compatible with the existing economic, socioeconomic, regulatory and legislative framework conditions;
- be cost-efficient, by providing the services required at reasonable cost;
- be flexible enough to adapt to changing framework conditions.

The policies which use tracking results are called *schemes*. According to the use of tracking results three types of schemes are allocated: disclosure, quantitative targets and support.

These different schemes define the information, which need to be tracked. This information is called the *attributes*, which usually is related with electricity generation. The fuel source “coal” used by fossil fuel

power plant is one of the attributes, which will be used, in the tracking system for disclosure purposes. Another attribute could be the specific CO₂ emissions from this power plant.

In order to reduce the barriers for cross-border tracking of attributes, all countries should agree on common (minimum) set of information. Tracking information based on the minimum list of attributes should be accepted within all countries, which are using proposed standard.

Within E-TRACK standard all tracking activities should be organized in *domain*. A domain is defined as a geographic region for the purposes of a policy scheme. It is recommended to have one domain per country. Issuing Body should be appointed as the main operator of the tracking system in the domain. A common “hub” should connect all domains.

The E-TRACK standard distinguishes two generic options for tracking: *explicit* and *implicit* tracking.

Explicit tracking is based on a mechanism, which creates a link between generation and consumption of electricity. It can be based on contracts and on certificates. In the case of *contract tracking*, all generation attributes are allocated to consumers based on bilateral contracts. *De-linked tracking* is in the case of certificates, i.e. it is possible to allocate attributes from generation to consumers independently from physical electricity market using *certificates*. Issue of each certificate is based on corresponding volumes and attributes of electricity generation. Certificates can be transferred independently for physical electricity. The attributes represented in each certificate are used by redeeming of certificate. After redemption certificates are removed from the market.

Implicit tracking is based on default set of attributes, this is meaning that statistical data or averages from a group of power plants is used as attributes for a certain volume of electricity.

The E-TRACK standard requires all domains to provide facilities for explicit and also for implicit tracking of the attributes of electricity generation. Implicit tracking should be introduced in order to reduce the burden of tracking for those parts of the market, where explicit tracking information is not available. However the E-TRACK standard aims to reduce the share of implicit tracking, i.e. implicit information should be used only where explicit evidence is not available.

Technically the E-TRACK standard requires to set up a *registry* system for handling of attributes. Registries will allow tracking the ownership of attributes and will support transfers of ownership within the registry and to other registries under the E-TRACK standard. A registry should provide as much open access as possible to provide transparency and support the accuracy of reported information. This suggests to have a web-enabled registry, which will be the most efficient solution offering a suitable broad coverage.

There are already a number of operation registries in different EU countries, some of which are handling Guarantees of Origin (GO) and other certificates. Most of these registries are connected to the European Energy Certificate System (EECS). This system is the most

comprehensive certificate system for electricity in Europe. However, almost none of them handle all forms of electricity sources yet. But it would not be necessary to build an entirely new registry infrastructure, only will be necessary to develop existing registries further.

Explicit tracking attributes will be recoded in the registry as transferable electronic certificate. The life cycle of certificate consist of three steps: issuing, transfer and redemption.

Issue of certificate will be based on information on electricity production devices, which will be held permanently in the registry, and additional information about certain generation episodes.

The issuing of certificate is voluntary for power plant owner and operator. They can decide whether to register their power plants in the registry or not. After registration, they can decide for each generation episode to issue certificates or not. Issuing of certificates should be normally based on full megawatt hours (MWh). Rounding up of part units of some generation episode should not be used because this discriminates small power plants. Any remaining part units should be forwarded into following generation episode.

Only current owner can use the attributes represented in a certificate. The seller must initiate transfers of certificates within the E-TRACK standard.

In order to make use of a certificate for one or several schemes, the owner must redeem the certificate. After redemption certificate will be removed from the market. The owner must specify for which scheme the redemption is made for and in case of disclosure, for which retailer and for which electricity product the attributes are redeemed. After redemption, the registry operator will produce a redemption statement, which gives proof of the volume of electricity generation and attributes.

Almost in all EU countries GO for RES-E and CHP-E are implemented as tracking certificates, which can be used for disclosure purposes. Therefore besides GO, certificates can be issued for any type of electricity production. This means that all GO should be integrated into a comprehensive system of tracking certificates. However, GO for RES-E and CHP-E retain their specific legal status.

In relation to GO, implicit tracking should not just be based on statistics of electricity production in certain region. This is important because explicit tracking, i.e. GO or support systems for RES-E or CHP-E, will cover part of the overall production in each domain. Therefore in order to avoid double counting of attributes should be used, so called, a *Residual Mix*, which corrects the generation statistics in a certain geographic region by all attributes. The Residual Mix represents all attributes in a certain region, which have not been allocated to final consumption of electricity based on explicit tracking.

In order to calculate Residual Mix, the lifetime of disclosure certificates must be limited. Only after the end of this lifetime, the Residual Mix calculation can be started. Any certificates, which have been issued, but not redeemed until the end of their lifetime, will expire and their attributes will become part of the Residual Mix.

The Residual Mix for a domain will be calculated based on following procedure:

- Attributes from all power generation in the domain
 - Attributes from all disclosure certificates issued in the domain
 - Attributes from power generation covered by GO or support systems
 - + Attributes from expired disclosure certificates (this includes the certificates which have been imported, but have not been used)
 - +/- An adjustment of the attribute volume in the domain with a superior European attribute mix
-
- = Residual Mix in the domain

The Residual Mix is then allocated to all electricity sold to final consumers in this region, for which no explicit attributes information is available. But in general explicit tracking should be used where possible.

One of the major purposes of the tracking standard is to make explicit and implicit transfers between domains possible, i.e. certificates issued in one domain can be transferred to another domain and can be redeemed there for one or several schemes.

The objective of the E-TRACK standard is to support the coordination between the tracking systems used across Europe. It is not aiming for one uniform tracking system in all countries, but if individual tracking systems will be developed in compliance with standard, these systems will deliver a reliable and cost-efficient service to the electricity industry, consumers, governments and regulators.

3. Currently implemented electricity tracking systems in Baltic States

As it was earlier mentioned several EU policies require to account for certain attributes of electricity generation. Directive 2003/54/EC requires that electricity suppliers should provide information to its consumers on primary energy sources usage, CO₂ emissions and nuclear waste. This information should be specified in the bills or in promotional materials and should be provided to each consumer. Currently implementation of these requirements in the Baltic States is still lagging behind. In general, information according to the requirements of this directive is readily available, but this information is still is not provided to the final consumers. Moreover, monopolistic suppliers, with control of distribution networks, dominate in electricity markets of all three countries; therefore there is no real competition among suppliers to the final consumers. Lack of competition in electricity markets is the main reason why Baltic countries are behind the required policy implementation.

Situation regarding GO for RES-E and CHP-E in all three countries are similar.

3.1. Lithuania

Lithuania already has in place legislation for implementation of GO for RES-E and CHP-E:

- GO for RES-E adopted on 14 October 2005 by Regulation of Ministry of Economy No. 4-346 "Rules on Issue of GO of Electricity produced from Renewable Energy Sources",
- GO for CHP-E adopted on 19 May 2008 by Regulation of Ministry of Economy No. 4-206 "Rules on Issue of GO of Electricity produced from High-efficiency Cogeneration".

According to these regulations Issuing Body of GO is Transmission System Operator (TSO). TSO is responsible for database administration, registration of new participants, issue of GO in response to request, reporting about RES-E production and about issued, transferred and used GO. But GO was not issued yet because there was no request for it.

Legislation regarding disclosure of generation attributes is not adopted in Lithuania.

Major part of electricity consumed in Lithuania is produced locally, therefore information about primary energy use for electricity production is easily available from several sources, including department of statistics. CO₂ emissions and nuclear waste also can be obtained, but it isn't readily available. Despite information availability it isn't currently presented to final consumers even on the TSO, DSO or suppliers websites.

3.2. Latvia

Latvia already has in place legislation for implementation of GO for RES-E and CHP-E:

- GO for RES-E adopted on 24 July 2007 by Regulation of Cabinet of Ministers No. 503 "Regulations on Electricity Generation from Renewable Energy Sources",
- GO for CHP-E adopted on 6 November 2006 by Regulation of Cabinet of Ministers No. 503 "Regulations Regarding Electricity Production in Cogeneration".

According to these regulations Issuing Body of GO is Ministry of Economy. Rules of GO issuing and the status with regard to the registry are still unclear. Therefore GO was not issued yet.

Legislation regarding disclosure of generation attributes is not adopted in Latvia.

Latvia is net electricity importer. It produces only around 2/3 of electricity consumed. Major part of electricity import comes from Lithuania and Estonia, some from Russia and Scandinavia (Finland). Latvian TSO, Latvenergo, provides information about local electricity generation and amounts of imported electricity. Information about CO₂ or nuclear waste is not available. Currently Latvia doesn't have plans on introduction of disclosure.

3.3. Estonia

Estonia already has in place legislation for implementation of GO for RES-E and CHP-E:

- GO for RES-E entered into force in January 2005 by amendment of the Electricity Market Act (11 February 2003);
- GO for CHP-E entered into force in February 2007 by Amendment of the Electricity Market Act (11 February 2003).

According to these regulations Issuing Body of GO is Estonian TSO. At the request of a producer TSO should issue to the producer GO. But currently nobody has applied for GO yet.

Estonia has legislation on disclosure since January 2005 according to the amendment of the Electricity Market Act (December 2004).

Major part of electricity consumed in Estonia is produced locally; therefore information about primary energy use for electricity production is available. Estonia is the only Baltic country that provides paper bills for electricity to its consumers. Limited information of electricity generation sources is available in these bills, but no information about CO₂ is provided.

4. Proposals for integration of tracking standard in Baltic States

Seeking to participate in common electricity attributes trading activities across Europe it is reasonable to introduce E-TRACK standard in Baltic States. Creating a common domain for these purposes would be preferable.

All three Baltic counties have already implemented GO for RES-E and CHP-E systems with database. Power plants that are currently not covered by GO are regular, usually big and producing only one type of energy (electricity). Adding them to the certificate system will cause less effort and will bear only marginal extra costs. Based on this we can assume, that introduction of E-TRACK standard in Baltic States could be done at minimal cost. It would allow not only to provide correct information to electricity consumers, but also enables participation in EU trade of generation attribute.

Currently there are very limited grid connections to outside of Baltic States (except from Russia), therefore major electricity exchanges goes only inside the region. Creating common domain for three countries, not only reduce the E-TRACK standard implementation cost, but also will make intra-region trade less complicated.

In other EU countries the most popular mean of disclosure is providing information on the bill or with the bill. In Baltic States only Estonia provides paper bills for electricity consumers, therefore sending personal information to each electricity consumer will cause extra costs. It leave only to mainstream information media: newspapers (which will also add extra cost) or electricity supply company's website, where information could be placed.

5. Position of stakeholders

From provided discussions with major stakeholders and from questionnaires it is evident that in Baltic States

there is no driving force for electricity tracking or value added electricity products creation.

Consumers, the main driving force in some EU15 countries, aren't very concerned about primary sources of electricity they use. Only small number of household consumers expressed willingness to buy green electricity products and pay extra. There are no strong consumer organizations in the region that could advocate preferences for green electricity. Preferences of industrial consumers are based mainly on price and reliability of supply. Industrial consumers understand the importance of eco-friendly electricity production, but in general are not willing to increase production costs by buying green electricity.

Regulators of Baltic countries expressed interest in the possible additional costs that implementation of the tracking system could impose. They are not entirely sure, if consumers will benefit from knowledge of primary energy sources used or pollution created by production of electricity they consumed.

Electricity suppliers don't see immediate benefits neither from informing the consumers nor from creating differentiated electricity products. Marginal number of consumers that are currently interested in it can't justify the cost of creating such products. Moreover, the general (country wide) information about primary energy sources used are freely available, therefore interested costumers, even now could find all information required by the directive.

Decision makers in general agree that EU legislation should be implemented locally, but they also don't see any immediate benefits for any of the involved parties.

6. Conclusions

1. Implementation of the proposed E-TRACK standard could be beneficial for all three Baltic States accommodating integration into EU electricity and it's attributes markets.
2. Taking into account current level of available information E-TRACK standard could be implemented at the relatively low cost.
3. Based on current electricity market structure of Baltic States it is preferable to have one domain for all three countries.
4. Despite current cautions of all stakeholders groups implementation of E-TRACK standard could have positive impact on RES-E electricity and overall market liberalization.

7. References

1. Konstantinavičiute I., Tarvydas D. Tracking Systems for Electricity. Energy – 2007, Nr. 3. P. 33–39.
2. A European Standard for the Tracking of Electricity. Final report from the E-TRACK Project. - August 2007. 114 p.
3. The E-TRACK Standard – August 2007, 22 p. www.e-track-project.org

TENDENCIES OF NUCLEAR FUEL UTILIZATION MODES

Gediminas ADLYS, Alvydas JOTAUTIS, Ramūnas NAUJOKAITIS Pranas KANAPECKAS
Kaunas University of Technology, Lithuania

Abstract: The nuclear fuel burn-up in power reactors have important influence on efficiency of nuclear power plant and on amount of radioactive waste. It depends on reactor type and on fuel enrichment. During the last thirty years fuel burn-up in power reactors was increased 2-3 times depending on reactor type. Physical limiting factor of the fuel burn-up in thermal reactors is increasing amount of the new produced neutron absorbing fission products during the reactor operation. The strongest neutron absorbers among fission products in nuclear fuel of typical PWR reactor have been calculated using codes APOLLO1 and PEPIN1. This paper presents an overview of the nuclear fuel origin for fusion and fission reactors, thermal and fast reactors, fuel conversion and breeding and trends in the evolution of nuclear fuel burn-up utilization. Possibilities to apply modern practices for nuclear fuel utilization are discussed.

Keywords: nuclear reactors, fuel, fuel burn up, fuel enrichment, fuel conversion, fuel utilization.

1. Introduction

Nuclear energy is released by the splitting or merging together of the nuclei of atoms. The conversion of one element into another is called transmutation process. The conversion of nuclear mass to energy is corresponding to mass-energy equivalence formula: $\Delta E = \Delta m \cdot c^2$, in which c is a speed of light in a vacuum. The actual mass of an atomic nucleus is not the sum of the masses of nucleons (protons and neutrons) of which it is composed. This mass difference is called mass defect. In this case the energy ΔE is the binding energy of the nucleons. Any process that results in nuclides being converted to other nuclides with the higher binding energy per nucleon will result in the conversion of mass into energy. The fusion of light atomic mass nuclides (e.g. hydrogen) is the basis for fusion reactor technologies. The splitting of very high atomic mass nuclides is the basis of the fission process for the release of nuclear energy and for fission reactor technologies.

2. Nuclear fusion and fission reactors

Fusion is a very promising future energy option, which is characterized by almost unlimited fuel reserves, favorable safety features and environmental sustainability.

Most promising nuclear reaction to be used for generation of fusion power is fusion of deuterium 2_1H and tritium 3_1H : ${}^2_1H + {}^3_1H \rightarrow {}^4_2He + {}^1_0n + 17,6 MeV$. This amount of energy corresponds to the recoil energy of helium nuclei and neutron. The energy of 17.6 MeV per fusion process in this reaction is distributed between the neutron and the helium nucleus as 4/5 and 1/5. It corresponds to 14 MeV and 3.6 MeV, respectively.

The biggest part of the reaction energy (14 MeV) is neutron kinetic energy to be used as heat source. To use the energy released by moderating of neutrons for electric power generation is an actual challenge.

Fusion technologies are in the experimental stage. The aim of International Thermonuclear Experimental reactor ITER is to prove the scientific and technical viability of fusion energy and to test the simultaneous and integrated operation of the technologies needed for a fusion reactor. One of main objectives is to achieve 500 MW fusion power for 300 seconds. Upon the expected success of the ITER, it is planned to build the DEMO - demonstration nuclear fission power plant. The size of ITER reactor coincides approximately with the size of 1000-1500 MW_e power commercial fission reactors. Later on, it is planned to build PROTO – prototype of commercial fusion reactor. However, according to the prognosis it will be very difficult to commission the first commercial-sized fusion reactor before 2050.

Almost all operating and new built nuclear reactors are nuclear fission reactors at present time.

The largest amount of the nuclear energy released during fission event is represented by the kinetic energy of the recoiling fission fragments. Contrary to the fusion reaction released neutral neutron, the fission fragments are heavy charged particles. The range of these particles in the fuel element is a fraction of a millimeter. Therefore the recoil energy is effectively deposited as a heat at the point of fission. Kinetic energy of prompt

and delayed neutrons and gamma radiation is deposited in the surrounding material. The fission energy released in material depends on heavy nuclei. Uranium and plutonium are the main isotopes used as a nuclear fuel in fission reactors. Releases of the total fission energy for the most important heavy nuclides in nuclear fuel calculated for one single fission event are presented in Fig. 1. It could be derived that elementary fission energy increases with the increasing mass number of nuclides.

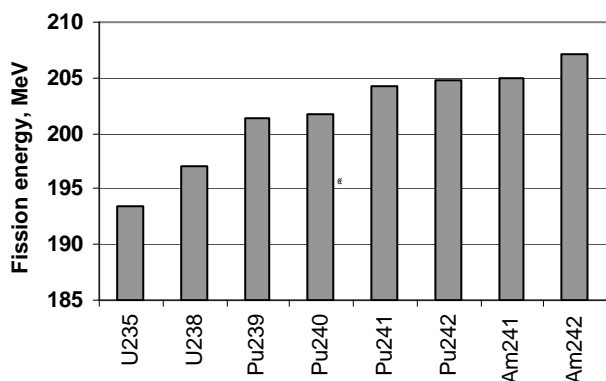


Fig.1. Fission energy of the main radionuclides in nuclear fuel

Such the fission energy and chain of such nuclear fission reactions is physical bases of nuclear fission reactors.

3. Features of thermal and fast neutron reactors

The advantage of nuclear chain reaction is that a number of prompt neutrons are produced for each bombarding neutron during the fission process of heavy nuclei. The average neutron number released per fission depends on bombarding neutron energies, thermal (T) or fast (F) and on heavy nuclide (Fig.2). This number increases when fission is induced by fast neutrons.

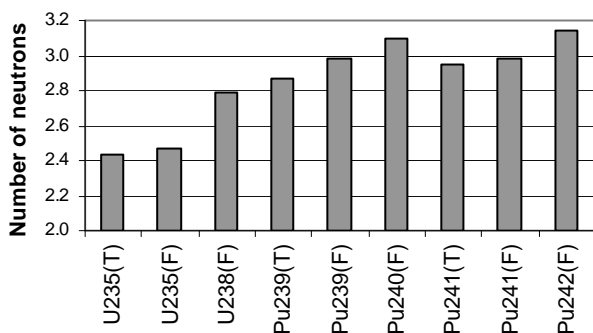


Fig.2. The average neutron number per fission

Thermal neutrons are characterized by a nominal energy of 0.0253 eV. The prompt fission neutrons have an energy spectrum in the range 0-10 MeV with the average energy of 1.5-2 MeV.

The probability of an interaction of neutron with nucleus is referred to as the neutron cross section, σ .

The values of nucleus fission cross sections for thermal and fission neutrons for most important heavy nuclides are presented in Table 1. For some nuclides (e.g. $^{233}_{92}\text{U}$, $^{235}_{92}\text{U}$, $^{239}_{94}\text{Pu}$, $^{241}_{94}\text{Pu}$), the fission probability is sufficient enough and a chain reaction is possible when the bombarding neutron has very low kinetic energy. Such nuclides are referred to as fissile. Operating under these circumstances reactors are thermal reactors.

Table 1. Fission cross sections, σ , for heavy nuclides

Nuclide	Thermal neutron (0,025 eV) σ , b	Fission neutron σ , b
U235	584,4	1,235
U238	$1,177 \cdot 10^{-7}$	0,3284
Pu238	17,89	1,994
Pu239	747,4	1,800
Pu240	0,0588	1,357
Pu241	1012	1,648
Pu242	$2,557 \cdot 10^{-3}$	1,127
Am241	600,4	0,2296
Am242	2100	1,756

1 barn ($1b = 10^{-24} \text{ cm}^2$)

In thermal reactors a moderator is integrated into reactor core to reduce the neutron energy from the MeV region to thermal energies. Neutron moderation is achieved by successive elastic collisions with light nuclei. Moderator is low atomic mass material: hydrogen as a part of light (ordinary) water, deuterium as a part of heavy water, carbon as graphite. Ideal in this respect is hydrogen, except that it can absorb neutrons. Heavy water and carbon are other good moderators because of their small neutron absorption probability.

Nuclides $^{238}_{92}\text{U}$, $^{240}_{94}\text{Pu}$, $^{242}_{94}\text{Pu}$ are non-fissile in respect of thermal neutrons but can undergo fission induced by fast neutrons.

Reactors designed to operate with fast neutrons are called fast-neutron reactors or fast reactors. The average fission neutron energy is of the order of 0.5 MeV to 1.0 MeV. The fission threshold for ^{238}U is 1.0 MeV. There is no need to slow down neutrons in the fast reactors; thus there is no need to integrate moderator. The nuclear fuel composition depends on reactor type, on moderator and coolant physical features (Table 2). In some reactors types, one substance serves both functions: to assist in neutron slowing and to remove the fission heat. Others involve one material for moderator and another for coolant. Moderators are light water, heavy water, graphite, and beryllium. Coolants are light water, carbon dioxide, helium, liquid metal.

The condition of the coolant serves as further identification. The pressurized water reactor (PWR) provides high-temperature water to a heat exchanger that generates steam, while the boiling water reactor (BWR) supplies steam directly. RBMK-1500 type reactor operating in Ignalina nuclear power plant is light water BWR reactor with graphite moderator. In high-temperature gas cooled reactors HTGR gas is used as a coolant, but in fast neutron reactors (FBR) liquid metal is used at present time (Table 2). Liquid metal

transports heat very efficiently and only lightly moderates the neutrons from fission. Sodium is used as the most common form of liquid metal for these reactors.

Table 2. Characteristics of nuclear power reactors.

Reactor type	Fuel	Moderator	Coolant
PWR	UO ₂ enriched U235	Light water	Light water
CANDU	Natural UO ₂ (0.7 % U235)	Heavy water	Heavy water
BWR	UO ₂ enriched U235	Light water	Light water
HTGR	UO ₂ (~ 8-19 %)	graphite	Gas
FBR	UO ₂ /PuO ₂ (~ 16-20 %)	none	Liquid metal

The distribution of reactors types in the world is shown in Fig.3. Figure 4 presents a number of power reactors which are under construction or are planned to start operation until 2016. Baltic-1 (Russia) 1200 MWe PWR type reactor is planned to be built by Energoatom.

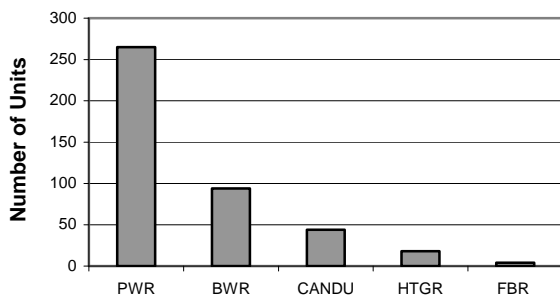


Fig.3. Distribution of operating reactors by type

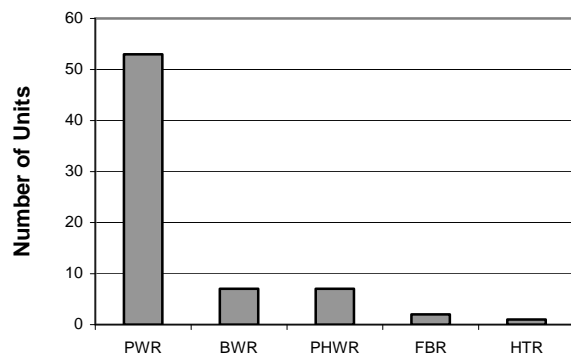


Fig.4. Power reactors under construction (or almost so)

Pressurized light water reactors are dominant type of reactors.

The Canadian firm, Atomic Energy of Canada Limited (AECL), has developed a modified pressurized heavy water reactor PHWR (the ACR series) which would only use heavy water as a moderator. Light water would cool this reactor. In earliest version of PHWR reactors,

CANDU, heavy water was used for both functions: moderation and cooling. The CANDU-9 has been developed on the base of the existing design.

High-temperature gas-cooled reactors (HTGR or HTR) are graphite moderated, helium cooled reactors.

High temperature reactors HTR can potentially use thorium-based fuels, consisting of uranium with thorium, plutonium with thorium.

A Pebble Bed Modular Reactor (PBMR) is advanced version of high temperature reactors (HTR). It utilizes a helium cooled and graphite-moderated nuclear core as a heat source.

4. Fuel conversion and breeding

If a neutron is absorbed by uranium ²³⁸U, then the nucleus after two successive β^- decays is converted into plutonium ²³⁹Pu, which is fissile. Because of subsequent neutron captures plutonium isotopes ²⁴⁰Pu, ²⁴¹Pu, ²⁴²Pu are formed. Plutonium isotopes ²³⁹Pu and ²⁴¹Pu are fissile in the thermal reactor.

Production of plutonium isotopes was evaluated for the nuclear fuel of typical PWR reactor (enrichment 3.3 % of ²³⁵U) and for RBMK-1500 reactor (enrichment 2.4 % of ²³⁵U + Er) fuel. The evaluation was performed using APOLLO1 neutron code. The actinides ²³², ²³⁴⁻²³⁶, ²³⁸U, ²³⁶, ²³⁸ - ²⁴² Pu, ²³⁷Np, ²⁴¹⁻²⁴³ Am and ²⁴²⁻²⁴⁴ Cm were used as an input data for the performed calculations. The composition of plutonium isotopes in typical PWR reactor fuel after 40 MWd/kg burn-up is shown in the Fig. 5. and in the case of RBMK-1500 reactor fuel after 20 MWd/kg burn up - in Fig.6. Production of these isotopes is an important factor for reactors economics.

The ratio of the rate of creation of new fissile isotopes to the rate of destruction of fissile isotopes is defined as conversion ratio. When this ratio is > 1, it is called "breeding" ratio. The conversion ratio for the light water PWR and BWR reactors is 0.6, for heavy water reactor CANDU - 08. The breeding ratio for fast breeder reactors can vary from 1.06 to 1.60.

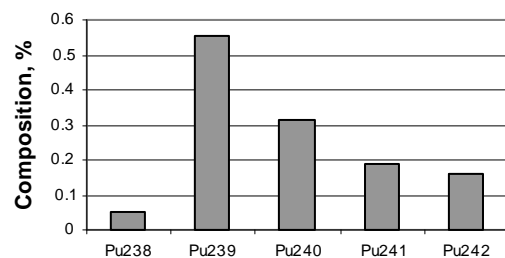


Fig. 5. Composition of plutonium isotopes in spent nuclear fuel of typical PWR (40 MWd/kg burn up)

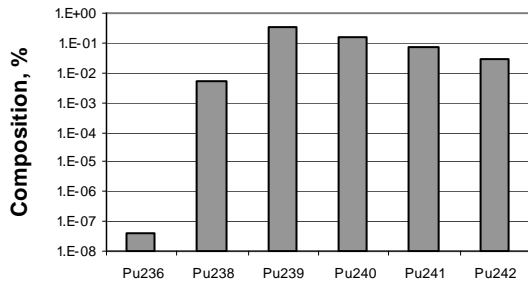


Fig. 6. Composition of plutonium isotopes in spent nuclear fuels of RBMK-1500 reactor (20 MWd/kg)

5. Nuclear fuel burn up

The economics of nuclear power is strongly affected by the efficiency of fuel utilization to produce power. The amount of produced power is related to the fuel burn up. The most commonly used measure of fuel burn up is the fission energy release per unit mass of fuel. It is characterized as the fission energy release in megawatt-days divided by the total mass of fuel nuclei existing in the initial loading.

Fuel burn up depends on fuel composition and changes during reactor operation. For thermal reactors typical fuel burn up is from 30 MWd/kg to 50 MWd/kg. Fuel burn up in fast reactors is projected from 100 MWd/kg to 150 MWd/kg. A burn up of 3 MWd/kg to 6 MWd/kg is attained when natural uranium fuel is used. The higher fuel burn up produces more actinides and fission products with the large thermal neutron cross sections. Higher discharged burn-up of light water reactor fuel leads to a more economical fuel cycle and reduced amounts of spent nuclear fuel [6]. To reach higher burn-ups higher fuel enrichment is necessary. At present time fuel enrichment approaches the 5 % ^{235}U level.

6. Nuclear fuel composition

The use of thermal nuclear reactors for energy production is based on the ability of certain fissile nuclei, such as uranium-235, plutonium-239 and plutonium-241, to maintain fission chain reactions.

Pressurized water reactors (PWR) and boiling water reactors (BWR) use light water as a coolant and moderator. Due to the neutron absorption by hydrogen, it is necessary to use uranium fuel enriched to about 3% of ^{235}U , when hydrogen is thought as a moderator. Raising the uranium ^{235}U content the possibility of fission increases. If light water is replaced by heavy water as a moderator, the reactor can be operated using natural uranium as it is in the case of CANDU reactor. Natural uranium contains about 0.7 % of ^{235}U and 99.3% of ^{238}U .

The CANDU-9 has flexible fuel requirements ranging from natural uranium through slightly-enriched uranium, recovered uranium from reprocessing spent PWR fuel, mixed oxide fuel, direct use of spent PWR fuel, to thorium. The advanced CANDU reactor ACR-700 will run on low-enriched uranium (about 1.5-2.0%

^{235}U with high burn up, extending the fuel life by about three times and reducing high-level waste volume accordingly. PHWRs have been popular in several countries because they use less expensive natural (not enriched) uranium fuels, and can be built and operated at competitive costs.

The fuel for high temperature reactors HTR is in the form of particles. Each has a kernel of uranium oxycarbide, with the uranium enriched up to 9 % ^{235}U . This is surrounded by layers of carbon and silicon carbide, giving a containment for fission products which is stable to 2000 °C.

A Pebble Bed Modular Reactor (PBMR) fuel consists of approximately 10 %enriched uranium triple-coated isotropic particles contained in a molded graphite sphere. A coated particle comprises a kernel of uranium dioxide surrounded by four ceramic layers. A fuel sphere consists of some 15,000 particles and has a diameter of 60 mm. The total mass of a fuel sphere is 210 g and uranium mass is 9 g. During normal operation the PBMR core contains a load of 456,000 fuel spheres [7]. Fuel pebbles, having 5-6 % enrichment, reaches burn-up of 80 MWd/kg. Target of burn-up is 200 MWd/kg.

It is expected that a particle keeps inside all fission products during all accident conditions, and hence requires no separate containment building.

7. Re-enriched and reprocessed nuclear fuel

After a burn-up of 50 MWd/kg spent nuclear fuel contains about 0.7 % ^{235}U and 0.6% ^{236}U . Such reprocessed uranium can be re-enriched. In addition, also fresh enriched ^{235}U can be added to attain a necessary mixture. By such a mode low enriched uranium fuel with 5.52% ^{235}U , 3.0% ^{236}U and 91.48% ^{238}U can reach a discharge burn-up of 60 MWd/kg [8].

Furthermore, the substantial quantities of plutonium remain in the spent fuel removed from the reactor (Fig.5 and Fig.6). This plutonium may be recovered by the chemical reprocessing of the spent nuclear fuel, and may be reused after mixing it with uranium in the form of mixed fuel oxide (MOX). Modern thermal reactors can be loaded by MOX fuel for 0-100 %.

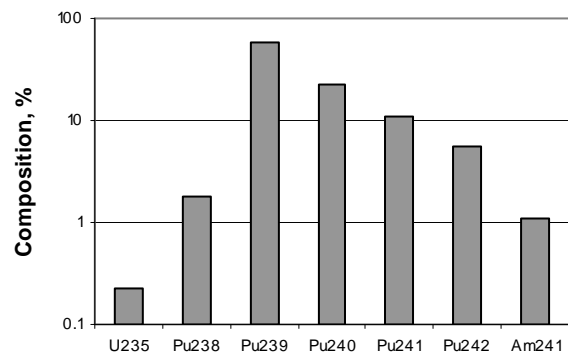


Fig.7. Composition of MOX fuel

Plutonium can be used more efficiently by reducing the quantity of uranium or by altering the moderating ratio. The latter approach has been adopted in the Advanced Plutonium Assembly (APA) in which the neutron moderation has been increased to enable a more efficient use of plutonium in a PWR than it is in the case with MOX recycling. Plutonium, produced by conversion of ^{238}U in a thermal reactor, after separating procedure could be used as the fuel in the fast breeder reactor. So, the breeder reactor can complement the thermal reactor.

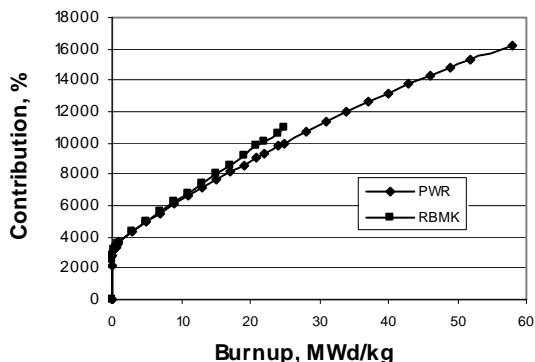


Fig. 8. Relative contribution of fission products to neutron absorption in nuclear fuel

The fission process leads to the reduction of the number of fuel nuclei and a big variety of actinides (Fig. 5 and Fig. 6) and fission products are produced, many of which have a large neutron capture cross sections. The buildup of fission product poisons in the fuel eventually leads to the loss of the efficiency. Figure 8 represents the total relative contribution of all fission products to neutron absorption in the fuel of PWR and RBMK reactors respectively. Presented distributions were obtained from the modeling results, which were performed using the French code APOLLO1.

8. Problems of fast fission reactors

The fast reactor has no moderator and relies on fast neutrons alone to cause fission. This process is less efficient than using slow neutrons.

Table 3. Generation IV nuclear reactors

Type	Neutron	Coolant	Fuel	Power, MWe
GCFR	fast	helium	U238	288
LCR	fast	Pb-Bi	U238	50-1200
MSR	Epi-thermal	Fluoride salts	UF in salt	1000
SCR	fast	sodium	U238, MOX	150-1500
SWCR	Thermal or fast	water	UO ₂	1500
VHTR	thermal	helium	UO ₂	250

As its basic fuel a fast reactor uses plutonium or relatively highly-enriched uranium (about 20% ^{235}U).

At the same time the number of neutrons produced per fission is 25% more than from uranium (Fig. 2), and this means that there are enough neutrons to maintain the chain reaction and also to convert ^{238}U into fissile plutonium. The use of liquid sodium as coolant avoids any neutron moderation and provides a very efficient heat transfer medium. So, the fast reactor during its operation can produce plutonium. It can operate as fast breeder reactor FBR.

The FBR was originally conceived to extend the world's uranium resources, and could do this by a factor of about 60. But until now and in nearest future too it is enough natural uranium for producing nuclear fuel and fast reactors are not competitive. Another factor which blocks the FBR development is changed utilization of plutonium separated from reprocessing used light water reactor fuel. It was originally envisaged for FBRs, but now is used as mixed oxide (MOX) fuel in conventional reactors. The economics of FBRs depends on the value of the plutonium fuel which is bred, relative to the cost of fresh uranium.

Fast neutron reactors have a high power density and are normally cooled by liquid metal: sodium, lead, or lead-bismuth. Liquid metal is characterized with high conductivity and boiling point and no moderating effect.

An international task force is developing six nuclear reactor technologies for deployment between 2020 and 2030. Four are fast neutron reactors (Table 3). In the table: GCFR – gas cooled fast reactors, LCR – lead-cooled reactors, MSR – molten-salt reactors, SCR- sodium-cooled reactors, SWCR- supercritical water-cooled reactors, VHTGR- very high temperature gas reactors

9. Worldwide marketed reactors

At present time reactors suppliers in North America, Japan, Europe, Russia and South Africa have a set of new nuclear reactor designs at advanced stages of planning while others are at the research and development stage.

In the Figure 9 there are number of contracts for nuclear power reactor construction or completion projects around the world to 2008 shown.

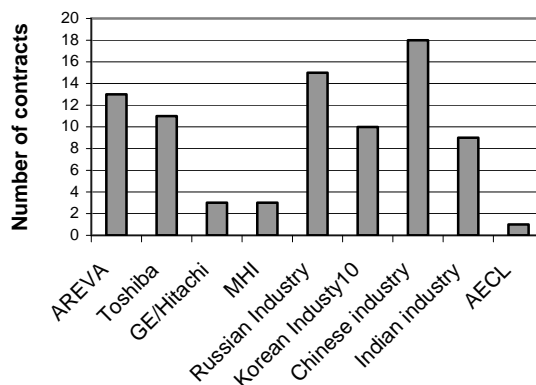


Fig. 9. Contracts around the world

Asia will see most of the nuclear plant construction, with over 45 nuclear reactors being built or planned for the near future. The Western companies (AREVA, Toshiba, Ge/Hitachi, MHI and AECL) account for about one quarter of the currently ongoing reactor construction projects.

Table 4 provides a list of reactors that are currently being marketed worldwide.

Table 4. A list of marketed reactors

No	Name	Power, MWe ₁	Available for construction
1	ABWR		Yes
2	APR-1400	1400	From 2010
3	AP-600	600	Yes
4	AP-1000	1000	Yes
5	ESBWR	1520	From 2010-2011
6	APWR	1538	Yes
7	US-APWR/EU-APWR	1700	From 2012
8	ATMEA	1100	Not yet
9	EPR	1600-1750	Yes
10	SWR 1000	1200-1290	Yes
11	Advanced BWR	1500	Not yet
12	AES-92 (VVER-1000)	1000	Yes
13	AES-2006 (VVER-1200)	1150-1200	Yes
14	VVER-1500	1500	Not yet
15	CANDU-9	925-1300	Yes
16	Enhanced CANDU-6	750	Yes
17	ACR-700	700	Not yet
18	ACR-1000	1080-1200	Not yet
19	PBMR	165	After 2013
20	GT-MHR	285	Not yet

The type of reactors provided in the Table 2 are: boiling water reactor BWR (1, 5, 10, 11), pressurized water reactor PWR (2-4, 6-9, 12-14), heavy water reactor HWR (15-18) and high temperature gas cooled reactor HT-GCR (19, 20). The vendors of the reactor construction are: Areva (8-10), AECL (15-18), Eskom (19, 20), General Electric (1, 5), Hidropress (12-14), Hitachi (1, 5), Mitsubishi (6, 7), MHI (8), South Korea (2), Toshiba (1, 11), Westinghouse (3, 4).

10. Trends in nuclear fuel utilization

The majority of the reactors in operation worldwide are light water reactors (LWRs), both of pressurized or boiling water (PWR or BWR) types.

For a given energy output the mass of the fresh fuel loaded and the mass of the spent fuel discharged are inversely proportional to the average discharge burn up [4]. For an individual country, the optimum of the achieved burn up with respect to the fuel cycle costs may vary, depending on the specific technical, licensing and economic conditions, but the gain of a higher amount of energy from the same amount of fuel with increased burn up clearly indicates a strong economic benefit. Other ways to improve fuel utilization in a

LWR can be introduction of longer fuel cycles, partial reload of fuel with UO₂/PuO₂ mixed oxide assemblies, introduction of low leakage core loading patterns, etc. Many utilities are increasing the initial fuel enrichment usually to more than 4% ²³⁵U (Fig. 10) and are usually burning the fuel to leave about 0.5% ²³⁵U at the end of fuel life.

Due to the higher enrichment and the higher burn up the fuels remains in the reactor longer time.

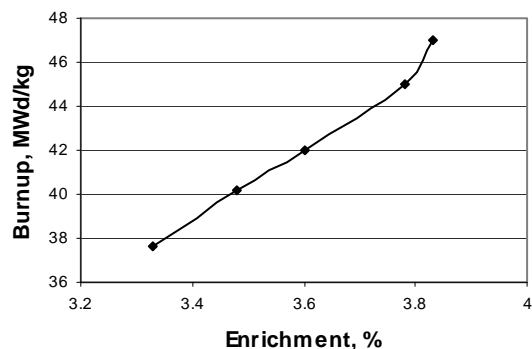


Fig.10. Worldwide trends of enrichment and burn up in the period of 1990 to 2010

11. References

1. W.M. Stacey. Nuclear reactor physics. John Wiley and Sons, Inc. 2007. 735 p.
2. A.R. Foster, R.L. Wright, Basic nuclear engineering. Boston. 1993. 611 p.
3. D. Bodansky. Nuclear energy. Principles, practices and prospects. Springer, 2004. 701 p.
4. H-D Berger, High Fuel Burn-ups and related safety consideration, Presentation at 2006 FJOHSS, 23 August – 1 September, 2006.
5. WNA information on Uranium Markets, www.world-nuclear.org
6. W.Goll, Ch.Hellwig, P.B.Hoffmann, W.Sauser, J.Spino, C.T> Walker. UO₂ Fuel Behavior at Rod Burn-ups up to 105 MWd/kg HM. International Journal for Nuclear Power, 2007 No 2, 95-102 p
7. G.Brahler, K.Buttner, K. Froschauer, W. Kress. PBMR fuel sphere production facility project Pelindaba, South Africa. International Journal for Nuclear Power, 2006 No 11, 701-704 p
8. C.H.M. Broeders, G. Kessler. The generation of denatured reactor plutonium by different options of the fuel cycle. International Journal for Nuclear Power, 2006 No 11, 711-716 p
9. S.Niesen. Do we live a nuclear renaissance? International Journal for Nuclear Power, 2008 No 5, 317-319 p.

NUCLEAR ENERGY MIX IN THE BALTIC SEE REGION

Gediminas ADLYS*, Olegs LINKEVIČS**, Saulius RAILA*, Rūta ADLYTĖ*, Helmut ALT ***
 *Kaunas University of Technology, Lithuania; **Latvenergo, Latvia;
 ***FH Aachen Fachbereich Elektrotechnik, Germany

Abstract: Nuclear energy is a key component of low-carbon and secures energy supply policy in the context of the increasing demand of energy, depletion of fossil resources, increasing energy prices, growing energy dependence and greenhouse emission.

This article presents the overview of the electricity generation mix in the Baltic Sea region. It is based on the analysis of the nuclear energy contribution to the total electricity generation in different countries.

Keywords: electricity generation, energy mix, nuclear power, interconnections.

1. Introduction

As of 2008 nuclear generation capacity in the world represented around 393 GW. There are 439 nuclear power reactors in operation around the world, operating in 31 countries. Most of the nuclear power plants which are operating until now were built between 1970 and 1990 (Fig.1).

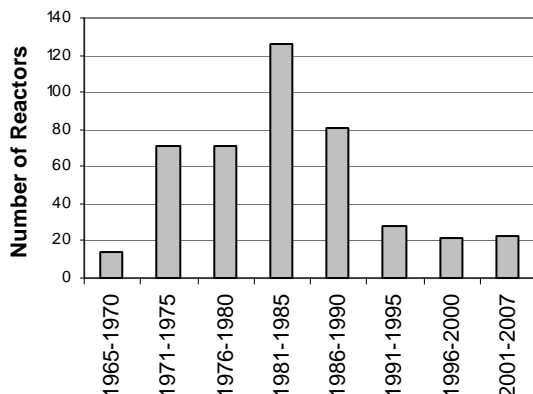


Fig. 1. Number of installed nuclear power reactors versus time

Despite the fact that after this period there was a sharp decrease in the number of nuclear power reactors put into service, nuclear's share of global electricity generation all time was increasing (Fig.2).

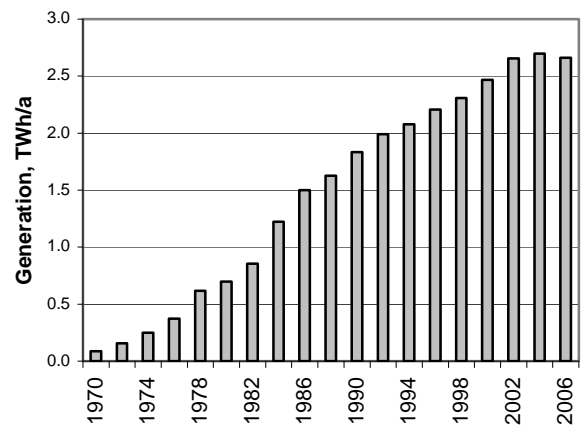


Fig. 2. Nuclear electricity production worldwide

From 1990 to 2006, world capacity rose by 44 GW_e due to net addition of new plants and uprating some established ones. The relative contributions to this increase were: new constructions - 36%, uprating -7% and availability increase - 57%. The increase over the last five years (210 TWh) is equal to the output from 30 large new nuclear plants.

Nuclear energy takes important place in electricity generation around the world. As of 2005, nuclear power provided 6.3% of the world's energy and 15% of the world's electricity.

At present time 44 reactors with a net electrical capacity 41.5 GW_e are under construction in 14 countries. Most of them are being built in Russia, China, India and Korea.

2. Nuclear energy tendencies in European Union

New nuclear power plants have been planned or are already being built across Europe: two units at Belene in Bulgaria to be built by 2014 and 2015, the third and fourth units of the nuclear power plant at Mochovce, southern Slovakia to be constructed by 2013 and

Cernavoda NPP's units 3 and 4 to be completed by 2014 and 2015 in Romania [1].

The construction of a European pressurized water reactor (EPR) will begin at Penly/France, on the Channel coast near Dieppe, in 2012. It will be connected to the European energy grid in 2017. Penly has already two operating 1300 MW PWRs. The new EPR will be the second unit of its kind in France, after Flammanville, and the third in Europe after Olkiluoto, Finland. The government of UK has announced the building of a new fleet of reactors (around 8) and it has already developed its action plan for the construction. In Finland, three companies (TVO, Fortum and Fennovoima) are seeking for the potential building of three reactors in total. The Baltic States agreed to jointly build a new Visaginas NPP in Lithuania. The Polish government adopted a Resolution on nuclear power, which sets the conditions to construct one or two NPPs by 2020.

On 24 February 2009 an agreement between France and Italy was signed which paves the way for the building of nuclear power plants in Italy, using French technology and the participation of Italian Electricity Utility in the construction of NPPs in France. Italy phased-out its nuclear power plants after being forced to abandon its nuclear energy programme following a referendum in 1987. Therefore, Italy is the world's largest electricity importer and electricity prices in Italy are 45% higher than the European average. In the framework of the Italian-French agreement a study of the feasibility of constructing at least four EPR units is planned. The first EPR reactor in Italy should come into operation by 2018.

3. Nuclear energy situation in European Union

Nuclear energy provides 30% of the electricity from the total energy production of the European Union.

Many European countries are relying on nuclear energy. In terms of electricity generated by nuclear energy in 2007, France holds the top position with a share of 76.9% followed by Lithuania with 64.4 %, Slovakian Republic and Belgium with 54% and Sweden with 46.1%. (Fig. 3).

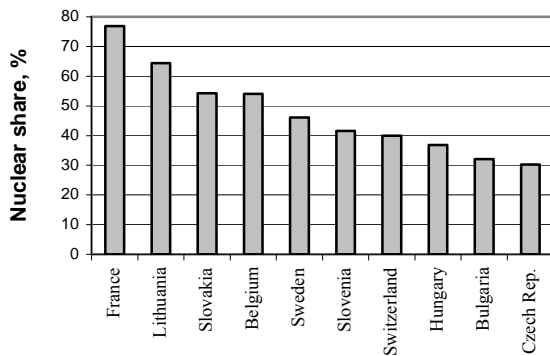


Fig.3. European countries with nuclear share in electricity generation > 30 % in 2007

As of November 2008, there were 197 nuclear power plant units with an installed electric net capacity of

169,891 MW_e in operation in Europe and 14 units with 12,817 MW_e were under construction in five countries.

4. Energy mix in Baltic States

The power systems in the three Baltic countries differ considerably. The Estonian power system is purely thermal; the Latvian system is based on hydro and thermal technologies, and the Lithuanian system is dominated by nuclear power production [2]. The big differences in the power systems create potential benefits to be gained from electricity trade between the countries [3].

In 1990, Estonia, Latvia and Lithuania produced more than 50 TWh of the electrical power in total (Fig. 4). In 2006 it was only 27 TWh [4].

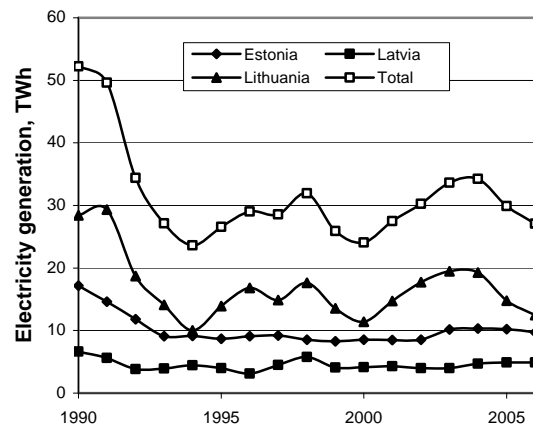


Fig.4. Electricity generation in Baltic States

The drop down in electricity consumption after 1990 mainly caused by the economical recession and restructurization of the economy was the main reason for the decrease of the generated power capacity. A change in energy export capacities to neighboring countries (Kaliningrad district, Russia and Belarus) was the second reason.

The numbers of the annual net export of electricity from each Baltic country during the time period from 1990 to 2006 are provided in Fig.5.

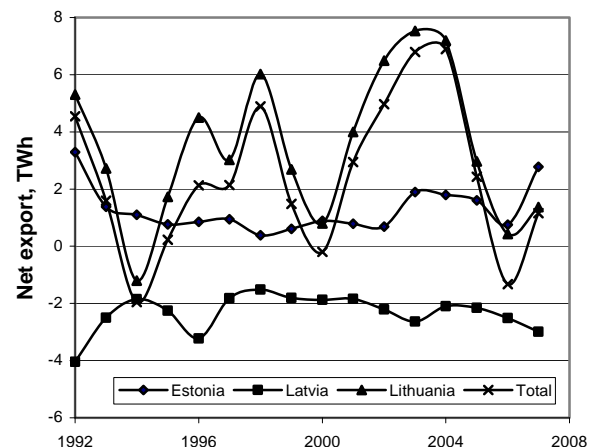


Fig. 5. Net export of electricity in the Baltic States

Negative numbers indicate a net import of electricity. Latvia is a net importer of electricity while Estonia and Lithuania are net exporters of electricity.

The total net export out of the three Baltic countries was ranging from 0.4 to 6.8 TWh per year in the period from 1999 to 2003. These numbers include an import from Russia and export from Lithuania to Belarus and Kaliningrad. The energy balance from year 2003 is illustrated in Fig.6.

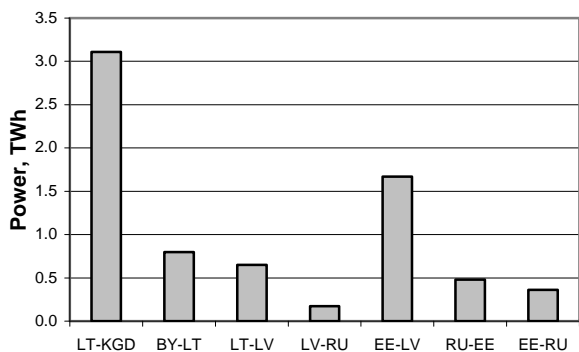


Fig. 6. Annual electricity exchange between Baltic and neighboring countries

In October 1998, an agreement on co-operation in the energy sector between the three Baltic States was signed, and a Baltic Energy Strategy was approved by the Baltic Council of Ministers. In 1999, the strategy stipulated the creation of the Common Baltic Electricity Market as a long-term energy policy goal.

The share of different kinds of energy in The Baltic States energy system is shown in Fig.7.

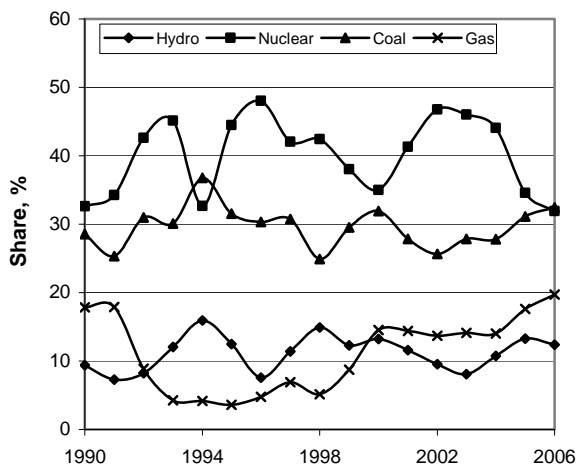


Fig.7. Coal, nuclear, gas and hydro share in Baltic States energy system

The Estonian electricity sector is characterized by the large share of oil shale power. Thermal power stations dominate in the Estonian electricity generation. Two largest plants are Eesti PP and Balti PP. Estonia generates approx. 30% of the total power generation in the three countries.

Latvia accounts for 11-18% of the power generation in the Baltic States, which is mainly produced by hydro power and the CHP plants in Riga.

Hydro power represents about two-third of the installed power capacity Latvia (Fig.8). The three major hydroelectric plants of Latvia are set on the Daugava River: Kegums Hydro Electrical Station (HES), Plavinas HES and Riga HES. Kegums HES consists of two hydroelectric plants with at total capacity of 264.1 MW. Plavinas HES consists of 10 hydroelectric units and was put into operation in 1968 with a total capacity of 825 MW. Plavinas is the largest hydroelectric plant in the Baltic States by its capacity.

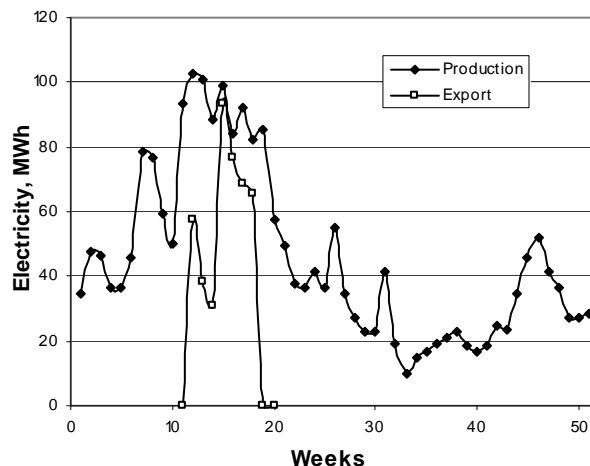


Fig. 8. Annual fluctuations of power production by Daugava HPP

In 2004 Lithuania accounted for the largest power generation in the three countries, i.e. 48-60%. The power generation in Lithuania is highly dependent on the Ignalina nuclear power plant, which will be closed at the end of 2009.

5. Energy mix in Nordic Countries

The Nordic (Sweden, Finland, Norway) power system is highly integrated in terms of physical connections and system stability. The Nordic electricity market and the exchange of electricity with neighboring countries (Fig.9) are of crucial importance for Sweden's electricity supply [5]. Therefore the project to join Sweden and Baltic States electricity systems by underwater cable and to form common Baltic Sea countries energy market is of high priority.

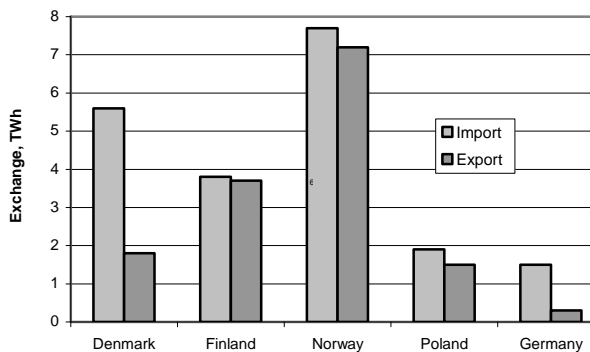


Fig.9. Electricity exchange between Sweden and neighboring countries in 2006

Electricity generation in Sweden is dominated by CO₂-free hydro and nuclear power (Fig.10).

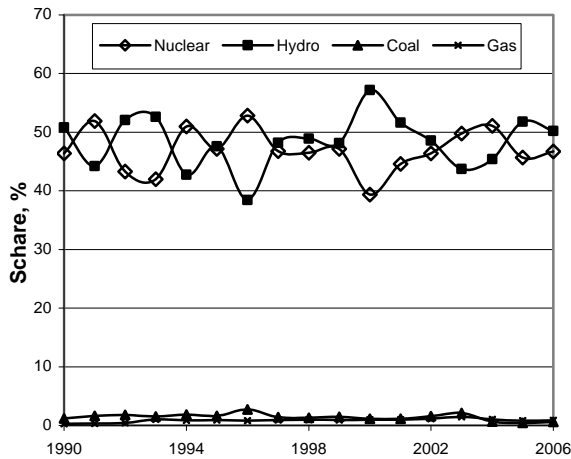


Fig.10. Electricity mix in Sweden

The Swedish government announced recently, that it intends to reverse the country's long-standing ban on nuclear energy and allow the building of new nuclear reactors to gradually replace its existing nuclear fleet. The nuclear phase-out policy was brought in following a national referendum in 1980.

The contribution of the nuclear energy is nearly 30% of the total energy production in Finland

6. Nuclear energy in Germany

The electricity generation share by fuel type in Germany is presented in Fig. 11.

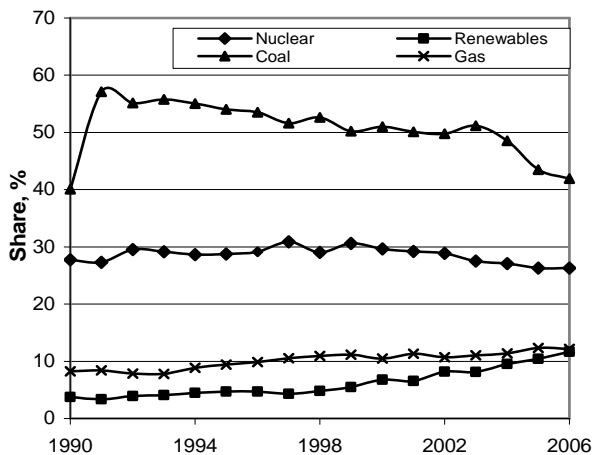


Fig.11. Electricity generation share by fuel type in Germany

17 nuclear power plants units with an electric gross output of 21,457 MW are in operation in Germany (Table 1). Total generated electric power capacity was 140 billion kWh in 2007.

It is to point out that the operation time of almost all nuclear power plants in Germany is restricted by the life design time: most of the nuclear power plants were commissioned 20-30 years ago. The shutdown of the last unit is foreseen in 2022.

Table 1. Operating nuclear power plants in Germany

Nuclear power plant	Year	GC, MWe	NC, MWe	REC, TWh
Biblis A	1975	1225	1167	13.7
Biblis B	1977	1300	1240	23.0
Brokdorf	1986	1440	1370	128.4
Brunsbüttel	1977	806	771	11.0
Emsland	1988	1400	1329	141.8
Grafenrheinfeld	1982	1345	1275	69.6
Grohnde	1985	1430	1360	113.8
Gundremmingen B	1984	1344	1284	79.7
Gundremmingen C	1985	1344	1288	89.1
Isar-1	1979	912	878	24.2
Isar-2	1988	1475	1400	139.1
Krümmel	1984	1402	1346	88.6
Neckar-1	1976	840	785	10.2
Neckar-2	1989	1400	1305	152.2
Philippsburg-1	1980	926	890	28.7
Philippsburg-2	1985	1458	1392	113.5
Unterweser	1979	1410	1345	43.6

GC – gross capacity, NC – net capacity, REC – residual electricity quantity

The last column of Table 1 indicates residual electricity generation quantities of the individual nuclear power plants in accordance with the Atomic Energy Act. (The situation on 01-01-2008 is shown).

The Atomic Energy Act was voted in 2002 after consensus talks (the „Atomkonsenz“) between operators and the government in Germany. According to the Act each nuclear power plant is allowed to generate a fixed quantity of electricity and these quantities may be transferred under special conditions from one nuclear power plant to another. As soon as a nuclear power plant has reached its volume of electricity production, it must be withdrawn from the grid.

It seems that the only way for Germany to secure power supply in the country in the future is to follow an example of Swedish and Italian governments and to disclaim nuclear power phased-out politics.

7. References

1. The Nuclear relaunch in Europe. European Atomic Forum, Brussels, 2008
2. Power sector development in a Common Baltic Electricity Market. Final Report. June 2005.
3. Z. Krishans, A.Mutule, I. Oleinikova, A. Kutjuns. Application of Risk Assessment Method for Baltic States Power System Development Optimization. 9th International Conference. KTH, Stockholm, 2006.
4. BALTSO. Annual Report 2007. Riga. 48 p.
5. The Electricity Year 2007. Annual report. Svensk Energi. Stockholm. 47 p
6. Analyses of Energy Supply Options and Security of Energy Supply in the Baltic States. IAEA-TECDOC-1541. Vienna, 2007. 323 p

PERSPECTIVES OF NUCLEAR COGENERATION TECHNOLOGIES

Gediminas PETRAUSKAS*, Gediminas ADLYS*, Diana ADLIENĖ*, Kęstutis GEDIMINSKAS**,
Algimantas VALINEVIČIUS*

* Kaunas University of Technology, Lithuania; **Ignalina nuclear power plant, Lithuania

Abstract: Energy is one of the most challenging issues that currently many countries are facing, including Lithuania and Baltic States. Increasing energy prices, concerns about dependency on foreign energy sources, climate change have led to a nuclear energy renaissance. Modern nuclear technologies are good basis to use nuclear energy not only for base load electricity production but also for safe district heating in the cogeneration nuclear power plants.

Features of cogeneration heat and electricity production analysis and the review on properties and perspectives of small size nuclear reactors for cogeneration power plants is provided in this article.

Keywords: nuclear energy, cogeneration plants, small size nuclear reactors, greenhouse gas emissions.

1. Introduction

Generation of the heat within the reactor core is a result of the nuclear fission process. The heat can be applied to the generation of electricity or used in providing hot water or steam for industrial or space heating purposes. Practically nuclear power reactors were applied to generate electricity and to produce the heat for industry or district heating at the same time from the very beginning of their commissioning. The first nuclear power reactor at Calder Hall in the United Kingdom provided electricity to the grid and heat to a neighboring fuel reprocessing plant. The Agesta reactor in Sweden provided hot water for district heating to a suburb of Stockholm.

In 1973-1976 in Bilibino, Chukotka four power units of the nuclear heat and electricity generating plant were sequentially commissioned. They were provided with water-graphite reactors. Each unit's capacity was 12 MWe, each of them was supplying heat for Bilibino central heating system at a rate up to 25 Gcal/hour.

Romania has two nuclear reactors generating almost 20% of its electricity. The first unit also provides district heating for Cernavoda town. 148 TJ were supplied in 2003.

Switzerland operates 5 nuclear reactors generating 40% of its electricity [1]. A national vote has confirmed

nuclear energy as a part of Switzerland's electricity mix. Both Beznau nuclear power plant and Gösgen nuclear power plant are supplying the district heating in addition to power generation. Refuna district heating system supplied from Beznau nuclear power plant consists of 35 km of the main network and 85 km of local distribution pipelines. It has become an integrated part of the regional infrastructure. The REFUNA district heating network sells about 130 000 MWh of energy every year and is thus the largest district heating system of Switzerland.

Visaginas town district heating system is supplied by Ignalina nuclear power heat (Fig. 1) too.

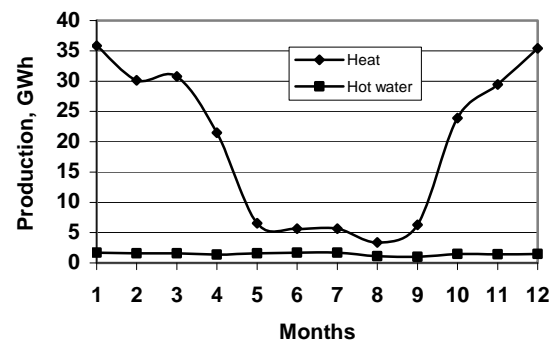


Fig. 1. Heat and hot water production for Visaginas town by Ignalina NPP in 2008

District heating accounts for about 50 per cent of the total heating market in Finland. 4/5 of it is being produced in combined heat and power plants. The City of Helsinki is going to prepare its own feasibility study of the nuclear energy involvement to cover the district heating demands of different districts of the capital in the Great Helsinki area. A new unit at Loviisa (site, with two existing 488 MW reactors) will be able to cover the heating demands of the entire metropolitan area.

2. Features of cogeneration

Cogeneration – or combined heat and power (CHP) – means using both: the electricity and heat produced together. Compared to separate generation of heat in

boilers and power in condensing plants, CHP systems offer considerably higher energy efficiency levels. Cogeneration leads to wasting less energy in production, increasing efficient utilization of primary energy resources and for reducing CO₂ emissions. Surplus heat from an electric power plant can be used for industrial purposes, or for the heating of space and water. Otherwise, when steam or hot water is produced for an industrial plant or a residential area, power can be produced as a by-product [2].

Significant differences exist between the applications of electricity and of heat. [2]. Transport of the heat from its generation places to the end-user is complicated and expensive. Compared to heat, the transport of electricity is easy and cheap, even to large distances measured in hundreds of kilometers. The key to successful CHP is to design the plant according to the heat demand of the system. These systems can also be installed close to users, reducing power transmission losses.

According to the definition of the European Communities Commission of 19.11.2008, a cogeneration unit operating with maximum technically possible heat recovery is said to be operating in full cogeneration mode. The heat has to be produced at the site pressure and temperature levels required for the specific useful heat demand of market. In the case of full cogeneration mode, all produced electricity is considered as combined heat and power (CHP) electricity. If the plant does not operate in full cogeneration mode under normal conditions of use, it is necessary to identify separately the amount of the electricity and heat which was not produced under cogeneration mode, and to distinguish it from the CHP production [3].

3. Cogeneration and greenhouse gas emission

Cogeneration is a highly efficient and environment-friendly way of producing electricity and heat simultaneously. Practically the entire heat market is supplied by burning coal, oil, gas, or wood. Greenhouse gas (GHG) emissions for fossil fuel technologies comprise the direct (stack) emissions from the combustion process and the indirect emissions originating among others from the fuel supply chain. Fuel use for mining, processing and transport, plant construction and decommissioning are included into the full energy production chain. The emissions depend on generating technology too. Typical results for different technologies (including CO₂, CH₄, N₂O, etc.) are shown in Table 1 [4]. The principal emissions are related to the power plant, and only some 10-20% of the emissions are related to other steps in fossil fuel chains. Conversely, for nuclear and renewable energy chains, there are no GHG emissions from the power plant. But there are some emissions from the other steps of the chain.

Hydro power related emissions depend on reservoir size. Nuclear power is one of the less carbon intensive generation technologies, amounting to only about 2.5-5.7 grams of GHG per kWh of electricity produced (gC_{eq}/kWh) as it is indicated in Table 1. Some 105 to

366 gC_{eq}/kWh are calculated for fossil fuel chains and 2.5-76 gC_{eq}/kWh - for renewable energy.

Table 1. Range of total GHG emissions (gC_{eq}/kWh) from electricity production chains

Energy source	Plant emissions	Other	Total
Lignite	217-359	11-14	228-366
Coal	181-278	25-79	206-357
Oil	121-215	28-31	149-246
Natural gas	90-157	16-31	106-188
Hydro	0	6.3-64.6	6.3-64.6
Biomass	0	8.4-16.6	8.4-16.6
Solar PV	0	8.2-76.4	8.2-76.4
Wind	0	2.5-13.1	2.5-13.1
Nuclear	0	2.5-5.7	2.5-5.7

The main greenhouse gases are carbon dioxide and methane. Burning of fossil fuels for electricity and heat production results to the increased carbon emissions in the form of carbon dioxide.

The biggest part of the primary energy sources in Lithuania is used for the energy industry. The energy industry consists of the public electricity and heat production, petroleum refining and other energy production industries (liquefied gas, peat, etc). Comparison of the utilizations structure of energy sources in Lithuanian and EU-27 [5] in 2006 is provided in Fig.2. The indications in the Fig.2 are: EI - for energy industry, I - for industry, T- for transport, H - for household, S - for service, O - for others.

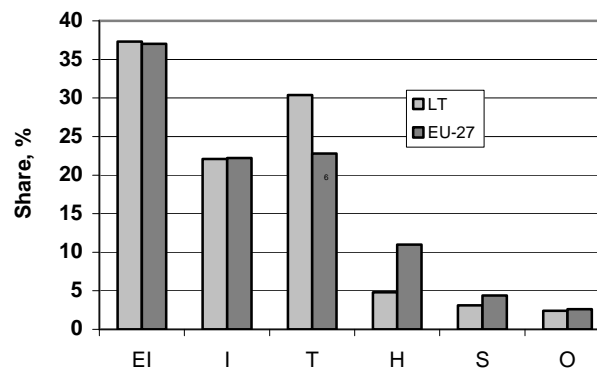


Fig.2. Primary energy utilization structure in Lithuania and EU-27 in 2006

4. Situation in the Baltic States

The possibility of significant climate change, largely caused by greenhouse gas emissions from fossil fuel burning, especially carbon dioxide, presents a fundamental challenge to the goals of sustainable development. Variations of CO₂ emissions during the years in three Baltic States are shown in Fig.3. It could be assumed that emissions in Latvia and Lithuania remained almost constant during the last years and were lower as compared to the emissions in Estonia, where the main contribution to the emissions is attached to the burn up of the oil shale.

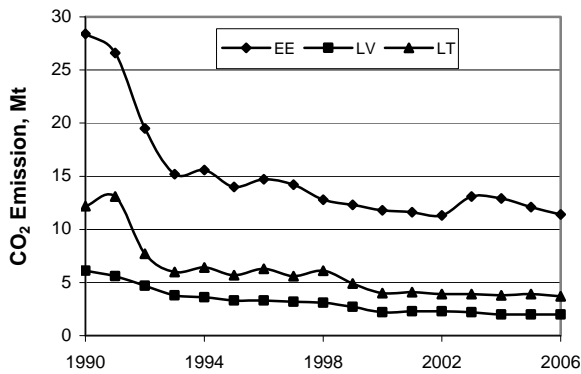


Fig. 3. CO₂ emissions in the Baltic States

CO₂ emissions in Denmark, Estonia, Latvia, Lithuania, Finland and Sweden in 2006 are provided for the comparison (Fig.4)

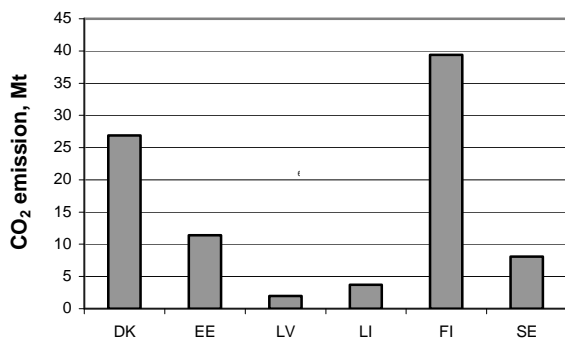


Fig.4. CO₂ emissions in the Baltic region countries

About 75% of the primary energy supply in Estonia is domestic — mostly oil shale, wood and peat.

Oil shale is a main fuel for electricity and heat generation in Estonia and represents the largest fossil resource of the Baltic region. Russian oil and Russian gas are imported.

Latvia, contrary, is importing about three quarters of its primary energy (natural gas, coal and oil products). Biomass, peat and hydropower are domestic resources. Two large CHP plants, TPP-1 with an installed electric capacity of 144 MW and TPP-2 (390 MW), are located in the city of Riga. CHP is produced mainly in cogeneration mode, according to the heat-load curve. During the heating season, when there is a substantial demand for heating and hot water, Riga CHP plants produce approximately 80% of the total annual production volume, while during summer time the volume of energy production reduces. Operation at full load during the summer (partly in condensing mode), is not reasonable from an economic point of view. It is the feature of cogeneration plant.

About 75% of residential houses in Lithuania's towns are supplied with heat from district heating systems. Energy supply to Lithuania is vulnerable, as about 90% of primary energy is imported from a single supplier [6]. It will decrease after the closure of the Ignalina nuclear power plant. The reliable supply of natural gas can be jeopardised by politically driven interruptions in the same way as it has already occurred in both Lithuania and in Latvia concerning oil supplies.

The share of renewable and indigenous energy resources (wood, peat, various combustible wastes, etc.) in the primary energy balance has so far not been sufficiently used (Fig. 5).

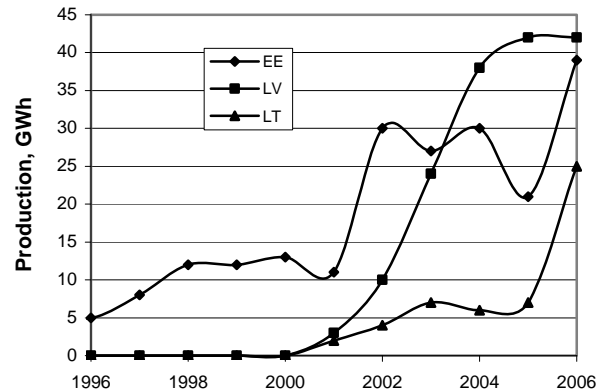


Fig.5. Electricity generation from biomass in the Baltic states

The use of natural gas as a fuel to generate electricity and provide district heating, despite its favourable characteristics, represents a supply security risk and rising prices.

5. Nuclear energy as a heating source

Energy production and consumption give rise to significant health and environmental impacts. Besides commercial energy sources, large volumes of non-commercial wood and other biomass are burned for energy supply. Acid gas and particulate emissions from fossil fuels degrade local and regional air quality. Non-carbon sources such as nuclear energy and renewable energy sources can make a vital contribution to reducing emissions.

Use of nuclear energy as a heating source is greatly challenged by the economic factor since the nuclear heating reactors have relative small size and often characterized as having the lower plant load factor. District heating networks generally have installed capacities in the range of 10 to 50 MWth in towns and small communities. 600 to 1200 megawatt-thermal (MWth) are installed in large cities. Due to the size effect, nuclear economics are, in general, improved for larger units. But current design small and medium size reactors are not scaled down versions of large commercial reactors. They are intended to be economically competitive.

Potential radioactive contamination of the district heating networks is avoided by appropriate measures, such as intermediate heat exchanger circuits with pressure gradients which act as effective barriers. No incident involving radioactive contamination has ever been reported for any of the reactors used for these purposes [2]. Heating of Visaginas town from Ignalina Nuclear Power Plant is an example of a good praxis in Lithuania.

6. Small-sized nuclear reactors

The IAEA defines small reactors as reactors with power levels between 0 and 300 MW_e while medium size reactors have power levels between 300 and 700 MW_e. The requirements for worldwide deployment of small reactors include: nonproliferation assurances; passive safety; efficient utilization of uranium resources; as well as simple and reliable plant operation [7]. These new opportunities are provided by advanced high-temperature and fast neutron reactors.

Fast reactors typically use liquid metal coolants, such as lead, lead-bismuth, or sodium, instead of water.

USA has developed a concept called STAR, the secure transportable autonomous reactor. The main goal of the implementation of this concept is to provide reliable and cost-effective electricity, heat, and freshwater. The reactor design could also be adapted to produce hydrogen for use as an alternative fuel for passenger cars. The STAR proliferation-resistance features include 30 full power years between whole-core refueling [7]. Fuel cycle services and waste management is planned at centralized facilities operated under international safeguards oversight.

A set of STAR reactors is under development: SSTAR (20 MWe, 45 MWth) for small towns; STAR-LM (181 MWe, 400 MWth) for cities and STAR-H. The latest is a high temperature version of STAR-LM reactor for production of hydrogen. STAR-LM is modular reactor with a sequence of clustered modules installed over time as required for growing electricity demand. SSTAR is a small, sealed, transportable, autonomous reactor.

The small fast reactor 4S has been under development in Japan since 1988. It is thought to contribute to a multipurpose utilization of nuclear power as an electrical power supply, heat supply, and desalting of seawater, especially where the power transmission infrastructure cannot be maintained. The 4S reactor is designated as a nuclear battery. The reactor core would be constructed and sealed at a factory, then shipped to the site. It can be removed and replaced when the power is depleted. Core lifetime of 4S reactor is 30 years. Toshiba proposed to test their new 4S (Super Safe, Small and Simple) reactor in Galena, Alaska.

Table 2. Selected characteristics of liquid metal cooled nuclear battery reactors

Type	Outlet, °C	Circulation	Power, MWth
4S	485	Forced	30
SVBR-75/100	480	Forced	280
ENHS	<600	Natural	60-400
STAR-LM	590	Natural	400
STAR-H	800	Natural	400
SSTAR	570	Natural	45

The Encapsulated Nuclear Heat Source (ENHS) is developed at the University of California. ENHS is a liquid metal-cooled modular reactor concept of 125 MWth. It incorporates a fast neutron spectrum core with a 15-20 year core life. The core is at the bottom of a

metal-filled module sitting in a large pool of secondary molten metal coolant. The whole reactor sits in a 17 meter deep silo. This reactor is designed for developing countries and is highly proliferation-resistant.

Some selected characteristics of liquid metal cooled nuclear battery reactors are provided in Table 2.

Concept of creating nuclear power plant with floating power source was developed in Russia. It is carried out on the basis of existing ice-breaker reactor plant and established shipbuilding technologies. Floating power unit - KLT-40C reactor plant for heat and power generation is two-circuit system with pressurized water reactor.

Table 3. Small and medium reactors at advanced development stage

Reactor	Power, MWe	Country
CAREM	27	Argentina
MRX	30-100	Japan
KLT-40	35	Russia
IRIS-50	50	USA
Modular SBWR	50	USA
SMART	100	Korea
NP-300	100-300	France
FUJI	100	Japan, Russia, USA
RSR	100	USA
PBMR	165	South Africa
GT-MHR	285	USA, Russia
BREST	300	Russia

Recently Rosatom/ Russia decided to accelerate the development of the SVBR-75/100 reactor. SVBR-75/100 is a lead-bismuth fast reactor with power level between 75 and 100 MW_e, transportable, having 7- to 10-year refueling interval.

7. References

1. Nuclear power in Switzerland. Country nuclear power profiles. IAEA, 2003
2. B.J.Csik, J.Kupitz. Nuclear cogeneration: supplying heat for homes and industries. IAEA. 2002.
3. Commission of the European Communities Brussels, C (2008) 7294 Commission decision of 19.11.2008
4. Nuclear Energy and Kyoto Protocol. NEA OECD 2002. 53 p.
5. EU Energy in Figures 2009. CO2 Emissions* by Sector, EU-27. European Commission. DG TREN, 2009, 67 p.
6. National energy strategy. Lithuanian Energy Institute, 2003, 44 p.
7. J.J. Sienicki, D.C. Wade. Nonproliferation features of the small secure transportable autonomous reactor (SSTAR) for worldwide sustainable nuclear energy supply.

ALLOCATING PRODUCTION COST OF CHP PLANT TO HEAT AND POWER

Viktorija NEIMANE*, Antans SAUHATS**, Guntars VEMPERS***, Inga TERESKINA***

*Vattenfall Research & Development, Sweden; **Riga Technical University, Riga, Latvia;

*** Riga Technical University, JSC "Siltumelektroprojekt", Riga, Latvia

Abstract: This paper is dedicated to the task of cost determination for heat and power energy production for small size cogeneration plants. Cogeneration of heat and power is only possible if there is a demand for both types of energy. The consumers of both heat and power are considered as members of the coalition having a goal to gain additional revenues due to reduced investments and increased efficiency of power production. The suggested approach uses the cooperative game theory for distribution of the additional revenues between the members of the coalition. The examples of energy tariffs determination in the market environment show the rationality and efficiency of using the considered approach.

Keywords: energy supply, distributed energy resources, cogeneration, district heating, game theory, decision-making.

1. Introduction

Awareness of the global society regarding issues related to production, distribution and consumption of both thermal and electrical energy is mainly induced by the following three factors [1]:

- Global reserves of primary energy resources are limited
- Mankind activities increasingly influence the global climate changes
- The demands of modern society towards reliable energy supply without interruptions are increasing.

In the countries of North-Eastern Europe the issues of enhanced efficiency and reliability of energy supply are especially important due to climatic, historical and economic reasons. What are the prerequisites there?

- Rapid economic development goes along with increasing energy demand.
- The existing energy supply system was built based on condition that there are inexpensive primary energy resources available. This system appears to be inefficient in a new

situation due to low efficiency of the energy production sources, high transportation losses and utilization of excessively energy demanding technologies and buildings. Furthermore, a number of energy sources appear to be inefficient from the environmental and safety viewpoints.

- Due to climatic conditions (cold winters) there is especially high demand towards reliability of energy supply.
- There is considerable number of industrial and domestic constructions and there is a need for upgrade of energy production sources, which creates the possibility for utilization of progressive technologies for energy production and consumption.
- The systems of district heating are extensively used in the cities of North-Eastern Europe. These systems are suited for efficient utilization of cogeneration in combined heat and power plants (CHPs).

The intention for fuller utilization of fuel as well as the obvious advantages of cogeneration resulted in creating such equipment that provides for constructing CHPs with small capacities (in the order of tens kWe and larger). Such power plants can be located near the energy consumers, which can result in the essential reduction of energy losses in the heat and electricity supply networks.

The companies owning CHPs (which can include the consumers of the energy) have two possibilities to increase the incomes:

- By increasing the heat energy tariffs
- By increasing electricity power energy tariffs.

The strategy chosen by the owners of CHP influences considerably the costs and behavior of the customers. High heat energy prices stimulate saving measures, for example better isolation in houses etc. Simultaneously measures for saving of electrical energy are not prioritized. It is obvious, that for the rational development of energy supply systems the objective relation between the prices on heat and electrical energy

is needed. The methods for determination of costs and tariffs on different kinds of energy in case of cogeneration are known [2], [3], [4].

These methods are based on calculation of the summary revenue R_{Σ} that is sufficient for normal functioning of CHP. R_{Σ} is gained from selling thermal energy W_Q and electrical energy W_E , proceeding from the given rate of profit. The revenue that is gained from the production of each type of energy, R_E and R_Q respectively, is distributed on the basis of physical laws, for example, proportionally to the produced energy as follows:

$$\begin{aligned} R_E &= \left(\frac{W_E}{W_Q + W_E} \right) \times R_{\Sigma} \\ R_Q &= \left(\frac{W_Q}{W_Q + W_E} \right) \times R_{\Sigma} \end{aligned} \quad (1)$$

In this case, the unequal value of thermal and electrical energy is not taken into account.

The method of *Exergy* is a more common method, by means of which a different value of energy is accounted for by coefficient β , that changes depending on energy production technology used.

$$\begin{aligned} R_E &= \left(\frac{W_E}{\beta W_Q + W_E} \right) \times R_{\Sigma} \\ R_Q &= \left(\frac{\beta W_Q}{\beta W_Q + W_E} \right) \times R_{\Sigma} \end{aligned} \quad (2)$$

For the steam cycle, for example, $\beta=0.6$ [2] is assumed. The main disadvantage of this method is the impossibility of objectively assessing the value of the coefficient β . It is obvious that this coefficient is different for different power systems. For example, in case of ample water resources, resulting in production of cheap electrical energy, the larger value of this coefficient should be selected.

When selling electrical energy via the power system grid, its price is determined by market. Hence, using (1) or (2), we can determine R_{Σ} and R_Q . However, in case of small CHPs, the consumers can receive the electrical energy from CHP, not using the power system grid. In this case, the conditions that are dictated by the global market become non-obligatory for these consumers. Even more, the considered approaches are not giving any advantage to the customers whose consumption profile suits cogeneration profile of heat and power best. Thus, the contribution of the heat energy consumers to the operational efficiency from the point of view of fuel savings and exhaust gases emission when producing two types of energy is not taken into consideration in the price setting.

The method based on the cooperative game theory, which overcomes the limitations described above, is presented in this paper. First the mathematical base for

the method is given, and then the task of power supply is formulated as a game with participation of coalition with several players. Case study based on real-life data used in planning of power supply of Riga (Latvia) is presented. A business plan for construction of a CHP utilizing wood waste as the main fuel is considered.

2. The theoretical background

2.1. Game- theoretical approach to the planning task

Let us imagine the task of power supply development planning in the form of a static game with complete information [5]. The game is presented in normal form as following:

$$\{I, S = \prod_i \{S_i\} i \in I, R = \{R_1, R_2, \dots, R_n\}\} \quad (3)$$

i.e. a list of players I , all situation combinations $\{S = \prod_i \{S_i\} i \in I$ and revenues R of each player at all his strategies and at each combination of the competitors' strategies.

It is assumed that the list and number of the players, i.e. competing companies, is known; also, that each player knows the competitors' strategies, i.e. the list of their possible structures and parameters, as well as the revenues at any combination of structures and parameters of all the players.

It is known [5] that the solution of the game task, presented in the form of (3), is a collective choice of equilibrium strategies. The most often used is the Nash equilibrium [5], i.e. such a set of strategies $s \in S$ that for all players i and each alternate strategy $s_i' \in S_i$, the following condition is fulfilled:

$$\forall i, \forall s_{-i} \in S_{-i} \quad R_i(s_i, s_{-i}) \geq R_i(s_i', s_{-i}) \quad (4)$$

i.e. the equilibrium is formed by such a set of strategies, with which the decision of one of the players to deviate from such set may only diminish his revenues.

The search for the equilibrium includes the following:

1. Forming the set of all the possible strategies, excluding the dominated strategies, i.e. strategies s_i' of player i , for which the following condition is fulfilled [5]:

$$\forall s_{-i} \in S_{-i} \quad R_i(s_i, s_{-i}') \geq R_i(s_i', s_{-i}') \quad (5)$$

i.e. the player's strategies are excluded, if there is a strategy that is better, irrespective of the competitors' actions.

2. Search for the equilibrium using (3). Let us suppose that as a result of such search the only set of strategies that complies with the Nash equilibrium conditions is determined. Theoretically, there may be many such equilibriums; however, some methods are known [5] that make it possible to diminish their number.

3. Considering the rationality and possibility of organizing a coalition among the players.
4. Choosing the methods for organizing the coalition and distributing additional revenues among the participants of the coalition.

If the possibility to form a coalition is taken into account, the formulation of the optimization task is modified once more. Due to the need to consider not only the strategies of individual companies, but also those of possible coalitions in various combinations, the dimension of the task increases considerably. Resulting from the solution of this task, the set of the sub-optimum plans for each company and their coalitions at various combinations of possible competitors' plans can be obtained.

2.2. Distribution of the gain between the members of the coalition – Shapley value

In case of cooperative behaviour, there is a problem of revenue distribution between the members of the coalitions. The simple approach would be to give to each player his contribution c_i :

$$c_i = R(S \cup \{i\}) - R(S) \quad (6)$$

where $R(S)$ is the revenue of the coalition S , $R(S \cup \{i\})$ is the revenue of the coalition S with participation of the actor i .

However, such an approach is not anonymous, i.e. ordering of the players makes difference in the amount they are rewarded.

In game theory, a Shapley value [6] describes one approach for the fair allocation of gains avoiding the mentioned drawback. Fair allocation ensured by selecting uniformly a random ordering and rewarding each player his expected marginal cost in ordering. Since players can form $n!$ possible random orderings, the probability of set S being ranked exactly before player i is: $|S|!(n-1-|S|)!/n!$. Thus the additional amount that the player i gets is:

$$\phi_i = \sum_{i \notin S \subseteq N} \frac{|S|!(n-1-|S|)!}{n!} (R(S \cup \{i\}) - R(S)) \quad (7)$$

where n is the total number of players, $|S|$ is size of the set S , the sum extends over all subsets S of N not containing player i .

In the simplest case, when only two players participate in the game, the expression (7) is simplified and obtains the following form:

$$\phi_1 = \phi_2 = (R(S \cup \{i\}) - R(S)) / 2 \quad (8)$$

The Shapley value describes the fair (in a sense determined by the accepted axioms) [6] distribution of additional gains in case of formation of the coalition. In particular, the definition is based on the assumption that

possible combinations of the players who form the coalition are equally probable.

3. Examples of formation of the additional gains distribution

The district heating plant (DHP) "Z" is situated in one of the districts of Riga. At present, the equipment is in satisfactory condition; however, the growth of heat loads is expected. Let us assume that there is a search for the best schematic of power supply to this district "Z". There is a great number of variants for this schematic (the preventive variant – repair work of the boiler house equipment; individual (consumer) boiler houses; electrical heating, etc.). Let us suppose that as a result of comparing these variants, the dominating strategies have been rejected. In order to increase the efficiency of power supply, it has been decided to reconstruct DHP "Z" into a combined heat and power plant (CHP) (Fig. 1), which will allow for providing the consumers of the district not only with heat but also with electricity. Based on the State support of CHP, it has been decided to use wood waste as the main type of fuel. Part of electric energy can be exported or imported via the distribution grid. Reconstruction of the existing boiler house that produces only heat energy for the consumers serves as an alternative for the power supply schematic presented on Fig. 2.

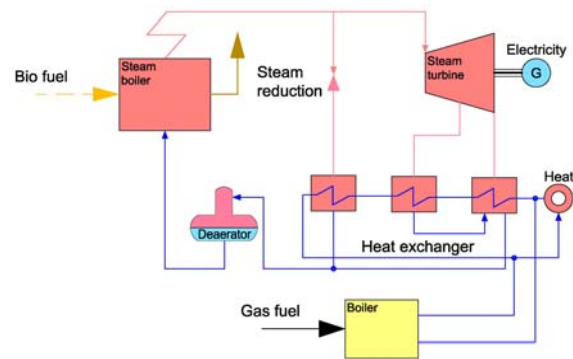


Fig. 1. The simplified structural schematic of CHP

In this case, all the electricity is imported by the district in question (let us call this power supply variant as "Variant A"). In Variant A, electricity is imported from the grid, and its price is fully dictated by market. In this case, the price for heat is mainly determined by the price for fuel, capital costs for boiler house construction, operating costs and credit payment terms.

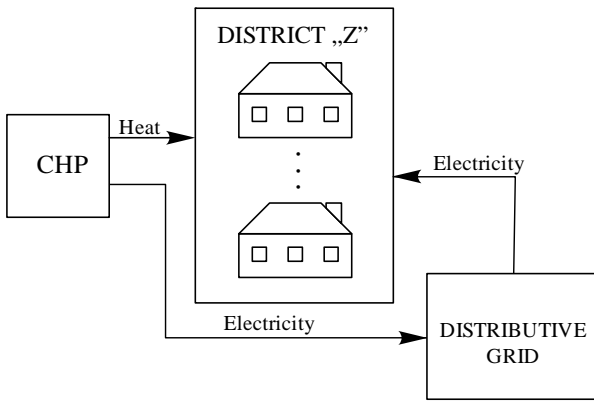


Fig. 2. The schematic of power supply to district “Z” (Variant B1)

In the event of CHP construction, two more variants of power supply appear:

- Variant B1 (Fig. 2.): CHP supplies heat to district “Z”, and electricity is exported to the grid; the district, in its turn, imports the necessary electricity from the grid.
- Variant B2 (Fig. 3.): CHP supplies both types of energy (heat and electricity) to district “Z”, i.e. a coalition of consumers has been formed within the district. Such coalition is possible, if its expenses E_k are less than the summary expenses $E_1 + E_2$ of the consumers of heat (E_1) and electricity (E_2), acting independently, i.e., if:

$$E_k < E_1 + E_2 \quad (9)$$

The heat consumers provide the conditions for the functioning of a cogeneration plant. They are interested in the formation of a coalition with electricity consumers, provided that the sale price is fixed higher than the price of energy that is exported to the grid. At the same time, the power consumers will be interested in a coalition, if the electricity price is lower than the price of energy imported from the grid. A question about fixing reasoned tariffs emerges.

The principal data used in calculations are presented in Table 1. When calculating investments, it was taken into account that the State support is 30% of the expenses necessary for construction of CHP. In this paper it is assumed that it is possible to calculate the costs associated with providing energy supply for district “Z”. In the considered Variant A, electricity is imported from the grid, and its price is fully dictated by market. In this case, the price for heat will be mainly determined by the price for fuel, capital costs for boiler house construction, operating costs and credit payment terms.

In Variant B1, when all the electricity is exported, its price is also determined by market. On condition that there is a task for gaining the normalized profit, the revenue from selling electricity makes it possible to reduce the price for heat supply. However, in this case, the district is forced to purchase the relatively expensive electricity from the grid. In power supply Variant B2,

the coalition of the consumers of both types of energy gains the additional revenue at the expense of difference in the prices for imported and exported electricity.

Table 1. The principal data used in calculations.

No.	Name	Amount, Measuring units
1	Investments	6834 thous. EUR
2	Summary costs of fuel (per hour)	980622 EUR
3	Price of electricity exported	105 EUR
4	Price of electricity imported	126 EUR
5	Amount of heat supplied to the grid	183,6 thous. MWh
6	Amount of electricity supplied to the grid	16,6 thous. MWh

It is possible to distribute the additional revenue, using (7) and (8), which will reduce the prices to an even greater degree.

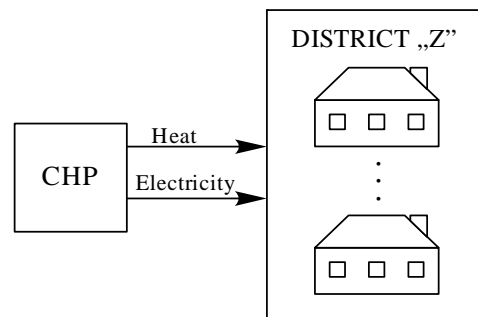


Fig. 3. The schematic of power supply to district “Z” (Variant B2)

In price calculation, it was assumed that the district is fully consuming the electricity produced. In case if some part of electricity is exported to the grid, the difference between Variants B1 and B2 will diminish. Such dependence indicates that the coalition is interested in consuming the electricity of its own production. The considered approach regarding the distribution of the additional revenue can serve as a basis for creating an appropriate procedure of calculation with the consumers, depending on their heat and electric load charts. Notice that the results shown on Fig. 4 have been obtained, using the real prices for fuel and equipment. Hence, these results substantiate, in the first instance, the efficiency of using small-capacity cogeneration plants, especially, with high prices for energy carriers.

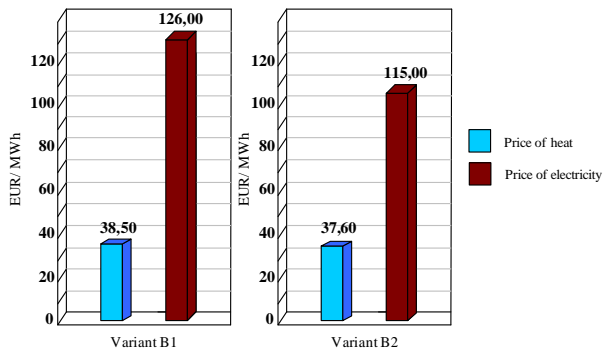


Fig. 4. Comparison of heat and electricity tariffs in Variants B1 and B2 (with the State support)

Fig. 4 schematically shows the comparison of heat and electricity tariffs in Variants B1 and B2. The mentioned prices, for which the consumers of district “Z” will buy the thermal and electric energy, differ markedly from one another. Hence, the application of the method based on the game approach results in electricity prices that are sufficiently close to the market prices as well as to relatively low heat prices. It appears that such price ratios stimulate the extensive application of cogeneration processes in energy production.

Fig. 5 represents the prices of heat and electricity, excluding the State support. In this case, the heat prices appear to be higher than the average heat prices in Riga. Hence, the considered Variant turns out to be non-competitive.

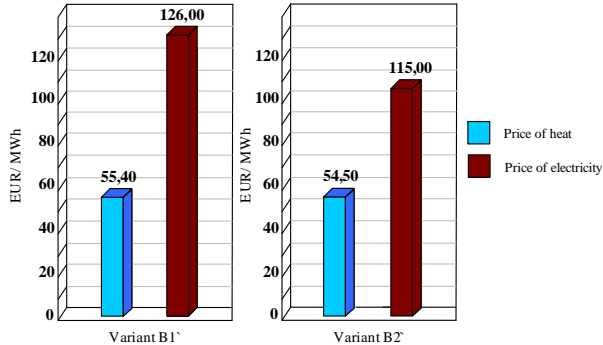


Fig. 5. Comparison of heat and electricity tariffs in Variants B1 and B2 (without the State support of investments)

4. Conclusions

1. Methods based on the game theory can contribute to making the right decision about the development of energy supply sources. In particular, the cooperative game taking into consideration the possibility of building the coalition should be used. In due course, this approach will result in a more efficient energy supply system and acceleration of DER implementation in power systems.
2. The known methods of determining tariffs for energy produced in the cogeneration mode are poorly adapted for application in the market environment.

3. Construction of CHP and formation of a coalition of heat and electricity consumers makes it possible to essentially reduce tariffs for both types of energy.

The formation of a coalition of energy consumers for the construction of CHP with increased capacity may result in the additional reduction of energy tariffs.

5. Acknowledgements

The research activity presented in this paper is supported by the European Union through the SES6-CT-2003-503516 project "EU-DEEP".

6. References

1. Directive 2001/77/EC of the European Parliament and of the Council of 27 September 2001 on the promotion of electricity produced from renewable energy sources in the internal electricity market.
2. N.A.Slavina, E.M.Kosmatov, E.E.Barikin. Methods of CHP production costs allocation. Power stations Nr. 11, 2001, p.p.14-17 (in Russian) Thermoflow. Comprehensive Thermal Engineering software. Thermoflow Inc. April 2002.
3. Viktoria Neimane, Antans Sauhats, Guntars Vempers, Inga Tereskina, Galina Bocharjova. Approach for Power Supply System Planning Based on Cooperative Game Theory, The 5th International Conference on the EUROPEAN ELECTRICITY MARKET - EEM 08, Lisbon, Portugal, May 28-30, 2008, ID#206.
4. V. Neimane, A. Sauhats, J. Inde, G. Vempers, G. Bockarjova. Using Cooperative Game Theory in energy Supply Planning Tasks, 16th Power Systems Computation Conference- PSCC2008, Glasgow, Scotland, July 14-18, 2008, ID#220.
5. Osborne, M.J. and Rubinstein, A. „A Course in Game Theory”, MIT Press (Chapters 13, 14, 15), 1994.
6. Lloyd S. Shapley. A Value for n-person Games. In Contributions to the Theory of Games, Volume II, by H.W. Kuhn and A.W. Tucker, editors. Annals of Mathematical Studies v. 28, pp. 307-317. Princeton University Press.

CROSS-BORDER CAPACITY AUCTIONS

Rimantas DEKSNYS*, Robertas STANIULIS*, Giedrius RADVILA**

* Kaunas University of Technology, Lithuania,

** AB „Lietuvos energija“, Lithuania

Abstract: Paper is actual because of perspective strategy of Baltic-Nordic and Baltic-Polish electricity systems connections, which could lead to the integration of Baltic electricity system and market into united European transmission system UCTE and European electricity market. The main task of this paper is to summarize the cross-border capacity allocation mechanism applied in European countries and to evaluate the possibilities of new Baltic interconnections.

Keywords: electricity market, congestion, cross-border capacity, capacity auction, explicit auction, implicit auction.

1. Introduction

With the development of international relations in electricity trade, with the increasing gross domestic product, import and export, integration of separate power systems is growing, which enables the development of common electricity market. In this stage of development of energy systems common system infrastructure is being developed, i. e. cross-border links, which connect separate energy systems with each other, enable connection of smaller energy systems to the bigger ones, more effective utilization of energy resources and appearance of market elements in energy systems. Together with infrastructure organizational requirements of cross-border flows control without discrimination and with understandable and reliable principles are growing. The most important role falls for transmission system operator in this process. Transmission system operators under strict governmental regulation have to ensure reliable and qualitative supply of electricity, ensure free third party access to the network and ancillary services, which are related with energy quality and reliability of supply. Other important task for transmission system operators is network development, which could meet electricity quality, control, technical, organizational and market needs. Determining those needs, objective parameters are needed, which could show economic benefit of

network development and return on investment. Investment security and benefit are showing the parameters determined through effective utilization of power network, market development level, possibilities of electricity market expansion and connection. Therefore one of the most important indicators is satisfaction to the market situation of cross-border capacity, controlled by transmission system operators, and mechanisms of congestion management and congestion income formation. In continental part of Europe historically cooperation of big companies, which were the main industrial consumers, and foreign generators was developed by buying electricity on the basis of mutual agreements. Therefore later with the development of free and organized market mechanisms, the task of system control for transmission system operators has emerged. Therefore mechanism of explicit auctions for cross-border capacity allocation and control was introduced in continental part of Europe. Nordic countries, where electricity generation is diversified, have chosen more advanced implicit auction mechanism for cross-border capacity allocation.

This paper is actual because of perspective strategy of Baltic-Nordic and Baltic-Polish electricity systems connections, which could lead to the integration of Baltic electricity system and market into united European transmission system UCTE and European electricity market. The main task of this paper is to summarize the cross-border capacity allocation mechanism applied in European countries and to evaluate the possibilities of new Baltic interconnections.

2. Methods of cross-border capacity allocation

Auctions are well known market mechanism, which are used for distribution of limited resources, in this case cross-border capacity. Auctions are transparent and efficient as they allocate capacities to those that value it the most.

At present, a variety of different capacity allocation methods are in use in electricity market. Although each method is unique, but they can be grouped as follows [1, 2]:

1. First come first served: capacity is allocated according to the order in which the transmission requests have been received by the TSO. Starting from the earliest request, all requested amounts of capacity are fully granted until the available capacity is used up.

2. Pro rata: all requests are partially accepted in the way that each applicant is granted a fixed share of his requested capacity amount, the share being equal to the amount of available capacity divided by the sum of all requested capacity amounts.

3. Explicit auction: along with the requested capacity amount, the applicants have to declare how much they are willing to pay for this capacity. These bids are ordered by price and allocated starting from highest one until the available capacity is used up. In contrast to the previous methods, network users incur cost for obtaining transmission capacity (usually the price is set to the bid price of the lowest allocated bid).

Variations in auction design are possible with regards to the bidding mechanisms or the time periods, which are auctioned (days, weeks, months, years). Explicit auctions separate energy flows from transmission capacity. Hence, once interconnection capacity has been secured by a market participant, the participant will need another transaction for energy. This can be done on the bilateral market or on a power exchange.

4. Implicit auction: with all previously described methods, the electricity spot markets are separated from the transmission capacity allocation procedure and close after the transmission capacity has been allocated. With implicit auctioning transmission capacity is managed implicitly by the spot markets: network users submit purchase or sale bids for energy in the geographical zone where they wish to generate or consume, and the market clearing procedure determines the most efficient amount and direction of physical power exchange between the market zones. Hence congestion management model is integrated with the energy market and a separate allocation of transmission capacity is not required.

Since this method does not separate energy flows from transmission capacity, the process is simpler for market parties. Such system creates revenue for the market operator equal to the size of the interconnector capacity times the price difference. The revenues which the market operator collects should in theory, be the same as the revenues from an explicit auction. The main drawback of this option is that it requires an organized market to function in the downstream side of each congested interconnection. This is currently an important practical limitation in many countries where a liquid and stable organized electricity markets have not yet developed.

Especially in the initial stages of market development, this has included non-market-based methods, such as the first-come-first-served principle, retention or a pro-rata allocation, which have been gradually replaced by auction-based mechanisms over the past few years.

Although explicit auctions can still be regarded as the prevailing methods for the time being, implicit auctions are generally regarded as being the most efficient

solution and can be expected to become of increasing importance as regional market integration proceeds.

3. Economics of cross-border trade

The benefit from the cross-border trade could be obtained two ways. First, because of cheaper imported electricity, average electricity price in the importing country is decreasing and generators of the exporting country are earning more money. Second, because of limited cross-border capacity additional incomes are earned by the owners of interconnection.

Congestion incomes could be calculated evaluating electricity price difference between interconnected parties, duration of congestions and capacity of interconnection:

$$R = \Delta MC \cdot T \cdot ATC ;$$

where: R – congestion revenues; ΔMC – difference of marginal electricity prices between interconnected parties; T – duration of congestions; ATC – available transfer capacity of interconnection.

Economic principles of cross-border trade between regions A and B are shown in Fig. 1. Without interconnection between those regions in region A electricity price would be $MC A1$ and in B region – $MC B1$, and $MC A1 > MC B1$.

If available transfer capacity exists between those regions, marginal price of A region would decrease till $MC A2$ and in B region would increase till $MC B2$. In case that there are no congestions between regions, electricity price would be equal $MC AB$ in both regions.

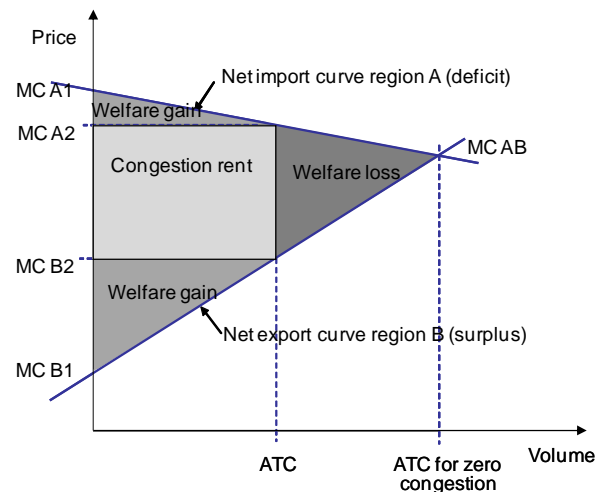


Fig. 1. Economics of cross-border trade

In Fig. 1 different areas show distribution of benefit between regions A and B, when limited interconnection capacity ATC exists. In A region electricity price decreases from $MC A1$ till $MC A2$ and the benefit of A region consumers is equal to the area above the line $MC A2$ shown in the figure. In B region because of increased electricity price from $MC B1$ till $MC B2$, benefit of B region generators is shown below $MC B2$ line in the figure. Area of the congestion rent is showing the benefit of interconnection operators because of the price

difference between the regions. This benefit is usually divided between operators in proportion to the amount of shares or by other methods. Reduction of social benefit, which represented by the area in the figure, is appearing because of limited transfer capacity between the regions. Maximum social benefit is obtained in the case then there are no cross-border trade limitations between the regions.

4. Simulation of new interconnections in the Baltic region

Success, economic and social benefit of cross-border interconnection projects between separate electricity markets depend on the electricity market conditions and system control possibilities, because these subjects let objectively evaluate pay-back time of the investments, its security, social and economic benefit in the long run. To solve those problems evaluation of technical level and future interconnection projects, current and future analyzed and surrounding countries market situation, evaluation of market isolated situation, perspective market development tendencies, simulation of market based interconnection capacities auction mechanisms are needed.

Simulation of new interconnections between two regions could be done by three scenarios described below.

4.1. First scenario – market isolation

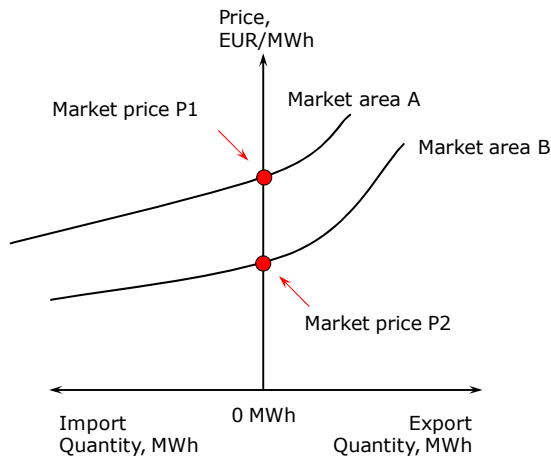


Fig. 2. Electricity price formation with the isolated electricity market

Marginal electricity price in the isolated electricity market, without physical connection or with available transfer capacity equal to zero, would be developing independently from the price of neighboring countries. Import and export activities would not be possible and only supply and demand of internal market players form electricity price.

So in this case:

Internal market price $MC2 \neq$ External market price $MC1$.

Analyzing the influence on generation and consumers, it is necessary to state that in this case there is no crucial effect on their costs and revenues. Social and economic benefit of common electricity market is not achieved

and benefit is obtained only through the deployment of internal market resources and internal competition.

4.2. Second scenario – sufficient interconnection capacity

Equal electricity price in the common electricity market is formed simulating the interconnection according to the second scenario, when there is some certain available transfer capacity ATC between the markets, which is available for the common electricity market.

But this price is being formed only until import or export through the available interconnection is not restricted by larger supply amounts from the lower to higher price region.

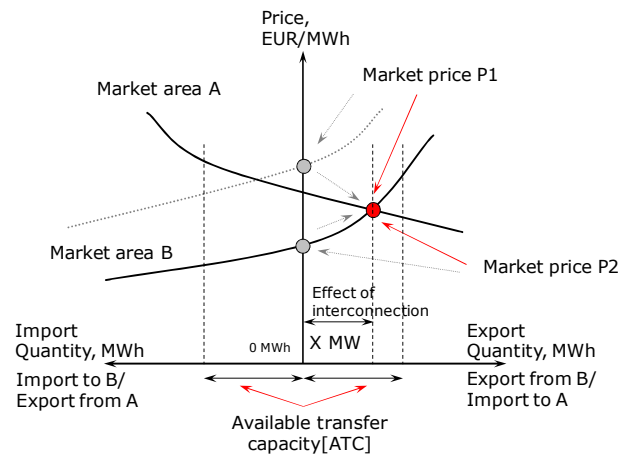


Fig. 3. Electricity price formation in the common electricity market with sufficient interconnection capacity

The main assumption of this scenario is that available transfer capacity is larger than actually needed capacity (X) for electricity import and export.

The influence of interconnection capacity could be simulated as the additional possibility of lower price region market players (in this case internal market) to sell electricity and for higher price region market players (in this case neighboring external market) to buy cheaper electricity that is proposed in the isolated market.

So in this case:

Internal market price $MC2 =$ External market price $MC1$.

With the condition that available transfer capacity ATC is higher than actually needed capacity X.

Investigation of market price changes, using marginal price methodology, having interconnection and possibilities to import and export electricity shows that generators in the exporting country could increase their revenues, but costs for consumers would be higher. And on the contrary, consumers' costs would be lower in the importing country, because of the lower electricity price. Revenue of importing country generators would be lower, because they will have to compete with cheaper imported electricity. Simulation shows that there is no congestion rent for interconnection operator, because there is no price difference between the markets due to sufficient interconnection capacity.

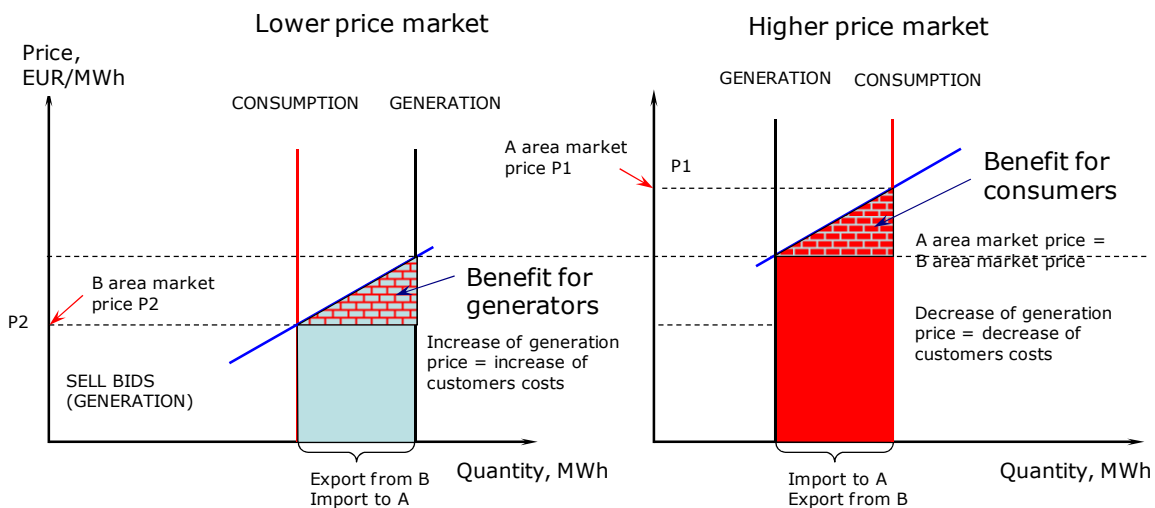


Fig. 4. Relation of revenue and costs for generators and consumers

In the situation when electricity is exported from the market, the greatest benefit would get exporting generators, because of the possibility to sell their energy in the high electricity price markets. In the importing region benefit would be gotten by electricity consumers, because more expensive local generators would be replaced by cheaper electricity import.

4.3. Third scenario – limited interconnection capacity

The third scenario is simulated for the situation when the quantity of sell bids in the higher price region is higher than available transfer capacity of interconnection. In this case different price areas would develop.

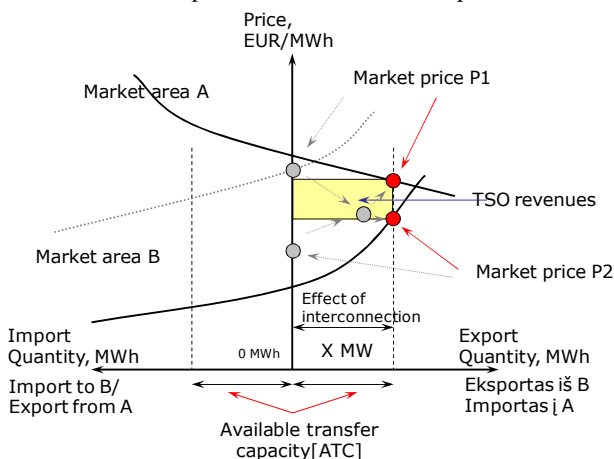


Fig. 5. Electricity price formation in the common electricity market with limited interconnection capacity

In the third scenario the situation is analyzed when all available transfer capacity of the interconnection is used by market players.

The influence of interconnection capacity is maximal, because all available transfer capacity is used for needs of higher price area. In this case bigger benefit is for exporting market, because sell bids are cleared fully utilizing interconnection capacity.

The tendency of electricity price changes would depend on the customers' elasticity, when customers are reacting to indicative electricity price and change their consumption behavior. But the tendency of revenue and costs distribution is the same as in the second scenario. In this case:

Internal market price $MC2 \neq$ External market price $MC1$.

With the condition that available transfer capacity ATC is equal to actually needed capacity X. Available transfer capacity ATC is lower than the quantity of proposals to sell electricity using interconnection capacity, what is corresponding to demand curve in the higher price area.

Having price difference between external and internal market, congestion rent is being cumulated by electricity exchange, which could be distributed among transmission system operators at the end of the year. The level of congestion rent is indicating how often congestions occur and is it necessary to increase interconnection capacity. On the other side, these revenues could guarantee the return of investments of new interconnection, therefore further analysis of interconnection return of investments is related with possibility to forecast electricity price in two analyzed markets and to distribute congestion rent for the investment.

5. Simulation of interconnection return of investments

Simulating the return of investments of Baltic–Swedish interconnection certain assumptions have to be done which influence calculation results. One of the main assumptions – is the forecast of electricity price difference in Baltic and Nordic electricity markets for the pay-back period, which is equal to 7 years. It was assumed that interconnection is simulated for the period from 2013 to 2019. This period includes big changes not only in the Baltic, but also in neighboring markets:

Table 1. Forecast of Nord Pool electricity physical exchange price in 2010–2019, EUR/MWh

Year	2010	2011	2012	2013	2014	2015	2016	2017	2018	2019
Maximal Nordic electricity market price	53.0	55.1	54.0	56.2	55.0	57.2	56.0	58.2	57.0	59.3
Minimal Nordic electricity market price	37.9	38.1	41.0	45.0	46.0	47.8	49.8	51.7	53.8	56.0

Table 2. Forecast of Baltic electricity physical exchange price in 2010–2019, EUR/MWh

Year	2010	2011	2012	2013	2014	2015	2016	2017	2018	2019
Maximal Baltic electricity market price	98.0	101.9	106.0	110.2	114.6	119.2	124.0	129.0	134.1	139.5
Minimal Baltic electricity market price	72.1	75.0	78.0	81.1	84.3	87.7	91.2	94.9	98.7	102.6

1. Closure of Ignalina nuclear power plant.
2. Start of operation of new Visaginas nuclear power plant in 2018.
3. Russian electricity market growth, development and integration into other markets.
4. Installation of new capacities in the Baltic region and annual growth of demand by 4 %.
5. Buy-out of Estlink interconnection from shareholders in 2014 and further exploration as infrastructural project.
6. Estonian electricity market opening in 2013.
7. Closure of Estonian oil-shale power plants.
8. New period of quotas distribution of greenhouse gases emission in 2013.

Taking into account the forecast of long-term physical market contracts, the most probable that electricity price in the physical electricity market Nord Pool would reach 53 EUR/MWh in 2010 (Table 1) [4]. Correction factors, related with economic indicators of different markets, could more precisely set the margins of electricity price increase, but to set this tendency more precise economic evaluation and officially confirmed forecasts of development scenarios are needed. In the price forecast annual inflation rate of 4 % is assumed. Assumptions are evaluated taking into account historical data for 8 years period, therefore minimal forecasted margin is set taking into account prices of futures, and the maximal price – forecast of spot market electricity price.

Taking into account generation structure and annual energy generation in the Baltic countries, after closure of Ignalina NPP indicative electricity price in Baltic countries will be formed by Estonian and Lithuanian condensing power plants. Forecasted electricity price in the Baltic countries for the period from 2010 to 2019 is provided in the Table 2. Annual inflation rate of 4 % was assumed in this forecast. In Baltic and in Nordic countries seasonal factor has a big influence on electricity prices. During the tide effectively using Latvian Daugava hydro power plants, Lithuanian Kruonis hydro storage power plant and importing the rest of energy from neighboring countries, influence of condensing power plant on indicative electricity price could be eliminated. Taking into account seasonal factor, energy import possibilities and redistribution of generation sources, electricity prices in the annual perspective could decrease by 30 %, because during this

time Estonian and Lithuanian condensing power plants could be eliminated from the market.

Using electricity price forecast in Baltic and Nordic countries and modeling the return of investments of Baltic–Nordic interconnection, it could be stated that Baltic electricity market will be an importing market. For the formation of revenues from the interconnection, two assumptions have to be fulfilled:

- interconnection has to be an infrastructural or by other means free access to use interconnection capacity for market players has to be ensured;
- sufficient electricity price difference and market liquidity, ensuring sufficient amounts of electricity sell and buy bids on both sides of interconnection.

Total annual consumption in Nordic countries is 412.8 TWh, while in the Baltic countries it is 25.8 TWh, therefore possibilities for Baltic countries to use the advantages of Nordic electricity are much bigger than the opposite way. Calculating the return of investments using forecasted electricity prices for the period 2013–2019, it is necessary to determine the capacity of interconnection. According to the future plan of interconnection, two scenarios of interconnection capacity are reasonable – 700 MW and 1000 MW. Therefore further calculations will be for two interconnection capacity scenarios.

Duration of congestions depends on the price difference between the markets and technical reliability of the interconnection. To evaluate technical inaccessibility of the interconnection due to annual maintenance and fault conditions could be done by knowing projected utilization factor of interconnection. Usually this factor is equal to 97 %, therefore duration of congestions is decreased by 3 % of annual operation of the interconnection. Evaluating the tide period, when situation in the Baltic market is similar to Nordic market, it is advisable to decrease the period of congestions by two months, when there will not be buy bids in Nordic countries, though interconnection capacity will not be totally used (second scenario). To ensure system security minimum generation level in the system will be set, which could ensure hot operational reserve, guarantee sufficient regulation range for generation and consumption balance.

With the varying maximum price difference between Baltic and Nordic electricity markets from 65.2

EUR/MWh (2013) till 83.5 EUR/MWh (2019) maximum possible annual congestion revenue with 700 MW interconnection capacity vary from 320 to 410 mill. EUR, and with 1000 MW interconnection capacity – from 501 to 821 mill. EUR. With the varying minimum price difference between Baltic and Nordic electricity markets from 36.1 EUR/MWh (2013) till 46.7 EUR/MWh (2019) minimum possible annual congestion revenue with 700 MW interconnection capacity vary from 177 to 229 mill. EUR, and with 1000 MW interconnection capacity – from 253 to 327 mill. EUR. Not adequate situation in the Baltic market is being formed after closure of Ignalina NPP. Big price difference between the markets is causing high level of congestion revenues, which are equal to big countries – France, Germany and Italy – revenues. Physically isolated Baltic electricity market with high electricity price has enough potential to initiate new interconnection projects, which pay-back could be guaranteed by market connection and integration with Nordic electricity market.

6. Conclusions

1. Success, economic and social benefit of cross-border interconnection projects depend on the electricity market conditions and system control possibilities, because these subjects enable objectively evaluate pay-back time of the investments, its security, social and economic benefit in the long run.
2. Marginal electricity price in the isolated electricity market according to the first analyzed scenario, without physical connection would be developing independently from the price of neighboring countries. Social and economic benefit of common electricity market is not achieved and benefit is obtained only through the deployment of internal market resources and internal competition.
3. Simulation of interconnection according to the second scenario with sufficient interconnection capacity shows that generators in the exporting country could increase their revenues, but costs for consumers would be higher. And on the contrary, consumers' costs would be lower in the importing country, because of the lower electricity price. There is no congestion rent for interconnection operator, because there is no price difference between the markets due to sufficient interconnection capacity.
4. Simulation of interconnection according to the second scenario with limited interconnection capacity shows that different price areas would develop. Having price difference between external and Baltic market, congestion rent is being cumulated by electricity exchange, which could be distributed among transmission system operators at

the end of the year. The level of congestion rent is indicating how often congestions occur and is it necessary to increase interconnection capacity. Also, these revenues could guarantee the return of investments of new interconnection.

5. Simulating the return of investments of Baltic–Swedish interconnection the forecast of electricity price difference in Baltic and Nordic electricity markets for the 7 year pay-back period from 2013 to 2019 is needed. The most probable electricity price in the physical electricity market Nord Pool would reach 53 EUR/MWh in 2010 and 59.3 EUR/MWh in 2019. Forecasted maximal electricity price in the Baltic countries in 2010 could reach 98 EUR/MWh and in 2019 – 140 EUR/MWh.
6. Using electricity price forecast in Baltic and Nordic countries and modeling the return of investments of Baltic–Swedish interconnection, it could be stated that Baltic electricity market will be an importing market. For the formation of revenues from the interconnection, interconnection has to be an infrastructural or by other means free access to use interconnection capacity for market players has to be ensured and also sufficient electricity price difference and market liquidity, ensuring sufficient amounts of electricity sell and buy bids on both sides of interconnection, have to be guaranteed.
7. Big price difference between the Baltic and Nordic markets is causing high level of annual congestion revenues, which vary from 177 to 410 mill. EUR for 700 MW interconnection and from 253 to 821 mill. EUR for 1000 MW interconnection and are equal to big countries revenues. Physically isolated Baltic electricity market with high electricity price has enough potential to initiate new interconnection projects, which pay-back could be guaranteed by market connection and integration with Nordic electricity market.

7. References

1. Analysis of Cross-Border Congestion Management Methods for the EU Internal Electricity Market. Study commissioned by the European Commission. CONSENTEC, Final report, June 2004.
2. Market Operator (Regulatory Oversight), Final Version. Energy Regulators Regional Association (ERRA), Prepared by KEMA International B.V., December 2007.
3. Towards a common coordinated regional congestion management method in Europe. Study commissioned by European Commission, CONSENTEC, October 2007.
4. Market information. www.nordpoolspot.com, 2008.

THE NEURAL NETWORK AS THE INDUCTIVE ENGINES STATES ANALYSER

Boguslaw TWAROG, Zbigniew GOMOLKA
University of Rzeszow, Institute of Technology, Poland

Abstract: The idea of object diagnostics with use artificial neural network and the method of computer simulation vibrate processes of inductive motor is proposed. Information about system is contained in vibration signals or in the current load flow, that allows to define its state. Changes of air gap and one-sided forces of magnet attraction are taking into consideration. The integration of differential equations is realized by Gear implicit method. Using neural networks as diagnosis instrument we can determine different degree of damages.

Keywords: mathematical model, diagnostic, inductive engine, Fourier transform, spectrum of signal, neural network, back-propagation.

1. Introduction

The system of defect detection has to shown on-line that failure occurs. Usually in techniques we have two categories of detection and error diagnosis: estimation methods and pattern recognition methods.

Estimation methods require knowledge of mathematical model, which reflect real process. Model cannot be too complicated because diagnostics is realized on-line and solution of model equations shouldn't take too long time. When error of device functioning or its failure occur diagnostic system should detect it immediately. Next kind of error and his location should be properly classified. If it is possible should isolate influence of failure in system.

In second category of recognition methods there is no mathematical model, process of diagnostic and error classification. There is representation space of process from measurements to space of decision. Traditional recognition and classification is divide to three levels: measurement, analysis, classification. Artificial neural networks can realize such classification tasks in very efficient ratio. It connects to choice of network architecture, which depends on problem which realize. In that case chosen characteristics of object determine number of neurons in input, output and hidden layer.

Structure of neural network depends as well on complexity of solving problem. Possibility of generalization is important advantage of artificial neural network over traditional diagnostic methods. If neural network is teach by representative set of data then it is able to work properly even for cases don't considered before [2].

2. Architecture of diagnostic system

In our case an electric engine is the object of analysis. The proposed method is non interference and using artificial neural network. It allows to detect first symptoms of failure what is important for assuring lasting work without damages. The measurement signal is vibration signal of working engine which contain information about object state.

The proposed system consists of three main parts: measurements sub-system, sub-system of artificial intelligence, presentation sub-system.

Realization of such measurement system (working in real time) was done on laboratory standing with IBM PC computer and PCI 1711 series measurement module equipment [5]. That module enables to make measurement of electric variables or representing by them physical variables using analog-digital converter. Advantage of measurement module is tuning possibility of input and output voltage range. Proper adjustment of input and output voltage range can prevent over tuning and increase measurements accuracy. Especially measurement system contains:

1. microprocessor system: analog interface for system protection, serial interface for communication with another computers, microprocessor card with analog/digital and digital/analog converters,
2. software system: sampling and estimation, taking decision, error classification.

Described systems have high sensitivity, non complicated construction and universal applications. The artificial intelligence systems, which used neural network, detects failures or their symptoms. That detection bases on spectrum of object vibrations. The

$$a = \frac{(1+TN)M - TS^2}{\Delta}; \quad c = \frac{(1+TM)N - TS^2}{\Delta};$$

$$M = b \int_0^{2\pi} \frac{\cos^2 p_0 \eta}{\delta(\eta)} d\eta; \quad S = b \int_0^{2\pi} \frac{\sin p_0 \eta \cos p_0 \eta}{\delta(\eta)} d\eta;$$

$$N = b \int_0^{2\pi} \frac{\sin^2 p_0 \eta}{\delta(\eta)} d\eta; \quad T = \alpha_S + \alpha_R + \frac{\pi p_0}{3w^2} \rho;$$

$$\Delta = (1+TM)(1+TM) - TS^2; \quad b = \frac{S}{\Delta}$$

There $b = 3wa\mu_0/(\pi p_0)$ is constant coefficient; ρ is magnetic resistance of main magnetic circuit of electric machine with the exception of resistance of air gap; w is number of effective windings of phase stator; μ_0 magnetic constant; $p_0\eta$ is angle coordinate of stator; $\delta(\eta)$ is function dependence of value of air gap from angle η

$$\delta(\eta) = \sqrt{x_R^2 + y_R^2 + R_1^2 - 2R_1\sqrt{x_R^2 + y_R^2} \cos\eta} - R_2 \quad (8)$$

where R_1 is inner radius of stator; R_2 is external radius of rotor.

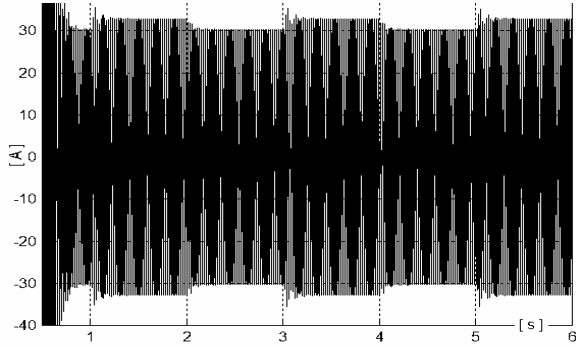


Fig. 2. The time run of the current changes of the stator of phase A

Electromagnetic moment

$$M_E = \frac{3}{2} p_0 (\psi_\xi i_{S\xi} - \psi_\chi i_{S\chi}) \quad (9)$$

The one-sided forces of magnet attraction in immovable co-ordinate axes will be

$$F_x = F_\xi \cos\gamma_R - F_\chi \sin\gamma_R; \quad F_y = F_\xi \sin\gamma_R + F_\chi \cos\gamma_R \quad (10)$$

where

$$F_\xi = c_0 \int_0^{2\pi} \frac{\varphi_\eta^2}{\delta(\eta)^2} \cos\eta d\eta; \quad F_\chi = c_0 \int_0^{2\pi} \frac{\varphi_\eta^2}{\delta(\eta)^2} \sin\eta d\eta, \quad (11)$$

There

$$\varphi_\eta = \left(\frac{3w}{\pi p_0} (i_{S\xi} + i_{R\xi}) - \frac{\rho \psi_\xi}{w} \right) \cos p_0 \eta + \left(\frac{3w}{\pi p_0} (i_{S\chi} + i_{R\chi}) - \frac{\rho \psi_\chi}{w} \right) \sin p_0 \eta, \quad (12)$$

where $c_0 = R_1 l \mu_0 / 2$ is constant coefficient; l is length of stator.

The velocities of rotor movement we obtain from general equation of dynamic

$$\frac{dv_{xm}}{dt} = \frac{1}{m} (F_x - c_x x_R - v_x (v_{xm} + \varepsilon \omega \sin\gamma));$$

$$\frac{dv_{ym}}{dt} = \frac{1}{m} (F_y - gm - c_y y_R - v_y (v_{ym} - \varepsilon \omega \cos\gamma)); \quad (13)$$

$$\frac{d\omega}{dt} = \frac{1}{J} \left(M_E - M_M + m \frac{dv_{xm}}{dt} \varepsilon \sin\gamma - \left(m \frac{dv_{ym}}{dt} + mg \right) \varepsilon \cos\gamma \right)$$

where M_M is resistance moment; c_x, c_y are stiffness of rotor supports; v_x, v_y are dissipation coefficients; g is gravitations constant.

The system of 11 differential equations (1), (3), (4), (13) are integrated simultaneous and joint. As result of integration we find full linkage magnetic fluxes $\Psi_{S\xi}, \Psi_{S\chi}, \Psi_{R\xi}, \Psi_{R\chi}$, co-ordinates of centre of rotor mass x_m, y_m , angles of rotor turn γ and movable co-ordinate system γ_R , linear velocities of movement of centre of rotor mass, v_{xm}, v_{ym} and angle rotor velocity ω .

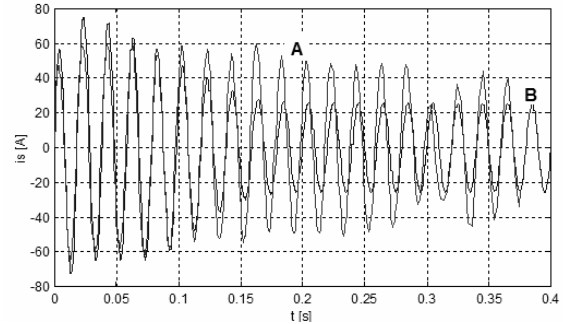


Fig. 3. The time run of the current changes of the stator of phase A of the eccentricity of the rotor of the inductive engine $\varepsilon = 5.0e-05$ (A) and $\varepsilon = 2.0e-04$ (B)

Because of high frequency vibrations of mechanical system the differential equations are very stiff [3]. They are integrated by implicit numerical Gear method including the formulas of 6-th order. For this aim we obtained the analytical formulas of Jacobi matrix, because it is very complicated we here do not given.

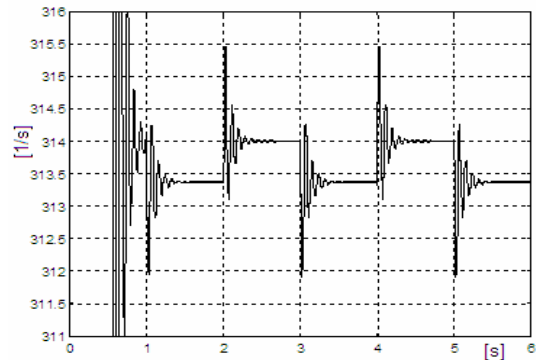


Fig. 4. The time run of the changes angular speed

Obtained results confirm that mathematical model can reach steady state thus can work properly Fig. 4. Further experiments will realize with using neural network for

engine with different defects, which can obtain setting up appropriate conditions in mathematical model. Proposed diagnostic system allow to elimination of a human being from participation in measurements. Entire diagnostic process is realized automatically by kit of suitably equipped personal computer. In presented system measurement signal is submitted to Fourier Transform and results, after appropriate treatment, are feed as input signal to neural network.

4. The system with the artificial neural network

Because of the lack of the occurrence of non-linear relations between the changes of the analyzed quantity and their causes the non-linear artificial neural networks have been used in the researches. Such tasks require solving the problem of the right transformation of the runs describing the object as well as carrying out experiments in the range of choosing the right architecture and data for teaching to obtain the ability of the network to generalize. The direct pass of the current flow on the receptors of the neural network is connected with the necessity of the digitizing of this flow, whereby the lowest the digitizing step the more precisely the flow will be represented. There is a necessity of the initial converting of the current flow stator, that is a modulated flow. In order to do this there has been the current distribution into the Fourier series applied. The frequency value and the component amplitude of the particular spectrum are the result of the solution of the mathematical model equations for the steady work state. The quantitative evaluation of the spectrum will be done by using the neural networks. This kind of approach does not need the division of the spectrum of the stator current into particular component sets, characteristic of the particular eccentricity kind. At the neural input there is a vector given, including the amplitudes and particular phases of the components related to the value of the grooved component. Different winding eccentricity values generate different spectrums (amplitude values and phase angles) of the winding current components, that is why these changes can be used in research with the application of the artificial neural networks.

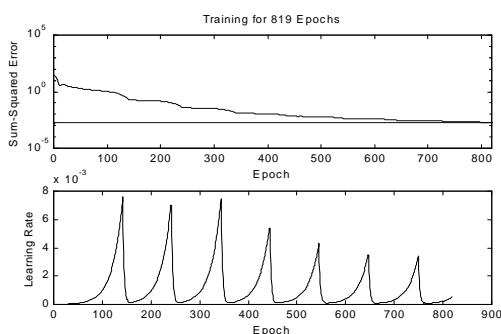


Fig. 5. The course of teaching error in the function of the stages number necessary to achieve the established error level

In this case there has been the non-linear neural network applied for the purpose of the experiment made up of one hidden layer. For teaching the networks Fig. 5, the

gradient method of Levenberga Marquardt has been applied in connection with the back-propagation algorithm, implemented in the programming language of Matlab for Windows [4]. For the final evaluation of the activity quality of the network there has been the independent, evaluation sequence used, made up of 80 input vectors Fig.6.

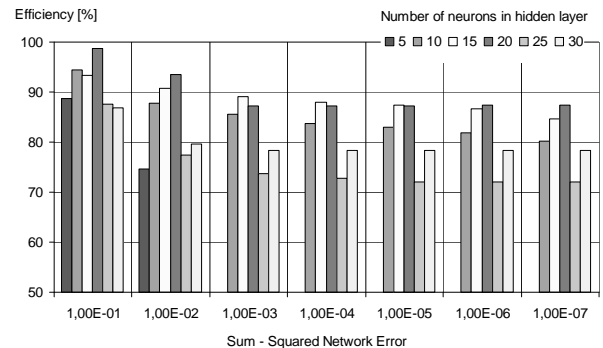


Fig. 6. Effectiveness of the neural network depending on the number of neurons in the hidden layer

5. Conclusions

The main virtues of using the artificial neural networks in the diagnostic testing of the technical system result from the attractive network properties, such as the ability of the parallel information processing, effective approximation of free nonlinearity, teaching and tutoring the networks on the basis of the object signals. Moreover, using the specialized mathematical model and advanced computational technology led to the proper network training and allowed for the precise evaluation of the device state like the induction motor. Below there are the detailed conclusions that are the result of the task realization: the special approach has been proposed for the analysis of the dynamic stresses in the induction motors considering the mechanical and electromagnetic vibratory effects, the analytical relations have been received for the defining of the size of the air-gap in the induction motor that allow for the mutual interaction of the mechanical and electromagnetic subsystems in the motor, the mathematical models have been compared in terms of the usefulness in computer simulations, the effectiveness of the artificial neural network application has been shown for the analysis of the non-linear object state using among others: their virtues for example the abilities to generalize, low sensitivity on possible damages (breaking certain number of the joints between the neurons), the ability of the parallel processing and the work in the actual mode.

6. References

1. Tchaban V. Mathematics modeling of electro-mechanical processes. Lviv, 1997.
2. Kościelny J. M. Diagnostyka zautomatyzowanych procesów przemysłowych. Wyd. EXIT/2001
3. Fortuna Z. i inni. Metody numeryczne. WNT/2005
4. Demuth H, Beale M. Neural Network Toolbox User's Guide. The Math Works Inc.

INVESTIGATION OF THE INDUCTION MOTOR START UP PROCESS USING STAR-DELTA START

Marina KONUHOVA, Karlis KETNERS, Elena KETNERE, Svetlana KLUJEVSKA
Riga Technical University, Faculty of Power and Electrical Engineering, Latvia

Abstract: This investigation is concerning mathematical modeling of the induction motor start up mode using stator windings switching from star to delta connection. Mathematical model of induction motor realized by Park-Gorev equations. The analyses of presented start up mode show, that at the switching time there is rotor rundown of induction motor. Speed of rotation of the induction motor due to rotor rundown decreases and in case of prompt switching in delta connection remaining rotor flux, which could not drop to zero immediately, it may be current rush up to 20 times more than rated current and that is not acceptable for induction motor. In this investigations there are provided recommendations for optimal switching time determination for star – delta start up mode of induction motor.

Keywords: analysis, induction motor, mathematical model, modeling, Park-Gorev equations, star-delta start.

1. Introduction

Induction squirrel-cage rotor motors (IM) are most commonly used motor type on the market. They are relatively cheap and have not expensive service [1].

Generally in asynchronous drive there appear transient conditions: electromagnetic, resulted by induction motor windings electromagnetic lag and mechanical, resulted by the motor mechanical lag [2].

Transient current in the motor rotor and stator during motor start process vary according to complicated fluctuating rules and inducted by that electromagnetic torque is of waving mode and is in complicated time dependence [2].

Full voltages start up of the induction motor entail two adverse factors i.e.: inrush current big repetition factor, exceeding 6-10 and fluctuating damping type of motor starting torque. Consequences of these factors effects are:

-big inrush current leads to large drop of the voltage of the substation main bus-bar (if the power of transformer and motor are commensurable) thus destroying normal work of other consumers and motor itself dragging out its start;

-big inrush current cause large windings thermal overload thus accelerating insulation ageing, its damaging and finally turn-to-turn fault;

-large fluctuation of motor torque in the beginning of start exceeding 4-5 times of nominal torque create adverse conditions for mechanical part (kinematics chain).

Due to provided obstacles in industry it is widely used star-delta start (reduced-voltage start). This solution allows limit inrush current [3].

2. Induction motor star-delta start features

Induction motor star-delta start is possible for the motors intended for operation with delta connection of stator windings. This mode of start is acceptable only if the starting torque of the driven mechanism is not big. If motor has big load, the torque might be too short for acceleration of the motor up to the speed for switching of delta connection. For instance, the motors driving pumps and ventilators in the start moment have small torque and increase proportionate to rotation speed squared. When the speed exceeds 80-85% of nominal speed, the torques of motor from one side and torque of the load become even and acceleration ends [1].

Inrush current in circuit when start is star switching is triple smaller then when delta switching used. That is a large advantage of considered start mode. Taking in consideration that the on star switching of stator windings the voltage is $\sqrt{3}$ smaller than on delta switching, the start torque M decreases 3 times.

Disadvantage of this mode is absence of smooth of start, having only two starting steps and increased start process.

Starting with use of start-delta switch presented on the Fig.1.

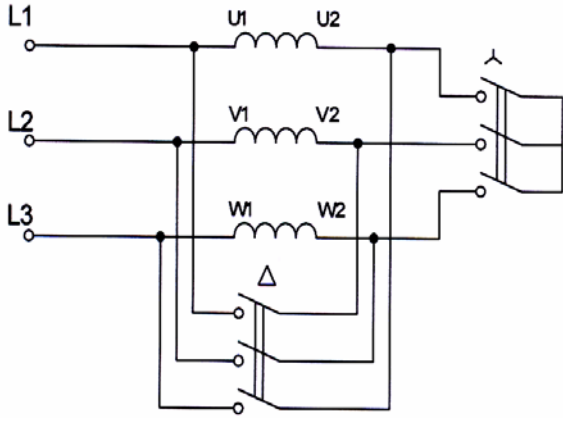


Fig. 1. Connection scheme of stator windings starting

At the switching moment, stator windings are switched off for a while and then switch on again. Switch in starting position switching stator windings in star and in working position in delta. For switching usually apply different automatic schemes (relays, contactors, actuators).

3. Mathematical model of star-delta start for induction motor

Developed program allows to model: induction motor start up mode under undervoltage conditions (switching stator windings in star), rundown mode of induction motor (switching time) and induction motor switching on full voltage (switching stator windings in delta). IM reduced-voltage start and repeated switching on full voltage modeling is implemented using IM mathematical model described by Park-Gorev equations, which are putted down in coordinates rotating synchronously with stator field (coordinates d, q) [4]:

$$\left. \begin{aligned} U_{1d} &= R_1 i_{1d} - \omega_{0el} \psi_{1q} + \frac{d\psi_{1d}}{d\tau} \\ U_{1q} &= R_1 i_{1q} + \omega_{0el} \psi_{1q} + \frac{d\psi_{1q}}{d\tau} \\ U_{2d} &= R_2 i_{2d} - (\omega_{0el} - \omega) \psi_{2q} + \frac{d\psi_{2d}}{d\tau} \\ U_{2q} &= R_2 i_{2q} + (\omega_{0el} - \omega) \psi_{2q} + \frac{d\psi_{2q}}{d\tau} \end{aligned} \right\} \quad (1)$$

$$T_M \frac{d\omega}{d\tau} = [M_{em} - M_l], \quad (2)$$

$$\left. \begin{aligned} \psi_{1d} &= X_1 i_{1d} + X_{ad} i_{2d} \\ \psi_{1q} &= X_1 i_{1q} + X_{ad} i_{2q} \\ \psi_{2d} &= X_2 i_{2d} + X_{ad} i_{1d} \\ \psi_{2q} &= X_2 i_{2q} + X_{ad} i_{1q} \end{aligned} \right\} \quad (3)$$

where T_M - time constant of the machine in electrical radians;

$M_{em} = X_{ad}(i_{2d}i_{1q} - i_{2q}i_{1d})$ - the electromagnetic torque;

$u_{1d}, u_{1q}, u_{2d}, u_{2q}$ - are components of stator and rotor voltage;

$u_{2d} = u_{2q} = 0$ for induction motor with a squirrel-cage rotor;

$\psi_{1d}, \psi_{1q}, \psi_{2d}, \psi_{2q}$ - are components of flux linkages;

$i_{1d}, i_{1q}, i_{2d}, i_{2q}$ - are components of stator and rotor currents;

ω - is angular rotation speed of rotor;

ω_{0el} - is angular rotation speed of coordinate system;

$X_1, X_2, X_{ad}, R_1, R_2$ - are parameters of the induction motor;

M_{em}, M_l - are electromagnetic torque and load torque.

For IM rundown process (switching time) modeling we solve the equation (1) by substitution of equation (3) concerning derivative currents.

As far the current in stator of IM on rundown immediately drops to zero, it is necessary to make such an admission:

$$i_{1d} = i_{1q} = 0. \quad (4)$$

Taking into consideration above mentioned, from the combined equations, which are modeling IM start up we receive differential equations, which determine IM rundown conditions:

$$\frac{di_{2d}}{dt} = -\frac{R_2}{X_2} \cdot \frac{1}{X_1 - \frac{X_{ad}^2}{X_2}} \cdot X_1 i_{2d} - \left(\frac{1}{X_1 - \frac{X_{ad}^2}{X_2}} \cdot X_1 \omega - \omega_{0el} \right) \cdot i_{2q}, \quad (5)$$

$$\frac{di_{2q}}{dt} = \left(\frac{1}{X_1 - \frac{X_{ad}^2}{X_2}} \cdot X_1 \omega - \omega_{0el} \right) \cdot i_{2d} - \frac{R_2}{X_2} \cdot \frac{1}{X_1 - \frac{X_{ad}^2}{X_2}} \cdot X_1 i_{2q}, \quad (6)$$

$$\frac{d\omega}{dt} = -\frac{1}{T_M} M_l. \quad (7)$$

Voltage induced by damped rotor field on the stator terminal is following:

$$U_{1d\ res} = -\frac{R_2 X_{ad}}{X_2} i_{2d} - X_{ad} \omega i_{2q}, \quad (8)$$

$$U_{1q\ res} = X_{ad} \omega i_{2d} - \frac{R_2 X_{ad}}{X_2} i_{2q}, \quad (9)$$

where $U_{1d\ res}, U_{1q\ res}$ - are residual voltage on stator terminal.

Elaboration of this model allows researching electromagnetic, mechanical and energetic parameters for induction motor and completing electrical drive as well.

4. Modeling and obtained results analysis

For induction motor switching from star to delta mode of start up analysis it was used induction motor (4A355M4Y3) possessing following parameters [7]: $P_{2N}=315\text{kW}$; $P_{2N}=315\text{kW}$; $X_{\mu}=5.7$; $R'_1=0.012$; $X'_1=0.099$; $X_S=5.799$; $R''_2=0.014$; $X''_2=0.14$; $X_{k.p.}=0.16$; $R_{2p}=0.027$; $R_{k.p.}=0.039$.

Curves of rotation speed, current and torque of induction motor depending on time during induction motor star-delta start and direct start are presented on Fig.2 – Fig.4.

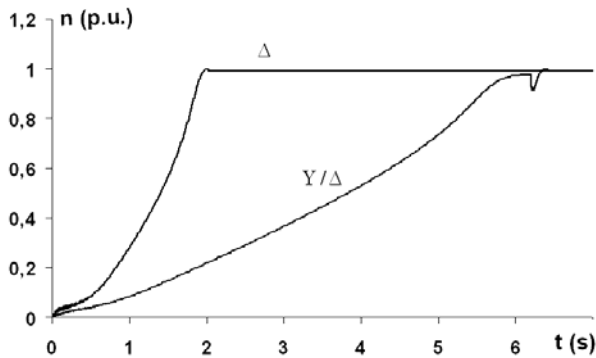


Fig. 2. Induction motor rotation speed curve starting

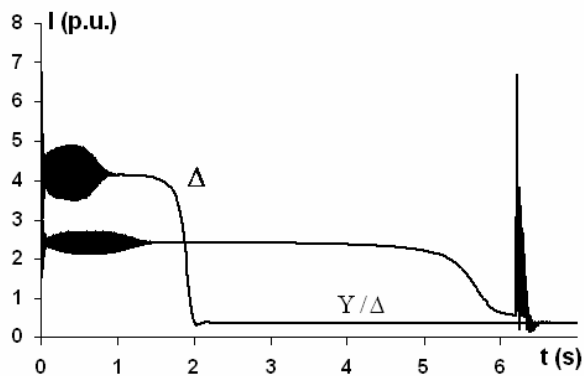


Fig. 3. Induction motor current curve starting

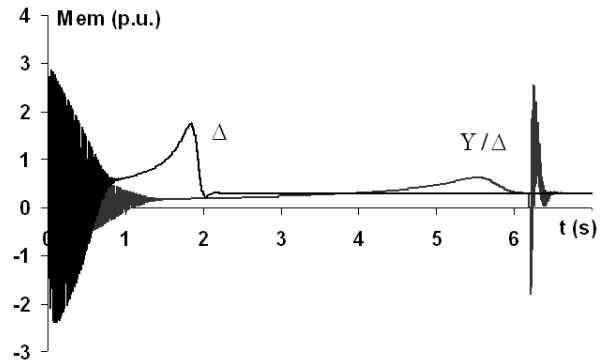


Fig. 4. Induction motor electromagnetic torque curve starting

At the time of starting between breaking and switching from star to delta power supply interrupted, thus rotation speed under the action of resistance of the driven mechanism decreases. Rundown process of induction motor in details is shown on the Fig.5.

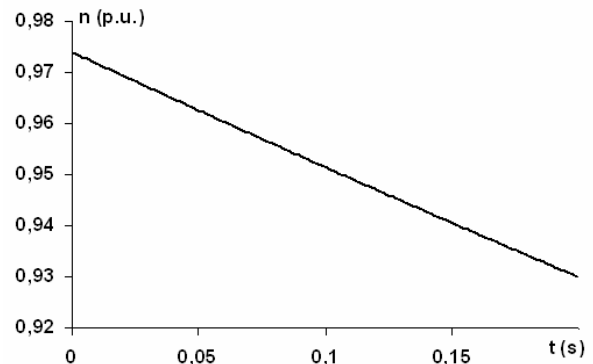


Fig. 5. Rundown mode of induction motor

Every IM possesses own rundown characteristics because of dependence of load parameters and of driven mechanism mechanical characteristics, finely of IM parameters. The bigger moment of inertia and initial rotation speed and the smaller motor load, the slower rotation speed decrease during rundown time [5].

IM switching off from power supply, inducing residual EMF in stator windings on rundown time. Since IM magnetic flux couldn't instantly break off, the presence of this flux exert negative influence to transients and cause maximal transitional torques increase [6]. Relying on IM rundown process modeling we obtained hodographs of rotor current and of a voltage on stators terminals (see Fig.6 & Fig.7), which shows EMF attenuation process. Traced analysis shows that the prompt switching from star to delta in case of adverse switching phase (antiphase) may result with inrush current amount to multiple nominal current rates. Observed $25 I_N$ inrush current on switching to delta in conditions of adverse phase (see Fig.8) another time closing on favorable phase inrush current was lack (see Fig.9).

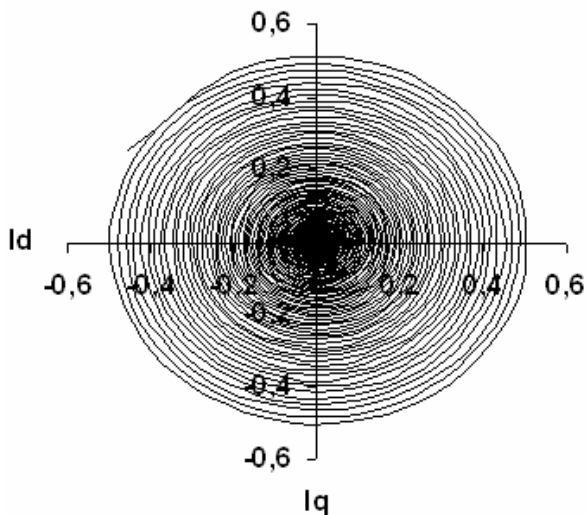


Fig. 6. Hodograph of a rotor current

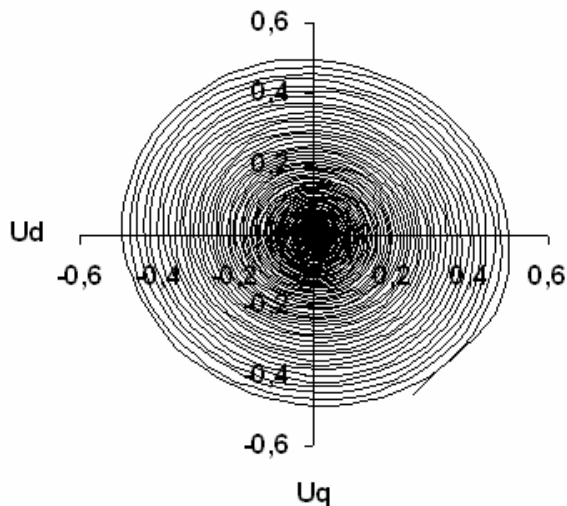


Fig. 7. Hodograph of a voltage on stators terminals

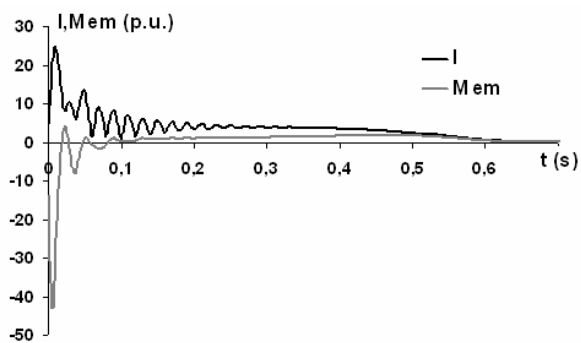


Fig. 8. Curves of current and electromagnetic torque depending on time. Process unsuccessful

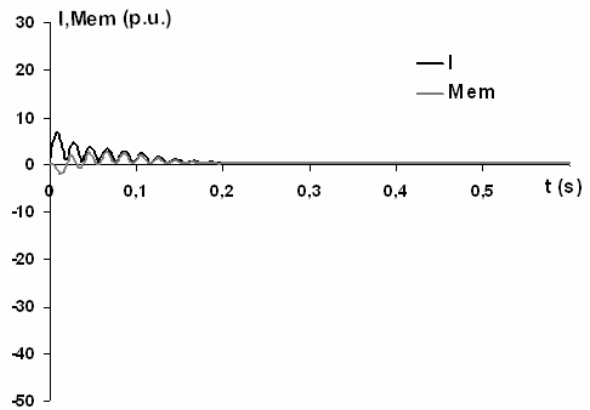


Fig. 9. Curves of current and electromagnetic torque depending on time. Process successful

So, applying present model there is opportunity to analyze IM safe start by star-delta start mode, since residual voltage presence on IM stator at the windings switching in delta might result with significant windings thermal overloading, such way processing untimely its insulation deterioration, injury and finely turn-to-turn fault.

5. Conclusions

Provided mathematical model of IM allows to make complete switching process analysis if chosen motor start to make in star-delta start mode. Analysis of proceeded investigations shows that using this mode of start up it is not useful to apply fast-acting automatic machinery since each motor has different EMF attenuation process time interval depending on its own characteristics and load parameters. If apply fast-acting automatic machinery for switching, there is risk to close in antiphase. In such conditions the injury of the IM is inevitable.

6. References

1. Softstarter handbook, ABB Automation Technology Products AB, Control, February 2003.
2. Москаленко В.В. Электрический привод, М.: издательский центр «Академия», 2004.
3. Austin, H. (2006) Electric Motors and Drive (3rd ed.). Published by Elsevier Ltd, UK.
4. Копылов И.П. Математическое моделирование электрических машин. Учебник для вузов.-3-е изд.-М.:высшая шк.,2001.
5. Голоднов Ю.М. Самозапуск электродвигателей - 2-е изд., перераб. И доп.-М.:Энергоатомиздат, 1985.
6. Ketnere E., Ketners K., Kļuevska S., Koņuhova M. „The research into the self-starting mode of the induction motor”. RTU, ”Energētika un elektrotehnika” 4. Sērija, 20. Sējums, Rīga, 2007.
7. Асинхронные двигатели серии 4А: Справочник / А.Э.Кравчик, М.М.Шлаф, В.И.Афонин, Е.А.Соболевская.- М.:Энергоиздат, 1982.

RATIONAL GEOMETRY OF A MAGNETIC CIRCUIT OF AXIAL INDUCTOR GENERATOR

Svetlana ORLOVA*, Vladislav PUGACHOV*, Nikolaj LEVIN*, Edmunds KAMOLINS**
 *Institute of Physical Energetics, Latvia; **Riga Technical University, Latvia

Abstract: Axial inductor generator (AIG) is considered together with tooth windings in the present work. This generator is being manufactured by plant RER for power supply of carriages. In order to define the optimal geometry of tooth zone and magnetic circuit, an estimation of electromagnetic field in the generator was performed together with the application of a complex of programs "QuickField". The analysis of the results was performed with the help of an objective function which characterizes the relation of nominal power to the generator's mass. The recommendations concerning the choice of rational geometry of the generator realization, which will allow improving mass-dimensions indices, are given on the basis of the analysis of magnetic fields.

Keywords: axial inductor generator, objective function, software "QuickField".

1. Introduction

Inductor generators are devices belonging to the type of brushless electrical machines, which have been widely used in different industrial fields. Inductor generators often have been used in the systems of electrical supply of trains, planes and ships, in wind-driven power plants systems, as well as in modern technologies of electric arc welding, induction heating etc. This type of equipment is characterised by the diversity of its structural variations, scheme and modifications. In the present paper the inductor generator with axial excitation is examined. The main feature of this type of machines is that by rotating rotor the flux in the teeth of the rotor doesn't change the direction.

Axial inductor machines (AIM) have a simple construction (see Fig. 1.) and a high degree of reliability as well as they have some advantages in comparison with common constructions of synchronous machines:

1. Absence of rotating windings and the rotor made like a tooth-type cylinder. In this case, magnetic flux density in every surface point of the armature bore of an inductor machine changes only in its value, but the direction remains the same.

2. Owing to the fact, that the magnetic flux is created by one unmovable coaxial excitation coil situated in the space between the rotor packets, inductor machines requires a significantly lower expenditure of copper and power of excitation, which makes the excitation system and regulation of the machine simpler.

3. The inductor machine used for alternating current of heightened frequency has a possibility to perform significantly smaller tooth points on the rotor in comparison with clearly polar synchronous machine of the same diameter.

4. Absence of rotating windings saves the machine from any contact, and this feature constitutes its most important advantage [2].

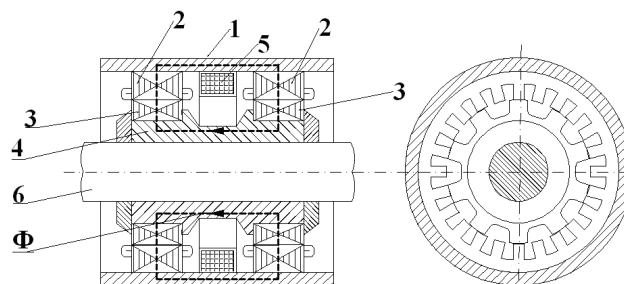


Fig. 1. Two-core axial inductor machine: 1 – body, 2 – armature cores with windings, 3 – rotor cores, 4 – rotor shell, 5 – excitation winding, 6 – shaft, (Φ is a magnetic flux)

The main disadvantage of axial inductor machine is low mass-dimensional magnitude, therefore designer shall take a special attention to the rational selection of geometry of teeth area of generator.

2. Modeling of magnetic field of an axial inductor machine

AIM owing simple constructions have an electromagnetic system that principally differs from other synchronous machines and magnetic fields in them and preserves clearly three-dimensional character. However, with the help of some simplifications the solution can be reflected in two two-dimensional tasks: the field in an active zone (a core of the stator, a rotor

and a main air gap) is flat parallel, but outside the borders of the active zone (in an axial core) can be received as symmetrical to the axis. Complexity in modeling of a magnetic field in the active AIM zone is that it is necessary to model an absent source of the excitation field, as the coaxial excitation coil is situated in the space between the cores of the stator and the rotor [1].

The magnetic field, in the cross-section of the machine is defined by a vector magnetic potential and is described by a differential equation (1) in quotient derivatives:

$$\frac{\partial}{\partial x} \left(\frac{1}{\mu_y} \cdot \frac{\partial A_z}{\partial x} \right) + \frac{\partial}{\partial y} \left(\frac{1}{\mu_x} \cdot \frac{\partial A_z}{\partial y} \right) = -j_z, \quad (1)$$

where components of the tensor of magnetic permeability μ_x and μ_y , A_z is a vector magnetic potential, j_z is density of the current on the co-ordinate, which coincides with the axis of machine rotation.

When AIM is no-load, the source of the field is – an excitation coil, which is situated outside the calculation area between the two cores of the stator and the rotor.

In case when the calculation area is half of the machine (Fig. 2), boundary conditions are set in the following way:

1. Boundaries AB and CD are axes of symmetry of the magnetic field and a boundary condition of the 1st line should be set for them: $A_{AB} = \text{const}$; $A_{CD} = \text{const}$, where A_{AB} , A_{CD} are the values of a vector potential on the boundaries of AB and CD.

As the magnetic flux is defined with the help of the expression (2):

$$\frac{\Phi}{2} = (A_{AB} - A_{CD}) \cdot l = \Delta A \cdot l, \quad (2)$$

where l is the length of a machine.

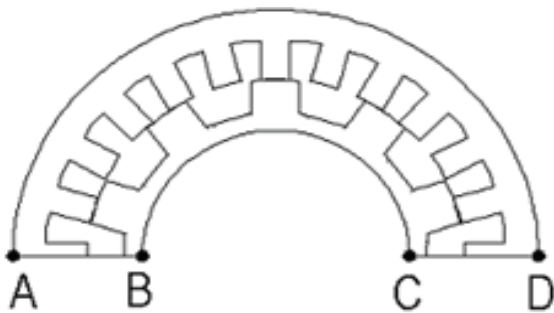


Fig. 2. Calculated geometrical model of magnetic system in cross-section for AIM with teeth 24/10

The value of a vector magnetic potential can be chosen freely on one of the boundary, in this particular case: $A_{CD} = 0$ and $A_{AB} = \Delta A$.

2. Boundary conditions of the 2nd line are set on the outer (AD) and inner (BC) circumferences, as the boundaries under consideration have only normal constituent of flux density ($B_{\tau} = 0$) [3].

In case of optimisation the investigations on numerical modelling of magnetic fields in AIM presented are not complete, as it is necessary to take into account the distribution of magnetic flux if the geometry of tooth zone is different. Program «Quick Field» [4] is used in the present work for estimation of magnetic field in the machine's cross-section, allowing to get a real picture of magnetic field and on this basis to perform optimisation of the machine's magnetic system on the higher level and to avoid the disadvantages mentioned before. It is necessary to take into account the dependence of vector magnetic potential (VMP) and magnetic flux on geometric parameters of the tooth's zone in the optimization tasks for the AIM magnetic circuit. Fig. 3 shows an illustration of cross-section of magnetic field of AIG, where $Z_1 = 24$; $Z_2 = 10$; $\gamma = 1,45$.

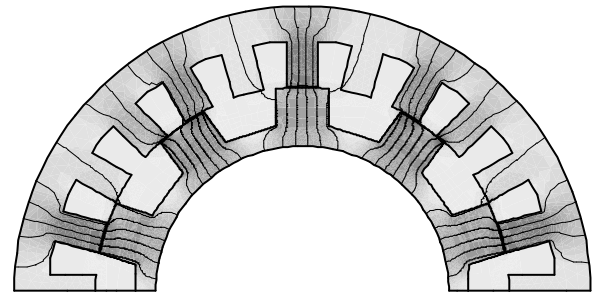


Fig. 3. Cross-section of magnetic field of AIG with $Z_1 = 24$; $Z_2 = 10$; $\gamma = 1,45$

The present work considers methods of definition of vector magnetic potential and magnetic flux for changeable parameters of the tooth's zone for the condition of permanent current in the machine's excitation windings which are outside the investigation area as it was already stated above. The methods proposed allow connecting the picture of magnetic field in cross-section of the machine with magnetomotive force of excitation winding. Special values of vector magnetic potential are chosen (that is in our case A_{AB}) for each geometry of the machine. The relation between the number of teeth of stator (Z_1) and rotor (Z_2), ratio of the width of slot to the width of the tooth of the rotor (γ) were chosen as changeable parameters for the solution of optimization issues. In all cases the magnetomotive force of excitation winding remains permanent even if geometrical values are changed. The algorithm of gaining of vector magnetic potential with the help of software «Quick Field» is presented below:

1. Optionally predetermine the value of vector magnetic potential (A_{AB}).
2. Find magnetomotive force within the tooth's zone (F_i) and total magnetic flux (Φ) for the predetermined value A_{AB} .
3. Calculate magnetomotive force values in axial magnetic core (F_c).
4. Sum up magnetomotive force values found in the tooth's zone and in the axial magnetic core; gain magnetomotive force of the excitation winding (F_{exc}) under the predetermined vector potential.
5. The value of electromotive force is known and by using Newton's interpolation we can obtain the

necessary values of vector magnetic potential, electromotive force of excitation winding and total flux. The present algorithm of gaining of vector magnetic potential should be estimated in each separate case, as in case of changes in the geometry of the tooth's zone, the zones change themselves as well as magnetomotive force values in the tooth's zone and in the magnetic core.

3. Objective function used for calculation of an axial inductor generator

In order to obtain optimal geometry of teeth area of two-core inductor generator having axial excitation and toothed windings it has to be used objective function, representing correlation between generator's nominal power and it's mass (3):

$$C = \frac{mU_N I_N}{G}, \quad (3)$$

where m is a number of phases; U_N , I_N are the nominal voltage and the current of a generator; G is a generator's mass.

If a generator runs at its nominal conditions (4), by reaching maximal power at active load the voltage is

$$U_N = \frac{E_0}{\sqrt{2}} \quad (4)$$

and the current (5)

$$I_N = \frac{I_k}{\sqrt{2}} = \frac{E_0}{x_S \sqrt{2}}, \quad (5)$$

In that case objective function is represented as follows (6):

$$C = \frac{mE_0^2}{2x_S}, \quad (6)$$

where E_0 is an electromotive force of no-load stroke; I_k is a short-circuit current; X_S is a synchronous resistance. Electromotive force of no-load stroke can be calculated by equation (7):

$$E_0 = \sqrt{2} \pi w_k f n_k k_{wl} \frac{\Phi_{\max} - \Phi_{\min}}{2}, \quad (7)$$

where w_k is a number of turns in toothed coil of armature winding; f is a frequency; n_k is a number of coils in each parallel branch; k_{wl} – winding coefficient; Φ_{\max} , Φ_{\min} – max and min magnetic flux of excitation, corresponding to disposition of stator tooth in relation to rotor tooth and in relation to rotor slot.

The following equation is true for synchronous resistance (8):

$$x_S = 2\pi f n_k w_k^2 \frac{\lambda_a}{a}, \quad (8)$$

where a is a number of parallel branches in armature windings; $\lambda_a = \frac{\Phi_{\max(k)} + \Phi_{\min(k)}}{2F_k}$ is an average

permeance ensured by magnetic flux of tooth, which is linked with the coil of armature winding dislocated on it and which is induced by short-circuit peak current ($F_k = \sqrt{2} w_k I_k$).

Since the frequency (9) is

$$f = \frac{Z_2 n_N}{60}, \quad (9)$$

but the number of coils in the parallel branch of a two-core generator (10) is

$$n_k = \frac{2Z_1}{ma}, \quad (10)$$

where Z_1 is a number of stator teeth; Z_2 is a number of rotor teeth; n_N is a nominal rotational speed.

The final expression of equitation is as follows (11)

$$c = \frac{\pi}{120G} k_w^2 n_N Z_1 Z_2 \frac{(\Phi_{\max} - \Phi_{\min})^2}{\frac{\Phi_{\max(k)} + \Phi_{\min(k)}}{F_k}}, \quad (11)$$

It has been assumed that, by choosing geometry of toothed area the higher harmonic components of magnetic flux of excitation are reduced up to "0".

Analysis of said expression shows that by increasing the number of stator and rotor teeth the nominal power of inductor generator also should increase. However if Z_1 and Z_2 values increase, the difference of magnetic flux ($\Phi_{\max} - \Phi_{\min}$) decreases in quadratic equitation. Therefore these values cannot increase indefinitely, i.e., optimal values for Z_1 and Z_2 do exist, which give maximum result of objective function. It brings to conclusion that in order to design optimal geometry of inductor generator both by size and by the shape of rotor and stator teeth it is necessary to carefully analyze magnetic field in the air gap of electrical machine and to determine conditions under which objective function, i.e., specific power of electrical machine reaches it's maximum.

4. Analysis of results obtained from objective function of inductor generator

The present paper shows calculation of objective function for obtaining the most rational geometry of axial inductor generator with power of 32 kW, produced by RER which has been used for power supply of carriages. The rated values of the basic type model are given below:

- nominal power – 32 kW;
- number of stator teeth – 24;
- number of rotor teeth – 10;
- ratio of the width of slot to the width of the tooth of the (γ) – 1,45;

- nominal rotational speed – 1000 RPM;
- excitation current – 3A;
- number of turns of the excitation winding – 1500;
- number of cores – 2;
- length of stator/rotor core – 115 mm;
- winding – three phases tooth winding;
- outer stator diameter – 458,3 mm;
- stator bore diameter – 329,3 mm;
- height of stator tooth – 36 mm;
- width of stator tooth – 25 mm;
- steel grade of the stator and the rotor – 2211.

The basic dimensions of the machine are as follows: the number and form of armature teeth, data about the winding, dimensions of axial magnetic core and excitation winding remain without changes. The parameters changed were: the number of teeth of the rotor, and their relative width. Modeling of the electromagnetic field was performed for the value of the teeth of the inductor $Z_2=8,10,11;12;13;14,16,17$ in case of ratio of the width of slot to the width of the tooth of the rotor $\gamma=1,2;1,4;1,45;1,5;1,55;1,7;1,9$. Optimum had been reached with values $Z_1=24; Z_2=14\div 16$, however when $Z_2=16$, due to the lack of distribution effect of winding the shape of curve of electromotive force becomes worse, and when machine is running it increase noise and vibration. Therefore $Z_2 = 14$ as an optimal number of inductor teeth was selected. Fig. 3 shows a curve of objection function in relation to excitation current, where $Z_2=10, \gamma=1,45$ – for basic sample, and if $Z_2=14; \gamma=1,7$.

The Fig.4 shows, that optimum has been reached when $Z_2=14; \gamma=1,7$. Meanwhile, if teeth are has been changed from $Z_2=10, \gamma=1,45$ to $Z_2=14, \gamma=1,7$, it allows to increase the specific power of generator by 12 %.

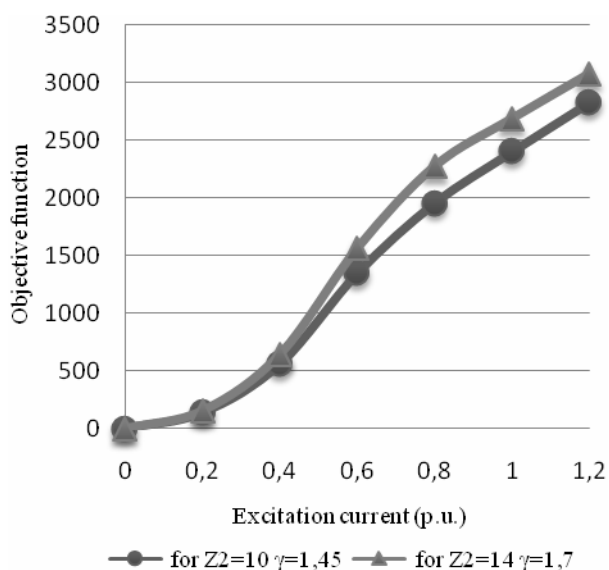


Fig. 4. Curves of dependence objective function of excitation current for $Z_2=10 \gamma=1,45; Z_2=14 \gamma=1,7$

5. Conclusion

The present paper describes the results of modelling of teeth area of the inductor generator with power of 32 kW. There is also illustrated the type of modelling of magnetic field, taking into account relation between vector magnetic potential and magnetic flux and geometrical parameters of teeth area. Proposed methodology allows defining relation between cross-section of magnetic field and electromotive force of the excitation winding. In order to obtain optimal geometry of teeth area of two-core inductor generator with axial excitation and toothed coils it has to be used objective function, representing correlation between generator's nominal power and it's mass. The calculation of objective function shows, that if the number of inductor teeth reaches 14, the specific power of axial inductor generator can be increased by 12 %.

6. References

1. Браканский У.К., Зайцев А.И., Звиедрис А.П. Некоторые методологические вопросы численного моделирования магнитных полей в аксиальных индукторных машинах. Latvian Journal of Physics and Technical Science, Riga, 1991, Nr.1, pp.87-94.
2. Домбур Л.Э. Аксиальные индукторные машины. Изд-во «Зинатне», Рига 1984, стр.247.
3. Orlova S., Pugachov V., Levin N. Magnetic field in the tooth zone of an axial inductor machine (AIM). 5th annual Conference of Young Scientists on Energy Issues – 29 May, 2008, Kaunas, Lithuania, CD proceedings. II-20 – II-27
4. QuickField User' Guide, version 5.5. WEB <http://www.quickfield.com>

THE EDGE EFFECTS INFLUENCE ON THE BRAKING FORCE OF LINEAR INDUCTION MOTOR

Bronius KARALIŪNAS, Edvardas MATKEVIČIUS
Vilnius Gediminas Technical University, Lithuania

Abstract: The main peculiarity when determining the difference between linear induction motors (LIM) and rotary motors is considered to be expressed in longitudinal and transversal edge effects. These effects in LIM appear due to the finite length and width of magnetic system of motors. Because of the mutual correlation of both effects, internal electric and magnetic asymmetry in linear motors is formed. Rotary type of motors does not have the characteristics of such asymmetry.

The work presents the research carried concerning the influence of longitudinal and transversal edge effects on the braking force of a LIM. The theoretical study is based on spectrum analysis method for magnetic fields and on Maxwell equations and Fourier integral changes. The same method is exercised in the assessment of the influence of longitudinal and transversal edge effects on the characteristics of a LIM and on transitional processes.

Keywords: linear induction motor, longitudinal effect, transversal effect, magnetic field, braking force, Reynolds's magnetic number.

1. Introduction

In new technologies there are widely used both rotary motors of common structure and linear electric motors. In cases when special technologies require linear or sliding motion there are applied LIM with the secondary element shorter than an inductor. Such an executing device with the help of a sliding magnetic field not only expels the secondary element conductive to electricity from the active zone of the inductor but has the capacity to perform the functions of an electromagnetic brake, a damper, a spring, an absorber and executes the other functions of an energy converter [1, 2]. The motors mentioned above could be successfully installed in compressors, in repulsion and shock hammering mechanisms, in aggressive and hazardous technologies such as for extraction of conductive metallic parts when utilizing and decontaminating mercury, luminescence, daylight lamps and other gas – discharge tubes.

In LIM because of their open magnetic circuit there are manifested the so called longitudinal and transversal edge effects. Because of that the characteristics and energy indexes of a LIM are worse than the indexes of analogous rotary type motors.

LIM practically are confronted with the phenomenon of braking the secondary element or the other moving parts. From all the known modes of electric braking the most extensively investigated is the mode of dynamic stationary braking, considering that the velocity of the secondary element at the moment of braking is constant [3]. However, the influence of edge effects on to the braking characteristics of a LIM is not sufficiently analyzed. The main parameter describing the efficiency of any braking mode is the braking force generated by a LIM.

The objective of the article is to investigate the influence of longitudinal and transversal edge effects on to the braking force of a LIM as well as to present the results of the computations processed.

2. Studies on edge effects of linear induction motors

When solving the problems of braking regarding a LIM, the main attention is devoted to the analysis of an electromagnetic field in respect to the influence of longitudinal and transversal edge effects. The available literature sources usually present the description of various reasonable mathematical models.

The processes of a stationary dynamic braking in a double – sided linear induction motor are also analyzed in work [4]. The influence of edge effects is assessed there when solving the problem of one – dimensional electromagnetic field by means of corresponding marginal conditions. There are some researchers who assess only longitudinal edge effect when analyzing the dynamic mode of braking, but the influence of transversal effect is suggested to be assessed by applying the correction coefficients of A. Voldek, Russell – Norsworthy or Preston – Rice. These coefficients do not depend on the operational mode of a motor i.e. on the change of velocity of the secondary element or on its slip. V. Skobelev [5] proposed the

empirical coefficient which depends only on the geometric measurements of a LIM:

$$K_F = \frac{1}{1 + \frac{0,63\tau^2}{2c(2b-2c)}}; \quad (1)$$

where $2b$ – is the width of the secondary element; $2c$ – is the width of the active zone (inductor); τ – is the pole pitch of an inductor.

H. Bolton [5] suggested a better way. He stated that the transversal edge effect depends not only on the parameters of a motor but on the slip s :

$$K_F = \frac{1 - \operatorname{Re} th(c\alpha_1 \sqrt{1 - is\varepsilon_0}) - sv\varepsilon_0}{1 - sv\varepsilon_0 + s^2\varepsilon_0^2 \operatorname{Re} th(c\alpha_1 \sqrt{1 - is\varepsilon_0})}; \quad (2)$$

where Re – is a real part of a complex number; th – a hyperbolic tangent; $i = \sqrt{-1}$ – imaginary unit; ε_0 – Reynolds's magnetic number; v and s – is the velocity of the secondary element and its slip; $\alpha_1 = \frac{\pi}{\tau}$ – is a special frequency of braking current and primary magnetic field.

S. Jamamura [6] determined the boundaries, when trying to reduce hazardous influence of transversal effect on the characteristics of a motor, the boundaries up to which it is advisable to widen the secondary element. Its coefficient is rather simple:

$$K_F = th \frac{\pi(b-c)}{\tau}. \quad (3)$$

The difference $(b - c)$ in the expression (3) indicates the size of ones sided widening of the secondary element in respect to the active zone c of a motor. When changing the argument, the value of hyperbolic tangent (3) gradually approaches unit one. Starting from the values 1.3 and more of an argument, K_F slightly differs from unit one, then comes the following:

$$\frac{\pi(b-c)}{\tau} \approx 1.3. \quad (4)$$

Then the relative value of widening of the secondary element will be the following:

$$\frac{b-c}{\tau} \approx 0.41. \quad (5)$$

The achieved result (5) indicates that single – sided widening of the secondary element behind the boundaries of an inductor has to be not higher than 41% from the pole pitch τ . There is no need to widen the secondary element, because this measure does not give a positive effect and doesn't have any possibility for practical application.

The influence of the edge effects on such technologies is evaluated by the brought in resistances of the

resultant scheme as well as by the coefficients of correction.

3. Computation of braking force

In this work the braking force is calculated following the theoretical simulation model of a LIM which is presented in sources [7, 8]. According to the model, for the analysis of all electric modes of braking there is applied spectrum method based on the equations of the electromagnetic field and Fourier integral transformations along the longitudinal axis of a motor.

At first, in accordance with the assumed wave of volume density of braking current there is calculated complex amplitude \underline{H} of the strength of the total magnetic field. There was obtained that the magnetic field in the air gap of a motor is comprised of two components:

$$\underline{H} = \underline{H}_1 + \underline{H}_2; \quad (6)$$

where \underline{H}_1 – is the complex amplitude of the primary or inductor generated magnetic field; \underline{H}_2 – is the complex amplitude of the magnetic field generated by the induced currents in the secondary element.

By applying spectrum method together with the expressions of theory of residuum, it is possible to calculate by analytic method magnetic fields \underline{H}_1 and \underline{H}_2 concerning any electric braking mode. Then an electromagnetic braking force generated within the active zone boundaries of a motor is easy to calculate by means of the following type of volume integral:

$$F_{elm} = -\frac{\mu_0}{2} \operatorname{Re} \int_{(V)} \underline{H}_2 \underline{j}(x,t) dV; \quad (7)$$

where $\mu_0 = 4\pi 10^{-7}$, H/m – is magnetic permeability of the secondary element; $\underline{j}(x,t)$ – is the joint complex of volume density of the braking current; V – is the volume of the secondary element where the braking force is generated and according to which expression (7) is integrated.

After solving integral (7) for any braking modes there are derived rather complicated mathematical expressions indicating that braking force consists of three components:

$$F_{elm} = F_1 + F_2 + F_3; \quad (8)$$

where F_1 – is the braking force component, estimating only transversal edge effect as well as the change of velocity of the secondary element and validated for a motor with an infinite long active zone; F_2 – is a free component of the braking force, existing only during the transitional process; F_3 – is force component evaluating longitudinal and transversal edge effects and their mutual correlation.

In case of dynamic braking, when the direct current

flows through the inductor windings, the following expression is derived to calculate component F_3 :

$$F_3 = -F_0 \operatorname{Re} \frac{1}{p\pi^3} \sum_{k=0}^{\infty} \frac{\varepsilon_0 v_{0n} \sin^2 \left[\frac{\pi(2K+1)}{2\xi} \right]}{\xi \left(\frac{c}{\tau} \right)^2 \sqrt{(\varepsilon_0 v)^2 + n_K^2}} \times$$

$$\times \left\{ \frac{1 - \exp \left[-\pi p \left(-\varepsilon_0 v + \sqrt{(\varepsilon_0 v)^2 + n_K^2} \right) \right]}{\beta_{K3} (\varepsilon_0 v_{0n} - \beta_{K3}) (1 - i\beta_{K3})^2} + \right.$$

$$\left. + \frac{1 - \exp \left[-\pi p \left(\varepsilon_0 v + \sqrt{(\varepsilon_0 v)^2 + n_K^2} \right) \right]}{\beta_{K4} (\varepsilon_0 v_{0n} - \beta_{K4}) (1 - i\beta_{K4})^2} \right\}; \quad (9)$$

where F_0 – is an ideal braking force of a LIM without the edge effects; p – is the number of pairs of an inductor poles; v_{0n} – is the initial velocity of braking of the secondary element; c/τ – is relative width of an active zone; $\xi = b/c$ – is relative width of the secondary element; β_{k3} and β_{k4} – are the roots of the characteristic equation:

$$\begin{cases} \beta_{K3} = \frac{\varepsilon_0 v - \sqrt{(\varepsilon_0 v)^2 + n_K^2}}{2}; \\ \beta_{K4} = \frac{\varepsilon_0 v + \sqrt{(\varepsilon_0 v)^2 + n_K^2}}{2} \end{cases}; \quad (10)$$

$$n_K = \frac{2K+1}{\xi c/\tau}; \quad K = 0; 1; 2; 3; \text{ and etc.}$$

In the expressions of force components F_1 and F_2 the influence of transversal edge effect is evaluated by coefficient h_s . For a LIM model, where the secondary element is wider than the active zone of an inductor ($b > c$), there was derived the following expression of the coefficient of transversal edge:

$$h_s = \operatorname{Re} \left\{ 1 - \frac{\operatorname{sh}(\pi c/\tau \sqrt{1 - i\varepsilon_0 v})}{\pi c/\tau \sqrt{1 - i\varepsilon_0 v}} \times \right.$$

$$\left. \times \frac{\operatorname{ch} \left[\pi c/\tau (\xi - 1) \sqrt{1 - i\varepsilon_0 v} \right]}{\operatorname{ch} \pi (c/\tau) \xi \sqrt{1 - i\varepsilon_0 v}} \right\}; \quad (11)$$

where v – is the velocity of the secondary element at the moment of braking.

4. The results of computations

In order to analyze the edge effects, it is very comfortable to calculate all the components of the braking force by relative units. For that purpose braking force F_0 of an ideal motor is taken by the basic quantity. Following the derived expressions (9) – (11) there were calculated dependencies of relative forces F_3/F_0 and coefficient h_s on the parameters of a motor and geometric measurements by means of software Mathcad 2001 Professional.

Dependencies of braking forces F_3/F_0 on the width c/τ of an active zone of a motor are presented in Fig. 1.

Fig. 2 presents the curves indicating the variation of force F_3/F_0 which depends on number p of the pairs of poles of a motor. Analogous dependencies on the relative width ξ of secondary element are presented in Fig. 3.

Dependencies of coefficient h_s on width c/τ of a motor are presented in Fig. 4.

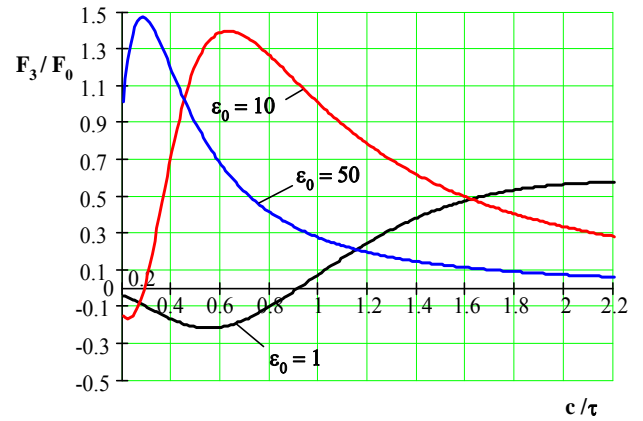


Fig. 1. Dependencies of relative braking force F_3/F_0 on the width c/τ of an active zone, when Reynolds's numbers are different and $p=1,0$; $v_{0n} = 1,0$; $\xi = 1,4$

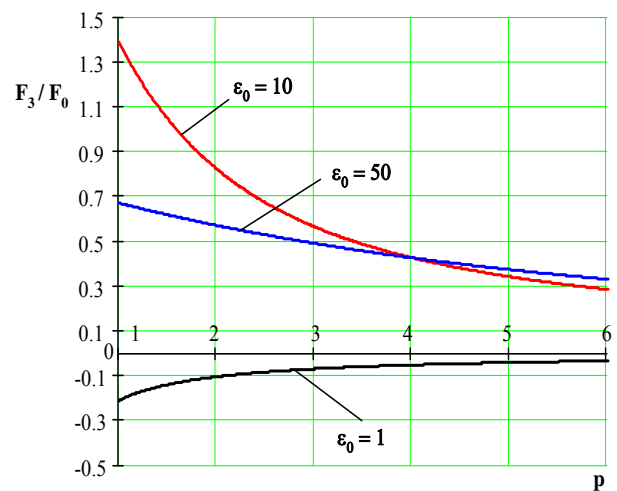


Fig. 2. Dependencies of relative braking force F_3/F_0 on the number of pairs of poles of a motor, when Reynolds's numbers are different and $v_{0n} = 1,0$; $c/\tau = 0,6$; $\xi = 1,4$

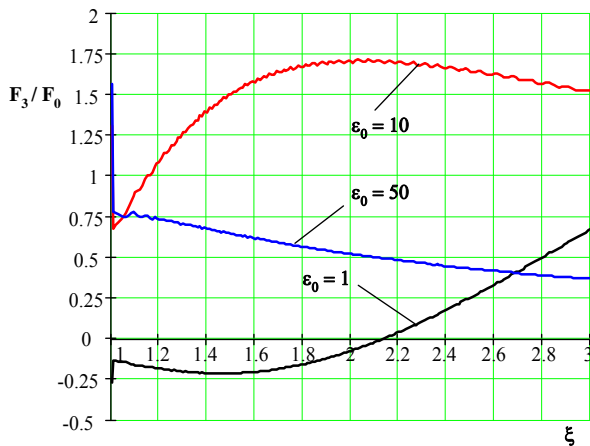


Fig. 3. Dependencies of relative braking force on relative width of the secondary element, when Reynolds's numbers ε_0 are different and $p=1,0$; $v_{0n} = 1,0$; $c/\tau = 0,6$

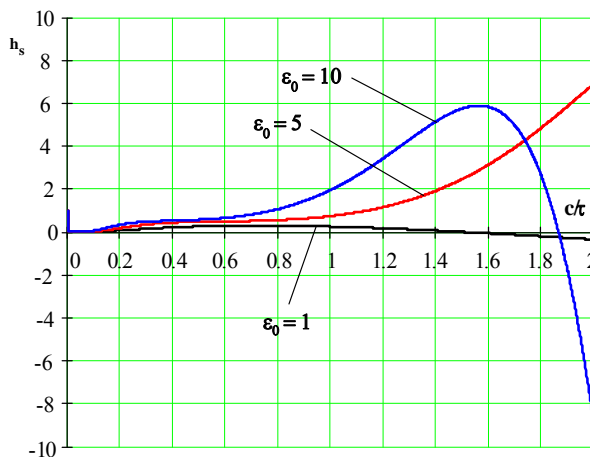


Fig. 4. Dependencies of coefficient h_s of the transversal effect on the width of a relative active zone when Reynolds's numbers ε_0 are different and $\nu=0,8$; $\xi = 1,4$

The results of computation indicate that components F_1 and F_2 of the braking forces depend on the transversal edge effect, which is characterized by coefficient h_s given in expression (11). Due to that the longitudinal edge effect for the mentioned above components has no influence.

From the submitted curves it is obvious that the most significant influence onto the relative force F_3/F_0 is caused by transversal and longitudinal edge effects and their mutual correlation. However, the influence onto the motors with different Reynolds's numbers is not equal. When Reynolds's numbers are low ($\varepsilon_0 \leq 3,0$), the edge effects weaken the braking force and therefore, the braking of these types of motors is not efficient. When Reynolds's numbers are increasing the transversal edge effect exhibits itself in the most significant way in relatively narrow sized motors where $c/\tau \leq 0,8$. Widening of the secondary element behind the boundaries of an active zone ($\xi > 1,0$) tends to weaken the transversal edge effect as well.

5. Conclusions

1. To calculate braking force of a LIM the authors applied spectrum analysis of magnetic fields which is based on Maxwell equations and Fourier integral transformations along the longitudinal axis of a motor.
2. There is determined that electromagnetic braking force is generated by three components in which there is assessed the influence of transversal and longitudinal edge effects, their mutual correlation as well as the change of velocity of the secondary element at the moment of braking.
3. The results of calculations made indicate that the influence of edge effects of a LAM with different Reynolds's numbers is irregular. The transversal edge effect is the most intensively expressed in relatively narrow motors. The widening of the secondary element behind the boundaries of the active zone of a motor enables to reduce the influence of transversal effect on the braking force. By increasing the number of pairs of inductor poles the influence of longitudinal effect on the braking force has a tendency to be weakened. If $p > 4,0$, then it is possible not to consider the longitudinal edge effect in braking force calculations.
4. The derived results could be implemented in designing a new LAM and in compiling the most optimum systems of their braking .

6. References

1. Laitwaite E. R. A History of Linear Electric Motors. London, 1986. 178 p.
2. Boldea I. Linear Electric Actuators and Generators. IEEE Transactions of Energy Conversion, vol. 14, No. 3, 1999. p. 712-716.
3. Скрябина Г. И. Исследование характеристик линейной асинхронной машины в двигательном и тормозных режимах. Дисс. канд. техн. наук. Ленинград, 1978. 252 с.
4. Nonaka S. Simplified Fourier Transform Method of LIM Analysis Based on Space Harmonic Method. Proceedings of Second International Symposium on LDIA'98, Tokyo, Japan, 1998. p. 187-190.
5. Karaliūnas B. Trinties jėgų komprnsavimas lėktuvo valdymo sistemoje. Elektronika ir elektrotechnika, Nr. 1(19), Kaunas, 1999. p. 53-56.
6. Ямамура С. Теория линейных асинхронных двигателей. Ленинград, 1983. 180 с.
7. Karaliūnas B. Non Stationary Processes in the Electric Machine Converters of Energy. Proceedings of Electrotechnical Institute, vol. 200/99, Warszawa, Poland, 1999. p. 99-112.
8. Darulienė O., Karaliūnas B. Mathematical Model of Non – Stationary Processes of Electromechanical Power Converters. Proceedings of 11-th International Conference on Power Electronics and Motion Control, EPE – PEMC'2004, vol. 3, Riga, Latvia, 2004. p. 415-419.

MODELING OF TWO-MASS SYSTEM WITH ELASTICITY

Sigitas JURAITIS, Roma RINKEVIČIENĖ, Jonas KRIAUCIŪNAS
Vilnius Gediminas Technical University, Lithuania

Abstract: Dynamics of two-mass electromechanical system with clearance and elements capable to deform is considered. Model for investigation of influence of elasticity and clearance is presented. Induction motor is used to drive two-mass system. Speed responses of the system are presented and analyzed. Influence of elasticity and clearance to speed response is considered.

Keywords: two-mass electromechanical system, influence of elasticity and clearance, simulation.

1. Introduction

Electromechanical system as object of investigation comprises electrical and mechanical parts. Electromechanical power converter and its control system depends to electrical part as well as all moving masses coupled between themselves form mechanical part. Electromechanical system includes various mechanical chains, with infinite or finite elasticity and clearance. Systems with infinite stiffness and without clearance are one-mass systems and are quite well analyzed [1, 2, 3]. Systems with capable to deform chains and clearance are more complex. They are described by high order nonlinear differential equations, and without essential simplifying of problem they cannot be solved in analytical way. In these cases computer models of solved program must be developed, using specialized software, and system responses simulated.

Some problems of two-mass system were considered in [4, 5, 6, 7, 8, 9, 10].

The paper presents general model of two-mass system, developed in Simulink. Results simulations at different stiffness of two-mass system and different clearance are presented and considered. Dependences of maximal speed values against elasticity factor and clearance are formed and presented.

2. Model of two-mass system with clearance

Two-mass system is described by set of equation:

$$\begin{cases} M - M_{st1} - M_{12} = J_1 \frac{d\omega_1}{dt}; \\ -M_{st2} + M_{12} = J_2 \frac{d\omega_2}{dt}. \end{cases} \quad (1)$$

Torque of elasticity is calculated as:

$$M_{12} = c_{12} \cdot (\varphi_1 - \varphi_2), \quad (2)$$

where c_{12} is stiffness of elastic mechanical part. All other notations are as in [4].

Rotational stiffness c_{12} is given by:

$$c_{12} = \frac{M}{\theta}, \quad (3)$$

where M is the applied torque, θ is the rotation angle. Rotational stiffness is typically measured in newton-metres per radian. In general, elastic modulus is not the same as stiffness. Elastic modulus is a property of the constituent material, stiffness is a property of a solid body. That is, the modulus is an intensive property of the material, stiffness, on the other hand, is an extensive property of the solid body dependent on the material and the shape and boundary conditions.

Differentiating equation (2) yields:

$$\frac{dM_{12}}{dt} = c_{12} \cdot \left(\frac{d\varphi_1}{dt} - \frac{d\varphi_2}{dt} \right) = c_{12} \cdot (\omega_1 - \omega_2). \quad (4)$$

Equation (4) in frequency domain looks like this:

$$\begin{cases} M - M_{st1} - M_{12} = J_1 s \omega_1; \\ -M_{st2} + M_{12} = J_2 s \omega_2; \\ s M_{12} = c_{12} (\omega_1 - \omega_2). \end{cases} \quad (5)$$

Portion of two-mass system with kinematic clearance is shown in Fig. 1, a. Due to the clearance, dependence $M_{12} = f(\Delta\varphi)$ is nonlinear (Fig. 1, b).

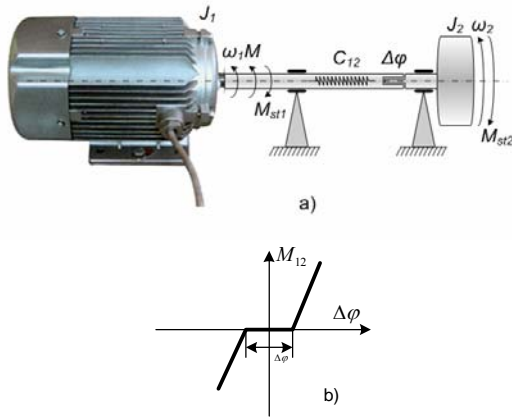


Fig. 1. View of two-mass system with clearance (a) and dependence $M_{12} = f(\Delta\varphi)$ (b)

Two-mass system movement equations in frequency domain can be expressed as [4]:

$$\begin{cases} M - M_{st1} - M_{12} = J_1 s \omega_1; \\ -M_{st2} + M_{12} = J_2 s \omega_2; \\ M_{12} = c_{12} \left(\varphi_1 - \varphi_2 - \frac{\Delta\varphi}{2} \right), \text{ when } |\varphi_1 - \varphi_2| > \frac{\Delta\varphi}{2}; \\ M_{12} = 0, \text{ when } |\varphi_1 - \varphi_2| \leq \frac{\Delta\varphi}{2}. \end{cases} \quad (6)$$

Equation 6 shows both system masses moving independently one from other while system operates in the clearance zone.

At starting of the drive with load three stages of response can be separated. In the first stage, while $M_{12} = 0$, the speed of second mass ω_2 also is equal to zero. Due to this effect the speed of the first mass rises quickly because torque, developed by motor M is greater than load torque M_{st1} . Afterwards the second stage of starting begins. Clearance already is absent, but speed ω_2 remains equal to zero, while increasing torque M_{12} becomes greater than M_{st1} . Afterwards speed begins to rise. This speed influences dynamic load of the second load.

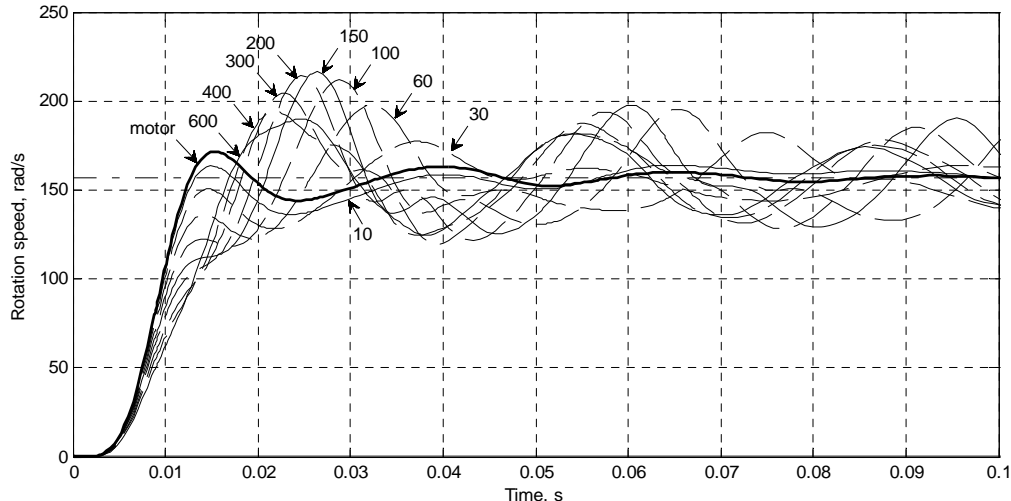


Fig 3. Speed transients at different elasticity

3. Development of model and simulation of the system

Computer model is elaborated for a motor, which parameters are presented in Table 1.

Table 1. Parameters of a motor

Parameter	Value
Motor power, kW	1,1
Number of pole pairs	2
Phase voltage, V	230
Power factor	0,81
Rated torque, N·m	7
Rated current, A	3,56
Inertia, kg·m ²	0,00262

The second mass is chosen freely. Let it will be by cylindrical shape body, fastened along mass center (see Fig. 1). Its inertia is calculated in this way:

$$J = \frac{m \cdot r^2}{2}, \quad (7)$$

where m is mass of cylinder and r is radius of cylinder. It is assumed in simulation $J=0,0025\text{kg}\cdot\text{m}^2$.

Model of induction motor operating with two-mass system is presented in [7]. The general simplified form of model is presented in Fig. 2.

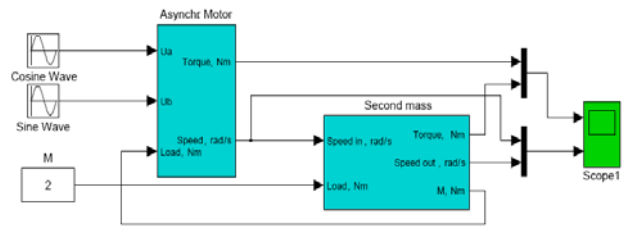


Fig. 2. Model of two-mass electromechanical system

Response of motor speed at different values of stiffness is presented in Fig.3.

Simulation results are compared with results of one-mass system operating at no-load for exploring dependences of system parameters influence. Clearance is determined by time duration after which the first mass (motor) starts to move the second mass. Stiffness value was chosen freely for getting dependences of speed maximum value against stiffness. Comparison of simulation results indicate motor speed lag in two-mass system, depending on stiffness, with speed of motor, operating in one-mass system. That depends on the load torque, developed by second mass. After the shaft dislodges the second mass, the motor speed reaches the greater value than that at no load due to inertia of the second mass accelerating the motor. Oscillations of speed in steady-state also are greater because elasticity of the shaft. The shaft under rotation of motor is being twisted and deformed. In this way it accumulates energy and delays the influence of the

second mass, causing oscillations of the speed. Dependence of the speed against elasticity is presented in Fig. 4. The greatest values of the first and second maximum are marked in this figure. The solid thick line corresponds to motor speed at no-load. With increasing of stiffness the greatest speed approaches the speed transient of one-mass system. At first the second amplitude of oscillations reduces, then increases and reaches the maximum value, afterwards it begins to reduce again. According to simulation results, the system reaches the greatest value at proper elasticity, which is undesirable due to great speed oscillations. On the other way, if the elasticity is small, maximum speed is smaller. This operation mode can be used to avoid speed impact during starting.

Speed response at constant elasticity and different clearance values is presented in the Fig. 5.

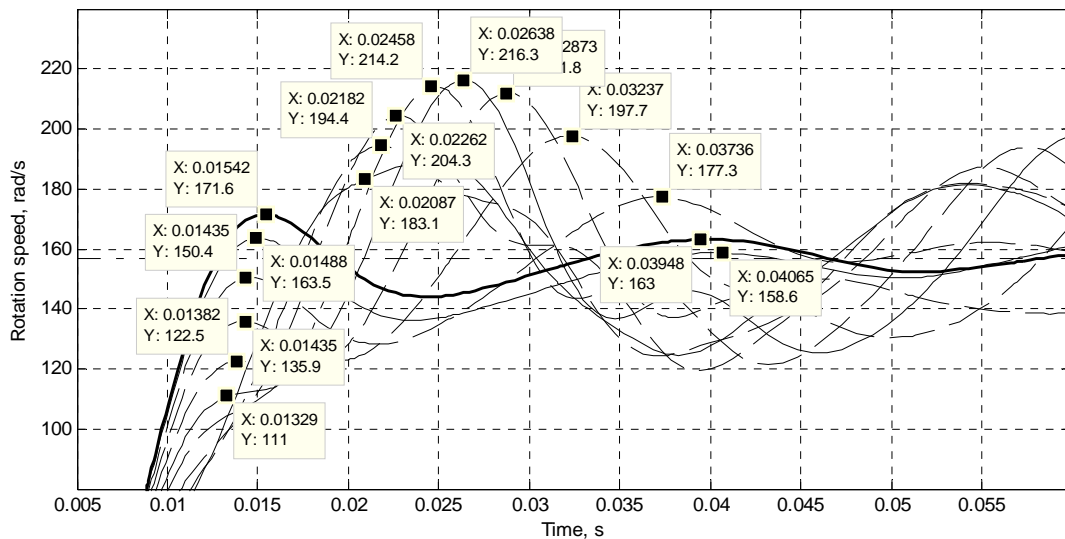


Fig 4. Speed transients maximum values at different elasticity

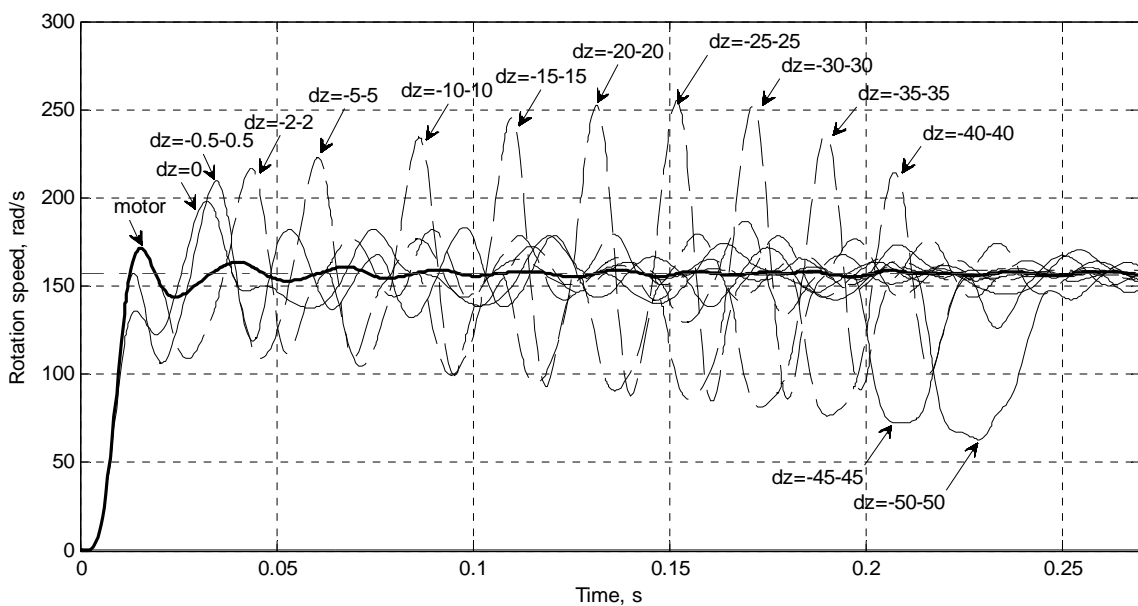


Fig 5. Speed transients maximum values at different clearance

Curves, presented in Fig. 4 indicate the shorter time required to reach the speed maximum with increasing elasticity and greater oscillations frequency as well as longer set-up time. Fig. 6 presents the peak speed values at varying elasticity factor, obtained from simulation results in Fig. 4.

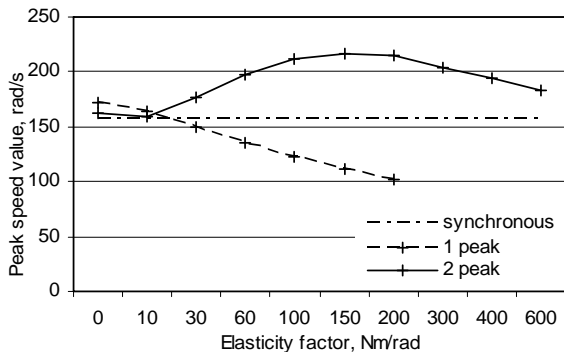


Fig 6. Dependence of the speed maximum against elasticity

Dependence of peak speed values, obtained from Fig. 5, is presented in Fig. 7.

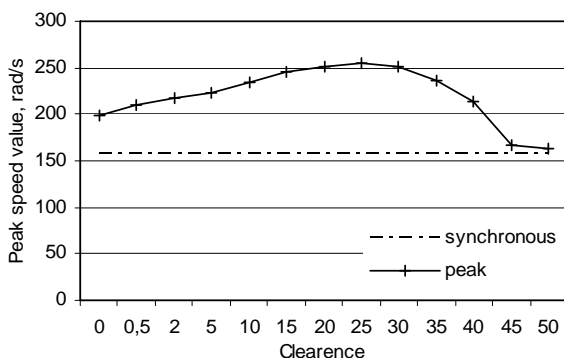


Fig 7. Dependence of the speed maximum against clearance

Peak speed value reaches its maximum at clearance factor, approximately equal to 25.

Dash line in Fig. 7 denotes synchronous speed of motor. The greatest peak speed exceeds synchronous speed approximately 45 percent. Motor at this time operates in regenerative mode.

4. Conclusions

1. Finite stiffness causes angular speed oscillations of two-mass system, which amplitude, frequency and set-up time depends on value of stiffness.
2. Value of finite stiffness can reduce undesirable speed overshoot; otherwise this phenomenon can be used to reach the greatest value of speed.
3. In the system with clearance beginning of starting transients corresponds to starting transients of the drive at no load. During this time motor speed increases by exponential law.
4. Clearance causes dynamic torques in electromechanical system, whose values increase with the increase of clearance.

5. The maximum speed value increases proportionally to clearance. At the great clearance, when the movement to second mass is transmitted at steady-state speed of the motor, the maximum speed during transients is not significant.

5. References

1. Schönfeld R., Hofmann W. Elektrische Antriebe und Bewegungsteuernungen. Vde - Verlag. 2005. s. 454.
2. Vogel J. Elektrische Antriebstechnik. 5. bearb. Aufl. Hüttig, Buchverlag, 1991.
3. Masteika R. K. Mechanics of electric drives. Kaunas: Technologija, 1996. 40 p. In Lithuanian.
4. Smilgevičius A., Rinkevičienė R. Simulation of transients in the Mechanical part of Electromechanical system // Mathematical Modelling and Analysis Proceedings of the 10th International Conference MMA2005&CMAM2, Trakai. 2005. p. 155-162.
5. Rinkevičienė R., Batkauskas V. Modelling and Investigation of Vector Controlled Induction Drive. Elektronika ir Elektrotechnika. Electronics and Electrical Engineering. 2008 No.1 (81). p. 53 - 56.
6. Smilgevičius A., Rinkevičienė R., Savickienė Z. Operation of electric motor with elastic load. Elektronika ir elektrotechnika. Electronics and Electrical Engineering. 2006, Nr. 6(70), p. 15 -18.
7. Juraitis S., Rinkevičienė R., Smilgevičius A. Dynamic properties of two-mass electromechanical system. 6th International Symposium „Topical Problems in the Field of Electrical and Power Engineering“. Kuressaare 2009, p. 18-21.
8. Feiler M., Westermaier C., Schroder D. Adaptive speed control of a two-mass system.//CCA 2003. Proceedings of 2003 IEEE Conference on Control Applications, 2003.Vol. 1, 23-25 June 2003, p. 1112 – 1117.
9. Kara T., Eker I. Experimental nonlinear identification of a two mass system. CCA 2003. Proceedings of IEEE Conference on Control Applications, 2003.Vol. 1, 23-25 June 2003, p. 66 – 71.
10. Bolognani S., Venturato A., Zigliotto M. Theoretical and experimental comparison of speed controllers for elastic two-mass-systems.//IEEE 31st Annual Power Electronics Specialists Conference, 2000. PESC 00. Vol. 3, 18-23 June 2000. p. 1087 – 1092.

THE MEANS OF ELECTROMAGNETIC FLOW METER MAGNETIC CIRCUIT TESTING

Valdas Jonas PAKĖNAS, Juozapas Arvydas VIRBALIS
Kaunas University of Technology, Department of Electrical Engineering, Lithuania

Abstract: The measurement accuracy of electromagnetic fluid flow meter depends on parameters of magnetic circuit and distribution of magnetic field inside of transducer active zone. The stability of magnetic circuit parameters and magnetic field distribution can be monitored by control coils or using for monitoring one of magnetic field exiting coils. The magnetic circuit parameters can vary because of three main reasons. The reasons are the following: the magnetic admixtures inside fluid, the magnetic sediments on channel wall and the variation of circuit permeability. When two control coils are used, the unwarrantable variation of magnetic flux and the reason of this variation can be set.

Keywords: Electromagnetic fluid flow meter, magnetic field distribution, control coil.

1. Introduction

The quantitative characteristics of fluid flow: local and mean velocity, the mass and volume flow and quantity are important for many technological processes and commercial accounts. Its measurements compose about 40% of all technological measurements which are performed in industry. The conventional problems are the accounting of drinking and industrial water and heat measurement. The actual problems with arising of ecology requirements are the accounting of sewages, the batching of different special fluids and other. The significant part of meters using for this purposes are the electromagnetic fluid flow meters EMFM. The EMFM are convenient for use in different informational and control systems and in the devices, intended for different combined measurements, par example, in heat meters. The modern EMFM are intellectual devices, in which the microcomputers are used for measurement cycle organization, for subsidiary parameters calculation, for parasitic signals suppressing, for measurement error diminishing.

The mean advantages of EMFM are absence of resistance to fluid flow, practically non-inert measurement, linear transfer characteristic and small measurement uncertainty. There is what for commercial

accounting of fluid and transporting by fluid heat practically only EMFM and ultrasonic meters are used.

When fluid flows in non-moving magnetic field the electric field arises. The electric field strength E by Faraday's law of electromagnetic induction in any point of flow can be expressed as vector product flow velocity vector v and magnetic flux density vector B in this point: $E_F = v \times B$. If the electrodes are mounted in the walls of channel, the difference of potentials U_i arises in the electrodes. It can be expressed when fluid is directed by channel axis, i.e, the flow velocity in any flow point has only one component $v = v_z v_z$, this way:

$$U_i = \int_{\tau} v_z W_z d\tau. \quad (1)$$

There $d\tau$ is element of EMFM sensor active zone volume τ , W_z is weight function. Active zone is flow volume in which electrode signal is forming, i.e, magnetic field is acting. The weight function is proportional to component of magnetic flux density B_y , perpendicular to flow and to the line which connects the electrodes: $W_z = K_v B_y$. Usually EMFM are used for measurement of volume fluid flow Q . By (1) electrode signal of EMFM must depend on distribution of velocity in cross-section of channel. But superabundance of experimental investigations shows [1], that when the distribution of magnetic field in active zone is close to uniform, we can suppose that electrode signal is proportional to fluid flow in all diapason of flow values. The transfer coefficient of EMFM is not depended on flow and proportional to total magnetic flux Ψ , which passes via EMFM transducer:

$$U = KQ, \quad K = K_1 \Psi, \quad (2)$$

where $K_1 = \text{const}$. The transfer coefficient K is setting when EMFM is calibrated and it must be constant along all time between two metrological assessments. Coefficient K_1 depends on geometrical dimensions of device and it is practically constant. Therefore the stability of EMFM transfer coefficient depends on

stability of magnetic flow Ψ and on its distribution in EMFM active zone. We can guarantee the EMFM measurement results metrological reliability when stability of magnetic flow Ψ will be constantly monitored.

2. Magnetic circuit of EMFM and means of its monitoring

Typical magnetic circuit of EMFM is presented in Fig. 1. The particularity of this circuit is the large air gap. The rectangular current pulses are used for magnetic field excitation in the most of all electromagnetic flow meters. The frequency of these pulses is not exceeded some Hz. The invariability of EMFM transfer coefficient will be warranted when the magnetic flux Ψ and its distribution inside sensor active zone will be invariable.

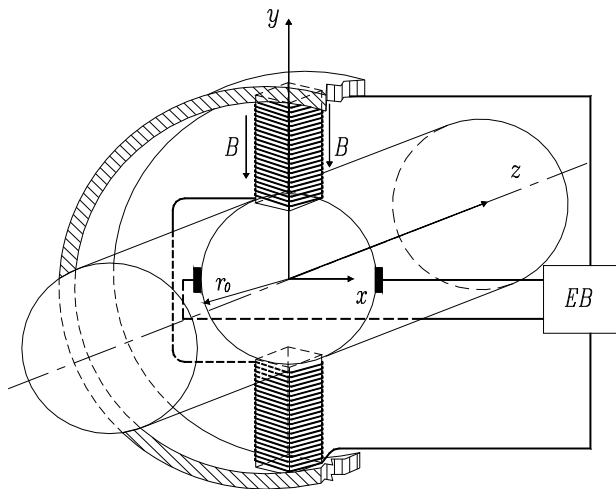


Fig. 1. Magnetic circuit of EMFM sensor

The merest way of magnetic flux monitoring is the use of one or two complementary control coils CC1 and CC2. They can be mounted between one of magnetic field excitation coil and channel as it is showed in Fig. 2. The voltages U_{r1} and U_{r2} , proportional to magnetic flux of sensor active zone, arise in the coils CC1 and CC2, correspondingly.

But this way is suited to the case, when sensor is designing. When the EMFM sensor is produced without the control coil, the magnetic flux inside the EMFM sensor can be monitored by one of excitation coils. In this case we can measure the control coil voltage instead of the flow measurement.

The possible excitation current generation circuit is showed in Fig. 3 by bold lines. The switch S is in the 1 position. In this case the magnetic field excitation current is directed via both excitation coils EC1 and EC2, when the pulse with amplitude U_e acts on the input of voltage to current converter VCC. The flow is measuring in this case.

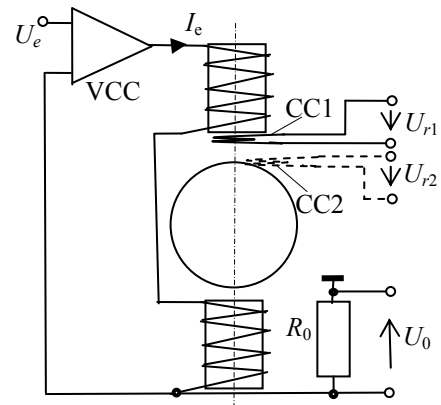


Fig. 2. The EMFM sensor with control coils

When the switch is turned into position 2, the excitation current is directed via only one excitation coil EC1. The voltage U_r , which arises in the excitation coil EC2 can be used for magnetic flux monitoring.

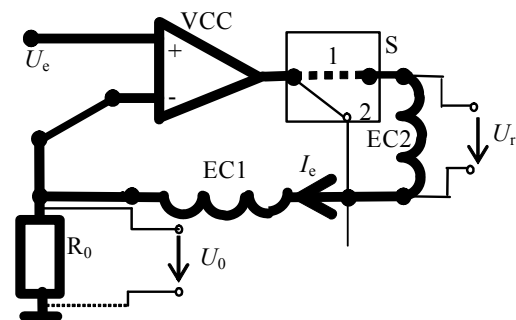


Fig. 3. The use of excitation coil for magnetic flux monitoring

The some part Ψ_r of common flux Ψ passes via control coil independently on chosen monitoring technique: using the special control coils or using one of the excitation coils. This part is proportional to common magnetic flux. In turn the common magnetic flux Ψ is proportional to excitation current i_e . Therefore we can write:

$$\Psi_r = K_{\Psi} i_e, \quad (3)$$

where $K_{\Psi} = \text{const}$ is coefficient of proportionality. The processor of EMFM forms the series of pulses with amplitude U_e . The timescale of pulse T_m is equal to the timescale of pause T_p . The pulse and the pause compose one measurement cycle. When the pulse with amplitude U_e begins to act in input of voltage to current converter (see Fig. 3 and Fig. 4) the excitation current arises exponentially:

$$i_e = I_0 (1 - e^{-\frac{t}{\tau_e}}); \quad (4)$$

where $\tau_e = L_e / R_r$ is time constant of exciting circuit, L_e and R_r are the total inductivity and resistance of exciting coil (or coils), correspondingly. After time interval $\Delta t = (4 \div 5) \tau_e$ the magnetic field excitation current

practically becomes equal to I_0 . The excitation current time diagram of one cycle is showed in Fig 4.

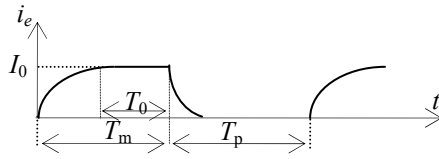


Fig. 4. The form of exciting current

The electrodes signal is measured in the time interval when the excitation current $i_e=I_0$. By (2) and (3) we can write:

$$U=K_1K_\psi I_0 Q. \quad (5)$$

We can suppose, that transform coefficient is constant when coefficient K_ψ value is not varied with respect to value $K_\psi=K_{\psi 0}$ obtained in the moment of EMFM calibration. Therefore the monitoring of coefficient K_ψ must be performed.

3. The monitoring technique

The monitoring technique is the same in the both cases: when there are used the special control coils or one of excitation coils for magnetic flux measurement.

For the accurate coefficient K_ψ evaluation two measurements are performed. In the first measurement cycle the basic voltage U_0 is measured and in other cycle the voltage of control coil is measured.

The monitoring circuit is presented Fig. 5.

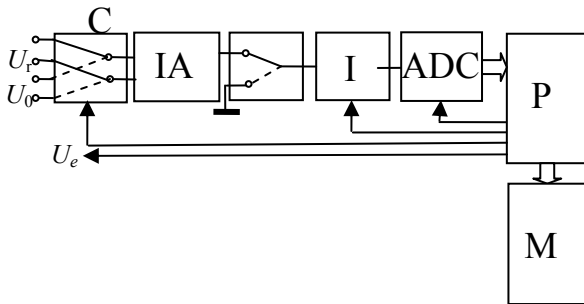


Fig 5. The monitoring circuit

There are in this circuit: IA – input amplifier, I - integrator, ADC converter analog-to-digital, P - processor, C – commutator, M – memory unity.

At first the voltage $U_0=R_0I_0$ is connected via commutator C to amplifier IA input. This voltage acts in resistor R_0 (see Fig. 2 or Fig. 3), when the transient process is finite and excitation current i_e is equal to I_0 (interval T_0 in the time diagram, presented in Fig. 4).

Therefore the voltage U_0 is connected to IA input during the interval T_0 . This voltage amplifies into amplifier IA and integrates during all interval T_0 . After the end of interval T_0 the integrator output voltage is equal:

$$U_{I0}=K_{IA}I_0R_0T_0/\tau_i, \quad (6)$$

where τ_i is integrator time constant, K_{IA} – amplification coefficient of IA.

The potential equal to zero connects to integrator input and the integrator output connects to ADC input in this moment. We obtain in the ADC output the number N_0 :

$$N_0=K_{ADC}U_{I0}=K_{ADC}K_{IA}I_0R_0T_0/\tau_i, \quad (7)$$

where K_{ADC} is transfer coefficient of converter ADC. The number N_0 is stored into memory M, and integrator output is setting to zero.

The second measurement performs when other current cycle begins. The voltage U_r of control coil connects to IA input. The integration of amplified voltage begins with current pulse beginning in this case.

The control coil voltage U_r is equal to derivative of total magnetic flux which passes via this coil. We obtain evaluating (3) and (4)

$$U_r = \frac{d\Psi_r}{dt} = K_\psi \frac{di_e}{dt} = \frac{K_\psi I_0}{\tau_e} e^{-t/\tau_e}. \quad (8)$$

This voltage after amplifying is integrating along all excitation current pulse T_m . The integrator output voltage will be equal after integration:

$$U_{Ir} = \frac{1}{\tau_i} \int_0^{T_m} \frac{K_{IS}K_\psi I_0}{\tau_e} e^{-t/\tau_e} dt = \frac{K_{IS}K_\psi I_0}{\tau_i} e^{-t/\tau_e} \Big|_0^{T_m} = \frac{K_{IS}K_\psi I_0}{\tau_i}. \quad (9)$$

This voltage analogically to voltage U_{I0} is converted to number N_r in ADC:

$$N_r=K_{ADC}U_{I0}=K_{ADC}K_{IA}K_\psi I_0/\tau_i. \quad (10)$$

This number is stored into processor memory, too and the ratio N_r/N_0 is computed. The coefficient K_ψ can be expressed of (7) and (10) via this ratio:

$$K_\psi = R_0T_0 \frac{N_r}{N_0}. \quad (11)$$

The numbers N_r and N_0 must be measured immediately after calibration and $K_{\psi 0}$ must be computed. The monitoring measurements must be repeated periodically for example one time during day (or during week dependently on EMFM working conditions) and obtained value of K_ψ must be compared with $K_{\psi 0}$. It is useful to store the data-bank in memory.

4. The advantage of two control coil use

The coefficient K_ψ which relates excitation current with passing via control coil magnetic flux depends on two groups of reasons. The first group consists of the geometrical reasons: the geometrical dimensions of magnetic circuit, the dimensions of control coil and its

position. The external sensor part is immobile. Therefore, the probability of the geometrical variation is very small in normal conditions. The second group of reasons is related with magnetic resistance of magnetic circuit variation or magnetic field redistribution. There are three factors, which can vary magnetic resistance or magnetic field distribution: variation of relative permeability of magnetic circuit, magnetic sediments on channel internal walls and magnetic admixtures in flow [2, 3]. We can see of Fig. 6, that any of these three factors can be characterizes by specific magnetic field distribution in active zone of EMF sensor.

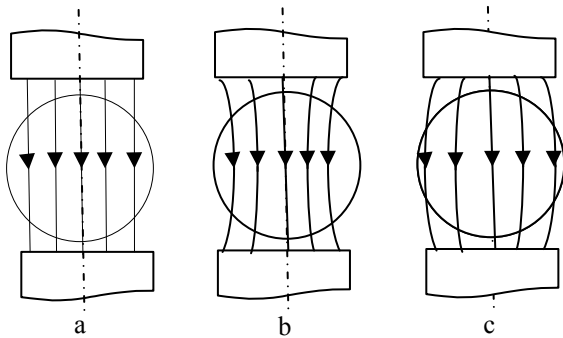


Fig.6. The distribution of magnetic field in active zone of EMFM : a) when channel is pure, b) flow with magnetic admixtures. c) channel walls with magnetic sediments

When the two control coils are mounted we can not only observe the variation of transfer coefficient, but we can understand the reason of this variation. It is usefully to mount the coils CC1 and CC2, as it is showed in Fig. 2: one under the central part of magnetic core, other – under the edge of excitation coil. When the signals of both coils decrease, therefore, we can suppose, that permeability of magnetic circuit decreases. When the signal at least of one coil increases and the signal of central coil increases more than the signal of peripheral coil, therefore, the magnetic admixtures appear in the flow (see Fig. 6, b). When, contrary, the signal of peripheral coil increases more than the signal of central

coil, therefore, the magnetic sediments are formed on the internal walls of channel (see Fig. 6, c).

The accumulation of magnetic sediments and decrease of permeability are the inertial and monotonic processes. But the magnetic admixtures can appear sharply and be episodic or, contrary, the long time the concentration of magnetic admixtures can be constant. Examining the dependences $K_{\psi_{CC1}}(t)$ and $K_{\psi_{CC2}}(t)$ stored in the data-bank we can understand, as the processes develop and we can surely solve about the variations about metrological characteristics of EMFM.

5. Conclusions

1. The measurement accuracy of electromagnetic fluid flow meter depends on parameters of magnetic circuit and distribution of magnetic field inside of transducer active zone.
2. The stability of magnetic circuit parameters and magnetic field distribution can be monitored by control coils or using for monitoring one of magnetic field exiting coils.
3. When two control coils are used, the unwarrantable variation of magnetic flux and the reason of this variation can be set.

6. References

1. Virbalis J.A. Elektromagnetiniai impulsiniai skysčio debito ir kiekio matuokliai // Elektrotechnika: Mokslo darbai. – Kaunas, Technologija, 1996. – Nr.20(29). – p.121-128.
2. Padegimas R., Virbalis J.A. Nuosėdų įtaka elektromagnetinio skysčio srauto matuoklio signalui // Elektronika ir elektrotechnika.- Kaunas: Technologija, 2002.- Nr.5 (40).- P.59-64.
3. D. Baltušninkas, J. A. Virbalis “Magnetinių dalelių poveikis elektromagnetinio skysčio srauto matuoklio magnetinei grandinei”.// “Matavimai” 2002 Nr.1 (21). - P. 24 – 28. ISSN 1392 – 1223.

THE ATTENUATION OF THE ELECTRIC REACTOR MAGNETIC FIELD STRENGTH

Jevgenij MOROZIONKOV, Juozapas Arvydas VIRBALIS

Kaunas University of Technology, The Department of Electrical Engineering, Lithuania

Abstract: The electromagnetic field in which electrical devices spread out can be dangerous for human. The special attention is given to a magnetic component of an electromagnetic field of industrial frequency. Electric reactors with the air core concern to the electromagnetic devices which create the strong electromagnetic field. For reduction of the magnetic field influence to the person organism the following measures should be taken for: shielding of workplaces; use of shielding waistcoats; exception of long exposure in places with the raised level of the industrial frequency magnetic field. Recently many new materials with unique properties have been developed. Therefore, the shielding is one of the most perspective approaches to the solution of the problem on decrease in inadmissible levels of electromagnetic fields.

Keywords: magnetic field, the electric reactor, electric shielding of magnetic fields, the limiter of a shock current.

1. Introduction

The discussions about an influence of the industrial frequency magnetic field on the person health are sharp in the last years. There are two opposite sights of scientists and experts to this question. The opinion dominates that existent standards of limiting values of the magnetic fields intensity danger to the person, are quite sufficient and there is no basis for their revision. However recently the publications appear which prove the negative influence of relatively small industrial frequency magnetic fields on a human.

According to Instruction 2004/40/EB of the Parliament and Council of Europe from 2004.04.29, the strength of the industrial frequency magnetic field on a workplace should not exceed 400 A/m. In Lithuania the basic document regulating limiting influences of electromagnetic fields on a human body is hygienic norm HN110:2001 "The electromagnetic field of industrial frequency (50 Hz) on a workplace. Admissible numerical values of parameters and the requirement to measurements" operating since January,

1st, 2002. According to this document the action on a human body of the industrial frequency magnetic field strength should not exceed 900 A/m in the working day (8 hours) [1]. Acceptance of the norms specified in the Instruction of Parliament and the Council of Europe 2004/40/EB, in Lithuania is postponed till April, 30th, 2012. Thus, a tendency to decrease in maximum-permissible specifications of influence of magnetic fields it is not observed yet. Now many experts consider that maximum permissible size of a magnetic flux density must be equal to 0,2 - 0,3 μ T. These values are equivalent to magnetic field strength values 0,16 - 0,24 A/m.

Electric reactor is one of the most powerful sources of magnetic fields of industrial frequency in power plants. Therefore, the adequate attention must be given for attenuation of the reactor magnetic field.

2. The three-phase electric reactor of vertical installation

In high-voltage networks short circuit currents can reach very large values and it is not obviously possible to pick up installations which could sustain the electrodynamic forces arising by these currents. The main destination of electric reactor is to restrict the shock current of a short circuit [2].

Usually the air electric reactor is placed in the ground floor room of the indoor switch-gear, i.e., in the small area room. In the first floor under the reactor there can be situated the sectionalized bars, disconnecting switches and cases with the electronic equipment (equipment of relay protection and automatics).

The three-phase electric reactor of vertical installation (see Fig. 1) consists of three single-phase reactors. Axes of the phases A, B and C windings coincide. Distance between end faces of phase windings is equal to g [2].

The magnetic field, created by currents of the three-phase reactor, has elliptic polarization. The effective value of the total magnetic field on the big semi axis of an ellipse is defined by this expression [2]:

$$H_{\max} = \sqrt{(H_z^2 + H_r^2)^2 + \sqrt{(H_z^2 + H_r^2)^2 - 4H_z^2 H_r^2 \sin^2(\psi_z - \psi_r)}}, \quad (1)$$

where ψ_z and ψ_r are the phase angles of total components magnetic field strength on the coordinate axes.

The approached calculation of magnetic field strength, H , A/m, created along an axis of the reactor; can be performed by expression [3]:

$$H = \frac{In}{2} \cdot \frac{r^2}{(r^2 + x^2)^{1.5}}, \quad (2)$$

where r - reactor radius, m; x - distance on an axis of the reactor from its centre to a measurement point, m; I - the reactor current, A; n - number of coils.

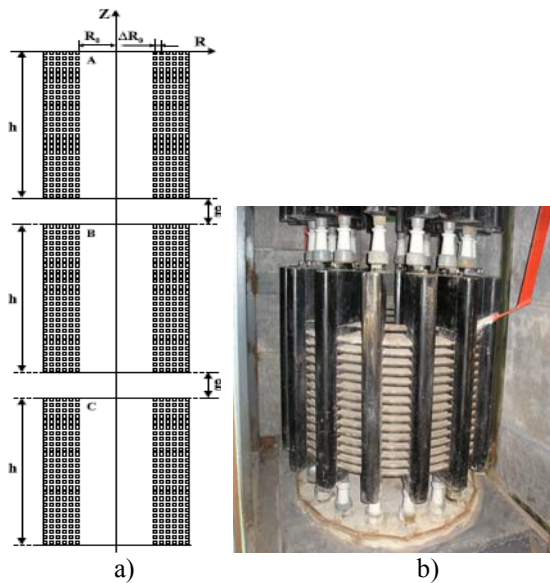


Fig. 1. Distribution of reactor phase coils (a) and the photo of a phase "C" of the air electric reactor (b)

The approximate calculation of magnetic field strength, H , A/m, created by the reactor in a horizontal plane on distances more than two diameters of the reactor, can be performed by the expression [2]:

$$H = \frac{In}{4\pi} \left[\int_0^{2\pi} \frac{rx \cos \beta}{(r^2 + x^2 - 2rx \cos \beta)^{1.5}} d\beta - \int_0^{2\pi} \frac{r^2}{(r^2 + x^2 - 2rx \cos \beta)^{1.5}} d\beta \right], \quad (3)$$

where β is the angle between the abscise axis and the vector directed from the centre of the reactor to the point in which the field is calculated.

3. Estimation of influence of the electromagnetic field on the workers at service of the electric reactor

Last years the increasing attention is given to such mechanism of magnetic field influence on a human body, as the currents induced in it. The induced currents values depend on the magnetic field frequency, on the direction and the value of the magnetic field strength, on the conductivity of the tissues and on the form of the

person body. The average electric conductivity of the person tissues are equal about 0,04 S/m. The numerical analysis of this influence can be performed using Maxwell equations.

There is estimated by such analysis that when the magnetic field acts to the human body in different directions, the greatest density of the induced current is observed around a thorax. The maximum value of the induced density current is obtained 100,3 $\mu\text{A}/\text{m}^2$, when the magnetic field strength is equal to 80 A/m [4].

The influence of small currents induced by the magnetic field as on internal organs, as on whole person body is not known till now. In the absence of such information the normative documents contain only the limiting values of magnetic field strength.

At carrying out of the electric reactor repair the person is in immediate proximity from current carrying parts of the other reactors which are in the next cells under loading. The certain position of the person near the reactor can have the essentially influence to the density of the currents induced in its body.

The distribution of magnetic field strength was computed by means of package ANSYS in the reactor and around it. The magnetic field strength on distance 0,5 m from a reactor winding was obtained equal to 49576 A/m and on distance 1 m was obtained equal to 25083 A/m, when reactor is loaded by rated current (see Fig. 2).

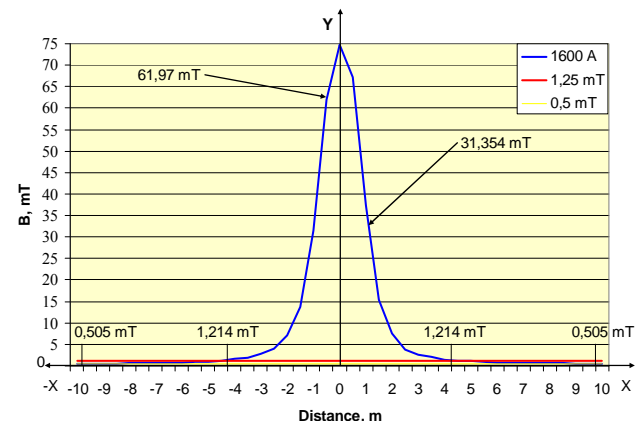


Fig. 2. The distribution of magnetic flux density created by the electric air reactor at loading $I=1600$ A and distance from the reactor axis equal to 10 m.

The obtained results show that for such workplaces additional actions are required for the magnetic field strength decrease.

4. Limiters of a current rush

The application of the reactors raises not only the enlarged level of magnetic field strength, but also the voltage losses. The self-start problem of powerful electric motors arises caused by this phenomenon. These problems can be solved using the current rush limiters which are established in parallel to electric reactor. Such limiters are developed and produced in Germany (ABB-Color Emag – «Is-limiter»), in the USA (G&W Electric Company – «CLiP») and in the other countries [6].

When the reactor operating conditions are normal the voltage losses are not exceeded the 3 – 4 % in comparison with the voltage rate value. That is quite admissible. The maximal value of short circuit current rush can be calculated by expression [5]:

$$i_m = 2.54 I_N \frac{100}{X_r \%}, \quad (4)$$

where I_N is network rated current; X_r is the reactor reactance.

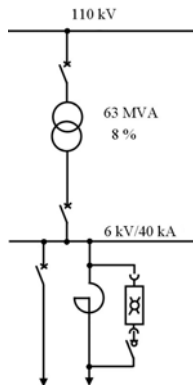


Fig.3. Is-limiter and the reactor connected in parallel

In Is-limiter the bus rupture occurs only in one point, in CLiP - in several points (on 10 kV four ruptures). With more quantity of the rupture intervals the speed of a current switching from the basic bus to a parallel safety fuse increases. The electric durability of the disconnecting device improves after full transition of a current to a safety fuse [6].

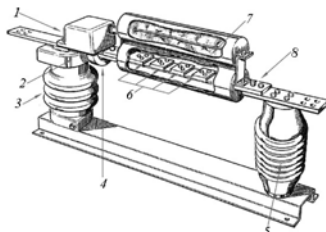


Fig. 4. Device CLiP: 1 - logic schemes, 2 - input, 3 - the dividing transformer, 4 - the current transformer, 5 - a basic insulator, 6 - rupture points on the copper bus, 7 - a safety element, 8 - replaced disconnecting device

In CLiP the signal on switching-off arises only when the instant value of current I_s achieves the threshold size, in Is-limiter the system of definition I_s by the speed of increase of a current di/dt is applied.

In the normal conditions the current flows by the copper bus. When the current rush is beginning the electronic control device switches the disconnecting device which tears the bus on some sites. The current is switched to in parallel connected safety fuse. The safety fuse begins to melt, providing restriction of the current within the first half-cycle of current to the first peak [7].

The current limiters are produced in various executions, both for external installation and in the form of sliding cells of complete switch-gears.

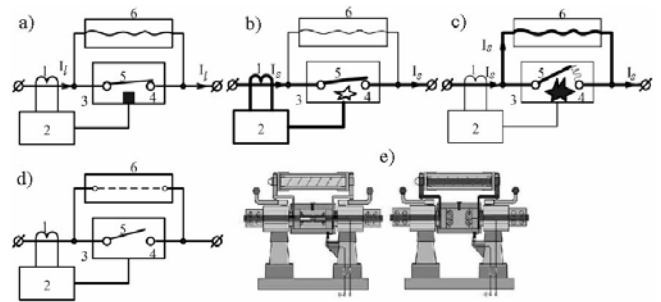


Fig. 5. The circuit of Is-limiter and a principle of its work: a) in a normal operating mode; b) at the moment of giving of an initiating impulse on a charge; c) at the moment of current interruption in an explosive breaker; d) the rupture chain; e) the cross-section of Is-limiter in an initial condition and after operation [6]



Fig. 6. Is-limiter: a) Truck mounted Is-limiter in a switchgear panel; b) Is-limiter connected in parallel with a reactor (fixed mounted)

5. Application of electromagnetic screens

The electromagnetic screens can restrict the magnetic field strength created by electric reactor, too. This variant of shielding can be used, when the new electric reactor is designing, manufacturing or installing. This method does not suited to reactors already being in operation because of the design features of the offered screen. The winding of screen coil K is placed over the winding of the phase coil N (see Fig. 7, a). The axes of shielding and phase coils coincide [3].

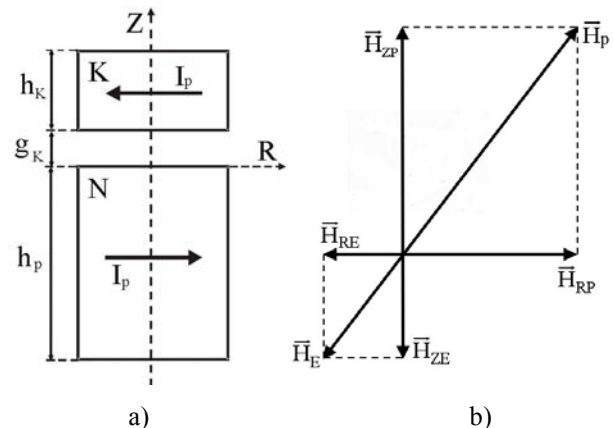


Fig. 7. The scheme of a shielding winding K arrangement over the winding N of phase coil (a) and the vector diagram of magnetic field strength components created by the phase coil winding and the shielding winding (b)

The turns of winding K are reeled up in opposite direction to phase coils N and both windings are connected in series. The components of magnetic field strength created by currents in windings N and K are directed in opposite directions (see Fig. 7b). The magnetic field strength of shielding winding compensates some part of the magnetic field created by reactor. The total values of magnetic field strength are defined by expressions (5) and (6) [3]:

$$H_{ZPK} = \frac{I_{\varphi} R_0}{4\pi} \sum_{i=0}^{N-1} \int_0^{2\pi} \frac{R_0 - R \cos \varphi}{\left(\sqrt{(z+in)^2 + R^2 + R_0^2 - 2RR_0 \cos \varphi} \right)^3} d\varphi - \quad (5)$$

$$- \frac{I_{\varphi} R_{0EK}}{4\pi} \sum_{j=0}^{K-1} \int_0^{2\pi} \frac{R_{0EK} - R \cos \varphi}{\left(\sqrt{(z-g_K - jk)^2 + R^2 + R_{0EK}^2 - RR_{0EK} \cos \varphi} \right)^3} d\varphi,$$

$$H_{RPK} = \frac{I_{\varphi} R_0}{4\pi} \sum_{i=0}^{N-1} \int_0^{2\pi} \frac{(z+h_p) \cos \varphi}{\left(\sqrt{(z+in)^2 + R^2 + R_0^2 - 2RR_0 \cos \varphi} \right)^3} d\varphi - \quad (6)$$

$$- \frac{I_{\varphi} R_{0EK}}{4\pi} \sum_{j=0}^{K-1} \int_0^{2\pi} \frac{(z-g_K - h_k) \cos \varphi}{\left(\sqrt{(z-g_K - jk)^2 + R^2 + R_{0EK}^2 - 2RR_{0EK} \cos \varphi} \right)^3} d\varphi$$

Using the shielding winding mounted on the top of the reactor the magnetic field strength over the reactor decreases almost in 5 times. Sideways from the reactor the magnetic field strength decreases only in 1,2 times. Its greatest value is on the area of the reactor winding middle.

For the magnetic field shielding in the horizontal plane, the shielding winding V can be mounted outside of the reactor winding as it is showed in Fig. 8. This winding is reeled up in opposite direction to coils of the reactor winding, too. The coils of the reactor and of the winding V are connected in series [3]. When the shielding windings K and V are used the magnetic field strength over the reactor decreases to 30 times, and sideways from the reactor to 6 times.

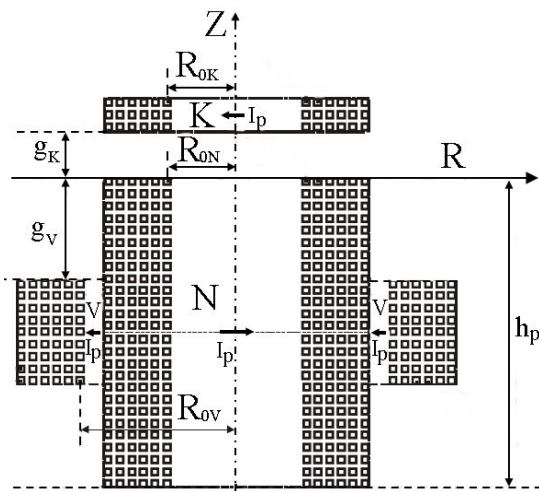


Fig. 8. An arrangement of shielding windings K and V outside of the reactor winding N

The inductive resistance of the winding N of the reactor is equal to $X_p = 0,35 \Omega$.

The inductive part of the full resistance of the reactor with shielding windings K and V is defined by expression [3]:

$$X_{p\Sigma} = X_p + X_K + X_V - 2\omega M_{PK} - 2\omega M_{PV} + 2\omega M_{KV}. \quad (7)$$

When the V shielding winding is installed the full inductive resistance of the reactor will decrease to 33 %.

6. Conclusions

1. Despite the overestimated norms the values of the electric reactor magnetic field strength in normal conditions are considerable and must be decreased.
2. At parallel connection of the reactor with limiters of a shock current, the loading current flows bypassing the reactor. Therefore the reactor magnetic field is insignificant in normal conditions. The values of the magnetic field strength exceed maximum permissible only during short circuit in a network after operation of the shock current limiter.
3. Installation on the electric reactor of shielding windings allows to lower considerably the levels of magnetic field strength created by the air reactor.

7. References

1. Lietuvos higienos normos HN 110: 2001 „Pramoninio dažnio (50 Hz) elektromagnetinis laukas darbo vietose. Parametrų leidžiamos skaitinės vertės ir matavimo reikalavimai“.
2. Мисриханов М.Ш., Рубцова Н.Б., Токарский А.Ю. Магнитные поля электрических реакторов. // Обзор эффективных экологических проектов, внедренных на предприятиях ОАО РАО «ЕЭС России», 2007. - выпуск № 2. - С. 108 - 113.
3. J. Morozionkov, J.A.Virbalis. Magnetic Field of Power Plant Air Core Reactor. // Electronics and Electrical Engineering. - Kaunas: Technologija, 2007. - No. 7(79). - P. 67 - 70.
4. Кадомская Л.П., Степанов И.М. Влияние конструкций воздушных линий высокого напряжения на интенсивности магнитных полей по их трассам.// материалы 3-ей Российской с международным участием научно-практической конференции ЛЭП2008, 2008. - С. 81-90.
5. J. Schaffer. Commutating Current-Limiters - an effective alternative for high current protection.// NETA World, vol. 18, Winter 1996-97. - No. 4. - P. 7-18.
6. Мисриханов М.Ш., Рубцова Н.Б., Рябченко В.Н., Токарский А.Ю. Электромагнитные экраны для электрических реакторов. // материалы IX-го Симпозиума "Электротехника 2030. Перспективные технологии элек-троснабжения.", 2007.
7. ABB AG. Calor Emag Medium Voltage Products. Is-limiter.// Leaflet no. DEABB 2243 08 E Leaflet no. DEABB 2243 08 E. - Germany, 2008. - P. 24.

DIGITALLY SELECTED SPEEDS FOR A DIRECT CURRENT (DC) MOTOR'S APPLICATIONS

Sambwa ADOKO*, Onyekachi ADOKO**

*Asa-Lambda Technology Ltd., Nigeria;

** Benson Idahosa University, Nigeria

Abstract: The authors present a digitally selected speed for a DC motor using pulse width modulation (PWM). The 555 timer which generates a PWM output, is interfaced by a multiplexer channel and a switching regulator, to digitally select the speeds and position for DC motor's applications. Although, it is an open loop controller with great level of precision and simple to configure and design.

Keywords: Pulse generator, switching regulator circuits design, and applications.

1. Introduction

Ideally, the motor speed controller represents a module which is used to drive a motor at a pre-determined speed. In some cases, it measures such speed, hence the difference between feedback speed controller and open loop speed controller. The adopted speed controller circuit in this work does not necessary assume the above mentioned objectives rather, it is designed to efficiently control the DC motor's speed to a pre-set values as shown in Fig. 1.

In thru perceptive, the DC motor speed controller is a variable power supply. This is accomplished by simply adjusting the voltage sent to the motor. Visibly, such technique may seem highly inefficient to perform.

Consequently, the process being adopted in this work is an ON – OFF switching technique, which is performed by a 555 timer (IC) as pulse generator, coupled with a switching regulator made of power transistor that can turn very large currents ON and OFF under the control of a signal width.

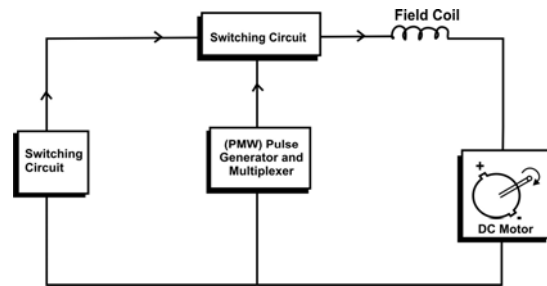


Fig. 1. Basic DC motor's speed controller topology

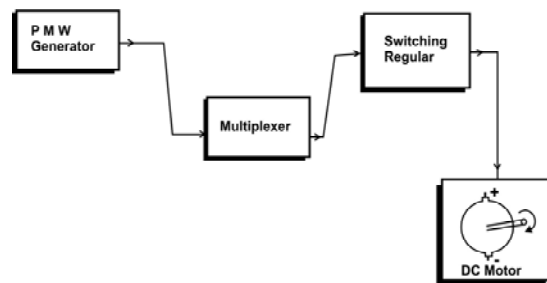


Fig. 2. Proposed speed controller topology

The time that it takes a DC motor to vary its speeds under switching conditions is dependant on the inertia of the rotor, and how much friction and load torque there is [1]. The objective of this work has been and remains the realization of the principle of switch mode speed control.

Thus, the speed is governed by PWM – Pulse width modulation, following the general principles governing DC motors in which the speed of a DC motor is directly proportional to the supply voltage [2]. There exist several methods and procedures establishing such proportionalities. Hence, the introduction of electronically controlled DC motor's speed, as shown in Fig. 3.

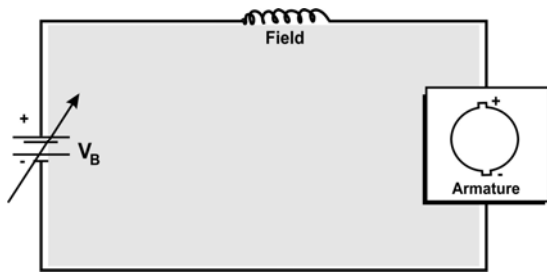


Fig. 3. Basic DC motor speed controller using a variable supply

If the above stated principles are justified, then the main objective of this work will be to design a regulated supply and create a sub-circuit which will function as a variable switching regulator. That is, a regulated supply having a variable regulated output. This scenario is necessary as to create a working environment where the output stage regulator's function will be to change the input supply voltage to another voltage level. The second stage regulator is the DC motor's speed controller. In other words, the supply voltage will remain constant while the second regulator will vary its output to match with the pre-selected motor's speeds. It then creates a voltage of different magnitude from the voltage that power it, and the process is done digitally through switching regulator.

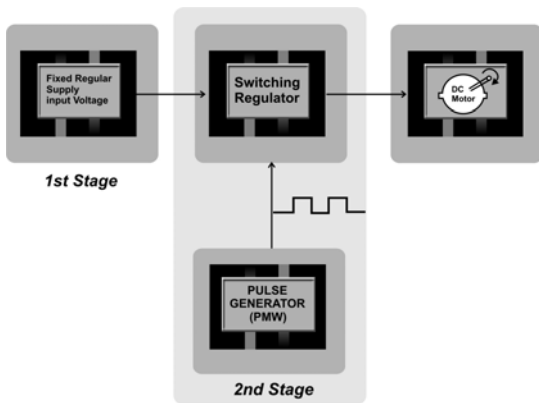


Fig. 4. DC – to – DC Converter as DC motor's speed drive

2. Pulse generator (PWM)

The simplicity of this work lies in the selection of the pulse generator which produces a digital signal. The width of the modulated signal is critical for the motor speed control, by adjusting the pulse width, the speed of the DC motor can efficiently be controlled without larger linear stages.

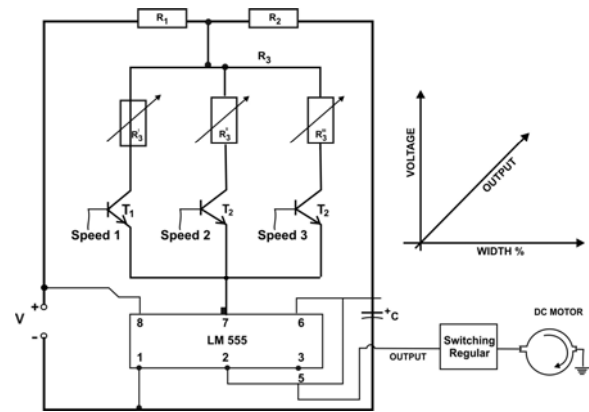


Fig. 5. Integrated pulse generator unit

The above circuit diagram as described in Fig. 5 can be built into a capture/compare/ PWM (CCP) Peripheral. Configured for a single PWM output, while the step up regulator is designed to produce the unique output for the motor's control. If cost and availability remain a critical design factor as it is the case in the sub-Saharan – Africa, used and unserviceable apparatus remain one of the best alternative options.

3. LM 555 (IC) timing analysis

The basic elements of a 555 timer (IC) are shown in Fig. 6. The switching unit is commutated to the supply, via the pulse generator. The 555 timer has been re-arranged to be analysed as a T-Network configuration, using the existing basic techniques.

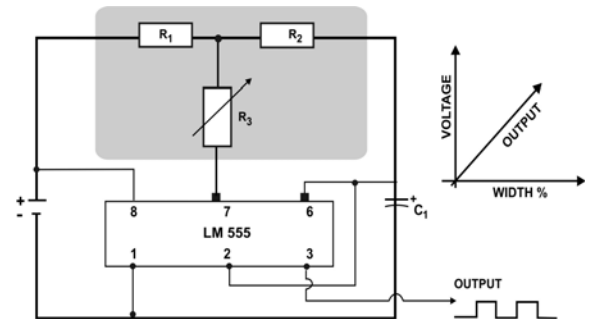


Fig. 6. The project's clock generator circuit

4. Switching regulator

In view of maintaining a constant output voltage, an adoption of a switching regulator became apparent and appropriate for this work. As it can be shown in Fig. 7, the primary filter capacitor (c) has been placed on the output of this regulator. Such arrangement has been confirmed by several authors as an efficient arrangement in switching regulators [3].

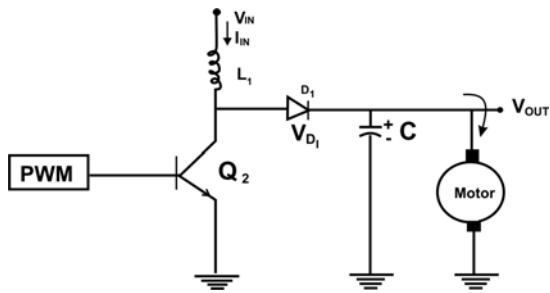


Fig. 7. Switching regulator topology

Keeping the fact of having a constant voltage and constant current output, a step up switching regulator remains an ideal consideration [3]. Modulated by an external pulse generator, the adopted regulator in this work, functions as shown in Fig. 8-10, that is, the switching regulator uses a power switch (transistor), an inductor, and a diode to transfer energy from, input to the motor. The sequences of such transfer constitute the main objective of this work. The regulators components perform special role in their individual characteristics.

5. A charging stage

At this stage, the inductor [L], main assignment is to limit the current slew rate through the power switch. It creates a fast energy storage which is expressed as follows:

$$E = 0.5LI_L^2. \quad (1)$$

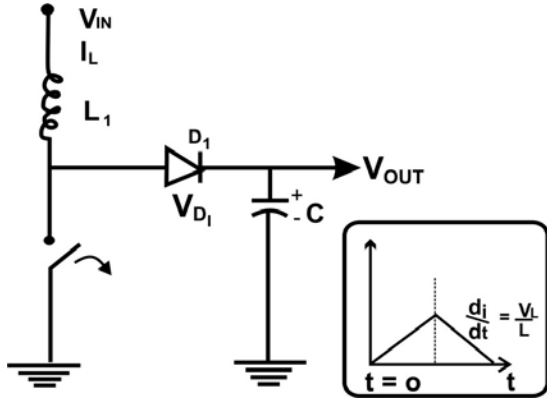


Fig. 8. Regulator's charging stage

As stated in the engineering theories, the inductor's current I_L is 90 degrees out of phase with the voltage [4]. This will facilitate the recovery of the stored energy during the discharge phase of the switching cycle. The Engineering beauty is the fact that this process produces less heat at an acceptable efficiency.

6. Discharging

At the instant when the switch closes, V_{IN} is impressed across the inductor L. The capacitor C discharges its energy to the load. The current I_L through the inductor rises linearly with time at a rate proportional to the input voltage divided by the inductance.

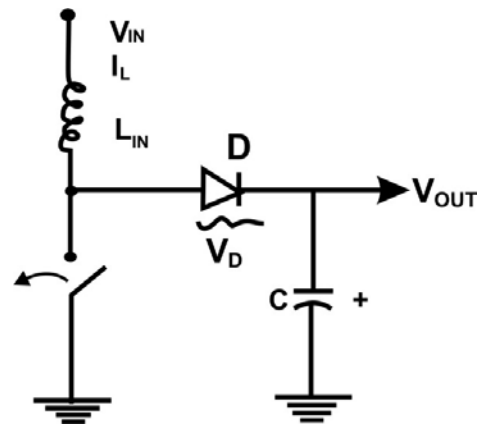


Fig. 9. Discharging stage of the switching regulator

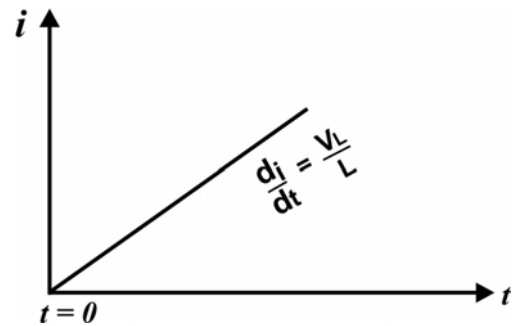


Fig. 10. A graph diagram of the current (i) at a time $t=0$

$$\frac{di}{dt} = \frac{V_L}{L} \quad (2)$$

Contrarily, as shown in Fig. 8, when the switch opens, the inductance voltage is expressed as

$$V_L = L \frac{di}{dt}.$$

For a DC motor's operating environment, it will be advisable to maintain the current through the inductor in a steady state mode. Hence, for a given charge time t_{ON} , and a given input voltage with a lossless energy circuit, there will be a specific discharge time t_{OFF} , for an output voltage.

The correlation between the above sequence and the clock transition period needs to be established. In the interim, the switching circuit can equally be calculated as follows:

$$V_{IN} = \frac{t_{OFF}}{t_{ON}} \times \frac{V_L}{L}. \quad (3)$$

Working in the steady state mode, we have

$$V_{OUT} = V_{IN} \left(1 + \frac{t_{ON}}{t_{OFF}} \right). \quad (4)$$

Then, the duty circle is

$$D = \frac{t_{ON}}{(t_{OFF} + t_{ON})}, \quad (5)$$

$$V_{OUT} = \frac{V_{IN}}{(1 - D)}. \quad (6)$$

From the above analysis, the adopted controller can be classified as a voltage mode controller (VMC). The pre-selected pulses detect the shape and width of the output voltage, hence controlling the speed of the DC Motor. A current mode control (CMC) can equally be used.

7. Applications

With the trend of power electronics where the speed and power handling capabilities of semi conductors have improved substantially in the last few years in the field of portable power supply and electric motor's speed control. This development has considerably enhanced some complex real time algorithms often required in industries.

In addition, the development of renewable energy has been made possible through such innovations as DC-DC converters as an added values from some powerful low cost semi-conductor devices.

As mentioned by B.K. Bose, that "Electrical machine control was one of the first research fields to take advantage of this continuing development with both AC and Dc machines" [5]. Although the applications of DC motor's speed controller have spread in several avenues, among them are, the robots, electrical vehicles, and renewable energy technologies, to mention but a few.

Equally, there seem to be some unanswered questions in PWM techniques for DC motor's speed control. This puzzle lies on the load torque and speed relationship.

It has been established that, as the load torque of a DC motor increases, the speed drops [6]. This is a general occurrence for an open loop speed control as it is the case in this work. It will be assumed that PWM under a constant speed will have its torque equal to the load torque. But, when the load increases, the motor torque and load torque have to be balanced out immediately with the current I_L and the equivalent torque value on the torque current T_L . But, obviously speaking, the speed demand is a DC voltage which is fed to the PWM generator for motor. This drives motor at the speed required on the demand voltage, but not on load torque. Possibilities to incorporate special devices/sensors to the circuit can be a positive aspect with tremendous advantages [7].

8. Conclusion

DC motor's speed control technique has been hitherto very difficult and energy wasteful method to implement. The modern switching technique as adopted in this work

can be applied in a wide range of applications. It offers better efficiency, smaller components and cost effective. This simplicity has been demonstrated in the work where it was possible to design and construct a complete circuit using the components recovered from the unserviceable apparatus and the final results are satisfactorily.

While there exists, some buckets of problems in DC motor's speed control, the works done by C. Schaefer [7], J.P. Karunadasa [8], and N. Matsoi [9] illustrate useful contributions in this issue of engineering importance.

9. References

1. Marcel P.J., Gaudreau P.E., Casey J.A. , Hawkey T.J., Kempkes M.A., Mulvaney J.M., Ver Planck P. Solid State High Voltage DC Power distribution and control. In proceeding of the Particle Accelerator Conference, New York, 1999.
2. Adoko S. Effective Paradigm for direct current (DC) distribution using light emitting diodes (LEDs) in architectural lighting system. The 3rd Regional World Renewable Energy Congress (AISEC-10), Kuwait City, Kuwait, 2008.
3. Adoko S., Irowa O. Integrated power supply's design and construction practice for solar lighting applications. Energy and Environment (EE09) WSEAS Conference, Cambridge, UK, 2009.
4. Theraja B.L., Theraja A.K Textbook of Electrical Technology. Ninja Construction & development Co. (p) Ltd Ram Nagan, New Delhi, 1997.
5. Bose B.K. Adjustable speed AC Drives– A technology status review. IEEE Trans Ind. App., 1982, vol. 70, no. 2. p. 116-135.
6. Herrit B., Morogavel R. PWM DC Motor Control Using Timer – A of the MSP 430. Application Report SLAA 120 Texas Instruments – December 2000.
7. Schaefer C. Field Weakening of Brushless Permanent Magnet Motors with Rectangular Current. Proc. Env. Conf. Power Application (EPE), Florence, 1991, vol. 3, p. 429-434.
8. Karunadasa J.P., Renfrew A.C. A flexible fast Digital Controller for a Brushless DC motor. 4th Int. Conf. Power Electronic and Variable speed Drives, 1990. p. 429-434.
9. Matsoi N. Sensorless PM Brushless DC Motor Drives. IEEE Trans Ind. Electronics, April 1996, vol. 43, no. 2. p 300-308.

INTENSIFICATION OF HEAT EXCHANGE IN REFRIGERATION TECHNOLOGIES BY USE OF CORONA FIELD

Stasys ŽEBRAUSKAS*, Irmantas BENIULIS**

* Kaunas University of Technology; Lithuania, **Lithuanian University of Agriculture, Lithuania

Abstract: Experimental results of the influence of corona field on the heat exchange in domestic freezer processes are discussed. Average freezer condenser surface temperature influenced by negative corona field at the end of compressor operating cycle decreases by 2.4 K in comparison with the temperature without corona field. This decrease is 4.0 K at the end of compressor pause cycle. Decrease of condenser surface temperature causes the reduction of compressor operating cycle, and consequently the reduction of freezer energy consumption by 14 %. Use of negative corona field for cooling of water from 289 K to 273 K in the freezer reduces the duration of the process and freezer energy consumption by 35 %. Heat exchange processes intensification and energy saving is caused by small corona device energy consumption.

Keywords: rate of temperature changing, corona field.

1. Introduction

Direct current corona field is widely used for heat and mass transfer enhancement. In this technique, application of high voltage to an electrode with a small radius of curvature ionizes air molecules, which are propelled by the electric field, transferring part of their energy to neutral air molecules, thus creating airflow and cooling effects. It is shown in [1] that the increase of convection heat-transfer coefficient is linearly proportional to the applied voltage for all tested air-gap separation distances. Experimentally and by means of modeling is determined that velocities of airflow initialized by ion movement in the space between electrodes are of values up to 4 m/s, and maximal value of convection heat transfer coefficient is 280 W/(m²·K) [2]. Because ionic wind can generate flow with no moving parts and have low energy consumption, it offer an attractive method for enhancing convection heat transfer from a surface. An increase of more than 200 % in the local heat transfer coefficient is observed due to the ionic wind for a power input of only 68 mW [3]. In the presence of a bulk flow ionic wind distorts the

boundary layer with a still air, reducing its thermal resistance and increasing the heat transfer from the wall. Experiments demonstrate the ability of ionic wind to decrease the wall temperature substantially in the presence of a bulk flow over a flat plate, corresponding to local enhancement of the heat transfer coefficient by more than twofold [4]. This technology to increase the heat transfer coefficient, which describes the cooling rate, by as much as 250 %, is unique, because other experimental cooling enhancement approaches might give you a 40-50 % improvement [5]. It is sufficient to create ionic wind with a velocity of 0.1-0.3 m/s to demonstrate such an effect [6].

2. Corona fields in cooling and freezing processes

During the last twenty years daily energy consumption of domestic coolers and freezers is reduced from 1.5 kWh to 0.5 kWh. This is achieved due to use of more perfect constructions and new heat insulating materials. There are several processes in each cooler or freezer which effectiveness may be enhanced by use of the corona field: cooling of the product from room temperature to 0 °C, deep-freezing or icing of the product, storage of the product in deep-frozen state, defreezing of the product or the ice, cooling of the condenser of cooler or freezer, heat exchange on the surface of evaporator, evaporation of refrigerant, condensing of refrigerant, separation of oil from refrigerant in the compressor, production of artificial snow, control of the moisture in refrigerating product, antiseptic action to refrigerating product. Effectiveness of using the corona field is caused by small energy consumption of corona field arrangements. The results of cooling the surface of condenser and cooling and freezing of water in domestic freezer by use the corona field are discussed in this article.

3. Cooling of the surface of condenser

Domestic refrigerator of power, equal to 180 W and overall length of condenser tube 8.4 m is used for

testing in direct current or 50 Hz corona field. The temperature of ambient air is 296 K. Diameter of condenser tube is 6.5 mm. Corona wire which diameter is 0.050 mm is attached at the distance from the tube surface equal to 15 mm. Refrigerator is connected to supply network through watt-hour meter. Formulas for computation of volt-ampere characteristic in electrode system “wire parallel to the cylinder” are given in [6] and [7]. Operating corona voltage is determined from computed volt-ampere characteristic and is equal to 6 kV. Linear corona current density is 100 $\mu\text{A}/\text{m}$. Condenser tube surface temperature is measured at the beginning of the tube, at the end and at the other 4 points on the surface of the tube separated by distances 168 cm. Freezing chamber contains a vessel with 5 l of water. The best effect is detected for negative corona field. Variation of condenser tube surface temperature at the 1 point is presented in Fig. 1. Condenser surface temperature at the end of compressor operating cycle is 309 K, at the end of pause is 298 K for negative corona field, and correspondingly 311 K, 302 K for control test. Average duration of operating cycle is 3.5 min for corona field and 4.0 min at control test. Average energy consumption

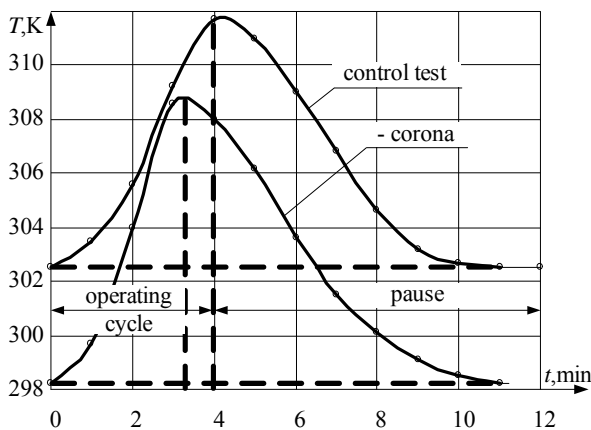


Fig. 1. Variation of temperature at the beginning of condenser tube

is 1.45 kWh/day for corona field, and 1.65 kWh/day for control test. Energy consumption of corona device is 0.1 kWh/day. Reduction of condenser surface temperature by 1 K corresponds to a day energy consumption by 4 %.

Dynamics of temperature variation at all 6 points of condenser tube surface is given in Fig. 2 – Fig.5. During compressor pause average meaning of condenser surface temperature influenced by corona field decreases from 309 K to 298 K (Fig. 2) and from 311 K to 302 K at a control test (Fig. 3), correspondingly. Temperature decrease wave passes from the end of condenser tube to the beginning. The rate of this decrease during the first minute of pause influenced by corona field exceeds 1.7 time the corresponding rate at the control test.

Condenser surface temperature increase dynamics at all 6 points for operating cycle of compressor influenced by corona field and during the control test is shown in Fig. 4 and Fig. 5.

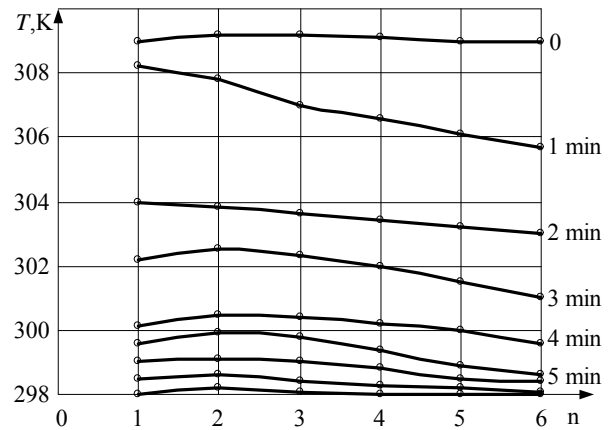


Fig. 2. Variation of temperature at 6 equally distant points in overall length of the condenser tube influenced by negative corona field for pause of the compressor operation

Average meaning of condenser surface temperature influenced by corona field rises from 298 K at the beginning of operating cycle of the compressor to 309 K at the its end. Corresponding values for control test are 302 K and 312 K.

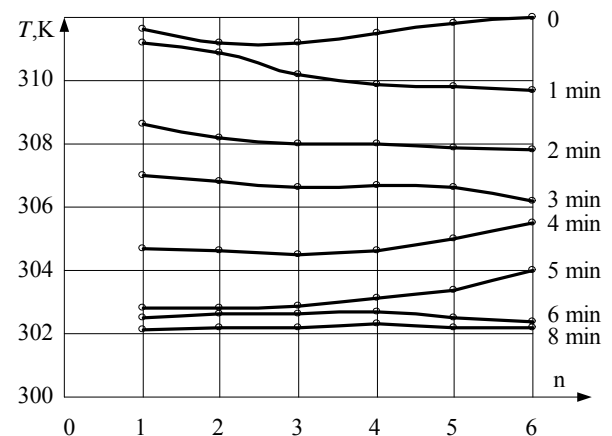


Fig. 3. Variation of temperature at 6 equally distant points in overall length of the condenser tube during the control test for pause of the compressor operation

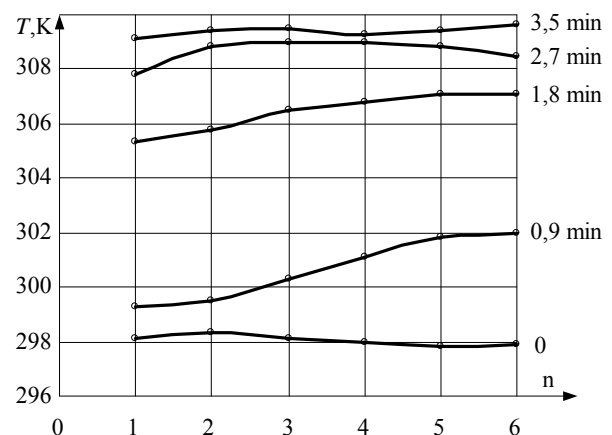


Fig. 4. Variation of temperature at 6 equally distant points in overall length of the condenser tube influenced by negative corona field for operating cycle of the compressor

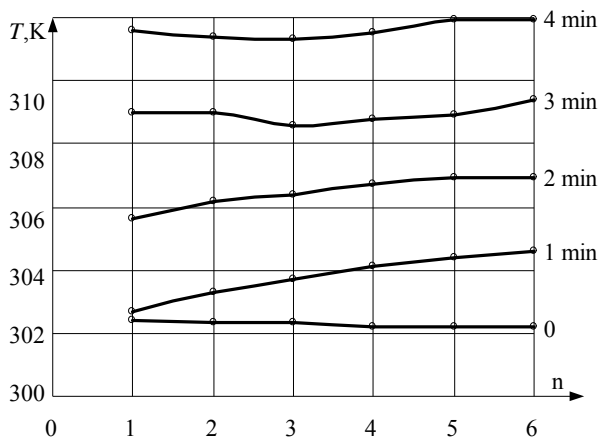


Fig. 5. Variation of temperature at 6 equally distant points in overall length of the condenser tube during the control test for operating cycle of the compressor

Temperature rise wave passes from the end of condenser tube to the beginning. The rate of this increase during the first minute of operating cycle influenced by corona field exceeds 1.75 time the corresponding rate at the control test.

4. Cooling and freezing of water in freezing chamber of domestic freezer

Freezing chamber of domestic freezer which power is 180 W contains of a vessel with a 1000 ml of water. The area of the open surface of water is 490 cm². A net of parallel corona wires of 0.1 mm diameter is arranged 10 mm above the surface of water. The distance between neighbouring wires is 15 mm. Area of the net with corona wires is 314 cm². Formulas for computation the volt-ampere characteristic are the same as in [8]. Operating value of corona voltage $U = 10$ kV is selected from computed characteristic. It corresponds to 400 μ A of average corona current value and 4 W corona arrangement power. Cooling water temperature decrease process from 289 K to 273 K is shown in Fig. 6. Positive corona field practically has no effect to the rate of temperature decrease. 50 Hz corona field demonstrates negative effect. No effect is detected also for electrostatic and quasistatic 50 Hz electric field. Only negative corona field demonstrates the cooling rate enhancement effect. Water cooling from initial temperature to 273 K is 25 min under control test conditions, and 18 min influenced by negative corona field. It corresponds to 240 kJ (67 Wh) energy consumption without a field, and 177 kJ (49 Wh) with a corona field (35 % decrease). Energy consumption of corona field arrangement is only 1.2 Wh. Constant temperature values for $t > 30$ min correspond the freezing point.

Freezing water temperature changing curves in the interval 275 K – 263 K are shown in Fig. 7. Duration of water freezing to ice in negative corona field (at 263 K temperature) is 5 h. It corresponds to 20 % reduction in comparison with control test conditions. Duration of the process influenced by the positive corona field reduces by 15 % in comparison with control test. 50 Hz corona field demonstrates the least effect to freezing process.

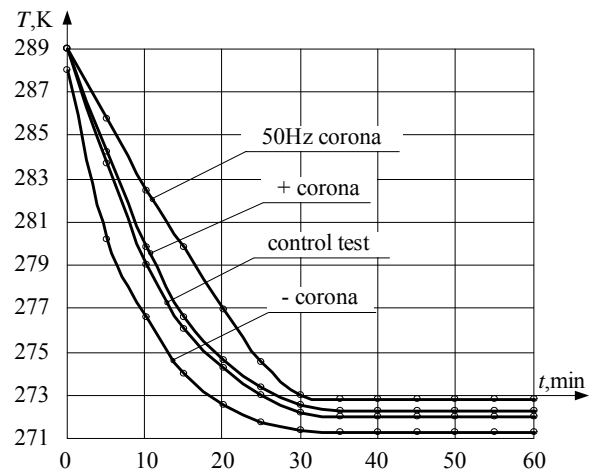


Fig. 6. Variation of freezing water temperature

Energy consumption of the process is 3400 kJ (0.944 kWh) for control test conditions, and 2900 kJ (0.805 kWh) for negative corona field conditions (17% reduction). Energy consumption of corona field arrangement is 20 Wh.

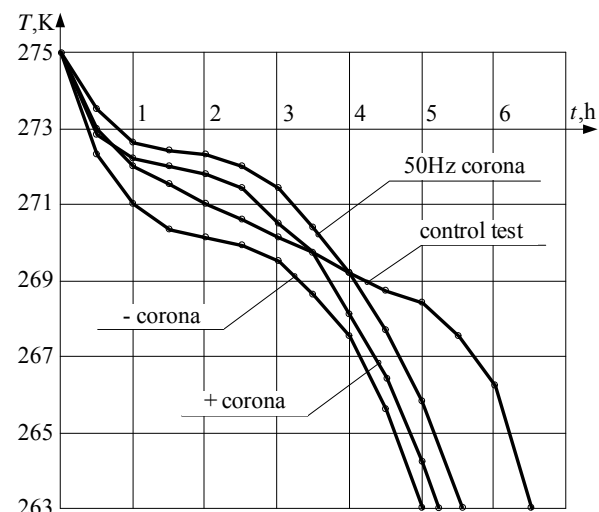


Fig. 7. Variation of frozen water temperature

Ice melting temperature rise curves in the interval 263 K – 283 K are shown in Fig. 8. Contrarily to cooling and freezing tests the most substantial influence to the rate of ice melting temperature rise has the positive corona field. Duration of ice melting process corresponding to temperature rise from 263 K to 283 K is 4.5 h under control test conditions. Duration of the process influenced by positive corona field is 3.7 h (60 % reduction). Flat part of characteristics correspond to specific solution heat.

5. Conclusions

1. Average freezer condenser surface temperature influenced by negative corona field at the end of compressor operating cycle decreases by 2.4 K in comparison with the temperature without corona field. This decrease is 4.0 K at the end of compressor pause cycle.

6. References

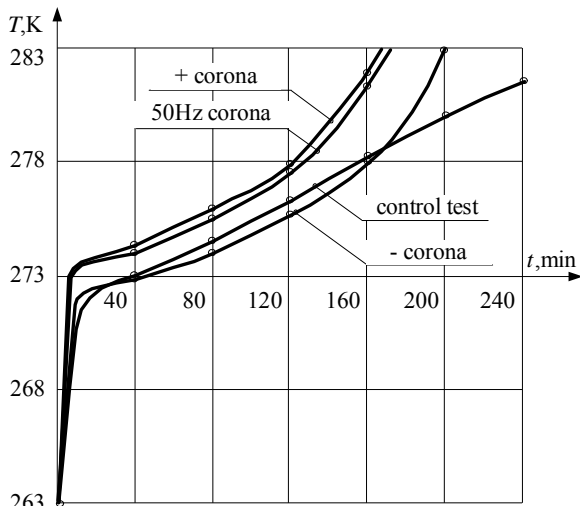


Fig. 8. Variation of melting ice temperature

2. Decrease of condenser surface temperature causes the reduction of compressor operating cycle, and consequently the reduction of freezer energy consumption by 14 %. Decrease of condenser surface temperature by 1 K corresponds to the reduction of energy consumption by 4 %.

3. Use of negative corona field for cooling of water from 289 K to 273 K in the freezer reduces the duration of the process and freezer energy consumption by 35 %.

4. Use of negative corona field for freezing of water to ice causes the decrease of process duration and freezer energy consumption by 17 %.

5. Heat exchange processes intensification and energy saving is caused by small corona device energy consumption in comparison with freezer energy consumption.

1. Hsu C. P., Jewell-Larsen N. E., Krichtafovitch I. A., Mamishev A. V. Heat-Transfer-Enhancement Measurement for Microfabricated Electrostatic Fluid Accelerators. *Journal of Microelectromechanical Systems*, Vol. 18, No. 1, February 2009, p. 111-118.
2. Jewell-Larsen N. E., Krichtafovitch I. A., Montgomery S. W., Dibene J. T., Mamishev A. V. CFD Analysis of Electrostatic Fluid Accelerators for Forced Convection Cooling. *IEEE Transactions on Dielectrics and Electrical Insulation*, Vol. 15, No. 6, December 2008, p. 1745-1753.
3. Go D. B., Maturana R. A., Fisher T.S., Garimella S.V. Enhancement of External Forced Convection by Ionic Wind. *International Journal of Heat and Mass Transfer*, Vol. 51, 2008, p. 6047-6053.
4. Go D. B., Garimella S. V., Fisher T.S. Ionic Winds for Locally Enhanced Cooling. *Journal of Applied Physics*, Vol. 102, 053302, 2007, 8 p.
5. McHale. Purdue Researchers Demonstrate New Chip-Cooling Technology. *Military and Aerospace Electronics*, November 2007, p. 3.
6. Žebrauskas S., Marčiulionis P. Elektrodoų sistemos "laidas šalia cilindro" vienpolio vainikinio išlydžio elektrinis laukas. *Electronics and Electrical engineering*, 2006, No. 1(65), p. 43-47
7. Žebrauskas S., Marčiulionis P. Elektrodoų sistemos "laidas šalia cilindro" elektrostatinis laukas. *Electronics and Electrical engineering*, 2005, No. 6(62), p. 32-36
8. Žebrauskas S. Barčiauskas R. Using of Corona Fields in Building Material Industries. *Proceedings of International Conference "Electrical and Control Technologies – 2009"*, Kaunas, 2009 p. 247-250.

USING OF CORONA FIELDS IN BUILDING MATERIAL INDUSTRIES

Stasys ŽEBRAUSKAS, Ričardas BARČIAUSKAS
Kaunas University of Technology, Lithuania

Abstract: The experimental results of clay panel drying rate enhancing in direct current corona field are discussed. Using the direct current corona field for clay panel drying process increases the rate of 100 % moisture evaporation 3.2-fold in comparison with natural drying process in the air. The duration of drying to 80 % moisture evaporation reduces 10 times, and the duration of 50 % moisture evaporation reduces 20 times. Energy consumption of 100 % drying is 1.5 kWh to 1 m² of clay panel area. It takes 0.6 kWh/m² for 80 % drying, and 0.3 kWh/m² for 50 % drying. Using the direct current corona field to drying process increases the drying quality. Rate of moisture evaporation in all points of drying material volume becomes more uniform. Intensification of drying may be enhanced by increasing the corona voltage, but it will increase the energy consumption.

Keywords: clay-straw panels, moisture content, corona field.

1. Introduction

Modern building technologies as a part of a common industrial technologies ought to meet ecological requirements. One of new (and ancient) kinds of buildings is the straw bale one [1]. There are many advantages inherent to straw bale constructions: excellent heat insulation quality, reduced heating and cooling costs, suitability to use local renewable materials, cheap and fast mounting procedure [2]. Plaster as well as plaster-cartoon panels are used usually for finishing. There are proposals to use clay-straw panels in straw bale buildings which are more preferable in comparison with plaster-cartoon ones for some advantages [3]. The main disadvantage limiting the usage of clay-straw panels is comparatively long drying duration of panels after the formation procedure. One of successful methods of drying is the freeze-drying [4]. The moisture content of humus decreases to 22 % from an initial value of 44 % wet basis after 2 h of electro-osmosis at 50 V across a 2.9-cm-thick bed in electro-osmotically enhanced drying of biomass [5]. The well-known method of water removal from the paper is electromagnetic paper drying using the microwave

frequencies [6]. Moisture content can be reduced by using the chilling and heating method [7]. The speed of water evaporation may be enhanced by using the corona field. Ion-driven movement of air influences the rate of mass exchange processes of evaporation. Absolute rate of water evaporation from porous material increases up to 15 times by using the corona field [8]. We discuss there the results of clay panel drying enhancement by using the direct current corona field.

2. Experimental arrangement

We use the direct corona electrode system “a set of parallel corona wires above the plane electrode” (Fig.1) Plane electrode is represented by the surface of drying clay panel. Test drying clay sample is a plate of 1 cm thickness and of 10x10 cm² area. Radius of corona wires is $r_0 = 0.05$ mm, the step of the grid $d = 15$ mm, and the height h is variable in the interval 10-14 mm.

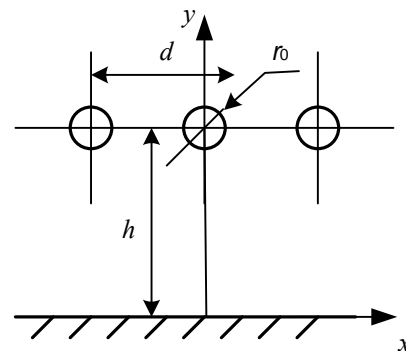


Fig. 1. Electrode system of the experimental device

We use the calculated data for volt-ampere characteristics of corona in the discussed electrode system at several values of the height h to determine the proper values of test voltage and current corresponding the source voltage ≤ 10 kV and the current ≤ 1200 μ A. The used formulas are the same as in [9]. Initial field strength of the discharge depends upon the radius of the wire r_0 and the relative air density δ .

$$E_0 = 3030000\delta(1 + 0,0298/\sqrt{(r_0\delta)}), \quad (1)$$

the relative air density being determined by the formula:

$$\delta = pT_0 / p_0T, \quad (2)$$

where p is the atmospheric pressure, p_0 is equal to p for normal conditions, $p_0 = 101.325$ kPa; T is the thermodynamic temperature, T_0 is equal to T for normal conditions, $T_0 = 293.15$ K. Relative air density equals to 1 if $p = p_0$, $T = T_0$. Onset voltage of the discharge:

$$U_0 = r_0E_0 \left(2\pi \frac{h}{d} - \ln 2\pi \frac{r_0}{d} \right). \quad (3)$$

Discharge index depends upon the voltage U :

$$\gamma = \left(\frac{U}{U_0} - 1 \right) \left(2\pi \frac{h}{d} - \ln 2\pi \frac{r_0}{d} \right). \quad (4)$$

Linear density of discharge current:

$$I_0 = 1,6k\varepsilon_0 \left(1 + 1,12 \frac{d}{h} \right) \left(\pi E_0 \frac{r_0}{2h} \right)^2 \gamma^{1,5}, \quad (5)$$

where k is the ion mobility, $k_- = 2.20 \cdot 10^{-4} \text{ m}^2/\text{Vs}$ for negative discharge, and $k_+ = 1.80 \cdot 10^{-4} \text{ m}^2/\text{Vs}$ for positive discharge, ε_0 is the permittivity constant, $\varepsilon_0 = 8.85 \cdot 10^{-12} \text{ F/m}$. Initial field strength determined from (1) for $r_0 = 0.05$ mm and $\delta = 1$ is $E_0 = 158.0$ kV/cm. The dependence of initial voltage U_0 determined from (3) on the height h is given in Table 1.

Table 1. Dependence of initial voltage on the height h

h , mm	10	11	12	13	14
U_0 , kV	6.36	6.69	7.02	7.35	7.68

Computed volt-ampere characteristics for negative and positive discharge are shown in Fig. 2 and Fig. 3. The values of height h are given in mm. The greater values of voltage are needed for the same values of current if the values of height h are increased.

The greater values of the discharge current for negative corona are determined by the greater negative ion mobility. The value of height of corona wires above the plane electrode is selected equal to 10 mm for experimental arrangement.

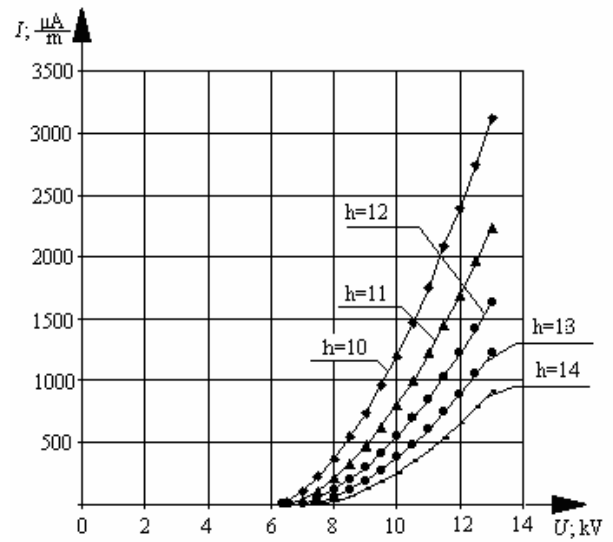


Fig. 2. Computed volt-ampere characteristics for negative corona

Data of volt-ampere characteristics at the value of height $h = 10$ mm are used for choosing the proper high voltage source.

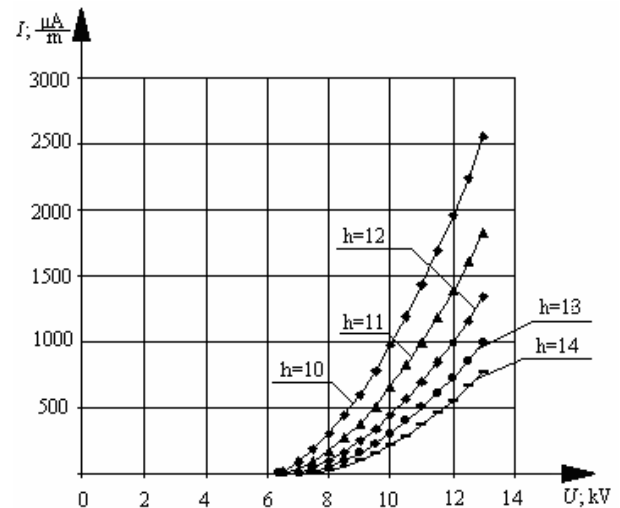


Fig. 3. Computed volt-ampere characteristics for positive corona

Comparison of computed and experimental volt-ampere characteristics for discussed electrode system is shown in Fig. 4 and Fig.5. Experimental curves differ from the computed ones due to the roughness of corona electrode and the errors of measurement. The discharge voltage shouldn't exceed the value $2U_0$ because it is related with a risk of a spark discharge.

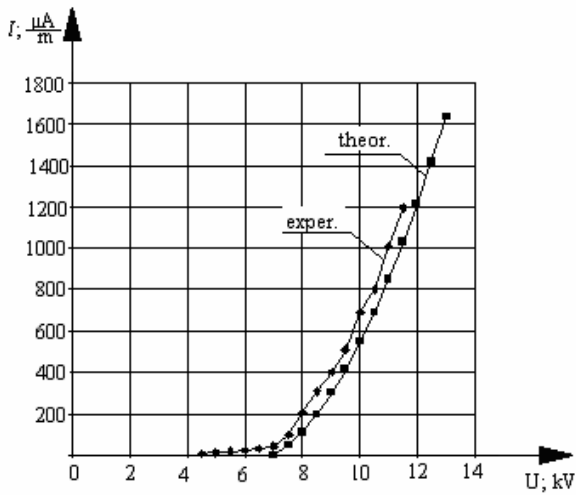


Fig. 4. Comparison of computed and experimental volt-ampere characteristics for negative corona

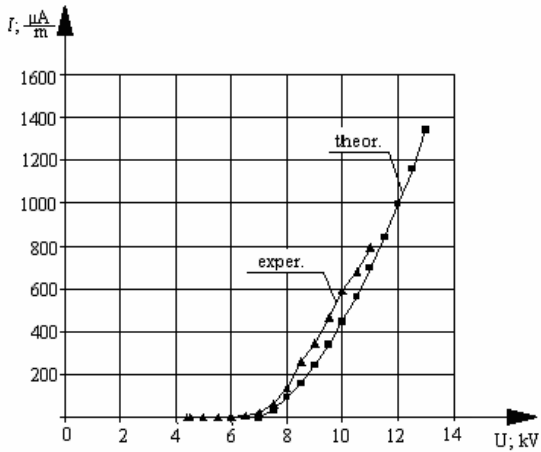


Fig. 5. Comparison of computed and experimental volt-ampere characteristics for positive corona

3. Results of an experiment

Drying test is performed at 19 °C ambient air temperature, 45 % relative humidity and 101-102 kPa of an atmospheric pressure. Drying clay sample is arranged horizontally on the grounded aluminium sheet. Initial weight of wet clay sample is 0.241 ± 0.001 kg. Periodicity of sample weighing is 1 h. Each drying session is performed twice: under free convection conditions and with a sample subjected by direct current corona field. Total discharge current is adjusted to 200 μ A at the voltage 7.5 kV (approximately, the value of the voltage is slightly increased to compensate the increasing of resistance of drying clay sample). Final weight of dry clay sample is 0.206 ± 0.001 kg. Total weight of water in wet clay sample is 0.035 kg. Curves of drying process with negative and positive corona field in comparison with natural drying conditions in still air are presented in Fig. 6 and Fig. 7. Letter m denotes the mass of drying clay sample, and t is the time measured from the beginning of drying. Drying experiment is finished at 10 h from the beginning when the sample drying in corona field has no moisture.

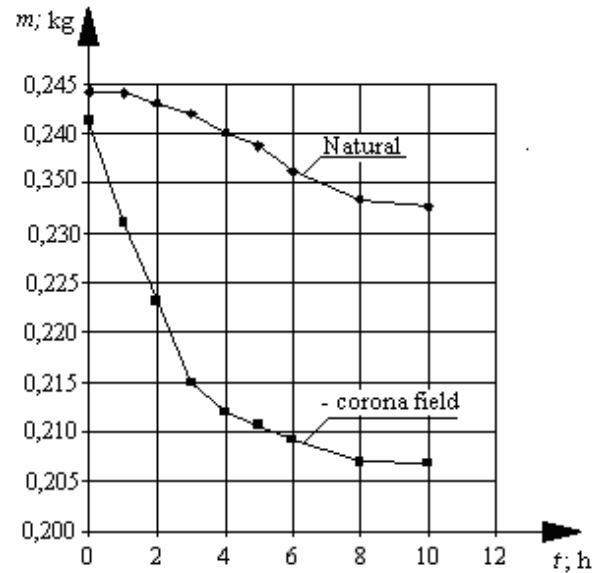


Fig. 6. Drying process in negative corona field

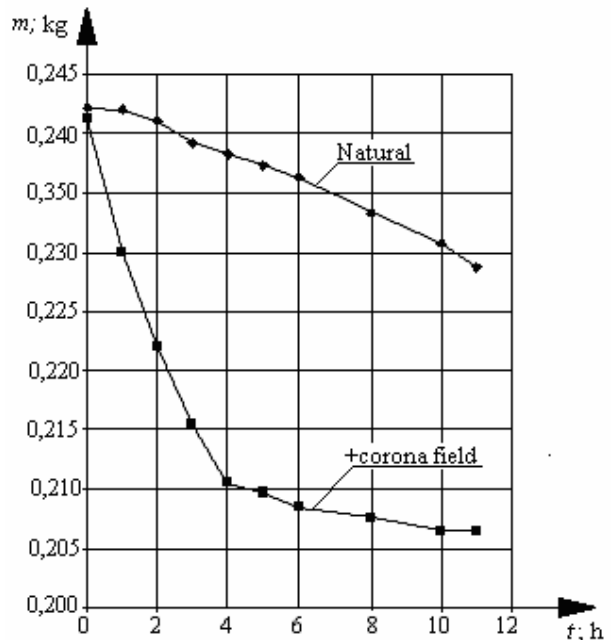


Fig. 7. Drying process in positive corona field

Parameters of the drying process with the corona field and without it are given in Table 2.

Table 2. Parameters of drying process

t , h	m_{nd} , %	m_{+cd} , %	m_{-cd} , %	r_{+} , times	r_{-} , times
1	0.6	31.0	28.6	51.7	47.7
2	2.8	54.0	51.4	19.3	18.3
4	8.6	88.6	82.8	10.3	9.6
6	14.3	94.3	91.4	6.6	6.4
8	22.8	97.1	97.1	4.3	4.3
10	31.4	100.0	100.0	3.2	3.2

Meanings of symbols used in Table 2 are the following: m_{nd} is the quantity of naturally evaporated water from drying clay sample, m_{+cd} and m_{-cd} are the quantities of evaporated water from drying clay sample with positive and negative corona discharge, r_{+} and r_{-} is the increase of drying rate actuated by positive and negative corona

field, respectively, in comparison with natural drying rate.

Positive corona field influences slightly better to the rate of moisture evaporation at the beginning of drying process in comparison with the negative corona field, but the influence of both corona modes to the overall drying process is the same. The duration of 100 % drying under the action of direct current corona field is 10 h, the increase of the drying process rate to evaporate all the moisture content is 3.2-fold in comparison with natural drying conditions. The duration of 80 % drying actuated by corona field is 4 h, the increase of the drying process rate to evaporate this content of moisture is more than 10 times. The duration of drying process to evaporate 50 % of moisture content is 2 h, using the corona field it reduces by 20 times. Intensification of the drying process is determined by the ion-driven wind (electric wind) of the corona discharge and by the phenomenon of electro-osmosis in the drying material [5]. Using of corona field improves the quality of drying because of more uniform moisture evaporation in all the volume of the material. Under the conditions of naturally drying process the moisture evaporates more intensively in the layer near the surface.

Energy consumption of 100 % drying is 1.5 kWh to 1 m² of clay panel area. If drying process ends at 80 % of moisture evaporation it takes 0.6 kWh/m², and the consumption of energy for 50 % moisture evaporation is 0.3 kWh/m².

Experiment of drying is performed at the relative corona voltage $U/U_0 = 1.67$. Intensification of drying may be enhanced by increasing the relative corona voltage but it will increase the energy consumption.

4. Conclusions

1. Using the direct current corona field for clay panel drying process increases the rate of 100 % moisture evaporation 3.2-fold in comparison with natural drying process in the air. The duration of drying to 80 % moisture evaporation reduces 10 times, and the duration of 50 % moisture evaporation reduces 20 times.
2. Energy consumption of 100 % drying is 1.5 kWh to 1 m² of clay panel area. It takes 0.6 kWh/m² for 80 % drying, and 0.3 kWh/m² for 50 % drying.
3. Using the direct current corona field to drying process increases the drying quality. Rate of moisture

evaporation in all points of drying material volume becomes more uniform.

4. Intensification of drying may be enhanced by increasing the corona voltage, but it will increase the energy consumption.

5. References

1. Nekrošius L. Architektūros ir aplinkos darna: šiaudinis namas. <http://www.spec.lt>
2. Milutienė E., Jürmann K., Keller L. Straw Bale Building – Reaching Energy Efficiency and Sustainability in Northern Latitudes. International Conference “Northern Sun 2007”, 2007-05-30 – 2007-06-01, Rīga, 6 p.
3. King B. Design of Straw Bale Buildings. The State of Art. New York, Green Building Press. 2006. 218 p.
4. Kaneko T., Hamada K., Chen M. Q, Akashi M. Freeze-Drying of Soft Nanoparticles with Projection Coronas Forms Three Dimensional Microstructs. *Advanced Materials*, 2005, Vol. 17, p. 1638-1643.
5. Banerjee S., Law S. E. Electroosmotically Enhanced Drying of Biomass. *IEEE Transactions on Industry Applications*, 1998, Vol. 34, No 5, p. 992-999.
6. Monzon J. C. Electromagnetic paper drying. *IEEE Transactions on Microwave Theory and Techniques*. 1995, Vol. 4, No 2, p. 299-305.
7. Mishima H., Yasui T., Mizuniwa T., Abe M., Ohmi T. Particle-Free Wafer Cleaning and Drying Technology. *IEEE Transactions on Semiconductor Manufacturing*, 1989, Vol. 2, No 3, p. 69-75.
8. Панченко М. С., Панасюк А. Л., Мосиевич А. С., Панченко И. М. К интенсификации испарения влаги из сырьевого шлама с помощью электрического поля. *Электронная обработка материалов*, 1990, No. 56 с. 49-53.
9. Remeikis M., Žebrauskas S. Heat exchange in the corona field. Proceedings of the 2nd international conference on electrical and control technologies, ECT-2007. Kaunas, Technologija, 2007, p. 209-212.

A COMPARATIVE STUDY BETWEEN SMALL TRADITIONAL INDUCTION MOTORS AND SMALL CONDUCTING SLEEVE INDUCTION MOTORS USING 3D FINITE ELEMENT TRANSIENT ANALYSIS

Seyed Mohsen HOSSEINI*, Javad S. MOGHANI*, Akram HOSSEINI*

* Amirkabir University of Technology, Iran

Abstract: In this paper, transient modeling of a small induction motor with conducting sleeve is presented. Conducting sleeve Induction motor has a solid rotor which is composed of two parts: ferromagnetic core and conductor hollow cylinder. After two dimensional finite element transient analysis of the motor, its performance is compared with traditional induction motor. Then, for the precision study of the motor, three dimensional finite element transient simulation is also presented and compared with two dimensional results. Two and three dimensional finite element results are relatively similar. It is shown that in small sizes, the performance of the conducting sleeve induction motor is better than traditional squirrel cage induction motor.

Keywords: conductor sleeve, eddy current, finite element analysis, induction motor, traditional, transient analysis, three dimensional, two dimensional.

1. Introduction

Conducting Sleeve Induction Motor (CSIM) is a special induction motor with a solid rotor which is made of two parts: ferromagnetic core and hollow conducting cylinder. The material of hollow conducting cylinder could be copper or aluminum. This motor has particular applications such as helical motion induction machines [1], [2], [3], [4]. In helical motion induction machines, induced currents on the rotor must move in helical direction, so squirrel cage structures can not be used. Therefore using solid structure for the rotor is unavoidable. One of important application of solid rotor induction machine is high speed motors. Due to solid rotor and low cost, solid rotor induction motors are a good choice for high-speed applications comparative to other kinds of motors [5]. Conducting sleeve structure of the rotor is the good counterpart of the wholly ferromagnetic rotor. The wholly ferromagnetic rotor structure presents lower torque than the conducting sleeve structure. In the recent years a

number of methods are proposed for analysis of solid rotor induction motors like finite element and analytical methods [6, 7], but no work present transient analysis of conducting sleeve three phase induction motors. In this paper, with finite element method, transient simulation of the CSIM is done. First two dimensional transient simulation of the CSIM is done and its performance is compared with the performance of traditional induction motor. Then for precision study of the CSIM, three dimensional model is analyzed with finite element method. Results from two and three dimensional finite element analysis are compared with each other. These results are agreed together. It is shown that in small size, the performance of CSIM is relatively better than traditional induction motor.

2. Introduction to the Three Phase CSIM Structure

Fig.1 shows three and two dimensional views of a three phase CSIM structure.

The stator of the CSIM is similar to the traditional structure.

As shown in Fig.1, the rotor has a ferromagnetic core that is surrounded by a conducting sleeve.

The material of conducting sleeve may be copper or aluminum.

3. Transient Finite Element Analysis

Governing equations are as following [8]:

$$\nabla \times B = \mu J \quad (1)$$

$$\oint B \cdot dl = \mu \int J \cdot ds \quad (2)$$

$$\nabla \times J = -\sigma \frac{dB}{dt} \quad (3)$$

$$B = \nabla \times A \quad (4)$$

Where B , J and A are magnetic flux density, current density and magnetic vector potential respectively.

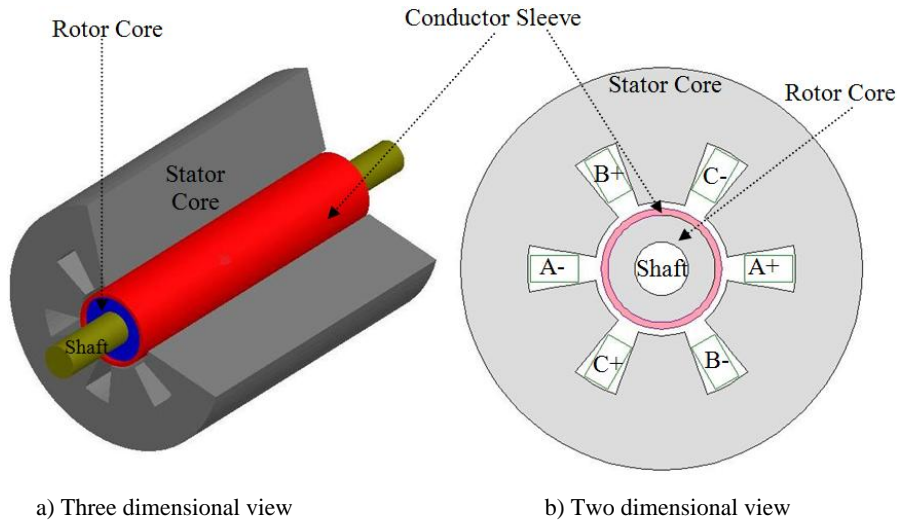


Fig. 1. Three and two dimensional views of a three phase CSIM structure

σ and μ are electrical conductivity and magnetic permeability. The following equation directly results from the above equations:

$$\nabla \times \frac{1}{\sigma} \nabla \times H + \frac{\partial B}{\partial t} = 0 \quad (5)$$

The final result is a formulation where vector fields are represented by first order edge elements and scalar fields are represented by second order nodal unknowns. Field equations are coupled with circuit equations for conductors, because in transient simulations supply voltages are applied and currents are unknown. For the nonlinearities, the classical Newton-Raphson algorithm is used.

The major difficulty for transient simulation is that induced currents on the rotor conductor must be calculated in each step, and then the torque must be calculated. The mentioned procedure is time consuming and need high memory especially in three dimensions.

4. Two Dimensional Finite Element Transient Simulation

Table 1 summarizes the characteristics of the CSIM. The designed CSIM has small dimensions.

Table 1. Design Data

inner radius of rotor	2 (mm)
outer radius of rotor	4 (mm)
outer radius of stator	15 (mm)
air gap	1 (mm)
conducting sleeve thickness	0.5 (mm)
relative magnetic permeability of stator core	2000
relative magnetic permeability of rotor	250
conductor sleeve conductivity	5.8e+7 (S/m)
number of slots	6
slot wide	20°
current density in stator slot	3 (A/mm ²)
pole numbers	2
frequency	50
number of phases	3

Copper is chosen to be used in conducting sleeve motor. In every step of transient simulation, induced currents on conducting sleeve due to stator excitation is calculated first. Fig.2 shows induced currents on conducting sleeve at time t=0.05 second.

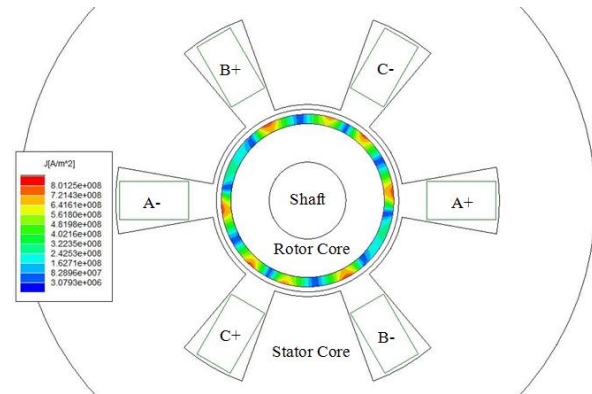


Fig. 2. Induced currents on conducting sleeve at t=0.05 second

Fig. 3 shows flux lines at t=0.05 second.

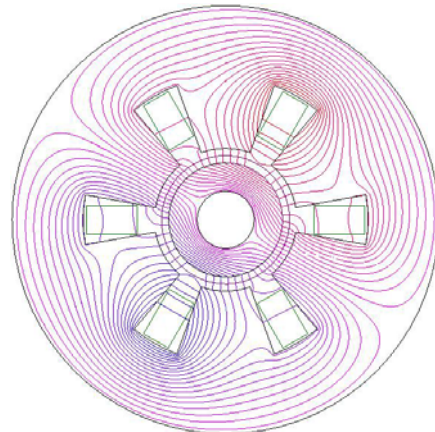


Fig. 3. Flux lines at t=0.05 second

After reaching to the steady state condition, the transient torque and speed are obtained and shown in Fig. 4 and

Fig. 5 respectively. Note that simulations are done at free acceleration.

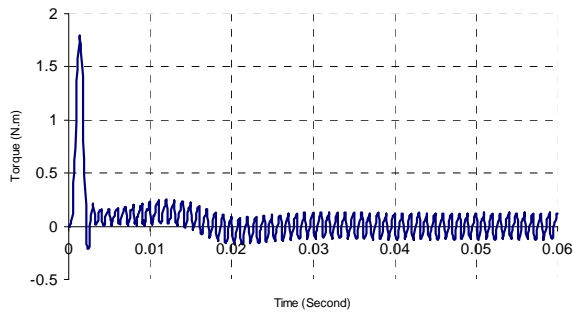


Fig. 4. Transient torque in free acceleration

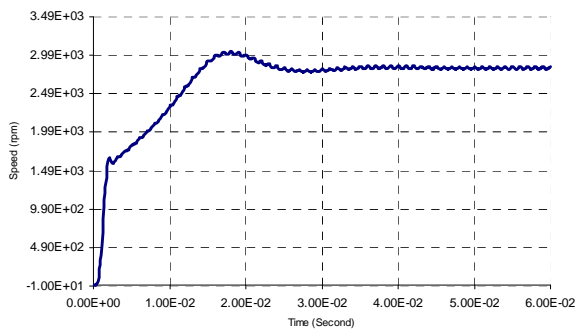


Fig. 5. Transient speed in free acceleration

As shown in Fig. 5, reaching to slips under 5% is impossible even at no load. No load currents are shown in Fig. 6.

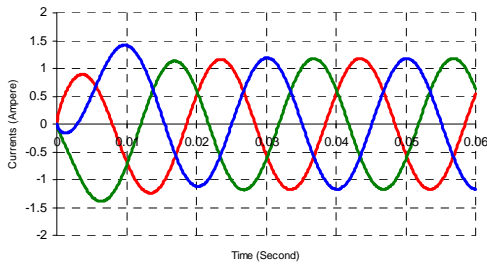


Fig. 6. Transient currents in free acceleration

For comparison with a traditional induction motor, a traditional induction motor with similar characteristics to CSIM is designed and simulated.

Fig.7, Fig.8 and Fig.9 show transient torque, speed and currents in free acceleration respectively.

Fig. 10 shows flux lines in the traditional induction motor at t=0.05 second.

Fig.4 depicts the pulsating torque in CSIM has lower amplitude in comparison with traditional induction motor (Fig.7).

Fig.8 illustrates that the traditional motor speed has larger amplitude vibration with respect to CSIM speed (Fig.5)

It is clear from Fig.6 and Fig.9 that the CSIM no load currents are greater than traditional no load currents.

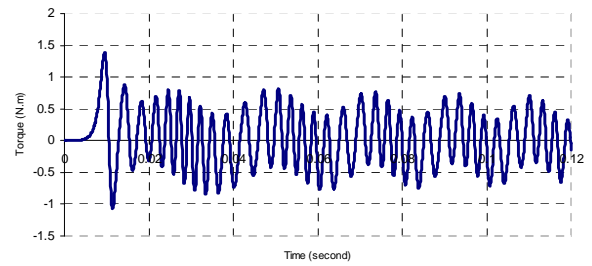


Fig. 7. Transient torque in free acceleration

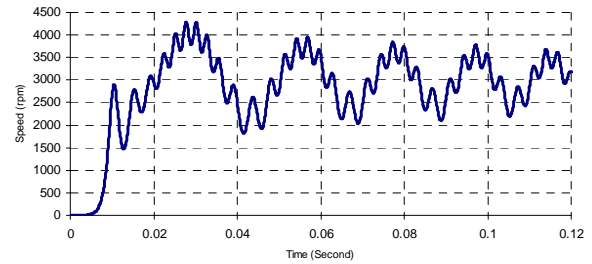


Fig. 8. Transient speed in free acceleration

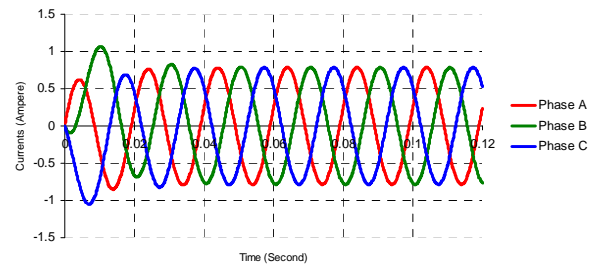


Fig. 9. Transient currents in free acceleration

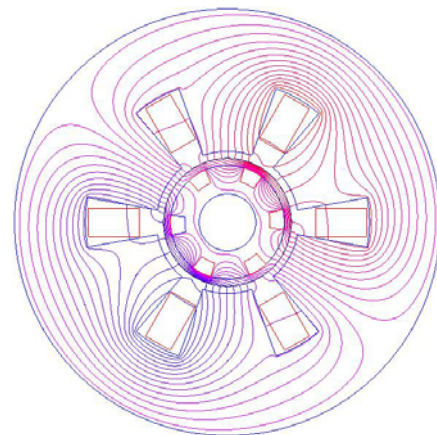


Fig. 10. Flux lines at t=0.05 second

From transient analysis results one can conclude: In small scale and few pole numbers CSIM has relatively better performance in comparison with traditional induction motor. Moreover in small scale manufacturing process, a CSIM has lower cost and easier process than the traditional induction motor.

5. Three Dimensional Finite Element Transient Simulation

In this section for precision study of the CSIM three dimensional finite element transient analysis is presented.

As mentioned before, in each step of transient analysis, eddy currents induced on rotor conducting sleeve should be calculated first. In three dimensions, this takes longer time and needs high memory.

Fig.11 illustrates eddy currents induced on rotor conducting sleeve at $t=0.05$ second.

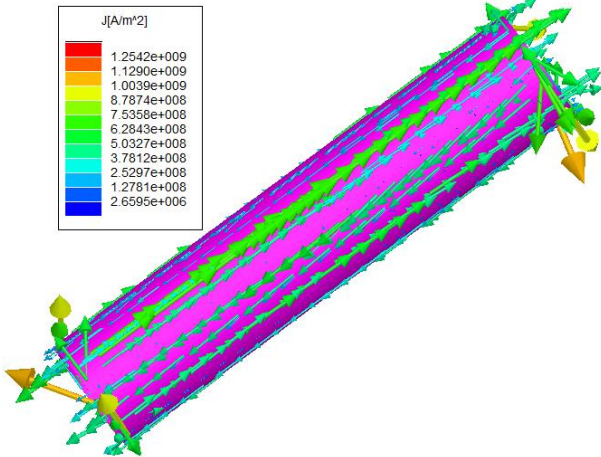


Fig. 11. Induced currents in three dimensional model of the rotor conducting sleeve at $t=0.05$ second

Fig. 12 and Fig.13 depict transient torque and speed in free acceleration, respectively.

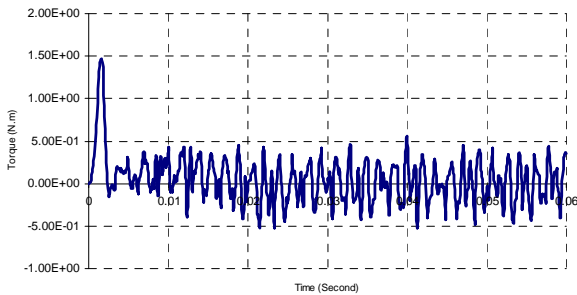


Fig. 12. Transient no load torque curve results from 3D finite element analysis

No load currents are shown in Fig. 14.

Three dimensional results are in good agreement with two dimensional results.

Fig. 12 shows more oscillation in comparison with Fig.4, because in 3D finite element analysis the real model of the motor is used while in 2D the length of the motor is assumed too long.

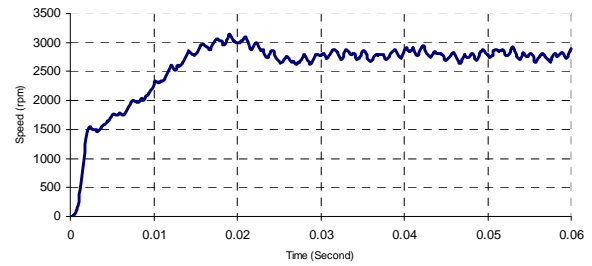


Fig. 13. Transient no load speed curve results from 3D finite element analysis

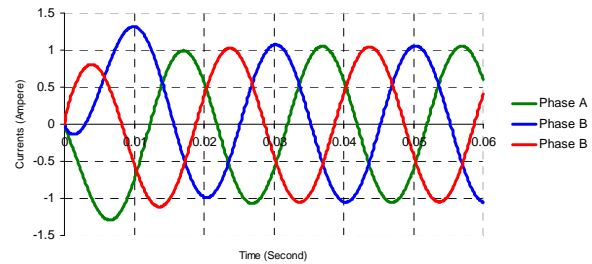


Fig. 14. Transient no load currents

As shown in Fig.14, no load current is slightly less than 2D result (Fig.6).

Torque versus speed curve in 2D and 3D simulations are shown together in Fig. 15. As expected, the peak of transient torque from 3D finite element analysis is lesser than 2D result.

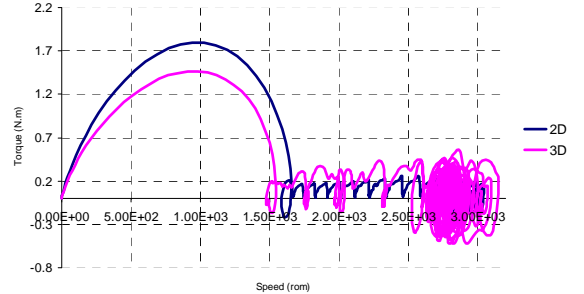


Fig. 15. Torque versus speed curve from 2D and 3D transient finite element simulations

6. Conclusions

In this paper, transient simulation of a small scale conducting sleeve induction motor is presented. Simulations are done with finite element method both in 2D and 3D. Results from 2D and 3D simulations are in good agreement with each other. This ensures the results validity.

Transient finite element simulation of a traditional induction motor is presented, too. Results show that in small scale and low pole number motors, CSIM has relatively better performance in comparison with traditional induction motor. Moreover in small scale manufacturing process, the CSIM has lower cost and easier to process than the traditional induction motor.

7. References

1. Cathey J. J. Helical Motion Induction Motor. Proceedings of IEE, Mar. 1985, vol. 132, pt. B, no. 2, pp. 112-114.
2. Onuki T., Jeon W. J. and Tanabiki M. Induction Motor with Helical Motion by Phase Control. IEEE Transaction on Magnetics, September 1997, Vol. 33, No. 5, pp.4218-4220.
3. Alwash J. H. H., Mohssen A. D. and Abdi A. S. Helical Motion Tubular Induction Motor, IEEE Transaction on Energy Conversion, September 2003, Vol. 18, No. 3, pp. 362-369.
4. Becherini G. and Tellini B. Helicoidal Electromagnetic Field for Coilgun Armature Stabilization, IEEE Transaction on Magnetics, January 2003, Vol. 39, No. 1, pp. 108-111.
5. Hupponen J. High Speed Solid Rotor Induction Machine–Electromagnetic Calculation and Design, Thesis for the degree of Doctor of Science, 2004, Lappeenranta University of Technology, Finland.
6. Jagiela M., Bumby J. R. and Spooner E. Modeling of High Speed, Solid Rotor Induction Machines Using Adaptive Finite Elements Procedures. Proceeding of International Conference "Electrical Machines (ICEM)- 2004" , Lodz, Poland, 2004.
7. Davey K.R. Analytic Analysis of Single and Three Phase Induction Motors. IEEE Transaction on Magnetics, 1998, Vol. 34, No. 5, pp. 3721-3727.
8. Bianchi N. Electrical Machine Analysis Using Finite Element. CRC Press, 2005, pp. 3-24.

GRAPHICAL METHOD OF ESTIMATING OPTIMUM VALUES FOR THE MAIN DIMENSIONS OF A D.C. MACHINE

C. EASWARLAL*, V. PALANISAMY**, M.Y. SANAVULLAH***

*Sona College of Technology, India,

** Principal Info Institute of Engineering, India

*** K.S.R. College of Technology, India

Abstract: Design is based on the assumption of values for the variables. However, the machine is expected to have minimum cost, weight, volume and losses. The above factors are conflicting with one another. However, all the factors are dependent upon the machine dimensions. In practice, only one of the above factors is taken as objective and optimum design is arrived at. But in this paper, the variables are categorized carefully as free and fixed variables. The values for the fixed variables are selected from the range of values available. The value for the free variables is estimated under specified constraint, resulting in optimum values for the free variables. The main dimensions of a DC machine are treated as free design variables. The objective is suitably stated along with the constraint. Thus the design problem is changed to an optimization problem. Graphical method is used for obtaining optimum values for the main dimensions besides care is bestowed to obtain rated power as output. A design problem is taken for illustration and obtained results both by conventional and graphical method are compared. The optimality of the graphical method is verified by popularly available optimizing method.

Keywords: power, armature diameter, armature core length, optimum values, graphical method.

1. Introduction

Design may be defined as a creative physical realization of theoretical concepts [1]. Engineering design is application of science, technology and invention to produce machines to perform specified task with optimum economy and efficiency. Engineering is the economical application of scientific principles to practical design problems. If the items of cost and durability are omitted from a problem, the results obtained have no engineering value. The problem of design and manufacture of electric machinery is to build, as economically as possible, a machine which fulfills a certain set of specifications and guarantees.

The design is subordinated to the question of economic manufacture. The major considerations to evolve a good design are:

- I. Cost
- II. Durability
- III. Compliance with performance criteria as laid down in specifications.

In most of the situations, it becomes difficult to design a machine which meets all the performance indices and also satisfies the cost and durability criteria because these requirements are usually conflicting. It is impossible to design a machine which is cheap and is also durable at the same time. This is because a machine which is to have a long life span must use high quality materials and advanced manufacturing techniques which obviously make it costly. The performance indices have to be met for certain. However, a compromise between cost and durability can be had. In order to achieve optimality of an objective, the values that are used for the variables should be optimum besides assuming which of the variables are free and fixed variables suitably.

The main dimensions of a d.c.machine can be expressed in terms of the rated power output, desired magnetic and electric loadings and speed of the machine in the form of an equation, which is known as output equation of the machine. The choice of specific magnetic and electric loadings is made based on performance factors, such as:

- I. Maximum flux density in iron parts of the machine
- II. Magnetizing current
- III. Core losses

for specific magnetic loading and

- I. Permissible temperature rise
- II. Voltage
- III. Size of machine
- IV. Current density

for specific electric loading.

It is clear that these specific loadings are design variable. Similarly the main dimensions are also design variables. Speed of the machine may be treated as fixed variable or constant. Hence the power output for a constant or fixed speed machine can be expressed in terms of the above four variables. The general procedure in design is to assume some variables as known and fixed and some variables as independent or free variables and evolve. Since the specific loadings are dependent on the main dimensions, the specific loadings are treated as fixed variables and the main dimensions are treated as independent or free variables. To find optimum values for the free design variables, an objective function and constraint, if any is required in terms of free design variables. The objective must be such that the machine dimensions are minimum or optimum. [2] P.RUpadhyay and K.R.Rajagopal considered efficiency as the objective function whereas temperature rise and motor weight are the constraints and the slot electric loading, magnet-fraction, slot-fraction, air gap and air gap flux density are the design variables. [3] Messine, F (et.al) showed the advantage of a deterministic global-optimization method in the optimal design of electromechanical actuators. The numerical methods classically used are founded either on nonlinear programming techniques (i.e., augmented Lagrangian, sequential quadratic programming) or on stochastic approaches which are more satisfactorily adopted to global optimum research (i.e., genetic algorithm, simulated annealing). However, the later methods only guarantee reaching this global optimum with some probability. In this paper, the non-linear design variables are limited to two in number. Further the power output is taken as constraint. The constraint equation is modified in terms of the same two design variables, which helps to use [4], [5], [6] a simple graphical method for getting optimum values for the design variables. The values are obtained simultaneously, which is a special feature of this method and satisfy the objective.

2. Symbols

P_a	=	Power developed by armature, kW
D	=	Armature diameter, m
L	=	Armature core length, m
n	=	Speed in rps
B_{av}	=	Specific magnetic loading, Wb/m ²
ac	=	Specific electric loading, A
P	=	Rated power output, kW
η	=	Efficiency
Ψ	=	Ratio, pole arc to pole pitch
τ	=	Pole pitch = $\pi D/p$
C_o	=	Output coefficient
b	=	Pole arc
b_p	=	Width of pole body
λ	=	Lagrange multiplier
L_f	=	Lagrangian function
X	=	A constant
p	=	Number of poles

3. Description of design problem

[1] To find the optimum values for the main dimensions of a 5 kW, 250 V, 4 pole, 1500 rpm simplex lap wound D.C. shunt generator. The loadings are: Average flux density in the gap = 0.42 Wb/m² and ampere conductors per metre = 15,000 A. Assume full load efficiency = 0.87.

4. Solution by conventional method

Design makes use of assumptions, empirical relations derived out of experience, approximations, etc., Neglecting friction, windage and iron losses, the power developed by the armature in general can be written as

$$P_a = P/\eta = 5.75 \text{ kW.}$$

$$\text{Speed, } n = 25 \text{ r.p.s.}$$

Output equation,

$$P_a = \pi^2 B_{av} ac D^2 Ln \times 10^{-3} \quad (1)$$

The output coefficient,

$$C_o = \pi^2 B_{av} ac \times 10^{-3} \quad (2)$$

On substitution, $C_o \approx 62.1$.

From equation (1), $D^2 L = P_a / C_o n$.
Substituting the values,

$$D^2 L = 0.0037037 \text{ m}^3 \quad (3)$$

or

$$D^2 L \approx 0.0037 \text{ m}^3 \quad (4)$$

The value as a product in terms of D^2 and L is obtained for D and L . In order to separate D and L , one of the following techniques depending upon the requirement is adopted.

- Square pole section ($L = b_p$)
- Length equaling twice the width of pole body ($L=2 b_p$)
- Square pole face ($L = b$)

The above indicates only pole proportion of the machine. Let us take the case of square pole face such that the armature core length equals pole arc.

For a square pole face, core length/pole arc = $L/b = 1$ or $L/\Psi \tau = 1$. Taking, $\Psi = 0.64$, $L = \Psi \times \pi D / p = 0.50265D$, i.e.,

$$L \approx 0.503D. \quad (5)$$

Substituting eqn. (5) in eqn. (4) and solving,

$$D \approx 0.195 \text{ m}$$

$$\text{and } L \approx 0.1 \text{ m} .$$

Thus the values for the main dimensions are found analytically one after another. Further the values for the main dimensions would be different for different

requirements. Unique and optimum values can not be expected.

5. Optimum value by graphical method

[4] Optimization is a process of finding the conditions that give the maximum or minimum value of a function. For any optimization problem, an objective is compulsorily required along with constraint, if any is to be specified. Here the conditions refer to the values for the free design variables, namely D and L such that the objective function is made maximum or minimum. The function refers only to

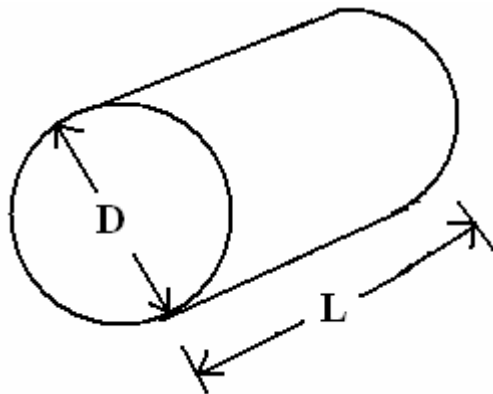


Fig. 1. Armature of a D.C. Machine

the objective function. The aim now is to bring in an objective function. The armature of a d.c. machine labeling D and L is as shown in “Fig.1”. Whenever we refer armature diameter, D it reminds only a circle, whereas armature core length, L may be thought of a linear distance. The circle (i.e. armature) diameter is also considered as a linear distance with a linear distance of D. Hence the objective function may be written in terms of D and L, which are variables, as

$$f(D,L). \tag{6}$$

The armature is viewed in terms of its main dimensions namely D and L. The objective is to minimize the sum of linear distances of armature and hence the objective function equation is written as

$$D + L = X; \tag{7}$$

where X is a constant, which must be minimum.

The design problem is now stated as to find the values for D and L such that total linear distance in the machine is optimum (i.e. minimum) and at the same time delivering the rated power. Thus the output equation which governs the power output is the constraint equation, and it is expressed in terms of D and L. The corresponding equations for the design problem are equation (7) and equation (4) which are rewritten as

$$D + L = X \quad \text{(objective function)}$$

$$\text{and} \quad D^2 L = 0.0037 \text{ m}^3 \quad \text{(constraint equation).}$$

The above equations contain only two variables. The constraint is an equality constraint type. Since there are two variables, a simple graphical method is used.

The graph for constraint equation is drawn first. The values for D are obtained for different assumed values of L and a graph between D and L is drawn. The shape of the graph is obviously non-linear and takes the form of a parabola as shown in “Fig.2”. The readings for the graph are as shown in “Table 1”.

To draw the objective function graph, a constant value for X is assumed. Then for different assumed values for L, the corresponding values for D are obtained. It is a straight line graph. This process is repeated for different X. The points for objective function graph for different value of X are given in “Table 2”, “Table 3” and “Table 4” as examples. The objective function is thus represented as a series of straight line graphs as shown in “Fig. 2”. It may be noted or seen that some graphs may be above the constraint graph and some may be below it. But at the same time, one straight line graph may become tangent to the constraint graph.

Table 1. Readings for L and D (constraint equation)

L, m	0	0.01	0.02	0.05	0.07	0.09	0.1	0.12	0.14	0.16	0.2	0.25	0.3	∞
D ² , m ²	∞	0.37	0.185	0.074	0.053	0.041	0.037	0.0308	0.026	0.023	0.0185	0.0148	0.0123	0
D, m	∞	0.608	0.43	0.272	0.23	0.202	0.192	0.1756	0.162	0.152	0.136	0.121	0.111	0

Table 2. D + L = X (= 0.2)

D,m	0	0.2
L,m	0.2	0

Table 3. D + L = X (= 0.3)

D,m	0	0.3
L,m	0.3	0

Table 4. D + L = X (= 0.4)

D,m	0	0.4
L,m	0.4	0

The constraint graph and the objective function graphs are shown in “Fig.2”. One objective function graph become tangent to the constraint graph. From the tangent point, the values for D and L are obtained as

$$D = 0.192 \text{ m ;}$$

$$L = 0.1 \text{ m .}$$

which are optimum values for D and L, irrespective of the requirement of pole proportions.

6. Optimality by lagrangian method

The objective function is $D + L = X$
 and constraint equation is $D^2L - 0.0037 = 0$.
 The Lagrangian function L_f can be written as
 $L_f(D,L,\lambda) = D + L + \lambda(D^2L - 0.0037)$.

The necessary conditions for optimum are

$$\frac{\partial L_f}{\partial D} = 0 \tag{8}$$

$$\frac{\partial L_f}{\partial L} = 0 \tag{9}$$

$$\frac{\partial L_f}{\partial \lambda} = 0 \tag{10}$$

On solving, the optimum values are

$$D = 0.1948\text{m}$$

and $L = 0.0974\text{m}$.

7. Comparison of results

The values for armature diameter and core length obtained by all methods are given in “Table 5” for comparison.

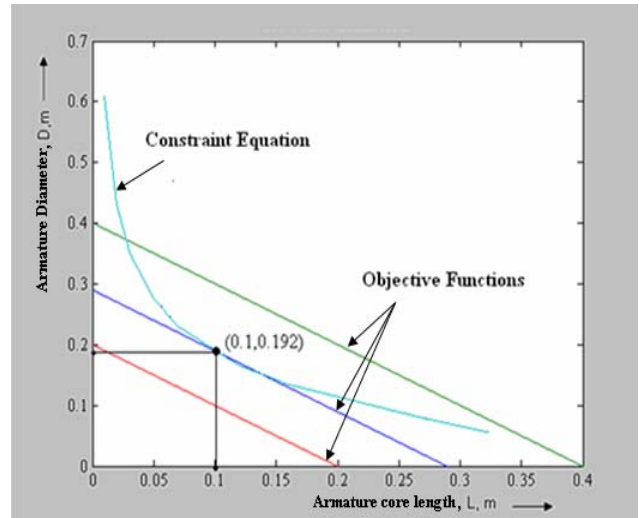


Fig. 2. Graphical Method

Table 5. Comparison of values

Design variables	Methods		
	Conventional	Graphical	Lagrangian
D, m	0.195	0.192	0.1948
L, m	0.100	0.100	0.0974
(D+L), m	0.295	0.292	0.2922

It is seen that the sum of armature diameter and core length is less in graphical method than that obtained by conventional method which indicate that the values for D and L are optimum. It is verified with the help of Lagrangian method.

8. Conclusions

A d.c.machine design problem is solved by conventional method, which employs assumptions, approximations, etc., Further it requires an equation in terms of pole proportions for the separation of D and L, which results in different values for D and L depending upon the separating condition equation. None of these values would be optimum. Hence the conventional design problem is converted as an optimization problem. The procedure for estimating optimum values for the main dimensions are explained with the help of graphical method. The values are verified with the values obtained by popularly available optimizing method. The values are agreeable. The speciality of this method is that optimum values for both the free design variables are obtained simultaneously. Such method can be used in intermediate steps in the process of design of an electric machine, provided the constraint equation and objective function contain only two same variables. The example may be the estimation of window dimensions of a transformer. The performance of the d.c. machine would improve because the optimum values are estimated at the first step itself which will be used in further calculations. Hence such graphical method may be adopted for obtaining optimum values for the two variables at the time of design of an electric machine at appropriate places.

9. References

1. Sawhney A. K. A course in Electrical machine Design. Dhanpat Rai & Co (p) Ltd, Delhi-110006, 2001.
2. Upadhyay P. R., Rajagopal K. R. Genetic algorithm based design optimization of a permanent magnet brushless dc motor. J.Appl.phys.97, 10Q516(2005); D.O.I : 10.1063/1.1860891.
3. Messine F., Nogarrede B., Lagowanelle J.L. Optimal design of electromechanical actuators: a new method based on global optimization. IEEE Transactions on Magnetics, Vol.34, Issue 1, Jan 1998, PP.299-308, D.O.I:10.1109/20.650361.
4. Singirasu S. Rao. Engineering optimization theory and practice. 3rd Ed., New Age international (p) Lt, New Delhi-110002, 1999, pp.11-15.
5. Easwarlal C., Palanisamy V., Sanavullah M.Y., Gopila, M. Graphical Estimation of optimum weights of iron and copper of a transformer. ISBN:0-7803-9772-X/06/\$20.00©2006 IEEE.
6. Easwarlal C., Palanisamy V., Sanavullah M.Y. Optimim full load losses of a Transformer by graphical method, International Journal of Electrical and Power Engineering. (3):359-362, 2007, ©Medwell journals, 2007.

10. Biographies



C. Easwarlal was born in 1947. He studied his B.E (Electrical and Electronics Engineering) degree course and M.Sc (Engg) (Electrical Machines) degree course at PSG College of Technology, Coimbatore - 641 004 and received the degrees in the years 1971 and

1973 from University of Madras. He has worked as an Electrical Engineer in a company for two years. Then he took up the teaching assignment. He has put in 28 Years of experience. Currently he is working towards his Ph.D degree in Anna University, Chennai, India. He is a professor of Electrical and Electronics Engineering, Sona College of Technology, Salem – 636 005, India. His area of interests is design of Electrical Machines, optimization in design, power system analysis.



V. Palanisamy received the B.E. degree in Electronics and Communication Engineering, from PSG College of Technology, Coimbatore in 1972, the M.E. degree in Communication systems in 1974 from University of Madras and the Ph.D. in Antenna Theory in 1987 from IIT Karagpur, India.

Since 1974 he has been working in various capacities of Technical Education in Tamilnadu, and he is retired Principal of Government College of Technology, Coimbatore, India. Currently he is holding the post of Principal at Info Institute of Engineering, Coimbatore. His interest includes Neural Network, Fuzzy Logic and Optimization.



M. Y. Sanavullah was born in 1942. He received the B.E degree in Electrical & Electronics Engineering and M.Sc degree in Power System Engineering in the years 1965 and 1967 from the University of Madras, Ph.D degree in High Voltage

Engineering in 1987 from Anna University, Chennai. He guided a candidate at Ph.D level in Periyar University, Salem during 2001 – 2005. At present he is guiding four candidates leading to Ph.D in Vinayaka Mission's University, Salem. He has 38 Years of teaching experience. He is currently a Professor and Dean with K.S Rangasamy College of Technology, Tiruchengode 637 209, India. He is interested in finite Element Method.

THE RESEARCH OF CAUSES AND CONSEQUENCES OF PARAMETERS CHANGES OF GROUNDING ELECTRICAL INSTALLATIONS

Marina KIZHLO, Arvids KANBERGS
Riga Technical University, Institute of Power Engineering, Latvia

Abstract: This paper introduces the resistance of the ground (soil resistivity) and measurements of the soil resistivity. It is well known that the resistance of the ground electrode is heavily influenced by the soil resistivity in which it is driven and as such, measurements of the soil resistivity are an important parameter when designing grounding installations. Knowledge of the soil resistivity at the intended site, and how this varies with parameters such as moisture content, temperature and depth, provides a valuable insight into how the desired ground resistance value can be achieved and maintained over the life of the installation with the minimum cost and effort.

Keywords: resistance of the ground, soil resistivity, grounding system, measurements of the soil resistivity.

1. Introduction

The electrical characteristics of the ground have an effect on the resistance of the grounding system, and therefore to the electrical safety of the personnel, which operates electrical devices. One of the main objectives of grounding electrical systems is to establish a common reference potential for the power supply system, building structure, plant steelwork, electrical conduits, cable ladders and trays and the instrumentation system. To achieve this objective, a suitable low resistance connection to the ground is desirable. However, this is often difficult to achieve and depends on a number of factors:

- Soil resistivity;
- Stratification;
- Size and type of electrode used;
- Depth to which the electrode is buried;
- Moisture and chemical content of the soil.

The conductivity of surface layer substantially influences the value of the touch voltage and step voltage. The resistivity of the ground changes in the very wide range depending on the geological structure of the ground. By changing the spacing of the grounding electrodes, it is possible to develop a profile of the soil resistivity at various depths, which can be used to

identify the most appropriate ground electrode design. However, even on the area, selected for the construction of the grounding system, the ground vary most frequently in terms of significant heterogeneity in the vertical and horizontal sectional views; therefore the soil resistivity, which satisfies the high accuracy of calculation can be obtained only by direct measurements. In cases when the high accuracy of calculation is not required, it is possible to use tabular values of the soil resistivity of the ground. It is known that all substances according to their electrically conducting properties are divided into:

- conductors $\rho \leq 10^{-5} \Omega \cdot m$;
- insulators $\rho \leq 10^{+8} \Omega \cdot m$;
- semiconductors $10^{-5} \Omega \cdot m < \rho < 10^{+8} \Omega \cdot m$.

The rocks, different structures of the ground and natural aqueous media, as a rule, relate to the semiconductors.

2. Soil resistivity

The property of resistivity can be defined for any material. As applied to soil, resistivity is an indication of a given soil's ability to carry electric current. The flow of electricity in the soil is largely electrolytic, determined by the transport of ions dissolved in moisture. The soil resistivity is the resistance measured between two opposing surfaces of a $1m^3$ cube of homogeneous soil material, usually measured in $\Omega \cdot m$. The soil resistivity has a direct effect on the resistance of the grounding system. The typical features of soils with certain resistivity values are shown in Table 1. These changes are caused by the influence of admixtures and by different structure of the mineral grains, on which the measurements were conducted. Microscopic cracks and oxidations of surface within the limits of individual grains produce significant changes in the values of the measured resistances. The values of the resistivity of the ground water are given in Table 2.

Table 1. Classes of soil and their resistivity

Classification	Resistivity ρ ($\Omega\cdot m$)	Features
Low resistivity zone	$\rho < 100$	Lowland at the mouths of rivers or by the sea. Usually abundant in water.
Medium resistivity zone	$100 \leq \rho < 1000$	Midland plains where ground water is not so difficult to obtain.
High resistivity zone	$\rho \geq 1000$	Hilly zones, piedmont districts and high lands, where drainage is good.

The resistivity of rocks depends also on temperature. For the water-containing rocks the temperature effect on the resistance of rocks is the same as the temperature effect on the electrical resistance of the located in the rocks water and the temperature range between the points of its freezing and boiling.

Table 2. Resistivity of water (approximate values)

Type of water	Resistivity ($\Omega\cdot m$)
Pure water	200000
Distilled water	50000
Rain water	200
Tap water	70
Well water	20 ~ 70
Mixture of river and sea water	2
Sea water (inshore)	0.3
Sea water (ocean 3%)	0.2 ~ 0.25
Sea water (ocean 5%)	0.15

Table 3 demonstrates evidently a sharp increase of the resistivity of the rocks with the freezing of pore moisture. The resistivity of soil varies with changes in temperature and the rate of its increase as temperature declines. The moisture content of the soil in Table 3 is 15.2% of its total weight. The resistivity of the soil at $-15^{\circ}C$ is 45.9 times higher than the resistivity of the same soil at $+20^{\circ}C$. The resistivity of soil is, in fact, influenced by many factors and it fluctuates constantly. It is lower in summer and higher in winter. Table 4 gives the recommended values of the resistivity of the upper layer of the ground with a thickness of up to 50 m for the use in the design calculations.

Table 3. Soil temperature vs resistivity

Temperature	The ground resistivity ($\Omega\cdot m$)	Rate
$20^{\circ}C$	72	1.0
$10^{\circ}C$	99	1.4
$0^{\circ}C$	130	1.8
$0^{\circ}C$ (ice)	300	4.2
$-5^{\circ}C$	790	11.0
$-15^{\circ}C$	3300	45.9

3. Measurements of the soil resistivity

When designing the grounding system to meet safety and reliability criteria, an accurate resistivity model of the soil is required. The purpose of the soil resistivity testing is to obtain a set of measurements which may be

interpreted to yield an equivalent model for the electrical performance of the ground. However, the results may be incorrect or misleading if adequate investigation is not made prior to the test or the test is not correctly undertaken. To overcome these problems, the following data gathering and testing guidelines are suggested.

Table 4. Classes of soil and their resistivity

Class of soil	Resistivity ($\Omega\cdot m$)
Paddy of clay and swamps	10 ~ 150
Farmland of clay	10 ~ 200
Seaside sandy soil	50 ~ 100
Paddy or farmland with gravel stratum	100 ~ 1000
Mountains	200 ~ 2000
Gravel, pebble seashore or parched river bed	1000 ~ 5000
Rocky mountains	2000 ~ 5000
Sandstone or rocky zone	$10^4 \sim 10^7$

Data related to nearby metallic structures, as well as the geological, geographical and meteorological nature of the area is very useful. For instance the geological data regarding strata types and thicknesses will give an indication of the water retention properties of the upper layers and also the variation in resistivity to be expected due to water content. By comparing recent rainfall data, against the seasonal average, maxima and minima for the area it may be ascertained whether the results are realistic or not. For measuring the parameters of the electrical structure of the ground - the thickness of the layer and of resistivity of each layer the two methods are recommended: the method of the trial vertical electrode and the method of the vertical electrical sounding. The selection of the method of measurement depends on the characteristic of the ground and necessary accuracy of measurement. The following sections outline the major practical aspects of the measurement procedure and result interpretation.

4. Method of trial vertical electrode

The method of the trial vertical electrode can be used in the electrical devices up to 20 kV, if the ground in the region of electrical device is characterized by a relatively low specific resistance. As a rule, in such electrical devices the grounding system is calculated by the permissible resistance, moreover significant in the value standardized permissible resistances can be obtained with a comparatively low accuracy of the determination of the soil resistivity of the ground. The method is based on the measurement of the resistance of the trial electrode, whose geometric dimensions correspond to those accepted for designing the grounding system, immersed at the calculated depth at different points of the selected area. Resistivity is determined on the basis of the formulas, which characterize the resistance of the grounding conductor of the corresponding form. For example, for the pivotal trial grounding conductor specific resistance is calculated by the formula (1):

$$\rho = \frac{Rl}{0,366 \cdot \lg \frac{2l}{d}}, \quad (1)$$

where R – resistance of the grounding conductor in the form of electrode, obtained by the measurement, [Ω];

l – depth of the laying of trial electrode, [m];

d – the diameter of trial electrode, [m].

Obtained result of measurement of the soil resistivity represents a certain averaged value (2), which calculates the heterogeneity of the ground on the basis of vertical line. In order to consider the uniformity of the ground along horizontal, one should conduct several measurements at different points of the selected area and for the calculations use arithmetic mean of the results of measurements:

$$\rho_{avg} = \frac{\rho_1 + \rho_2 + \dots + \rho_n}{n}, \quad (2)$$

where R – soil resistivity, obtained as a result of measurement at different points of the area, [$\Omega \cdot m$];

n – number of measurements.

A change of the soil resistivity along the horizontal is not considerable with the small sizes of areas and it is possible to limit to conducting one measurement. Climatic conditions in the region of the construction of the grounding system cause, as a rule, the essential fluctuations of the soil resistivity of the ground in the course of the year as a result of freezing, moistening and drying soil; therefore it is necessary to carry out the measured specific resistance ($\Omega \cdot m$) to the design conditions by means of the seasonal coefficient (3):

$$\rho_{eq} = \rho_{avg} k, \quad (3)$$

where ρ_{eq} – calculated equivalent soil resistivity, (it corresponds to the most unfavourable climatic condition of the ground), [$\Omega \cdot m$];

k – seasonal coefficient, which considers an increase the resistance of the ground.

Seasonal changes in the soil resistivity depend on climatic conditions in the region of the grounding system and depth of the ground layer for accounting for seasonal changes, the entire territory of Latvia is divided into four climatic zones (Table 5). Seasonal coefficients are selected depending on climatic conditions in the period, which precedes measurements. In this case accept different coefficients for vertical (Table 6) and horizontal grounding conductors (Table 7). Different influence of climatic conditions on the surface and deep layers of the ground thus is considered. The method of the trial vertical electrode is characterized by simplicity of measurements, and it also requires the use of a minimum quantity of minimum number of measuring equipment and calculations.

Table 5. Climatic zones

Characteristic of the climatic zone	Climatic zones			
	I	II	III	IV
Average long-standing lowest temperature of air (January), °C	-20 ÷ -15	-14 ÷ -10	-10 ÷ 0	0 ÷ +5
Average long-standing highest temperature of air (July), °C	16 – 18	18 – 22	22 – 24	24 – 26
Average annual amount of precipitation, cm	40	50	50	30 – 50
Duration of the freezing of water, days	190 – 170	150	100	0

Table 6. Seasonal coefficients for the design conditions of the soil resistivity for the calculation of the resistance of trial vertical grounding conductors

Climatic zones	Value of coefficient k with the submersion depth of electrode					
	2 – 3 m			4 – 5 m		
	For the moisture of soil or amount of precipitation in the period before the measurements					
	Increased	Average	Lowered	Increased	Average	Lowered
I	1,85	1,65	1,50	1,45	1,35	1,30
II	1,60	1,45	1,30	1,30	1,25	1,20
III	1,45	1,30	1,20	1,25	1,15	1,10
IV	1,30	1,10	1,0	1,20	1,10	1,0

Table 7. Seasonal coefficients for the design conditions of the soil resistivity for the calculation of the resistance of trial horizontal grounding conductors

Climatic zones	Value of coefficient k with the length of grounding conductor					
	2 – 3 m			4 – 5 m		
	For the moisture of soil or amount of precipitation in the period before the measurements					
	Increased	Average	Lowered	Increased	Average	Lowered
I	5,4	3,2	2,3	4,3	2,6	2,0
II	3,8	2,2	1,7	3,2	2,0	1,5
III	3,1	1,7	1,4	2,6	1,5	1,3
IV	2,0	1,3	1,1	1,8	1,2	1,0

Its basic deficiency is complexity of sinking the measuring electrodes at the calculated depth, especially under the conditions of the solid ground. However, the method is not practically acceptable for the measurements on areas with the high specific resistance of the surface layers of the ground (rock, permafrost and so forth). The need for immersing grounding conductors at the significant depth under such conditions can arise and, to determine the calculated specific resistance it is necessary to use the method of vertical electrical sounding.

5. Method of vertical electrical sounding (VES)

For the measurements four electrodes (Fig. 1), immersed at the small depth 40-50 mm are used. Measuring the strength of the current I , that flows from the source through the current electrodes 1, 4, and the

voltage between the potential electrodes 2, 3, determine the resistance (4)

$$R = U / I , \quad (4)$$

which is equal to the resistance of a certain volume of the ground, which adjoins the measuring unit. Conditionally this volume is taken as the equal to the hemisphere with the diameter, determined by the distance between the current electrodes. The measured soil resistivity carries to the point of the ground on the vertical axis of the hemisphere at the depth, equal to fourth of its diameter. Consequently, for measuring the soil resistivity at the depth h it is necessary that the distance between the current electrodes would compose $l_{1-4} = 4h$. In this case if the potential electrodes divide the distance between the current electrodes into equal parts $l_{2-3} = 1/3l_{1-4}$, the soil resistivity ($\Omega \cdot m$) can be calculated according to the formula (5)

$$\rho_{VES} = 2\pi Ra , \quad (5)$$

where $a = l_{1-2} = l_{2-3} = l_{3-4}$ – distance between the adjacent electrodes, [m];

R – measured resistance, [Ω].

Changing the distance between the current electrodes, the conditional soil resistivity ρ at the different depth h for the different layers of the ground is measured. If the distance between the potential electrodes composes $l_{2-3} < 1/3l_{1-4}$, it is possible to transpose the current electrodes only, leaving the potential electrodes constant. In this case the value of the soil resistivity is calculated from the formula (6)

$$\rho_{VES} = \frac{\pi}{2} R \left(\frac{l_{1-4}^2 - l_{2-3}^2}{2l_{2-3}^2} \right). \quad (6)$$

For obtaining the minimum error it is not allowed to take a too small distance between the potential electrodes. It should be assumed $l_{2-3} = (0,41 \div 0,43)l_{1-4}$. The measured soil resistivity by the method of vertical electrical sounding is a conditional value. For bringing it into the calculations, use the special graphs - theoretical templates for the multilayer ground, used in geophysics. In this case it is necessary to attempt to reduce the results of vertical electrical sounding to a smaller number of layers. If bringing the result to the design conditions, the structure of the ground has several layers, accept it as the two-layered ground. The tentative depth of the laying of the horizontal and vertical conductors of the grounding system is selected for this; moreover, it is necessary to select the length of vertical electrodes proportional to the layer depth of the ground with the high conductivity. As the first equivalent layer, accept the layer, which penetrates vertical electrodes. All the remaining layers of the ground are taken as the second equivalent layer.

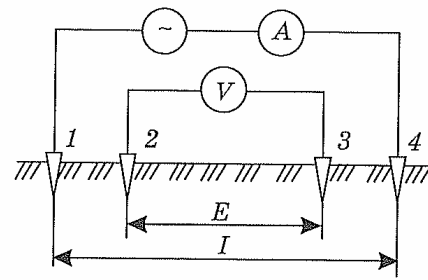


Fig. 1. Method of vertical electrical sounding

However, the obtained equivalent soil resistivity of two-layered structure of the ground cannot be used directly for calculating the resistance of the grounding system. In fact, the grounding system consists of different type of the grounding conductors, which occupy different position relative to the equivalent layers of the ground of the calculated two-layered structure of the ground. Therefore for the basic types of grounding conductors and grounding system tables and drawings have been developed. That makes it possible to calculate the equivalent soil resistivity respecting the soil resistivity of two-layered structure of the ground and relative placement of the grounding conductors in it.

6. Conclusions

The soil resistivity data is the key factor in designing a grounding system for a specific performance objective. All soil conducts electrical current, with some soils having good electrical conductivity while the majority has poor electrical conductivity. The soil resistivity varies widely throughout the whole territory of Latvia and changes dramatically within small areas. Factors that affect the soil resistivity may be summarised as:

- Type of the ground.
- Stratification; layers of different types of soil.
- Moisture content; resistivity may fall rapidly as the moisture content is increased.
- Temperature; the ground resistivity is lower in summer and higher in winter.
- Chemical composition.
- Topography; rugged topography has a similar effect on the resistivity measurement as the local surface resistivity variation caused by weathering and moisture.

Factors such as maximum probe depths, lengths of cables required, efficiency of the measuring technique, cost (determined by the time and the size of the survey crew) and ease of interpretation of the data need to be considered, when selecting the test type.

7. References

1. Kizlo M., Kanbergs A., The special features of the grounding equipment, master paper, Riga, RTU, 2008. 120 p.
2. Маньков В.Д., Заграничный С. Ф. «Защитное заземление и зануление электроустановок» Л.: ПИ 2005.г
3. IEEE Std 80-200 (Revision of IEEE Std-1986), LVS valid from 12.07.2004.

4. Sverko R. E., Ground measuring techniques: electrode resistance to remote earth and soil resistivity, ERICO, Inc. Facility Electrical Protection, U.S.A.
5. Armstrong, H. R., „Grounding electrode potential gradients from model tests”, IEEE Transactions on Power Apparatus and Systems, pp.618-623, 1960.
6. Switzer, W. K., Practical guide to electrical grounding, ERICO
7. Soil resistivity testing. Four point wenner method, LEP-1001, Lyncole XIT Grounding
8. Internet sources: www.building.lv, www.likumi.lv, www.vdi.gov.lv.

A SIMPLE TRANSIENT-BASED WIDE-AREA SELECTIVITY TECHNIQUE FOR EARTH-FAULTS IN ISOLATED AND COMPENSATED NEUTRAL MEDIUM VOLTAGE NETWORKS

Mohamed F. ABDEL-FATTAH and Matti LEHTONEN

Department of Electrical Engineering, Helsinki University of Technology (TKK), Espoo, Finland

Abstract: This paper presents a simple selectivity technique for earth-faults in isolated and compensated neutral medium voltage networks. It is based on investigations on the flow of the residual currents in the network during the earth fault. The fault weight is calculated as the transient RMS residual current ratio between the feeder/section and the background network. The fault indicator will be activated for higher fault weights; around 100%. The faulted feeder can be detected easily and the faulted section can be selected accurately. The proposed technique is less dependent on the fault resistance and the faulted feeder parameters; it mainly depends on the background network. The MV network is simulated by ATP/EMTP program. Extensive simulations that cover different fault conditions are performed to validate and realize the technique.

Keywords: earth faults, transient based protection, residual current, isolated and compensated neutral medium voltage distribution networks.

1. Introduction

As a result of climate change, windiness and thunder storms in particular are considerably increasing. This in turn leads to a higher fault probability. Together with the climate change, the modern society's growing dependence on uninterrupted power supply will greatly influence the development of distribution networks and organizations. Therefore, the requirement of reliable and efficient protection system is increased. Earth faults detection in isolated and compensated neutral medium voltage distribution networks presents a challenge to protection system due to small levels of fault currents that can not be detected by conventional relays [1].

Although several techniques have been proposed, and much progress has been made, a reliable and flexible solution has still not been found. Transient-based protective schemes utilize the transient component in the fault signals, which provides fast information about

the possible disturbance in the system. It can detect high-impedance and intermittent arcing faults; leading to improvement in the reliability and power quality. Many research works have been done in this area in the last few years, but the goal is still not fulfilled [2-9].

In this paper, a simple selectivity technique for earth fault detection is proposed. It is transient current-based technique. The fault weight factors will be calculated as the ratio between the transient residual currents. It will be used for detection of the faulted feeder (first stage) and selection of the faulted section (second stage). A wide-area communication link is required for the coordination between the two stages. A 20 kV, 251 km medium voltage distribution network is simulated by ATP/EMTP program. Extensive simulations are performed to validate and realize the technique, for different fault conditions; different fault inception angles, fault locations and high fault resistances.

2. Transient RMS Frequency Response

The transient period is the first few milliseconds directly after fault incidence. The fault detection window is proposed to be the most sensitive part of the transient period, in which the polarity comparison technique is verified. The window width is not constant; it varies according to the fault characteristics, mainly depends on the fault resistance and incidence angle. Ref. [2] proposes a sensitive varying fault detection window, in which the average values of the transient voltage and current are calculated. In practical application, the constant sliding window is preferred, which makes some limitation to the average calculations that are highly affected by opposite polarities contained in the fault detection window. In this paper, it is proposed to use the transient RMS values which are not affected by polarity changing, and can be used with constant sliding fault detection window technique. The transient RMS value will be calculated in a constant sliding window. The width of the window will be very

small; about few milliseconds to be able to extract the transient features from the considered waveform. The residual value is equal to the summation of the instantaneous phase values (a , b and c) as given by (1). The residual currents are very small in normal operation and become meaningful in fault condition. They are very sensitive for earth faults and from practical point of view, it can be measured easily by one sensor for each feeder; hence it is suggested to be used for fault detection.

$$i_r(t) = i_a(t) + i_b(t) + i_c(t). \quad (1)$$

The transient RMS value of the residual current (I_r) will be calculated using the following equation:

$$I_r = \sqrt{\frac{1}{N} \sum_{k=1}^N (i_{r,k})^2}. \quad (2)$$

Where: $i_{r,k}$ is the instantaneous value of the residual current at sample k , calculated from (1) and N is the total number of samples in the window. Equation (2) is calculated in the constant sliding fault detection window which starts at sample ($k=1$) and terminates at sample ($k=N$). If T_s is the sampling time, then the width of the fault detection window will equal to $N \times T_s$. The sliding (moving) window will be updated after collecting the new samples, after constant time step T_s . The smaller value of the sampling time enables to cover high frequencies contained in the waveform which increases the sensitivity of the detection. A sampling frequency of 25 kHz is used.

Ground fault signals consist of different frequency components, which result from charging or discharging of the network capacitances. The range of these frequencies is varying from few hundreds to few kilo Hertz. According to practical experience, the frequencies of discharge and charge components vary in the range $500\text{-}2500 \text{ Hz}$ and $100\text{-}800 \text{ Hz}$ respectively. The amplitude of the discharge component is relatively small, typically only about $5\text{-}10 \%$ of the amplitude of the charge component [10].

The evaluation of the frequency response of the transient RMS values should be investigated for different frequency components contained in the transient period. This can be achieved by calculating the transient RMS value for a sinusoidal signal with different frequencies. After that, investigate if the RMS value of each frequency can be estimated by the transient RMS method or not. The transient RMS value will be estimated in a constant width sliding window and the effect of the sliding window width will be determined to propose the suitable value of it.

Fig. 1 and 2, present the transient RMS frequency response for different values of the sliding window width (0.5 , 1.0 , 1.5 , 2.0 & 2.5 ms), at sampling frequency of 25 kHz . From preliminary analysis, it is investigated that the response of the transient RMS is highly affected by the lower frequencies (less than 2000 Hz) but the error is small for higher frequencies.

Therefore, the response will be investigated only for frequencies up to 5000 Hz .

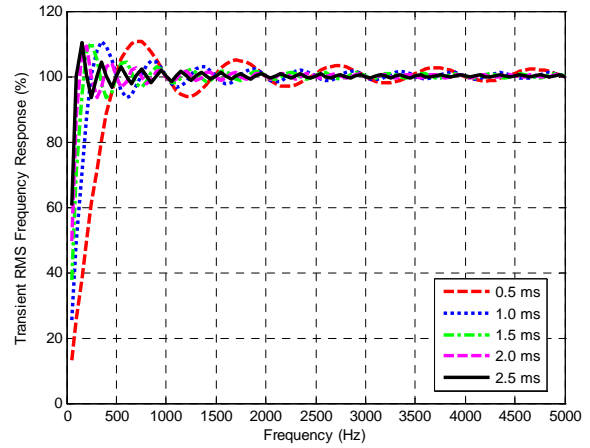


Fig. 1. The transient RMS frequency response for different values of the sliding window width (0.5 , 1.0 , 1.5 , 2.0 & 2.5 ms), up to 5 kHz , at sampling frequency of 100 kHz

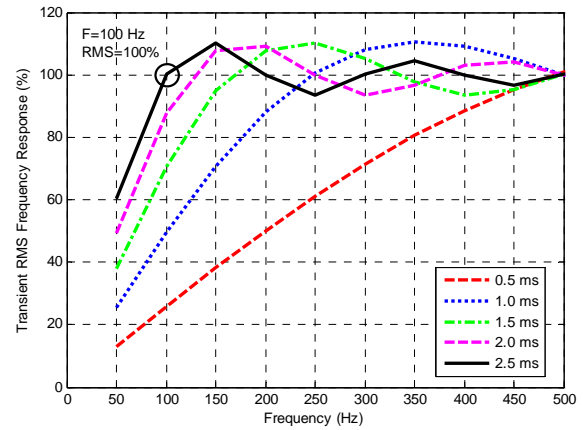


Fig. 2. Enlarged view, up to 500 Hz , for the transient RMS frequency response shown in Fig. 1

The response is evaluated as a percentage ratio between the estimated RMS value and the actual expected RMS value. From Fig. 1 and 2, it can be seen that, the lower frequency components can be estimated by the transient RMS calculations using a suitable sliding window width. The performance is highly improved by increasing the window width but more calculations are required considering the same sampling frequency.

A suitable minimum window width of 2.5 ms is adequate and proposed to cover the minimum transient frequency of 100 Hz by 100% (as shown in Fig. 2). The sampling frequency is mainly related to frequency components contained in the transient period. To cover different frequency components up to 10 kHz , the minimum required sampling frequency is 20 kHz .

3. The Simulated Network

A 20 kV , 251 km medium voltage distribution network is simulated by ATP/EMTP program. A single line diagram of the simulated network is presented in Fig. 3.

The network consists of a 66 kV supply connected to a 66/20 kV substation transformer.

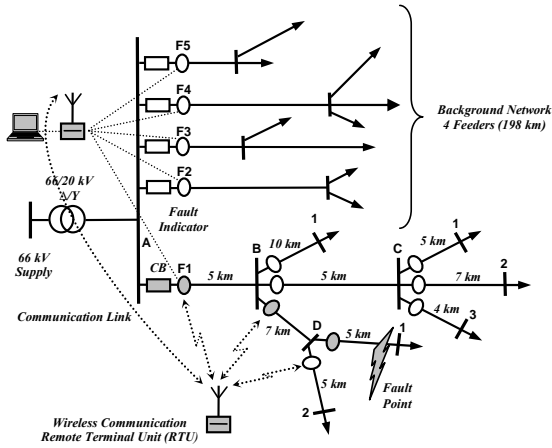


Fig. 3. The simulated, 20 kV, 251 km, medium voltage distribution network

The transformer feeds five 20 kV-overhead line feeders. Each feeder is terminated by a 0.4 kV load through 20/0.4 kV transformer. The network is implemented using ATP (Alternative Transients Program), version of EMTP program where the circuit was realized using ATPDraw [11]. The transmission line frequency dependent model of EMTP program is intentionally selected to account for the unsymmetrical faults. The feeder lines are represented using the frequency dependent JMarti model. The two cases of isolated and compensated neutral of the main transformer are simulated. A sampling frequency of 25 kHz is used. The ATPDraw circuit and the configuration of the feeders are given in Fig. 10 and 11 in Appendix.

4. The Proposed Technique

The proposed technique is based on the investigations on the flow of the residual currents in the medium voltage distribution network during the earth fault. The transient residual currents for each feeder and section are calculated and used to detect the faulted feeder (first stage) and select the faulted section (second stage) without voltage measurements. Considering the simulated network in Fig. 3, the flow of the earth fault residual currents, during a single line to ground (SLGF) fault is presented in Fig. 4.

The earth fault residual current, for the faulted feeder, is composed of the residual currents flowing through the earth capacitances of background network, and hence should be equal to the summation of the residual currents in all healthy feeders as shown in Fig. 4. The other impedances of the network components are small compared to those of the earth capacitance and hence can be neglected. The earth capacitance of the network depends on the types and lengths of the lines connected in the same part of the galvanic connected network. In practice, for radial medium voltage distribution networks, it is the area supplied by one HV/MV

substation transformer. The connected high-voltage and low-voltage networks do not affect the fault currents.

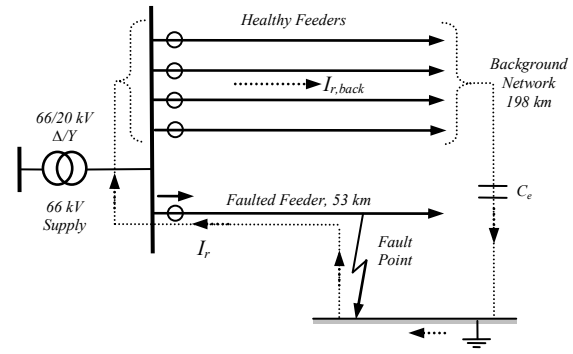


Fig. 4. The flow of the earth fault residual currents, during a single line-to-ground fault

In the first stage, the faulted feeder will be detected. For each feeder, the transient RMS residual current (I_r) will be calculated using (2), and the transient RMS background residual current ($I_{r,back}$) which is equal to the summation of the residual currents in the other background feeders will be calculated using (3).

$$I_{r,back} = \sum_{back\ feeders} I_r \quad (3)$$

It can be concluded that, for faulty feeder the residual current should equal to the background residual current but for healthy feeder they are not equal. The fault weight factors are proposed to be used as fault indicators. It will be calculated as the percentage ratio between the residual current of the feeder and the residual current of the background network as in (4), considering availability of all residual currents at the substation.

$$W = \frac{I_r}{I_{r,back}} \times 100 \quad (4)$$

For the faulted feeder, the fault weight should be equal to 100%. For the healthy feeder, the fault weight should be small. It will depend on the number of feeders in the considered network and its lengths. Assuming network of n number of equal feeders, then the fault weight for healthy feeder will be given by (5).

$$W_{hf} = \frac{1}{2n-3} \times 100 \quad (5)$$

Where n is the number of feeders in the assumed equal feeder networks. Considering the simulated network shown in Fig. 3, and assuming equal five feeders, then the fault weight for the healthy feeder should be equal to 1/7 (i.e. 14.29%). For higher number of feeders in the networks, the fault weight will be very small which improves the performance of the proposed technique and enhances its selectivity. Once the faulted feeder is

diagnosed, the proposed technique will continue to select the faulted section in the faulted feeder.

In the second stage, the fault weight factors for all sections in the faulted feeder will be calculated using the residual current of the background network for the faulted feeder as a reference, considering the availability of suitable wide-area communication link between the fault indicators for all sections and the substation, as shown in Fig. 3. The fault weight for the faulted section should be higher than 100% due to the extra circulated residual currents through the branched sections. The faulted section can be selected easily by following the radial flow of the active fault indicators. For the healthy section, the fault weight should be very small. It will depend on the number of sections in the in the faulted feeder, its lengths and its configuration. Assuming feeder of m number of radial equal sections, then the fault weight for healthy section will be given by (6).

$$W_{hs} = \frac{1}{m(n-1)} \times 100. \quad (6)$$

Where m is the number of radial equal sections and n is the number of radial equal feeders in the networks. Considering the simulated network shown in Fig. 1, and assuming equal nine sections in the faulted feeder (F1), then the fault weight for the healthy section should be equal to $1/36$ (i.e. 2.78%). For higher number of sections in the feeder, the fault weight will be very small which improves the performance and selectivity of the proposed technique.

5. Results and Setting

For the simulated network shown in Fig. 3, the instantaneous feeder residual currents are directly measured or calculated from the phase values (using (1)) at the substation measuring points; F1, F2, F3, F4 and F5. Fig. 5 shows the waveforms of the instantaneous feeder residual currents for a single line to ground fault on feeder 1 (section D1). The waveforms for all healthy feeders (F2, F3, F4 and F5) are in phase and approximately the same but the situation is different for faulted feeder (F1); higher magnitude with opposite polarity, which confirms the suitability of using transient RMS method. The waveforms are equal to zero before the fault incidence at 3 ms. The transient RMS values of the residual feeder currents are calculated in the proposed sliding window (2.5 ms) using (2). The waveforms of the transient RMS values, in time domain, are shown in Fig. 6. The transient RMS background residual currents for each feeder are calculated, in the sliding window, using (3). Then, the fault weights for each feeder are calculated, as the percentage ratio between the residual current of the feeder and the residual current of the background network, using (4). The fault weights results in the sliding window for each feeder and section are shown in Fig. 7 and 8. It can be seen that; for the faulted feeder, the fault weight is about 100% but for the

healthy feeders, the fault weight are less than 20%, which presents a high selectivity performance of the proposed technique.

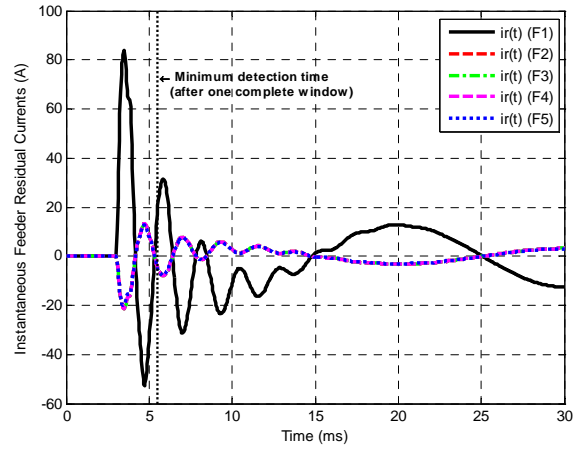


Fig. 5. The waveforms of the instantaneous feeder residual currents for a single line to ground fault on Feeder 1 (section D1) after 3 ms incidence time and 10 Ω fault resistance

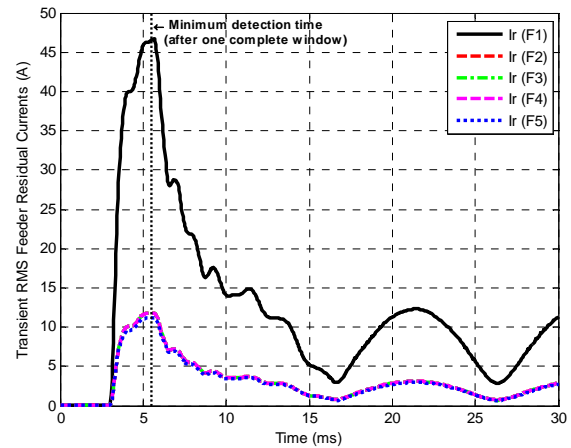


Fig. 6. The waveforms of the transient RMS feeder residual currents for a single line to ground fault on Feeder 1 (section D1) after 3 ms incidence time and 10 Ω fault resistance

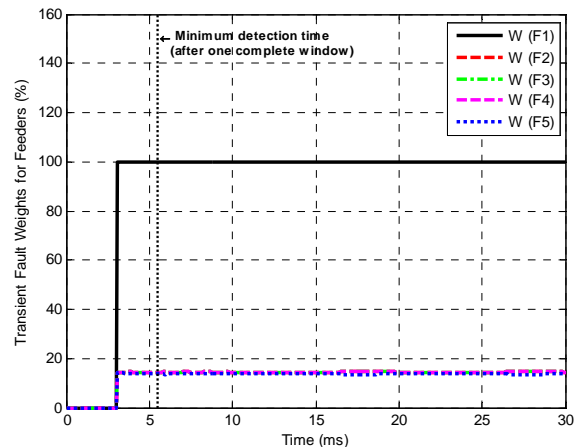


Fig. 7. The percentage transient fault weights for all feeders for a single line to ground fault on Feeder 1 (section D1) after 3 ms incidence time and 10 Ω fault resistance

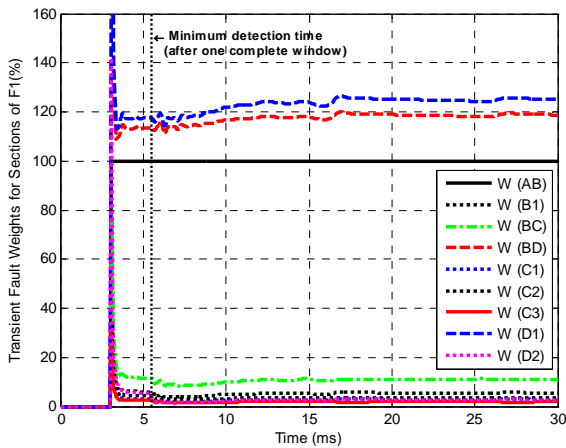


Fig. 8. The percentage transient fault weights for all sections of the faulted feeder (F1) for a single line to ground fault on section D1 after 3 ms incidence time and 10 Ω fault resistance

As shown in Fig. 8, the fault weights for all faulted sections (AB, BD and D1) are greater than or equal to 100%. The faulted section can be selected easily by following the radial flow of the higher fault weights (active fault indicators). Actually, the highest fault weight is for the faulted section. For all healthy section, the fault weights are less than 20 %.

For compensated networks (Peterson coil/resonance grounded/earthing networks), the impedance of the compensation coil is relatively high at transient frequencies. Consequently, the transients are about similar in both of isolated and compensated neutral networks. This is clearly investigated from the results of the simulation data. The effects of the fault resistance (up to 100 kΩ) for both of isolated and compensated networks are investigated.

The threshold fault weight limits are shown in Fig. 9. There is an adequate isolating gap between the healthy and faulty condition, and no overlapping between the two conditions. The setting value of the critical fault weight is proposed to be at the middle of the isolating gap, which is equal to 60%.

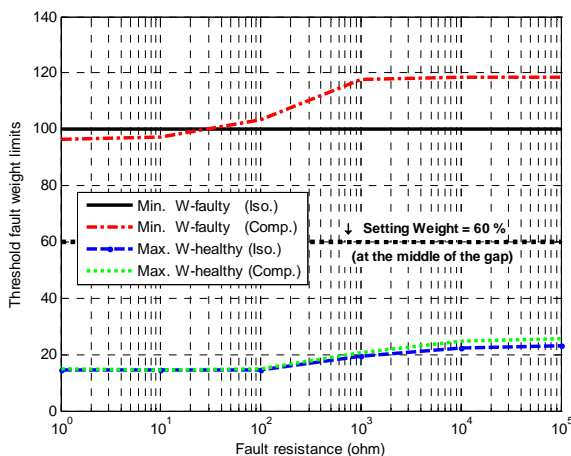


Fig. 9. The threshold fault weight limits for isolated and compensated neutral networks for a SLG fault with higher fault resistance up to 100 kΩ

6. Conclusions

A simple transient-based technique for earth faults in isolated and compensated neutral medium voltage networks is proposed. The proposed technique is used to detect the faulted feeder and select the faulted section exactly without any voltage measurements. Transient RMS values of the residual currents are calculated in a moving sliding window of 2.5 ms and then the fault weights are determined for all feeders and sections. The higher fault weights indicate the faulted feeder and section. Extensive simulations using ATP/EMTP are performed to validate the proposed technique for isolated and compensated networks. The proposed algorithm is simple and applicable

7. Appendix

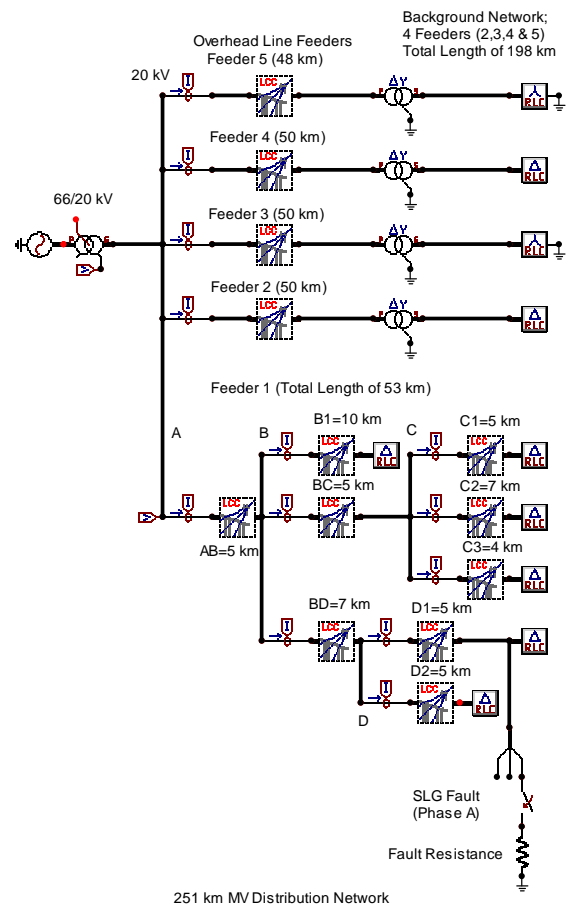


Fig. 10. The ATPDraw circuit of the simulated, 20 kV, 251 km, medium voltage distribution network

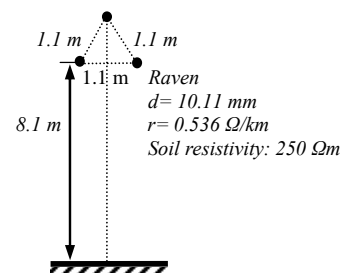


Fig. 11. The configuration of the feeders in the simulated medium voltage distribution network

8. References

1. L. Kumpulainen et al., "Distribution network 2030, Vision of the future power system," *Technical Research Centre of Finland (VTT)*, Research Report VTT- R-03835-07, Espoo, Finland, May 2007.
2. M. F. Abdel-Fattah and M. Lehtonen, "A Transient Fault Detection Technique with Varying Fault Detection Window of Earth Modes in Unearthed MV Systems," *Power Quality and Supply Reliability, 6th international conference (PQ2008)*, Pärnu, Estonia, 27-29 August 2008, pp. 181-186.
3. N. I. Elkalashy, M. Lehtonen, H. A. Darwish, A.-M. I. Taalab and M. A. Izzularab, "DWT-Based Detection and Transient Power Direction-Based Location of High-Impedance Faults Due to Leaning Trees in Unearthed MV Networks," *IEEE Transactions on Power Delivery*, vol. 23, no. 1, Jan. 2008, pp. 94-101.
4. W-Y. Huang and R. Kaczmarek, "SLG Fault Detection in Presence of Strong Capacitive Currents in Compensated Networks," *IEEE Transactions on Power Delivery*, vol. 22, no. 4, Oct. 2007, pp. 2132-2135.
5. X. H. Zhang, H. X. Ha, Z. C. Pan and B. Y. Xu, "Grounding faulty line selection in non-solidly grounded systems using transient energy," *International Power Engineering Conference (IPEC 2007)*, 3-6 Dec. 2007, pp. 1147-1150.
6. Q. Yilong, T. Weipu, C. Shuan and Y. Yihan, "Study on Fault Line Selection based on Transient and Mathematical Morphology in Resonant Grounded System," *International Conference on Power System Technology (PowerCon 2006)*, 22-26 Oct. 2006, pp. 1-5.
7. W-Y. Huang and R. Kaczmarek, "Line-to-ground fault location in compensated distribution networks by 3 parameters least-squares curve fitting without voltage measurements," *IEEE Power Tech, Russia*, 27-30 June 2005, pp. 1-4.
8. H. Belka and M. Michalik, "Application of the continuous wavelet transform to intermittent high impedance ground fault detection in MV networks," *Eighth IEE International Conference on Developments in Power System Protection*, vol. 2, 5-8 April 2004, pp. 473-476.
9. J. Lorenc, K. Musierowicz and A. Kwapisz, "Detection of the intermittent earth faults in compensated MV network," *IEEE Power Tech 2003 Conference Proceedings*, Bologna, vol. 2, 23-26 June 2003, pp. 1-6.
10. M. Lehtonen and T. Hakola, *Neutral Earthing and Power System Protection - Earthing Solutions and Protective Relaying in Medium Voltage Distribution Networks*, ABB Transmit Oy, Vassa, Finland, FIN-65101, 1996.
11. L. Prikler and H. Høidalen, "ATPDraw User's Manual", *SINTEF Energy Research*, TR A4790, Nov. 1998.

9. Biographies

Mohamed F. Abdel-Fattah was born in Qualiobia, Egypt on June 11, 1972. He is a lecturer and researcher at Zagazig



University, Egypt. He received his B.Sc. with distinction and first class honors, M.Sc. and Ph.D. degrees from Zagazig University (Faculty of Engineering, Department of Electrical Power and Machines Engineering) in 1995, 2000 and 2006, respectively.

He is a member of *IEEE*. Currently, he is a Post-Doctoral Fellow at Helsinki University of Technology (TKK), Department of Electrical Engineering, Espoo, Finland.

His main research interest is protection of electrical power systems including fault diagnosis and location of high-voltage transmission lines, transient/ultra-high-speed and wide-area protective schemes and compensation of the high resistance effect in earth faults. (e-mail: mohamed.abdel-fattah@tkk.fi , mohamed.f.abdelfattah@ieee.org).

Matti Lehtonen (1959) was with VTT Energy, Espoo, Finland from 1987 to 2003, and since 1999 has been a professor at the Helsinki University of Technology (TKK), where he is now head of Power Systems and High Voltage Engineering.



Matti Lehtonen received both his Master's and Licentiate degrees in Electrical Engineering from Helsinki University of Technology in 1984 and 1989, respectively, and the Doctor of Technology degree from Tampere University of Technology in 1992.

His main activities include power system planning and asset management, power system protection including earth fault problems, harmonic related issues and applications of information technology in distribution systems (e-mail: matti.lehtonen@tkk.fi).

SENSORS FOR ON-LINE PARTIAL DISCHARGE DETECTION IN COVERED-CONDUCTOR OVERHEAD DISTRIBUTION NETWORKS

G. Murtaza HASHMI*, Matti LEHTONEN*, Mikael NORDMAN**, Muzamir ESA*

*Power Systems and High Voltage Engineering, Helsinki University of Technology (TKK), Espoo, Finland

**Ensto Utility Networks, Porvoo, Finland

Abstract: The covered-conductor (CC) overhead lines have been frequently used in medium voltage (MV) networks in Finland for a long time. The falling trees produce PDs, which may cause the insulation of the conductors to deteriorate with the passage of time. In this paper, the Rogowski coil is proposed as a partial discharge (PD) sensor for this application. This sensor is non-intrusive and superior to the conventional PD detecting methods. The PD measurement methodology is introduced. The concept of wireless sensors and challenges to implement it for on-line condition monitoring are also described.

Keywords: covered-conductor, medium voltage, partial discharge, Rogowski coil, and wireless sensors.

1. Introduction

The CC lines have been used in MV networks throughout the world since 1970 [1]. One compelling reason to use CC lines is that they are more compact and environment-friendly than bare conductors. The CC line also withstands clashing and fallen trees for a considerable time without interruption to the power supply. In this way, the line can continue to function despite the tree contact and the removal of the trees can be scheduled appropriately. A drawback of CC lines in distribution networks is that falling trees on the line can neither be detected with normal protection relays nor be localized by advanced high impedance relays because the fault current is approximately nothing due to the CC insulation and tree resistances. However, these leaning trees produce PDs in the insulation of the CC lines as mentioned in the previous chapter, which may rupture after the passage of a certain time, resulting in different kind of faults being introduced into the network. By monitoring these PDs on-line, progressive deterioration of the insulation can be indicated. Early detection of developing faults leads to better power quality and increased customer satisfaction. PD monitoring involves an analysis of materials, electric fields, arcing characteristics, pulse

wave propagation and attenuation, sensor spatial sensitivity, frequency response, calibration, noise, and data interpretation.

For electric power distribution industries, continuous monitoring of installed and operating HV apparatus is of particular importance from the point of view of safety and reliability. The relatively new and challenging application is conducting on-line high frequency PD measurements for the monitoring of falling trees on the CC overhead distribution lines [2]. The advantage of on-line PD monitoring allows for conductor insulation diagnostics during normal operation, and specifically, when the trees are leaning on the conductors. The falling trees produce PDs, whose magnitude increases when trees cause the surface of the conductors to deteriorate. Automatic detection of the falling trees will reduce visual inspection work after storms and it will improve reliability and safety of the distribution system. Recently, a great interest has been shown by electric utilities using CC system in distribution networks in Finland to develop an on-line automatic system that should be capable of detecting falling trees on the lines. The system can be planned to be integrated into the distribution automation system to reduce the overall costs of the CC lines [3].

For the development of the on-line PD measuring system using a Rogowski coil to detect falling trees on the CC lines, the following few experiments were conducted to investigate the PD wave propagation over the CC line as well as to analyze the behavior of the Rogowski coil for high frequency measurement

2. Conventional PD detectors and their limitations

When a PD occurs, a current pulse is produced and this current pulse interacts with the insulation capacitance as well as the external elements in the test circuit. Consequently, a voltage pulse is superimposed on to the high voltage (HV) supply. The conventional detection methods generally employ matching impedance consisting of resistors, inductors and capacitors in the PD current path. The measuring

resonant circuit expands the discharge current pulses in the time domain for easier detection. In the event of PD taking place, a quantitative parameter is required to decide whether the apparatus needs to be repaired or replaced. This means that the detected signal needs to be accurately calibrated. In most cases, calibration is done by injecting a known amount of charge and measuring the voltage amplitude from the detector. There are following two different methods of conventional PD investigation [4].

- i) Straight detection including direct and indirect methods
- ii) Balance detection method (bridge circuit)

The conventional PD detection technique can identify discharges in short isolated cable lengths only. Unfortunately, it has insufficient sensitivity for a long circuit because of the large capacitance involved. It is also required to isolate the cable from the circuit. PD testing requires, besides the PD detector, additional HV components such as a test-voltage supply and a coupling capacitor, which are heavy and expensive and not suitable for on-site tests [5]. The capacitor is a very high impedance to the high ac voltage, while being a very low impedance to the high frequency PD pulse currents. The PDs are detected via a high-pass filter established by this capacitor and the resistive measuring impedance [6]. This method has two main disadvantages for on-line application:

- a) Since the HV capacitors have to be connected to the phase conductors, the cable has to be switched off, and power delivery is interrupted.
- b) The HV capacitor has to be connected for a long measuring time, or even permanently. HV capacitors are not always reliable in the long term and can, therefore, become a cause of faults themselves [6].

Instead of installing a lumped component, capacitive coupling can also be realized through a metal electrode, e.g., a plate can be installed at a certain distance from a phase conductor. The obtained capacitance, however, is now highly dependent on the geometry of the substation, cable termination, and positioning of this electrode. Furthermore, the capacitance is relatively low. In modern substations, a capacitor is sometimes integrated in the switchgear to detect the power frequency voltage on each phase conductor. The use of this capacitor for measuring small signals like PDs is in practice hard, due to its small value (usually <100pF). Moreover, this method would not be very universal, since it depends on the presence of this particular type of switchgear. In short, these conventional techniques experience severe limitations when it comes to on-line monitoring due to the influence of background noise, absence of non-intrusive sensors and processing facilities. They are, therefore, restricted to testing in a laboratory environment.

Recent studies have shown that radiation from PDs is impulsive in nature and consists of individual high-energy, wideband impulses of a few μs in length. The digital storage oscilloscopes and advanced digitizers enable study of the PD signals more closely using

window processing, zooming and auto-advance features. Such techniques promise to be superior to the currently used conventional PD detector methods. Additional benefits may be gained if monitoring can be performed as a continuous on-line measurement with automatic PD data analysis [7]. Costs and need for personnel expertise are reduced and the reliability of condition assessment is improved [8]. Recently, the PD detection frequency range has been extended up to the radio frequency band with the development of new sensors e.g., Rogowski coils.

3. Rogowski coil as a PD sensor

In 1912, the Rogowski coil was introduced to measure magnetic fields. Since the coil output voltage and power were not sufficient enough to drive measuring equipments, it has been widely used for measuring fast, high-level pulsed currents in the range of a few mega-amperes rather than in power system [9]. With the improvement of today's microprocessor-based protection relays and measurement devices, the Rogowski coils are more suitable for such applications. They have generally been used where other methods are unsuitable [10]. They have become an increasingly popular method of measuring current within power electronics equipment due to their advantages of low insertion loss and reduced size as compared to an equivalent current transformer (CT) [11]. They are the preferred method of current measurements having more suitable features than CTs and other iron-cored devices.

The coils have also been used in conjunction with protection systems particularly high accuracy systems or where there are direct current (DC) offsets which would degrade the performance of CTs. This is useful when measuring the ripple current, e.g., on a DC line. The features of the Rogowski coils which make them particularly useful for transient measurements stem from their inherent linearity and wide dynamic range.

3.1. Construction of Rogowski coil

A Rogowski coil is basically a low-noise, toroidal winding on a non-magnetic core (generally air-cored), placed around the conductor to be measured, a fact that makes them lighter and smaller than iron-core devices. To prevent the influence of nearby conductors carrying high currents, the Rogowski coil is designed with two wire loops connected in electrically opposite directions [12]. This will cancel all electromagnetic fields coming from outside the coil loop. The first loop is made up of turns of the coil, and the other loop can be formed by returning the wire through the centre of the winding as shown in Fig. 1, where d_1 , d_2 , and d_{rc} are the internal, external, and net diameters of the Rogowski coil, respectively. The coil is effectively a mutual inductor coupled to the conductor being measured and the output from the winding is an electromotive force proportional to the rate of change of current in the conductor. This voltage is proportional to the current even when measuring complex waveforms, so these transducers are good for measuring transients and for

applications where they can accurately measure asymmetrical current flows.

The self inductance of the coil is fixed, and its mutual inductance with the HV test circuit varies to some extent (or slightly) depending on the position of the coil in relation to the conductor. But once the coil is clamped and held stationary, the mutual inductance remains constant. Usually the coil is not loaded and the voltage appearing across it is used as PD measurement signal. Under this condition, the coil voltage is directly proportional to the derivative of the current in the conductor. Owing to the small value of the mutual inductance it acts as a high pass filter; the sensor, therefore, attenuates the power frequency component of the current in the conductor and minimizes EMI at lower frequencies. However, the PD signals are in the range of MHz generally and induce sufficiently large voltage in the range of mV.

The coils are designed to give a high degree of rejection to external magnetic fields, e.g., from nearby conductors. The coils are wound either on a flexible former, which can then be conveniently wrapped around the conductor to be measured or are wound on a rigid former, which is less convenient but more accurate. Both of these transducer types exhibit a wide dynamic range, so the same Rogowski coil can often be used to measure currents from mA to kA. They also exhibit wideband characteristics, working well at frequencies as low as 0.1 Hz, but are typically useful up to hundreds of kHz, too. All this with low phase error and without the danger of open-circuited secondary (as could happen in case of CT). A typical mutual inductance of a standard flexible Rogowski coil (used in this research work) is up to 200-300 nH and its resonant frequency lies in the high frequency spectrum [13], [14].

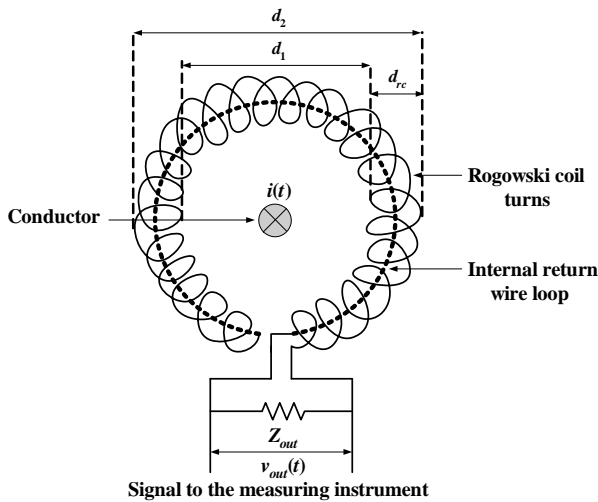


Fig. 1. Geometry and construction of the Rogowski coil

3.2. Working principle of Rogowski coil

The Rogowski coil operates on the basic principle of Faraday's law. The air-cored coil is placed around the conductor, where current pulses produced by PDs are to be measured. This variable current produces a magnetic field and the rate of change in current induces a voltage in the coil given as:

$$v_{rc}(t) = -M \frac{di(t)}{dt} \quad (1)$$

where $v_{rc}(t)$ is the voltage induced in the coil by the current $i(t)$ flowing in the conductor due to the mutual inductance M between the main current and the coil, which is practically independent of the conductor location inside the coil loop.

For simplified analysis, the behavior of the Rogowski coil with terminating impedance Z_{out} can be represented by its equivalent circuit of the lumped parameters as shown in Fig. 2 [15], where R_l , L_l , and C_l are the lumped resistance, inductance, and capacitance of the coil, respectively. The high frequency behavior of the coil, in particular its bandwidth and susceptibility to high frequency oscillations, is significantly influenced by the terminating impedance Z_{out} . There is a trade-off between the bandwidth and the sensitivity of the coil. The transfer function (V_{out}/V_{rc}) of the Rogowski coil lumped parameters model (see Fig.2) can be calculated as:

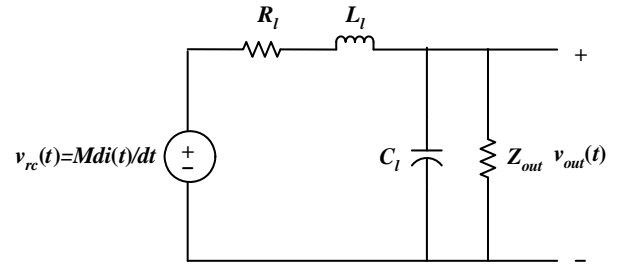


Fig. 2. The Rogowski coil equivalent circuit (lumped parameters model)

$$\frac{V_{out}}{V_{rc}} = \frac{Z_{out}}{s^2 L_l Z_{out} C_l + s(L_l + R_l Z_{out} C_l) + (R_l + Z_{out})} \quad (2)$$

Usually the air-cored coil is used in combination with large load impedance, i.e., $\omega L_l \ll Z_{out}$. ω is the angular velocity (rad/s), where $\omega = 2\pi f$, and f is the frequency (Hz) of the propagated signal. By assuming that the Rogowski coil has negligible resistance, the approximate measured voltage at terminals becomes:

$$v_{out}(t) \approx v_{rc}(t) \approx -M \frac{di(t)}{dt} \quad (3)$$

So the output voltage at the terminals of the winding wound around the toroidal coil is proportional to the time derivative of the current flowing in a conductor passing through the coil. An integrator is incorporated with the coil, which integrates the output voltage $v_{out}(t)$ according to the following equation to convert it into the current following through the conductor,

$$i(t) = -\frac{1}{M} \int v_{out}(t) dt \quad (4)$$

3.3. Advantages of using Rogowski coil

In the conventional PD sensor, the test circuit capacitance determines the frequency bandwidth and it is usually not very wide compared with this sensor. The frequency bandwidth of the Rogowski coil is not influenced by the capacitance of the test circuit. It is determined largely by the self inductance and the capacitance of the coil and signal cables. It has the following advantages:

- i) The frequency response of the Rogowski coil sensor is very wide.
- ii) There is no conductive coupling between the coil sensors and the HV test circuits. Furthermore, the coil installation does not necessitate disconnection of the grounding leads of the test objects and therefore becomes a non-intrusive sensor which is a very important aspect for on-site, on-line monitoring.
- iii) It has the advantage of possessing high signal to noise ratio (SNR) with wide frequency bandwidth.
- iv) There is no saturation due to air-cored coil; therefore, it is not damaged by over current.
- v) It has very good linearity due to the absence of magnetic materials.
- vi) The Rogowski coil based PD measurement system is a low cost solution and can be easily implemented on-site due to its light weight.

These advantages are essential for on-line PD measurements; therefore, the Rogowski coils are preferred over conventional PD sensors to take measurements for detecting falling trees on CC overhead distribution lines.

4. PD measurement methodology

The PD data captured by the Rogowski coil is essentially an oscillatory voltage pulse, which needs to be processed to obtain PD characteristics such as peak value, apparent charge, phase position, repetition rate, and PD energy. The apparent charge $q(t)$ entering into the system due to PDs is given as:

$$q(t) = \int i(t)dt = -\frac{1}{M} \iint v_{out}(t)dt^2 \quad (5)$$

where $v_{out}(t)$ is the oscillating voltage appearing at the output terminals of the sensor, M is the mutual inductance of the Rogowski coil (which is taken as 200 nH in this case), and $i(t)$ is the current flowing in the conductor due to PDs.

The fast Fourier transforms (FFTs) of the acquired pulses show the spectrum of frequency contents present in the signals. An infinite impulse response (IIR) band-pass filter (Butterworth type) of order 16 having frequency band (1-6 MHz), depending on the frequency contents of the interferences and disturbances in the signal, is applied for noise elimination. Using the above steps and mathematical expression of equation (5), the following Simulink

model can be used to measure the PD magnitude by the Rogowski coil (see Fig. 3).

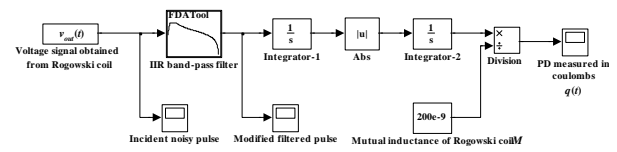


Fig. 3. Simulink model for PD measurements

5. Wireless sensors concept for on-line PD measurements

5.1. Motivation for wireless sensors

The rapid development in electronics, microcontroller performance, digital signal processing, and wireless communication has opened up possibilities to implement new industrial sensor solutions on the process level. One such promising concept is the wireless sensor [16]. Wireless sensors can be used in several applications like environmental monitoring, medical diagnosis, and different industrial condition monitoring applications. The wireless sensors may become a key technology, especially in on-line condition monitoring, as they are cheap and can easily be embedded in the processes (also as retrofit). They do not need wiring, which is a source of noise and unreliability [17].

The motivation for using wireless sensors in power system instrumentation is generally twofold: economy and safety. From a system operation perspective, wireless sensors give an opportunity to safely and cost efficiently increase measurement coverage of the network, including locations where wiring is impossible. Hence, more extensive and accurate real-time information regarding the state of the system becomes available to the operator. This means that the components and the network can safely be run closer to their technical limits and that vital information for condition based maintenance of the network assets can be elicited.

Today, one of the biggest shortcomings in distribution automation is the lack of simple and cheap instrumentation solutions that are easy to implement and are applicable in system refurbishment. The cost of instrumentation in a distribution automation system with a high degree of automation is approximately 25% [18]. The overall cost of installing and wiring a sensor exceeds the cost of the sensor by more than ten times [19]. Using wireless communication, installation costs are significantly reduced; no problems appear with damaged signaling cables that would need maintenance, and instrumentation is possible in applications where wiring is unfeasible [17]. Typically these relate to rotating machines as well as medium and HV environments. In these environments, isolation becomes a problem and maintenance activities can be dangerous [19]. In addition, refurbishment and installation without de-energizing the power network is possible. This favors wireless over power line communications (PLC), although PLC has similar advantages to wireless technologies for sensor communication in industrial environments [20].

5.2. Challenges in on-line condition monitoring using wireless sensors

Wireless sensor networks in general pose considerable technical problems in data processing, communication and system management. These problems are typically caused by a harsh and dynamic environment; combined with bandwidth and energy constraints that affect the communication, data, and signal processing that can be done. One of the biggest limitations is the fact that the wireless sensors are self-powered (the power is drawn from a battery or from energy harvested from the environment). This means that the energy resources are scarce (especially as the sensors should be small, easy to embed in components and economical); only very low frequency sampling and limited data processing can be done in the sensor [17], [21], [22].

For on-line monitoring, especially of fast phenomena like PDs, this means that the sensor has many design challenges. For example, the design of the signal processing filters must be very energy efficient and the designer must know which frequency component are the important ones for the application (to reduce the impact of noise). Also the analogue-to-digital (A/D) conversion is difficult to implement because the A/D converters working at high frequencies have rather high energy dissipation. The samples received from the conversion must be processed by the microcontroller, which means that the requirements on processing and memory capabilities are high.

Minimizing the power consumption is the most important design aspect for wireless sensors. In addition to optimized components and functionality, "shut-down" and power management strategies are used. In wireless sensors for power systems, minimized energy dissipation is essential for the feasibility of integrating the sensor within equipment and components. A light, small sensor is easy to integrate and thus minimizes the impact the sensors have on the power system reliability and operability. To achieve this goal, wireless sensors in power systems should not operate continuously. They instead need properly designed "shut-down" strategies and the means to minimize the pre-processing done by the sensor. However, they must preserve functionality, i.e., the capability to participate in, for example, state estimation and fault management [16].

Hence, it is clear that the design of a wireless sensor for the measurements of PDs in CC overhead lines needs a totally new design philosophy. To be able to find the right solutions for the design of the critical sensor components, and to be able to find the trade-off that must be made between energy dissipation and functionality, a generic model of the sensor and the PD behavior should be created.

6. Conclusions

The use of CC lines has been expanding in MV networks throughout the world over the last 30 years. CC systems are developed to reduce failure rates compared to bare wire MV networks and hence, to improve the security of the supplies. One compelling

reason to use CC lines is that they are more compact and environment-friendly than bare conductors. The additional investment cost is often fully compensated by savings in line spacing, reduced maintenance, and a better quality of network. A drawback of CC lines is that falling trees on the line cause a very high impedance fault which cannot be detected with normal or advanced protection relays. However, these leaning trees produce PDs in the insulation of the CC lines, which may rupture after the passage of a certain time, thus introducing different kinds of faults in the network.

A relatively new and challenging application is conducting on-line high frequency PD measurements for the monitoring of falling trees on CC lines. The advantage of on-line PD monitoring allows for conductor insulation diagnostics during normal operation, and specifically, when the trees are leaning on the conductors. By monitoring these PDs on-line, progressive deterioration of the insulation can be indicated. Early detection of developing faults leads to better power quality and increased customer satisfaction. PD monitoring involves the analysis of materials, electric fields, arcing characteristics, pulse wave propagation and attenuation, sensor spatial sensitivity, frequency response, calibration, noise, and data interpretation.

The measurements are taken using a wired Rogowski coil, which can be converted into a wireless sensor in the future. Due to limited computation capacity and energy constraints in wireless sensors, signal processing techniques can not be implemented as is possible in the case of the wired Rogowski coil. We must collect PD energy over a long period of time at a specific bandwidth. This PD energy will be sensed by the sensor to detect the intensity of PDs. Wireless technology is fairly inexpensive and it can be integrated into modern protection relays and to the distribution automation systems for detecting falling trees on CC lines. The proposed system will improve the safety of CC lines and make them more attractive to utilities due to reduced maintenance costs and visual inspection work.

7. References

1. P. Heine, J. Pitkänen, and M. Lehtonen, "Voltage Sag Characteristics of Covered Conductor Feeders", *38th International Universities Power Engineering Conference (UPEC 2003)*, Thessaloniki, Greece, September 1-3, 2003.
2. G. M. Hashmi, M. Nordman, and M. Lehtonen, "A Partial Discharge Detection Concept for Wireless Sensors in Covered-Conductors Distribution System", *Europe's Premier Conference on Electrical Insulation (INSUCON2006)*, Birmingham, UK, May 24-26, 2006.
3. P. Pakonen, V. Latva-Pukkila, M. Björkqvist, and T. Hakola, "Condition Monitoring and Fault Detection of Medium Voltage Covered Conductor Lines", *4th Nordic Distribution Automation Conference (NORDAC)*, Trondheim, Norway, May 22-23, 2000.

4. IEC60270, *High-Voltage Test Techniques – Partial Discharge Measurements, CEI/IEC 60270, third edition*, 2000-12.
5. N. H. Ahmed and N. N. Srinivas, “On-line Partial Discharge Detection in Cables”, *IEEE Transaction on Dielectrics and Electrical Insulation*, Vol. 5, N0.2, April 1998, pp.181-188.
6. P. C. J. M. van der Wielen, J. Veen, P. A. A. F. Wouters, and E. F. Steennis, “Sensors for On-line PD Detection in MV Power Cables and their Locations in Substations”, *7th International Conference on Properties and Applications of Dielectric Materials*, Nagoya, June 1-5, 2003.
7. P. Pakonen and V. Latva-Pukkila, “On-line Partial Discharge Measurements on Covered Conductor Lines”, *Nordic and Baltic Workshop on Power Systems*, Tampere, Finland, February 4-5, 2002.
8. B. A. Lloyd, S. R. Campbell, and G. C. Stone, “Continuous On-line Partial Discharge Monitoring of Generator Stator Windings”, *IEEE Transaction on Energy Conservation*, Vol. 14, No. 4, December 1999.
9. G. Xiaohua, L. Jingsheng, Z. Mingjun, and Y. Miaoyuan, “Improved Performance Rogowski Coils for Power System” *Transmission and Distribution Conference and Exposition, 2003 IEEE PES*, Wuhan, China, 7-12 September 2003.
10. D. A. Ward and J. L. T. Exon, “Experience with using Rogowski Coils for Transient Measurements”, *Pulsed Power Technology, IEE Colloquium*, February 20, 1992, pp.61-64.
11. Z. Mingjuan, D. J. Perreault, and V. Caliskan, “Design and Evaluation of an Active Ripple Filter with Rogowski Coil Current Sensing”, *Power Electronics Specialists Conference, PESC99, 30th Annual IEEE*, Vol. 2, 1999, pp.874 -880.
12. L. A. Kojovic, “Rogowski Coil Transient Performance and ATP Simulations for Applications in Protective Relaying”, *International Conference on Power Systems Transients (IPST'05)*, Montreal, Canada, June 19-23, 2005.
13. D. A. Ward and J. La T. Exon, “Using Rogowski Coils for Transient Current Measurements”, *Engineering Science and Education Journal*, June 1993.
14. L. A. Kojovic, “Rogowski Coil Suit Relay Protection and Measurement of Power Systems”, *IEEE Computer Applications in Power*, Vol. 10, No. 3, July 1988, pp.47-52.
15. M. Argueso, G. Robles, and J. Sanz, “Implementation of Rogowski coil for the Measurement of Partial Discharges”, *American Institute of Physics, Review of Scientific Instruments*, 76, 065107, June 2005.
16. M. Nordman, “An Architecture for Wireless Sensors in Distributed Management of Electrical Distribution Systems”, *Doctoral dissertation, Helsinki University of Technology (TKK)*, Finland, November 2004.
17. T. Brooks, “Wireless Technology for Industrial Sensor and Control Networks”, *Sensors for Industry Conference, Sicon'01*, Rosemount, Illinois, USA, 5-7 November 2001.
18. E. Antila, “Developing Distribution Automation in Medium Voltage Networks”, *Master's Thesis, Helsinki University of Technology (TKK)*, Finland, February 2003.
19. G. Shamble, J. Schutz, and C. Apneseth, “Novel Wireless Power Supply System for Wireless Communication Devices in Industrial Automation Systems”, *IEEE Annual Conference of the Industrial Electronics Society (IECON02)*, Sevilla, Spain, 5-8 November, 2002.
20. J. Ahola, “Applicability of Power-line Communications to Data Transfer of On-line Condition Monitoring of Electrical Drives”, *Doctoral dissertation, Lappeenranta University of Technology (LUT)*, Finland, 2003, ISBN: 951-764-783-2.
21. A. Sinha and A. Chandrakasan, “Dynamic Power Management in Wireless Sensor Networks”, *IEEE Design & Test of Computers*, Vol. 18, March-April 2001.
22. D. Wentzloff, B. Calhoun, R. Min, A. Wang, N. Ickes, and A. Chandrakasan, “Design Considerations for Next Generation Wireless Power-aware Microsensor Nodes”, *International Conference on VLSI Design*, Mumbai, India, January 2004.

FAILURES AND DIAGNOSTICS OF POWER TRANSFORMERS

Sandra VITOLINA, Janis DIRBA
Riga Technical University, Latvia

Abstract: The situation in the field of power transformers' diagnostics is analyzed, focusing mainly on the most frequent causes for transformer outages in Latvian distribution system. Classification of diagnostic tests according to a fault type as well as some aspects of control parameter's selection is given. A version of condition appraisal system is also given in this article.

Keywords: control of technical condition, diagnostics, power transformers, reliability.

1. Introduction

Power transformer is one of the main elements of energy system determining largely the reliability of electric supply. Effective control of technical condition is one of the ways how to reach and to maintain high reliability of the unit.

It has been proved that in many cases prolonging power transformer's lifetime for a 20-30 years is economically more profitable than replacement of the old unit with the new one. The use of rather expensive control and diagnostics systems is considered as appropriate. The expenses of diagnostic systems amount to 10% of costs of a power transformer [1]. Thus a conversion from previously scheduled repair system to a more operative repair system based on units' technical condition prognosticating also unit's work with acceptable risk level is prerequisite.

Sudden failure of a power transformer can cause high expenses. For example, in year 2002 transformer fire caused by a failure in one of the 345kV bushings was experienced in Labadie power plant in the USA (Fig.1). This transformer was put into operation in 1968 and served one of the four generators in the plant with 600 MW rated generating power. Estimated loss at this point is \$ 5 million, including \$ 1.5 million business interruption. 15 days were needed for a primary repair to set up a spare unit and to proceed generation [2]. Experts clarified the reason of the fire after this accident. Investigation showed that the fire was caused by small fault in one of the high voltage bushings that caused subsequent failures. Severe failures of power transformers are very rare in Latvian power system

however small and initially insignificant defects are frequently determined. This confirms that a well timed detection of the faults in their early stage is extremely important as it provides high coefficient of readiness, reduces outages and costs for repair, as well as prolongs the working life of the power transformer.

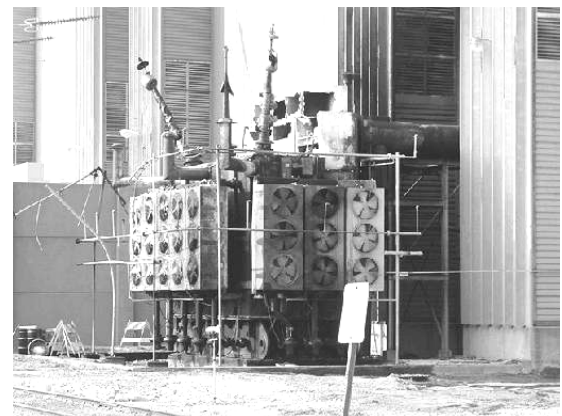


Fig. 1. Transformer fire caused by a failure in high voltage bushing and aftereffects of the transformer fire

2. Control parameters, measuring methods and diagnostic tests for power transformers

Generally power transformers are affected by outer factors or abnormal conditions in power system. It is considered that material deterioration, construction imperfections, manufacture faults, as well as inadequate maintenance strategy and not sufficiently performed

repair works are the factors that mostly reduce reliability of transformers.

Determination of the unit's technical condition can be divided into 3 stages:

1. Selection of control parameters that characterise ongoing processes in the unit;
2. Measurement of chosen control parameters;
3. Condition assessment of the unit based on gained data analysis.

The main control parameters for oil-filled power transformers are following:

- Concentration of dissolved gases in oil, interfacial tension, acid number, dielectric strength, moisture, density of mechanical admixture, concentration of soluble acids and many other oil parameters;
- Cellulose insulation parameters – cellulose polymerization degree, moisture and mechanical strength;
- Oil-cellulose dielectric parameters including dielectric loss, conductivity, capacitance, resistance, absorbability etc.;
- Unit's heating parameters such as hottest point temperature, temperature apportionment in the winding, temperature of local overheating in the winding;
- Mechanical qualities of the winding – condition of pressing, short circuit impedance of the winding, frequency characteristics etc.;
- Parameters of partial discharges – intensity, incidence, continuance, primary voltage of partial discharge, medium current value, discharge power etc.

Thus there are very many diagnostic control parameters. The larger half of mentioned control parameters is measured accomplishing the complex diagnostic of the unit. However complex diagnostic of the unit is time-consuming and very expensive, thus optimization of choosing control parameters is done in two stages. In the first stage minimum obligatory characterizing parameters are measured, allowing determining origination of faults in transformers. After determining the existence of the fault the second diagnostic stage is started in which extra control parameters are measured, fault type and it's stage of development are designated. This approach is cost-effective, but it isn't possible yet to nominate optimal minimum obligatory control parameters whose measurement results could show origination of all type faults.

One of the basic requirements for measuring control parameters is high metering precision. The accuracy of the gauge has to be higher for at least an order than acceptable value of measuring parameter prescribed in standards. It is very important to ensure reiterative measurements which means to provide conditions as equal as possible when measurements are carried out. Thus it is possible to compare the results to the accumulated diagnostic data from previous tests. Another aspect is necessity to gain data in the most suitable form for unit's technical condition assessment. For example, it's hard to make a decision if only total mass of mechanical alloy in oil is given, because there can be a lot of small and harmless particles as well as

paucity of large particles that are hazardous for the transformer. In this case for determining mechanical alloy in oil lasers are used to screen off alloy groups in order of their proportions.

The second stage of diagnostics is the measurement of chosen control parameters. For the needs of diagnostics it is necessary to choose such metering methods that can be applied for a loaded transformer. This requirement reposes on several aspects. Firstly in many cases it is substantially to intensify supervision of unit's technical condition by increasing frequency of periodical inspections or by using automatic on-line monitoring systems, and that means that measurements have to be done for loaded transformers. Secondly several parameters as for example dielectric loss of paper – oil insulation measured for loaded transformers give larger and more reliable diagnostic information.

The third stage of diagnostics is condition assessment based on gained data analysis. Determination of transformer's technical condition that is based on gained data analysis is a very complicated diagnostic stage that requires comprehensive knowledge about ongoing processes in the unit and diagnosing experience. In the last 15-20 years tendency to apply expert systems for diagnosing the transformer can be observed [3].

The most characteristic faults of power transformers, their caused problems as well as diagnostic test techniques are briefly summarized in Table 1[4].

Table 1. Selection of diagnostic test according to a fault type

Fault type	Problems caused by a fault	Diagnostic test
Dielectric fault of insulation	Winding inter-turn short circuit	Turns-ratio measurement
	Winding shorted to core	Insulation resistance measurement
	Leads shorted to tank	
	OLTC failure due to short circuit	Insulation and winding resistance
Electrical connection fault	Gas generation	Dissolved gas analysis (DGA)
	Overheating between defective contacts at terminal bushings	Thermography
Winding failure	Winding open circuit	Winding resistance measurement
	Winding deformation or displacement	Frequency response analysis
Tank leakage, mechanical fault	Oil leaks	Visual inspection
	High impurities or moisture content	Oil quality analysis, Tan delta test
Bushing fault	Cracked bushing	Tan delta, inspection
OLTC failure	OLTC not functioning	Tap changer functional tests
Cooling system failure	Overheating of winding and insulation	Thermography, fans functional test
	Paper degradation	Furfural analysis Degree of polymerization

3. Analysis of the most frequent causes for transformer outages

The specificity of power transformers' diagnostics is the use of paper-oil insulation. High voltages and rated powers prescribe high operation ratio of active materials. These materials must resist heightened heat, considerable strength of electric and magnetic fields, as well as mechanical strokes during short circuits. Since condition of insulation is the main factor determining working life of the transformer, it is substantially to control ageing of insulation during exploitation. Important tasks are also periodical fixation of windings, avoiding additional moisture and air from environment and other preventative activities.

The combination of chemical and electrical diagnostic testing can provide a better assessment on the condition of the transformer. Any fault in the transformer core, winding, tap changer or any other part can be diagnosed by various parameters as described previous.

With so much data provided by several diagnostic parameters and diagnostic techniques engineers have difficulties to evaluate the risks and proposing corrective solutions on problematic transformers.

Many energy companies and institutes such as US Bureau of reclamation have developed the algorithm for testing and evaluating transformers using condition index [4, 5, 6]. However equipment and situations is very different so it is impossible to use their experience directly, development of an algorithm appropriate for a particular power system is required.

The most frequent causes of transformer outages are:

1. Material deterioration (aging);
2. Construction imperfections and manufacture failures;
3. Inadequate maintenance;
4. Outer and unpredictable stress (such as atmospheric overvoltages);
5. Not sufficiently performed repair works;
6. Environmental effects.

The proportion of the above mentioned outages for the power transformers of Latvian distribution network for the time period from 1998 to 2008 is given in Fig.2.

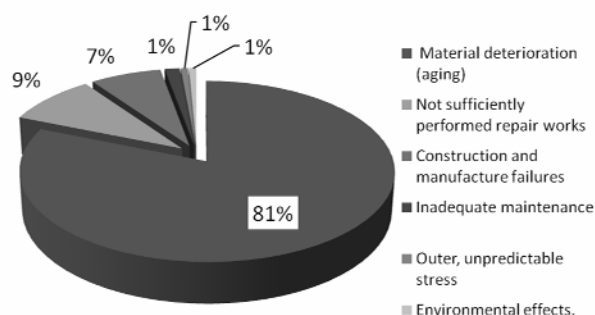


Fig. 2. The most frequent causes of transformer outages in Latvian power system in a time period from 1998 to 2008

Fig. 2 shows that the most severe problem is aging and deteriorating of insulation materials (81.13%). This aspect is not anything extraordinary considering age

distribution of in-service power transformers (more than 40% of all power transformers have served more than 30 years)

Outages caused by inadequate maintenance as well as by outer and environmental effects occur comparatively rare (respectively 1.45%, 0.72% and 0.72% of whole proportion). Construction imperfections and manufacture failures (6.97%) are external factors. However high proportion of outages is caused by not sufficiently performed repair works (9.01%), which suggests that higher reliability can be achieved by increasing the quality of repair works.

Reliability level of power transformers maintenance generally can be evaluated by outage flow parameter which characterizes the number of outages in definite time period

$$\omega(t) = \frac{n(t)}{N \cdot \Delta t}, \quad (1)$$

Where $n(t)$ – the number of outages;

N – total amount of power transformers;

Δt – time period (generally $\Delta t = 1$ year).

Reliability level of power transformers maintenance can be also evaluated by such parameter as probability of no-failure operation

$$p = 1 - \omega(t). \quad (2)$$

Table 2 shows values of these parameters for Latvian distribution system power transformers in the time period from 1998 to 2007.

Summarizing power transformer outages in the last decade (see Fig. 3) it is obvious that the highest intensity of outages are semi-season stages (March-May and August-October), which characterizes with changes of electrical load and accordingly with changes of operational and environmental temperature.

Table 2. Estimated outage flow and probability of no-failure operation values

Year	Number of outage $n(t)$	$\omega(t)$, per 1 year	p
1998	3	0.03	0.97
1999	3	0.03	0.97
2000	3	0.03	0.97
2001	5	0.05	0.95
2002	2	0.02	0.98
2003	4	0.04	0.96
2004	2	0.02	0.98
2005	3	0.03	0.97
2006	6	0.06	0.94
2007	3	0.03	0.97

4. Selection of power transformer's diagnostic techniques

A complete condition evaluation of a power transformer should include several subsequent steps (proposed version of this article is shown in Table 3). Each one of these steps has several elements which promote diagnostic data evaluation process, as well as many

times identify defects, some of which may be avertable thus leading to transformer life extension.

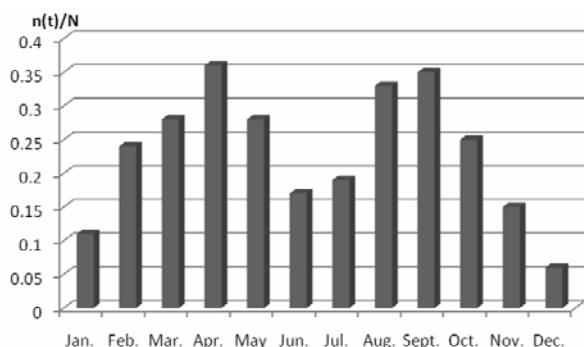


Fig. 3. Time chart of detection of defective power transformers

Table 3. Proposed transformer condition appraisal system

Level	Diagnostic method	Use
Basic level	Design analysis: <ul style="list-style-type: none"> • manufacturer; • winding configuration; • materials etc 	Database
	Operating environment: <ul style="list-style-type: none"> • protection scheme; • ambient temperatures; • lightning level ect. 	Database
	Maintenance: <ul style="list-style-type: none"> • loading and overloads; • fault frequency; • previous repairs etc. 	Database
Level 1	Dissolved gas analysis	On-line
	Oil quality analysis	On-line
	Infrared thermography	On-line
	External inspections: <ul style="list-style-type: none"> • cooling system; • bushings; • tank; • lightning arresters ect. 	On-line
Level 2	Turns-ratio measurement	Off-line
	Winding resistance measurement	Off-line
	Tan delta measurement	Off-line
	Insulation resistance measurement	Off-line
	Internal inspection: <ul style="list-style-type: none"> • coils and clamp; • LTC switch; • oil level ect. 	Off-line
Level 3	Furfural analysis	On-line
	Degree of polymerization	Off-line
	Frequency response analysis	Off-line
	Partial discharge analysis	On-line

Basic condition appraisal level provides a starting point condition which is very important and increase the effectiveness of technical condition assessment and predictive maintenance.

The other three levels subdivide diagnostic techniques used in Latvian power system, starting with on-line methods and external inspection of the unit (Level 1)

followed by off-line methods included in the Level 2 and internal inspections. Level 3 consists of additional diagnostic tests the results of which allow drawing to conclusions about reducing the load, preparing for major repairs or even considering replacement. Since most severe problem is aging and deteriorating of insulation materials this appraisal level includes several techniques devised for cellulose insulation technical condition assessment.

5. Conclusions

The stated material allows concluding that:

- It is hard to nominate optimal minimum control parameters whose measurement results could show origination of all type faults in power transformers. Research in this field to improve diagnostic parameters continues.
- The most severe problem of Latvian power system transformers is aging and deteriorating of insulation materials (81.13% from all outages).
- Proposed condition appraisal system could be used to mark out transformers with higher probability of a defect which need an additional supervision. System could render assistance for such decision making as reducing the load, preparing for repairs or replacement of a certain unit.

6. References

1. Алексеев Б.А. Контроль состояния (диагностика) крупных силовых трансформаторов. // – М.: Изд-во НЦ ЭНАС, 2002.
2. Transformer fire. – The internet: <http://www.electrical-contractor.net/forums/ubbthreads.php/topics/114034/1>
3. M.Kosaki, M.Ieda, K.Itoh, Y.Tsutsumi, Application experience of expert system to insulation diagnosis of power apparatuses in Japan // CIGRE Session paper, 1990, Ref. No: 15/33-04.
4. Young Zaidey bin Yang Ghazali, Mohd Aizim bin Talib, Hannah binti Ahmad Rosli. Condition Assessment of Power Transformers in TNB Distribution System and Determination of Transformer Condition Index // 17th Conference on the Electric Power Supply Industry, October 27-31, 2008.
5. Facilities Instructions, Standards, and Techniques Vol. 3-31 // Hydroelectric Research and Technical Services Group, US Dept. of the Interior, Bureau of Reclamation, June 2003.
6. Franchek M.A., Woodcock D.J. Life cycle considerations of loading transformers above nameplate rating // Proceedings of the Sixty-Fifth Annual International Conference of Doble Clients, 1998, Sec 8-10.1

INFLUENCE OF THE DISTRIBUTION OF THE AXIAL, RADIAL AND CIRCUMFERENTIAL COMPONENT OF THE MAGNETIC INDUCTION VECTOR WITHIN THE SPACE BETWEEN SWITCHES ON RUPTURING CAPACITY OF VACUUM SWITCHES

Dr inż. Bogdan KWIATKOWSKI *, Dr Robert PEKALA **

* Rzeszow University , Technology and IT Institute; **Rzeszow University, Technology and IT Institute, Poland

Abstract: The paper presents experimental tests results of magnetic field distribution for highcurrent switch. Provided tests show influence of switch shape on field distribution to obtain sustained vitality of vacuum switch. The method shown in the paper let obtain all components of magnetic induction vector. There is aspired to gain the highest value of axial component designing switches shape. It warrants favorable influence on fixity and turn off ability of switch system. There are lower values of peripheral and radial components making bipolar field in space between switches.

Keywords: vacuum chamber, bipolar switch, magnetic field.

1. Introduction

There have been the results of experimental research of the magnetic field distribution on chosen vacuum switches construction (bipolar) presented in this article. The construction of switches, that generate the axial field is technologically difficult to perform in comparison with the switches with the radial field. Such a switch must consist of several parts that must provide the proper mechanical strength of the whole switch construction. The main element of the switch is the copper axle, where the crown is mounted, copper too that causes division of current flowing in the axle into the equal parts, where the switch cover is attached, made of the special copper and chromium alloy. Preparing such a connection is the most difficult one because its quality can not worsen the connection durability of the whole switch chamber.

2. Measure method of the magnetic field distribution

There are several measure methods of the magnetic field distribution known between the vacuum switches. The way of magnetic field distribution between the switches

surfaces presented in Figure 1 consists in applying the measurement probe. There has been the way of placing the probe towards the surface, where the field distribution is being measured, presented in Figure 1 below.

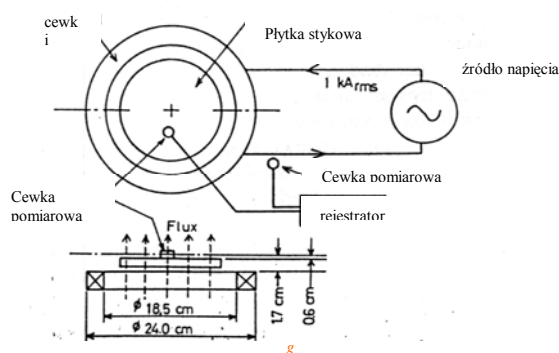


Fig. 1. Measurement of the field distribution with the use of the probe [1]

The switch cover is placed in the magnetic field in this method, which is generated by the coil shown in figure 1. The measurement has been done on the switch surface, and the measured tension has been compared with the coil tension of the frame of reference placed outside the measurement system

3. Description of the research system

There has been the HIOKI type „8841/42 MEMORY HiCORDER” recorder used for the laboratory measurements. In order to do measurements of the electromagnetic induction in the space between the switches there has been a measurement probe constructed, consisting of three coils. These coils are placed in a way that one can measure all components of the electromagnetic induction. The figure below shows the measurement probe. (fig. 2).

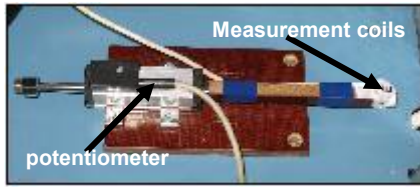


Fig. 2. measurement probe

There have been 50 coils rolled up on each measurement coil, the coil diameter is $\varnothing 8,7$ mm. The measurement probe together with the base was mounted to the device supporting switches (fig 3). This device enabled to lift and lower switches on a given height. Moreover, the table where the measurement probe was mounted, was equipped with the plate allowing the setting of the measurement probe every 150 on the circuit.

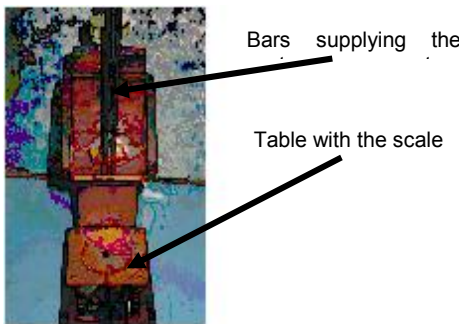


Fig. 3. Table with the plate with cuts

4. Measurement and results analysis

In the measurement method applied, the directly measured quantity is the voltage induced on measured coils. These coils are in the space between the switches while current is flowing through the switch system and are put from the outside to the inside of the switch plate. The measurement of the voltage induced on coils was done by the HIOKI recorder with the sample frequency $100 \mu s$. It allows for receiving about 25 thousand measurement points for each measurement probe location. The measurement probe in the initial phase of measurements of each switch system, is placed in so called zero position (0^0) and is successively moved every 150 on a switch plate circuit. The measurement method described here has been realized according to the following diagram (fig.4).

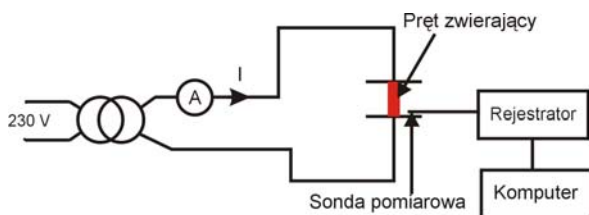


Fig. 4. Electric diagram of the measurement system.

While doing the measurements, the frequency of the sample recorder was $100 \mu s$ what gives at the network power supply the amount of 200 samples per period.

The electromagnetic induction was counted with the conversion of the following formula (1).

$$V_n = -S_n d \frac{B_n}{dt} \quad (1)$$

where: V_n - induced voltage on n - coil , S_n - switch field included by the n-coil, B_n -density of the electromagnetic field stream. So that is the final formula calculating the electromagnetic induction in the following form:

$$B = \frac{\sum_{i=1}^{200} abs(u - offset) * f_p}{4 * z * S} * \frac{\sqrt{2} * 50 * 10^3}{\max(abs(I))} \quad (2)$$

$$offset = \frac{\min(u) + \max(u)}{2} \quad (3)$$

where: u – voltage measured on measurement coils, $z=50$ – number of coils of the measurement coil, $S=59$ mm² – measurement coil surface, f_p – frequency of the sample recorder, I – current flowing through the switch system.

5. Measurement results of the chosen high-voltage switches

The construction of switches under test



Fig. 5. Bipolar switch

The main aim of the measurements was to show that there is a possibility of the evenness improvement of the magnetic field distribution through the choice of the construction and setting the switches towards themselves, in the vacuum chamber of the switch in order to achieve the best conditions of the magnetic field distribution and at the same time the conditions of the arc-quenching.

There were three field components measured: axial, circumferential and radial, measured with three probes at the same time from the outer edge of the switch into inside.

The choice of the axial component have been approached in these measurements with even field distribution on the switch surface, what gives the even diffusion arc distribution.

The circumferential component should be small because it focuses the diffusion arc and can cause excessive burning of the switch in its eg. Central part and forming the big amount of metal pairs.

The radial component influences the movement of the arc on the circuit and its values are big in the central part of the switches.

During measurements the current of 50 kA was flowing in. In order to standardize the nomenclature there is a switch setting shown in figures 6 and 7 towards themselves, for which the measurements were done.

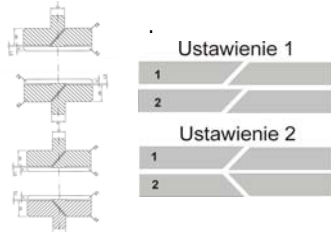


Fig. 6. Bipolar switch (setting 1, setting 2)

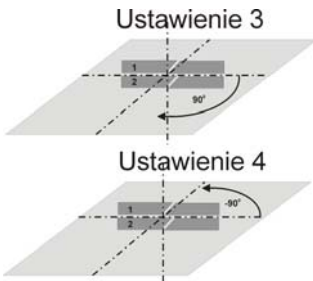
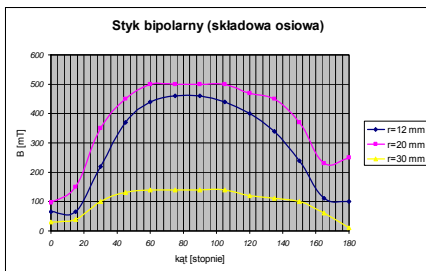


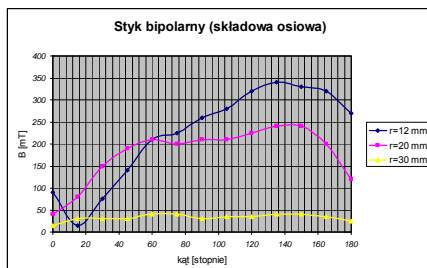
Fig. 7. Bipolar switch (setting 3, setting 4)

For each setting there have been the magnetic field induction components measurements done. The following routes have been presented in order to depict the influence of the switches location on the distribution and value of the magnetic induction components.

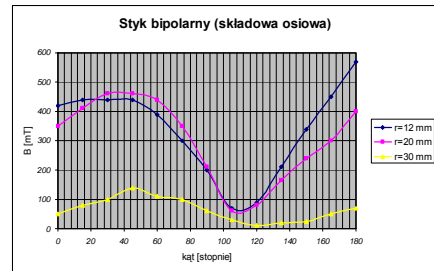
a)



b)



c)



d)

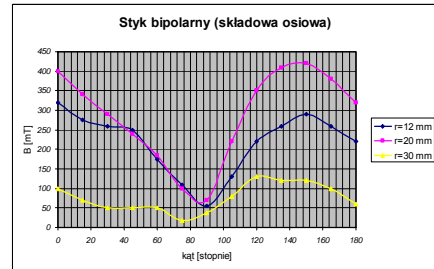
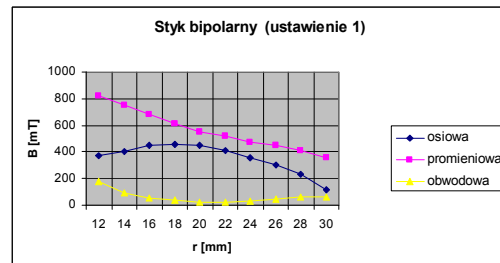


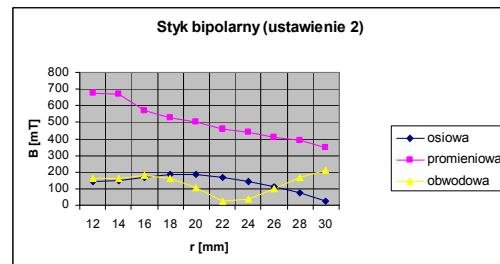
Fig.8. Magnetic field induction axial components distribution a)setting 1, b)setting 2,c)setting 3,d)setting 4

It appears from the following routes that the axial component has the biggest values for setting 1. In case of this setting this component has the most even distribution on the switch surface. The following routes show the distribution of the axial, radial and circumferential components of the magnetic induction for all settings of the measuring angle 45^0

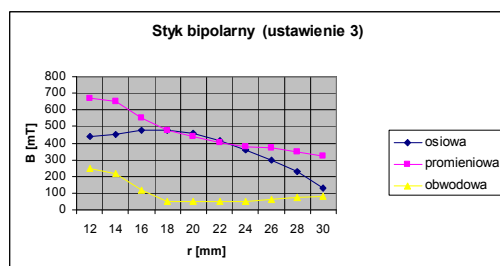
a)



b)



c)



d)

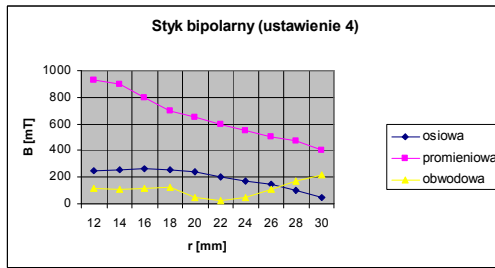


Fig.9. Magnetic field induction components distribution for the measuring angle 45° .

The axial component takes the biggest values for the setting 1 and setting 3 with small values of the circumferential component. This kind of proportion between the components is the most profitable between the diffusion arc switches in space. The next four routes show the magnetic induction components distributions for the following settings for the measuring angle 90° .

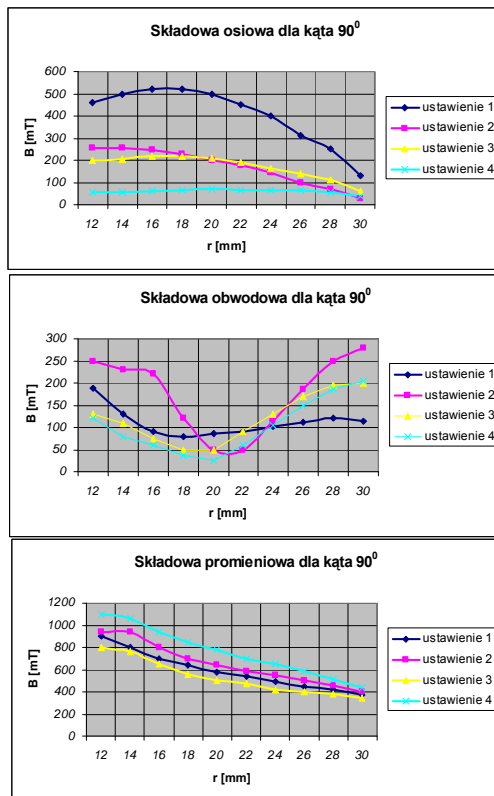


Fig.10. Magnetic field induction components distribution for the measuring angle 90° .

The axial component of the magnetic field reaches the high values for the „setting 1” and „setting 4”. In setting 4 there is the possibility of receiving, in the central part of the switch, small values of the circumferential component of the magnetic field strength and huge on the outer edges of the switch.

The value of the axial component of the field for the setting 4 is big – the biggest in the central part of the switch .

6. Conclusions

The presented construction of the vacuum switches construction does not exhaust all possibilities within this range. The research has been conducted in the world all the time on new interesting constructions that allow for the increase of the rupturing capacity and rated voltage often with the simultaneous decrease of the vacuum chamber size. There are works on new constructions and research methods of the switch systems done because vacuum switches are ecological, have huge mechanical and breaking capacity and allow for the switching off the huge short-circuit currents.

The measurements results done on a chosen switch system in the vacuum chambers of the switches shown that there is a huge influence of the switches setting towards themselves on magnetic field components distribution. The measurement results of the magnetic field distribution between switches used in the vacuum chambers of the switches determine the original approach in switch construction research. They also allow for the evaluation of the magnetic field strength value between switches and for the choice of the optimal field distribution on the switch surface for achieving the most profitable solution.

7. References

1. Yoshihiko Matsui, Hidemitsu takebuchi, Masayuki Sakaki, Akira Nishijima, Masami Takakura, Yasushi Noda, Analysys and Measurement of Axial Magnetic Field in Vaccum Interrupter, 19 Int. Symp. On Discharges and Electrical Insulation in Vacuum, Xian 2000, China
2. Homma M., Somei H, Niva Y., Yokokura, K.Ohsima, Physical and Theoretical Aspects of a New Vacuum Arc Control Technology - Self arc diffusion by electrode; SEDE, IEEE 18 International Symposium on Discharges and Electrical Insulation in Vacuum Eindhoven 1998
3. Dobrogowski J., Moscicka-Grzesiak H., Seidel S. Załucki Z., Podstawy wyładowań i wytrzymałość elektryczna w próżni, PWN Warszawa-Poznań 1983
4. Jimei Wang: Discussion on future development of vacuum switschgears, IEEE 18 International Symposium on Discharges and Electrical Insulation in Vacuum, Eindhoven 1998
5. M. Honma, K. Watanabe, M. Nishihara, I. Oshima, New Vacuum Arc Technology; SADE - Application to Vacuum Interrupters, IEEE 18 International Symposium on Discharges and Electrical Insulation in Vacuum, Eindhoven 1998.
6. H. Fine, M. Heimbach, W. Shang: A New Contact Design Based on Quadropolar Axial Magnetic Field and its Characteristics, European Trans, on Electrical Power Engineering, Vol.20. 2000, pp.75
7. Siemens Co.: Low Voltage Vacuum Circuit Breakers with Intelligential Functions, Siemens Product Specification, 1994.

THE RESEARCH OF THE INFLUENCE OF THE BOUNDARY CONDITIONS OF THE ATMOSPHERIC OVERVOLTAGES ON THE INSULATION OF HIGH VOLTAGE EQUIPMENT

Saulius GUDŽIUS, Linas Andronis MARKEVIČIUS, Alfonsas MORKVĖNAS
 Kaunas University of Technology, Lithuania

Abstract: The situation when difference characteristics protection devices against overvoltages are mounted in the same partly reconstructed substation frequently occur in the high voltage electric power network. The typical example of such situations is when dischargers near power transformers are replaced by arresters and the left part of the substation is protected using discharges. For the evaluation of such typical situation the model of power plant substation has been analyzed. The dangerous conditions for the insulation of the equipments mounted near incoming lines, when wave of the overvoltages rose by the lightning discharge arrive to the substation, has been analyzed during research and break-down data investigation.

Keywords: overvoltages, arresters, cable insertion.

1. Introduction

The strategy of the protection of the high voltage equipment insulation against overvoltages has been changed when overvoltages arresters started being used instead of dischargers. The valve dischargers can protect the insulation of the equipment mounted in the substation against violation in the zone of 100 – 120 m. for its feature during its switching on, when the discharge gap is broken down, to generate the returning electromagnetic wave of the opposite direction which dampers the overvoltages wave that comes from the line.

During the process of the replacement of valve discharges by overvoltages arresters in the electric energy system, there might be a situation when a valve discharger is left for the protection of the equipment insulation, and the overvoltages arrester is connected to the transformer. In such a combination of the protection devices, a dangerous level of overvoltages can occur in the case when the overvoltages arrester lowers the level of overvoltages and the valve discharger cannot switch on. In such a situation the insulation of the equipment, mounted in the substation near the incoming lines, can be damaged.

The aim of the work is to analyse the conditions of the possible violation of the insulation, to evaluate the change of the characteristics of the network elements

and the boundary characteristics of electromagnetic waves because of the overvoltages caused by a lightning discharge, when overvoltages arresters and dischargers are used for the protection of the substation equipment insulation.

The main attention in the work is assigned to the evaluation of the working conditions of the insulation of the equipment of the 110 kV substations and the investigation of the arresters efficiency and reliability.

2. The characteristic of the overvoltages calculation model

The calculation scheme of the substation consists of the parameters of the distributed buses segments and lumped parameters, which model the current and voltage instrumental transformers, power transformers and coupling capacitors.

The modelling scheme with five lines has been created for the electromagnetic transient processes analyser (Fig 1), meant for the investigation of the maximum overvoltages in the 110 kV electrical substation.

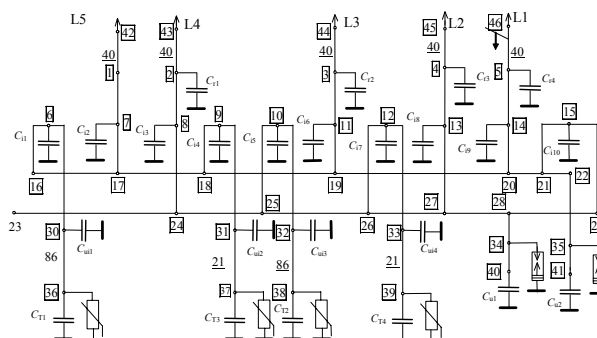


Fig. 1. Modelling scheme of the 110 kV substation: 40 – the length of the segment between the nodes (unshown lengths has been calculated according to the step of the cell 9 m); 10 – the number of the node

Because of their minor influence on the overvoltages, other apparatuses of the substation have been equivalented.

When analysing the transient processes of overvoltages, it is important to correctly calculate the scheme parameters, especially those which depend on the frequency because of the skin effect.

Partial line parameters capacities of aerial lines scheme are calculated as follows:

$$C = (C_{ik}) = \frac{1}{2\pi\epsilon_0} N, \quad (1)$$

ϵ_0 – dielectric air constant;

$\epsilon_0 = 1/36\pi 10^9$, F/m;

$N = (N_{ik})$;

$$N_{ii} = \ln \frac{2hi}{r_{ei}};$$

$$N_{ik} = \ln \frac{D_{ik}}{d_{ik}};$$

h_i , r_{ei} , d_{ik} , D_{ik} – average conductor hanging, geometric mean radius of the conductor, the distance between i and k conductor, the distance between the mirror reflection on the earth surface of the i and k conductor.

Partial line parameters inductivities of aerial lines scheme are calculated as follows:

$$L = (L_{ik}) = \frac{\mu_0}{2\pi} (N + F + M), \quad (2)$$

μ_0 – air magnetic permeability ;

$\mu_0 = 4\pi 10^{-7}$, H/m;

$F = (F_{ik})$;

$$F_{ik} = \frac{\pi}{2\eta_1} [H_1(\eta_1) - Y_1(\eta_1)] - \frac{1}{\eta_1^2} + \frac{\pi}{2\eta_2} [H_1(\eta_2) - Y_1(\eta_2)] - \frac{1}{\eta_2^2};$$

$$\eta_{1,2} = r_{ik} \exp(j(\psi \pm \theta_{ik}));$$

$$r_{ik} = D_{ik} \sqrt{-k_z^2 + k_0^2};$$

$$\Psi = \arg \sqrt{-k_z^2 + k_0^2};$$

$$\Theta_{ik} = \arctg \frac{|b_i - b_k|}{h_i + h_k};$$

$$k_0 = \omega \sqrt{\epsilon_0 \mu_0};$$

$$k_z^2 - k_0^2 = -\frac{j\omega\mu_0}{\rho_z};$$

H_1 и Y_1 – Struve function of the first type Struve and the second type Bessel function of the first type;

b_i – abscise of the i conductor;

ρ_z – specific ground resistance ($\rho_z = 100 \Omega\text{m}$);

ω – angular frequency rad/s;

$M = (M_{ii})$;

$$M_{ii} = \frac{k_1 \rho_1 J_0(k_1 r_i)}{j\omega\mu_0 r_i J_1(k_1 r_i) n_i},$$

$$k_1 = \sqrt{-j\frac{\omega\mu_1}{\rho_1}};$$

μ_1 и ρ_1 – conductor magnetic permeability and specific resistance;

r_i и n_i – the radius and number of the conductor in I wire.

The modeling of the electromagnetic processes has been carried out using special coordinates – p , q and θ for wave channel separation.

Voltage coordinates $\gamma = p, q, 0$ are calculated as follows:

$$(u_v)_{3 \times 1} = T_U^{-1} (u_\gamma)_{3 \times 1},$$

$v = p, q, 0$;

$\gamma = a, b, c$.

Current coordinates are calculated as follows:

$$(i_v)_{3 \times 1} = T_I^{-1} (i_\gamma)_{3 \times 1},$$

here: T_U^{-1} и T_I^{-1} – inverted modal and T_I matrix values.

Phase coefficients and decrement of dissipation are calculated as follows:

$$\text{diag}(G_v) = T_U^{-1} (LC) T_U, \quad (3)$$

Surge resistance:

$$\text{diag}(Z_v) = \text{diag}(G_v)^{-1} T_U^{-1} L T_U, \quad (4)$$

Specific scheme models parameters when current frequency is 200 Hz are equal:

$$C = \begin{pmatrix} 0.1188 & -0.0126 & -0.0027 & -0.0158 & -0.0029 \\ -0.0126 & 0.1194 & -0.0126 & -0.0092 & -0.0092 \\ -0.0027 & -0.0126 & 0.1188 & -0.0029 & -0.0158 \\ -0.0158 & -0.0092 & -0.0029 & 0.0660 & -0.0034 \\ -0.0029 & -0.0092 & -0.0158 & -0.0034 & 0.0660 \end{pmatrix} \times 10^{-10}, [\text{F/m}];$$

$$L = \begin{pmatrix} 0.1526 & 0.0633 & 0.0495 & 0.0733 & 0.0514 \\ 0.0633 & 0.1526 & 0.0633 & 0.0647 & 0.0647 \\ 0.0495 & 0.0633 & 0.1526 & 0.0514 & 0.0733 \\ 0.0733 & 0.0647 & 0.0514 & 0.2332 & 0.0557 \\ 0.0514 & 0.0647 & 0.0733 & 0.0557 & 0.2332 \end{pmatrix} \times 10^{-5}, [\text{H/m}]$$

$$R = \begin{pmatrix} 0.1639 & 0.1450 & 0.1440 & 0.1419 & 0.1410 \\ 0.1450 & 0.1639 & 0.1450 & 0.1417 & 0.1417 \\ 0.1440 & 0.1450 & 0.1639 & 0.1410 & 0.1419 \\ 0.1419 & 0.1417 & 0.1410 & 0.4301 & 0.1381 \\ 0.1410 & 0.1417 & 0.1419 & 0.1381 & 0.4301 \end{pmatrix} \times 10^{-3}, [\Omega/\text{m}].$$

3. The effect of the overvoltages on the insulation of the electrical equipments

The level of the overvoltages depends on the length of the electrical lines, their configuration, construction and load, the characteristics of the protection devices against overvoltages and voltage level in the network.

The situation in the power station 110 kV closed substation is being analysed, when two coupling capacitors exploded, when overvoltages occurred near

the substation after the lightning discharge in the aerial power line.

Up to 700 kV amplitude voltage wave ($10 \Omega \times 70 \text{ kA}$) might occur in the spot of the lightning discharge in the aerial line when the insulator garland is electrically recovered. When there are no protection devices against overvoltages, the voltage can exceed the tested voltage of the equipment insulation. Because of the overvoltage caused by the lightning discharge, a wave coming to the substation can evoke overvoltages which are dangerous for the equipment insulation. Fig. 2 shows the processes in in different spots of the power station 110 kV substation when there are no protection devices against overvoltages.

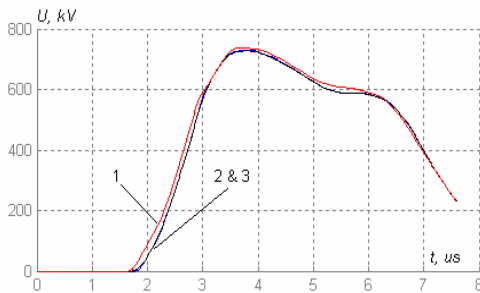


Fig. 2. Lightning overvoltages in the power plant 110 kV substation when the 700 kV 1,2/50 wave comes through the line L1; Overvoltages protection means are not intalled; 1- voltage in the coupling capacitor; 2, 3- voltage in the connection spot of the arrester and dischargers

The level of the overvoltages exceeds the specimen voltages guaranteed by the producer, that is why overvoltages lowering means must be installed in the substation. In the 110 kV voltage substation, discharges are erected next to the buses voltage transformers, and overvoltages arresters are erected next to the power transformers. In the scheme investigated, auxiliary power transformers are installed 21 meters and block power transformers are installed 86 meters from the main buses. Overvoltages arresters protect the insulation of the equipment which are beyond the connection spot. Because of their characteristics to evenly lower the voltage, overvoltages arresters practically do not protect the equipment which is in front of the arresters. The protection zone of the overvoltages arresters is rather narrow.

The arrester, which is the closest to the substation transformer, lowers the voltage next to the discharger, and the latter does not connect when the overvoltages wave comes from the line. The length and amplitude of the impuls are dangerous for the insulation of the equipment; in the case investigated, it is dangerous for the insulation of the coupling capacitors (Fig. 3); the longer the length of the impuls, the lower electric resistance of the inner insulation.

The valve dischargers can protect the insulation of the equipment mounted in the substation against violation in the zone of 100 – 120 m. for its feature during its switching on, when the discharge gap is broken down, to generate the returning electromagnetic wave of the opposite direction which dampers the overvoltages

wave that comes from the line. As it is seen from the results of overvoltages test (Fig. 3), the overvoltages arrester next to the transformer lowered the overvoltages level at the discharger connection spot, and the discharger did not connect.

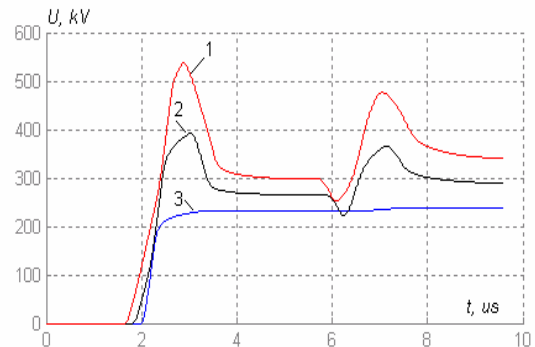


Fig. 3. Lightning overvoltages in the power plant 110 kV substation when the 700 kV 1,2/50 wave comes through the line L1; Overvoltages protection means are intalled; 1- voltage in the coupling capacitor; 2 - voltage in the connection spot of the dischargers; 3 - voltage in the connection spot of the arrester

If there were only a discharger in the substation, the lengths of the impuls influencing the insulation would be obviously shorter (Fig. 4)

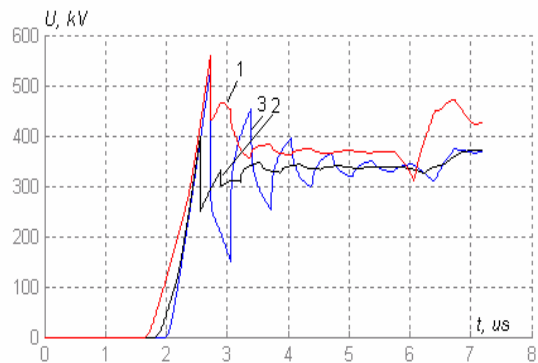


Fig. 4. Lightning overvoltages in the power plant 110 kV substation when the 700 kV 1,2/50 wave comes through the line L1; Only dischargers are installed; 1- voltage in the coupling capacitor; 2 - voltage in the connection spot of the dischargers; 3 - voltage in the connection spot of the arrester

As dischargers (near the buses) and overvoltages arresters (right next to the power transformers) were erected in the closed substation of the 110 kV voltage electric power station, the coupling capacitors were affected by the overvoltage higher than its impulsive resistance. It could have been the main reason why the coupling capacitor exploded. Besides, when the line L1 is connected from the other side, the highest overvoltages are formed at the end of the line, i.e. on the coupling capacitor. Because of these overvoltages and as it was damaged by the initial overvoltage caused by the lightning discharge, the insulation of the coupling capacitor was punched.

When overvoltages transient processes in the 110 kV voltage substation of the electric power station without arresters were modeled by a digital analyzer, a condition was accepted that overvoltages do not span the insulation of the substation equipment even if the impulsive resistance of the insulation is exceeded. In such a way the most dangerous spots in the substation are determined, in which the overvoltages of the highest amplitude are most likely to occur, when the wave comes from line L1.

When there are overvoltages arresters instead of the discharges, the levels of overvoltages in the 110 kV voltage substation of the electric power station are estimated for the same regimes electromagnetic wave forms as there are in the scheme without arresters.

When estimating and choosing the devices for the protection of the insulation of 110 kV voltage equipment in electric energy system the most attention must be paid to the overvoltages caused by a lightning discharge, and if the voltage is more than 110 kV, the attention must be paid to all the possible overvoltages. When the initial working voltage of the protection equipment against overvoltages is being lowered, it is necessary to take into account the energy which is absorbed by them, if switching overvoltages are limited. Valve discharges, which are used in the electric net up to 110 kV, do not react to switching overvoltages because their switching-on voltage is higher than the level of switching overvoltages.

The results of the research show that overvoltages arresters erected before the power transformers and in the place of discharges can not protect the insulation of all the substation equipment. Dangerous overvoltages of higher amplitude than the testing impulse voltage can influence the insulation of part of the current transformers and coupling capacitors.

4. Conclusions

1. The analysis of the accident shows that the failure in coupling capacitors could be caused by improperly tuned overvoltage protections. In 110 kV closed substation, the dischargers were mounted near the buses and surge arresters were mounted near the power transformers and the coupling capacitors were affected by overvoltage higher than impulse resistance. The main reason why the capacitor exploded was that the discharger didn't work. Furthermore, the highest overvoltages occur in the end of the line, i.e. at coupling capacitor during the line L1 switching. These overvoltages damaged the insulation of the coupling capacitor

which was affected by initial lightning overvoltage discharge.

2. The overvoltage levels in 110 kV substation of the power plant can have higher amplitude than pulse test voltage of equipment insulation if surge arresters are mounted instead of dischargers. The simulation results show that the surge arresters mounted before power transformers at the location of dischargers can not protect all the equipment of the substation. The insulation of part of the current transformers and the coupling capacitors can be affected by dangerous overvoltages higher than pulse test voltage, which secures reliable operation of equipment insulation.
3. The analysis shows that surge arresters must be mounted at the first supports of the overhead lines in order to protect the insulation of the 110 kV closed substation equipment of the power plant. Surge arresters are not necessary near power transformers in the closed substation.
4. The energy characteristics of surge arresters show that the dissipated amount of energy by surge arresters mounted near the first supports must be equal or larger to 5.8 kJ/kV. According to energetic capacity, additional surge arresters must be of the III class.

5. References

1. Gudžius S., Markevičius L., Morkvėnas A. Recursive method to examine electromagnetic transient processes in cable network // IV Simpozium, "Metody matematyczne W elektroenergetyce MMwEE'98", Zakopane, 1998. P. 235-244.
2. Gudžius S., Markevičius L., Morkvėnas A. The research of overvoltages arresters efficiency in high voltage substation // XI International Conference on Electromagnetic Disturbances: EMD'2001, Overvoltage in Power – Electronic – and Computer Engineering / Bialystok Technical University, Vilnius Gediminas Technical University, Kaunas University of Technology. Bialystok, 2001. P. 3–6.
3. Gudžius S., Markevičius L. A., Morkvėnas A., Navickas A. S., Stanionienė R. 110 kV kabelinių intarpų apsaugos priemonių nuo viršįtampių darbo sąlygų tyrimas // Elektros ir valdymo technologijos 2007. 2 tarptautinės konferencijos straipsnių lietuvių kalba rinkinys – Kaunas: "Technologija", 2007. P. 20-23.
4. Gudžius S., Markevičius L., Morkvėnas A., Navickas A., Stanionienė R., Rožanskas A. V. The influence of the overvoltages on the reliability of the 110 kV power line with cable insertion // XVII International Conference on Electromagnetic Disturbances: EMD'2007, 19-21 September 2007, Bialystok, Poland. Kaunas: "Technologija", 2007. P 187-190.

INSULATION LIMIT RESISTANCE PERFORMANCE ASSESSMENT MODEL

Alfonsas MORKVĖNAS, Renata STANIONIENĖ, Povilas VALATKA
Kaunas University of Technology, Electrical Systems Department, Lithuania

Abstract: In order to increase power grid reliability, it is necessary to use the cost-based evaluation tool which determines the impact of various characteristics in order to reduce the duration of the emergency interruptions, by using a properly chosen insulation protection from overvoltages and by monitoring characteristics which impact the equipment. In this paper, the analysis of factors which influence the electrical equipment and processes which take place in isolation during overvoltages is given. Also, there are defined the characteristics of factors which influence the nature of the parameters change. The digital model of the processes which take place in the equipment insulation is designed.

Keywords: grounding device, concentrated grounding device, specific resistance, coefficient of discharge.

1. Introduction

Reliable operation of the power system electrical equipment is a key factor in guaranteeing a reliable and economical operation of whole power system. Reliable operation of the electrical equipment is based on the appropriate equipment condition monitoring, scheduled repair tasks, and the nature of impact factors.

High-voltage equipment insulation condition and the reliable duration of working time is determined by various factors of the power system: overvoltages, partial discharges, overcurrents, vibrations and so on. Insulation aging rate and the appearance of defects mainly are caused by overvoltages, heating, and partial discharges. Duration of the Overvoltages and its amplitude can be various in the power system. Overvoltages and equipment operating temperature are the main factors of insulation aging speed [1, 2, 7].

During the maintenance of the high voltage substations equipment, which is effected by the high electric field, overvoltages, discharges, thermal effects, moisture, oxidation, vibration, aging and other factors, the various defects appear. The in operation equipment monitoring systems are applied for the high-voltage equipment, which monitors such characteristics, which analysis can give the answer of the inner insulation, and other units, technical condition and assess the accident risk. In most

cases it is the chromatographic analysis of the gasses which are dissolved in insulation [2, 9].

High-voltage equipment monitoring system monitors the characteristics which impact to the power system (overvoltage parameters and their duration, asymmetry, harmonics, parameters of the emergency regimes).

The aim of this work is to determine the limit of insulation resource according to two factors- voltage and temperature. To identify the impact factors influence to the consequences of exposure parameters.

2. Factors which effect the electrical insulation

During the maintenance of electrical equipment insulation is exposed to operating voltage, short-term overvoltages, temperature. The parameters of impact factors, which effect the equipment's isolation, depend on the equipment location in the network, load variation, the frequency of overloads, short-circuiting faults.

The electrical power system maintained equipment's insulation condition evaluation and prognosis of defects is relevant and quite a complex task involving the processes occurring in the network, and its insulation. This task determines the electrical equipment efficiency and reliable power system operation. The electrical equipment reliability, quite often is determined by insulation [1, 2]. In order to evaluate accurately the condition of electrical equipment and clarify the defect it should be investigated processes in the power system and in electrical equipment insulation, also to determine the impact factors influence to the consequences of exposure parameters and to identify their variation regularity. Analysis of the overvoltages caused changes in isolation can give the predicted insulation aging speed and the evolution of defects and also could allow to remove defects when necessary and prevent accidents and power system losses.

The reliable operation of electrical equipment and its insulation condition is determined by various factors (operation current and voltage, overvoltages, overcurrents, vibration, humidity, etc.) which appear in power system. The electrical equipment isolation (internal and external) must be resistant to long-term maximum permissible voltage, switching and

atmospheric overvoltages [1, 10]. Overvoltages transient process, if the insulation of electrical equipment is properly maintained and protected from overvoltages, can reliably serve all set time.

Because of the overvoltages impact in solid and liquid isolation begins or increases the partial discharge processes [3]. During the partial discharge processes deteriorates the insulating properties of electrical installations, increases quantities of gas in oil, increase the surfaces of micro cavities in solid insulation an also accelerates the aging process [2, 5, 9]. Overvoltages impact to the insulation may be considered according arranged insulation model, which evaluates the partial discharge process. The partial discharge process in the electrical equipment insulation increases during the overvoltages impact. Partial discharge level increases 5-8% per year [3].

Limit insulation resistance conditions are affected by the operating voltage, its influence time and temperature.

Overvoltages level and impact duration characteristics for insulation are studied by various authors [1, 7]. To evaluate insulation resources the experiments are done, where the insulation resistance was explored according to dependence on time and temperature [7]. Such studies are carried out in order to measure the insulation resistance to stress exposure duration (volt-second characteristic), and thus determine the limit of resource. In the power system equipment is installed in different locations and is exposed to the different factors with different parameters (amplitude of overvoltage, the duration of exposure, occur rate, overloads, etc.). Therefore, electrical equipment insulation aging processes take place differently. In addition, in various locations overvoltage parameters, because of network configuration, technical characteristics, ongoing complex physical phenomena, are dispersed uneven. Secondary electrical equipment insulation control in terms of qualitative characteristics, is performed periodically or permanently, and can evaluate the condition of the device, but the nature of the factors and the influence still remains unclear [3, 4, 5, 6, 8]. By registering the operating characteristics of the factors (overvoltages amplitudes and exposure duration), and simultaneously the consequences of impact (partial discharge characteristics: the apparent charge, discharge currents, the frequency of recurrence, etc.) it is possible to evaluate arising defects of equipment in the initial stage.

3. Limit insulation resistance characteristics

Maximum economically based equipment utilization effects on higher equipment's working temperature. Device temperature increase is limited by the insulating properties of the materials- at a higher temperatures increases materials thermal decomposition and aging. If the temperature is increasing the speed of chemical reactions accelerates. For organic type of insulation chemical processes often increases of two times when the temperature increases 10 °C.

The insulation break down is considered as a phase transition, which has been depended on energy density.

Energy density consists of thermal component and the part of electromagnetic field energy which had been converted into energy of molecular oscillations. The energy density of Thermo electromagnetic field H_{TEM} consist of the following components [7]:

$$\text{thermal } H_T = \rho \cdot c_v \cdot T; \quad (1)$$

$$\text{electrical } H_E = \frac{\varepsilon}{2} \cdot E^2; \quad (2)$$

$$\text{and magnetic } H_M = \frac{\mu}{2} \cdot M^2. \quad (3)$$

The thermo-electromagnetic field density can be written in the following expression:

$$H_{TEM} = \rho \cdot c_v \cdot T + \frac{1}{2} \cdot (\varepsilon \cdot E^2 + \mu \cdot M^2); \quad (4)$$

here ρ – density of insulating material;

c_v – isochoric heat capacity;

ε and μ – electric and magnetic permeability;

E and M – strengths of electric and magnetic fields.

The actual exploitation time for an insulating material starts at time t_s and ends at the time t_D . This time interval is considered as a resource:

$$R = t_D - t_S. \quad (5)$$

This value is directly proportional to its dimensionless modification:

$$t_D - t_S = (\tau_D - \tau_S) \cdot \rho_{am}^{1-\nu} \cdot z^{-1}. \quad (6)$$

On the other hand dimensionless conversion temperature at constant load is:

$$\Theta_C = \tilde{R} \cdot \left(T + \frac{r \cdot \varepsilon}{\rho \cdot c_v} \cdot E^2 \right) / w. \quad (7)$$

Expression in measured values can be assumed as:

$$R = (\tau_D - \tau_S) \cdot \rho_{am}^{1-\nu} \cdot z^{-1} \cdot e^{w / \left(\tilde{R} \cdot \left(T + \frac{r \cdot \varepsilon}{\rho \cdot c_v} \cdot E^2 \right) \right)}. \quad (8)$$

It can be noted that in (8) equation there are included parameters which depends on the properties of material and the activation energy for the reaction. One does not necessary to determine each parameter separately. To make a prognosis of the insulating service life it suffices to find experimentally such values:

Insulation scale time

$$R_\infty = (\tau_D - \tau_S) \cdot \rho_{am}^{1-\nu} \cdot z^{-1} = P_1, [h] \quad (9)$$

Activation temperature

$$T_a = w / \tilde{R} = P_2; [K] \quad (10)$$

here w – activation energy [J/mol];

\tilde{R} – universal gas constant 8,134 [J/mol·K].

The basic electrothermal constant is described as

$$B = \frac{r \cdot \varepsilon}{\rho \cdot c_V} = P_3; [\text{K} \cdot \text{m}^3 \cdot \text{J}^{-1}]. \quad (11)$$

Based on these values the insulation resource can be presented as

$$R = R_\infty \cdot e^{T_a / (T + B \cdot E^2)} = P_1 \cdot e^{P_2 / (T + P_3 \cdot E^2)}. \quad (12)$$

It can be noticed that at infinitely high conversion temperature the scale time $\lim_{T_c \rightarrow \infty} R = \tilde{R}$.

To determine the rates of three values R_∞ , T_a , B , one needs at least three experiments to be performed at three differing conversion temperatures and according to the test results it is necessary to solve system of equations according (11) equation. The solution of the system equations gives parameters R_∞ , T_a , B . It is noted that there can be done large number of experiments, so the solutions of equations may also be a very large number. A.N. Stepanov conducted a series of experiments to verify the conversion theory of insulation ageing [7]. There was investigated the breakdown time for two materials for temperatures +20 °C and +150 °C, and electric field strengths from 4 MV/m up to 12 MV/m with step of 2 MV/m. Under such conditions duration of tests made up from 2,7 to 728,5 hours [7]. According A.N. Stepanov tests results, and using of the above explained methods, the solution of equations according (11) gives us the parameters of digital resource model. For the correct parameters evaluation and selection it is necessary to perform a statistical evaluation of results.

According A.N. Stepanov experimental results and choosing the estimated model parameters according to the lowest average error of approximation, there was determined such parameters of the model:

First material $R_{1\infty} = 2,3 \cdot 10^{-3}$ h, $T_{1a} = 4633,4$ K, $B_1 = 2,126$ $[\text{K} \cdot \text{m}^3 \cdot \text{J}^{-1}]$;

Second material $R_{1\infty} = 70 \cdot 10^{-3}$ h, $T_{1a} = 3393,7$ K, $B_1 = 2,006$ $[\text{K} \cdot \text{m}^3 \cdot \text{J}^{-1}]$.

In figures 1 and 2 are shown insulation resource according A.N. Stepanov's measurement's results and the calculated ones according to the numerical model where two parameters, rated voltage and temperature, are involved.

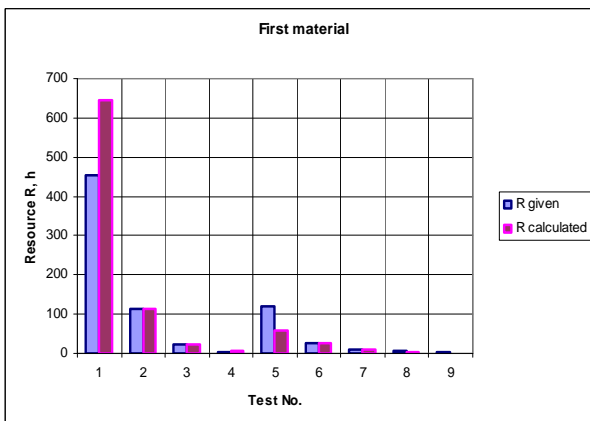


Fig. 1. First material's test results compared to the calculated according digital model

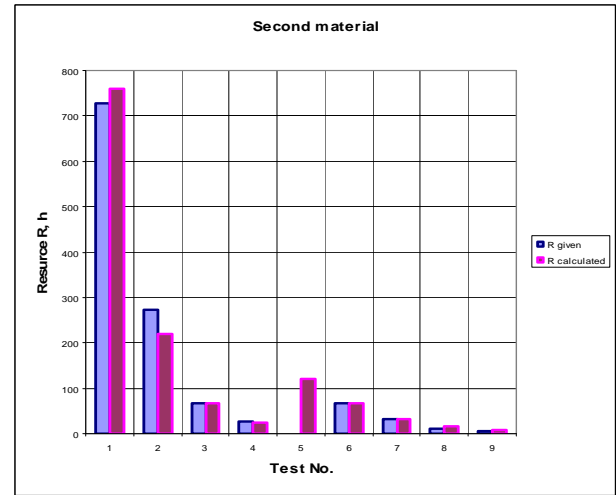


Fig. 2. Second material's test results compared to the calculated according digital model

In figure 3 and 4 are given material's model marginal insulation resource surfaces.

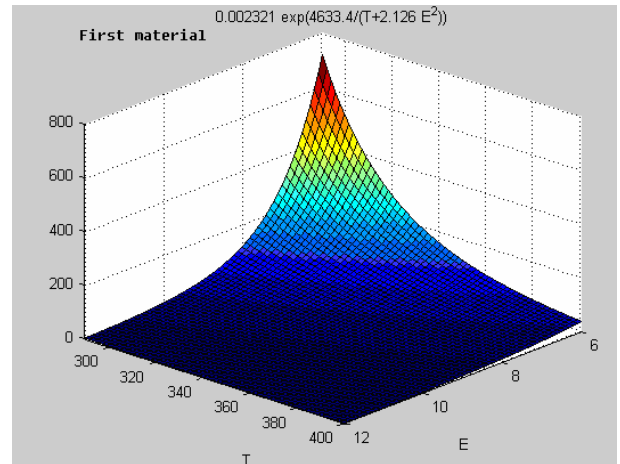


Fig. 3. First material's insulation resource marginal surface according to electric field strength and temperature

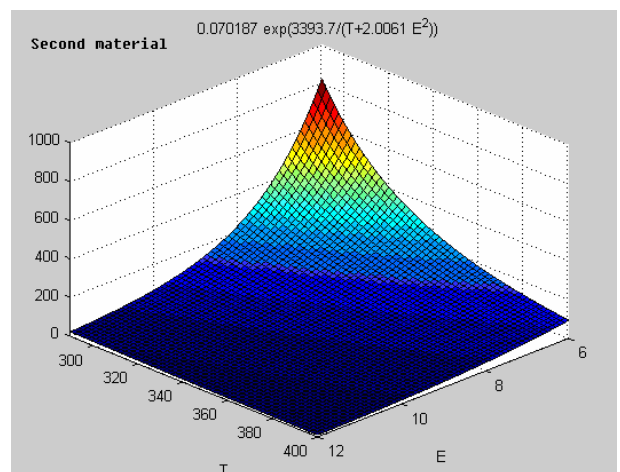


Fig. 4. Second material's insulation resource marginal surface according to electric field strength and temperature

The prognosis of electrical equipment insulation resource utilization can be determined by the recorded integral characteristics of the overvoltages impact [10].

More detailed resource usage model could be arranged if the two parameters of numerical model of resource were applied, where the integral characteristics of the overvoltages impact and the thermal component are implied.

4. Conclusions

1. It was arranged digital insulation resource model where the operating voltage and temperature are included.
2. According A.N. Stepanov experimental results it was calculated parameters of mathematical model and assuming the lowest average error of approximation the marginal insulation resource digital model parameters were set.

5. References

1. Тиходеев, Н.Н.; и Шур, С.С. Изоляция электрических сетей. Ленинград: Энергия, 1979. 304 с.
2. Сви, П. М. Контроль изоляции оборудования высокого напряжения. Москва: Энергоатомиздат, 1988. 128 с.
3. Kreuger, F. H. Partial discharges detection high voltage equipment. London: Butterworth & Co. Ltd. 1989, 192 p.
4. Aubin, J.; and Gervais, P. On-line monitoring of key fault gases in power transformers and shunt reactors. Sixty-second Annual International Conference of Doble Clients, 1995. P. 122 – 135.
5. Gibeault, J. P. On-line monitoring of key fault gases in transformer oil. 10th International Symposium on High Voltage Engineering, Montreal, 1997. P. 62-71.
6. Hamed, M.; and El Desouky, A.A. Computerized inspection for the high voltage insulating surfaces. Electric Power Systems Research, 2000, Nr. 53. P. 91-95.
7. Gerhards, J.; and Temkins, A. Prognostics of electrical insulation resources: Nordic Insulation Symposium Stockholm, 11-13 June 2001. P. 125-132.
8. Cavallini, C.M.; and Montanari, G.C. On-field partial discharge measurements: A feasible approach to noise rejection and defect assessment. The 9th INSUCON International Electrical Insulation Conference Messe Berlin, Germany, 18-20 June 2002, Berlin, 2002. P. 183-188.
9. Morais D. R.; and Rolim J. G. A hybrid tool for detection of incipient faults in transformers based on the dissolved gas analysis of insulating oil. IEEE Transactions on Power Delivery, April 2006, Vol.21, No.2. P.673-680.
10. Gudžius, Saulius; Markevičius, Linas Andronis; Morkvėnas, Alfonsas; Navickas, Algimantas Stanislovas; Stanionienė, Renata. The Analysis of the Integral Characteristics of the Overvoltages Effect Duration // EMD 2006: Proceedings of XVI International Conference on Electromagnetic Disturbances, September 27-29, 2006, Kaunas, Lithuania, Kaunas: Technologija. 2006. ISSN 1822-3249. P. 72-77.

THE MODELS OF SOURCES OF ELECTROMAGNETIC INTERFERENCES OVER UHV LINE FOR TRANSIENT PROCESSES INVESTIGATION

Linās A. MARKEVIČIUS, Vytautas ŠIOŽINYS
Kaunas University of Technology, Lithuania

Abstract: the conditions of surge development due to lightning strike are described in the article. The insulator breakdown model error is assessed comparing calculation results with electrode system rod – rod experimental voltage – time characteristics. The fault source model is described for transient electromagnetic processes analysis.

Keywords: electromagnetic transient, insulation, lightning, electromagnetic interference

1. Introduction

The assumption, that the fault source is the step voltage with rise time equal to calculation time step is made for transient processes calculation in electric power network. However, that simplicity is narrowing understanding about processes. It is worth to mention, that lightning current flow overcome difficult charge generation and neutralization processes via grounding impedance. Additionally, lightning current induced surge overlap insulator, which breakdown mechanism overtake streamer and leader propagation time. Probably, easiest way is to describe the lightning current magnitude, rise time, impulse time as the stochastic processes with exponential distribution. However, fault place circuit and the surge impedance could be modeled. So, the factors, which make influence on lightning surge and its parameters, should be known for the electromagnetic transient processes investigation.

2. Insulators flashover mechanism

Ionization process in the gap of electrode system rod – rod do not start if the applied voltage is less than corona inception voltage. The higher intensity and non uniform electric field strength area is created by space charge due to increased voltage which is higher than corona inception voltage. The later on, voltage increase raises higher intensity electric field strength area till leader has formed. This area could be described as streamer propagation time t_s [6]:

$$t_s = \frac{0.5}{\frac{u(t)}{g} - B}, \quad (1)$$

there $u(t)$ - the gap voltage; g - the gap length in m; B - constant 0.42 for positive voltage and 0.5 for negative. The leader propagation time t_l could be calculated from [4]:

$$\frac{dl}{dt} = k_l \cdot u(t) \cdot \left[\frac{u(t)}{g-l} - E_{str} \right], \quad (2)$$

there l - the leader length in m; E_{str} - initial electric field strength in the gap, before leader formation; k_l - leader coefficient or ion mobility [3], for the positive ion $k_l^+ = 1,2 m^2 kV^2 s^{-1}$, for the negative ion $k_l^- = 1,3 m^2 kV^2 s^{-1}$.

The gap flashover time, according to [24] and [25]:

$$t = t_c + t_s + t_l + t_n, \quad (3)$$

there t_c - corona inception time in s; t_n - the ion neutralization time in s.

Corona inception and ion neutralization time are neglected because of the shortest in all gap flashover mechanism.

Electric field strength inside the streamer according to [1, 4, and 5] varies in range for the positive discharge $E_{str}^+ \approx 5 \text{ kV/cm}$, and for the negative one $E_{str}^- \approx (6 \div 10) \text{ kV/cm}$. However the voltage gradient for the pulse voltage could seek $E_{str}^- \approx 10 \text{ kV/cm}$.

The assumption is made for leader propagation time calculation. The idea is that the leader stops develop, than the voltage gradient inside the unabridged part of gap drops below value E_{str} . If the applied pulse voltages rise time τ_f is short, than gap flashover time become equal to voltage pulse time. The voltage magnitude

should be raised to seek gap flashover. After that, than the pulse voltage rises till maximum value, the space charge move from rod and the voltage gradient significantly decreases. At the same time leader propagation is unfavorable due to decrease of generated amount of charge. The flashover propagation starts near the impulse voltage maximum at the voltage $u = U_{50\%}$ and its rise time equal to critical $\tau_f \approx \tau_{kr}$. Decrease of voltage rise time leads to gap flashover over the voltage maximum. The gap average electric field strength increase due to increase of impulse voltage magnitude and the leader propagation time decrease. In our point of view, the gap flashover starts at the maximum of impulse voltage and at the rise time for the higher voltage magnitudes as it is depicted in figure 1.

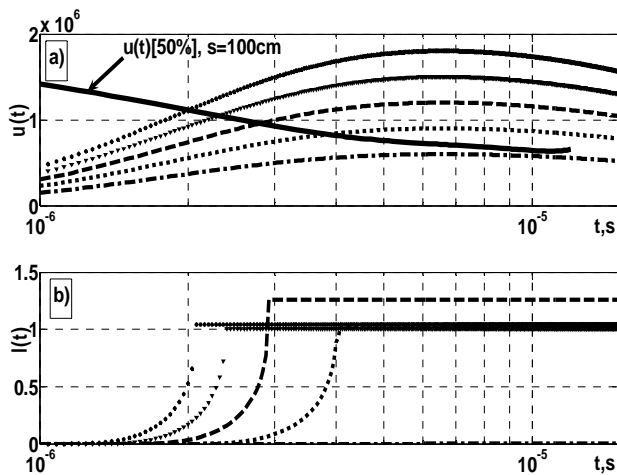


Fig. 1. Leader propagation upon time (b), after applied different magnitude impulse voltage (+1.5/40 μ s) (a)

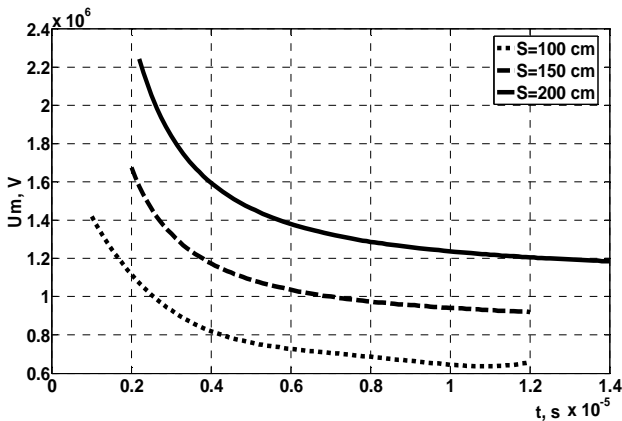


Fig. 2. The fifty percent full wave impulse (+1.5/40 μ s) flashover voltage - time characteristic for the gap rod - rod

The leader propagation speed and duration yield expression (2) after numerical integration for example with 4th order Runge - Kutte method. Numerical integration of expression (2) starts, than the condition $u(t) \geq U_0$ is met. There U_0 is the initial corona voltage. However another assumption was made - voltage drop $u(t)$ across gap through propagated leader are neglected.

The calculation results, dependences of leader length upon time, after impulse (1.5/40 μ s) voltage was applied, depicted in figure 1.

However another way to assess insulators flashover dynamics is to use the fifty percent impulse flashover voltage upon the time characteristic. The electrode system rod - rod voltage - time characteristics are equivalent to UHV line insulator voltage - time characteristics, as it could be seen from [5, 6]. The experimental electrode system rod - rod voltage - time characteristics after pulse voltage (+1.5/40 μ s) was applied are depicted in figure 2.

The leader propagation dynamics equations (1-3) simulation results satisfy electrode system rod - rod voltage - time characteristics for full wave voltage (+1.5/40 μ s).

The leader propagation calculation (2) starts after overall breakdown time $t \geq t_s$, there t_s is the streamer propagation time from (1).

3. The lightning as the source of electromagnetic wave in transmission line

From 60 to 100% of all lightning starts from negative charged clouds as it is described in [2, 5]. Step by step streamers in space and time forms leader which is heated up to a few thousands degree of Celsius. The same sign as cloud charge, space charge is generated by floating ions in conductive medium. After leader seek the ground the space charge surrounding channel neutralization process starts, due to formed new streamer with speed $v = 2 \cdot 10^7 \div 1,5 \cdot 10^8$ m/s. So the resistance of the lightning channel at the stage of formation and neutralization could be described by Tepler equation $R_K = 0,08/q[\Omega/m]$, there q - charge, formed in lightning channel.

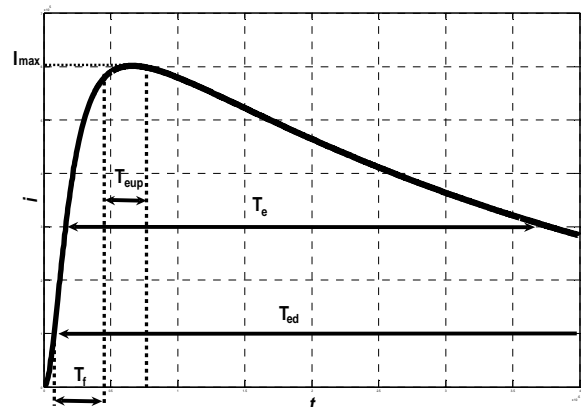


Fig. 3. Typical lightning discharge current

The minimal lightning current rise time could be calculated $T_f = H_l / c = 600 / 3 \cdot 10^8 = 2 \mu$ s assume, that the minimum cloud height from ground surface is $H_l = 600$ m. The typical lightning discharge current is depicted in figure 3. There [2] T_{eup} - electron spreading time in streamers, formed in upper lightning channel

layers on the moment of channel neutralization; T_e - electron spreading time in streamers, formed in the middle of channel; T_{ed} - electron spreading time in streamers, formed in the lower layers of channel.

The lightning discharge current could stop flow on time T_f , if the lightning channel could seat all neutralizing charge. However it is not possible and the opposite sign than lightning channel streamers are formed from ground surface. So the electromagnetic wave spreads from ground surface to the centre of charged cloud due formation of streamers.

The lightning current depends on sign of discharge, clouds height from ground surface [2]:

$$I_{\max}^- = 2 \cdot \pi \cdot \varepsilon_0 \cdot v_e \cdot (E_{str}^- + E_{str}^+) \cdot H_l = 10,8 \cdot H_l, \quad (4)$$

$$I_{\max}^+ = 4 \cdot \pi \cdot \varepsilon_0 \cdot v_e \cdot (E_{str}^- + E_{str}^+) \cdot H_l = 21,7 \cdot H_l. \quad (5)$$

The current steepness [22]:

$$a_{\max}^- = \frac{I_{\max}^-}{T_f} = 2 \cdot \pi \cdot \varepsilon_0 \cdot v_e \cdot v \cdot (E_{str}^- + E_{str}^+) = 3,25 \cdot 10^9 \text{ A/s} \quad (6)$$

$$a_{\max}^+ = \frac{I_{\max}^+}{T_f} = 4 \cdot \pi \cdot \varepsilon_0 \cdot v_e \cdot v \cdot (E_{str}^- + E_{str}^+) = 6,5 \cdot 10^9 \text{ A/s}. \quad (7)$$

The voltage gradient in streamers, electron movement speed $v_e = 1,5 \cdot 10^5 \text{ m/s}$ and wave propagation speed in lightning channel make influence on lightning current steepness as it could be seen from (6) and (7).

The discharge process change its view then lightning strikes to the high resistance earthed object. The potential difference between leader space charge and lightning channel decreases due to increase of potential on earth resistance. The decreased potential difference create slighter gradient. As the result charge neutralization process become slower and decreases the lightning current magnitude. The lightning current pulse duration increases, because the amount of total charge stays constant. Influence of equivalent earthing resistance z_Σ to the lightning current magnitude, steepness, impulse rise time is described as [2]:

$$I(R_{eq}) = I_{\max} / \left(1 + \frac{z_\Sigma}{z_{lightning}} \right), \quad (8)$$

$$a(R_{eq}) = a(R_{eq} = 0) / \left(1 + \frac{z_\Sigma}{z_{lightning}} \right), \quad (9)$$

$$T_f(R_{eq}) = T_f(R_{eq} = 0) \cdot \left(1 + \frac{z_\Sigma}{z_{lightning}} \right), \quad (10)$$

there $z_{lightning} \approx 300 \Omega$ lightning channel surge impedance.

The Heidler function [4] describes negative polarity lightning current:

$$i(t) = \frac{I_{\max}}{\eta} \cdot \frac{(t/T_f)^2}{1 + (t/T_f)^2} \cdot e^{-t/\tau}, \quad (11)$$

there τ - time constant, proportional to discharge duration, the time then discharge starts to discharge current seek 37% of magnitude;

η - correction coefficient.

The time constant T_f could be evaluated from [4]:

$$T_f = \begin{cases} 0,0834 \cdot I_{\max}^{0,828}, & I_{\max} \leq 20 \text{ kA}; \\ 0,154 \cdot I_{\max}^{0,624}, & I_{\max} > 20 \text{ kA}. \end{cases} \quad (12)$$

Discharge current magnitude is the main criterion for impulse rise time calculation as it could be seen from (12). Commonly statistical approach is used for assessment of discharge current magnitude. However, equation (11) mostly is used for statistical analysis of lightning process. The influence of full discharge circuit should be evaluated and equations (4-10) involved to electromagnetic transient on power network analysis.

4. UHV transmission line with rope

The earthing resistance makes influence on lightning discharge current shape, as it was described above. That's why processes at the fault place should be well known for fast transient processes over high voltage line investigation. The typical UHV line consists of phase conductor, steel or ferroconcrete tower and rope. Three calculation schemes are used for lightning generated transient processes calculations:

1. The lightning overlap phase wire, after that lightning overvoltage breakdown insulator at the tower;
2. The lightning overlap the tower, after that lightning overvoltage breakdown insulator;
3. The lightning overlaps the middle of the rope, after that lightning overvoltage breakdown the gap between rope and phase wires.

Than the lightning overlap phase wire, the voltage at the fault place:

$$u = \alpha \cdot u_0 = z_\Sigma \cdot I, \quad (13)$$

there $\alpha = (2 \cdot z_{line} / 2) / (z_{lightning} + z_{line} / 2)$ - wave refraction index; $z_{line} = 250 \div 400 \Omega$ - line surge impedance.

Equivalent lightning channel surge impedance before insulation breakdown:

$$z_\Sigma = \alpha \cdot (z_{lightning} / 2). \quad (14)$$

Then the wave propagates approximately $\approx 100 \text{ m}$ distance, insulation breakdown after $t = 3,3 \text{ ns}$ as it was described in part 2 starts. After insulator breakdown, tower and ground impedances should be involved in to the equivalent lightning channel surge impedance:

$$z_{\Sigma 1} = z_\Sigma \cdot 2 \cdot R_{earthing} / (R_{earthing} + z_{line}) \quad (15)$$

there $R_{earthing} = 10\Omega$ - tower grounding impedance.

Respectively, after the marginal value of impedance involved to equations (14) and (15) we acquire $z_{\Sigma} = 70 \div 120\Omega$, $z_{\Sigma 1} = 5 \div 7\Omega$.

After lightning overlap the tower, the equivalent surge impedance at the fault place:

$$z_{\Sigma} = z_{lightning} \cdot R_{earthing} / (R_{earthing} + z_{lightning}). \quad (16)$$

After an insulator breakdown, equivalent fault place impedance:

$$z_{\Sigma 1} = z_{lightning} \cdot z_x / (z_x + z_{lightning}) \quad (17)$$

there $z_x = z_{line} \cdot R_{earthing} / (R_{earthing} + z_{line})$.

After the marginal value of impedance involved to equations (16) and (17) we acquire $z_{\Sigma} = 9,7\Omega$, $z_{\Sigma 1} = 9,4\Omega$.

For the third transient calculation scheme, equivalent fault place surge impedance before an insulator breakdown:

$$z_{\Sigma} = z_{lightning} \cdot z_{rope} / (z_{rope} + 2 \cdot z_{lightning}) \quad (18)$$

there $z_{rope} \approx 400\Omega$ rope surge impedance.

After an insulator breakdown:

$$z_{\Sigma 1} = z_{lightning} \cdot 2 / (1 + z_{x1} \cdot z_{lightning}) \quad (19)$$

there $z_{x1} = 2 \cdot (z_{rope} + z_{line}) / (z_{line} \cdot z_{rope})$.

The marginal values of impedances for equations (18) and (19) yields $z_{\Sigma} = 120\Omega$, $z_{\Sigma 1} = 120 \div 150\Omega$.

It is worth to mentioned, that the lightning current surge shape is influenced by equivalent lightning channel surge impedance.

The surge wave is half wave, then the lightning strikes to phase wire. The lightning current steepness could be evaluated according (9) and (14). The impulse time would be restrained by the time from lightning current flow starts till insulator breakdown as depicted in figure 1. The lightning current magnitude is calculated according (9), (11) and (14).

The surge voltage in the tower rises slowly due to many second wave reflections from grounding, then the lightning strikes to tower. The insulation breakdown after voltage magnitude seeks the breakdown voltage. The surge in the line rise time is equal to insulator breakdown time.

Equation (8) and (18) describes the lightning current magnitude, then lightning strikes to the middle of the rope. The surge rise time is proportional to insulator breakdown time – leader propagation time, as depicted in figure 1b.

5. Acknowledgment

The research was supported by Lithuanian State Science and Studies Foundation.

6. Conclusions

1. The experimental rod – rod voltage – time characteristics with in high accuracy could be modeled using equations which describes leader propagation dynamics.
2. The general commutation law states, that charge can not change on bounce. The equivalent surge impedance before and after insulation breakdown should be evaluated for precise surge rise time evaluation.
3. The factors which make influence on lightning current rise time, impulse time and magnitude are described above. Because of that, these factors should be appended to classical lightning current versus time equation for the electromagnetic transient processes identification task.

7. References

1. Резинкина, М. М.; Князев, В. В.; Кравченко, В. И. Статическая модель процесса ориентировки лидера молнии на наземные объекты. Журнал технической физики, Том 75, вып. 9, 2005, p. 44-51.
2. Александров, Г. Н. Главная стадия разряда молнии: механизм и выходные характеристики. Журнал технической физики, Том 76, вып. 12, 2006, p. 101-105.
3. Левитов, В. И. Корона переменного тока. Издательство „Энергия“, Москва, 1975.
4. Dudurych, I. M.; Gallagher, T. J. EMTP analysis of the lightning performance of a HV transmission line. IEE Proc. Generation Transmission Distribution. Vol. 150, No. 4, July 2003, p. 501-506.
5. Костенко, М. В. Техника высоких напряжений. Издательство „Высшая школа“, Москва, 1973.
6. Shindo, T. Suzuki, T. A New Calculation Method of Brekdown Voltage – Time Characteristics of Long Air Gaps. IEEE Trans. on Power Aparatus and Systems. Vol. PAS-104, No. 6, June 1985, p.1556-1563.

APPLICATION OF ACTUAL POWER DEFICIENCY VALUE ON LOAD-SHEDDING

Vladimir CHUVYCHIN, Nikolay GUROV, Santa KIENE
Riga Technical University, Faculty of Power and Electrical Engineering, Latvia

Abstract: Paper considers the emergency load shedding process in power system using the calculated active power deficiency value as control impact.

Power deficiency value is continuously determined on the busbars of power plants during real time. Disturbance in power system related with deficiency appearance and subsequent frequency decline is eliminated with the operation of load shedding system. Calculated active power deficiency is implicated in the under-frequency load shedding system.

Keywords: active power deficiency, under-frequency load shedding.

1. Introduction

Frequency is one of the most important parameters describing power system, and frequency control is one of the main power system control tasks [1].

Successful operation of power system requires that frequency is constant and close to nominal value. Frequency deviation limits and duration is rationed and different for separate power systems. Parameters for normal and emergency operational conditions in different power systems are quite distinctive. Distinctive is assessment of quality of electrical energy, as well as the allocation and characterization of severity of frequency emergency operational condition. Requirements for electrical energy quality are more rigorous in European (UCTE, NORDEL) power systems in comparison with Russian IPS/UPS.

Frequency is determined with the balance of generated and consumed power. Any change in power balance causes frequency deviation [1].

At normal operational condition frequency within acceptable limits is kept by providing primary and secondary frequency control, which accomplishes generation control at power plants.

At emergency conditions, when fast frequency changes take place, in order to eliminate frequency drop and to prevent frequency avalanche the involvement of spinning reserves or under-frequency load shedding automation are activated. If governor action cannot

activate spinning reserve quickly enough to restore the system to its normal operating frequency, frequency actuated automatic load shedding (UFLS) serves as a last-resort tool to prevent the system from collapse [2,3].

Existing UFLS automation has drawbacks, which limit adaptability of emergency automation to a change of under-frequency situation in a power system. UFLS tripping frequency settings are selected for some specific emergency situation, which is considered more probable for specific power system. It is not possible to foresee all situations that can occur in the power system. Problem of value of a load to be shed is also very topical [4].

This papers deals with the determination of necessary amount of load to be shed in order to improve the operation of under-frequency load shedding system during real emergency time.

2. Power deficiency determination method

This section is devoted to the description of power deficiency determination method.

Power deficiency determination is provided for single machine power system considering the equation of motion, which is expressed as follows:

$$T_J (d\Delta\omega_s/dt) = P_{meh} - P_{el}, \quad (1)$$

where T_J – generator inertia time constant in seconds, $\Delta\omega_s$ – rotor speed deviation in per units, P_{meh} and P_{el} – mechanical and electrical power at current frequency in per units accordingly.

When there is a load change, it is reflected instantaneously as a change of electrical power of the generator. This causes a mismatch between the mechanical and the electrical power which in turn results in speed variations as determined by the equation of motion (1). System frequency varies depending on an active power [5].

However, use of expression (1) is not rational for determination of power deficiency, since the power balance between mechanical and electrical power can reinstate at frequency different from nominal value. Here, power system will be balanced, but at emergency deficient operational condition, reason of which is the

dependence of values P_{meh} and P_{el} on frequency. In order to restore the power balance at nominal frequency, current parameters of equation (1) are to be reduced to nominal frequency, and then the power deficiency value could be determined at any level of frequency.

As it is known, the governor speed droop R characterizes the ratio of speed deviation ($\Delta\omega_*$) or frequency deviation (Δf) to change in power output (ΔP) [5]. Mechanical power change due to frequency deviation can be expressed as $\Delta P_{meh} = (-\Delta\omega_*/R)$. Also the power system load has the frequency sensitivity, which is characterized with the load damping constant D . Load change after frequency deviation can be expressed as $\Delta P_{el} = \Delta\omega_* \cdot D$ [5].

Equation of rotor motion in an extended way taking into account the effects of governor speed droop R and the frequency sensitivity of load D on the net frequency change can be expressed as:

$$T_J (d\Delta\omega_*/dt) = (P_{meh} - \Delta\omega_*/R) - (P_{el} + \Delta\omega_* \cdot D). \quad (2)$$

This means that an increase of system load results in a total generation increase due to governor action and a total system load reduction due to its frequency sensitive characteristic.

Consequently, from expression (2) the power deficiency value taking into account frequency change can be derived as

$$\Delta P = T_J (d\Delta\omega_*/dt) + \Delta\omega_*/R + \Delta\omega_* \cdot D. \quad (3)$$

Power deficiency value from expression (3) allows determining the exact power impact value to the power system in order to restore the nominal frequency.

3. Mathematical simulations of load shedding

This section deals with the analysis of under-frequency load shedding (UFLS) operation in power system consisting of three parallel operated thermal power plants connected via long 330 kV power transmission lines with remote load centers. Operational condition of considered power system with respective parameters is represented in Fig. 1.

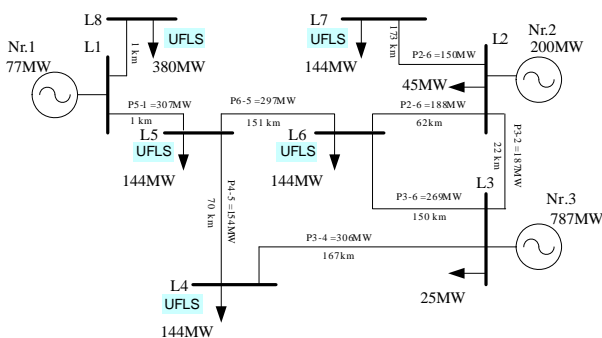


Fig. 1. Examined power system model

Detailed model of power system is provided in PSCAD software including speed governors and excitation systems for all power plants.

As it is seen from Fig. 1, most generation is concentrated in eastern part of power system, though power consumption is located mostly in western part of power system causing power flows at great distance.

In order to analyze the operation of UFLS in mathematical power system model the emergency situation is examined, when at time moment $t = 50s$ the generated power of amount 120MW, 200MW, and 300MW is tripped at power plant Nr.3, which causes active power deficiency of 11%, 19%, and 28% of total power system load.

UFLS operation is examined both for existing operating principle and new – the active power deficiency application principle.

3.1. Operation of UFLS under existing principle

To simulate the operation of existing UFLS the load shedding system used in Baltic countries was modeled. UFLS in Baltic countries consists of different types: UFLS-I, UFLS-II and special setting of UFLS.

The aim of the special setting of UFLS is to increase the spinning reserves of power system at first moment of frequency emergency by shedding less important consumers. Practice shows that amount of load connected to the special setting of UFLS is in range of 3-10% from maximal power system load and actuation time is in range of 0.2-0.5s.

UFLS-I is fast-acting automation, the aims of which are fast preventing of deep frequency drop by shedding consumers with small portions, as well as keeping frequency within allowable frequency-time limits. Practice shows that amount of load connected to the UFLS-I automation is in range of 30-50% from maximal power system load. Actuation time is in range of 0.1-2.0s, usually the settings of 0.4s or 0.5s are used. Actuation frequency is in range of 49.1-47.0Hz.

UFLS-II is slow-acting automation, the main purposes of which are the automatically restoration of frequency to rated values by shedding consumers with small portions and large actuation time, as well as automatically restoration of frequency to rated value in order to synchronize parts of power system. Practice shows that amount of load connected to UFLS-II automation is in range of 12-40% of maximal power system load, and actuation time settings are in range of 10s up to 80-120s.

It should be noted that UFLS-II automation is used only in the power systems of former USSR, in other power systems frequency restoration is provided manually by dispatcher instructions. In most of European power systems only fast-acting UFLS system for preventing deep frequency decline is used.

For simulation of frequency emergency processes it is sufficient to consider only fast activation of spinning reserves (primary frequency control), which is involved at emergency initial period. Spinning reserves are in average about 3-5% of actual power system load and they are evenly distributed along the power system.

Further, frequency response processes in power system considering operation of UFLS are simulated using data of UFLS automation of Baltic countries in 2003. In addition, in this paper is simulated only prevention of

deep frequency decline, which is realized with operation of special setting of UFLS and UFLS-I. Operation of UFLS-II here is not analyzed.

Amount of load connected to UFLS automation in power systems of Baltic countries in year 2003 is given in Table 1.

Table 1. Amount of load connected to fast-acting UFLS automation in power systems of Baltic countries in 2003

Parameters of UFLS	Units	Amount of load at UFLS		
		Estonia	Latvia	Lithuania
Load maximum	MW	1200	1200	1580
Special setting of UFLS, $f_{act} = 49.2\text{Hz}$, $t_{act} = 0.5\text{s}$	MW	36	36	47
	%	3	3	3
UFLS-I, $f_{act} = 48.8 - 47.2\text{Hz}$, $t_{act} = 0.5\text{s}$	MW	504	504	664
	%	42	42	42

In power systems of Baltic countries special setting of UFLS consists of one setting with connected load of 3% from load maximum. Actuation frequency $f_{act} = 49.2\text{Hz}$ and actuation time $t_{act} = 0.5\text{s}$.

Current UFLS-I has 9 settings with actuation frequency $f_{act} = 48.8 - 47.2\text{Hz}$ and setting step -0.2Hz . Actuation time of each setting is $t_{act} = 0.5\text{s}$. Total amount of load connected to automation in percents of forecasted maximum is 42%, in addition, average load of one setting is 4.67%.

In experimental model realized in PSCAD software the data of Latvian UFLS automation are used, and control actions are performed in 5 load centers (substations). Load connected to special setting of UFLS at each substation is following:

$$\Delta P_{UFLS(i)} = P_{UFLS_sp}/k = 36/5 = 7.2 \text{ MW}, \quad (4)$$

where P_{UFLS_sp} – total amount of load connected to special setting of UFLS (from Table 1), $k = 5$ – number of substations prescribed for operation of UFLS.

One setting of UFLS-I at each substation disconnects load in amount of

$$\Delta P_{UFLS-I(i)} = P_{UFLS-I\%}/(n \cdot k) = 504/(9 \cdot 5) = 11.2 \text{ MW}, \quad (5)$$

where $P_{UFLS-I\%}$ – total amount of load connected to UFLS-I automation (from Table 1), $n = 9$ – amount of UFLS-I settings.

From (5) it can be determined that one setting of UFLS-I realizes disconnection of load in amount of 56MW.

Frequency response during emergencies as trip of 120MW, 200MW, and 300MW generation capacity at power plant Nr.3 taking into account operation of UFLS under existing principle is showed in Fig. 2.

Emergency trip of 120MW causes frequency drop to 48.94Hz, which actuates special setting of UFLS automation, which in turn sheds 36MW of load. Remainder deficiency of about 84MW keeps frequency at 49.6Hz level. Emergency trip of 200MW causes frequency drop to 48.34Hz and actuation of 4 UFLS settings. UFLS automation performs load shedding in amount of 204MW. Frequency restoration process with

some overcorrection takes place and after about 7 seconds frequency stabilizes at value 50.07Hz. Emergency trip of 300MW causes frequency drop to 47.32Hz and actuation of 7 settings of UFLS automation, which perform load shedding in amount of 428MW. Redundant tripped load creates 0.5Hz over-frequency situation in power system.

Change of active power deficiency taking into account operation of UFLS under current principle is represented in Fig. 3.

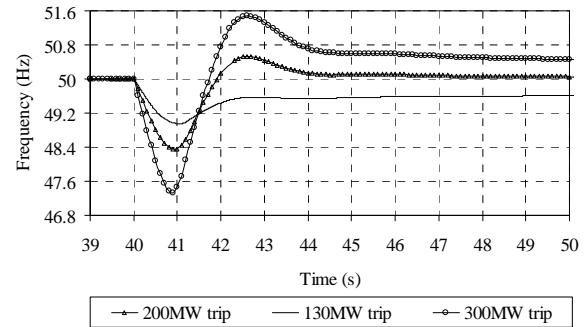


Fig. 2. Frequency change during emergency processes considering the operation of UFLS under existing principle

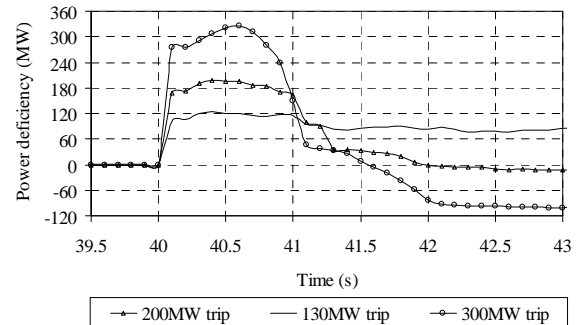


Fig. 3. Active power deficiency change after emergency processes considering the operation of UFLS under existing principle

After emergency impact deficiency sharply increases close to the tripped capacity value. Deficiency change process characterizes the operation of existing UFLS automation.

Frequency restoration and deficiency elimination processes using current UFLS automation of Baltic countries showed that UFLS automation is not adaptive during different emergency situations. The main problem is the proper selection of load to be shed.

3.2. Operation of UFLS under new principle

New operational principle of UFLS automation is based on the application of calculated deficiency (3) to the UFLS automation as actuating parameter.

To avoid frequency drop in considered power system below 49.7Hz, deficiency value for actuation UFLS automation is determined in accordance with following expression [1]:

$$\Delta P_{UFLS_act} = (\Delta f \cdot P_{\Sigma}) / (f_0 \cdot s) = 60 \text{ MW}, \quad (6)$$

where P_{Σ} – total power system generation (1060MW), Δf – frequency deviation (0.3Hz), f_0 – nominal frequency, s – average droop of all rotation speed governors in power system (10%).

Number of actuated settings is determined as follows:

$$n = \Delta P / P_{UFLS_act}, \quad (7)$$

where ΔP – actual calculated deficiency value (3) in power system.

One setting of UFLS is ordered to shed the amount of load equal to actuated deficiency value, which is 60MW according to (6). One setting at each substation is ordered to shed the load in amount of

$$\Delta P_{UFLS(k)} = P_{UFLS_act} / k = 60 / 5 = 12 \text{ MW}. \quad (8)$$

Therefore, appearance of 120MW of active power deficiency according to (7) actuates 2 settings of UFLS, which performs load shedding of about 120MW. Appearance of 200MW power deficiency in power system causes actuation of 3 UFLS settings. Load to be shed is 180MW or 90% of deficiency. Appearance of 300MW power deficiency in power system causes actuation of 5 UFLS settings. Load to be shed is 300MW or 100% of deficiency. Frequency response during emergency process taking into account operation of UFLS under new principle is showed in Fig. 4. Actuation time of settings t_{act} is assumed 0.5s.

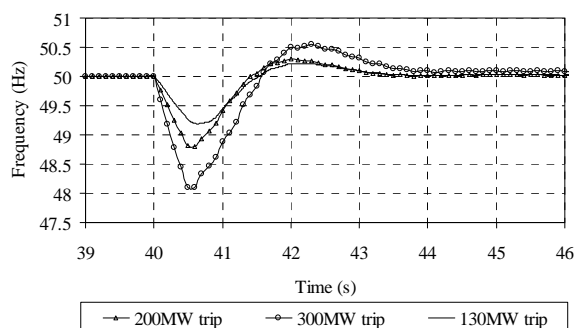


Fig. 4. Frequency response during emergency process considering the operation of UFLS under new principle

Operation of UFLS automation limits frequency drop to 49.2Hz, 48.8Hz, and 48.1Hz after emergency trip of 120MW, 200MW, and 300MW generated capacities accordingly. Fast load shedding and frequency restoration process is followed. After about 4 seconds frequency is restored to acceptable limits for all considered emergency situations.

Change of active power deficiency considering operation of UFLS under new principle is showed in Fig. 5.

In order to decrease possible inaccuracy of deficiency calculation, initial value of calculated deficiency provided to the UFLS automation could be decreased for 20-40% and selected with portions using the law of geometrical progression [6].

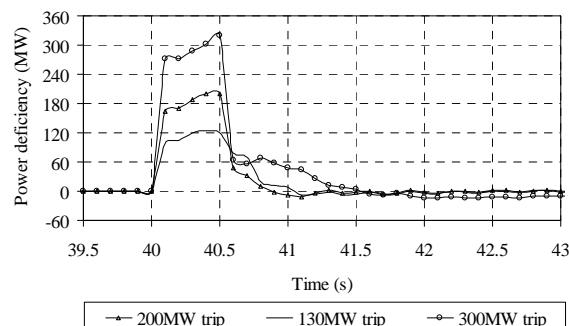


Fig. 5. Active power deficiency change after emergency considering the operation of UFLS under existing principle

Efficiency of operation of new UFLS automation can be characterized with the depth of frequency drop, duration of power deficiency elimination and frequency restoration process, and restored frequency value. Above mentioned parameters of the efficiency criteria were improved with operation of new UFLS.

4. Conclusions

Under-frequency load shedding operation during emergency situation was analyzed using current operating principle of UFLS automation in Baltic power systems, as well as new suggested by authors active power deficiency application principle.

Results showed that UFLS operating under new principle more efficiently prevents frequency drop, faster and more accurately restores frequency to rated values, as well as prevents from frequency overcorrection.

Proper selection of load to be shed can improve the operation of UFLS automation preventing deep frequency drop and avoiding over-frequency situation after control.

5. References

1. Sterninson L.D., Transient Processes During Power System Frequency and Power Control, Moscow, "Energija" 1975, 216 p (in Russian).
2. Rabinovich R.S., Automatic Frequency Actuated Load Shedding System, Moscow, "Energija", 1980, 344 p (in Russian).
3. IEEE Status Report on Methods Used for System Preservation During Underfrequency Conditions. „IEEE Transactions on Power Apparatus and System”, Vol. PAS-94, 1975.
4. Chuvychin V., Gurov N., Rubcov S., Adaptive underfrequency Load Shedding and Underfrequency Load Restoration System, International Conference Power Tech'05, Saint-Petersburg, 2005.
5. Kundur P., "Power System Stability and Control", Tata McGraw-Hill, New Delhi, 2008.
6. Chuvychin V., Gurov N., Kiene S., "Frequency Control and Determination of Controlling Actions to Enhance Stability of Power System", Proceedings of 4th Scientific Symposium "Elektroenergetika-2007", Slovakia, pp 709 – 712.

TECHNICAL ADVANCE IN THE AUTOMATION OF DISTRIBUTED NETWORK CONTROL

Virginijus RADZIUKYNAS, Arturas KLEMENTAVIČIUS, Sigitas KADIŠA, Algimantas LEONAVIČIUS, Neringa RUTKAUSKAITĖ, Antanas NEMURA, Feliksas BIELINSKIS, Viktorija NEZVANOVA
Lithuanian Energy Institute, Lithuania

Abstract: The paper presents short review of state-of-art and recent technical advance in automation of distribution network control. It covers issues of intelligent grids, substation automation, ICT, automated meter reading, feeder automation, SCADA. A number of new automation technologies are referred to. With permanent technology changes in process, the distribution networks move towards digital distribution networks, with widespread intelligence (microprocessors, controllers) across the networks and high-speed communications between intelligent devices. Both expectations and reservations from distribution network operators related to further automation are discussed.

Keywords: distribution networks, automation, technical advance, intelligent networks, control, communications.

1. Introduction

Network operators and power utilities “are transitioning from labor-intensive electromechanical power system designed and built in the mid-20th century to the advanced technology of 21st century; nowhere is this more evident as in the distribution system” [1].

The advanced distribution technology relies on distribution automation (DA) and is aimed at higher reliability of power distribution. The improvements of DA are steadily bringing it closer to its ideal functionality: to monitor, protect and control all processes and equipment in distribution substations and on feeders remotely, with minimum intervention of supervising dispatchers.

2. Contemporary problems of automation and innovations in distribution networks

First and foremost, distribution network operators (DNOs) quite positively envisage the further automation of networks and their progress to intelligent (smart) grids. Sometimes operators prefer monitoring the network versus operating the network. It means that more activities are expected to be performed

automatically. Operators really want to monitor the grids and to respond to troubles, less to control.

Despite of the market forces pressing on DNOs to become more operationally efficient, there are several barriers for long-term extension of DA and practical steps onto smart grids. As it seems, the psychological and awareness barriers are principal ones, associated with missing of the visionary views. DNOs often too much adhere to risk management strategies that overshadow the innovation strategies.

To pursue the objectives of intelligent grids, a lot of new devices and ICT technologies should be integrated. This is a challenge for DNOs – how to realize such fundamental changes. One of their responses – the architecture of intelligent grids shall be developed on “plug-and-play” basis. The concept of “plug-and-play” is probably best defined by Microsoft Corporation: it denotes “A combination of hardware and software support that enables a computer system to recognize and adapt to hardware configuration changes with little or no intervention by the user (www.microsoft.com).. Nevertheless, DNOs use connotation of this concept similar to “effortless for a user” and sometimes expect the ICT and equipment industries should do all job in developing and implementing major solutions..

It is observed that sometimes names of concepts might give a pretext to DNO personnel to underestimate the concept and visions. For instance, the name of automated metering reading (AMR) system is often understood as AMR only, with scepticism for other capabilities to be get out of the system. Anyway, the clue to resolve the hesitations as mentioned above is to take a leap of faith and develop consistent visions and plans for future intelligent grids. As for other barriers, regulatory views also play significant role. Whereas distribution business is regulated, the regulators, not DNOs, set energy tariffs for customers. A DNO cannot invest to DA projects, unless the tariffs ensure recovering of capital costs. Another characteristic barrier in DA field is technical and economical feasibility of automation projects in rural areas.

The moving to more intelligent grids promises for DNOs to get more out of the grid – to “mine” additional distribution capacities from the same grid infrastructure. Meanwhile customers expect to benefit another value – to get a higher reliability of delivery, particularly those in low-density areas. However, the operation of intelligent grid will call for new skills and new knowledge from operating staff. There are real challenges for DNOs to integrate information from variety of sources and to cope with existing information systems. Actually, some standard branches of DNOs are rather slow for innovations. They face data overload and, with the growth of information flows, their ability to interpret the data has decreased. On the other hand, there is a technical expansion need, mainly for standard protocols, more communication bandwidths, and more communication tools for remote sites [10].

3. Intelligent networks

The general trend in modern development of DA is its combination with distributed intelligence. It lays foundations for upgrading the distribution networks up to intelligent (smart, digital) grids. Therein electricity is linked with communications and computer control. Major features thereof will be „densely“ deployed sensors, monitors, controllers, high-speed communications and data-trading software. The intelligent grids will offer such values as greater reliability, increased capacity, choice, safety and flexibility. Intelligent networks are expected to be “self-healing”, with self-monitoring feeders problems anteriorly they happen.

Since the concept of intelligent network is rather vague for a lot of customers and even DNO employees, it can be defined, in simplistic mode, as an electric network, that will monitor, think, act, repair and prepare itself to respond quickly to customer needs.

The intelligent network features combination of high-speed computers, intelligent electronic devices (IEDs) and intelligent software.

The state-of-art of intelligent networks today might be seen as lying between visions and emerging networks. Majority of intelligent devices and technologies are available on the market. The current types of information systems will continue to overlie networks in their progress to intelligent ones. The principal systems seem to be SCADA/EMS (Supervisory Control and Data Acquisition/Energy Management System), SCADA/DMS (distribution management system), OMS (outage management system), AMR systems and WMS (work management system).

4. Substation automation

Historically, automation of distribution substation (HV/MV) might be loosely classified to following levels of technical advance:

- 1) electromechanical protection and control relays, initially without a remote terminal unit (RTU) of SCADA system in a substations;
- 2) electromechanical relays as data transducers to a microprocessor-based RTU in a substation;

- 3) solid-state (semiconductor-type) relays;
- 4) digital protection relays and microcontrollers;
- 5) programmable logical controllers (PLC) and IEDs, integrated into local area networks (LAN), with advanced logic, monitoring (including video surveillance), multiple control functions, sensing and extended communications between substations and between RTU and SCADA masters and central stations;
- 6) digital distribution substations of the next future featuring smart sensing and telemetering, and data traffic in various high-speed communication media, high intelligence, smart decisions, automated or not, extended monitoring with two-way communication between distribution substations, local substations (MV/LV), feeder switches, distributed generators, electricity storage units and customer loads.

4.1. Substation intelligence

If intelligence in substations is referred to as digital intelligence (computer intelligence), in the period of electromechanical and solid state relays there was no substations intelligence, only logic of protection and control. This logic was composed from a number of relays, each having one or two protective functions, reaching sometimes a rather complex logic.

In a digital relay, many functions are implemented by the microprocessor programming. A digital relay can analyze whether the relay should trip or restrain from tripping based on current or voltage magnitude, complex parameters set by the user, relay contact inputs, the timing and order of event sequences.

The modern versions of digital relay will contain advanced metering and communication protocol ports, allowing the relay to be a focal point in SCADA system. Digital relays are classified to IEDs – microprocessor-based controllers of power system equipment. Other types of IEDs include load tap changer controllers, circuit breaker controllers, capacitor bank switches, recloser controllers, voltage regulators etc.

Typically, IED contains around 5-12 protection functions, 5-8 control functions controlling separate devices, an autoreclose function, self monitoring function, communication functions etc.

Several IEDs can jointly control a distribution substation. Another control alternative is PLC. In contrast to IEDs, PLC relies on a processor, not on microprocessor. It contains more extended software and much more functions as an IED does. Unlike general-purpose computers, the PLC is designed for multiple inputs and output arrangements, extended temperature ranges, immunity to electrical noise.

Like IEDs, PLC receives inputs from sensors (analog or digital signals) and power equipment. Where substation design includes IEDs, inputs come from IEDs as well. PLC issues outputs to actuators such as relays, electric motors, pneumatic or hydraulic cylinders etc. Some input/output arrangements provide external communication with SCADA network (via RTU) and other computer networks as LAN or WAN (wide area network). Embedding the intelligence into substations needs more sensors, i.e. devices that measure physical quantities and

convert them into signals that can be read by intelligent devices. Here noteworthy seems to be recently developed so-called Esubstation model (Cooper Power Systems) – a new approach to distribution substation real-time monitoring of equipment and feeders. Based on Cannon Yukon software platform, it provides the dispatchers with a complete real-time picture of substation using integrated browser-based application with Cannon's equipment sensors.

The sensors located on substation's transformers measure (or monitor, as it is said) loadings, critical temperatures, cooling equipment status, combustible gas etc. Those located on substation's power circuit breakers monitor vital functions such as gas pressure, density and temperature along with the tripping status. Other Esubstation sensors can be installed in control house to monitor feeder loading, relay targets, voltage regulation and batteries [2]. In addition to sensor data, Esubstation offers a video surveillance opportunity that could replace on-site surveillance by a field crew.

The IEDs in Esubstation poll the sensors via fiber-optic (transformer data) and wireless (circuit breaker data). IEDs exchange data (aggregated and not) with RTU. IEDs and RTU are integrated into Substation Advisor Gateway of Esubstation. The Gateway communicates with dispatchers via SCADA and internet.

There is a lot of innovative, low-cost voltage and current sensors today in the market. Furthermore, new smart sensing technologies are introduced, maybe marking a threshold of a new sensor generation. For instance, classical current transformers might be replaced by one new IED model that acts as noncontact device and simultaneously measures 3 phases. Here classical sensors would need a contact with the bus works [3]. Similarly, another new current-monitoring device is used in top-pole applications and also has no contact with a conductor [2].

As for other smart sensing technologies, at least two of them rely on insulators. First one is defined as current- and voltage- monitoring insulators for use on switches and lines to monitor in remote locations. The second one refers to high-accuracy line-post current sensors that feature a line-post insulator with an embedded coil to measure currents through an inductive coupling. As for contact devices, a faulted-circuit indicator has been designed that clamps on the phase wire to indicate the exact location of a fault [2].

It can be credibly envisaged that substation equipment manufacturers will continue to develop proprietary technologies. Therefore, from manufacturers' and DNOs' perspective, the major problem related to intelligent substations will be to ensure the interoperability of substation devices [3] (see section 5).

4.2. Substation integration

Significant benefit of substation automation (SA) is reduction of substation space. DNOs (with other stakeholders in the sector) have undertaken customized substation integration projects aimed at development of optimal integrated design.

National Grid's company (Massachusetts, USA) has designed an integrated design model for breaker-and-a-half substation, which is most common in high-density load areas serviced by the company. The design pursued objectives to reduce the total-life cost of the secondary systems within substation and to replace electromechanical devices by IEDs. The design themes were adopted [4] as follows:

- 1) modularize the control and protection subsystems (two formerly vis-à-vis located protection and control bays A and B should be integrated into one modular cabinet, say, bay A located over bay B).
- 2) maximize the use of protective relay data (data should be collected once and used many times to provide information for various sources);
- 3) minimize the amount of hardware and wiring;
- 4) improve the functionality of substation user interface;
- 5) enhance remote diagnostics, data collection and test capabilities.

As a result, with the fewer cabinets in the modular design, the footprint of substation was diminished from 17 m² to 7 m². The control system design brought cost saving of 42 % over the previous design.

The new design retained an operator desk with human-machine interface (HMI), so substation is referred to as a control house. The computer of operator desk communicates with RTU and PLC within the substation's LAN. Considering the outside of distribution substations, it seems there is too much wiring and too many devices there. According to some experts (Mark Dudzinski, GE Energy) "more work is required on defining communication standards and architecture outside the substations to support the advanced distribution infrastructures and the vision of intelligent grids" [5].

5. Information and communication technologies

In a vision of intelligent network, a vast amount of the automated control actions will be co-ordinated by intelligent devices in real-time. The major condition for successful co-ordination will be existence of extended robust communication infrastructure and its high-speed functioning. Switching decisions, for instance, require sensor data sampling rates faster than 1 msec.

Bandwidth is a key technical factor for both the amount and speed of communicated data – analog and digital signals. Any set of data other than simple text message is very large against a message. Radio medium does not suit for transferring video (surveillance) data.

State-of-art of communications in distribution companies covers variety of physical media. Wired options include twisted pairs (copper cable), telephone line, coaxial cable, fiber-optic cable, power line carrier (PLCr) and broadband over power line (BPL). Wireless options include paging, radio, cellular, wireless fidelity (Wi-Fi), satellite and microwave. Most of the wired media have distance limitations, unless the amplifiers are added. Wireless media often have signal strength limitations [5].

In a substation environment twisted pair and fiber-optics are major physical media to carry sensor data to local meters, controllers and RTUs. First medium is

inexpensive, but rather sensitive to intensive electromagnetic interference, contrary to more costly second medium. Somewhere Wi-Fi and PLCr have been installed for communications inside a substation.

Computer-to-computer communications usually function on fiber-optic, coaxial or copper cable, because computers are interconnected typically as a LAN or WAN.

The RTUs access the SCADA central stations over dedicated telephone and all other wired media. In rural areas, pole-top mounted RTUs on rural feeders communicate with central sites via radio, cellular or satellite.

If not overestimated, the BPL has enormous potential in next coming years. One recent study envisages the potential of broadband network to reach app. 2 billion rural inhabitants (number of electricity customers will be several times less) around the globe who are still unreachable for modern voice and data services and who otherwise would remain without access to modern, high-speed telecommunication services [6].

Since more than 3 decades, the interoperability of various protection devices and controllers in both substations and power grids was largely restricted by different communication standards embedded into them by different manufacturers.

The existence of different communication protocols required from an operator to implement large amounts of commissioning efforts with subsequent adverse effects on matching the multi-protocol equipment to newly added devices in future. Therefore there have been only few substations where devices and controllers of different origin were good interfaced.

By now most installations in substations, LANs and WANs today communicate via DNP3 serial protocol, followed by older protocol Modbus. Often the proprietary protocols (not serial, i.e. standardized by IEC) still are used. SCADA central stations and RTUs communicate on DNP3 as well. The emerging option to DNP3 is nonserial Internet protocol/Ethernet. New IEDs, RTUs as well as video cameras are Ethernet-based devices. Ethernet-core substation networks are considered as modern technical structures. The emerging services in ICT market just include assistance in gradual modification of substations with low-bandwidth media and serial protocols to higher bandwidth and Ethernet.

Nevertheless, the Internet protocol/Ethernet is not the long-term benchmark. In the first half of 2004 the unique communication standard IEC 61850 for substation automation was released. It ensures smooth exchange of data with one another because all the connected devices communicate a common language.

The first substation in distribution networks (and first substation in world as such) with complete IEC 61850-based control was installed in a 16-kV substation in Switzerland, 6 months after the issue of the standard. It was done by Siemens Power Transmission and Distribution, the same entity that was protagonist in the development of a new standard. The old protection and control system was replaced by new one of SICAM type (it is Siemens equipment family consisting of products for digital power automation). The new communication

standard ensured the required interoperability in the substation.

6. SCADA/EMS and SCADA/DMS

The SCADA history begins with the advent of digital computers in the mid 1960-ties. Those computers were capable for real-time control. Prior to that time, the remote control existed but it was incapable to cover a power system (network), just only single objects, e.g. a larger power plant. Since then SCADA had a long history of efficient use on the transmission grid, while the predominantly radial distribution network has not generally benefited to the same extent.

Today SCADA is categorized to SCADA/EMS and SCADA/DMS. SCADA/EMS supervises, controls, optimizes and manages generation and transmission systems (so-called Generations and Transmission SCADAs). SCADA/DMS performs the same functions for distribution networks (so-called Distribution SCADA). Both systems enable DNO to collect, store and analyze data from hundreds of thousands of data points in national networks, perform network modeling, simulate power operation, detect faults, prevent outages, and participate in energy trading markets [7].

Nowaday SCADA/DMS is just getting into wide-spread usage. It covers MV&LV distribution networks and improves customer service by providing accurate and prompt information about maintenance and outages. SCADA/DMS masters communicate with substation and feeder RTUs, smart relays and SA systems to monitor the real-time status of the network and provide remote control of devices such as switches, capacitor banks and voltage regulators.

It can be concluded from the SCADA definitions referred to that SCADA/DMS is conceived as covering the MV and LV network points, but excluding distribution substations (HV/MV). Thus the above-mentioned statement "SCADA had a long history of efficient use on the transmission grid" implies namely the HV part of distribution substation! Therefore, conceptually, distribution network is "shared" by Transmission SCADA and Distribution SCADA.

Smart Energy Alliance (UK) refers to 9 primary benefits to installing a Distribution SCADA system: 1) monitoring&control; 2) advanced power flow analysis; 3) network switching; 4) load management; 5) fault detection, isolation, and restoration; 6) volt/VAR control; 7) integrated outage management systems; 8) integrated trouble call system; 9) mobile workforce management.

Since SCADA is, first of all, a system consisting of many objects (network points), the minimal threshold of system might be an issue. The technology developers are providing to the market microSCADA for minor applications – for selected number transmission and distribution substations.

The SCADA systems had developed from conventional architecture as "RTUs of distribution substation – SCADA masters in central stations with HMI" to contemporary innovative architecture as "conventional architecture plus distribution substation automation

systems plus feeders RTUs plus selected IEDs and digital relays in MV/LV network equipment”.

Substation RTUs collect sensor data on substation equipment and transmit it to SCADA masters and central stations in batch mode on periodic basis, app. each second (it is *data acquisition*). SCADA masters (computers, servers) analyze data and automatically monitor the process (it is *supervisory control*) and, when necessary, issue switching orders to RTUs in response to the process (it is *active or direct control*). Similarly, a dispatcher via HMI monitors the process (*supervisory control*) and intervenes (*active control*).

Some RTUs also perform control of substation equipment, but it is considered that PLCs do it better, while RTUs more suit for communication with masters.

Distribution SA systems do not have RTUs. They communicate to SCADA masters from PCLs or from IEDs. It is called SA/SCADA systems integration. It adds new or, at least, unconventional functions to SCADA system (additional SCADA dispatch centers, adaptive relay settings, access to substation metering data, feeder automation support, automatic load restoration, power quality monitoring etc. [8]).

As yet SCADA coverage on distribution substation level is practically completed: each larger substation in high-density areas typically has a RTU. Small substations and those in low-density areas do without it. Presumably, only limited potential for SCADA coverage extension can be envisaged therein. However SCADA systems on this level will extend in data flow dimension, because of new SA schemes, SCADA/DSM extension and cooperation/integration with other grid control systems. Considering compatibility issues, new SCADA architecture need adaptation to old substations and old RTUs, and *vice versa* new SA schemes require adaptation to old RTUs.

Today geographical data are embedded in SCADA systems, after their alignment with GIS.

It should be noted that SCADA is not the one and exclusive system of distribution network control. There are some other dispatching, telemetering and monitoring systems that do work without SCADA masters, e.g. AMI (see section 7). They can be integrated with SCADA.

Considering the future of remote distribution control, it is still vague whether intelligent networks will be a driver or a barrier for SCADA, despite of the growth of remote data traffic. Some uncertainties arise from recent reporting on BPL breakthrough and perspectives. Many observers see BPL as eventually able to replace other forms of remote asset management that include supervisory control and data acquisition, teleprotection and the use of narrow-bandwidth forms of PLCr [6].

7. Automated meter reading

The conventional practice of manual meter (electromechanical) reading is superseded by AMR (solid-state) systems. AMR enable DNOs to track customer energy usage, and to improve billing. In the last decade various AMR systems were implemented and tested. Such systems work as information networks that connect the

customer meters with central processing units of DNO. They perform the functions of gathering, transport and dissemination of metering data. Started with larger customers, AMR technology is currently coming to residential customers. In result, some DNOs declare that AMR have decreased the meter-related billing complaints, inaccurate billing and work order errors by half.

The wire-based networks have proved their value but recently the wireless networks seem be a winning technology. Particularly, then wireless technology is combined with new generation of meters.

The previous wireless network architecture was based on the huge amount of data collectors, for instance, hundreds or even thousands in urban area of 500 km². Modern network architecture, referred to as a new advanced AMR, is implemented in various power utilities in USA. It allows endpoint meters to communicate directly with AMR base stations. For the area of the mentioned above, the coverage is ensured by 3 tower-mounted base stations, with total elimination of complex, intermediate tier pole-top or roof-top-mounted data collectors. These new AMR systems provide synchronized hourly read interval data, including demand data. The integration of meter reads to billing systems is entirely automated [9].

Albeit the current AMR practice proved its technical and economical feasibility in urban areas, the analogous statement still hardly can be fitted for rural applications: as in general, DA of rural networks is complicated.

Nonetheless, the function of automated reading might be seen as only incipient application of AMR systems. The monitoring of customer's energy usage enables dispatchers to have a more comprehensive real-time monitoring of network operation. A next application might be recording of outages and customer interruptions. Further the monitoring of power quality, if advanced meters send power quality data to network dispatch centers, can be envisaged.

The next function would be based on two-way communication between a meter and a control center. Introduction of such communication will transfer an ARM system to higher level of advanced metering infrastructure (AMI). It will provide the remote connect-disconnect service of a customer. Finally, the AMI concept might be extended to include home portals for customers. Such a portal will be able to deliver price signals and to motivate a customer to engage to demand response. Moreover, a portal could provide information on outages and power quality. [10].

Eventually, one unexpected driver for AMI deployment might appear. It is BPL communication technology, still being in its infancy. It 2006 it covered only 1.3 million electricity customers worldwide, with forecasts o 20 and 70 million in 2008 and 2010, respectively [6].

8. Feeder automation

Feeder automation deals with automatic load transfer from failed feeder to a backup feeder. This transfer is carried out by circuit breaker or other change-over switch located either in a substation or in remote feeder

section. According to some estimation, the automation at feeder level in North America is less than 20% [1].

As for restoration of interrupted feeders, majority of utilities still rely on first call from a customer reporting on interruption, even with AMI systems installed (with capability of two-way communication). AMI or other monitoring technologies should be used to notify dispatchers on customers out of service. Having entire picture of outage, dispatcher can adequately choose the actions of remote control and dispatch field crews [1].

As yet customers served via a fuse-protected feeder usually experienced a sustained interruption after fuse had blown due to the momentary disturbance, e.g. the tree limb touching a power line. In 2007, advanced protection technology was successfully applied – so-called TripSAver Dropout Recloser. This device senses the severity of the problem and restores the delivery if the problem no longer exists. It proved to decrease outage time significantly.

The value of high-scale feeder automation in terms of outage duration can be quite impressive. Naperville (Illinois, USA) DA project (providing 70 % of distribution network with automation) demonstrated good response to out-of-power accident of one 138-kV distribution substation in Naperville city (normally, the city is supplied from 4 such substations). In an instant, 25% of Naperville customers, i.e. app. 13,600, lost power. In less than 2 minutes, 9100 customers (67%) regained electricity service – it was restored automatically. 5845 thereof were re-energized by switches in remote feeder sections, while the rest 3255 customers – by automatic load transfer process at the substation level.

Later on another 4380 customers (32%) regained service in the next 14 minutes by means of dispatcher control actions to operate substation bus ties and distribution assets (via SCADA). The remaining 1% of customers (143) was re-energized by repair crews within 81 minutes after the accident. Hence the automated feeders drastically reduced the number of customers exposed to a typical outage. That accident has completely validated the significant investment into city's DA [11].

As for urban environment, the optimum distribution circuit design is considered to consist of 2 feeders (MV), with 10 km total length (mainline), each feeder (5 km) fed from different substation. There are 3 circuit breakers installed on this circuit: at the open point between feeders and at the mid-point of each feeder. Thus the circuit is sectionalized into 4 sections. The total circuit can be fed from either substation in emergency case. The embedded auto-sectionalizing and reconfiguring intelligence allows the switches to reconfigure for faults and loss of power. A faulted feeder section is isolated automatically and the half the faulted circuit is restored within 60 sec. On a monthly basis, maintenance crews shall attend each circuit breaker to ensure that it is intact and all automated functions are in "ready-to-transfer status" [11].

If feeder automation is aimed at reduction of SAIDI minutes, the design of optimal distribution circuit might rely on sectionalizing feeders to maximum number of segments [2].

9. Conclusions

1. Automation, as it is in process, will transform distribution networks to digital (intelligent) distribution networks where computer (microprocessor) network will overlie power network.
2. Intelligent network vision is gradually turning to emerging network technologies that will help convert data to intelligence, intelligence to knowledge and knowledge to intelligent business decisions.
3. The major difficulty related to future intelligent substations and networks is referred to as interoperability of proprietary devices (different manufacturers keep to different communication protocols).
4. Sometimes views of distribution system operators on future intelligent networks are overcome by apprehensions of complexity in introduction and operation of intelligent technologies. Operators desire to implement "plug-and-play" type technologies and are apprehensive of superabundant information flows.
5. Distribution automation, particularly on feeders, has proved its high effectiveness in urban areas in terms of reliability performance (SAIDI minutes).
6. Automated meter reading systems are progressing to advanced metering infrastructures (AMI) featuring two-way communications for switching control applications.
7. With the communication technology advance leading to low-cost products, the automation of rural distribution networks, including Distribution SCADA or micro-SCADA, is entering into cost-effective applications.

10. References

1. Wolf G. The road to assets management. *Trans.&Distr. World*, April 2007. p. 8-10 (in supplement *Digital distribution*).
2. Wolf G. Embedded intelligence. *Trans.&Distr. World*, April 2007. p. 3-7 (in supplement *Digital distribution*).
3. Wolf G. Substation intelligence. *Trans.&Distr. World*, November 2007. p. 12-16 (in supplement *Digital transmission*).
4. Gwyn B. and Panas W. IEDs: Enhanced monitoring and control in a tiny package. *Trans.&Distr. World*, February 2005. p. 41-48.
5. Tani M. Critical connections. *Trans.&Distr. World*, April 2007. p.12-14 (in supplement *Digital distribution*).
6. Research firm releases study on broadband over power lines and power-line-carrier communications technologies. *Trans.&Distr. World*, Aug. 2007. p. 10.
7. <http://www.abb.com>.
8. Carpenter D., Foster V. and McDonald J. Kentucky utility fires up its first SCADA system. *Trans.&Distr. World*, February 2005. p. 33-39.
9. Alabama Power begins trial of 500 AMDS Meters. *Trans.&Distr. World*, February 2005. p. 14.
10. Bush R. and Musser P. Focus on efficiency. *Trans.&Distr. World*, February 2005. p. 44-49.
11. Geynisman O. and Schaub J. Automated switching benefits customers. *Trans.&Distr. World*, September 2007. p. 46-50.

DISTRIBUTED GENERATORS: DEFINITION IDENTIFICATION

Dainius SLUŠNYS
Kaunas University of Technology, Lithuania

Abstract: Electricity supply structures and energetic institutions associated with installation, exploitation and development of distributed energy resources have different definitions for distributed generation. Different types of generators are installed in electric power systems. Those units can be either high or low power, installed at customers' or far from them, traditional or renewable. Large amount of generating units and different definitions for distributed generators leads to problematic definition for real and exact distributed generators. Sometimes it can be a reason of misunderstanding.

Keywords: distributed generators, distributed generation, definition.

1. Introduction

Power of generating units in electricity supply system varies from few kilowatts to hundreds megawatts. Those units can be a part of small, large and interconnected electric power systems. Generating unit connection to the grid can be different. Unit can be connected straight to the load, both to the load and to the distribution network, only to the distribution network and to the transmission network. If unit is connected to the electricity supply system, consumer can be near, not far and far away. This variety is the problem for exact definition identification for distributed generators. Electricity supply structures and energetic institutions give very different definitions for distributed generators. The reason of different distributed generators definitions is a diverse understanding of traditional big power units. Mostly, if unit or units are not recognized as a traditional, they are called distributed generators. Sustaining definitions of electricity supply structures and energetic institutions, it is not possible to detect exact limits for the definition of distributed generators. Definitions are selected by subjective understanding. Objective definition must be chosen by arguments and proofs.

2. Review of definitions for distributed generators

The largest electricity supply structures and energetic institutions give different definitions for distributed generators. Let us have a look at some of the existing definitions [1, 5]:

1. By CIGRE (International Conference on High Voltage Electric Systems) distributed generators are called:

- ✓ Power less than 100 MW;
- ✓ Connected to the distribution network;
- ✓ Decentralized;
- ✓ Amount of electric energy is not planned.

2. By IEA (International Energy Agency) distributed generators are called:

- ✓ Connected to the distribution network;
- ✓ Connected straight to the load;
- ✓ Small scale (internal-combustion generators, small power gas turbines generators, micro turbines, fuel cells and solar units).

3. By DPCA (Distributed Power Coalition of America) distributed generators are called:

- ✓ Connected to the consumer;
- ✓ Small scale generators;
- ✓ Connected to the consumer network, distribution network or to the transmission network.

4. By „US Department of Energy” distributed generators are called:

- ✓ Connected straight to the load;
- ✓ Small scale generators.

5. By „Swedish Electric Power Utilities” distributed generators are called:

- ✓ Power is not important;
- ✓ Connected directly to the distribution network or at the customer site.

Other electricity supply structures and energetic institutions suggest that distributed generators have the following features [5]:

1. Standardized and modular generation source using renewable energy source in a range of up to one MW (Austria);
2. Source connected to the Distribution network (Norway);

3. Source less than 10 MW, not centrally planned and connected to the distribution network (Bulgaria);
4. Source not operated by utility (Czech Republic);
5. Source less than 50 MW for local consumption and/or for selling to the utility (Estonia);
6. Source less than 20 MW, not centrally planned and not centrally dispatched, and connected to the distribution network (Finland);
7. Integrated or stand-alone modular source close to the point of consumption (Germany).
8. Generation not active in system balancing (Netherlands).
9. Electricity or heat source connected to the user (Poland).
10. Decentralized source less than 50 MW rating (Romania).
11. Source less than 100 MW, not centrally planned and dispatched, and connected to the distribution network (Slovakia).
12. Source connected to the distribution network or to the customer site (Sweden).
13. Source not connected to the transmission network (Great Britain).

All those definitions are a proof of different understanding of distributed generators and distributed generation. It means that distributed generators definition is not identified exactly. Large number of definitions already exists and there is no clear consistency between them.

Lithuanian terminology vocabularies have no comments about distributed generation definition. Some international terminology vocabularies have comments about distributed generators but without exact limits and descriptions.

3. Distributed generators indeterminations and comments

Definitions prove that there are no exact limits between traditional generators and distributed generators. In definitions above distributed generators are identified by certain characteristics, which are as follows:

1. Power.
2. Generation unit type.
3. Connection location.
4. Generating unit distance to the load;
5. Load connection to the generating unit;
6. Generating unit status in the power system (centralized or decentralized);
7. Planning and forecast of power (planned or not planned energy amount);
8. Dependence of generating unit on the power system (generating unit operating in the power system, autonomous operation of generating unit, but with possibility to be connected to the power system and only autonomous operation of generating unit).

The following four criteria can be distinguished that have a prominent influence on the definition of distributed generators origin:

1. Generating unit power and amount of electric energy.
2. Generating unit type and connection location.

3. Generating unit status in power system;
4. Loads location.

Mostly distributed generators are identified as a result of correspondence to one of the criterions.

4. The aims of distributed generators establishment

The main goals for the establishment of distributed generators are [2, 3, and 4]:

1. To reduce electricity transmission losses.
2. To increase electricity supply reliability.
3. To make a convenience of renewable resources.
4. Electricity market liberalization.

5. Distributed generators definition and proof

The first step is to identify affinities of the distributed generators. For the objectiveness, certain criterions must be chosen: range limits, critical values and correlation.

The first of criterions is generating unit power and amount of electric energy. In already existing definitions, value of power varies from some kilowatts to one hundred megawatt. The amount of electric energy is taken into account only for renewable resources. Here we can see that the existing definitions of generating power unit greatly differ. It means that electricity supply structures and energetic institutions associated with distributed energy have different view point to the distributed generation. The explanation of it may be that various countries, electricity supply structures and energetic institutions have different installation and novelty levels of distributed generators. Projection, planning, designing, application, and management of distributed generators are in quite highly different levels too. The highest defined power of distributed generators is known as one hundred megawatt (CIGRE). The highest power is defined by load range limit possibility, but the demand, production and loads of electric energy is always increasing and it is the reason to increase defined power of distributed generators. For example, distributed network load is 150 MW (such high loads are possible in industry plants), generating unit – 130 MW, last 20 MW part is covered by electric system. Question is, is it possible to call 130 MW generating unit as a distributed generator even if the power is over limited? There is an important relation between load and generating unit. 130 MW generating unit uses all his power to cover local load. It is possible to satisfy three of four aims of distributed generators establishment. That is the reason to call 130 MW generating unit as a distributed generator even if the power is over limited. The development of distributed generators and simple examples provide a conclusion of power definition: **power and electric energy amount can not be a direct criterion for the identification of distributed generators definition.** The power of generation unit alone does not correspond to the goals of distributed generators establishment.

There are many types of generating units. The type of generator completely depends on demand and primary energy resources. In most cases, generators are divided into two groups: traditional and renewable energy.

Traditional generators can be built almost everywhere considering the demand. Renewable energy generators can be built only at renewable energy resources. The renewable energy unit power depends on amount of primary energy resources. The traditional generators can be connected to the electricity network almost everywhere. Meanwhile, the renewable energy generators can be connected to the network only at renewable resources places or close to them. The connection of generating unit to the net depends on power, stability of energy production, load location and load power. If to remember the example above, 130 MW can be either separate generating units, groups of generating units or different types. A conclusion can be made regarding the type of generator: **generator type can not be a direct criterion for the identification of distributed generators definition, but it can be a reason of connection location.** Generating unit can be connected to the electricity network in three ways:

1. Directly to the load.
2. To the distribution network.
3. To the transmission network.

A generator or a group of generators connected directly to the load can satisfy all four goals of distributed generators establishment or at least three of them.

If a generator or a group of generators are connected to the distribution network, all four, three, two, one or none of the goals of the distributed generators establishment can be satisfied.

A generator or a group of generators connected to the transmission network can satisfy only one or none of the goals of the distributed generators establishment.

The goals of distributed generators establishment are directly influenced by a connection location of a generator or a group of generators. Here a conclusion can be made regarding the connection location of the generator or the group of generators: **the location of connection of a generator or a group of generators is one of the main factors for the identification of distributed generators definition.**

Independent generators can be connected to the electricity grid, if electricity market is liberalized. The type and power of the generator or the group of generators is not important and can be neglected in this case. Those generators can be centralized and decentralized. The amount of electric energy can be centrally planned or not planned. A Centralized, decentralized, centrally planned or not centrally planned generator or a group of generators can be connected to the power network in all three mentioned ways. Here a conclusion can be made regarding the status of the generator or the group of generators in power system: **the status of the generator or the group of generators in the power system can not be a criterion for the identification of distributed generators definition.**

Load locations are available everywhere in the distribution grid. A single load power can vary from few watts to the ten megawatts and more, while groups of loads can reach hundreds of megawatts. Electric energy demand is changing all the time. Technological processes, various industrial requirements and anti-

pollution standards can be a reason for load location in the area. Load location and generator location can be the same. In most cases, loads are connected to the distributed network. A load supply voltage can vary from 0.4 kV to 10 kV (in exceptional cases load supply voltage can be higher). If a generator and load location are the same or close, it may be a distributed generation case. Here a conclusion regarding loads location can be made: **loads location is one of the main factors for the identification of distributed generators definition.**

Various definitions of distributed generators, proofs, criterion associations and the aims of distributed generators establishment suggest an objective conclusion that: **there are two main direct criteria for the identification of distributed generators definition – a connection location of a generator or a group of generators and a location of loads.** Other criterions are only secondary factors for the identification of definition.

Main criterions it suggest that there is an important distance between generating unit and load. Both criterions are sufficient for the identification of definition, but there are two indeterminations:

1. Definite greatest distance between generator and load in the distribution network.
2. Definite greatest power of generating units or definite greatest power proportion ratio in comparison with loads.

Both indeterminations must be researched and the conjunction between them defined.

The distances between loads and distribution points are selected to satisfy range of work parameters at loads. Distribution network can be divided into one, two or three steps of voltage. The generator can be connected to each of them in the distribution network. At generator and voltage step, a load or loads can be connected to the following voltage steps:

1. Connected to the same voltage step as a generating unit.
2. Connected one voltage step down.
3. Connected one voltage step up.
4. Connected two voltage steps down.

The first goal of the distributed generators establishment says that electric power losses must be reduced by using distributed generators. It is the main object to research. If a load is in the same voltage step as generator or generators, power losses are at the minimum and a generator or generators can be called distributed. If load is at one voltage step up or down as a generator or generators, power losses increase but less than in transmission. It means that generator or generators can be called distributed in this case. If load is at two voltage steps down like a generator or generators, power losses are almost the same as in the transmission. It means that generator or generators can not be called distributed in this case.

In the first three cases a generator or generators can be called distributed, if they correspond to other conditions mentioned above. Here a conclusion regarding the greatest distance between a generator and a load in the distribution network can be made: **the distance**

between a generator or generators and load in the distribution net is not important, but a generator or generators and a load must be connected in the same voltage step or not further than one voltage step up or down.

Usually power supply in the distributed network is obtained from the transmission network. All electric power transmission and distribution components are selected to supply a load power with required reserve. The power of a generator or generators can be selected to supply loads and to transfer the rest of the power to the transmission network. It means that the selected power of connected generator or generators can be double as it is in the load. Here a conclusion regarding the greatest power of a generator or generators can be made: **a generator or generators can be called distributed if the selected power is not greater than double as the one in loads.** If the power of a generator or generators is higher than double as the one in the loads, and if the distribution network is modified to transfer more power to the transmission network, then the generation can not be called distributed.

On the grounds of logic objectives, distributed generators definition can be exactly identified and represented as follows: **a distributed generator or generators are electric energy sources connected to the distributed network to the same voltage step or not further than one voltage step as loads, operating in normal conditions, power is not higher than double as the one of load and have a possibility to be connected to the system and partially or completely cover load demand.** Other factors are not important for the identification of distributed generators definition.

A distributed generator or generators are units with the following features:

1. Generator or generators connected to the distributed network.
2. Generator or generators connected to the same voltage step or not further than one voltage step as loads.
3. The power of a generator or generators must be not higher than double as the one in load and have a possibility to be connected to the system; and the same as load without a possibility to be connected to the system.
4. Generator or generators partially or completely cover load demand.
5. Normal operation conditions.

A generator or generators satisfying the conditions mentioned can be called distributed generators and electric energy produced by them can be called distributed generation.

If a generator or a group of generators are similar to both distributed and the traditional generators, and the definitions of distributed or traditional generators can not be applied, such generator or generators can be defined as dispersed generators. Electric energy produced by dispersed generators can be called dispersed generation. A definition of dispersed generators can be applied for generator or generators with the following features:

1. Small scale generator or generators connected to the transmission system (for example: wind farms, hydro power plants, etc.)
2. Generator or generators remote from the load more than one voltage step.
3. Generator or generators connected to the distribution network with power greater than double in comparison with a load (it can be all types of renewable energy power plants).
4. Large amount of small scale generators in the quite large area.

6. Conclusions

1. Generator or generators type, status in electric power system, centrally planned or not centrally planned, can not be a reason for distributed generators definition identification.
2. Generator or generators total power can be only secondary reason for distributed generators definition identification.
3. Location of connection and load of a generator or a group of generators are the main criteria in identification of distributed generators definition.
4. Distributed generator or generators are electric energy sources connected to the distributed network to the same voltage step or not further than one voltage step as loads, operating in normal conditions, power is not higher than double as the one of load and have a possibility to be connected to the system and partially or completely cover load demand. Other factors are not important for the identification of distributed generators definition.
5. If a generator or a group of generators are similar to both distributed and the traditional generators, and the definitions of distributed or traditional generators can not be applied, such generator or generators can be defined as dispersed generators. Electric energy produced by dispersed generators can be called dispersed generation.

7. References

1. CIGRE, Working Group 37.23. Impact of Increasing Contribution of Dispersed Generation on the Power System, 1999.
2. Vaclovas Miškinis, Egidijus Norvaiša. Paskirstytoji elektros energijos gamyba Europoje ir Lietuvoje. ENERGETIKA. 2007. T. 53. Nr. 4. P. 1–8.
3. Distributed generation in liberalized electricity market, IEA Publications, 2002.
4. ENIRDGnet, D2, Concepts and Opportunities of DG, WPI - concepts and opportunities of DG: the driving european forces and trends.
5. A.A. Bayod Rujula, J. Mur Amada, J.L. Bernal-Agustin, J.M. Yusta Loyo, J.A. Dominguez Navarro. Definitions for Distributed Generation: A revision. International Conference on Renewable Energies and Power Quality. 2005.
6. Ackermann T., Andersson G., Soder L. Distributed generation: a definition // Electric Power Systems Research. 2001. Vol. 57(3). P. 195–204.

NEW ACCURATE FAULT LOCATION METHOD FOR MULTI-TERMINAL POWER LINES

Przemyslaw BALCEREK*, Marek FULCZYK*, Jan IZYKOWSKI**, Eugeniusz ROSOŁOWSKI**,
 Murari Mohan SAHA***

* ABB Corporate Research Center, Krakow, Poland; ** Wroclaw University of Technology, Wroclaw, Poland;
 *** ABB Power Technology Systems, Vasteras, Sweden

Abstract: This paper presents a new method for locating faults on multi-terminal power lines, based on three-phase current from all (n) terminals and additionally three-phase voltage from the terminal at which a fault locator is installed utilization. The fault location algorithm consists of (2n-3) subroutines designated for locating faults within particular line sections and a procedure for indicating the faulted line section. Testing and evaluation of the algorithm has been performed with fault data obtained from comprehensive ATP-EMTP simulations. Sample results of the evaluation are reported and discussed.

Keywords: ATP-EMTP, current differential relay, fault location, simulation, multi-terminal line.

1. Introduction

Accurate location of faults on overhead power lines for the inspection-repair purpose [1]–[4] is of vital importance for operators and utility staff for expediting service restoration, and thus to reduce outage time, operating costs and customer complaints.

A system and a method for fault location on a multiple-terminal parallel transmission line is known from [1]. In that method a multi-terminal transmission system is equivalented to a three-terminal transmission system, for which differential current amplitudes are calculated in each station. Then, the distance to the fault point is calculated from their relations. A method for fault location using voltage and current phasor measurement in all stations at the ends of a multi-terminal line has been presented in [2]. That method relies on reducing a multi-section transmission line into systems of two-terminal lines assuming that the fault is located in one of these sections and then hypothetical fault locations are calculated for this assumption. Next, calculations of successive hypothetical fault locations are made assuming that the fault is located in further successive sections of the line. One value, which is contained in a

specific interval of expected values and which indicates the actual place of the fault, is selected from the hypothetical locations calculated in this way.

Use of yet another set of the fault locator input signals, which differs from those applied in the cited approaches [1]–[2], is proposed in this paper. Three-phase current acquired synchronously [5] at all line terminals and additionally three-phase voltage from the terminal at which the fault locator (FL – Fig. 1) is installed, are taken as the input signals. Such specific availability of measurements for locating faults has been assumed with the aim of simple adding the fault location function to current differential relays for multi-terminal lines.

After derivation of the fault location algorithm, the results of its evaluation with use of the ATP-EMTP [6] simulation data are delivered and discussed.

2. Fault Location Techniques

Modern microprocessor-based current differential relays exchange the locally measured current phasors over long distances. For this purpose different forms of communication means are utilized.

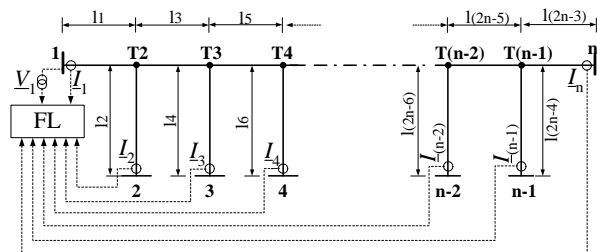


Fig. 1. Fault location on multi-terminal line with the assumed input signals

The current differential protection principle requires synchronization of digital measurements performed at different line terminals. This is accomplished using the well-known Global Positioning System (GPS) or the other techniques [5]. Phasors of three-phase current

from all line terminals: I_1, I_2, \dots, I_n , together with the locally measured three-phase voltage phasor (\underline{V}_1) are taken as the fault locator input signals (Fig. 1). In natural way, these measurements are considered further as synchronized.

The developed fault location algorithm consists of (2n-3) subroutines – designated for locating faults on particular line sections (as depicted in Fig.1) where ‘n’ is the number of terminals. Since the position of a fault is a random factor, the faulted line section is not known in advance. Therefore, the valid subroutine (for the faulted section) will be chosen using a special selection procedure.

2.1. Fault location algorithm – subroutine SUB_A

The subroutine SUB_A, designed for locating faults within the line section L1 (between nodes: 1, T2) (Fig. 2), is based on the following generalized fault loop model [4]:

$$\underline{V}_{1p} - d_1 \underline{Z}_{iL1} \underline{I}_{1p} - R_{iF} \underline{I}_F = 0 \quad (1)$$

where

d_1 unknown distance to fault distance to fault from the beginning of the line to the fault point (p.u.);

R_{iF} unknown fault resistance;

$\underline{V}_{1p}, \underline{I}_{1p}$ fault loop voltage and current;

\underline{Z}_{iL1} positive sequence impedance of the section L1;

\underline{I}_F total fault current (fault path current).

Fault loop voltage and current are composed accordingly to the fault type, as the following weighted sums of the respective symmetrical components of the measured signals:

$$\underline{V}_{1p} = a_1 \underline{V}_{11} + a_2 \underline{V}_{12} + a_0 \underline{V}_{10} \quad (2)$$

$$\underline{I}_{Ap} = a_1 \underline{I}_{11} + a_2 \underline{I}_{12} + a_0 \frac{\underline{Z}_{0L1}}{\underline{Z}_{iL1}} \underline{I}_{10} \quad (3)$$

where

a_1, a_2, a_0 - weighting coefficients (Table I);

$\underline{V}_{11}, \underline{V}_{12}, \underline{V}_{10}$ - symmetrical components (the second lower index) of voltages measured in station 1 (the first lower index);

$\underline{I}_{A1}, \underline{I}_{A2}, \underline{I}_{A0}$ - symmetrical components (the second lower index) of currents measured in station 1 (the first lower index);

$\underline{Z}_{0L1}, \underline{Z}_{iL1}$ - zero, positive sequence impedance of the line section L1.

Fault loop signals (2) and (3), and also those used in the remaining subroutines, are expressed in terms of the respective symmetrical components. Use of such notation is convenient for introducing the compensation for line shunt capacitances, however, it is fully equivalent to the description traditionally used for distance protection [4]. Natural sequence of phases: a, b, c was assumed for determining the weighting

coefficients (Table I), as well as in all further symmetrical components calculations.

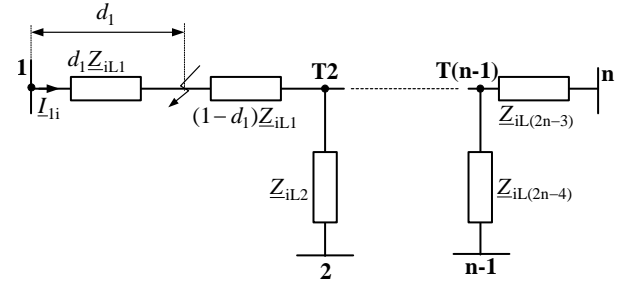


Fig. 2. Equivalent circuit diagram of the network for the i-th symmetrical component assuming that a fault is on the first line section

Table 1. Weighting Coefficients in Fault Loop Signals (2)–(3)

Fault type	a_1	a_2	a_0
a-g	1	1	1
b-g	$-0.5 - j0.5\sqrt{3}$	$0.5 + j0.5\sqrt{3}$	1
c-g	$0.5 + j0.5\sqrt{3}$	$-0.5 - j0.5\sqrt{3}$	1
a-b, a-b-g a-b-c, a-b-c-g	$1.5 + j0.5\sqrt{3}$	$1.5 - j0.5\sqrt{3}$	0
b-c, b-c-g	$-j\sqrt{3}$	$j\sqrt{3}$	0
c-a, c-a-g	$-1.5 + j0.5\sqrt{3}$	$-1.5 - j0.5\sqrt{3}$	0

It is proposed to calculate the total fault current from (1) by using the following generalized fault model:

$$\underline{I}_F = a_{F1} \underline{I}_{F1} + a_{F2} \underline{I}_{F2} + a_{F0} \underline{I}_{F0} \quad (4)$$

where

a_{F1}, a_{F2}, a_{F0} share coefficients (Table2).

The i-th sequence component of the total fault current is determined as a sum of the i-th sequence components of currents from all line terminals (1, 2, ..., n-1, n):

$$\underline{I}_{Fi} = \underline{I}_{1i} + \underline{I}_{2i} + \underline{I}_{3i} + \dots + \underline{I}_{(n-1)i} + \underline{I}_{ni} \quad (5)$$

where subscript ‘i’ denotes the component type: i=1–positive, i=2–negative, i=0–zero sequence.

From the analysis of the boundary conditions of faults [4] results that it is possible to apply different alternative sets of the coefficients, which are used in (4). In order to assure high accuracy of fault location, use of the particular set has been recommended. The following priority for usage of particular sequence components (the respective coefficient in (4) is not equal to zero) of measured currents is proposed (Table II):

- for phase-to-ground and phase-to-phase faults: use of negative sequence components;
- for phase-to-phase-to-ground faults: use of negative and zero sequence components;
- for three phase symmetrical faults: use of superimposed positive sequence components.

Excluding of the positive sequence components ($a_{F1} = 0$) from the total fault current (4) for all faults, except three-phase balanced faults, is characteristic for the share coefficients from Table II.

In case of three-phase balanced faults, only positive sequence components are contained in the signals

Table 2. Share Coefficients used in Fault Model (4)

Fault type	a_{F1}	a_{F2}	a_{F0}
a-g	0	3	0
b-g	0	$1.5 + j1.5\sqrt{3}$	0
c-g	0	$-1.5 - j1.5\sqrt{3}$	0
a-b	0	$1.5 - j0.5\sqrt{3}$	0
b-c	0	$j\sqrt{3}$	0
c-a	0	$-1.5 - j0.5\sqrt{3}$	0
a-b-g	0	$3 - j\sqrt{3}$	$j\sqrt{3}$
b-c-g	0	$j2\sqrt{3}$	$j\sqrt{3}$
c-a-g	0	$-3 - j\sqrt{3}$	$j\sqrt{3}$
a-b-c a-b-c-g	$1.5 + j0.5\sqrt{3}$	$1.5 - j0.5\sqrt{3}$ *)	0

*) $a_{F2} \neq 0$, however, negative sequence component is not present under three-phase balanced faults.

It is proposed to calculate positive sequence of the total fault current as the following sum of the superimposed (superscript: ‘superimp.’) positive sequence currents from the line ends 1, 2, ..., (n-1), n, respectively:

$$\underline{I}_{F1} = \underline{I}_{11}^{\text{superimp.}} + \underline{I}_{21}^{\text{superimp.}} + \dots + \underline{I}_{n1}^{\text{superimp.}} \quad (6)$$

Finally, negative-, zero- and superimposed positive-sequence components of the measured currents are used in calculation of the total fault current (4). This assures accurate calculation of the fault current flowing through the fault path resistance. This is so, since the positive sequence components, for which the shunt capacitance effect is the most distinct, are excluded.

After resolving (1) into the real and imaginary parts, and eliminating the unknown fault resistance (R_{1F}), the sought fault distance (d_1) is determined as:

$$d_1 = \frac{\text{real}(\underline{V}_{1p})\text{imag}(\underline{I}_F) - \text{imag}(\underline{V}_{1p})\text{real}(\underline{I}_F)}{\text{real}(\underline{Z}_{iL1}\underline{I}_{1p})\text{imag}(\underline{I}_F) - \text{imag}(\underline{Z}_{iL1}\underline{I}_{1p})\text{real}(\underline{I}_F)} \quad (7)$$

Having the fault distance calculated (7), the fault resistance R_{1F} can be also determined, as for example from the real part of (1) as:

$$R_{1F} = \frac{\text{real}(\underline{V}_{1p}) - d_1\text{real}(\underline{Z}_{iL1}\underline{I}_{1p})}{\text{real}(\underline{I}_F)} \quad (8)$$

2.2. Fault location algorithm – subroutine for locating faults on the end section of multi-terminal line

An analytic transfer of three-phase measurements: \underline{V}_1 , \underline{I}_1 , $\underline{I}_2, \dots, \underline{I}_{(n-1)}$, \underline{I}_n to the beginning of the section L2 is performed. The superscript ‘transf.’ is used to distinguish the analytically transferred signals from the measured signals. Certainly, such transfer has to be performed separately for each of the i th type of symmetrical component of three-phase voltage and current. Fig. 3 presents an equivalent circuit diagram of

the line for the i -th symmetrical component, assuming that the fault is located in the final section of a multi-terminal power line. Again, the subscript ‘ i ’ is used for denoting the respective: $i=1$ –positive, $i=2$ –negative and $i=0$ –zero sequence, components.

Transferring of voltage from the bus 1 to the tap point T2:

$$\underline{V}_{T2i}^{\text{transf.}} = \underline{V}_{1i} - \underline{Z}_{iL1} \cdot \underline{I}_{1i} \quad (9)$$

where

\underline{Z}_{iL1} impedance of section L1 respectively for the positive, negative and the zero sequence component.

Next, the voltages for symmetrical components: $\underline{V}_{T(n-1)1}^{\text{transf.}}$, $\underline{V}_{T(n-1)2}^{\text{transf.}}$, $\underline{V}_{T(n-1)0}^{\text{transf.}}$ in the end tap point T(n-1) are calculated:

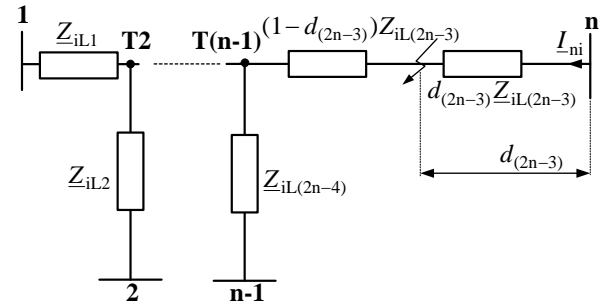


Fig. 3. Equivalent circuit diagram of a network for symmetrical components, under a fault on the end section of a multi-terminal line

$$\underline{V}_{T(n-1)i}^{\text{transf.}} = \underline{V}_{T(n-2)i}^{\text{transf.}} - \underline{Z}_{iL(2n-5)} \cdot \sum_{j=1}^{n-2} \underline{I}_{ji}, \quad (10)$$

$i=1,2,3$

where:

$\underline{Z}_{iL(2n-3)}$ impedance of line section L(2n-3) for the positive, negative, zero sequence components, respectively.

In turn, voltages at the k^{th} tap point $\underline{V}_{Tk1}^{\text{transf.}}$, $\underline{V}_{Tk2}^{\text{transf.}}$, $\underline{V}_{Tk0}^{\text{transf.}}$ are determined from the following formula:

$$\underline{V}_{Tki}^{\text{transf.}} = \underline{V}_{T(k-1)i}^{\text{transf.}} - \underline{Z}_{iL(2k-3)} \cdot \sum_{j=1}^{k-1} \underline{I}_{ji} \quad (11)$$

$i=1,2,3$

where:

$\underline{V}_{T(k-1)i}^{\text{transf.}}$ - calculated voltage at point (k-1),

$\underline{Z}_{iL(2k-3)}$ - impedance of line section L(2k-3) for the symmetrical components.

The values of current $\underline{I}_{T(n-1)n1}^{\text{transf.}}$, $\underline{I}_{T(n-1)n2}^{\text{transf.}}$, $\underline{I}_{T(n-1)n0}^{\text{transf.}}$, flowing from tap point T(n-1) to station ‘n’ in line section L(2n-3) are calculated, as follows:

$$\underline{I}_{T(n-1)ni}^{\text{transf.}} = \sum_{j=1}^{n-1} \underline{I}_{ji}, \quad (12)$$

$i=1,2,0$

The fault loop equation for faults on last line section has the following form:

$$\underline{V}_{T(n-1)np} - (1 - d_{(2n-3)})\underline{Z}_{iL(2n-3)}\underline{I}_{T(n-1)np} - R_{(2n-3)F}\underline{I}_F = 0 \quad (13)$$

where

$$\underline{V}_{T(n-1)np} = \underline{a}_1 \underline{V}_{T(n-1)1}^{transf.} + \underline{a}_2 \underline{V}_{T(n-1)2}^{transf.} + \underline{a}_0 \underline{V}_{T(n-1)0}^{transf.} \quad (14)$$

$$\underline{I}_{T(n-1)np} = \underline{a}_1 \underline{I}_{T(n-1)n1}^{transf.} + \underline{a}_2 \underline{I}_{T(n-1)n2}^{transf.} + \underline{a}_0 \frac{\underline{Z}_{0L(2n-3)}}{\underline{Z}_{1L(2n-3)}} \underline{I}_{T(n-1)n0}^{transf.} \quad (15)$$

where

$\underline{Z}_{1L(2n-3)}$ impedance of section L(2n-3) for the positive seq.,

$\underline{Z}_{0L(2n-3)}$ impedance of section L(2n-3) for the zero seq.

Writing (13) separately for the real / imaginary parts and after performing further mathematical transformations, the solutions for the searched fault distance $d_{(2n-3)}$ and fault resistance $R_{(2n-3)F}$ are obtained.

2.3. Fault location algorithm – subroutine for locating faults on tapped line section of multi-terminal line

Voltages for symmetrical components $\underline{V}_{Tk1}^{transf.}$, $\underline{V}_{Tk2}^{transf.}$, $\underline{V}_{Tk0}^{transf.}$ at the k^{th} tap point Tk (Fig.4) are calculated from the formula (11), by assuming for ‘k’ the number of the considered station, which is equal to the number of the tap point Tk, from which the faulted line goes to the station ‘k’.

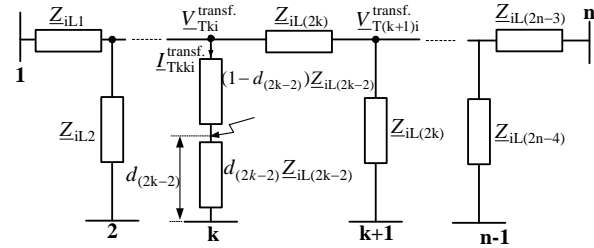


Fig. 4. Equivalent circuit diagram of a network for symmetrical components, assuming that the fault is located on a section of a tapped line

Then, the values of current $\underline{I}_{Tkk1}^{transf.}$, $\underline{I}_{Tkk2}^{transf.}$, $\underline{I}_{Tkk0}^{transf.}$ flowing from tap point Tk to k^{th} station in the tapped line section, labeled as L(2k-2), are calculated:

$$\underline{I}_{Tkk1}^{transf.} = \sum_{j=1, j \neq k}^n \underline{I}_{ji}^{transf.} \quad (16)$$

The fault loop equation takes the form:

$$\underline{V}_{Tkkp} - (1-d_{(2k-2)})\underline{Z}_{1L(2k-2)}\underline{I}_{Tkkp} - R_{(2k-2)F}\underline{I}_F = 0 \quad (17)$$

where:

$$\underline{V}_{Tkkp} = \underline{a}_1 \underline{V}_{Tkk1}^{transf.} + \underline{a}_2 \underline{V}_{Tkk2}^{transf.} + \underline{a}_0 \underline{V}_{Tkk0}^{transf.} \quad (18)$$

$$\underline{I}_{Tkkp} = \underline{a}_1 \underline{I}_{Tkk1}^{transf.} + \underline{a}_2 \underline{I}_{Tkk2}^{transf.} + \underline{a}_0 \frac{\underline{Z}_{0L(2k-2)}}{\underline{Z}_{1L(2k-2)}} \underline{I}_{Tkk0}^{transf.} \quad (19)$$

$\underline{Z}_{1L(2k-2)}$ impedance of line section L(2k-2) for the positive sequence component,

$\underline{Z}_{0L(2k-2)}$ - impedance of line section L(2k-2) for the zero sequence component.

After substituting (18)–(19) into (17) and the respective mathematical manipulations one obtains the searched distance to fault $d_{(2k-2)}$ and fault resistance $R_{(2k-2)F}$.

2.4. Fault location algorithm – for locating faults between two tap points

Symmetrical components of currents $\underline{I}_{T(k+1)1}^{transf.}$, $\underline{I}_{T(k+1)2}^{transf.}$, $\underline{I}_{T(k+1)0}^{transf.}$ flowing from the tap point Tk towards the tap point T(k+1) in the respective line section (Fig.5) are calculated:

$$\underline{I}_{T(k+1)i}^{transf.} = \sum_{j=1}^{k-1} \underline{I}_{ji}^{transf.}, \quad (20)$$

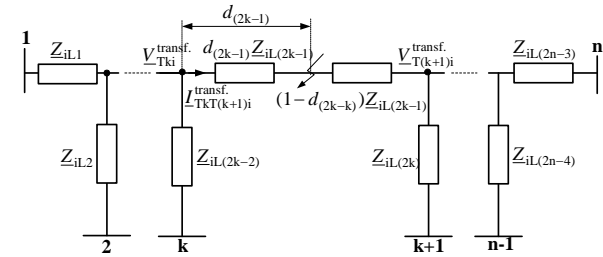


Fig. 5. Equivalent circuit diagram of network for symmetrical components, assuming that the fault is located between two tap points

Fault loop equation has the following form:

$$\underline{V}_{T(k+1)p} - (1-d_{(2k-1)})\underline{Z}_{1L(2k-1)}\underline{I}_{T(k+1)p} - R_{(2k-1)F}\underline{I}_F = 0 \quad (21)$$

where

$$\underline{V}_{T(k+1)p} = \underline{a}_1 \underline{V}_{Tk1}^{transf.} + \underline{a}_2 \underline{V}_{Tk2}^{transf.} + \underline{a}_0 \underline{V}_{Tk0}^{transf.} \quad (22)$$

$$\underline{I}_{T(k+1)p} = \underline{a}_1 \underline{I}_{T(k+1)1}^{transf.} + \underline{a}_2 \underline{I}_{T(k+1)2}^{transf.} + \underline{a}_0 \frac{\underline{Z}_{0L(k+1)}}{\underline{Z}_{1L(k+1)}} \underline{I}_{T(k+1)0}^{transf.} \quad (23)$$

$\underline{Z}_{1L(2k-1)}$ impedance of line section L(2k-1) for the positive sequence component,

$\underline{Z}_{0L(2k-1)}$ impedance of line section L(2k-1) for the zero sequence component,

k number of the tap point.

After substituting (22)–(23) into (21) and the respective mathematical manipulations one obtains the searched distance to fault $d_{(2k-1)}$ and fault resistance $R_{(2k-1)F}$.

3. Selection of valid results

The presented fault location algorithm consists of (2n-3) subroutines and only one of them – the valid subroutine, yields the results, which corresponds to the actual fault. The remaining subroutines give false results.

In the first step of the selection, the subroutine, which yields the distance to fault indicating the considered fault as occurring outside the section range (outside the range: 0 to 1.0 p.u.), or/and the calculated fault resistance of negative value, is surely rejected.

If the first step is not sufficient, then the remote source impedances (behind the terminals 2, 3, ..., (n-1), n in

Fig. 1), are calculated for the respective subroutines. For example, in case of considering the subroutine for locating faults on the end section (Fig. 3, Section IIB), the source impedance behind the bus n for the positive (negative) sequence is calculated as:

$$\underline{Z}_{2Sn} = -\frac{V_{-n2}}{I_{-n2}} \quad (24)$$

where:

$$\begin{aligned} \underline{V}_{-n2} = & V_{T(n-1)2}^{transf.} - (1 - d_{(2n-3)}) \cdot \underline{Z}_{2L(2n-3)} \cdot I_{T(n-1)n2}^{transf.} \\ & - d_{(2n-3)} \cdot \underline{Z}_{2L(2n-3)} \cdot (I_{T(n-1)n2}^{transf.} - I_{F2}) \end{aligned} \quad (25)$$

Note, in case of three-phase balanced faults the negative sequence quantities involved in (24)–(25) have to be changed into the incremental positive sequence quantities.

If the source impedance, calculated according to the considered subroutine, lays outside the Ist quadrant of the impedance plane, then this subroutine is false and has to be rejected. Otherwise, if there are still at least two subroutines remain, then the selection has to be continued. The particular subroutine can be rejected also if the calculated value of the remote source differs from the actual impedance. For this purpose certain knowledge about impedances of the actual equivalent sources behind the line terminals has to be possessed. In particular, such impedance can be calculated using pre-fault measurements, if there is no generation source at the line terminal.

4. ATP-EMTP evaluation

ATP-EMTP simulation program [6] was applied to evaluate performance of the developed fault location algorithm. Different multi-terminal networks were modeled for generation of fault data used in evaluation of the presented fault location algorithm.

In particular, the 130 kV four terminal network (Fig.1: $n=4$) including the line sections: 1–T2 (15.5km), 2–T2 (22.5km), 3–T3 (2.77km), 4–T3 (12.9km), T2–T3 (4.81km). The positive and zero sequence impedances for all sections: $\underline{Z}'_{IL} = (0.0276 + j0.3151)$,

$$\underline{Z}'_{0L} = (0.275 + j1.0265) \Omega/\text{km}.$$

Equivalent sources behind the terminals 1, 3 were modeled with EMFs and the impedances:

$$\underline{Z}_{1S1} = \underline{Z}_{1S3} = (0.7 + j10.5) \Omega, \quad \underline{Z}_{0S1} = \underline{Z}_{0S3} = (1.0 + j15) \Omega.$$

The EMF at the terminal 3 was delayed by: -30° with respect to the terminal 1. The loads at the terminal 2:

$$\underline{Z}_{1S2}^{actual} = 200 \Omega \text{ and at the terminal 4: } \underline{Z}_{1S4}^{actual} = 400 \Omega,$$

were also included. Current and voltage transformers were modeled as well.

Analogue anti-aliasing filters with the cut-off frequency of 350 Hz were included, and 1 kHz sampling frequency was used. Full-cycle Fourier orthogonal filters were applied for determining phasors of the processed signals Fig. 6 and Fig. 7 present the example of fault location on the four-terminal line: a–g fault at the section T2–2, fault distance: $d_2=0.7$ p.u., fault resistance: $R_{F2}=10 \Omega$.

Fig. 6 presents the wave-shapes of the fault locator input signals, while Fig. 7 the results for the subroutines SUB_2 and SUB_4, which indicate the fault as within their sections. The results of the remaining three subroutines are not visualized since yield the distance to fault exceeding the section range, and thus have to be rejected.

There is for selecting between the subroutine: SUB_2 (the results: $d_2=0.7035$ p.u., $R_{F2}=9.83 \Omega$) and SUB_4 (the results: $d_4=0.7006$ p.u., $R_{F4}=10.41 \Omega$). Both, distance to fault and fault resistance according to these two subroutines are not to be rejected. Calculating the source impedances behind buses: 2, 4 one obtains:

$$\text{SUB_2: } \underline{Z}_{1S2}^{SUB_2} = (198.2 + j0.26) \Omega, \text{ while } \underline{Z}_{1S2}^{actual} = 200 \Omega,$$

$$\text{SUB_4: } \underline{Z}_{1S4}^{SUB_4} = (576.6 - j3.41) \Omega, \text{ while } \underline{Z}_{1S4}^{actual} = 400 \Omega.$$

Therefore, the subroutine SUB_2 yielding the impedance more close to the actual one is selected correctly as the valid one, which gives the fault location, with acceptable 0.35% error. For the majority of the other considered fault cases the fault location error was kept below 1%. However, in case of faults on the shortest line section (T3–3) the maximum error slightly exceeded 2%, which for such short segment could be also treated as acceptable. For this selection knowledge of the actual effective load impedances is required. In field applications it will be done based on the experience of fault locator user, which is familiar with the level of effective load impedances at particular buses. In this case they were calculated by performing an analysis of pre-fault load flow.

5. Conclusion

In this work, the new algorithm designed for locating faults on a multi-terminal line has been presented. The specific set of the fault locator input signals: three-phase current from all line terminals and additionally the locally measured three-phase voltage, has been assumed. This fault location algorithm is intended for application with current differential relays protecting a three-terminal line.

The developed fault location algorithm consists of the subroutines, designated for locating faults within the respective line sections. The subroutines are formulated with use of generalized fault loop and fault models. Multi-criteria selection procedure is applied for selecting the valid subroutine, i.e. for indicating the faulted line section.

The simulation results show that the accuracy of fault location is acceptable under various fault types, fault resistances, fault locations, pre-fault loading conditions and source impedances. The evaluation also proves that the developed multi-criteria selection procedure allows reliable indication of the valid subroutine, i.e. indication of the faulted line section.

For the presented sample fault on the four-terminal line there are two subroutines (out of five subroutines), which indicate this fault as within their line sections. Indication of the faulted section is performed by

comparing the estimated impedances behind the respective line terminals with the impedances

determined from the pre-fault measurement.

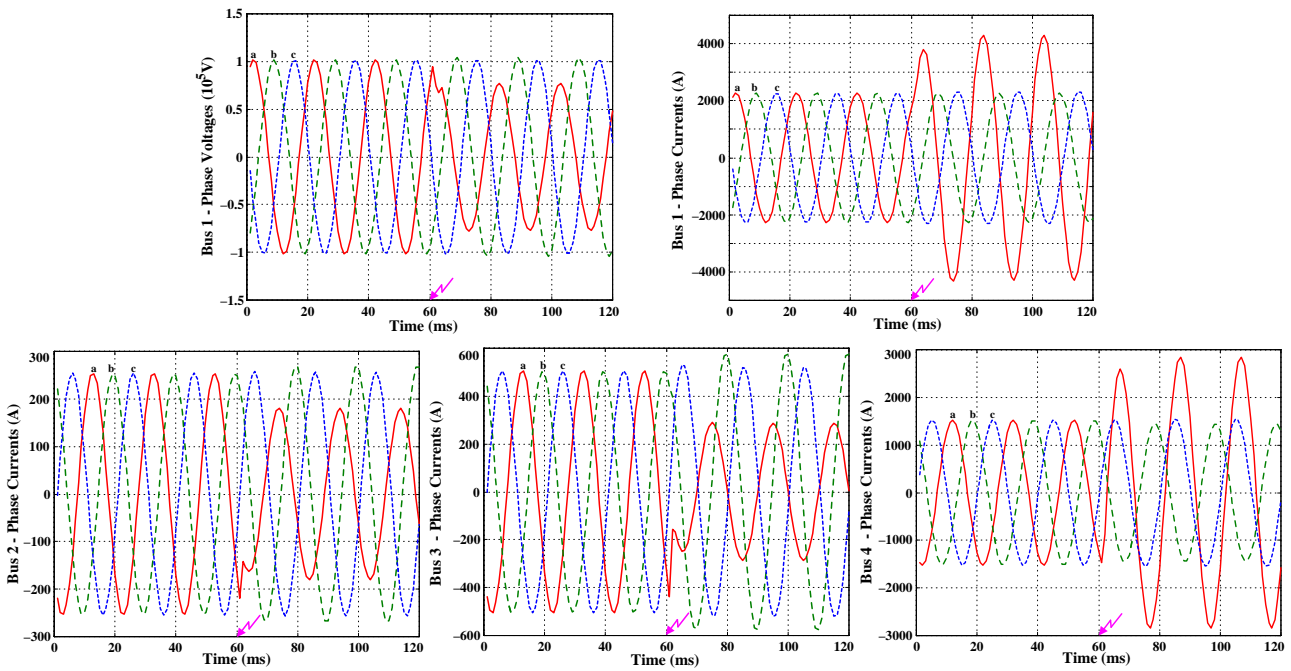


Fig. 6. Fault location on four-terminal network – the example: input signals of the fault locator.

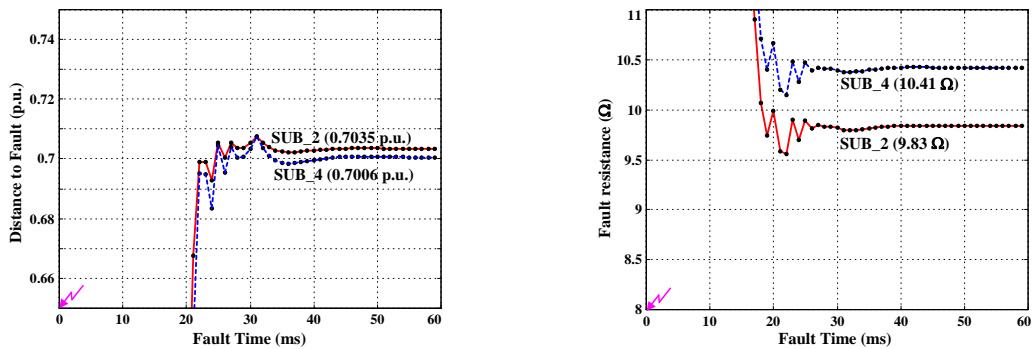


Fig. 7. Fault location on four-terminal network – the example: results of the subroutines SUB_2 (valid), SUB_4 (invalid).

6. References

1. Kenji Murata, Kazuo Sonohara, Susumo Ito, Kyoji Ishizu and Tokuo Emura, "Fault location method for a parallel two-circuit transmission line with n terminals", *US patent 5, 485,394*, Jan. 16, 1996.
2. Kai-Ping Lien, Chih-Wen Liu, Joe-Air, Ching-Shan Chen and Chi-Shan, "Novel Fault Location Algorithm for Multi-Terminal Lines Using Phasor Measurement Units" in *Proc. Thirty-Seventh Annual North American Power Symposium in Ames, Iowa, USA, October 23-25, 2005*.
3. IEEE Std C37.114: "IEEE Guide for Determining Fault Location on AC Transmission and Distribution Lines", *IEEE Power Engineering Society Publ.*, pp. 1-42, 8 June 2005.
4. J. Izykowski, E. Rosolowski and M.M. Saha, "Locating faults in parallel transmission lines under availability of complete measurements at one end", *IEE Gener., Transm. and Distrib.*, Vol. 151, No. 2, pp. 268-273, March 2004.
5. IEEE Std. C37.118: "IEEE Standard for Synchrophasors for Power Systems", *IEEE Power Engineering Society Publ.*, pp. 1-65, 22 March 2006.
6. H. W. Dommel, *Electro-Magnetic Transients Program*, BPA, Portland, Oregon, 1986.

TRANSIENT ANALYSIS OF VARIABLE SPEED WIND TURBINE

*Djilali KAIROUS, *Bachir BELMADANI, **Mostapha BENGHANEM

*Faculty of Science and Sciences Engineering, UHB, Chlef, Algeria, **Dpt. of Electrotechnics, UST, Oran, Algeria

Abstract: Large wind turbines are often equipped with Doubly Fed Induction Generator - DFIG.

Today the penetration level of wind power on the network is high. The power system stability defined as the ability of the system, for given initial operation condition, to regain a normal state of equilibrium after being subjected to a disturbance is the major problem.

In numerous papers the stability problems are pointed out and there are also many papers describing control strategies for wind turbine equipped with DFIG.

In this paper we study dynamic behavior of the DFIG during voltage sag. Also we study the ability of the control to improve the stability of the system.

Keywords: DFIG, stability, voltage sag, sliding mode control.

1. Introduction

Wind energy is one of the most important and promising sources of renewable energy due to its clean character and free availability. Many variable speed winds turbines have been used with induction generator, permanent magnet and eventually switched reluctance generators. Nowadays the market is oriented on the design of high power wind generation systems based on multi-pole synchronous machine or doubly fed induction generators (DFIG). The wind energy market (production) at present represents only a fraction of its potential 47.616.4 installed megawatts at the end of 2004. 80% of this is just located in four countries-Spain, Germany, United States and Denmark.

Power system stability has been recognized as an important problem for secure system operation [1]. The pining of the market of electricity obligates us to make production of the generators near their physical limits, for economic reason. It is thus necessary to evaluate these limits, in particular the risk of instability of network voltage.

This instability is often started by:

- Voltage recovery as fast as possible after clearance the grid faults and without wind turbine disconnection.
- Grid synchronisation for reconnection as fast as possible in order to feed maximum possible active power to the grid.

- Reactive power control by the excitation system to keep constant voltage.

- Reduce the mechanical torque by pitch angle control to avoid rotor acceleration.

Now doubly fed induction generator is well known. The advantage of the DFIG is that the rotor converter needs thus only to be rated for a fraction 25% (slip power) of the total output power. By controlling the bidirectional power flow in the rotor, the DFIG can operate as a motor or a generator, at sub and super synchronous speeds. The reactive power compensation can be supplied from both the supply side and the rotor side, and thus has potential to provide voltage support.

Different control strategies for such kind of generator have been proposed for active and reactive power control or voltage and frequency control. Direct field oriented control for active and reactive powers is presented in [2], [3].

In the proposed paper we present the control of the Active and reactive Powers by sliding mode. The system has the ability for simultaneous maximum wind power generation for large speed range of operation and achieves soft and fast synchronization to the grid. Power converters and associated control strategies are simulated using Simulink.

Some simulation results are presented to validate the theoretical analysis and to show the behaviour and performances of the proposed structure for power control.

2. Description of the studied system

The basic configuration of the whole system is presented in Fig. 1. The rotor of DFIG is connected to the grid through two back to back bridge converters. The grid side converter (GSC) is used to control the DC-link voltage and to keep it constant regardless to the magnitude and direction of the rotor power.

The DFIG is controlled by the rotor side in order to generate the optimal active power depending on the wind speed and turbine characteristics.

$$\begin{cases} V_{dqs} = R_s I_{dqs} + \frac{d\Phi_{dqs}}{dt} \mp \omega_s \cdot \Phi_{qds} \\ V_{dqr} = R_s I_{dqr} + \frac{d\Phi_{dqr}}{dt} \mp \omega_r \cdot \Phi_{qdr} \end{cases} \quad (6)$$

$$\begin{cases} \Phi_{dqs} = L_s I_{dqs} + M I_{dqr} \\ \Phi_{dqr} = L_s I_{dqr} + M I_{dqs} \end{cases} \quad (7)$$

By neglecting the stator resistance of the stator we can write:

$$\begin{cases} V_{ds} = 0 \\ V_{qs} \approx \omega_s \Phi_{ds} \end{cases} \quad (8)$$

$$\begin{cases} \Phi_{dr} = L_r \sigma I_{dr} + \frac{M}{L_s \omega_s} V_{qs} \\ \Phi_{qr} = L_r \sigma I_{qr} + \frac{M}{L_s \omega_s} V_{ds} \end{cases} \quad (9)$$

The general model of the machine is given by the following equations:

$$\begin{bmatrix} V_{ds} \\ V_{qs} \\ V_{dr} \\ V_{qr} \end{bmatrix} = \begin{bmatrix} R_s \Phi_{ds} - R_s c \left(L_r \sigma I_{dr} + \frac{M}{L_s \omega_s} V_{qs} \right) - \omega_s \Phi_{qs} + \frac{d\Phi_{ds}}{dt} \\ R_s \Phi_{qs} - R_s c \left(L_r \sigma I_{qr} + \frac{M}{L_s \omega_s} V_{ds} \right) + \omega_s \Phi_{ds} + \frac{d\Phi_{qs}}{dt} \\ R_b \left(L_r \sigma I_{dr} + \frac{M}{L_s \omega_s} V_{qs} \right) - R_r \Phi_{ds} - \omega_r \left(L_r \sigma I_{qr} + \frac{M}{L_s \omega_s} V_{ds} \right) + L_r \sigma \frac{dI_{dr}}{dt} \\ R_b \left(L_r \sigma I_{qr} + \frac{M}{L_s \omega_s} V_{ds} \right) - R_r \Phi_{qs} + \omega_r \left(L_r \sigma I_{dr} + \frac{M}{L_s \omega_s} V_{qs} \right) + L_r \sigma \frac{dI_{qr}}{dt} \end{bmatrix} \quad (10)$$

With: $a = \frac{1}{\sigma L_s}$, $b = \frac{1}{\sigma L_r}$, $c = \frac{M}{\sigma L_s L_r}$

The state model is put in the following form:

$$\dot{X} = f(x,t) + g(x,t) U_{dq} \quad (11)$$

$$U_{dq} = \begin{bmatrix} V_{ds} & V_{qs} & V_{dr} & V_{qr} \end{bmatrix} \quad (12)$$

$$g(x,t) = \begin{bmatrix} 1 & 0 & 0 & 0 \\ 0 & 1 & 0 & 0 \\ 0 & 0 & \frac{1}{\sigma L_r} & 0 \\ 0 & 0 & 0 & \frac{1}{\sigma L_r} \end{bmatrix} \quad \text{(III.31)} \quad (13)$$

$$f(x,t) = \begin{bmatrix} -R_s \Phi_{ds} + R_s c \left(L_r \sigma I_{dr} + \frac{M}{L_s \omega_s} V_{qs} \right) + \omega_s \Phi_{qs} \\ -R_s \Phi_{qs} + R_s c \left(L_r \sigma I_{qr} + \frac{M}{L_s \omega_s} V_{ds} \right) - \omega_s \Phi_{ds} \\ \frac{1}{\sigma L_r} \left(-R_b \left(L_r \sigma I_{dr} + \frac{M}{L_s \omega_s} V_{qs} \right) + R_r \Phi_{ds} + \omega_r \left(L_r \sigma I_{qr} + \frac{M}{L_s \omega_s} V_{ds} \right) \right) \\ \frac{1}{\sigma L_r} \left(-R_b \left(L_r \sigma I_{qr} + \frac{M}{L_s \omega_s} V_{ds} \right) + R_r \Phi_{qs} - \omega_r \left(L_r \sigma I_{dr} + \frac{M}{L_s \omega_s} V_{qs} \right) \right) \end{bmatrix} \quad (14)$$

The slip surfaces in the Park reference are defined to control the rotor currents.

They are given by the following equations [5]:

$$\begin{cases} \sigma_d = \lambda (I_{drref} - I_{dr}) \\ \sigma_q = \lambda (I_{qrref} - I_{qr}) \end{cases} \quad (15)$$

Where V_{dr} and V_{qr} are the two control vectors of, they force the trajectory of the system to converge towards surfaces $\sigma_{dq} = 0$.

The vector of Udqeq control is obtained by imposing $\sigma_{dq} = 0$

$$f(x,t) + g(x,t) V_{dq} = 0 \quad (16)$$

$$U_{dq} = \begin{bmatrix} - \left(-R_b \left(L_r \sigma I_{dr} + \frac{M}{L_s \omega_s} V_{qs} \right) + R_r \Phi_{ds} + \omega_r \left(L_r \sigma I_{qr} + \frac{M}{L_s \omega_s} V_{ds} \right) \right) \\ - \left(-R_b \left(L_r \sigma I_{qr} + \frac{M}{L_s \omega_s} V_{ds} \right) + R_r \Phi_{qs} - \omega_r \left(L_r \sigma I_{dr} + \frac{M}{L_s \omega_s} V_{qs} \right) \right) \end{bmatrix} \quad (17)$$

The Fig. 3 presents the global diagram for the DFIG with sliding mode control

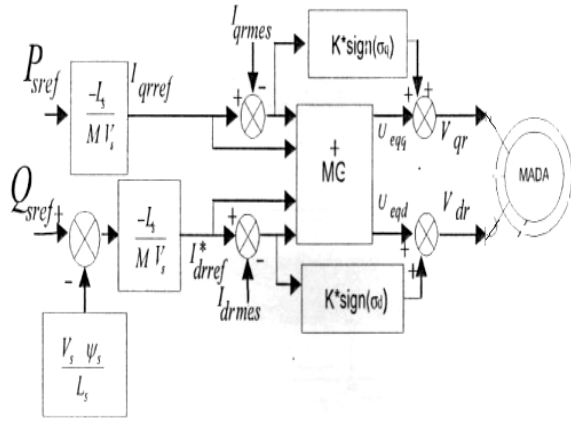


Fig.3. Sliding mode control of the DFIG

6. Simulation results

In this section we present the simulation results of the system presented in Fig.1. (The DFIG with PWM voltage sources converters).

The rotor voltage, the stator voltage, the speed and the powers are keeping at their nominal values. The DFIG used has a nominal power of 20kw.

The model is simulated between $t=0s$ and $t=1.6s$. We make a voltage sag of 50% during 200 ms (Between $t=0.45s$ and $t=0.65s$)

The results in the Fig.4 (figures of the currents, powers and the torque) prove the validity of proposed model, and the good stability of the system.

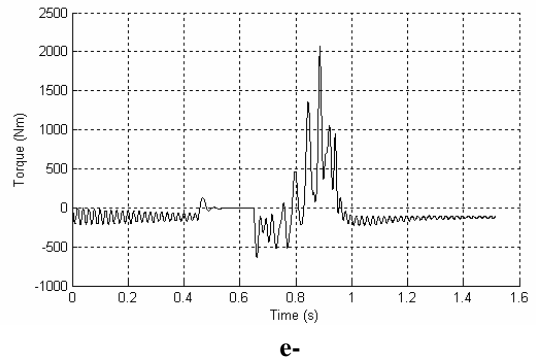
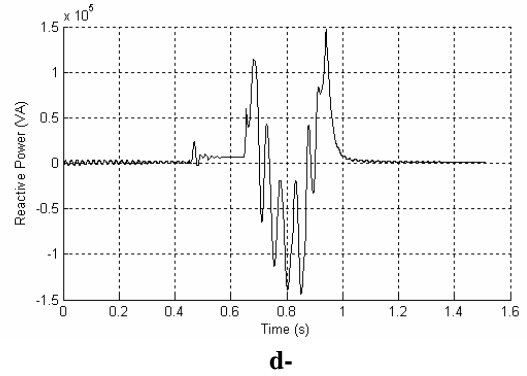
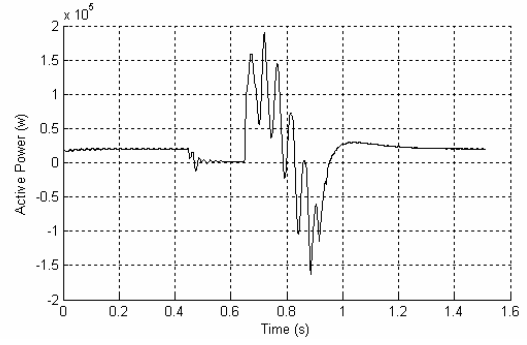
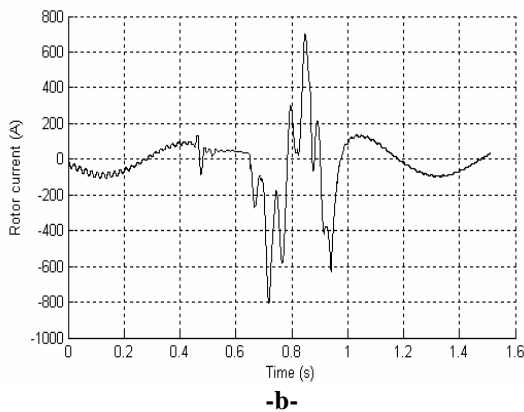
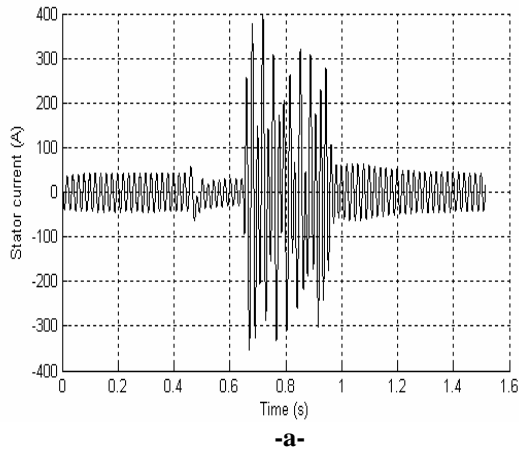


Fig. 4. Dynamic behaviour of the DFIG during Voltage sag of 50 %: a- Stator Current, b- Rotor current, c- Active Power. d- Reactive Power. e- Torque

7. Abbreviations

J, C_{fr} : Inertia and viscous friction

Ω : Mechanical speed

$\Omega_{turbine}$: is the turbine angular frequency

$V_{ds}, V_{qs}, V_{dr}, V_{dr}$ Tow-phase stator and rotor currents voltage

$\Phi_{ds}, \Phi_{qs}, \Phi_{dr}, \Phi_{qr}$: Tow-phase stator and rotor flux

$i_{ds}, i_{qs}, i_{dr}, i_{qr}$ Tow-phase stator and rotor currents

I_{dms}, I_{qms} Tow-phase measured rotor currents

C_r, C_e Prime mover and electromagnetic torque

R_s, R_r : Per phase stator and rotor resistance

M : Magnetising inductance

L_s, L_r : Total cyclic stator and rotor inductances

ω_s, ω_r : Pulsation

g : Generator slip

i_d, i_q : Tow-phase grid side converter currents

v_d, v_q : Tow-phase network voltages

v_{dc}, i_{dc} : Dc-bus voltage and current delivered by the grid side converter

P, Q : Active power delivered by the grid side converter and

i_m, P_m : Current and Active power delivered to the rotor side converter

C : Capacitance of the DC-link

R, L : Resistance and Inductance of the grid

P_s, P_r : Stator active power and rotor active power

Q_s, Q_r : Stator reactive power and rotor reactive power

$v_{ds}, v_{qs}, v_{dr}, v_{qr}$: Tow-phase stator and rotor

8. Conclusion

In this paper a doubly fed induction generator connected to the grid was presented.

The aim of the paper was to develop the decoupled d-q vector control technique of DFIG supply by a back-to-back PWM converter in the rotor side. The control strategy contains two control levels: DFIG control level (control of active and reactive power using sliding mode approach) and the control of the grid side converter.

The mathematical model of the system (DFIG-Converters-Grid) has been implemented in MATLAB & Simulink.

The main goal of the grid side converter control is to keep the dc-link voltage constant by balancing the real power on the machine side and on the grid side converter, and to compensate reactive power of the DFIG to get the unity power factor.

The control system is applied to the rotating reference frame fixed on the gap flux of the generator. It has been proved that this control system can control the active and reactive power independently and stably.

The simulation results show that we can make decoupling between active and reactive power and in the same time have a good stability in a case of voltage sag.

Also, the DC-link voltage was kept constant to the reference value. The torque has the same dynamic like the active power.

9. References

1. P. Kundur, J. Paserba, "Definition and Classification of Power System Stability", IEEE Transaction on Power Systems, Vol. 19, N°2, May 2004.
2. R. Pena, R.C. Clark, G.M. Asher, "Doubly Fed Induction Generator using Back-to-Back PWM Converters and its Application to Variable-Speed Wind-Energy generation", IEE Proc-Elect. Power Appl, Vol. 143, N°5. 380-387. 1996.
3. L. Mihet-popa, I. BOLDEA, "Control Strategies for Large Wind Turbine Application", Journal of Electrical Engineering, Vol. 7, Edition 3rd, ISSN 1582-4594. 2006.
4. P.C. Krause, "Analysis of Electrical Machinery", New York, McGraw-Hill. 1994.
5. B. Toufik, "Commande à Structure Variable et Etude de l'Integration d'Eolienne à base de Machine asynchrone à Double Alimentation sur le Réseau Electrique", PhD thesis (in French), University of NANTES, 2007.

SELECTED HIGH-FREQUENCY POWER SUPPLY SYSTEMS

Elzbieta SZYCHTA, Kamil KIRAGA
 Technical University of Radom, Faculty of Transport, Poland

Abstract: Principle of operation of basic power supply systems of induction heating equipment is presented. Principal inverter systems employed in induction heating, i.e. transistor voltage and current inverters, are discussed and design of E-class resonant inverter is presented.

Keywords: power supply systems, frequency, series inverter, parallel inverter, E-class inverter, MOSFET transistor.

1. Introduction

The frequency range of power supply to induction heating coils is very broad, starting from 16 $\frac{1}{4}$ Hz to as many as several mega Hertz. Therefore, designs and operating principles of power supply systems to such equipment are varied. The equipment supplied with the mains voltage frequency, i.e. 50 Hz, is the primary group of induction equipment. It will not be addressed in this paper, however.

The induction heating equipment of frequency increased to approximately 10 Hz deserves consideration. Originally, this equipment was supplied from such electromagnetic sources as electric mechanical generators or magnetic frequency multipliers. These solutions became obsolete, however, as inverters came into use [3, 7].

High-frequency equipment is supplied by means of transistor inverters including DC intermediary circuit. Employing IGBT transistors, power supplies of up to 50 kHz can be designed, while MOSFETs provide for frequencies of even 500 kHz. When E-class inverters (special transistor circuits) are utilised at low power, induction heating systems can operate at frequencies of up to 1 MHz [7].

Reduced frequency, e.g. 16 $\frac{1}{4}$ Hz, serves to supply power to induction equipment heating charges of very great dimensions, where highly uniform temperature distribution across the charge is required. Cycloinverters are used to supply power to this equipment.

Table 1 summarises the most common sources of power supply to induction heaters.

Table 1. Sources of power supply to induction heaters [6]

Source	Frequency range	Power range efficiency η	Advantages	Disadvantages	Comments
Cycloconvertors	16Hz 25Hz	Several dozen kW hundreds of kW $\eta = 70...80\%$	Simple desing of the power part and control system	Many valves	Rarely used – only to heat billets of greatest diameters, good power source for mixers
Power mains	50(60) Hz	Several dozen kW hundreds of kW MW	Easy access to the power source (mains), high power, easy choice of typical elements	Low frequency, low power density, non-symmetrical mains loading	
Static magnetic frequency multipliers	150Hz 450Hz	Several dozen kW hundreds of kW $\eta = 60...80\%$	Nature of the operation, simple design, low investment, high reliability, simple operation	Constant frequency, large dimensions, heavy weight	Rarely used, good power source for pool furnaces
Electric mechanical generators	960 Hz 2000 Hz 8000 Hz 10000 Hz	Hundreds of kW 2MW $\eta = 60...80\%$	High reliability	High investment, troublesome operation, large dimensions, heavy weight, necessary to build foundations, long start-up, water cooling, noise	The only medium-frequency power source until mid-1970s, superseded by semiconductor static inverters
Semiconductors statistical converters	300 Hz 500 Hz	Several kW Hundreds kW for MW $\eta = 90...95\%$	Completely static power and frequency, high reliability, small overall dimensions and weight, immediately ready to work	Requirements qualified persons for operation, Gentle	Basic sources of power supply to induction heaters
Lamp generators	300 kHz MHz	Tens of kW hundreds kW $\eta = 50...70\%$	Completely static operation, high reliability, immediately ready to work	Low power, constant frequency, lamp life 4000...6000h	The only high-frequency power source, now superseded by semiconductor static converters

A power supply system consists of a rectifier assembly with a smoothing filter, transistor direct voltage regulator, and a system of overvoltage or shorting safety switches. These subassemblies, depending on the inverter type, provide a current or voltage source of regulated capacity.

Both in the case of series and parallel inverters, non-control rectifiers are most commonly utilised, constituting a voltage source together with an appropriate filter. An LC filter in the DC circuit or a filter consisting of alternating voltage chokes and DC circuit capacitor may be employed.

With regard to high-power (over 25 kW) parallel inverters, thyristor control rectifiers including a smoothing choke acting as filter are utilised as well (the control rectifier also acts as a regulator) [7].

Series voltage inverter power supply circuits contain the classic buck voltage regulator. It has a voltage output in the case of series inverter and a current output in the case of parallel inverter.

IGBT transistor, mentioned before, is the most commonly used valve. Due to design considerations, chopper type insulated electric modules are best.

A properly designed transistor snubber enables to increase the switching frequency to several dozen kHz. This provides for reduced dimensions of the capacitor and choke regulator.

Resonant DC/DC buck inverter may be employed as regulator where a inverter must meet the additional condition of low electromagnetic interference (EMI).

2. Transistor voltage inverters

Transistor voltage inverters comprise a series resonant circuit and are powered from voltage sources, where the supplied direct voltage can be regulated. There are two designs of transistor voltage inverter most commonly used to supply power to induction equipment: one including a bridge circuit (Fig.1) and one including a half-bridge circuit and capacitance voltage divider, shown in Fig.2. Both the circuits can be modified by parallel connection of commutation capacitors.

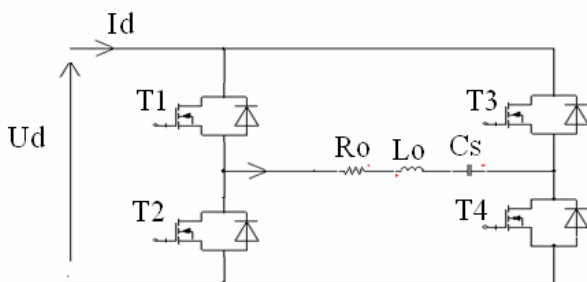


Fig.1. Design of voltage inverter supplying power to induction equipment [4]

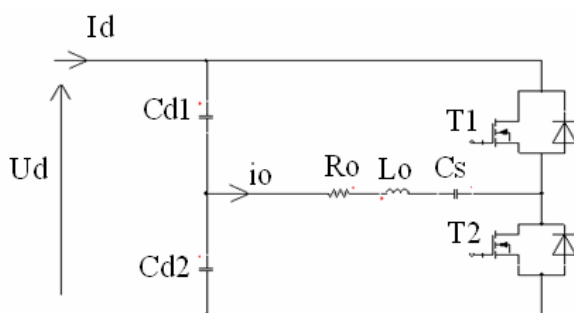


Fig.2. Design of voltage inverter supplying power to induction equipment – half-bridge circuit including a capacitance voltage divider [4]

The inverter in Fig.1 consists of four transistors (T1, T2, T3, T4) connected to form a bridge circuit. In addition, each transistor is shunted by means of a backward diode (in MOSFET inverters, backward diodes are included within the transistor's design). The series resonant circuit comprises: capacitor C_s and an inductor shown

with the aid of a receiver $R_o L_o$. The operating principle of this inverter is shown in Figures 3 a and b.

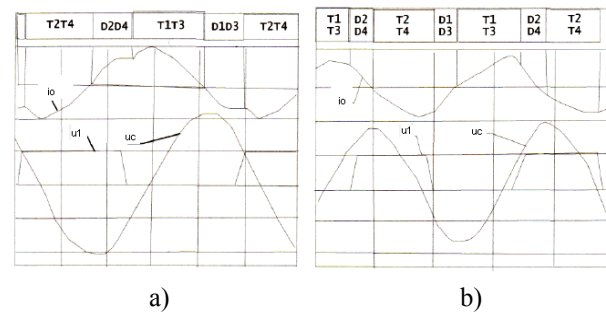


Fig.3. Waveforms of: current across the receiver - i_o , capacitor voltage C_s - u_c , and voltage across the transistor T1 - u_1 :

a) operating range II $0,5f_0 < f < f_0$

b) operating range III $f > f_0$

The inverter may operate in three frequency ranges:

- range one $0 < f < 0,5f_0$

- range two $0,5f_0 < f < f_0$

- range three $f > f_0$

The operating conditions are best at $f = f_0$ between the 2nd and 3rd working range. The load current is close to sinusoidal, the transistors are on and off at zero current. The backward diodes do not conduct the current. In effect, power losses across the semiconductor valves are the lowest [5].

The output power may be controlled using one of the three methods:

a) the amplitude method involves varying the average direct voltage U_d . This method is the most common, yet it requires application of a regular-value source of direct voltage.

b) the frequency method involves varying the frequency f of transistor switching in a range comprising the operation ranges, usually range 2 and 3, where U_d , for instance, remains constant. It is not employed in inverters working at high frequencies since the switching losses rise during resonant tuning.

c) the method of voltage pulse band width regulation at $U_d = const$. It involves an appropriate phase shift of the signals controlling the transistors T1 and T4 in relation to the signals for T2 and T3 at a constant frequency of their turn-on.

3. Transistor current inverters

Transistor current inverters contain a parallel resonant circuit and are supplied from direct voltage sources of a current nature, therefore, the shape of transistor current approximates a rectangle, and the form of the receiver's voltage is approximately sinusoidal.

Figures 4 a and b illustrate principal designs of the parallel current inverter.

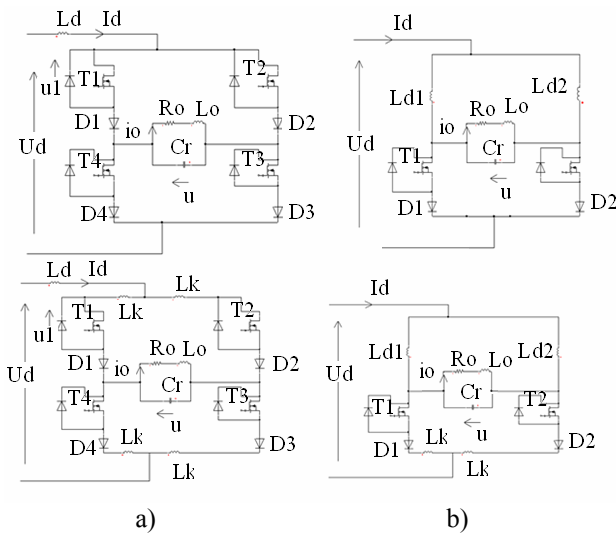


Fig.4. Designs of the parallel current inverter [7]:
a) basic design – a bridge circuit and, below, a bridge circuit including a shunt choke
b) half-bridge circuit including a double current source; below, a half-bridge circuit including a double current source and commutation chokes

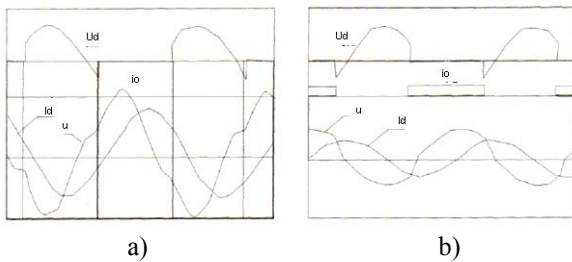


Fig.5. Waveforms of selected magnitudes in the parallel current bridge inverter:

- a) operating range $f < f_0$
- b) operating range $f > f_0$

Similarly to voltage inverters, transistor switching losses are lowest at the resonant frequency $f = f_0$.

It is impossible to decide clearly which of the inverters, voltage or current, is better suited to supply power to induction equipment. A final choice of a inverter depends on the following factors: power rating of the equipment, operating frequency, economics, types of transistors used, and manufacturer's research experience.

4. Single-transistor resonant (E-class) inverters

In E-class inverters, transistor switching losses are reduced to a minimum. This enables high-efficiency operation at very great frequencies of the input voltage (up to 1Mhz). It can be achieved by means of appropriate control techniques, so that the transistor should be switched when its voltages and/or currents are equal or close to zero [5].

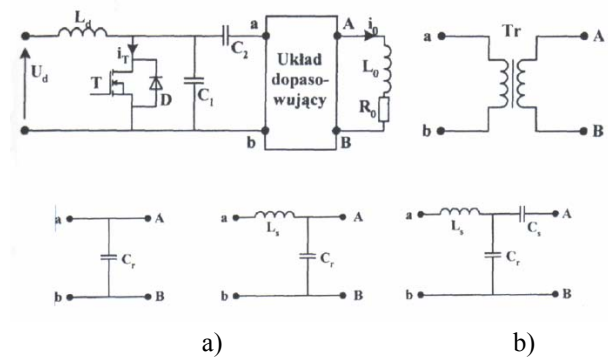


Fig.6. Basic designs of E-class inverter [1]:
a) main circuit of the inverter
b) possible solutions of the systems matching load parameters to the inverter

Single-transistor resonant inverters may implement three types of operations:

- a) optimum operation, where transistor switching is most beneficial: turn-on at zero current and voltage, turn-off at zero voltage and non-zero current[6].
- b) sub-optimum operation, where load resistance decreases, for example. The transistor is turned on and off at zero voltage and non-zero current. Switching power losses are somewhat greater than in the optimum operation.
- c) non-optimum operation, where the transistor is turned on at non-zero voltage and non-zero current and turned off at zero voltage and non-zero current. This operation may occur when parameters of the receiver change. Power losses are greater than in the sub-optimum operation, therefore it can be accepted at a relatively low load current [7].

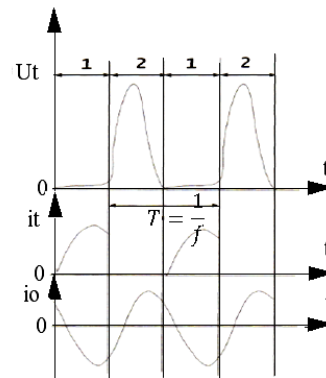


Fig.7. Voltage and current waveforms in the basic inverter circuit (without a matching circuit) during optimum operation
 U_T, i_T : transistor's voltage and current; 1 – the transistor is on, 2 – the transistor is off, $T = 1/f$ - operating interval of the inverter

5. Conclusion

This paper was intended to present methods of supplying power to induction heating systems in the range from medium to very high (MHz) frequencies. In practice, their designs vary. The differences are primarily determined by the intended use and operating conditions of the inverters, and by the type of power

electronic elements (their limitations and capabilities) used to design the inverters. Economics, or savings, are of major importance as well. With regard to inverters, this is related to reducing power losses in the process of transistor turn-on and switching. It is therefore essential to design the inverters in such a way that the power losses could be minimum with increased operating frequency of the transistor switching.

6. References

1. Junak J. Analysing Possible Application of E-Class Inverters Including MOSFET Transistors to High-Frequency Induction Heating.
2. Kempski A., Smoleński R., Strzelecki R. Common Mode Current Paths and their Modeling in PWM Inverter- Fed Drives "PESC 02", p. 1551- 1556.
3. Luft M., Szychta E., Szychta L. Method of designing ZVS boost inverter, Proceedings of the 13th International Power Electronics and Motion Control Conference, 1-3 September 2008, Poznań – Poland, p. 478-482.
4. Rodacki T., Kandyba A. Electrothermal Equipment, Gliwice 2002.
5. Skoczkowski T. Induction Heating, Przegląd Elektrotechniczny LXXII 10/1996.
6. Sajdek C., Samek E. Induction Heating, Wydawnictwo „ŚLĄSK” Katowice 1985.
7. Szychta E. Resonant Inverter Powered by DC Voltage Source, Automation and Control Technologies 2004, Proceedings of the V International Conference, Kaunas 2004, p. 26-30.

IDENTIFICATION OF PARAMETERS OF SYNCHRONOUS GENERATORS' DYNAMIC MODELS

Mindaugas AŽUBALIS*, Vaclovas AŽUBALIS*, Audrius JONAITIS*, Ramunas PONELIS***

*Kaunas University of Technology, Lithuania; **Lietuvos energija AB, Lithuania

Abstract: The identification technique for determination of parameters of synchronous generators' dynamic models for large scale power system stability studies is presented in the paper. The described methods allow to identify parameters according to field test data as well as to the data presented by manufacturers.

Keywords: synchronous generator, dynamic model, identification, power system stability.

1. Introduction

Accuracy of power system stability investigation and reliability of the study results depends on the accuracy of the used dynamic models of generating units. More accurate models ensure more reliable evaluation of maximum permissible capacities of power flows, loadings of separate generating units and possibilities of transient processes control.

Identification of dynamic models for power system stability and transient studies requires large amount of information about the equipment and its characteristics. The lack of data may make uncertainties in evaluation of dynamic models of generating units as well as simulation of operating conditions of power system.

The identification techniques for determination of parameters considering the field test data and data presented by manufacturers or operators are described in this paper.

2. Parameters of synchronous generator model

The producing of synchronous generator dynamic models and the calculation of their parameters need to know the type of generator, and the nominal total power S_N , active power P_N , nominal power factor of $\cos\varphi$, the nominal generator voltages and currents U_N and I_N , the field voltage and current U_{fN} and I_{fN} and the power diagram $Q_G=f(P_G)$.

The main generator dynamic parameters are the inductive reactances of direct-axis and quadrature-axis, time constants of field winding at open circuit (no load)

and short circuit and rotor inertia. The detailed list of parameters used in dynamic model is presented in table 1.

Table 1. Parameters of synchronous generator

<i>Inductive reactances and resistances, in p.u., at rated power and voltage S_N and U_N</i>		
1.	<i>d</i> -axis synchronous inductive reactance	x_d
2.	<i>q</i> -axis synchronous inductive reactance	x_q
3.	<i>d</i> -axis transient inductive reactance	x'_d
4.	<i>q</i> -axis transient inductive reactance *	x'_q
5.	<i>d</i> -axis subtransient inductive reactance	x''_d
6.	<i>q</i> -axis subtransient inductive reactance	x''_q
7.	Leakage reactance	x_ℓ
8.	Stator resistance	r_a
9.	Field circuit resistance **	r_f
<i>Field circuit time constants</i>		
10.	<i>d</i> -axis open circuit transient time constant **	T'_{d0}
11.	<i>q</i> -axis open circuit transient time constant *	T'_{q0}
12.	<i>d</i> -axis open circuit subtransient time constant	T''_{d0}
13.	<i>q</i> -axis open circuit subtransient time constant	T''_{q0}
<i>Total inertia of generator, turbine and exciter</i>		
14.	Inertia constant, s	T_J
15.	Moment of inertia, kgm^2 ($GD^2/4$) or	J
16.	GD^2 , kgm^2	GD^2
<i>Open circuit saturation</i>		
17.	Saturation at rated voltage U_N	$S(1.0)$
18.	Saturation at voltage $1.2U_N$	$S(1.2)$

Note: * – the parameter is not used for salient rotor (hydro) generators;

** – T'_{d0} and r_f are given at certain temperature of field winding during measurement.

Generator dynamic model parameters can be identified from the regime test or the frequency response test data.

3. Evaluation of dynamic model parameters according to field test data

3.1. Inductive reactances, resistances and time constants

The parameters of the synchronous generator can be identified according to two types of field tests:

- regime test – the disconnection of the generator loaded by only reactive load;
- frequency response test of the stopped generator.

It is possible to identify parameters of the generator d -axis using regime test data with sufficient accuracy.

During the test of unloaded generator which consumes the reactive power from the network, the terminal voltage and current are registered.

Processing of test data according to the voltage variation, the d -axis parameters x''_d , x'_d , x_d , T''_{d0} , T'_{d0} are determined.

Terminal voltage of the disconnected generator can be expressed as follows:

$$U(t) = U_\infty + (U'_0 - U_\infty) \cdot e^{-\frac{t}{T'_{d0}}} + (U''_0 - U'_0) \cdot e^{-\frac{t}{T''_{d0}}}, \quad (1)$$

or

$$U(t) = U_0 - I_0 \cdot x_d + (U_0 - I_0 \cdot x'_d - U_\infty) \cdot e^{-\frac{t}{T'_{d0}}} + (U_0 - I_0 \cdot x''_d - (U_0 - I_0 \cdot x'_d)) \cdot e^{-\frac{t}{T''_{d0}}}, \quad (2)$$

or

$$U(t) = U_0 - I_0 \cdot x_d + I_0 \cdot (x_d - x'_d) \cdot e^{-\frac{t}{T'_{d0}}} + I_0 \cdot (x'_d - x''_d) \cdot e^{-\frac{t}{T''_{d0}}}; \quad (3)$$

where U_0 , I_0 , U_∞ are initial voltage and current and the steady state voltage of the disconnected generator; U'_0 , U''_0 – initial values of transient and subtransient voltages, T'_{d0} , T''_{d0} – direct axis open circuit transient and subtransient time constants, x_d , x'_d , x''_d – direct axis synchronous, transient and subtransient inductive reactances.

The variation in voltage when the generator that is loaded with capacitive reactive load was switched off is shown in fig. 1.

The initial value of the subtransient voltage U''_0 can be expressed from the first voltage jump and a subtransient inductive resistance value can be found:

$$U''_0 = U_0 - I_0 \cdot x''_d; \quad (4)$$

$$x''_d = \frac{U_0 - U''_0}{I_0}. \quad (5)$$

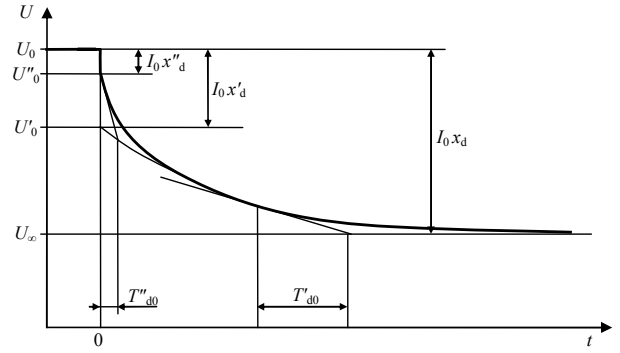


Fig. 1. The variation in voltage when the generator loaded with capacitive reactive load was switched off

At the subsequent voltage curve point (when the short-term voltage component extinct) derived tangent to the line that corresponds settled voltage U_∞ a direct axis transient time constant T'_{d0} can be determined.

Extrapolating the curve of the exponential transient voltage U' to the stoppage time the value of U'_0 is determined. According to it, the direct axis transient inductive resistance x'_d value is determined as follows:

$$x'_d = \frac{U_0 - U'_0}{I_0}. \quad (6)$$

The d -axis synchronous inductive resistance value is determined similarly:

$$x_d = \frac{U_0 - U_\infty}{I_0}. \quad (7)$$

The value of the d -axis subtransient time constant T''_{d0} is defined by extrapolating the tangent at certain point of the U''_0 curve to the derived U' curve.

The leakage resistance of the stator inductive x_ℓ value is not normally determined with the tests. It can be assessed in accordance with the manufacturers' data or approximately - according to longitudinal resistance x_d : $x_\ell \approx 0.08 \cdot x_d$.

Appropriate parameters of the q axis can be extrapolated in accordance to typical d and q axis ratios that is presented in table 2.

Table 2. Typical ratios for the d and q axis generators parameters

Parameters	Non-salient pole generator	Salient pole generator
x_q	$0.9 x_d$	$(0.6-0.7) x_d$
x'_q	$1.5 x'_d$	–
x''_q	x''_d	x''_d
T'_{q0}	$0.3 T'_{d0}$	0
T''_{q0}	T''_{d0}	T''_{d0}

In both cases of parameters' identification according to regime test and frequency response test of the stopped generator, the test temperature θ_B and the identified time constant T'_{d0B} must be taken into account and the value of excitation windings resistance r_{TB} need to be adjusted to the winding temperature of the nominal regime θ_N .

$$T'_{d0} = T'_{d0B} \cdot \frac{234.5 + \theta_B}{234.5 + \theta_N}; \quad (8)$$

$$r_f = r_{fB} \cdot \frac{234.5 + \theta_N}{234.5 + \theta_B}. \quad (9)$$

The data of the stopped generator frequency response test allows identify main parameters of the d and q axis: $x''_d, x'_d, x_d, T''_{d0}, T'_{d0}, x''_q, x'_q, x_q, T''_{q0}, T'_{q0}$ and resistances of the stator and rotor r_a and r_f .

The analyzed synchronous generator may be presented by the operator expressions for the direct and quadrature axes:

$$\Delta\Psi_d(s) = G(s) \cdot \Delta e_{fd}(s) - L_d(s) \cdot \Delta i_d(s), \quad (10)$$

$$\Delta\Psi_q(s) = -L_q(s) \cdot \Delta i_q(s), \quad (11)$$

Where $\Delta e_{fd}(s), \Delta\Psi_d(s), \Delta\Psi_q(s), \Delta i_d(s), \Delta i_q(s)$ are exciter voltage, the variation of flux linkage and current components, $G(s)$ – transfer function between rotor and stator, $L_d(s), L_q(s)$ – inductances in operator form of d and q axis.

The one-line diagrams corresponding to the (10) and (11) and representing the synchronous machine are shown in fig. 2. The variation of input and output signals are measured or simulated at the corresponding terminals of the blocks.

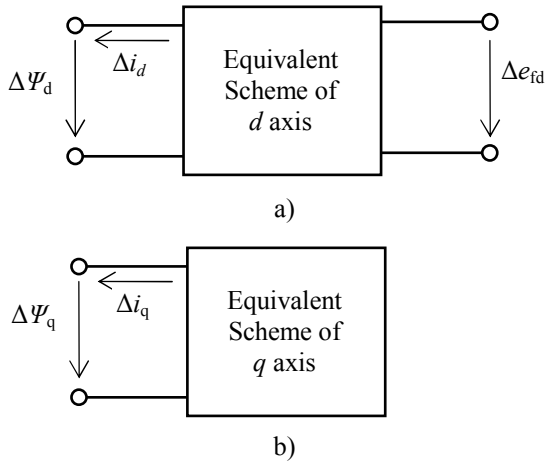


Fig. 2. Generalized schemes of the synchronous generator's direct axis (a) and quadrature axis (b)

From the expressions of the flux linkage generator transfer function and inductances expressions were made:

$$G(s) = G_0 \cdot \frac{1 + sT_{Id\ell}}{(1 + sT'_{d0}) \cdot (1 + sT''_{d0})}; \quad (12)$$

$$L_d(s) = L_d \cdot \frac{(1 + sT'_d) \cdot (1 + sT''_d)}{(1 + sT'_{d0}) \cdot (1 + sT''_{d0})}; \quad (13)$$

$$L_q(s) = L_q \cdot \frac{(1 + sT'_q) \cdot (1 + sT''_q)}{(1 + sT'_{q0}) \cdot (1 + sT''_{q0})}. \quad (14)$$

During the test, stator voltage and current and rotor current instant values were recorded.

During the test data processing complex input reactance of the d and q axis – $Z_d(s)$ and $Z_q(s)$; transfer function rotor-stator $s \cdot G(s)$ for the different frequencies ($s = j\omega = j2\pi f$) were determined. Operator values of the inductances $L_d(s)$ and $L_q(s)$ were determined estimating stator resistance

$$L_d(s) = \frac{Z_d(s) - r_a}{s}, \quad (15)$$

$$L_q(s) = \frac{Z_q(s) - r_a}{s}; \quad (16)$$

where r_a is the active resistance of stator windings, measured during the test at the temperature of windings.

With operator transfer functions and inductance values and expanded with polynomial ratio the dynamic parameters of $L_d, T'_{d0}, T''_{d0}, T'_d, T''_d$ and $L_q, T'_{q0}, T''_{q0}, T'_q, T''_q$ were determined. Parameters normally used to determine by frequency identification methods [1].

During the rapid changes of measured value, when $s = j\omega \rightarrow j\infty$, marginal values of the inductances $L_d(s), L_q(s)$ will be equal to transient inductance values L''_d and L''_q . According to (2.11)-(2.12) expressions, L''_d and L''_q expressed following:

$$L''_d = L_d(j\infty) = L_d \cdot \frac{T'_d \cdot T''_d}{T'_{d0} \cdot T''_{d0}}, \quad (17)$$

$$L''_q = L_q(j\infty) = L_q \cdot \frac{T'_q \cdot T''_q}{T'_{q0} \cdot T''_{q0}}. \quad (18)$$

Dynamic expressions of the inductances without the damping windings (the second rotor contour, contour with large time constants) will be less complicated and expressed as follows:

$$L'_d = L_d(j\infty) = L_d \cdot \frac{T'_d}{T'_{d0}}, \quad (19)$$

$$L'_q = L_q(j\infty) = L_q \cdot \frac{T'_q}{T'_{q0}}. \quad (20)$$

Rotor poles of the hydro units that are made of the steel sheets and the free currents closes through damping windings of rotor transverse axis. Hydro generators that is usually modelled with "2.1" model, now are designed with one contour in the transverse axis. In case, when damping windings time constants are smaller than the excitation windings time constants, it is considered that

there is no transient inductance or transient time constants, just transient inductance L''_q and the open circuit and short circuit time constants T''_{q0} , T''_q . Expression of the transient inductance L''_q is similar to the expression of the transient inductance of the turbogenerator:

$$L''_q = L_q(j\infty) = L_q \cdot \frac{T''_q}{T''_{q0}}. \quad (21)$$

The parameters of the transverse and direct axis equivalent schemes could be determined according to basic dynamic parameters values.

The test of the frequency response for the stopped generator is recommended only when the routine maintenance is completed and the generating unit is off for long time.

3.2. Inertia constant

The inertia time constant T_J of the generating unit is determined from the generator tripping test, where the initial speed $\left. \frac{d\Delta\omega_*}{dt} \right|_{t=0}$ is measured and the generator is loaded with low active load ΔP_* :

$$T_J = \frac{\Delta P_*}{\left. \frac{d\Delta\omega_*}{dt} \right|_{t=0}}. \quad (22)$$

The initial rotor speed should be recorded with sufficiently high sampling frequency, and the time interval should be within 0.01-0.1 s range.

3.3. Saturation characteristic

Generator saturation values of $S(1.0)$, $S(1.2)$ characteristics are determined by the open circuit (no load) characteristic (fig. 3).

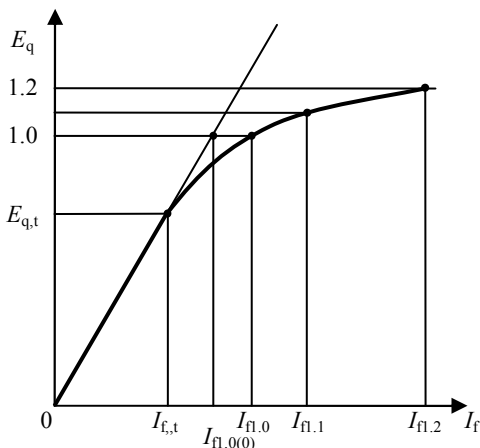


Fig. 3. Open circuit saturation characteristic

Any source voltage E_{qi^*} corresponding to the excitation current of I_{fi^*} can be expressed as follows:

$$I_{fi^*} = E_{qi^*} + D \times e^{C(E_{qi^*} - E_{qt^*})}, \quad (23)$$

and the values of the saturation curve:

$$S(E_{qi^*}) = \frac{D}{E_{qi^*}} \cdot e^{C(E_{qi^*} - E_{qt^*})}, \quad (24)$$

where E_{qi^*} and I_{fi^*} – source voltage and field current at i^{th} point of open circuit characteristic, in p.u.; E_{qt^*} – source voltage value at the end of linear characteristic, in p.u.; C and D – coefficients of the approximated characteristic.

Idle characteristic is usually measured to $1.1U_N$ and it continues to be extrapolated to $1.2U_N$.

According to the two nonlinear idling characteristic points K and M and the coordinates of the start of nonlinear approximation source voltage to find the coefficients C and D :

$$C = \frac{\ln \frac{I_{fK^*} - E_{qK^*}}{I_{fM^*} - E_{qM^*}}}{E_{qK^*} - E_{qM^*}}, \quad (25)$$

$$D = \frac{I_{fK^*} - E_{qK^*}}{e^{C(E_{qK^*} - E_{qt^*})}}; \quad (26)$$

where E_{qK^*} , E_{qM^*} , I_{fK^*} , I_{fM^*} , E_{qt^*} are source voltage values of the points of K and of M and the corresponding excitation currents and the values of the nonlinearity start in source voltage expressed in per units.

4. Evaluation of dynamic models according to data presented by manufacturers and operators

Almost all data necessary for identification of dynamic model can be listed in technical specifications of the modern generating units. The missing parameters may be identified according to startup tests. However, the list of required parameters in old generators' specifications usually is not sufficient. If there is no possibility to perform field tests, the parameters can be evaluated approximately. The main factors for determination of parameters are type of the synchronous generator, rated power, voltage and rotation speed.

The direct axis synchronous inductive reactance x_d can be evaluated according to ratio of field current's rated values I_{fN} and open circuit value I_{f0} and rated power factor $\cos\varphi_N$.

If the open circuit characteristic is known as well as rated values of field current and power factor, the x_d can be calculated considering the rated value of field current I_{fN^*} in per unit on base of field current value corresponding the source voltage at rated voltage of linearized characteristic ($I_b = I_{f,te1}$):

$$E_{qN*} = I_{fN*} = \frac{I_{fN}}{I_{f,te1}}. \quad (27)$$

The rated source voltage for non-salient pole generator equals

$$\underline{E}_{qN*} = \underline{U}_{N*} + \underline{I}_{N*} \cdot (r_{a*} + jx_{d*}), \quad (28)$$

and the absolute value is

$$E_{qN*} = \sqrt{(U_{N*} \cdot \cos\phi + I_{N*} \cdot r_{a*})^2 + (U_{N*} \cdot \sin\phi + I_{N*} \cdot x_{d*})^2}; \quad (29)$$

where U_{N*} and I_{N*} - rated voltage and current of synchronous machine, in p.u.; r_{a*} and x_{d*} - resistance and inductive reactance of the stator, in p.u.

At rated conditions, the voltage and current equals to one, then

$$x_{d*} = \sqrt{I_{fN*}^2 - (\cos\phi_N + r_{a*})^2} - \sin\phi_N. \quad (30)$$

Usually, the stator resistance is less than 0.5% of x_d and can be neglected. In this case x_d in p.u. can be written as

$$x_{d*} = \sqrt{I_{fN*}^2 - \cos^2\phi_N} - \sin\phi_N. \quad (31)$$

When the stator resistance is not taken into account, the source voltage of salient pole generator (hydrogenerator) E_{QN*} can be expressed via open circuit source voltage E_{qN*} and rated voltage and current of the generator:

$$\begin{aligned} E_{QN*} &= E_{qN*} - I_{dN*} \cdot (x_{d*} - x_{q*}) = \\ &= I_{fN*} - I_{dN*} \cdot (x_{d*} - x_{q*}), \end{aligned} \quad (32)$$

$$E_{QN*} = \sqrt{(U_{N*} \cdot \cos\phi_N)^2 + (U_{N*} \cdot \sin\phi_N + I_{N*} \cdot x_{q*})^2}. \quad (33)$$

Marking the ratio of x_q and x_d as

$$k_{qd} = \frac{x_q}{x_d}, \quad (34)$$

a quadratic equation can be written:

$$\begin{aligned} (U_{N*} \cdot \cos\phi_N)^2 + (U_{N*} \cdot \sin\phi_N + I_{N*} \cdot k_{qd} \cdot x_{d*})^2 - \\ - [I_{fN*} - (1 - k_{qd}) \cdot I_{dN*} \cdot x_{d*}]^2 = 0. \end{aligned} \quad (35)$$

For rated conditions, the (35) can be rewritten as

$$\begin{aligned} x_{d*}^2 \cdot [k_{qd}^2 - (1 - k_{qd})^2 \cdot I_{dN*}^2] + \\ + x_{d*} \cdot 2[k_{qd} \cdot \sin\phi_N + I_{fN*} \cdot (1 - k_{qd}) \cdot I_{dN*}] - (I_{fN*}^2 - 1) = 0. \end{aligned} \quad (36)$$

The value of d -axis synchronous inductive reactance of salient pole generator is the solution of (36):

$$\begin{aligned} x_{d*} &= \frac{-k_{qd} \cdot \sin\phi_N - I_{fN*} \cdot (1 - k_{qd}) \cdot I_{dN*} + \\ &+ \sqrt{\left[\frac{k_{qd} \cdot \sin\phi_N + I_{fN*} \cdot (1 - k_{qd}) \cdot I_{dN*}}{k_{qd}^2 - (1 - k_{qd})^2 \cdot I_{dN*}^2} \right]^2 + \frac{I_{fN*}^2 - 1}{k_{qd}^2 - (1 - k_{qd})^2 \cdot I_{dN*}^2}}. \end{aligned} \quad (37)$$

The majority of hydrogenerators has the ratio of reactances $k_{qd} \approx 0.6$ and $I_{dN*} = 0.75-0.8$, therefore, x_d can be approximately expressed as

$$x_{d*} \cong \sqrt{5I_{fN*}^2 + 3I_{fN*} - 2} - I_{fN*} - 2. \quad (38)$$

Also, the d -axis synchronous inductive reactance can be determined according to short circuit ratio K_{scr} :

$$x_{d*} = \frac{1.1}{K_{scr}}. \quad (39)$$

If the power factor is unknown, its value can be taken approximate: the power factor of turbogenerators under 120 MW and of hydrogenerators under 50 MW equals $\cos\phi_N = 0.8$, of turbogenerators 120-500 MW and hydrogenerators beyond 50 MW $\cos\phi_N = 0.85$, and of turbogenerators beyond 800 MW equals $\cos\phi_N = 0.9$.

According to x_d value, other parameters of synchronous generator can be determined. Approximate ratios of inductive reactances can be used (table 3) [3].

The approximate values of time constants are: $T'_{d0} = 6.0-9.0$ s, $T''_{d0} = 0,12$ s.

Table 3. Approximate ratios of inductive reactances of synchronous generators

Ratio	Turbogenerator	Hydrogenerator
x''_d / x_d	0.10	0.2
x'_d / x_d	0.16	0.3

Inertia constant of generating unit equals 5-10 s [4]. The data about unit's inertia can be given in three ways: value of moment of inertia $J = GD^2/4$, kgm^2 ; value of GD^2 , kgm^2 or inertia constant T_J , s.

Inertia constant can be determined according to the total moment of inertia of generator, turbine and exciter:

$$T_J = \frac{J_{\Sigma} \cdot \Omega_N^2}{S_N} = \frac{0.00274 \cdot GD_{\Sigma}^2 \cdot n^2}{S_N}, \text{ s} \quad (40)$$

where n - rotating speed in min^{-1} , $GD_{\Sigma}^2 = 4J_{\Sigma}$, kgm^2 and S_N - rated total value in VA.

In the literature of the post-Soviet countries, the value of inertia constant is given on base of the rated active power (T_{JPN}). The inertia constant on base of total power is calculated by

$$T_J = T_{JP_N} \cdot \cos \phi_N, \text{ s.} \quad (41)$$

The inertia can be described as a relative kinetic energy H of rotor of rated operating conditions, in s:

$$H = T_J / 2, \text{ s.} \quad (42)$$

5. Conclusions

The identification techniques of synchronous generators dynamic model's parameters are presented in the paper. The most accurate model can be identified if the special field tests of generating units are performed to obtain the data need for parameters' evaluation. If such tests are not available, the parameters can be determined approximately according to some data given by manufacturers.

6. References

1. Azubalis V., Virbickas D., Jonaitis A. and Azubalis M. Synchronous Generator and Excitation System Dynamic Model Parameters Investigation. Proceedings of International Conference "Electrical and Control Technologies – 2006", Kaunas, 2006. p. 110-113.
2. Kundur P. Power System Stability and Control. New York, 1993. 1176 p.
3. Neklepaev B.N., Krjuchkov I.P. Electrical part of power stations and substations. Moscow: Energoatomizdat, 1989. 608 p. (in Russian).
4. Sterninson L.D. Transient processes of frequency and power control in power systems. Moscow, 1975. 216 p. (in Russian).

POTENTIAL OF NON-TRADITIONAL ENERGY SOURCES FOR COLD RECOVERY IN ABSORPTION REFRIGERATING MACHINES

Michail G. BERENGARTEN*, Semyon I. VAINSHTAIN*, Aleksandr S. PUSHNOV*, Vytautas ADOMAVIČIUS**

*Moscow State University of Ecological Engineering, Russian Federation

** The Centre for Renewables Energy Technologies at Kaunas University of Technology, Lithuania

Abstract: Two types of refrigerating units for air conditioning systems – vapor compression and absorption types are examined in this paper. The examined equipment is applied for creation of special cooling systems in various large-scale objects (for example: the large area storages). Several advantages of the absorption refrigerating machines are shown there. There is emphasized that efficiency of such units may be increased by the substitution of individual boiler plant as a hot water source for the non-traditional energy source – solar collectors for water heating. It would result in savings of the fossil fuels and decrease in pollution of environment.

Keywords: air conditioning systems, absorption refrigerating machines, cogeneration, cooling, solar collectors.

1. Introduction

In many countries and regions the climate conditions require creating special refrigerating systems for various large-scale objects including storage and production workspaces with area up to 100.000 m². In several cases the mentioned above goal can be achieved by usage of air conditioning systems equipped with autonomous gas boiler plants in combination with absorption refrigeration units or vapor compression units.

2. Comparison of various types of refrigerating units

As indicated by calculations performed in reference [1], the outlay for usage of absorption refrigerating units and vapor compression units are three times better for absorption refrigeration units. The mentioned above comparative calculations [1] were made by taking the air conditioning system's capacity $Q=1000$ kW at the taken cooling coefficient $\varepsilon=3,0$.

Absorption refrigerating units have an important advantage in comparison with vapor compression units – they never consume the energy for the providing of

cooling cycle. The energy is necessary only for transportation of liquid and air – to make the pump and fan drives work.

Another serious feature of absorption refrigeration units are low operating costs. They are approximately two times lower in comparison with vapor compression units [1].

In line with the positions mentioned above the absorption refrigerating unit needs a source of hot water. For example, single-stage absorption cooling unit needs a hot water with temperature in a range $T_w=90\div 98$ °C.

Autonomous boiler plant traditionally is used as a hot water source for needs of absorption refrigerating unit. As an alternative there may be applied flue gas boiler, gas turbine or gas-piston cogeneration unit as a source of heating medium. The mentioned boiler units permanently are under further development and they are widely used around the world. They have a great capacity and minimal nitrogen oxide emissions into the atmosphere. Some technical features of modern back boilers are shown in Table 1.

Nevertheless, effective boiler plants WÄRTSILÄ that provide high capacity (up to 90÷94%) permanently need the fuel consumption – gas or liquid fuel that have a huge price at world market and is ranged. As for the efficient boiler plants BioEnergy produced by WÄRTSILÄ (Finland) that use the woodworking wastes, the peculiarity is following: this type of fuel isn't available everywhere in a sufficient amounts. The last WÄRTSILÄ design project is three-generation system that presumes production of the power and heat (hot water) in winter time and the cooling generation in summer as well.

But these units may be considered as the three-generation ones only taking into consideration the whole annual period, because during the season periods (summer or winter) they work as co-generation units, or in other words, they produce the power and heat in winter months and the power and cooling in summertime.

Table 1. Technical features of back boiler plants S3V produced by WÄRTSILÄ. Source: [2], [3]

Boiler plant	Overall dimensions, m		Fuel consumption			Efficiency, %
	length	width	Diesel fuel, kg/hour	Boiler oil 100 kg/h	Gas, nm ³ /h	
2x1 MW	5,3	9,8	198	200	220	92±2
2x2 MW	6,9	9,8	396	400	440	92±2
2x3 MW	6,9	9,8	594	600	660	92±2
3x5 MW	10,0	13,8	1485	1500	1650	92±2
4x15 MW	24,3	14,3	5940	6000	6600	92±2

3. Usage of solar energy

Alternative option of hot water source is usage of solar collectors for water heating.

As an example let's examine the single-stage absorption refrigerating unit using the hot water from autonomous boiler plant [1]. As a rule, the single-stage absorption refrigeration units are using hot water with temperature $T_w=90\div98$ °C have the following coefficient:

$$\eta = \frac{Q_0}{Q_h} = 0,75, \quad (1)$$

where Q_0 is refrigerating capacity, kW;
 Q_h – input of heat to refrigerating unit from the heating medium, kW.

It is required to burn the certain volume of natural gas in the boiler plant in order to get the necessary refrigerating capacity:

$$Q_g = \frac{Q_0}{\eta}, \quad (2)$$

where Q_g is heat capacity of the boiler running on natural gas, kW;
 η – the efficiency of the boiler.

Taking $Q_0 = 1000$ kW and efficiency 0,75 according to the formula (2) we get $Q_g = 1333$ kW.

Taking the boiler plant efficiency 0,92 as it is given in Table 4 [2], at calorificity of natural gas $\lambda=35\ 000$ kJ/m³ it is possible to calculate the common consumption of natural gas during the hot period of year (for example, 200 days):

$$V_g = \frac{24 \cdot Q_g \cdot \eta \cdot T \cdot k_l \cdot k_{md}}{\lambda}, \quad (3)$$

where T is the number of days when refrigeration is required, $N=200$;

k_l – loading factor of the refrigerating unit, (0,5);

k_{md} – coefficient of the dimensions' matching, ($3600 \cdot 10^3$).

After the substitution of the given above values of all parameters we get the total volume of the natural gas to be consumed:

$$V_g = 2\ 040\ 635\ \text{m}^3$$

The cost of such gas volume in Russia is the following:

$$C = 2040635 \cdot 1,85 = 3\ 775\ 175\ \text{roubles.}$$

Replacement of the traditional hot water source in an absorption refrigerating unit by the solar collectors for water heating of the adequate capacity gives a significant economy. In this case cost of the solar heat energy varies from 0,04 to 0,30 Euro for 1 kWh depending on solar energy resources in the particular region [5].

According to data of Lundh and Dalenbäck [4], for example, to Anneberg (Sweden) conditions (July, 2003) in period from 12.00 to 18.00 hours the large flat plate solar collector's array of 240 m² installed on a residential building may provide hot water of 60-70 °C temperature – that is adequate to 100-140 kW capacity of the array.

Usage of solar energy is limited in a flow of daytime and seasons of year and depends on the geographic latitude of the locality. So, for Central and Northern Europe the maximum of solar radiation goes to the period from April-May to September (look Table 2).

Table 2. Value of solar radiation in Europe, kWh/m² a day

	Central Europe	Northern Europe
January	1.7	0.8
February	3.2	1.5
March	3.6	2.6
April	4.7	3.4
May	5.3	4.2
June	5.9	5.0
July	6.0	4.4
August	5.3	4.0
September	4.4	3.3
October	3.3	2.1
November	2.1	1.2
December	1.7	0.8
Annually	3.9	2.8

We emphasize that the alternative variant based on solar collectors allows to get a somewhat lower potential of hot water $T_w=70$ °C in comparison with traditional autonomous boiler plant potential ($T_w=90$ °C). One of the possibilities to raise the temperature of hot water coming from solar collector is to use another available relevant heat source for backing up the solar installation.

Scheme of single-stage absorption refrigerating unit using the solar collector as hot water source is presented at Fig. 1.

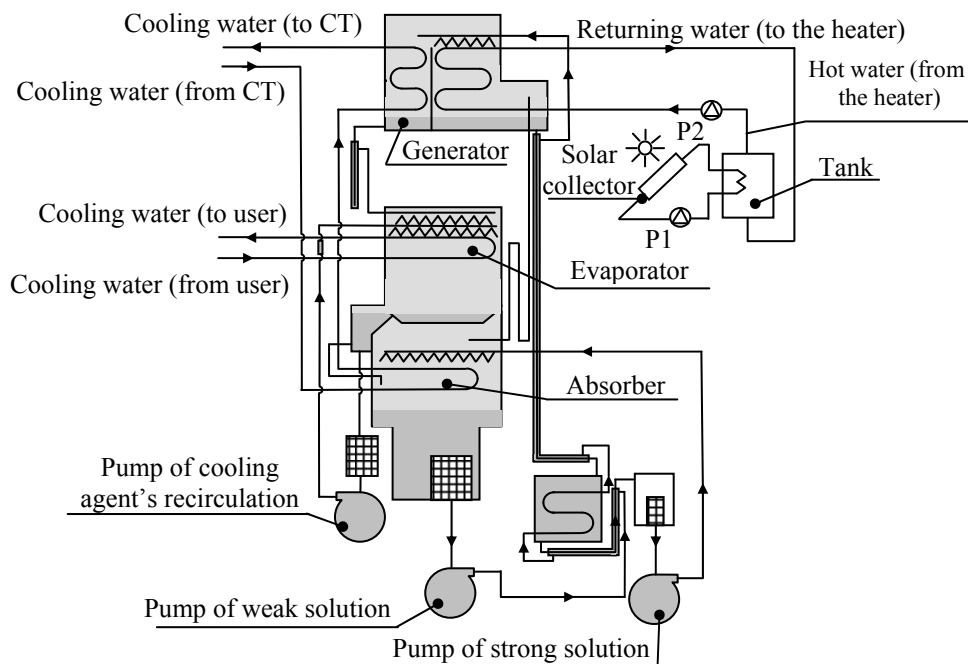


Fig. 1. Single-stage absorption refrigerating unit using hot water from the solar collectors

In order to upgrade the reliability of operation the suggested scheme of single-stage absorption refrigerating unit is additionally equipped with hot

water storage drums with vertical position of the polyethylene tubes $\text{Ø}32 \times 2,4$ mm in the seal laid down to the 100 meters depth (look Fig. 2).

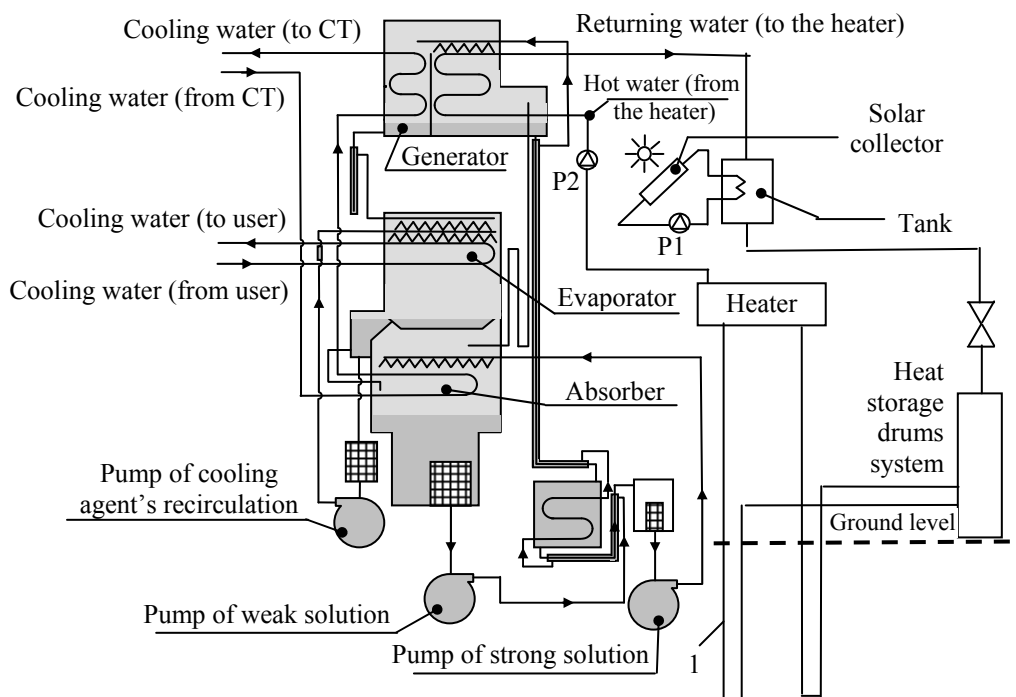


Fig. 2. Single-stage absorption refrigerating unit using hot water from the solar collector with heat storage drums system in the seal under ground; 1 – polyethylene tubes in the seal

Another solution of engineering, which can be used for the utilization of solar energy in order to diminish the expenditures for heat energy necessary to run the single-stage absorption refrigerating unit, is described in reference [6]. According to Seleznev patent [6], the solar energy accumulator made as a reservoir with mirror walls presumes can be implemented for this goal.

The scheme of such solar heat energy accumulator is presented in Fig. 3. Simple construction of the reservoir with integrated collector was suggested by Kučinskis and Liubarskiy [7]. The solar collector is combined there with the water accumulation reservoir. The specific capacity of the reservoir is recommended approximately $40\text{-}50 \text{ dm}^3$ per 1 m^2 of the collector's area.

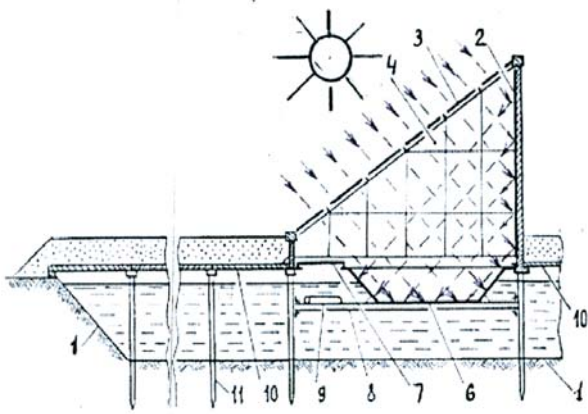


Fig. 3. Solar energy accumulator according to the patent [6]

During the period of low solar radiation the biogas energy may be used to get a hot water for the absorption refrigerating unit. In this case the hot water preparation block is operating in a sufficient way.

One of the possible variants of the scheme for production of hot water based on the biogas energy is shown in Fig. 4 [8]. In this case the hot water with temperature $T_w = 80-85^{\circ}\text{C}$ is discharged in the absorption refrigerating unit. The scheme includes the following constructions: methane tank, solar collectors, block of biogas cleaning, internal combustion engine and the heat pump. According to data of Rabinovych [8], capital costs could be returned in two years after the installation of this hot water system.

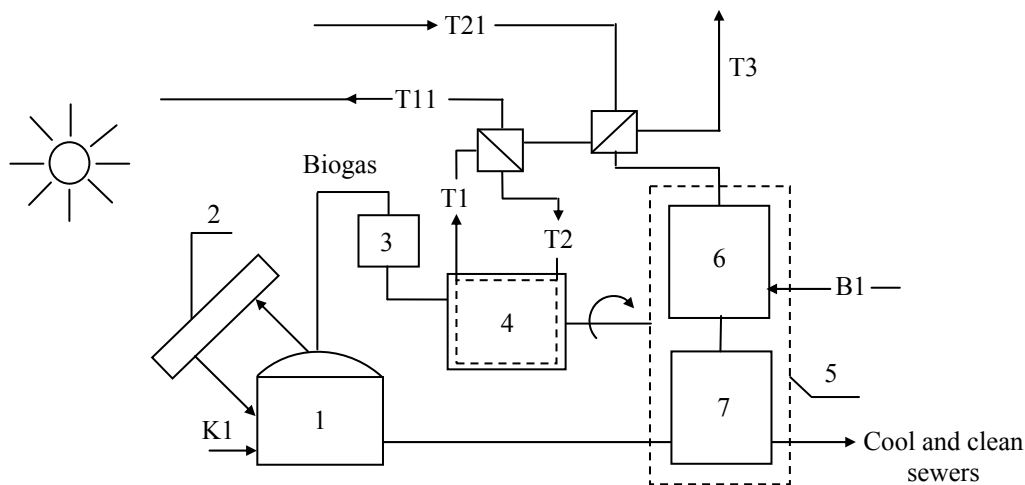


Fig. 4. Scheme of installation, which uses biogas and heat of sewage for the heat supply system: 1- methane tank; 2 – solar collectors; 3 – block of biogas cleaning; 4 – internal combustion engine; 5- heat pump plant; 6 – condenser; 7 – evaporator; T1 – water from cooling system of internal combustion engine; T11 – water in heating system, $t = 80-85^{\circ}\text{C}$; T21 – water from the heating system, $t = 55-60^{\circ}\text{C}$; T3 – hot water in hot water supply system, $t = 50-55^{\circ}\text{C}$; B1 – cool water from the running water supply system; K1 – sewage

4. Conclusions

1. Some alternative systems using solar and biogas energy for hot water supply to the absorption refrigerating unit are proposed in this paper.
2. Usage of the vertical tubes laid down up to the depth 100 meters under ground and the accumulating reservoirs are suggested here for the accumulation of hot water.
3. The biogas energy may be used to provide the absorption refrigerating unit with hot water with the temperature $T_w = 80-85^{\circ}\text{C}$ during the period of low solar radiation.

5. References

1. Бурцев С.И. О некоторых преимуществах абсорбционных холодильных машин // Инженерные системы. АВОК-Северо-Запад, №3(19), 2005. – p.p. 20-24.
2. www.wartsila.com (called on 02.16.2009).

3. Силловые станции: производственная программа WÄRTSILÄ.W-P 09.2004/Bock/s Office Waasa Graphics.
4. Lundh M. Dalenbäck J.-O. Solar heated residential area Anneberg – initial evaluation // LTMA mokslo darbai, №2. Klaipėda, Klaipėdos universitetas, 2005. – p.p. 142-153.
5. Kytra S. Atsinaujinantys energijos šaltiniai. Kaunas, KTU, 2007. – 140 p.
6. Селезнев Н.В. Аккумулятор солнечной энергии. Патент РФ №2267060.
7. Кучинскас В., Любарский В. Ресурсы и перспективы использования возобновляемой энергии в Литве. Энергосбережение в сельском хозяйстве. Труды 2-й Международной научно-технической конференции (2-3 октября 2000 г. М.-ВИЭСХ), Часть 2. М., 2000. – p.p. 405-410.
8. Rabinovych M.D. Renewable energy sources for sustainable development of historical cities. Environment Protection Engineering, vol.32, №1, 2006. Wroclaw, 2006. – p.p.81-86.

POSSIBLE PERSPECTIVES OF COOLING TOWER APPLICATION FOR ELECTRIC ENERGY PRODUCTION

Aleksandr S. PUSHNOV*, Michail G. BERENGARTEN*, Semyon I. VAINSHTEIN*, Vytautas ADOMAVIČIUS**

*Moscow State University of Ecological Engineering, Russian Federation

** The Centre for Renewables Energy Technologies at Kaunas University of Technology, Lithuania

Abstract: Possibilities of usage of the cooling tower combined with non-traditional power generating units were examined on the base of analysis of the aerodynamic situation in the cooling towers with natural draft. One of the schemes presumes the location of axial air flow turbine in alignment to air outflow on the axis of tower symmetry at its upper part. Another possible scheme presumes the location of several small wind turbines at the top of the cooling tower. The half of outer cover of the cooling tower oriented to south is proposed to blacken artificially in order to increase the power of the air flow inside the cooling tower. The discussion also deals with the installation of photovoltaic modules on the bulk of cooling tower: electric energy produced by them could support the feeding of cooling tower's pump equipment, which is used for the cooling of recycling water under normal exploitation mode.

Keywords: cooling towers with natural draught, non-traditional energy sources, wind turbines, electric energy.

1. Introduction

Ecological, economical and energy crisis currently taking place in the world makes us to look for new possibilities and new approaches in order to find out new energy sources for heat and power generation. First of all, we look for usage of renewable energy sources, which are universally available, free from payment and ecologically clean.

Some possible ways to use the cover of acting or suspended cooling tower for the installation of small scale wind turbines and (or) photovoltaic modules are described in this paper. The suggestions discussed below are based on the analysis of peculiarities in aerodynamic and heat situation in the cooling towers of various types.

General view and scheme of counter-flow cooling towers with natural draught are shown at Fig. 1 and Fig. 2.



Fig. 1. General view of counter-flow cooling tower HAMON (France)

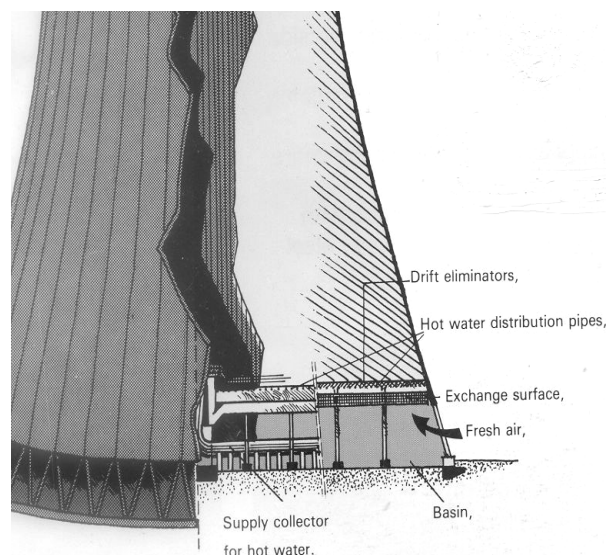


Fig. 2. Scheme of cooling tower

2. Aerodynamic situation in the cooling tower

As it is shown in a number of experimental and theoretical researches [1÷5], aerodynamic situation in

the cooling towers with natural draft is characterized by serious irregularities in cross view. There is also stressed a transformation of air speed field by the height of cooling tower.

The following peculiarities of speed field in the cooling tower are important from a viewpoint of possible use of this wind energy potential:

- symmetry of speed field with reference to the cooling tower block's axis of symmetry,
- presence of stable wall area of increased magnitudes of air speed's vertical constituent in the narrowest part inside the cooling tower; as this takes place, the said area of increased magnitudes of air speed near the tower walls survives by height becoming a little bit narrower at the point of the outgoing opening of the cooling tower.

The air flow pattern in the cooling tower is illustrated on the diagrams below and is taken from theoretical work of Gonzáles [3] with application of k-ε turbulence model (Fig. 3, 4). The design values of air speed's vertical and horizontal constituents in the cooling tower with height 150 m there is shown according to data [3].

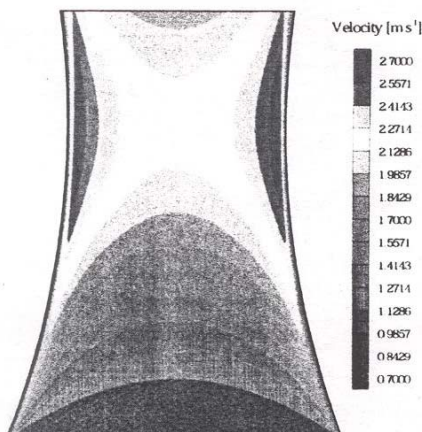


Fig. 3. Results of steady-state calculation of magnitude field with the k-ε turbulence model using wall functions for uniform vertical flow of moist air. Geometry of the tower is considered from the cooling pack position [3]

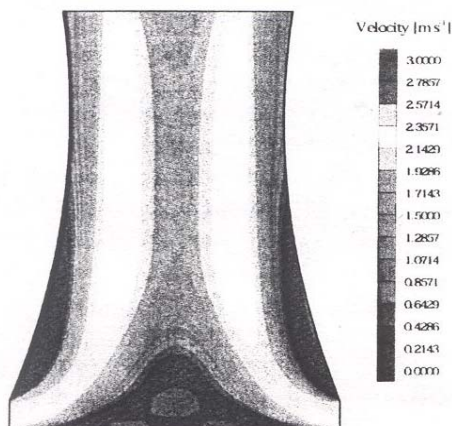


Fig. 4. Results of steady-state calculation of magnitude field with the k-ε turbulence model using wall functions for uniform vertical flow of moist air. All geometry of the tower is considered

3. Possible engineering solutions on the cooling tower's application for electric energy production

Let's examine the constructions and parameters of large ferroconcrete cooling towers with natural draft that are widely applied in power engineering. The capacity of such cooling towers on cooled recycled water is 100.000÷150.000 m³/hour.

Main geometrics of Russian-made and foreign modern counter-flow evaporative cooling towers are shown in Tables 1 and 2.

Table 1. Geometrics of some constructions of cooling towers

Reference	[7]	[4]	[6]	[13]			
	Gage diameter, m.	125	104,5	64,4	80	82	97
Height of offtake windows, m.	10	8	-				
Height of tower, m.	150	-	120	90	102	110	130

Table 2. Features of cooling towers by data [3]

No. of project	Height of the cooling tower, m.	Diameter of tower, m.		Height of offtake windows, m.	Material of tower frame
		On the upper level of nozzles	At the outgoing opening		
БГ-576-65	40	25,2	17,6	3,3	Steel
БГ-725-66	39	32,5	21,8	3,55	//
БГ-900-66	43,4	31,2	21,8	3,3	//
БГ-1520-70	53,5	47,6	25,6	3,3	Ferroconcrete
БГ-1200-70	48,3	40	26	3,3	Steel
БГ-2100-70	64,8	52,2	33	3,8	//
БГ-2600-70	71	58,2	37,9	4,3	//
БГ-3200-73	81	64,4	40,4	5	//
БГ-4000-71	91,5	72	41,6	5,5	//

3.1. Electric energy production by turbine placed in the cooling tower

A natural draft of air flow inside the cooling tower is a matter of primary interest from the standpoint of cooling tower usage. According to data of Ponomarenko and Arefyev [6] the air flow speed in the narrowest part of the cooling tower may be from 4÷5 up to 12÷13 m/s. Potential of this air flow may be used for generation of electric energy by the wind turbine placed in the upper part of the cooling tower. Possible engineering solutions

on positioning of one or several wind turbines of various types in the upper part of the cooling tower are shown at Fig. 5a-5d.

It's well known that some limits on air flow speed are determined by the demand to minimize the drop liquid drag-out from the cooling tower by upward air flow. The increase of air flow speed is integral with increase of such important cooling tower feature as depth of the recycled water cooling because of the intensification of heat and mass exchange processes [6].

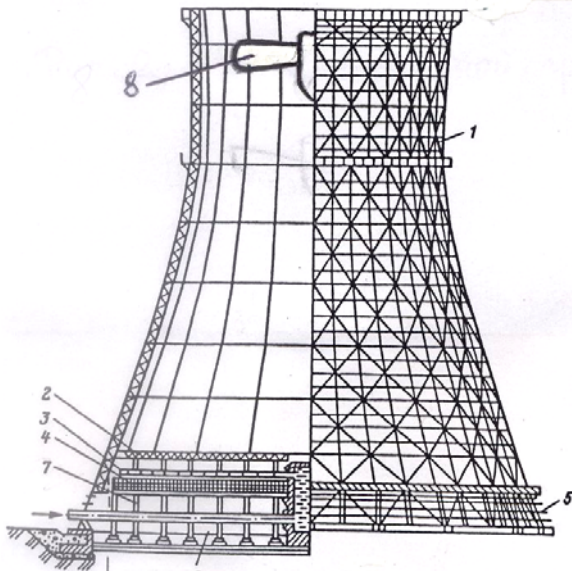


Fig. 5a. Scheme of the wind turbines' positioning in the upper part of the cooling tower: 1 – the exhaust tower; 2 – the water catcher; 3 – the water distributing system; 4 – the irrigation ditch; 5 – the air-regulating plant; 6 – the drainage; 7 – the load-carrying reference framework; 8 – the wind turbine.

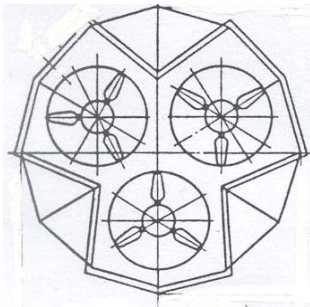


Fig. 5b. Scheme of three wind turbines positioning in outgoing opening of the cooling tower

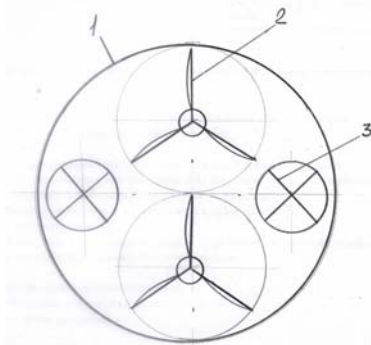


Fig. 5c. Scheme of cooling tower with small wind turbines of two types: 1 – cooling tower; 2 – two wind turbines; 3 – two smaller wind turbines.

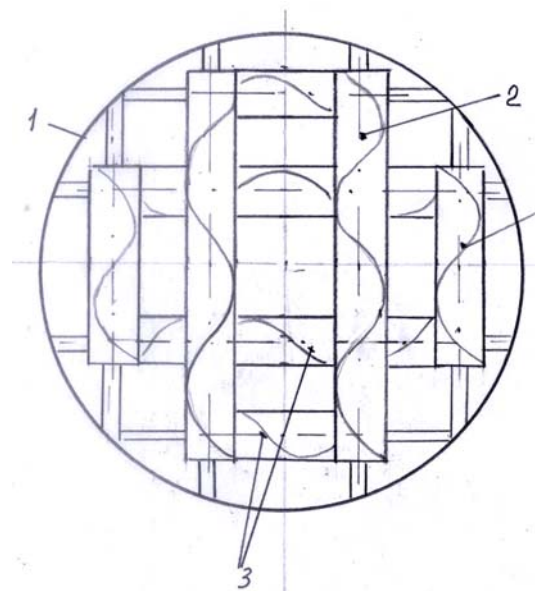


Fig. 5d. Scheme of the cooling tower with double-deck horizontal positioning of small wind turbines: 1 – cooling tower; 2 – up-level turbines; 3 – low-level turbines.

3.2. Possibilities to increase energy potential of air flow in the cooling tower because of increase of the natural draft intensity

It's known that a natural draft of the cooling tower is determined by:

- the tower's height and form;
- the level of the natural atmospheric air wind force in the cooling tower's surrounding space.

Nevertheless, at present a factor of possible increase of speed of air in the cooling tower following from additional heating is not taking into account. Let us examine this aspect more seriously because a few amount of heat air volume-up may become useful in order to increase the wind energy potential inside the cooling tower.

In reference [3] there are shown design data of air flow temperature in the cooling tower by its height (look at Fig. 6 and 7). It is shown that air flow temperature depending on the cooling tower height from 10 to 150 meters is from 29°C to 32°C. It's possible to provide additional heating of air flow inside cooling tower and increase of draft by artificial blackening of the outer cover of south-eastern side of the tower's ferroconcrete block.

During the hottest days in periods from 11³⁰ to 16⁰⁰ in summertime the blackened outer cover of the cooling tower may be heated up to 90 °C. Preliminary estimate analysis shows that the temperature of inside cover of cooling tower may be about 70°C in this case. The air in the cooling tower will be heated up under the air flow speed $W_0 = 4\div 12$ m/s. The heated up air will increase the natural draft (wind speed) inside the cooling tower what will contribute to the enhancement of the power of small-scale wind turbines, which could be installed in the tower.

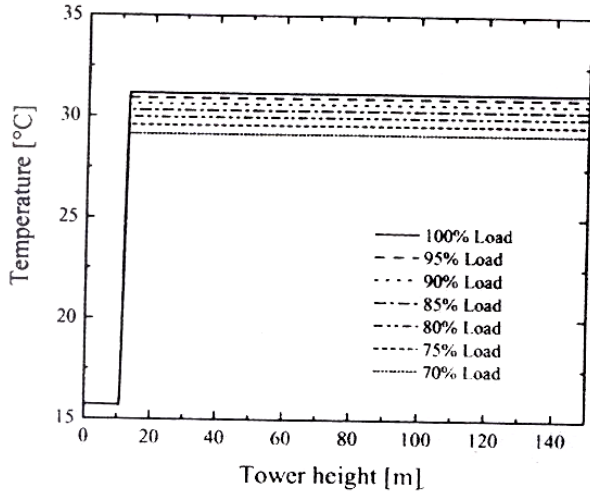


Fig. 6. Calculation results for the test case under summer atmospheric conditions at several values of heat load (variation of temperature)

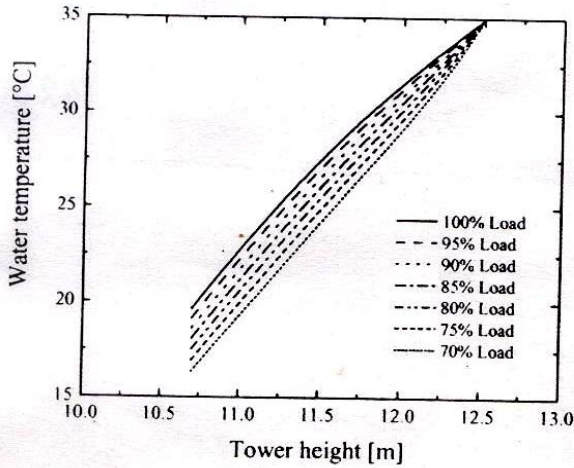


Fig. 7. Calculation results for the test case under summer atmospheric conditions at several values of heat load (variation of water temperature)

3.2.1. Calculation of heat leakage inside the cooling tower

Let's determine the heat leakage through the walls of cooling tower Q_1 compensating difference between the temperature of outer and inside covers of the cooling tower walls - Q_{1T} , and the heat leakage as a result of solar radiation's wall heat gain - Q_{1C} . The calculated scheme is shown at Fig. 8.

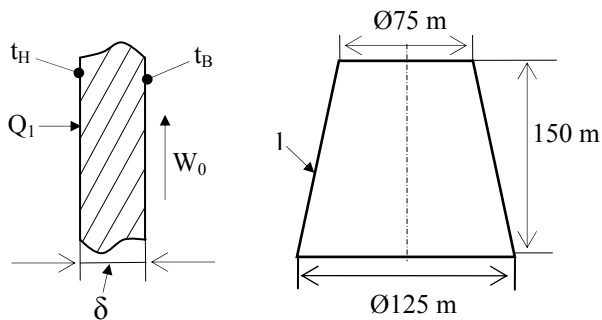


Fig. 8. Scheme of the cooling tower for calculations

$$Q_1 = Q_{1T} + Q_{1C}; \quad (1)$$

$$Q_{1T} = K_g \cdot F \cdot \Theta \cdot 10^{-3} = K_g \cdot F \cdot (t_H - t_B) \cdot 10^{-3}, \quad (2)$$

where Q_1 , Q_{1T} and Q_{1C} are the heat flows explained above, kW;

$t_H = 90$ °C is the temperature of the cooling tower outer wall;

$t_B = 32$ °C is the specified temperature of air flow inside the cooling tower according to Gonzales [3] calculations never accounting the heating of the wall by solar radiation;

$F = 35796$ m² is the area of the cooling tower outer wall;

$K_g = 3,56$ W/(m²·K) is the heat transfer coefficient of the cooling tower wall

$$K_g = \frac{1}{\frac{1}{\alpha_H} + \frac{\delta}{\lambda} + \frac{1}{\alpha_B}}, \quad (3)$$

where $\delta = 0,3$ m is the cooling tower wall thickness;

$\alpha_H = 23$ W/(m²·K) is the outer heat transfer coefficient [10];

$\lambda = 2,04$ W/(m·K) is the heat conductivity coefficient (ferroconcrete) [10];

$\alpha_B = 11$ W/(m²·K) is the inner heat transfer coefficient [10].

$K_g = 3,56$ W/(m²·K) was calculated after the substitution of the indicated above values into the equation (3).

The area of the cooling tower outer wall

$$F = \pi \cdot (R + r) \cdot l = \pi \cdot (62,5 + 32,5) \cdot 120 = 35796 \text{ m}^2. \quad (4)$$

The heat gained by the cooling tower bulk due to the solar radiation:

$$Q_{1C} = K_g \cdot F_C \cdot \Delta t_C \cdot 10^{-3}, \quad (5)$$

where K_g is the coefficient of heat transfer through the transparent covering of the blackened cooling tower's wall, W/(m²·K);

F_C is the area of the blackened cooling tower wall irradiated by sun, m²;

Δt_C is the excess difference of temperatures characterizing the impact of solar radiation in summertime, °C.

The following values are taken for the calculation:

$$F_C = 0,5 \cdot F = 0,5 \cdot 35796 = 17896 \text{ m}^2;$$

$$\Delta t_C = 90 \text{ °C} - 20 \text{ °C} = 70 \text{ °C};$$

$$K_g = 3,56 \text{ W}/(\text{m}^2 \cdot \text{K}) \text{ (look above).}$$

Eventually, using the data given above, all heat flows (1), (2) and (5) can be calculated:

$$Q_{1C} = 4460,2 \text{ W}; Q_{1T} = 7391,2 \text{ W};$$

$$Q_1 = Q_{1T} + Q_{1C} = 11851,4 \text{ W}.$$

3.3. Wind in bottom layer

Analysis of the meteorological parameters in bottom layer shows that its vertical dimension depends on intensity of turbulent baffling: in summertime under the well developed turbulence in may reach 50-90 m., in winter it decreases to 10-20 m.

Under equilibrium stratification of atmosphere, the wind speed profile in bottom layer is described by the following proportion from Karman and Prandtl theory of turbulence:

$$V_2 = V_1 \cdot \frac{\ln(z_2 + z_0)}{\ln(z_1 + z_0)}, \quad (6)$$

where V_1 и V_2 is the wind speed at altitudes z_1 and z_2 ,
 z_0 – altitude, where the wind speed goes to zero.

Proportion of the wind speeds for vertical profile is the following [15]:

$$V_1 = V_2 \cdot \left(\frac{z_1}{z_2} \right)^m, \quad (7)$$

where

$$m = 0,6 \cdot V^{-0,77}. \quad (8)$$

The cooling tower block is blown by wind with speed V . Wind pressure ΔP_v , to the cover positioned in perpendicular to velocity vector \vec{V} is equal to:

$$\Delta P_v = 0,5 \cdot \rho \cdot V^2. \quad (9)$$

Taking into account compensation factors used due to the non-perpendicularity of velocity vector to the slipped area, the wind pressure equation (9) will be the following:

$$\Delta P_v = \frac{k_1 - k_2}{2} \cdot \frac{\rho \cdot V^2}{2} \cdot K, \quad (10)$$

where ρ – air density, kg/m^3 ;

k_1, k_2 – aerodynamic coefficients from the windward and wind protected sides of the cooling tower block respectively;

K – coefficient that accounts increase of the dynamic pressure by altitude.

Values of coefficient K in equation (10) are shown in Table 3.

Table 3. Values of coefficient K

Altitude, m	10	40	100	200
K	1,0	1,55	2,1	2,6

So, by increasing the altitude from 10 to 200 meters the wind dynamic pressure increases 2,6 times.

For example: according to the conditions of the Jonava area (Lithuania), the calculated wind speed at the 10 m altitude is 20,6 m/s. Normative wind ram at the 10 m altitude is 27,0 kg/m^2 . Medium wind speed at the said altitude is 4,9 m/s in January and 4,3 m/s in June.

3.4. Energetic usage of atmospheric flows at the altitudes more than 40 meters

The wind pressure at the altitudes more than 100 m is higher in comparison with the heights of the majority of small and medium scale wind turbines [9]. Therefore this feature of atmospheric air flows at the altitudes in range of 80-140 m can be applied for the generation of power. For the said purpose the wind turbines of various types can be positioned for power generation at the adequate point of ferroconcrete construction of the cooling tower. One of the possible solutions of single wind turbine positioning on the top of cooling tower is shown at Fig. 9. Positioning of several wind turbines on the top of cooling tower is shown at Fig. 10. Towers of the wind turbines installed in one line should have different heights in order to mitigate the obstruction of wind for the next turbine.

Positioning of wind turbines at the altitude $H \geq 100$ meters significantly increases its energetic potential. Simultaneously there is a decrease of ecological impact to the environment that is traditional in case of standard height of wind turbine's tower [9].

Increase of the wind power potential following the growth of wind pressure under the exploitation of wind turbine at high altitudes is illustrated by data of S. Kytra [14]. Dependence of the wind power capacity on the wind turbine's hub height is given in Table 4.

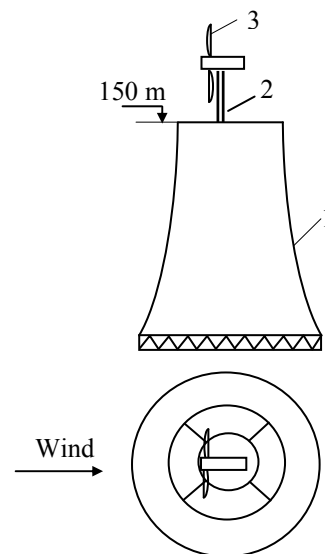


Fig. 9. Positioning of a single wind turbine on the top of cooling tower

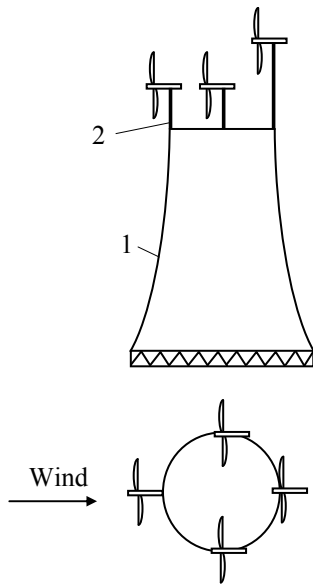


Fig. 10. Positioning of four small scale wind turbines on the top of cooling tower

Table 4. Dependence of the wind power capacity on the wind turbine's hub height and class of the locality's roughness [14]

Altitude, m	Parameters	Values of parameters depending on the locality's surface roughness			
		0	1	2	3
10	Wind speed, m/s	7,6	5,3	4,7	3,7
	Capacity, W/m ²	456	181	119	58
50	Wind speed, m/s	8,9	7,3	6,6	5,8
	Capacity, W/m ²	702	400	309	204
100	Wind speed, m/s	9,5	8,5	7,8	6,9
	Capacity, W/m ²	890	595	462	319

4. Conclusions

1. Constructions and parameters of large ferroconcrete cooling towers with natural draft are presented.
2. Possibilities of usage of the cooling tower for power generation by means of non-traditional power generating units were examined on the base of analysis of the aerodynamic situation in the cooling towers with natural draft.
3. Several options of small scale wind turbines positioning in the cooling tower with natural draft for electric energy production are proposed.

5. References

1. Гладков В.А., Арефьев Ю.И., Пономаренко В.С. Вентиляторные градирни // М.: Стройиздат, 1976. – 210 p.
2. Гончаров А.В. Натурные исследования башенной брызгальной градирни ТЭЦ Волжского автозавода // Известия ВНИИГ им. Б.Е. Веденеева, СПб, Том 236, 2000. – p.p. 242-247.
3. Israel Zúñiga-González. Modeling heat and mass transfer in cooling towers with natural convection. Summary of dissertation. Czech Technical University in Prague, faculty of mechanical engineering. Prague, 2005. – 23 p.
4. Hoffmann J.E., Kröger D.G. Analysis of heat mass and momentum transfer in the rain zone of a natural draft counter-flow cooling tower.// 7th COOLING TOWER AND SPRAYING POND SYMPOSIUM. Leningrad, USSR, May 29-June 2, 1990. – p.p. A10-(1÷8).
5. Grange J.L. A computer code for particular operating conditions of wet cooling tower// 7th COOLING TOWER AND SPRAYING POND SYMPOSIUM. Leningrad, USSR, May 29-June 2, 1990. – p.p. 8-(1÷11).
6. Пономаренко В.С., Арефьев Ю.И. Градирни промышленных и энергетических предприятий. Справочное пособие. // Под общей редакцией В.С. Пономаренко. М.: Энергоатомиздат. 1998. – 278 p.
7. Сухов Е.А., Шишов В.И. Труды ВНИИГ 2005г.
8. Kugelevičius J.A., Kuprys A., Kugelevičius J. Aplinkosauginių ir energetinių energijos gamybos rodiklių įvertinimai // Journal of Environmental Engineering and Landscape Management, 2005, Vol. XIII, №4. – p.p. 192a-199a.
9. Katinas V., Tumosa A. The possible usage of wind energy in Lithuania. Energy Agency, Directorate of the Energy Saving Programme, Kaunas, 1996. – 27 p.
10. Явнель Б.К. Курсовое и дипломное проектирование холодильных установок и систем кондиционирования воздуха. 3-е изд., переработанное и дополненное. М.: Агропромиздат, 1989. – 223 p.
11. <http://www.chv-praha.cz> (called on 02.02.2009)
12. <http://www.uniserv.com.pl> (called on 02.16.2009)
13. Федорович Л.А., Рыков А.П. Методика выбора тепломеханического оборудования ТЭС: Учебное пособие // М.: Издательский дом МЭИ, 2007. – 52 p.
14. Kytra S. Atsinaujinantys energijos šaltiniai. Kaunas, 2007. –140 p.
15. Безруких П.П., Стребков Д.С. Возобновляемая энергетика: стратегия, ресурсы, технологии. – М.: ГНУ ВИЭСХ, 2005. – 264 p.

APPLICATION OF RENEWABLE ENERGY SOURCES FOR FEEDING OF WATER RECYCLING SYSTEMS TECHNOLOGICAL EQUIPMENT

Michail G. BERENGARTEN*, Semyon I. VAINSHTAIN*, Aleksandr S. PUSHNOV*, Vytautas ADOMAVIČIUS**

*Moscow State University of Ecological Engineering, Russian Federation

** The Centre of Renewable Energy Technologies at Kaunas University of Technology, Lithuania

Abstract: The principal possibility to use non-traditional energy sources as a drive for water recycling systems technological equipment at large chemical enterprise is shown by example of the cooling tower with natural draft and cooling tower of type CK-400 having a single fan.

Keywords: Water recycling systems, renewable energy sources, PV power system, cooling towers with natural draft, cooling towers with fan.

1. Introduction

Water recycling systems of Russian Federation are using up to $160 \cdot 10^9$ m³ of recycled water. The said volume includes the usage of recycled water after cooling or purification. Up to $136 \cdot 10^9$ m³ of recycled water in Russia is used for cooling of various types of technological equipment. Let's examine the alternation dynamics of the whole volume of recycling and serial water supply in Russia and Belarus that is shown in Table 1.

Table 1. Total volume of recycling and serial water supply in Russia and Belarus [2]

Year	2000	2003	2004	2005
Russia, billions of cub. meters	133,5	135,6	135,0	135,5
Belarus, millions of cub. meters	6155	5842	6391	6369

Data on start-up of the recycling systems for the recycled water in Russia and Belarus are shown in Table 2.

Table 2. Start-up of the water recycling systems according to the data [2] (thousand of cub. meters a day)

Year	2000	2003	2004	2005
Russia	135	1130	786	1090
Belarus	0,05	163	8,4	0,5

Analyzing the data given in Table 2 we can to note that a significant feature of years 2003 and 2005 was a serious upgrade tendency in start-up of water recycling systems in Russian Federation. Supply of the recycled water by the industry branches according to the data [3] for the major Russian enterprises is shown in Table 3.

Table 3. Supply of the recycled water in major Russian enterprises

Industry	Supply of recycled water in major enterprises, thousands m ³ /hour	Temperature of recycled water °C	
		Cooling tower in	Cooling tower out
Oil refining industry	100	40...45	25-28
Chemical and petrochemical industry	100	40-45	25-30

Cooling of the recycled water at major enterprises of oil refining, petrochemical and chemical industries is realized at sectional and single fan cooling towers and also at cooling towers with natural draft.

The most part of energy consumption in recycling systems with fan cooling towers goes to the pumping equipment. In the fan type cooling towers energy is used also by fan drives.

The capacity of pumping and fan equipment of the cooling towers is shown in Table 4 according to the data given in reference [3].

The possibilities to use solar radiation by means of positioning of the photovoltaic (PV) modules mounted on the cooling tower's wall in order to produce electric energy are analyzed below.

The electricity produced by the photovoltaic power system can be used for baking up the main power source – electric grid. Consumption of electricity from the grid for feeding of fan and pump equipment of the tower could be reduced in this case. The best option in this case would be to install the grid-connected photovoltaic power system.

Table 4. Features of cooling tower fans

Fan mark	Electric drive capacity, kW	Rotation frequency, min ⁻¹
3VG25 (Russia)	11	365
2VG50 (Russia)	30	178
2VG70 (Russia)	75	178
1VG104 (Russia)	200	110
HEMA (Germany) fan diameter: 10,4 м	250	91
Balke (Germany) fan diameter: 10,4 м 20,0 м	250 800	127 65
06-300 № 8 (Russia)	3	1410
06-300 № 10 (Russia)	3	950
06-300 № 12,5 (Russia)	4	730

2. Fan cooling towers

Single fan cooling tower of type CK-400 have the largest area of the outer tower wall among the fan cooling towers. General view of such cooling tower and its scheme are shown at Fig. 1 and Fig. 2.

The scheme of possible positioning of the PV modules on the tower wall is shown at Fig. 3. In case of using efficient PV modules, the PV power system could supply over 100 kW power when sun is shining. This amount of power would be sufficient for running of some fans (Table 4) and would cover considerable part of power necessary for the most powerful fans.

It is appreciable that application of PV power systems is limited by weather conditions. But taking into account the fact that the hottest period of the year is also the most extreme one for exploitation of the cooling tower such an alternative to traditional energy sources may be rational in some situations. In any case, the use of PV power systems can help to reduce the load to traditional sources of power energy.



Fig. 1. Group of CK-400 cooling towers

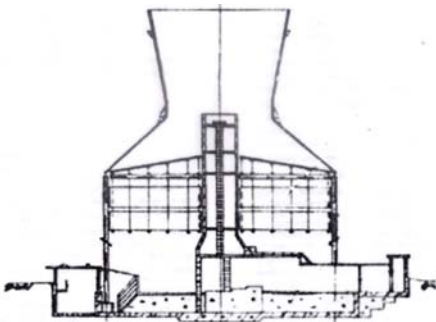


Fig. 2. Scheme of CK-400 cooling tower

3. Cooling towers with natural draft

The wall of cooling tower in some cases may become a perspective construction to mount the PV modules. The scheme of possible lining of PV modules on eastern and south sides of the tower wall is shown at Fig. 4. In this case up to 50 % of total tower wall area may be used for mounting of PV modules.

If half of the cooling tower (diameter – 125 meters, height – 150 meters) would be covered by the PV modules, the capacity of PV power system could make up about 1 000 kW. As it is shown at Fig. 4, axes of symmetry of all mounted PV modules are oriented vertically in alignment to the cooling tower axe of symmetry.

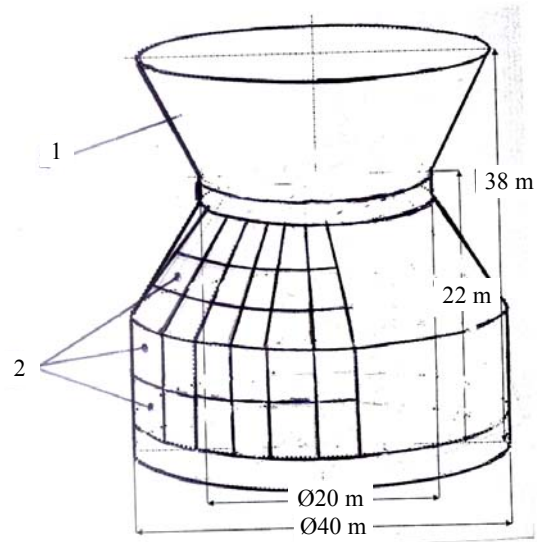


Fig.3. Scheme of positioning of solar collectors on the wall of CK-400 single fan cooling tower: 1 – the cooling tower wall; 2 – PV modules

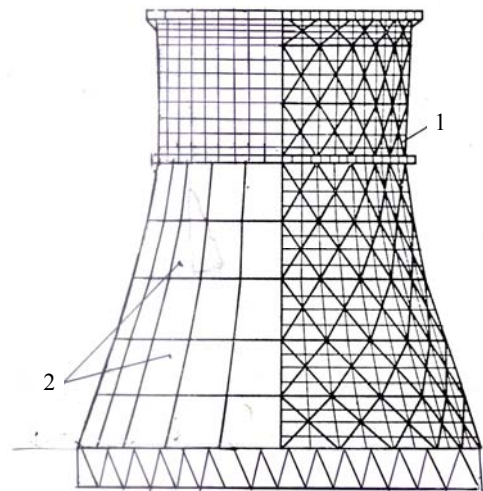


Fig. 4. Positioning of PV modules on the wall of reverse-flow cooling tower: 1 – the cooling tower wall; 2 – PV modules

The parabolic concentrators that are positioned on the outer cover of cooling tower in several decks by height also may be used there for increasing of efficiency. Analysis of operation of the parabolic-cylinder concentrators of solar radiation was made.

Symmetrical parabolic concentrator was made in Russian institute of agriculture electrification with application of technologies based on the principles of non-image forming optics. The unit belongs to the class of solar radiation reflecting concentrators. The concentrator may be defined as parabolic architecture formed by two parabolic curves branches – reflector. Usage of solar collectors positioned on the wall of tower provides the electric energy supply for operation needs of technological systems of industrial

enterprises. In focal sphere of the reflector there is positioned a solar module with double-sided working cover that consist commutated double-sided solar elements. The face side of module can reflect either non-concentrated or concentrated solar radiation in dependence on the angle between mid-plane of concentrator and Sun height. The wire side reflects concentrated flow of solar irradiation resulted by multi-reflection from the concentrator’s reflecting square.

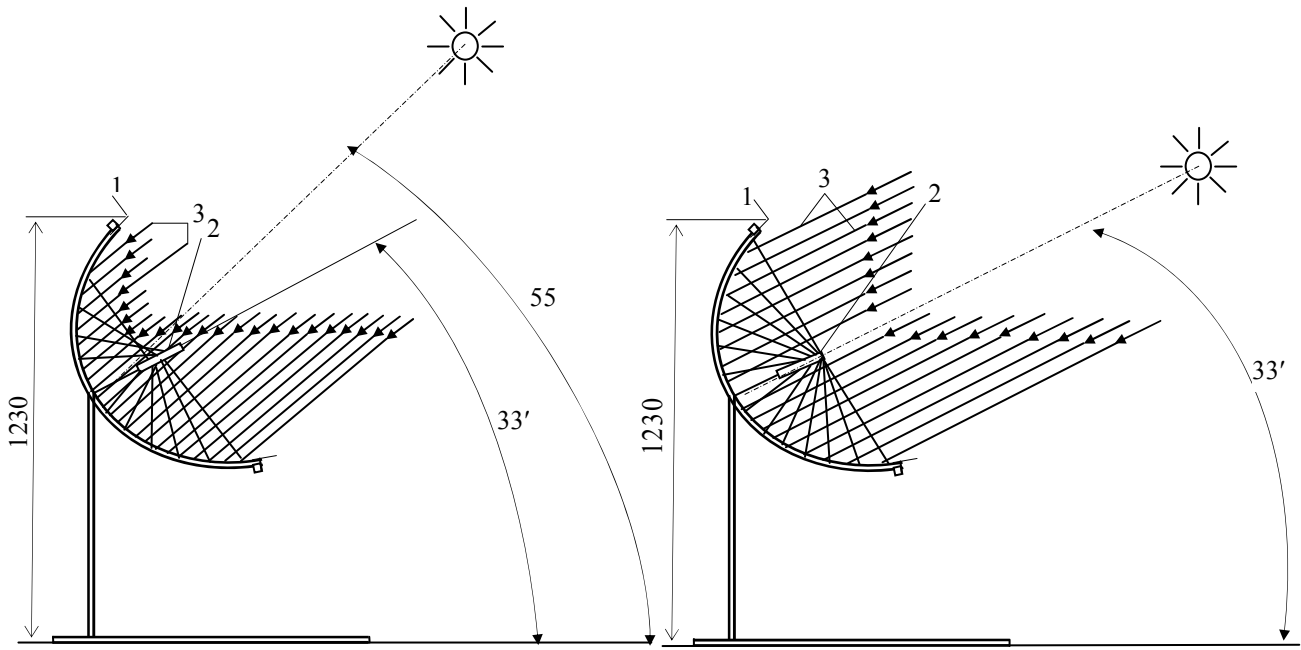


Fig. 5 Scheme of solar module operating activity with symmetric parabola-cylinder concentrator in stationary position under various Sun height: a) midday, June 1st, b) midday March 16 or 8.30 and 16.30, Moscow latitude; 1 – symmetric concentrating reflector; 2 – double-sided photoelectric module; 3 – solar rays path.

During the experiments conducted in cooperation with Russian institute of agriculture electrification the work of solar unit under various sun heights was modeled by changing of the plain angle in relation to horizon plain. The modeling sun height was:

$$h_m = h_0 + (90^\circ - \beta), \quad (1)$$

where $h_0 = \beta - \alpha$, (look Fig. 6);

α is angle of concentrator’s middle plain positioning in relation to solar rays path, angle grade;

β is angle of concentrator’s middle plain positioning in relation to horizon plain, angle grade;

h_m is modeling sun height, angle grade;

h_0 is actual sun height, angle grade.

Accounting the said above:

$$h_m = \beta - \alpha + (90^\circ - \beta) = 90 - \alpha \quad (2)$$

Position of solar unit symmetric parabolic-cylinder concentrator’s middle plain in relation to horizon plain is shown at Fig. 7.

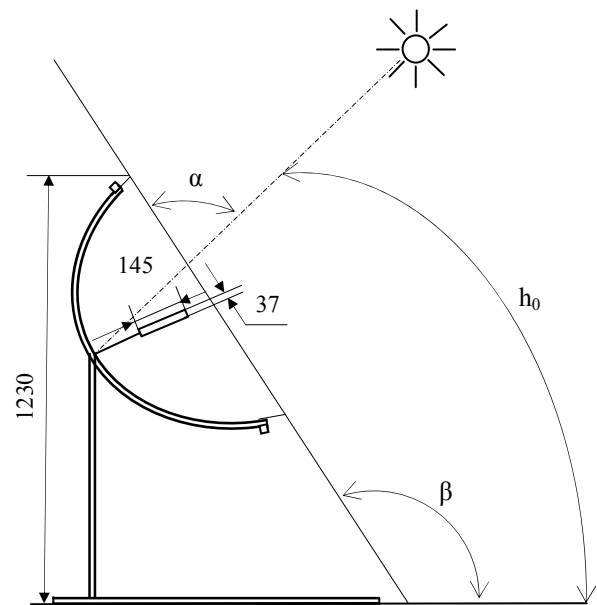


Fig. 6. Basic vertical position of the concentrator’s middle plain in relation to horizon plain

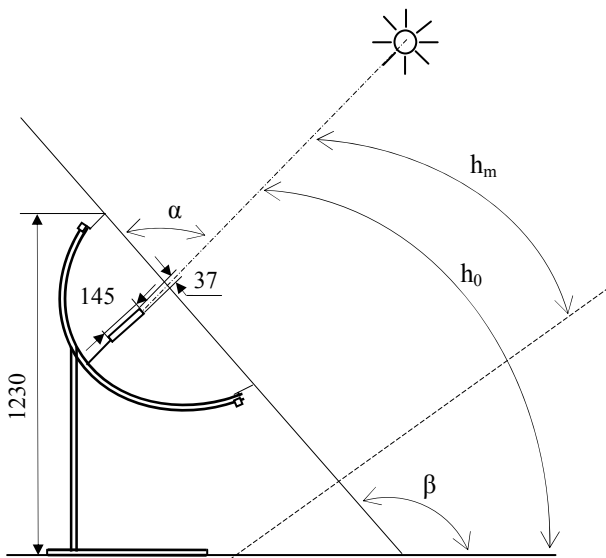


Fig. 7. Change of the concentrator's middle plain position in relation to horizon plain under experimental modeling of various sun heights

Electrical parameters of the solar unit were determined by design way under data got in Russian Institute of agriculture electrification in condition of natural solar radiation.

Overall geometry of the unit: $1.25 \times 0.73 \times 1.23 \text{ m}^3$, overall geometry of the solar module double glass – $1.2 \times 0.145 \times 0.037 \text{ m}^3$.

Design value of aperture angle of asymmetric parabolic concentrator unit $A = \pm 24$ angle grades.

Ability of the said concentrators to use the diffused radiation is in interest. So there were taken off the data in absence of direct solar rays. In this experiment there was applied solar module with solar elements with double-sided working surface. The research was guided separately with every side of solar module with opposite side closed.

The current-voltage characteristic of solar module with transverse width 0,145 m under $\alpha = 78$ angle grade is represented at Fig. 8.

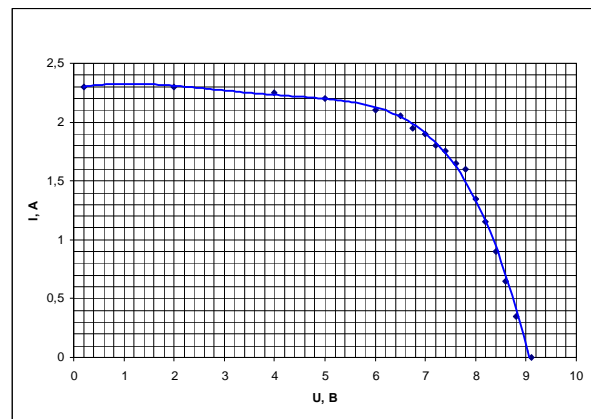


Fig. 8. Current-voltage characteristic of solar module with concentrator under $\alpha = 78$ angle grade

4. Conclusions

1. Application of PV modules positioned on the face side of cooling tower provides electricity supply for technological equipment of industrial water recycling.
2. Parabolic concentrators that are positioned on the outer cover of cooling tower in several decks by height also may be used there for efficiency increasing.

5. References

1. Рябушенко А.С. Градирни в системах обратного водоснабжения промышленных предприятий // Химическая техника. 2004, №10, С. 31-33.
2. Pushnov A., Berengarten M., Ryabushenko A. Influence of Aerodynamic Conditions I Cooling Tower or Losses of Water in System of Defensive Water in System of Defensive Water Supply. May 22-23, 2008. The 7-th International Conference Environmental Engineering, VGTU Press "Technika". - Vilnius, 2008. - P.290-296.
3. Пономаренко В.С., Арефьев Ю.И. Градирни промышленных и энергетических предприятий: Справочное пособие / Под общей редакцией В.С. Пономаренко. - М.: Энергоатомиздат, 1998. - 376с.

WIND POWER PLANT WITH REDOX FLOW BATTERY INVERTER – SYSTEM CONVERTER ENERGY CONVERSION PROCESSES RESEARCH

Povilas BALČIŪNAS, Povilas NORKEVIČIUS

Kaunas University of Technology, Faculty of Electrical and Control Engineering,
 Department of Electric Power Systems, The Centre of Renewable Energy Technologies, Lithuania

Abstract: Inverter-system converter (ISC) steady state and transitional character energy conversion processes of wind power plant with redox flow battery (RFB) are researched. Low intensity wind energy potential resources are fairly high in Lithuania. Such intensity wind energy potential can be better used installing ISC at wind power plants. RFB unique features and characteristics provide additional opportunity to store wind power plant generated stochastic character electrical energy effectively. Research data is used to create ISC prototype for wind power plant with vertical shaft.

Keywords: wind power plant, redox flow battery, inverter – system converter, energy, steady state, transient, conversion processes.

1. Introduction

Nowadays low intensity wind energy potential usage at wind power plants is problematic [4]. Successfully solved such problem and additionally effectively stored stochastic character electrical energy at RFB [1, 2] would create advantageous possibility to use existing long – term low intensity wind energy potential at Lithuania in significantly effective method. Possibility of innovative conception usage is researched for such problem solution. Here voltage system ($U=\text{const}$, $I=\text{var}$.) stochastic character electrical energy is converted to dual current system ($I=\text{const}$., $U=\text{var}$.) energy [3]. This concept practically has to be implemented by installing additional electrical energy conversion module – semiconductor inverter – system converter at wind power plant with synchronous generator structure. Such ISC steady state and transient operation modes research results are presented in this paper.

2. Wind power plant with RFB and ISC structure and features

Modified wind power plant structure with new features and functional possibilities is showed in Fig. 1. Vertical

shaft with sail wing type turbine WT rotates permanent magnet excitation system synchronous three phase generator SG. Generated stochastic character voltage system ($U=\text{const}$., $I=\text{var}$.) electrical energy is rectified by AC/DC inverter and transmitted to semiconductor ISC.

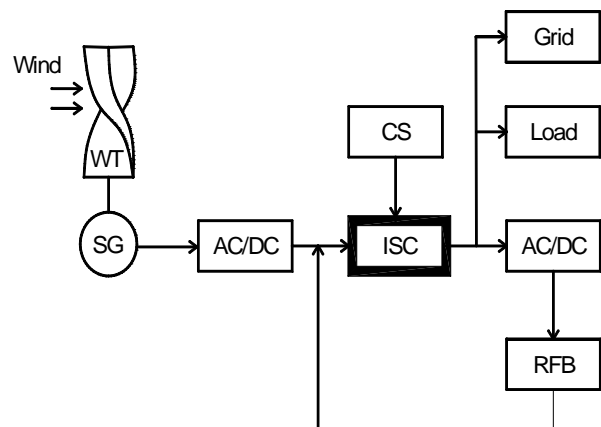


Fig. 1. Wind power plant with ISC and RFB electrical energy conversion structural scheme

Voltage system DC electrical energy of rectifier AC/DC is converted to AC dual system ($I=\text{const}$., $U=\text{var}$.) electrical energy at ISC. AC dual system ($I=\text{const}$., $U=\text{var}$.) electrical energy frequency f and phase φ is controlled by ISC control system CS.

Converted current system AC electrical energy can be used autonomously and for charging RFB through additional AC/DC rectifier simultaneously. Then stabilized AC voltage system energy is transmitted to autonomous load.

RFB can be connected to ISC input and transmit electrical energy to load continuously when wind turbine does not operate.

Modified wind power plant can be connected to grid and transmit electrical energy to load and grid. In this case Redox flow battery is disconnected. Wind energy

potential is used at the maximum when wind power plant operates autonomously or connected to the grid.

3. Steady state energy conversion processes simulation results

Simplified structural scheme for ISC energy conversion processes research is showed at Fig. 2.

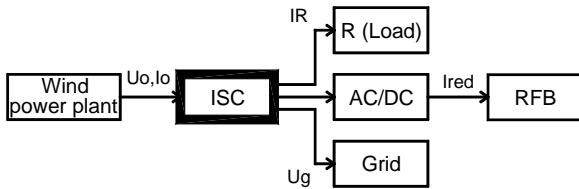


Fig. 2. Structural scheme of ISC energy conversion processes research

Energy conversion processes simulation is performed when ISC output is connected to active load R or grid or through AC/DC converter to RFB. Here I_o , U_o – wind power plant generated current and voltage, I_R – active load R current, I_{red} – RFB current, U_g – grid voltage is showed at Fig. 2.

Energy conversion processes simulation is performed with „MATLAB, Simulink“ software [5]. Simulation model is showed at Fig. 3.

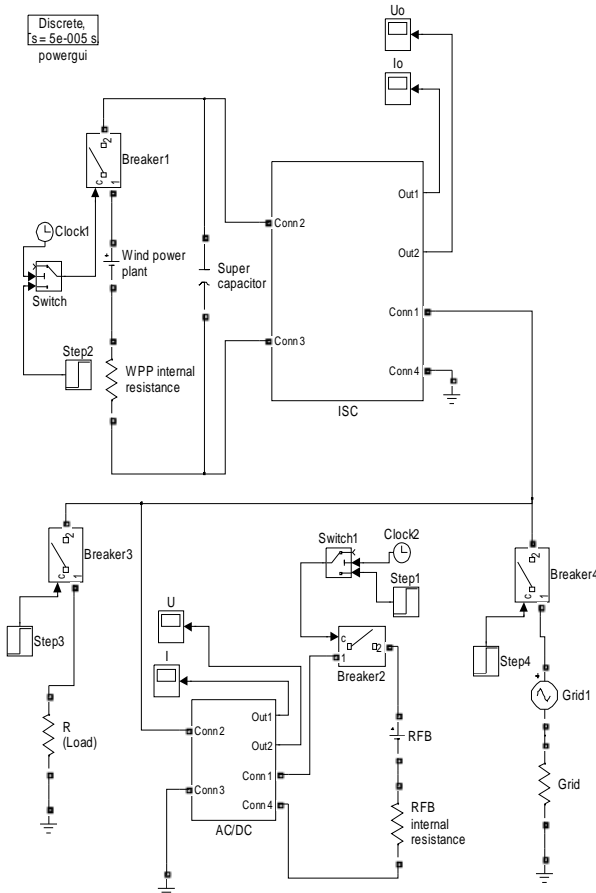


Fig. 3. ISC energy conversion processes simulation model

Wind power plant and RFB is simulated as DC voltage system source with internal active resistance block, ISC

and AC/DC inverter is simulated as subsystem block, load R as active resistance block, grid as AC source with internal active resistance block, currents and voltages are measured with I_o , U_o , I, U blocks.

Implemented super capacitor is used for excessive electrical energy storage from ISC semiconductors elements during transient processes.

ISC steady state energy conversion processes simulation with connected RFB is performed changing wind power plant generated voltage U_o from 5V to 120 V. RFB rated voltage is 230 V.

ISC steady state energy conversion processes simulation with connected R is performed changing R from 10 Ω to 500 Ω and U_o levels at 5 V, 24 V, 60 V.

ISC steady state energy conversion processes simulation with connected grid is performed changing U_o from 5 V to 120 V.

After steady state processes simulation of ISC with connected RFB performance I_{red} , $I_o = f(U_o)$, $\eta = f(U_o)$ dependences are compiled which showed at Fig. 4. and Fig. 5.

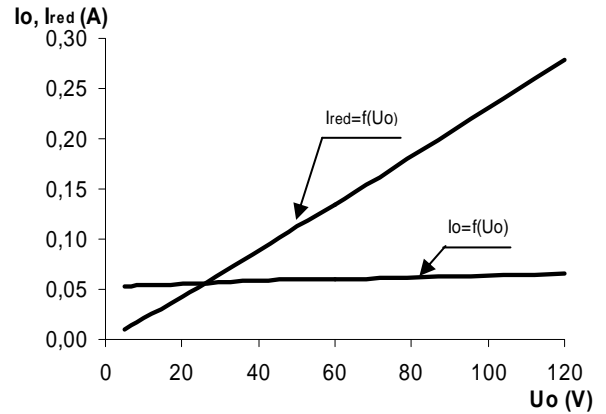


Fig. 4. Wind power plant generated current I_o , RFB charging current I_{red} dependence on wind power plant generated voltage U_o , I_{red} , $I_o = f(U_o)$

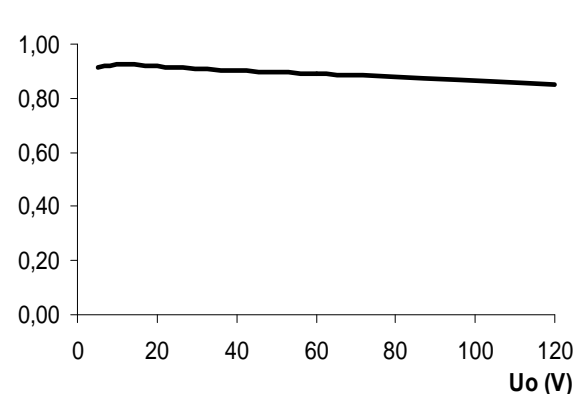


Fig. 5. ISC efficiency factor η dependence on wind power plant generated U_o voltage, $\eta = f(U_o)$

Fig. 4. shows that innovative ISC unique energy conversion characteristic allow to use low intensity wind energy potential. RFB charging process is possible

when wind power plant generated U_o is equal to any value.

Current I_{RED} increases linearly when wind power plant generated U_o increases. Here RFB charging duration is shorter when U_o increases. Wind power plant generated current I_o value does not depend on variation of voltage U_o from 5V to 120V. This dependence character shows that ISC converts wind power plant generated voltage system energy ($U=const., I=var.$) to dual current system ($U=var., I=const.$) energy.

Fig. 4 shows ISC efficiency factor η dependence on wind power plant generated voltage U_o character. ISC high efficiency factor η value is near 0,9 and decreasing insignificantly when voltage U_o increasing. Simulation results shows that ISC has low effect on wind power plant energy conversion structure efficiency.

After steady state processes simulation of ISC with connected R performance $I_R=f(R), \eta=f(R)$ dependences are compiled which showed at Fig. 6. and Fig. 7.

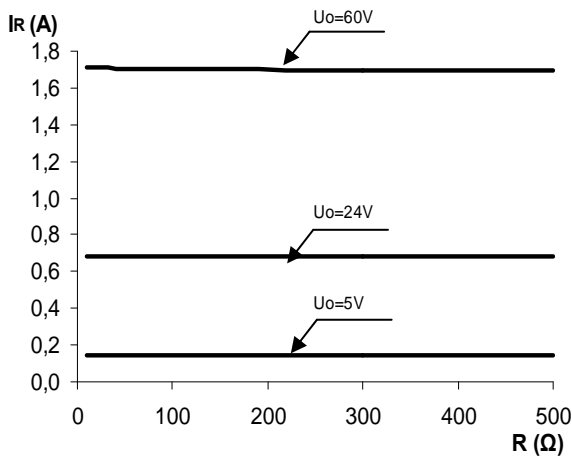


Fig. 6. Load current I_R dependence on load $R, I_R=f(R)$ at wind power plant generated different voltage U_o levels

Fig. 6 shows that ISC output has dual current system ($U=var., I=const.$) character. ISC converted current I_R has high stability factor. I_R character does not depend on R, U_o values when U_o varies 12 times and R 50 times. I_R stability factor γ when load varies from 10 Ω to 500 Ω when $U_o=5$ V, $\gamma=\pm 2$ %; $U_o=24$ V, $\gamma=\pm 5,8$ %, $U_o=60$ V, $\gamma=\pm 5,8$ %.

Fig. 7 shows that ISC operations is most effective when load R values is higher than 50 Ω and wind power plant generated voltage U_o value is higher than 24 V. ISC efficiency factor is high when load is varying at wide range.

Steady state energy conversion processes results shows that RFB connected to ISC input could determine autonomous load R RMS voltage value by selecting RFB rated voltage. R voltage can be steady when R value is changing.

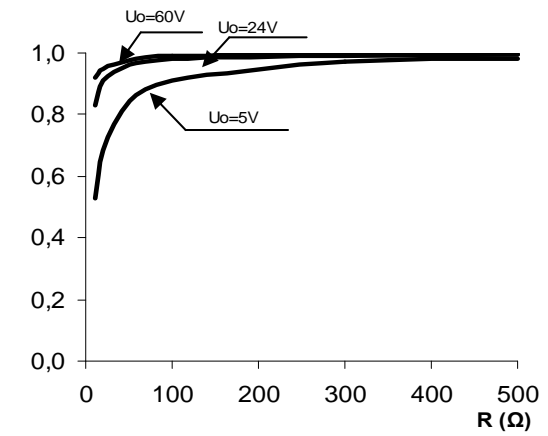


Fig.7. ISC efficiency factor η dependence on load $R, \eta=f(R)$ at wind power plant generated different voltage U_o levels.

Grid voltage U_g dependence on wind power plant voltage $U_o, U_g=f(U_o)$ is showed in Fig. 8. Stochastic character wind power can be steadily transmitted to grid after ISC and grid frequency f and phase ϕ synchronization when grid voltage U_g is equal to standard grid voltage RMS values ($U_g=230$ V; 400 V).

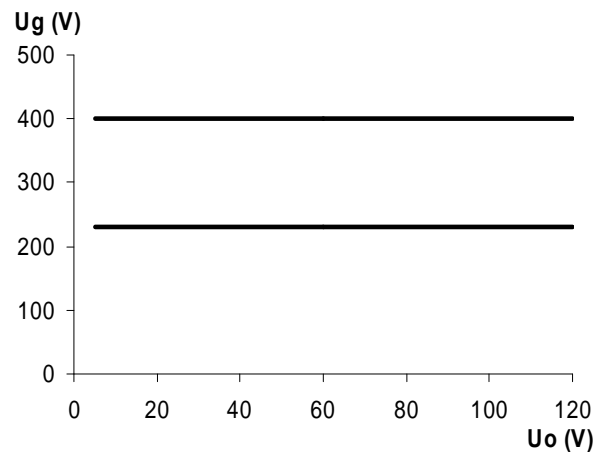


Fig. 8. Grid voltage U_g dependence on wind power plant voltage $U_o, U_g=f(U_o)$

4. Transient energy conversion processes simulation results

Transient process energy conversion simulation results are showed at Fig. 9, Fig. 10, Fig. 11, Fig. 12, when RFB permanently connected to ISC and wind power plant is connected at 1s of simulation time. RFB rated voltage is 230 V.

ISC reactive element voltage U_{Reak} dependence on time $t, U_{Reak}=f(t)$, when wind power plant is connected to ISC at rated DC voltage $U_{oR}=24$ V is showed at Fig. 9. and when wind power plant is connected to ISC at voltage $U_o=12$ V ($U_o=0,5U_{oR}$) is showed at Fig. 10.

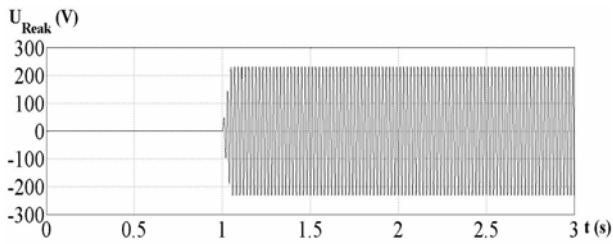


Fig. 9. ISC reactive element voltage U_{Reak} dependence on time t , $U_{Reak}=f(t)$, when connected wind power plant rated voltage $U_{oR}=24V$

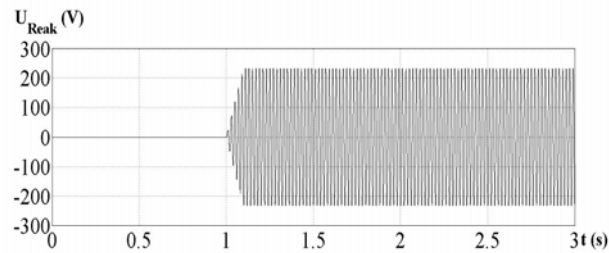


Fig. 10. ISC reactive element voltage U_{Reak} dependence on time t , $U_{Reak}=f(t)$, when connected wind power plant voltage $U_o=12V$

Peak value $U_{reakm}=231,7 V$ of steady state process when wind power plant rated voltage is U_{oR} and $U_{reakm}=230,6 V$ at $0,5U_{oR}$.

Peak value of transient process U_{om} is 0,8 times less than steady state value U_{Reak} at $0,5U_{oR}$ and U_{oR} . U_{reak} transient process duration at $0,5U_{oR}$ is 1,6 times longer than at U_{oR} .

ISC semiconductor element current I_{T1} dependence on time t , $I_{T1}=f(t)$, when wind power plant is connected to ISC at rated voltage $U_{oR}=24V$ is showed at Fig. 11 and when wind power plant is connected at $0,5U_{oR}$ is showed at Fig. 12.

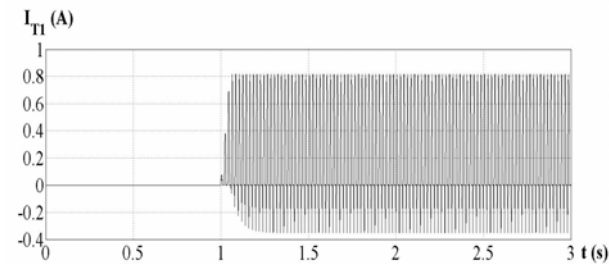


Fig. 11. ISC semiconductor element current I_{T1} dependence on time t , $I_{T1}=f(t)$, when connected wind power plant rated voltage $U_{oR}=24V$

Peak value $I_{T1m}=0,82 A$ of steady state process when wind power plant rated voltage is U_{oR} and $I_{T1m}=0,79 A$ at $0,5U_{oR}$.

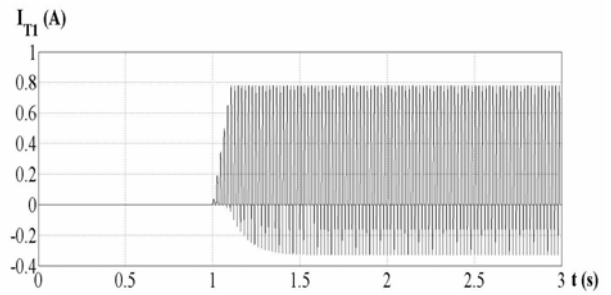


Fig. 12. ISC semiconductor element current I_{T1} dependence on time t , $I_{T1}=f(t)$, when connected wind power plant rated voltage $U_o=12V$

Peak value of transient process I_{T1m} is 1,2 times less than steady state value U_{reakm} at $0,5U_{oR}$ and U_{oR} .

I_{T1} transient process duration at $0,5U_{oR}$ is 1,8 times longer than at U_{oR} .

At Fig. 13., Fig. 14. Fig. 15., Fig. 16 is showed simulation results when specified value load $R=338 \Omega$ is permanently connected to ISC output and wind power plant is connected at 1s of simulation time. Here load R steady state effective voltage is standard value and equal to 230 V , wind power plant generated rated voltage $U_{oR}=24 V$.

ISC reactive element voltage U_{Reak} dependence on time t , $U_{Reak}=f(t)$, when wind power plant is connected to ISC at rated voltage $U_{oR}=24V$ is showed at Fig. 13. and when wind power plant is connected to ISC at voltage $U_o=12V$ ($U_o=0,5U_{oR}$) is showed at Fig. 14.

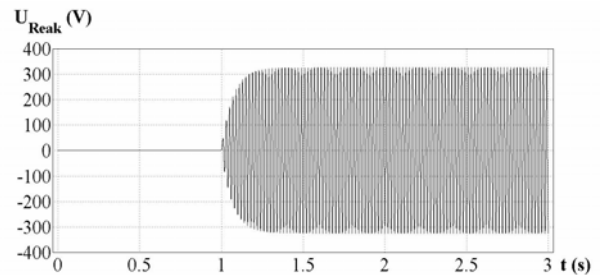


Fig. 13. ISC reactive element voltage U_{Reak} dependence on time t , $U_{Reak}=f(t)$, when connected wind power plant rated voltage $U_{oR}=24V$

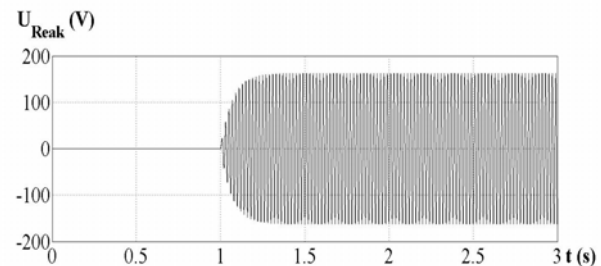


Fig. 14. ISC reactive element voltage U_{Reak} dependence on time t , $U_{Reak}=f(t)$, when connected wind power plant rated voltage $U_o=12V$

Fig. 13., Fig. 14., shows that U_{reak} transient process duration does not depend on wind power plant generated voltage U_o .

ISC semiconductor element current I_{T1} dependence on time t , $I_{T1}=f(t)$, when wind power plant is connected to

ISC at rated voltage $U_{oR}=24V$ is showed at Fig. 15 and when wind power plant is connected at $0,5U_{oR}$ is showed at Fig. 16.

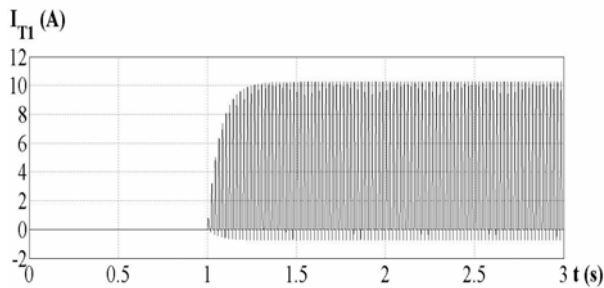


Fig. 15. ISC semiconductor element current I_{T1} dependence on time t , $I_{T1}=f(t)$, when connected wind power plant rated voltage $U_{oR}=24V$

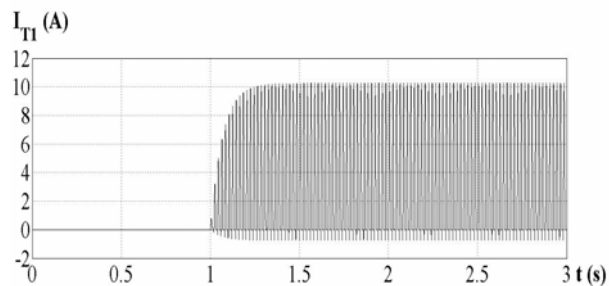


Fig. 16. ISC semiconductor element current I_{T1} dependence on time t , $I_{T1}=f(t)$, when connected wind power plant rated voltage $U_o=12V$

Fig. 15., Fig. 16., shows that I_{T1} transient process duration does not depend on wind power plant generated voltage U_o .

Fig. 13., Fig. 14. Fig. 15., Fig. 16 shows that transient process U_{reakm} , I_{T1m} values increases exponentially to steady state values independently on wind power plant generated voltage U_o value.

5. Conclusions

1. Research results confirmed voltage system ($U=const.$, $I=var.$) electrical energy conversion possibility to current system ($U=var.$, $I=const.$) electrical energy. Converter operates at inverter – system converter mode.
2. Wind energy generated voltage value variation has low effect on ISC efficiency factor at wind power plant with RFB.
3. Stochastic character wind power can be steadily transmitted to grid after ISC and grid frequency f and phase φ synchronization when grid voltage U_g is equal to standard grid voltage RMS values ($U_g=230 V$; $400 V$). Electrical energy steadily is transmitted to grid when U_o variation range is $-5 - 100\%$.
4. ISC can operate autonomously. In this case RFB have to be connected to ISC for energy storage. RFB set autonomous load AC voltage effective value.
5. Energy conversion processes results shows that RFB connected to ISC input could determine

autonomous load R RMS voltage value by selecting RFB rated voltage. R AC voltage can be steady when R value is changing.

6. ISC operation is steady when it operates autonomously or connected with grid. Electrical energy is transmitted steadily and uninterruptedly to grid or load when wind power plant voltage U_o varies at wide range.
7. ISC reactive element voltage peak value of transient process U_{om} is 0,8 times less than steady state value U_{Reak} at $0,5U_{oR}$ and U_{oR} . U_{reak} transient process duration at $0,5U_{oR}$ is 1,6 times longer than at U_{oR} when RFB is permanently connected and wind power plant connection performed to ISC.
8. ISC semiconductor current peak value of transient process I_{T1m} is 1,2 times less than steady state value U_{Reakm} at $0,5U_{oR}$ and U_{oR} . I_{T1} transient process duration at $0,5U_{oR}$ is 1,8 times longer than at U_{oR} when RFB is permanently connected and wind power plant connection performed to ISC.
9. ISC reactive element voltage and semiconductor current peak values of transient process increases exponentially to steady state values when ISC is connected to load R and wind power plant generated voltage varies from U_{oR} to $0,5 U_{oR}$.
10. Semiconductor element current I_{T1} and reactive element voltage U_{Reak} transient process duration does not depend on wind power plant generated voltage variation from U_{oR} to $0,5 U_{oR}$ when R is permanently connected and wind power plant connection performed to ISC.

6. Research results estimation and perspective activity

1. ISC energy conversion steady state, transient process analysis is presented at this paper.
2. ISC possible operation modes control algorithm has to be created for prototype model transient processes optimization.
3. ISC structure has to be optimized for transient process negative effect reduction on researched ISC structure elements.
4. ISC prototype model has to be created for theoretical research results adequacy verification.

7. References

1. P. Balčiūnas, P. Norkevičius. Wind micro power plant with redox flow battery conversion processes research. Energetika. 2009. Nr.1
2. Cigre technical brochure on modelling new forms of generation and storage. 2000. 139 p.
3. P. Balčiūnas. Aukšto dažnio įtampos – srovės galios keitiklių teorijos sintezė (monografija). Kaunas. Technologija. 1994. 272p.
4. C. Abbey, J. Chahwan, M.Gattrell, G.Joos. Transient modelling and simulation of wind turbine generator and storage systems. 21,rue d'Artois, F-75008 PARIS.
5. SIMULINK. Model-Based and System-Based Design. 2001. 846p.

HYBRID WATER HEATING SYSTEM BASED ON SOLAR COLLECTORS AND HEAT EXCHANGER FED FROM THE CENTRALISED HEAT SUPPLY GRID

Vytautas ADOMAVIČIUS*, Gytis PETRAUSKAS**

* The Centre for Renewable Energy Technologies at Kaunas University of Technology, Lithuania

** Department of Control Technology at Kaunas University of Technology, Lithuania

Abstract: Water heating is widely spread technology used for domestic and industrial purposes. Presently water heating is still based mostly on the fossil fuels although mature and cost-effective technologies running on the renewable energy sources already exist for this purpose. Water heating systems can run on renewables purely or partially. This paper describes concept of hybrid water heating systems based on solar collectors and heat exchanger fed from centralized heat supply grid, structure and sizing of the proposed system and principles for control of solar collectors.

Keywords: renewable energy, solar energy, solar collectors, water heating, hybrid systems.

1. Introduction

The last dramatic events in the crude oil market in 2008 when oil price increased up to 147 USD per barrel and in the natural gas market on the beginning of 2009 when Russia cut its gas supply for more than three weeks to many European countries have evidently proved the necessity to shift on more reliable and more predictable sources of energy in scale as large as possible and reasonable. First of all it could be the non-polluting renewable and other available local energy sources.

Water heating is widely spread technology used in the domestic sector and for the industrial applications including many small and medium enterprises. Considerable amounts of energy are used for this purpose. Presently water heating installations mostly are running on the fossil fuels or sometimes on electricity, which mainly is based on the fossil fuels as well. Substitution of the fossil fuels currently used for water heating could give the well-known benefits: increased energetic independence due to the reduction of imported fossil fuels, creation of more jobs and stimulation of local economic development, positive impact on mitigation of climate change and some other.

A huge and rather easily realizable potential for water heating by means of the renewable energy usage instead of fossil fuels exists in Lithuania and other countries all over the world. Solar collectors are one of the best

options for water heating due to solar energy universal availability and mature of this technology. However, as it is known, this source of renewable energy has one considerable disadvantage: energy of solar radiation is not constant over the time. Combined (hybrid) water heating systems can be used in order to compensate this shortage. They can be purely renewable or mixed when another water heater is based on the fossil fuel. There are many various sources of energy to choose for backing-up the solar collectors: wind [1], biomass, fossil fuels, centralized heat, electricity and other.

2. Concept of hybrid water heating systems based on solar collectors and backed-up on centralised heat

Often it is reasonable and convenient to use the water heating systems, which already exist in condominiums, enterprises or other users of hot water, and to combine it with solar collectors. The solar collectors could allow cutting bills for heat energy significantly.

As it is shown in Fig. 1, solar irradiation is not distributed evenly over the year in Lithuania. Therefore only in summer months solar collectors could cover all demands of hot water. In late autumn, winter and early spring the main producer of hot water will be the existing water heating appliances, which will cover shortage of solar energy in this period of year. Input of solar collectors then will not be significant (Fig. 1).

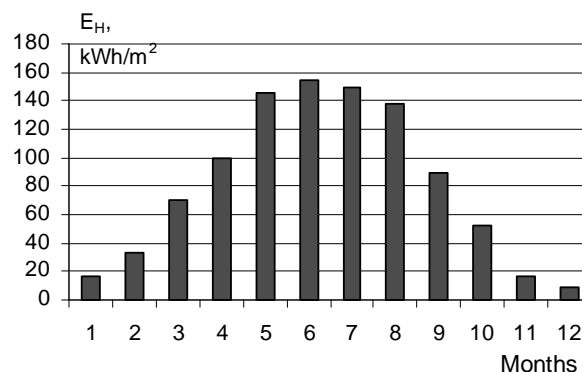


Fig. 1. Distribution of solar irradiation in horizontal plane over the year in Kaunas, Lithuania

Presently water heating systems running on centralized heat or natural gas prevail in cities and towns of Lithuania and other countries of Central and East Europe. In Lithuania water heating systems fed from the centralized heat supply grid are used mostly. Currently one type of hybrid water heating systems with solar collectors already exists. Solar collectors there are backed-up by means of electric water heaters [2]. However, electric energy is considerably more

expensive in comparison with energy from centralized heat supply grid. Therefore in many cases the best solution could be the hybrid water heating system based on solar collectors and the existing heat exchanger fed from the centralized heat supply grid. Structural scheme (Fig. 2) and description of this hybrid water heating system based on solar collectors and centralized heat source are presented below.

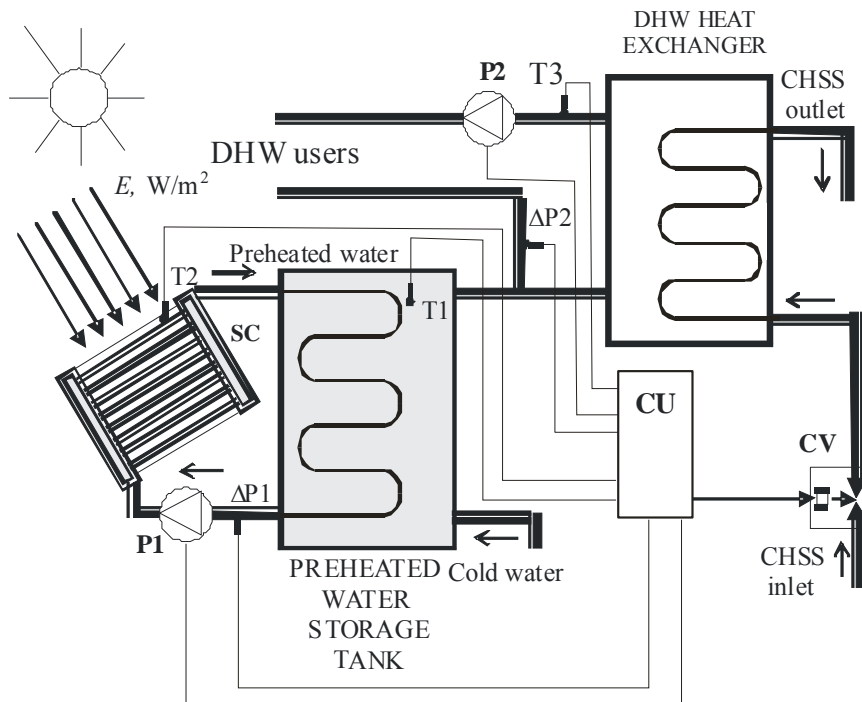


Fig. 2. Structure of hybrid water heating system based on solar collectors and centralized heat supply grid

3. Structure of the proposed hybrid water heating system

As it is shown in Fig. 2, the proposed hybrid water heating system is based on the solar collectors and the heat exchanger fed from the centralized heat supply grid. The system consist of the solar collectors SC, the preheated water storage tank, the collector pump P1, the sensors of temperature T1, T2 and T3, the ethylene glycol pressure switcher $\Delta P1$ and the DHW (domestic hot water) pressure switcher $\Delta P2$, the DHW pump P2, the DHW exchanger, the controlled valve CV and the control unit CU (integrated in to the building's management system). As a contemporary CU could be recommended the DDC4000 group controllers. It is a CU, which is used in building service systems for measuring, regulating, controlling, optimizing and monitoring. It is based on a 32-bit processor and functions according to the multitask principle. Its operating system is Linux. DDC4000 CU communicates via Ethernet (TCP/IP, BACnet). The DDC4000 is equipped with object oriented software and hardware modules, making available a large number of functions,

which can be activated and customized online without the need for additional tools.

In sunny days major part of heat energy, which is necessary for water heating up to the standard temperature (for example, 50-55 °C), will produce solar collectors.

If temperatures of water measured with thermometer T1 will be below the standard level, the DHW heat exchanger will boost it up to the necessary value according to the set up programme. In cloudy and dark days, especially in winter months, solar collectors SC will not develop sufficient heat capacity and therefore the main energy source for water heating will be the centralized heat supply grid.

Implementation of this hybrid water heating system would eliminate blackouts of hot water supply in every summer when heat energy from the centralized grid is cut due to the repairs in the grid. User's hated "snake" tax for the serpentine pipe, which heats bathrooms, would be eliminated in summer months as well and would be reduced in other months.

Efficiency and cost-effectiveness of the described water heating system are the most important targets to be achieved during the process of its implementation.

Successful achievement of these targets mainly depends on the following key factors:

- Type of chosen solar collectors,
- Correct sizing of the system,
- Correct (optimal) control of the system.

Vacuumed tubular or flat solar collectors can be chosen as the main heat suppliers for summer months. Industry currently produces both of them. However, superiority of the vacuumed tubular solar collectors is proven and well-known. Comparison of efficiency of vacuumed tubular solar collectors against flat collectors is presented in Fig. 3. As it can be seen on this figure, the vacuumed tubular solar collectors are approximately from 1.5 (in summer months) up to 3 (in winter months) times more efficient than the flat ones. Therefore it is recommended to use vacuumed tubular solar collectors in order to get better efficiency of solar energy conversion into heat.

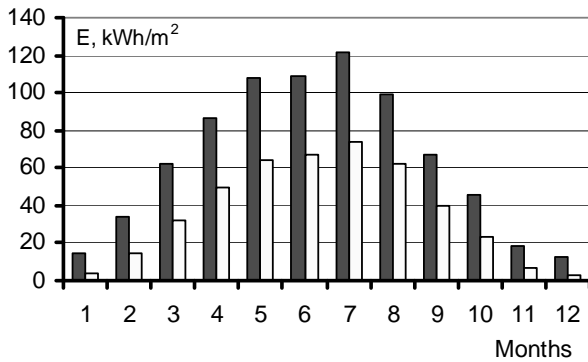


Fig. 3. Comparison of efficiency of solar collectors: vacuumed tubular (black columns) and flat (white columns)

The main principles of system's sizing and optimal control are presented below under the subsequent headings of this paper.

4. Sizing of the system

Determination of the optimal area of solar collectors' array and volume of the preheated water tank are the main tasks of the proposed hybrid water heating system sizing. Their sizes must correspond with capacity of the existing heat exchanger and DHW demands.

Capacity or area of solar collectors' array depends on the required volumes of hot water. If the system of hot water supply is being renovated and number of users remains the same, the volumes of necessary hot water can be determined by checking records of hot water consumption over the past years. In case of installing a new system in a new building, the necessary volumes of hot water should be calculated on basis of expected DHW users and their demands.

The energy required for water heating during the one summer month can be calculated by means of this equation:

$$E_{1S} = k_d \cdot c \cdot V_{1S} \cdot (T_1 - T_2), \quad (1)$$

where E_{1S} is the energy required for water heating during the one summer month, kWh,

$k_d = 0.278$ – coefficient for matching the dimensions,

$c = 4190$ – the specific heat of water, J/kg · K,

V_{1S} – the water demands in one summer month, m³,

T_1 – the temperature of hot water, K (°C),

T_2 – the temperature of cold water, K (°C),

We consider that this required energy for water heating in summer months must be covered mainly by solar collectors. Enlargement of solar collectors' area in order to have enough energy to meet all DHW demands in spring and autumn can not be justified because it would lead to the underused capacity in summer and to significantly increased expenditure. Only a small enlargement of solar collectors' area can be acceptable.

Heat energy produced by the solar collectors' array over the one chosen summer month approximately can be calculated in this way:

$$E_{SC} = \eta \cdot E_{1h} \cdot S_{SC}, \quad (2)$$

where E_{SC} is the energy produced by the solar collectors' array during the one summer month, kWh,

η – the average efficiency of water heating system based on solar collectors,

E_{1h} – the average perennial global solar irradiation over the one chosen summer month to the horizontal plane, kWh,

S_{SC} – the required area of the solar collectors' array, m².

The required area of solar collectors' array approximately can be expressed in shape of the following inequality by using the equations (1) and (2):

$$S_{SC} \geq \frac{k_d \cdot c \cdot V \cdot (T_1 - T_2)}{\eta \cdot E_{1h}} \quad (3)$$

In general, volume of the preheated water storage tank depends on the average DHW daily demands and on the possible number of dark (cloudy) days in turn. Possibility to use another heat source in the hybrid water heating system allows reducing of the tank's volume, however, the desire to maximize solar energy's share leads to the increase of this volume. Optimal decision can be found taking into consideration all necessary information including cost-effectiveness. Roughly volume of the preheated water storage tank can be chosen equal to the average DHW daily demands.

5. Principle of solar collector's control

Usually the control unit CU gives the signal to switch on the pump P1 (Fig. 2) when the difference between the temperatures T_2 and T_1 reaches the value ΔT set in advance. We suggest the variable ΔT depending on the solar irradiance E and the temperature of water in the preheated water storage tank T_1 in order to reduce consumption of power for feeding of the pump P1 and increasing of solar energy's share in the proposed hybrid water heating system. The calculation of the variable ΔT carries out the control unit CU. Calculation of the referable difference of temperatures ΔT can be based on the following equation:

$$\Delta T_{on} = \Delta T_{max} \cdot \left(1 - \frac{T_1}{T_{1N}}\right) \cdot \frac{E}{E_{ST}}, \quad (4)$$

where ΔT_{on} – the difference of temperatures for switching on the pump P1, °C,

ΔT_{max} – the maximal value of the difference of the temperatures, °C,

T_1 – the instantaneous temperature in the tank, °C,

T_{1N} – the rated temperature in the tank, °C,

E – the instantaneous solar irradiance, W/m²,

E_{ST} – the standard solar irradiance, W/m².

Value of the standard solar irradiance is generally received and is equal to 1 000 W/m² (one sun). The rated temperature in the tank for the DHW can be accepted 60 °C. The maximal value of the difference of the temperatures T_2 and T_1 can be accepted 30 °C. A new more convenient shape of the equation (4) can be deduced after the substitution of the mentioned above constant values in the initial expression:

$$\Delta T_{on} = \frac{E(60 - T_1)}{2000}. \quad (5)$$

The instantaneous solar irradiance can be measured by means of the pyranometer.

Values of the difference of temperatures for switching on the pump P1 can vary depending on values of the solar irradiance E and temperature in the preheated water storage tank T_1 .

Means of control and optimisation of the proposed hybrid water heating system based on solar collectors and heat exchanger in order to maximize solar heat energy's share are described in paper [4].

6. Conclusions

1. Combination of the solar collectors for water heating and various other water heating systems already existing in households, industrial enterprises or other hot water users and running on fossil fuels would be beneficial in many aspects.
2. Concept of hybrid water heating systems based on solar collectors and heat exchanger fed from centralized heat supply grid, principles of its sizing and system's control are presented.
3. A huge potential for installation of the described hybrid water heating systems exists in Lithuania and neighboring countries.
4. Simple methodology for determination of the recommended area of solar collectors' array and volume of preheated water tank is presented.
5. The proposed water heating system allows approximately twofold cutting of bills for the domestic hot water due to the partial substitution of the heat from centralized supply grid by energy of solar irradiation.
6. Installation of the proposed hybrid water heating system could allow avoiding of hot water supply blackouts in summertime when heat energy from the centralized grid is not supplied due to the repairs in the grid.
7. Principle of solar collector's control based on the variable reference value of the difference of temperatures in the solar collector and in the preheated water storage tank is proposed.

7. References

1. Adomavičius V., Watkowski T. Hybrid water heating systems based on solar and wind energy // Proceedings of International Conference "Electrical and Control Technologies – 2008". KTU, Kaunas, 2008. – P. 349-354.
2. Uken E-A. and Monyane D. Energy savings with a domestic solar-electric hybrid hot-water cylinder system. Proceedings of the 9th International Domestic Use of Energy Conference, Cape Town, South Africa, April 2001. P.159-162,.
3. Duffy J. A. and Beckman W. A. Solar Engineering of Thermal Processes. John Wiley and Sons, Inc., 2008. – 908 p.
4. Adomavičius V., Petrauskas G. Optimisation of hybrid water heating system based on solar collectors and heat exchanger in order to maximize solar heat energy's share // Proceedings of International Conference "Electrical and Control Technologies – 2009". KTU, Kaunas, 2009 (in press).

OPTIMISATION OF HYBRID WATER HEATING SYSTEM BASED ON SOLAR COLLECTORS AND HEAT EXCHANGER IN ORDER TO MAXIMIZE SOLAR HEAT ENERGY'S SHARE

Vytautas ADOMAVIČIUS*, Gytis PETRAUSKAS**,

* The Centre for Renewable Energy Technologies at Kaunas University of Technology, Lithuania

** Department of Control Technology at Kaunas University of Technology, Lithuania

Abstract: In principle, one of the main tasks for control of solar collectors in the hybrid water heating system, which is based on their combination with heat exchanger fed from the centralised heat supply grid, is to arrange operation of solar collectors in the way maximizing the capture of solar irradiation. Solution of this problem by means of programme packet for the designing of control systems Planning System 4000 is described in this paper.

Keywords: solar energy, solar collectors, water heating, hybrid system, optimization of operation.

1. Introduction

The world is making huge and rapid leaps towards a clean energy economy. Germany, Denmark, Spain and other countries were leaders in this sphere over the many years. Last time a large number of countries in Europe, America and Asia became seriously engaged in this process as well.

A Solar Grand Plan for the USA was proposed by Ken Zweibel, James Mason and Vasilis Fthenakis [1]. According to this plan, a massive switch from fossil fuels to solar power plants is anticipated in the nearest future. Solar power plants could supply 69 % of electricity and 35 % of total energy consumed in the US by 2050. 420 billions USD should be allocated to fund the realization of this plan.

Another bold plan is initiated by Nobel Prize winner former Vice-president Al Gore – to repower America with 100 % clean electricity within 10 years [2]. Under this plan it is intended to invest hundreds of billions USD for implementation of this idea. These investments will create high-paying new jobs for 5 millions Americans. It also will demonstrate the readiness of the decision makers of this nation to pave the way for clean energy across the country and provide long overdue solutions to the climate crisis.

The mentioned above and other steps in right direction to sustainable development made by the developed

countries are good examples for small countries currently lagging behind. Hopefully, Lithuania presently is already close to making important decisions in this sphere by creation the legal basis favourable for development of renewable energy technologies. Apart from other well known benefits, the worldwide expansion of renewables could lead to decrease of demands of fossil fuels and to keeping their prices on a moderate level. It could allow hoping to diminish probability of the new global financial-economic crisis similar to what we experience now.

“Think globally, act locally” - this is a popular catchword of the green movement currently ongoing worldwide. There are many possibilities to “act locally” in Lithuania and in every other country. Every cost-effective way to reduce our dependence on dirty fossil fuel should be seriously considered.

We suggest installing of the hybrid water heating systems based on solar collectors and heat exchanger running on the centralized heat supply grid in Lithuania and other countries having similar DHW systems. In Lithuania the heat exchangers usually exist in condominiums and other big buildings. Concept of this hybrid water heating system is described in paper [3]. Subject of the present paper is optimisation of operation of the proposed water heating system in order to maximize free solar energy share.

2. Object of research

The suggested experimental hybrid water heating system is intended to install in condominium (Fig. 1), which is located in Kaunas, Lithuania. The main technical characteristics of this condominium are given in Table 1.

Presently domestic hot water (DHW) is being prepared in the condominium only by means of heat exchanger running on the centralized heat supply grid. The main disadvantages of the existing DHW system are considerable price for water heating and blackouts of hot water supply in summertime when the system can

not operate due to the cutting off heat energy supply from grid because of the planned repair works. Usually it happens one time per year in May or June and duration of the blackout is about 7-15 days.



Fig. 1. The condominium where the experimental hybrid domestic hot water system is intended to install

Average monthly demands of domestic hot water in the condominium are presented in Fig. 2. Temperature of cold water coming from running water supply grid varies in Kaunas from 6 °C (in spring) to 10 °C (in autumn). Temperature of DHW at the outlet of heat exchanger is kept about 55 °C (standard value).

Table 1. Technical characteristics of condominium

Nr.	Parameters of house	Units	Values
1	Number of apartments	–	75
2	Number of stairwells	–	7
3	Number of stories	–	6
4	Number of dwellers	–	270
5	Total heated area	m ²	6 750
6	Total heated space	m ³	16 500
7	Length x width x height	m	60 x 20 x 14,60
8	Annual consumption of DHW	m ³	3 428
9	Average monthly consumption of DHW	m ³	285,67
10	Average daily consumption of DHW	m ³	9,39
11	Annual consumption of heat for DHW	MWh	175
12	Average amount of heat energy for production of 1 m ³ DHW, heat losses and 75 serpentine pipes	kWh/m ³	51
13	Tariff for water heating	Lt/m ³	12,19
Rate of Litas against Euro is constant and equal to 3,4528 LTL for 1 €			

The condominium has a flat roof, which is very convenient and proof enough for the installation and maintenance of solar collectors' array. The area of the roof makes up over 1 000 m² and this is more than enough for mounting the necessary array of solar collectors meeting the demands of DHW supply to the

dwellers of condominium in summer months. The heat exchanger could be switched out during this period of year. The next 8 months both parts of the hybrid water heating system have to operate – solar collectors and heat exchanger.

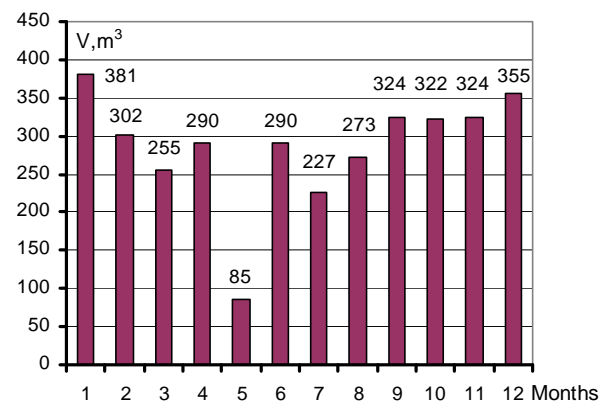


Fig. 2. Average monthly consumption of domestic hot water in the condominium

3. Parameters of the system under research

Structure of the proposed hybrid water heating system is given and described in paper [3].

With reference to the technical characteristics (Table 1) of the condominium it can be accepted the following parameters for sizing of the experimental hybrid water heating system:

- Average daily demand in summer (May – August) months is 10 m³/d;
- Average DHW demand in summer months is 300 m³ per month;
- Capacity of the preheated water tank is equal to the average daily demand – 10 m³.

Technical characteristics of heat exchanger are given below in Table 2.

Table 2. Technical characteristics of heat exchanger

Nr.	Parameters of heat exchanger ŠP 0,15 - 200	Units	Values
Producer – Joint Stock Company UAB Pergalės koncernas			
1	Rated thermal capacity	kW	200
2	Rated water flow	m ³ /min	0,15
3	Operating pressure	MPa	0,6
4	Testing pressure	MPa	1,25
5	Maximal operating temperature	°C	120
6	Length x width x height	cm	37 x 28 x 93
7	Weight	kg	280

The required number of vacuumed tubes of solar collectors array can be calculated according to the formulas given in paper [3]. The necessary number of tubes, which length is 1,80 m and diameter – 58 mm, in the array makes up 900 tubes. Orientation of the solar collectors' array is southward, tilt angle – 45 degrees. Total length of array will make up approximately 75 m.

It is recommended to split the array into the smaller subarrays in order to place them conveniently for mounting and maintenance.

4. Means of solar collector's optimal control

The DDC4000 control unit (CU) can be used for control of the proposed DHW system. This type of CU is often used for measuring, regulating, controlling, optimizing and monitoring purposes in building service systems. It

is based on a 32-bit processor and operates according to the multitask principle. The operating system is Linux. As it was described in [3], the optimal control of solar collectors' operation is based on the instantaneous calculations of the reference value ΔT – the difference between the temperatures T_2 (the temperature of the heat carrier in the solar collector) and T_1 (the water temperature in the preheated water storage tank). According to the formula (5) proposed in [3] for the calculation of ΔT , the reference value of ΔT will be high

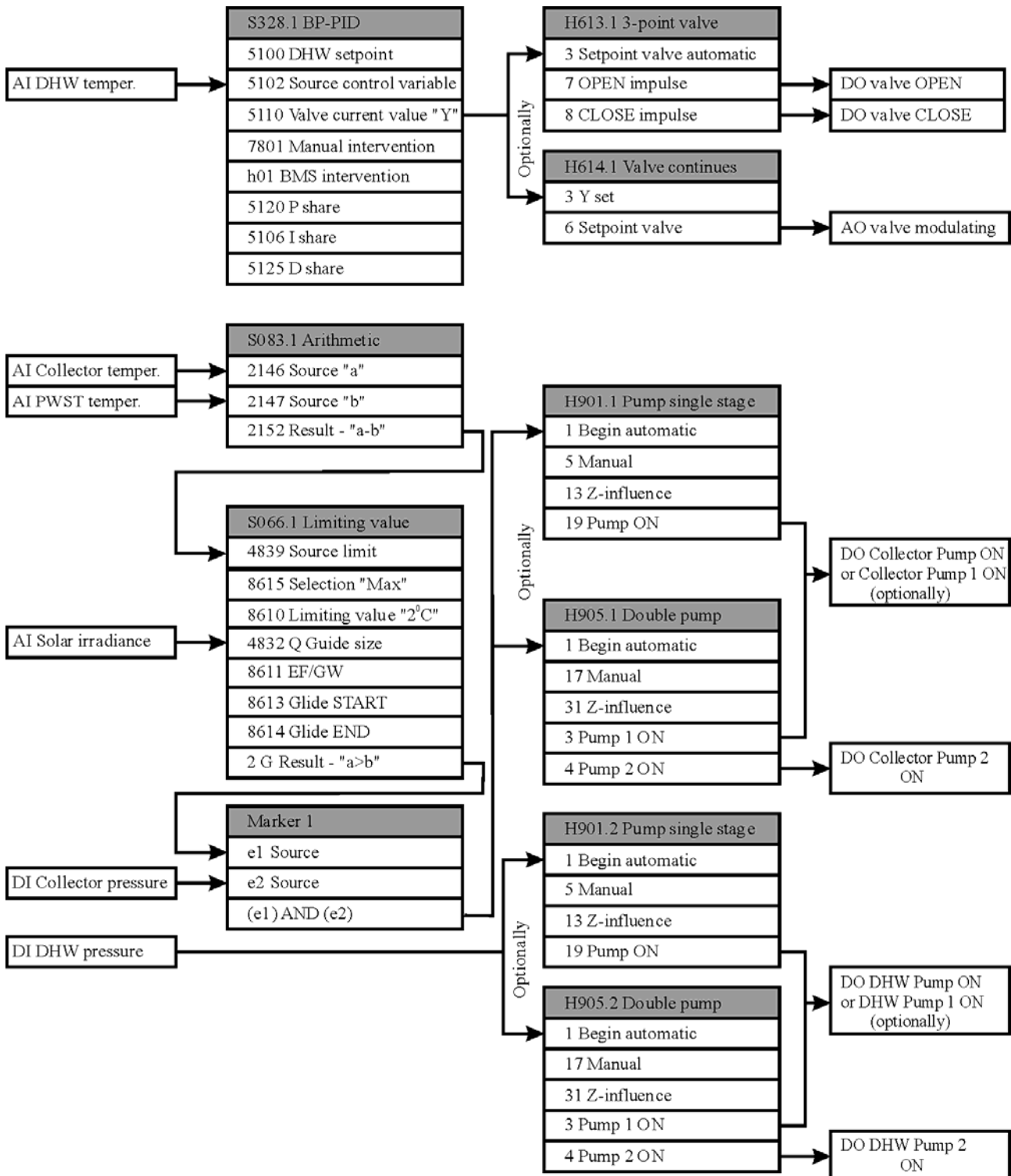


Fig. 3. Block diagram of control process for the hybrid water heating system

(over 20 °C) and frequency of switching operations of the pump P1 [3] will be low when the irradiance is high (close to 1 000 W/m²) and the temperature in the preheated water storage tank is low (about 10-15 °C). In the opposite case the reference value of ΔT will be low. Formula (5) can be made more exactly after the natural experiments. Optimal control of solar collectors can enlarge the share of solar heat energy in this system up to three times in comparison with not optimised cases of operation.

The DDC4000 CU is able to realise the described calculations and optimal control of water heating process. It communicates via Ethernet (TCP/IP, BACnet). The DDC4000 is equipped with object oriented software and hardware modules, making available a large number of functions which can be activated and customized online without the need for additional tools.

Using BACnet protocol DDC4000 allows the hybrid water heating system to be integrated in to the Building management system (BMS). The mentioned above software and hardware objects are summaries of control functions in a block with the input and output values.

The following DDC4000 software and hardware objects are used for the optimal control:

- S238 - Basic program PID;
- S083 - Arithmetic;
- S066 – Limiting value;
- H613 – Valve 3-point or H614 – Valve continues (optionally);
- H901 – Pump single stage or H905 – Double pump (optionally).

Block diagram of control process for the experimental hybrid water heating system is given in Fig. 3. Software object S328 - basic program PID control is used for the control valve position calculation. The control variable sensor (DHW temperature) is defined in parameter “5102 source control variable”. In parameter “5100 XS” the desired target value for the fixed value regulation is set – the DHW set point. The calculation of the Y output is used for CV control. The value of the Y output calculated by the basic program can be overwritten by manual intervention (7801 manual intervention), BMS intervention (h01).

The current value of the calculated Y output is displayed in the parameters “5110 Valve current value”. PID parameters “5120 P share”, “5106 I share”, “5125 D share” are available on operator level (Fig. 3). The value of calculated Y output is used by hardware objects H613 "3-point valve" and H614 "Valve continues" optionally. It depends on the kind of valve actuator – “three points” or “continues modulating”.

The hardware object H613 "3-point valve" controls a 3-point valve actuator using an analog signal of S238 Y output (0-100%). If the value of the Y output is to be increased, an OPEN pulse is created. The length of the OPEN and CLOSE pulses is calculated from the value of the change in the Y output and the actuator motor operating times “tMotAuf” or “tMotZu”. Also hardware object supports manual influence from DDC or BMS.

The hardware object H614 "Valve continues" controls a modulating valve actuator with target setting of S238 Y output 0-100%. Also hardware object supports manual influence from DDC in parameter “5 Manual” or from BMS in parameter “13 Z-influence”.

The software object “Arithmetic” carries out mathematic calculation of object sources – subtraction the temperature of water in PWST and the temperature of heat carrier in SC [3]. Parameter “2152 result” depicts the result of the arithmetic calculation. Analogous values (measured or calculated values) can be monitored for going above or below limiting values with the DDC software object S066 “Limiting value”. The value to be monitored is set in the “4839 Source limit” parameter. The stipulation of the min and max limiting value is made in the “8615 Selection” (Min-Max-infringement) parameter. If the value selected in the parameter “8610 limiting value” (set the difference between the temperature of water in PWST and the temperature of heat carrier in SC) has reached an internal contact, parameter “2 G Result” limiting value is set. It is the main premise for collector’s pump switching ON (Fig. 3). The switch back takes place with a switch back difference in line with parameter “8612 Xsd”. The parameter “8610 limiting value” is used to define the instantaneous difference between the temperature of heat carrier in collector and the temperature of water in PWST for turning collector pump on. The optimal difference of the temperatures has to glide depending on the solar irradiance in order to have the optimal hybrid water heating system. It is essential for the proposed hybrid water heating system control.

The software object S066 makes it to glide depending on the analogous command value – the solar irradiance, parameter “4832 Q Guide size”. This guidance signal (solar irradiance) lifts or lowers the limiting value set – the difference between the temperature of heat carrier in collector and the temperature of water in PWST. Impact of the command value only results in a change of the target value within a glide range. The glide range is stipulated by the parameters “8613 Glide START” and “8614 Glide END”, which are adapted to the actual hybrid water heating system. The influence of the guidance signal on the limiting value change is determined with the parameter “8611 EF/GW” (Fig. 4).

The current limiting value is indicated in the parameter “3 XS” as actual limiting value (Fig. 5). The value could be registered as a trend curve in DDC4000 control unit (Fig. 9). If gliding of limiting value is not active (command value invalid or EF/GW=0), the limiting value and “3 XS” actual limiting value are identical.

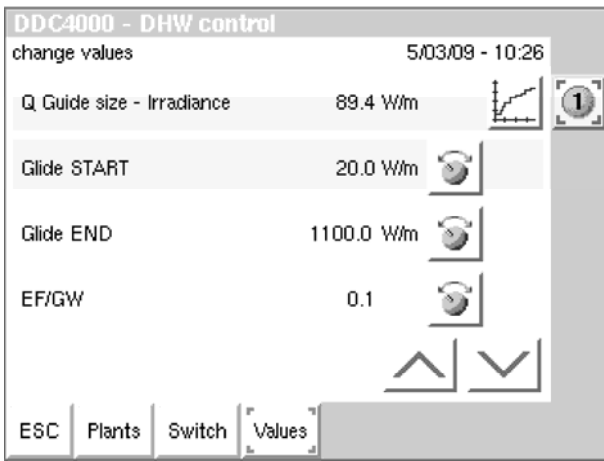


Fig. 4. Values of solar irradiance on CU screen for gliding of the difference of temperatures

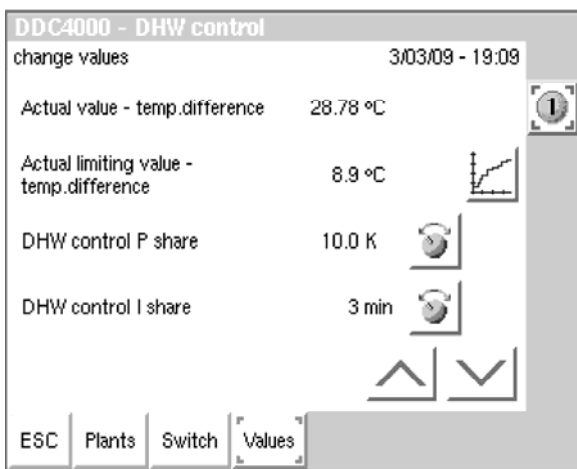


Fig. 5. Actual values of the difference of temperatures on CU screen

Hardware object H901 "Pump single stage" and H905 "Double pump" necessary for the collector pump and for the DHW circulation pump control are used optionally. It depends on the kind of pump. The hardware object H901 controls a single-stage pump. H901 supports:

- Switching delays;
- Pump blocking protection;
- Operating hours / limiting value;
- Command execution check;
- Malfunction catch / malfunction handling.

The hardware object H905 controls a switchable double pump (Fig. 2). It supports the same functions as H901 and pump switching function as well (varies with operating hours, per switching parameter or for malfunctions) [4].

For the visualization of situation in control process some indication lamps are set on CU screen (Fig. 6). DHW parameters are accessible in user or service levels. The limit of difference in temperatures used as signal for starting of solar collector's pump P1 [3] is set on the CU screen only in service level (Fig. 7).

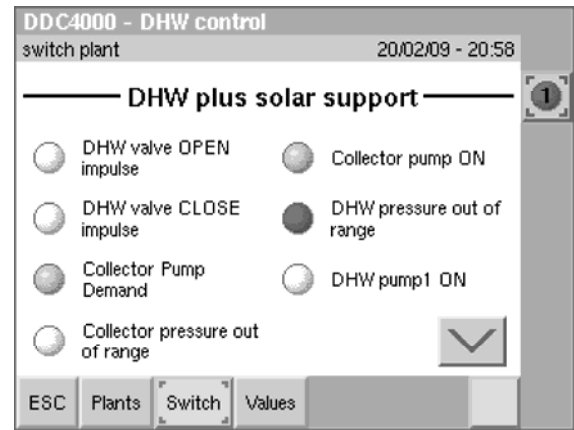


Fig. 6. View of signaling lamps on the CU screen

The deflection of parameters is represented as alarm message on CU screen and is accessible in users and service levels (Fig. 8).

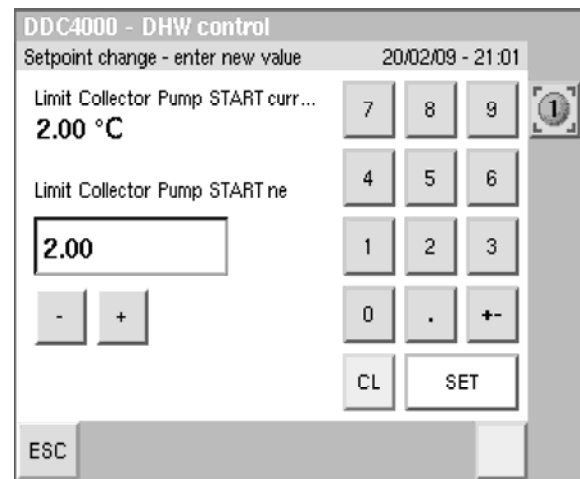


Fig. 7. The value setting view on the CU screen

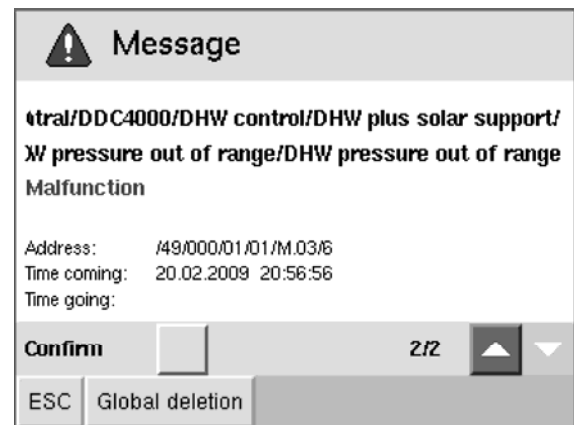


Fig. 8. View of CU screen in case of alarm message - collector pressure drop below the allowed value

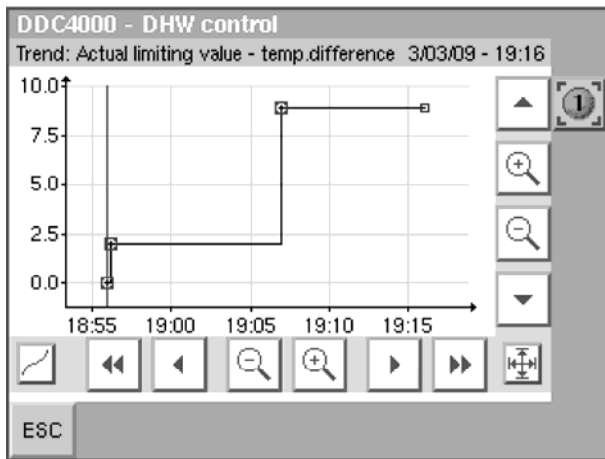


Fig. 9. View of trend curve on CU screen for actual difference of temperatures

The main decisions regarding this work were based on [4, 5].

5. Discussion

This paper was targeted for the preparation to install the proposed water heating system for a common DHW user in order to have a certain theoretical background before the renovation of the existing system. The experimental system is intended to install at first in one condominiums of Kaunas city. After this the research of the proposed hybrid water heating system is intended to continue at natural conditions. If the anticipated positive results will be achieved and disseminated, further implementation of these systems could be considerable. A large potential for implementation of the proposed hybrid water heating systems exists not only in Kaunas and Lithuania but also in other many countries, especially in Central and East Europe countries, where the centralized heat supply grid and buildings with flat roofs are common.

6. Conclusions

1. Presently there are many possibilities for substitution of the technologies based on dirty fossil fuels by technologies running on the renewables partially or entirely.
2. The hybrid water heating system based on solar collectors and heat exchanger fed from the centralised heat supply grid is proposed in order to shift partially on renewable solar energy and to

reduce the bills for domestic hot water in condominium.

3. One of the main tasks for control of solar collectors in the proposed hybrid water heating system is to arrange operation of solar collectors in the way maximizing the capture of solar irradiation.
4. Optimization of the proposed condominium's hybrid water heating system is carried out on the control unit DDC4000.
5. The object oriented software and hardware objects of DDC4000 make available a control program to be formed in way of objects activation and customization.
6. The optimal control of solar collectors' operation is based on the instantaneous calculations of the reference value of the difference between the temperature of the heat carrier in the solar collector and the temperature of water in the preheated water storage tank.
7. The gliding limit value for collector pump switching allows optimize control for maximum solar energy utilization.
8. Optimal control of solar collectors can enlarge the share of solar heat energy in this system up to three times in comparison with not optimised cases of operation.
9. The experimental hybrid water heating system described in this paper is intended to install at first in one of Kaunas city condominiums.

7. References

1. Zweibel K., Mason J. and Fthernakis V. A Solar Grand Plan // Scientific American Magazine. December 16, 2007.
2. Repower America 100 % clean electricity within 10 years. www.RepowerAmerica.org (called on 19.01.2009).
3. Adomavičius V., Petrauskas G. Hybrid water heating system based on solar collectors and heat exchanger fed from the centralized heat supply grid // Proceedings of International Conference "Electrical and Control Technologies – 2009". KTU, Kaunas, 2009 (in print).
4. Kieback&Peter GmbH & Co. DDC4000 engineering manual, 2009. – P. 73-85.
5. Duffy J. A. and Beckman W. A. Solar Engineering of Thermal Processes. John Wiley and Sons, Inc., 2008. – 908 p.

CONTROL OF ENERGY FLUXES IN THE GRID-TIED DOMESTIC POWER SYSTEM BASED ON WIND ENERGY

Česlovas RAMONAS*, Vytautas ADOMAVIČIUS**, Vytautas KEPALAS*

*Department of Control Technologies at Kaunas University of Technology, Lithuania

** The Centre for Renewable Energy Technologies at Kaunas University of Technology, Lithuania

Abstract: Control of energy fluxes in the grid-tied domestic power system based on wind energy is described in this paper. One object of control is the wind turbine itself. The load of wind turbine must be automatically controlled in order to maximize the power output. The produced electric energy must be divided between the electrical appliances, the power storage and the heat storage tank. Surplus of electricity can be supplied to the electric grid. Power from electric grid must be delivered to all domestic energy users in case of wind turbine breakdown or unexpected long term doldrums. Control system must safeguard energy distribution in all mentioned cases.

Keywords: control system, wind energy, wind turbine, domestic power system, grid-tied inverter.

1. Introduction

Up to this year (2009) International Energy Agency (IEA) and International Atomic Energy Agency (IAEA) were the main international organizations in sphere of energy affairs. However, mostly they were not among the diligent supporters of sustainable development. Therefore new international organization was necessary to coordinate and promote development of the renewables. Germany, Denmark and Spain were the leading promoters of this idea. The Conference on the establishment of the International Renewable Energy Agency was held in Bonn, Germany on 26 January, 2009 [1].

As it was reported in the conference, the International Renewable Energy Agency (IRENA) was founded to press ahead with the expansion of renewable energies in an even more comprehensive and targeted way [2]. German Federal Environment Minister Sigmar Gabriel declared that IRENA is “an expression of our conviction that in future we can cover the main share of our energy consumption with renewable energies” and “an expression of our awareness that renewable energies offer huge potential and that the technologies for their use are available”. But he also recognized that there are

some obstacles blocking the rapid expansion of renewable energies and that we have to join forces to overcome them. It will be done because the time is working in favour of renewables: “due to technological advances, renewable energies are often already a competitive alternative to conventional energy sources. And what's more, technological progress means they are cheaper from year to year. Renewables are developing into an important economic sector. In 2008 over 150 billion dollars were invested in renewable energies worldwide [2]”.

The foundation of IRENA will promote the expansion of renewable energies internationally. IRENA will encourage both industrialised and developing countries from all over the world to create their political and legal frameworks for the successful sustainable development. Creation of the right incentives and securities for investment are very important tasks of new organization. This process needs to be steered by governments, since a distorted market is not capable of initiating the transformation of energy systems. IRENA will act as a catalyst to facilitate technology and knowledge transfer, and to support capacity building [2]. Supporters of sustainable development now can expect to watch the acceleration of this process.

2. Research object

Small scale efficient wind turbines [3] of sufficient capacity can be used for the heating purposes as well [4]. Simplified scheme of wind turbine's power conversion system used for all domestic energy needs is shown in Fig. 1. The wind turbine (WT) has a permanent magnet synchronous generator SG. As it is shown in Fig. 1, the synchronous generator SG is connected to the electric grid over the rectifier, the shorting circuit, the inverter, the transformer and the grid's automatic switch 1Q,F. Shorting circuit consist of shorting transistor V_t , reactor L_d and disjunctive diode V_{at} . Wind energy converted by the WT is used for the domestic electrical appliances, for charging the battery, for the domestic hot water (DHW) preparation and

space heating. Surplus of electric power can be supplied into electric grid. Appliances for the DHW and space heating can be connected directly to the rectifier by means of the automatic switch 2Q,F. Capacity of the inverter can be reduced in this case and therefore the overall cost of the whole system will be reduced as well. The grid-connected inverter fed from the battery B some time can supply electricity for the most indispensable

users (lighting, refrigerator, radio, TV) in case of blackout and absence of wind simultaneously. Compatibility of the battery voltage and the grid voltage is an important task of the system's design. The voltage-matching transformer connected as the autotransformer is used in this case (Fig. 1). The required voltage of the transformer's secondary windings can be calculated by using this equation:

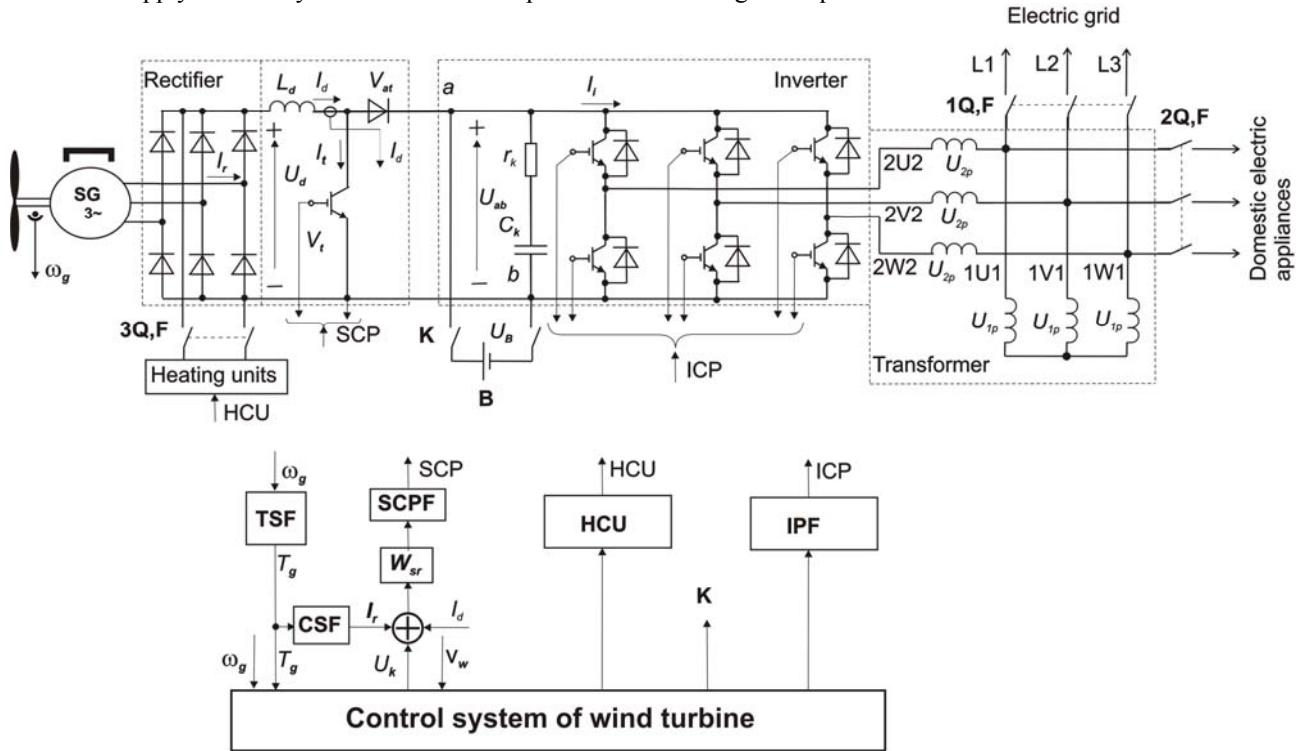


Fig. 1. Simplified scheme of wind turbine's power conversion system used for the domestic energy needs

$$U_{2p} = U_{1p} - \frac{U_B}{\sqrt{3} \cdot k_s}, \quad (1)$$

$$I_R = \frac{P_i}{k_{is} \cdot k_m \cdot \omega_g}, \quad (2)$$

where U_B – the battery voltage; U_{1p} – the phase voltage of the electric grid; U_{2p} – the phase voltage of the transformer's secondary winding; k_s – factor of the inverter's scheme.

The WT is controlled from its control system (Fig. 1). The control system generates pulses for the inverter control (ICP) and for the transistor of shorting circuit (SCP), performs discrete control of the heating units (HCU), the battery (B) and control of other units and appliances. Apart from this, the control system performs control of the WT's load over the shorting circuit.

Control system of the generator's load consist of the torque signal former TSF, the reference current signal former CSF, the shorting control pulse former SCPF and the current controller W_{sr} . The following signals operate in the control system: ω_g – signal of the angular speed, T_g – signal of the torque, I_r – signal of the reference current, I_g – signal of the rectified current, U_k – the control voltage, v_w – signal of the momentary wind speed. The reference current can be calculated in a similar way as in paper [5]:

In our case we have the only difference – the power share supplied into electric grid (P_i) is taken here instead of full power of the generator because we have to take into consideration that generator is (or can be) already loaded by heating units and (or) other electrical appliances. The generator's power share P_i supplied into electric grid can be described mathematically in this way:

$$P_i = P_m - \frac{U_d^2}{R_h}, \quad (3)$$

where in equations (1) and (2): k_m – torque factor; P_i – the generator's power share supplied into the grid; P_m – the power produced by wind turbine; k_{is} – is coefficient of rectifier's scheme (for the three-phase six-pulse rectifier $k_{is}=0.78$); U_d – the rectified voltage of the generator; R_h – the active resistance of the heating unit. The power produced by wind turbine P_m can be calculated by using power curve, which is given in the

WT's technical documentation. As a rule, polynomial of the n-th order is used for approximation of the power curve on purpose to have a sufficient adequacy of the mathematical description. So, the power curve of WT mathematically can be described by this equation:

$$P_t = a_n \cdot v_w^n + a_{n-1} \cdot v_w^{n-1} + a_{n-2} \cdot v_w^{n-2} + \dots + a_1 \cdot v_w + a_0 \quad (4)$$

As it can be seen in Fig. 1, the load of WT's generator can be controlled in discrete mode by changing the number of electricity users and gradually by adjusting the power supplied into electric grid. Algorithm of wind turbine's load control presented in Fig. 2 explains how it can be done.

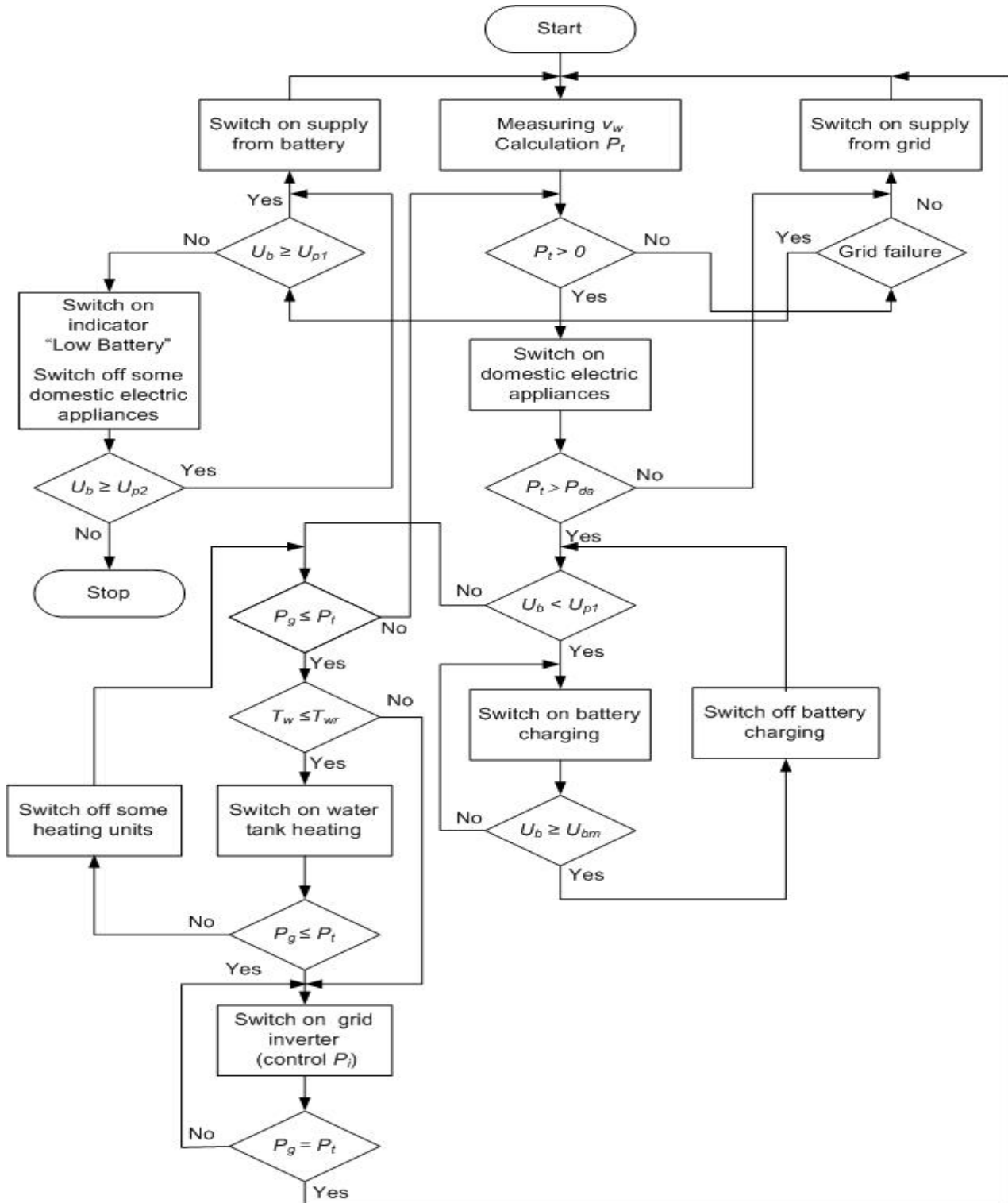


Fig. 2. Algorithm of wind turbine's load control

The presented algorithm of wind turbine's load control allows maximizing the utilization of power produced by the WT. As it is shown in Fig. 2, at first the wind speed v_w is measured and the power P_t produced by the WT is calculated. If the condition $P_t > 0$ is met, the control system allows switching on the domestic electrical appliances according to the presented algorithm. If the $P_t = 0$, the operation of the electric grid is checked (the grid failures can occur due to the blackouts, repair works, etc.). If the grid failure is not found, supply of electricity from the grid is switched on.

If the failure of grid exists, then the control system checks the level of the battery's charge. If the battery is charged enough ($U_b > U_{p1}$), the power supply from battery to the domestic electrical appliances is allowed. In contrary some domestic electrical appliances are switched off and the indicator „Low battery“ is switched on. The minimum permissible level of the battery discharge U_{p2} is also checked: if this level is reached, all domestic electrical appliances are disconnected. Fortunately, this case is hardly possible because the power supply is 3 times reserved (3 sources are used – the WT, the power grid and the battery. If the wind rotor is running ($P_t > 0$), then the control system checks the condition $P_t > P_{da}$ (capacity of the electrical appliances). If yes, further on the battery is checked if it is fully charged. If voltage of the battery is below the maximum value U_{bm} , the charging is switched on.

The water heating process is controlled as well: if the power of WT is high enough ($P_g < P_t$) and if the temperature of water is below the limit of the permissible value T_{WT} , the water heating is switched on. When the limit value is reached, the heating of water is switched off.

If the strong wind is blowing and a certain part of the WT's power is unused when the condition $P_g < P_t$ is met, the grid inverter is switched on and the surplus power is supplied into the electric grid.

If the wind is not blowing ($P_t = 0$) and grid failure exists, electricity is supplied from the battery only for the domestic power appliances. Two levels of the battery charge are checked: if the battery is full, all appliances are fed. If the battery charge level is below U_{p1} , some electric appliances are switched off and the indicator „Low battery“ is switched on.

3. Mathematical description of the proposed power system

Mathematical description of the system's power storage and inverting circuits (SIC) is set out well enough in the previous papers published by authors [5, 6], therefore it can be skipped in this paper. Only singularities of mathematical description depending on switching mode of the heating elements and the battery here will be presented. The average values of currents and voltages can be used for the description of these processes and non-stationary processes of the electromagnetic field alternations can be neglected [5, 6]. One-line scheme

presented in Fig. 3 will be used as the equivalent of wind turbine's circuitry (Fig. 1).

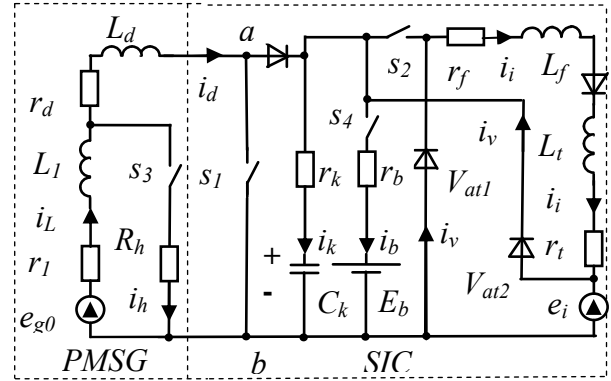


Fig. 3. Equivalent scheme of the system

Like it was described in reference [6], system of equations for the power inverting mode can be made up as follows:

$$\left\{ \begin{array}{l} \frac{di_d}{dt} = \frac{1}{L_d} (u_d - u_{ab} - r_d \cdot i_d); \\ \frac{di_i}{dt} = \frac{1}{L_i} (u_{ab} - e_i - r_i \cdot i_i); \\ \frac{du_c}{dt} = U_{c0} + \frac{1}{C_k} \cdot i_k; \\ u_d = e_{g0} - u_g - u_K - r_1 \cdot (i_h + i_d); \\ u_g = 2 \cdot r_1 \cdot (i_h + i_d) + 2 \cdot L_1 \cdot \frac{d(i_h + i_d)}{dt}; \\ u_K = \frac{m \cdot x_K}{2 \cdot \pi} \cdot (i_h + i_d); \\ U_{c0} = k_s \cdot E_{im}; \\ u_{ab} = u_c + r_k \cdot i_k; \\ i_b = \frac{1}{r_b} \cdot (u_{ab} - E_b); \\ i_k = i_d - i_b - i_i. \end{array} \right. \quad (5)$$

where e_i – the counteracting electromotive force of the grid; E_{im} – the maximum value of the grid's delta voltage; $r_i = r_t + r_f$ – the active resistance of the inverter circuit; r_t – the active resistance of the grid; r_f – the active resistance of the filter; $L_i = L_t + L_f$ – the inductance of the inverter's circuit; L_t – the inductance of the grid; L_f – the inductance of the filter; i_i – the inverted current; u_k – the voltage of the storing capacitor C_k ; i_k – the current of the storing capacitor C_k ; i_h – the current of the heating unit; i_b – the current of the battery; i_d – the current of the reactor; k_s – coefficient of the rectifier's scheme.

The counteracting electromotive force of the inverter e_i , electromotive force of the generator e_{g0} and other parameters can be calculated by using the method described in the preceding works of authors [5, 6, 7]. Synchronous generator with permanent magnets (PMSG) can be described like it was done in paper [5]:

$$\begin{cases} \frac{d\omega_g}{dt} = \frac{1}{J} \cdot (M_t - M_g - M_f); \\ M_t = \frac{P_{tm}}{\omega_g}; \\ M_g = k_m \cdot i_L \cdot \sqrt{\frac{2}{3} - \frac{\gamma}{3 \cdot \pi}}; \\ M_f = k_F \cdot \omega_g. \end{cases} \quad (6)$$

where M_g – the torque of generator; M_t – the torque of wind rotor; M_f – the combined torque of viscous friction of rotor and load; J – the combined inertia of rotor and load; ω_g – the angular velocity of the generator’s rotor; k_m – torque factor; k_f – friction factor; P_{tm} – the power produced by wind turbine; γ – the angle of the rectifier diodes’ commutation.

4. Mathematical model and simulation

Mathematical model of the proposed power system is shown in Fig. 4.

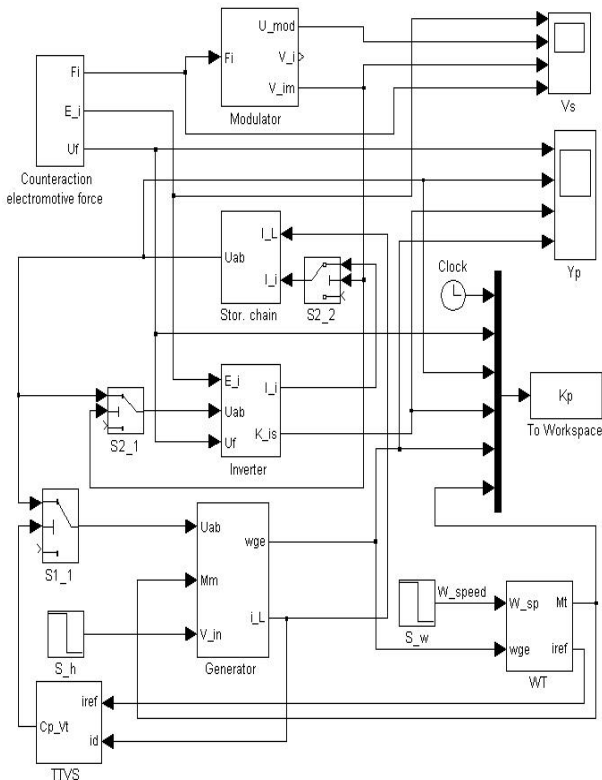


Fig. 4. Mathematical model for the WT’s power system

It was made up using the systems of equations (5, 6) and the equations (2÷4) as well. The storage chain “Storage Chain” and the inverting circuits “Inverter” of the mathematical model (Fig. 4) are made up by application of the previously published works of authors [5-7]. The mathematical model of wind turbine was worked out using the WT’s power curve, which can be described by means of the following equation:

$$P_t = -0.0461 \cdot v_w^6 + 2.1317 \cdot v_w^5 - 36.5307 \cdot v_w^4 + 271.5777 \cdot v_w^3 - 731.0533 \cdot v_w^2 + 531.6232 \cdot v_w + 8.5174. \quad (7)$$

Mathematical model of the wind-based domestic power system consists of three functional parts: the converter, which includes inverter, power storage circuit and control pulse former, the generator and the wind turbine. The control pulse former consists of the counteraction electromotive force unit and modulator. The TTVS unit performs the gradual control of the generator’s load. The load of generator is controlled by means of varying value of the stator’s rectified current. The reference rectified current is calculated in the model’s unit WT according to the (2) and (3) formulas.

The reference current i_{LR} reaches the TTVS unit through the inlet “iref” and the measured rectified current – through the inlet “id”. The control pulse formed by the controller TTVS on its output “Cp-Vt” controls the rectified current of the generator.

5. Results of research

As it was shown in Fig. 2, according to the proposed algorithm the system can supply the wind energy converted into the power to the water heating unit or into the electric grid, if the heat storage tank is fully charged. If generator produces more energy than heating units require, the surplus power can be supplied to the electric grid as well.

Quality of the load control in the proposed system was researched by means of mathematical simulation. Results of the research are presented below in Fig. 5 and Fig. 6.

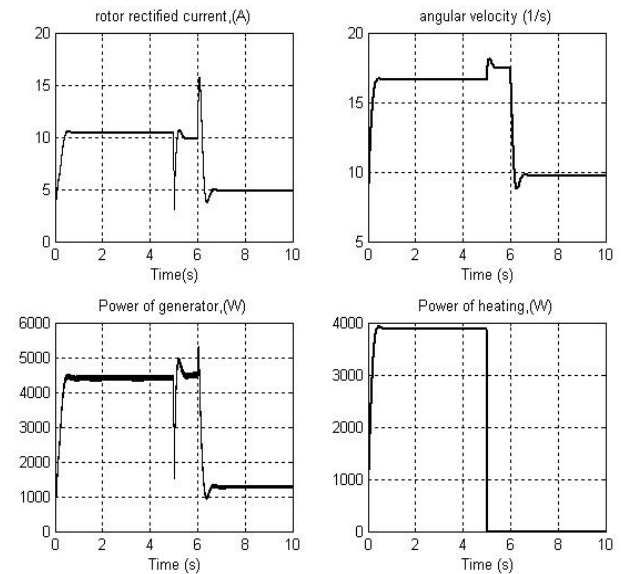


Fig. 5. Curves of the researched wind power system’s parameters at the following jumps of the action signals of generator: wind speed – $\Delta v =$ from 9 to 5 m/s, at $t = 6$ s; switch off heating unit at $t = 5$ s

Experimental curves are presented in Fig. 5 for the case when WT charges the heat storage tank and supplies electric energy into the electric grid. The process of control there is shown when the heating unit was switched off at the time 5 s and the wind velocity jumped down from 9 m/s to 5 m/s at the time 6 s.

As it is clearly shown on Fig. 5, the power of generator remains practically the same after the disconnecting of heating elements and the same share of power used for heating is then supplied into the electric grid (all power of the generator is supplied into the electric grid after 5 s). The rectified current of the generator slightly decreases and the rotational speed of the generator (and wind rotor) slightly increases due to the change of the current circuit configuration. Power of the WT sharply decreases after 6 s due to the wind speed jumping down. Therefore the angular speed of the wind turbine and the generator's rectified current accordingly decreases.

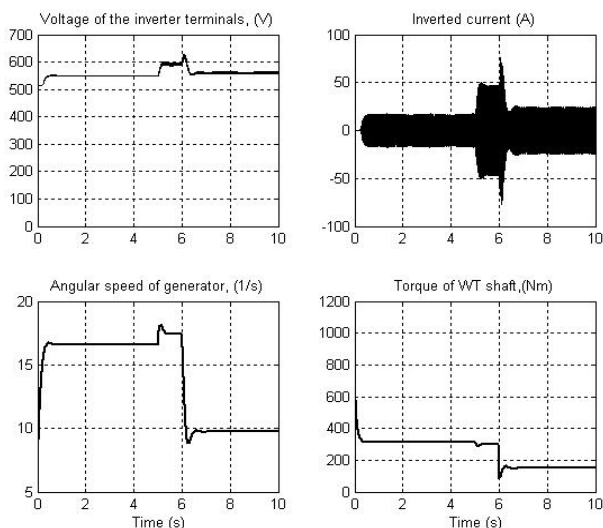


Fig. 6. Curves of the researched wind power system's parameters at the following jumps of the action signals of generator: wind speed Δv = from 9 to 5 m/s, at $t = 6$ s; switch off heating unit at $t = 5$ s

Alteration of the wind-based domestic power system's parameters depending on the change of wind turbines operation modes is shown in Fig. 6. There it can be noticed that at first the inverted current is not very strong because the major part of power produced by the WT's generator is used for the heating. After the disconnection of heating unit at the instant 5 s the voltage on the terminals of inverter slightly increases and sharply increases the inverted current. The load torque of the wind turbines practically remains the same. At the instant 6 s, when the wind speed jumps down, the rotational speed, the power of wind turbine and the inverted current decreases. It can be concluded that the experimental curves of the researched wind power system correctly reflect the electromagnetic processes taking place in the system's power circuits. The worked out mathematical model of the wind-based energy system allows researching the system's modes of

operation and more exact specifying of the power circuit's parameters (L_d, r_b, C_k).

6. Conclusions

1. Control of load and power fluxes in the grid-tied domestic energy system based on wind turbine is researched and algorithm of wind turbine's load control is worked out.
2. The proposed wind turbine's control system allows the meeting of electricity demands not only in case of low wind speed but also in cases of the blackouts and emergency.
3. The proposed wind turbine's control system also allows reducing capacity of the inverter and therefore the overall expenditure of the full system because only a part of power is supplied into the electric grid.
4. The presented mathematical model of the described energy system allows researching the system's modes of operation and more exact specifying of the power circuit's parameters.
5. The presented experimental curves confirm the correct operation of the researched domestic power system based on wind energy.

7. References

1. German Federal Ministry for Environment, Nature Conservation and Nuclear Safety. A milestone for future-oriented energy supply. Press release No. 023/09. Berlin, 26.012009.
2. Gabriel S. A pillar of clean energy supply. Founding Conference of the International Renewable Energy Agency (IRENA). Bonn, January 26, 2009.
3. Martinez F., Herrero L., Santiago P. and Gonzales J. Analysis of the efficiency improvement in small wind turbines when speed is controlled. 1-4244-0755-9/07/\$20.00©2007 IEEE.
4. Šefik M. Bajmak. Possible applications for the wind energy in the heating and air conditioning systems. Facta Universitatis. Series Mechanical Engineering Vol. 5, No.1, 2007.– pp.71-78.
5. Adomavičius V., Ramonas Č., Kepalas V. Control of wind turbine's load in order to maximize the energy output // Electronics and Electrical Engineering, 2008. Nr. 8(88). – P.71-76.
6. Kepalas V., Ramonas Č., Adomavičius V. Connection of the RES-based Power Plants into the Electric Grid // Electronics and Electrical Engineering, 2007. – Nr. 8(80). – P.67-72.
7. Paulauskas M., Kepalas V., Ramonas Č. Platininio asinchroninio ventiliinio kaskado dinamika // ISSN 1392 - 1215 Elektronika ir elektrotechnika, 1996. – Nr. 4 (8). – P. 56-58.

RESEARCH OF THE POWER CONVERSION PROCESSES IN THE SYSTEM OF POWER SUPPLY FROM A NUMBER OF WIND TURBINES OVER THE ONE GRID-TIED INVERTER

Česlovas RAMONAS*, Vytautas ADOMAVIČIUS**, Vytautas KEPALAS*

* Department of Control Technology, Kaunas University of Technology, Lithuania

** The Centre for Renewables Energy Technologies, Kaunas University of Technology, Lithuania

Abstract: Only one mutual inverter can be used in the power conversion system for a number of wind turbines having different capacities and installed close to each other. This is applicable both for stand-alone and grid-tied cases of wind turbines and for wide range of capacities. The proposed electrical scheme for power supply from the wind farm into electric grid allows using wind turbines of different types and capacity. Results of research of the power conversion processes in the system of power supply from a number of wind turbines over the one grid-tied inverter are presented in this paper. The main advantage of this scheme is cost-effectiveness of this power conversion system.

Keywords: wind farm, mutual grid-tied inverter, power conversion system.

1. Introduction

The wind-powered installations for electricity generation with rated capacity up to 100 kW are considered as small wind turbines. Small wind turbines are produced in more than 25 countries and over 300 different models already are available worldwide [1]. The global market of small scale wind turbines is led by the USA, the United Kingdom, China, Canada, Germany and other countries.

Presently price of small wind turbines usually varies between 3 and 5 USD per watt of capacity. However, sometimes price of this class wind turbines' is very high [2]. Price of electricity generated by the small wind turbines usually is about 10-15 cents (US).

Rate of development of small wind turbines global market is not as high as in case of large wind turbines – the annual increase makes up about 15-20 %. However, it is considered that business for small scale wind turbines can be big as well and that it was too long overlooked [3]. Indicators of small wind turbine's market for 2008 year confirm a considerable leap in this sector indeed.

Last year Lithuania started to produce small wind turbines as well. Number of installed small wind turbines in Lithuania is not booked. Approximately it could be about 10-20 installations per year during the last 2-3 years but considerable increase is predicted.

The degree of maturity of various wind turbines varies in a wide range. Manufacturers still have many possibilities to improve design of this class wind turbines in order to ensure operation capability in lower and higher wind speeds, to apply more advanced blade design and manufacturing methods, to decrease noise level, to make the wind turbines more visually attractive, to reduce their prices, etc. German researchers have a target to reduce price of small wind turbines up to 1 euro per 1 watt of capacity.

Design of power electronics' devices can be improved as well. First of all, the devices could be designed to meet stronger safety and reliability standards. The same model of wind turbine could be adaptable to either on-grid or off-grid use.

2. Research object and method

Sometimes many small scale wind turbines (WT) of the same type can be mounted on a parapet of big building or on the ground in order to produce more electricity [3]. In this case it would be reasonable to use only one inverter in the power conversion system on purpose to reduce expenditures on the power converting system. Research of the proposed system for power supply from the farm of small scale wind turbines into electric grid (EG) over one mutual inverter is described in this paper. Wind farms, which have wind turbines of different capacity and type, are applicable as well.

Elaboration of the proposed power conversion system for small wind turbines is based on the researches described in papers [4, 5, and 7].

Simplified electrical scheme of the system for power supply from the farm of small scale WTs into EG is presented in Fig. 1.

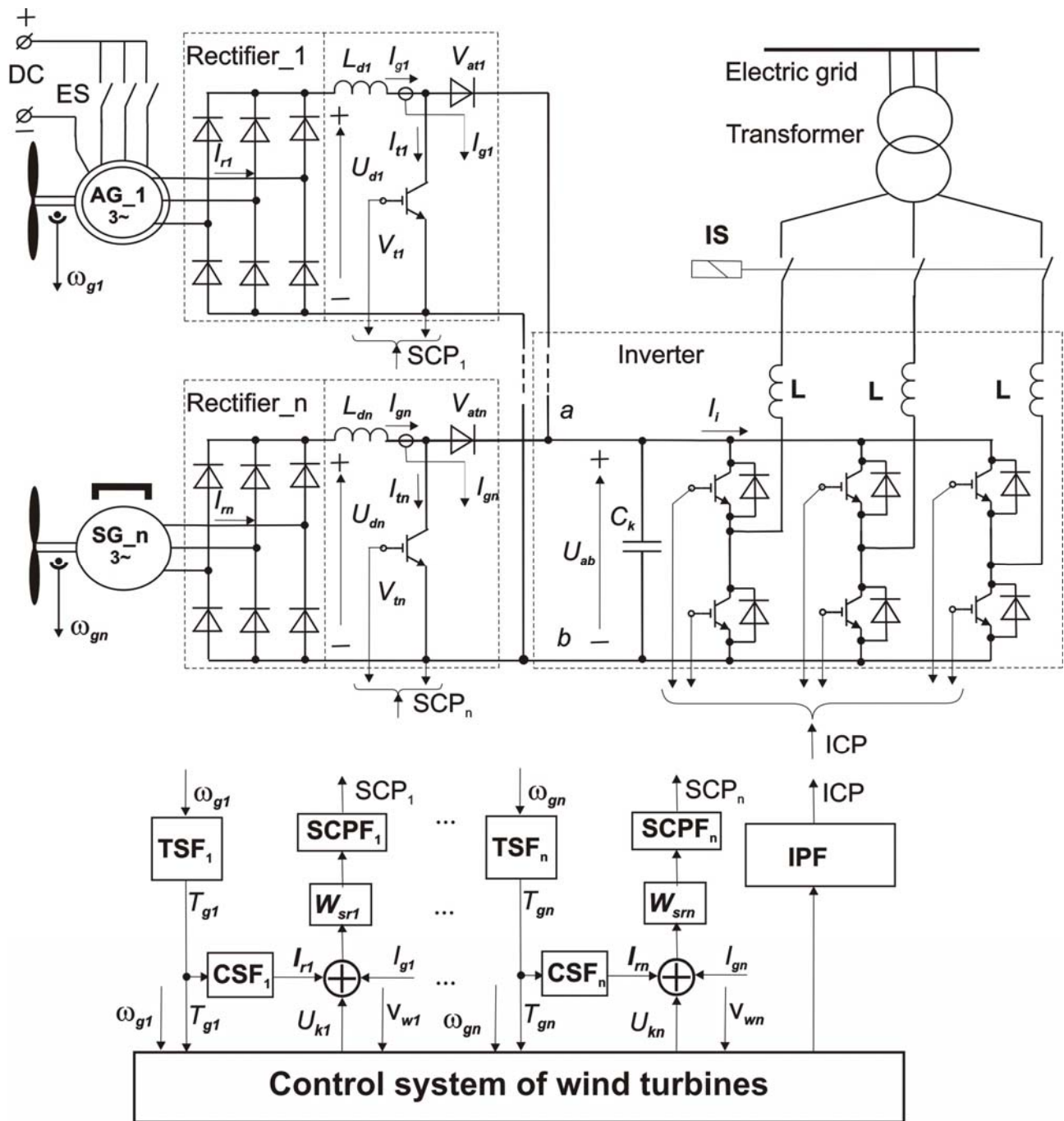


Fig. 1. Simplified scheme of power supply from park of small-scale WTs into EG over the one inverter

The suggested scheme has the power circuitry and the control system.

The system's power circuitry consists of "n" asynchronous and synchronous generators SG-1, SG-2... SG-n, "n" rectifiers, "n" shorting circuit units consisting of power storage reactors L_{dn} , transistors V_{tn} and disjunctive diodes V_{atn} , one mutual capacitor for power storage C_k , one mutual inverter, inverter's switch IS, transformer and of some other known elements. Control system of wind turbines operates together with "n" shorting circuit units, control pulse formers $SCPF_n$, current signal formers CSF_n , torque signal formers TSF_n and one inverter pulse former IPF. The following signals operate in the control system: ω_{gn} – signals of

the WTs' angular speeds, T_{gn} – the signals of the torques of the generators, I_{rn} – the signals of the reference currents of the generators, I_{gn} – the signals of the rectified currents of the generators, U_{kn} – the control voltages for the generators, V_{wn} – the signal of the momentary wind speed of the generators.

Mathematical simulation (MATLAB/SIMULINK) was used as a research method to check the operation abilities of the proposed electrical scheme. Initially the task was simplified by using only two wind turbines, two shorting circuit, one capacitor for power storage and one mutual inverter. The same method can be used for research of the system representing the wind park with any number of WTs.

3. Mathematical description and model of the proposed wind energy conversion system

Exact description of electromagnetic processes in circuits of power conversion system given in Fig. 1 is rather complicated task. Therefore some simplifications used in theory of converters' circuits and facilitating its mathematical description will be applied [4, 5, 7]. Power converter having electrical circuits with n-phases

is being substituted by the equivalent one phase scheme. Power switches in this scheme are being considered as ideal.

Equivalent scheme of the power converter presented in Fig. 1 is given in Fig. 2. The unmarked diodes show the directions of conductivities in this scheme. This scheme has the same n equivalent circuits of rectifiers, one mutual capacitor for power storage and one inverter.

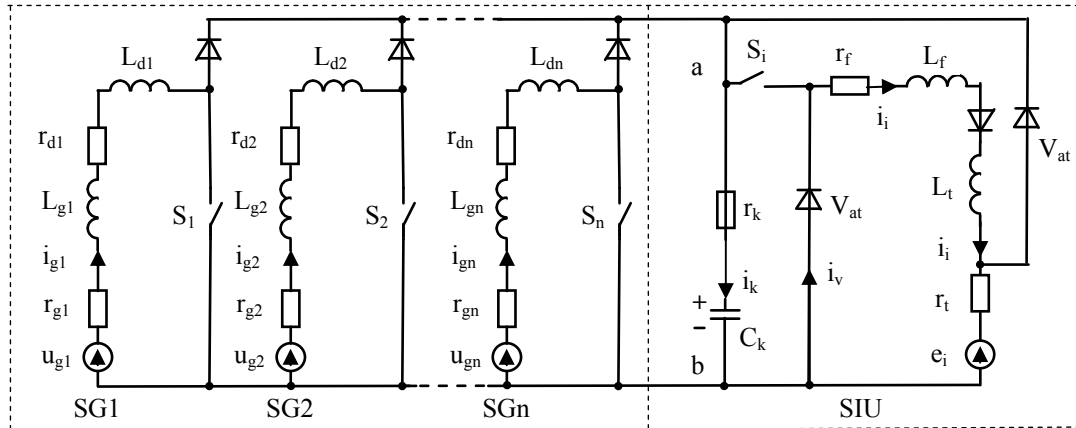


Fig. 2. Equivalent scheme of the system

When the wind turbines' generators $u_{g1}, r_{g1} - u_{gn}, r_{gn}$ are switched into the scheme of short circuit by means of the switches $S_1 - S_n$ (in case of AC the rectifier is necessary), the power is being stored in the reactors $L_{d1} - L_{dn}$. When the switches $S_1 - S_n$ are switched out, the power flows into the storing capacity C_k . If the S_i is switched on, the inverter I supplies the power into electric grid [7]. Pulse width modulation realised by means of the switch S_i is used in order to adjust voltages of the wind generators and the electric grid. The grid voltage is used for the modulation. In this way operation of converter is being synchronized with the electric grid. Carrier frequency of the modulated signal usually makes up from few to 20 kHz. Operation of the switches S_n can be synchronized with the electric grid or not. In our case switches $S_1 - S_n$ operate independently from the electric grid voltage.

Mathematical description of the system's power circuits was made up with reference to the equivalent scheme of the proposed system (Fig.2).

Every generator (Fig. 2) can operate in the two modes: shorting mode – when the switches $S_1 - S_n$ are switched on, and power inverting mode – when the switches $S_1 - S_n$ are switched out. When the generators are operating in the shorting mode ($S_1 - S_n$ are switched on), their power circuits are not related electrically (independent). Then currents of the generators' power circuits can be deduced from the following independent equations:

$$\frac{di_{gn}}{dt} = \frac{1}{L_n} (u_{gn} - r_n \cdot i_{gn}). \quad (1)$$

where u_{gn} – the voltage of the generator n ; i_{gn} – the rectified current of the generator; $r_n = r_{gn} + r_{dn}$ – the active resistance of the generator circuit; r_{gn} – the active resistance of the generator; r_{dn} – the active resistance of the reactor; $L_n = L_{gn} + L_{dn}$ – the inductance of the generator's circuit; L_{gn} – the inductance of the generator; L_{dn} – the inductance of the reactor.

When the generators operate in the inverting mode, the system of equations for calculating its power currents can be made up as follows:

$$\begin{cases} \frac{di_{g1}}{dt} = \frac{1}{L_1} (u_{g1} - u_{ab} - r_1 \cdot i_{g1}); \\ \frac{di_{g2}}{dt} = \frac{1}{L_2} (u_{g2} - u_{ab} - r_2 \cdot i_{g2}); \\ \dots \\ \frac{di_{gn}}{dt} = \frac{1}{L_n} (u_{gn} - u_{ab} - r_n \cdot i_{gn}); \\ \frac{di_i}{dt} = \frac{1}{L_i} (u_{ab} - e_i - r_i \cdot i_i); \\ U_{c0} = k_s \cdot E_{im}; \\ \frac{du_c}{dt} = U_{c0} + \frac{1}{C_k} \cdot i_k; \\ u_{ab} = u_c + r_k \cdot i_k; \\ i_k = \sum_{i=1}^n i_{gi} - i_i. \end{cases} \quad (2)$$

where e_i – the counteracting electromotive force of the grid; E_{im} – the maximum value of the grid’s linear voltage; $r_i=r_t+r_f$ – the active resistance of the inverter circuit; r_t – the active resistance of the grid; r_f – the active resistance of the filter; $L_i=L_t+L_f$ – the inductance of the inverter’s circuit; L_t – the inductance of the grid; L_f – the inductance of the filter; i_i – the inverted current; u_k – the voltage of the storing capacitor C_k ; i_k – the current of the storing capacitor C_k ; k_s – the coefficient of the rectifier’s scheme.

The counteracting electromotive force (EMF) of the inverter can be calculated by using the method described in the preceding works of authors [4, 7].

Apart from the shorting and inverting modes of operation, the proposed system of wind power conversion has the power storage mode of operation when the power from the generators is supplied into the storing capacity C_k . This mode of operation can be described by using the system of equations (2) without the fourth equation (counting from the top) taking into consideration that the inverting current is cut off ($i_i=0$). Mechanical part of the system (Fig.1) can be described by independent equations as follows:

$$\frac{d\omega_{gn}}{dt} = \frac{1}{J_n} \left(\frac{P_{in}}{\omega_{gn} \cdot i_n} - T_{gn}(i_{gn}) \right), \quad (3)$$

where T_{gn} – the torque of the n-th generator; P_{in} – the power produced by the n-th wind turbine; J_n – the moment of inertia of the n-th wind turbine; i_{gn} – the rectified current of generator; i_n – multiplication factor of the gear box of the n-th wind turbine; ω_{gn} – the rotational speed of the n-th generator.

Each generator’s torque T_{gn} depends on its rectified current i_{gn} . More detailed mathematical description of the generators of various types, including asynchronous and synchronous, is presented in the preceding authors’ works [4, 5].

Mathematical description of the WTs’ capacity depending on the wind speed is based on their power curves, which usually are given in the wind turbines’ technical documentation. Polynomial of the n-th order is used for the approximation of the power curve on purpose to have a sufficient adequacy the mathematical description.

Number of wind turbines and generators in the mathematical model of the system for power supply was limited up to two in order to facilitate the researches. The slip-ring asynchronous generator, type 4AHK355M12Y3, rated capacity 110 kW, rated rotational speed 500 rpm was taken as the first generator AG1. This generator is rotated by the wind rotor of wind turbine N27/150. The power curve of the wind turbine N27/150 mathematically is described by this equation:

$$P_t = -16.517 \cdot 10^{-5} \cdot v_w^5 + 0.01881 \cdot v_w^4 - 0.6797 \cdot v_w^3 + 9.1408 \cdot v_w^2 - 27.8 \cdot v_w + 4. \quad (4)$$

The second generator SG2 is synchronous machine with permanent magnets. Its type – GL-PMG-5, rated capacity – 5 kW. The power curve of this wind turbine of vertical axis mathematically is described by the following equation:

$$P_t = -16.517 \cdot 10^{-5} \cdot v_w^5 + 0.01881 \cdot v_w^4 - 0.6797 \cdot v_w^3 + 9.1408 \cdot v_w^2 - 27.8 \cdot v_w + 4. \quad (5)$$

Mathematical model (Fig. 3) for the wind power conversion system with 2 generators and one mutual inverter was elaborated on basis of the previous researches of authors [4, 5 and 7] and on the systems of equations (1 – 5).

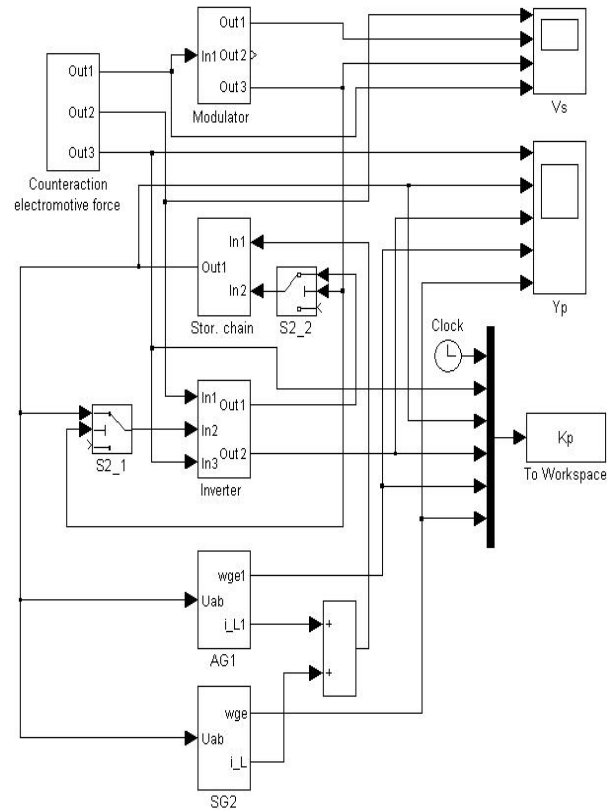


Fig. 3. Mathematical model for the power supply system with two different wind turbines (generators AG1 and SG2)

The same units can be found in the mathematical model of the proposed power supply system as in the electrical scheme (Fig. 2). Mathematical model of the power supply system with two different wind turbines consist of three functional parts:

- the converter, which includes inverter and power storage chain,
- the control pulse former (counteracting electromotive force unit and modulator),
- the two units of WTs.

The WTs units include control pulse formers used to control their short-circuiting transistors.

Mathematical model (Fig. 3) of the storage and inverting circuits (Storage chain, Inverter) was elaborated by the application of the same researches previously carried out by authors [4-7].

4. Research of the energy conversion processes in proposed wind energy conversion system

Processes of energy conversion in the system of power supply from park of small scale WTs into the EG over the one inverter were researched by means of mathematical simulation. Results of the researches are presented below in form of the experimental curves. Modes of operation of very different generators by type and capacity were researched when the one grid-tied inverter served for both of them.

Curves of response of the researched wind power system's parameters at the jumps of the action signals (explained below) are given in Fig. 4 and Fig. 5.

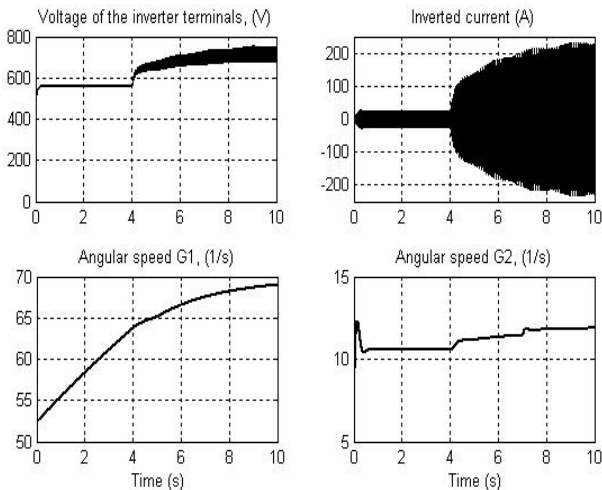


Fig. 4. Curves of the researched wind power system's parameters at the following jumps of the action signals of generators: **AG1**– $\Delta v_{G1}=10\div 14$ m/s, at $t_1=5$ s; $\Delta U_{G1}=3\div 1$ V, at $t_2=4$ s, **SG2** – $\Delta v_{G2}=9\div 12$ m/s, at $t_1=7$ s; $\Delta U_{G2}=3.0$ V, at $t_2=0$ s; ($C_k=2000$ μF)

There Δv_{G1} , Δv_{G2} – jumps of wind speeds accordingly for the first and the second wind turbines; ΔU_{G1} , ΔU_{G2} – jumps of control signals of control pulse formers for short-circuiting transistors of the corresponding circuits.

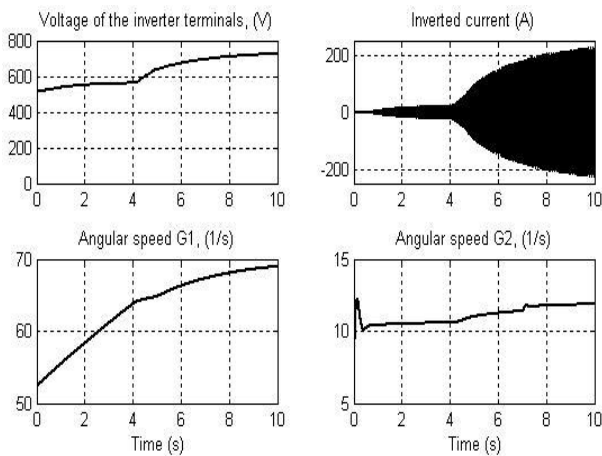


Fig. 5. Curves of the researched wind power system's parameters at the following jumps of the action signals of generators: **AG1**– $\Delta v_{G1}=10\div 14$ m/s, at $t_1=5$ s; $\Delta U_{G1}=3\div 1$ V, at $t_2=4$ s, **SG2** – $\Delta v_{G2}=9\div 12$ m/s, at $t_1=7$ s; $\Delta U_{G2}=3.0$ V, at $t_2=0$ s; ($C_k=200000$ $\mu\text{F} = 0.2$ F)

As it can be seen on Fig. 4 and Fig. 5, load of the generator AG1 suddenly starts to increase after the jump of the control signal of this generator (AG1) at the moment of time 4 s. Therefore the inverted current and voltage on the inverter terminals begin to increase after this moment. After this some impact originates on the operation of the second generator (SG2) – the angular speed of the SG2 slightly increases due to the increase of the voltage on the inverter terminals.

Additionally, as it can be seen on Fig. 4 and Fig. 5, changes of operation mode of small scale generator SG2 (rated capacity 5 kW) practically do not have any impact to the operation of the generator AG1 (rated capacity 110 kW).

Capacity of the power storing capacitor has a significant impact into the character of the voltage on the inverter's terminals and on the inverted current: their electromagnetic oscillations decrease considerably at high capacity C_k (Fig. 4 is for C_k capacity 2000 μF and Fig. 5 – for 0.2 F).

Inverted current in Fig. 6 has not a shape of real sine – it has a pulsating character and therefore the filter is necessary.

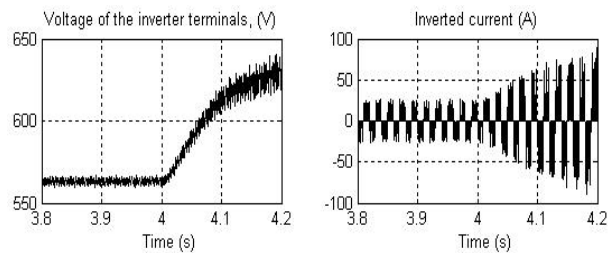


Fig. 6. Curves of the AG-1 generator parameters at the following jumps of the action signals of generators: **AG1**– $\Delta v_{G1}=10\div 14$ m/s, at $t_1=5$ s; $\Delta U_{G1}=3\div 1$ V, at $t_2=4$ s, **SG2** – $\Delta v_{G2}=9\div 12$ m/s, at $t_1=7$ s; $\Delta U_{G2}=3.0$ V, at $t_2=0$ s

Curves of the rectified current of the first wind turbine's generator (AG1), angular velocity and torque of the first wind turbine are presented in Fig. 7.

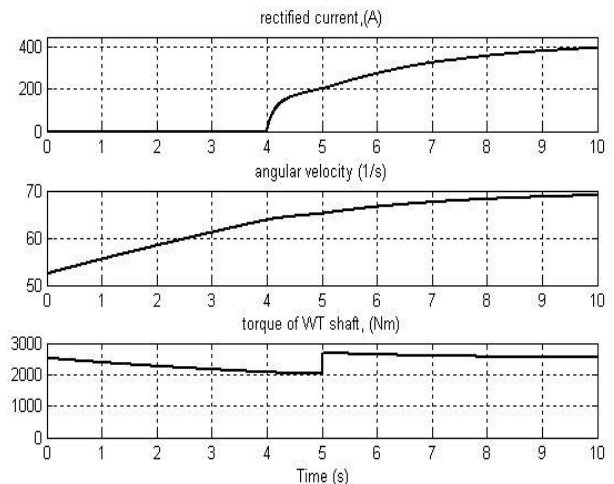


Fig. 7. Curves of the AG1 generator's parameters at the following jumps of the action signals of generators: **AG1** – $\Delta v_{G1}=10\div 14$ m/s, at $t_1=5$ s; $\Delta U_{G1}=3\div 1$ V, at $t_2=4$ s, **SG2** – $\Delta v_{G2}=9\div 12$ m/s, at $t_1=7$ s; $\Delta U_{G2}=3.0$ V, at $t_2=0$ s

The Fig. 7 shows how parameters of the generator AG1 are changing after the increase of its load. It also can be seen that after the sudden increase of the wind speed suddenly increases the torque generated by the turbine, but the angular speed of the wind turbine and the rectified current of the generator increase slowly due to the considerable moment of inertia.

Curves of the rectified current, angular velocity and torque of the WT shaft for the second wind turbine (generator SG2) are presented in Fig. 8.

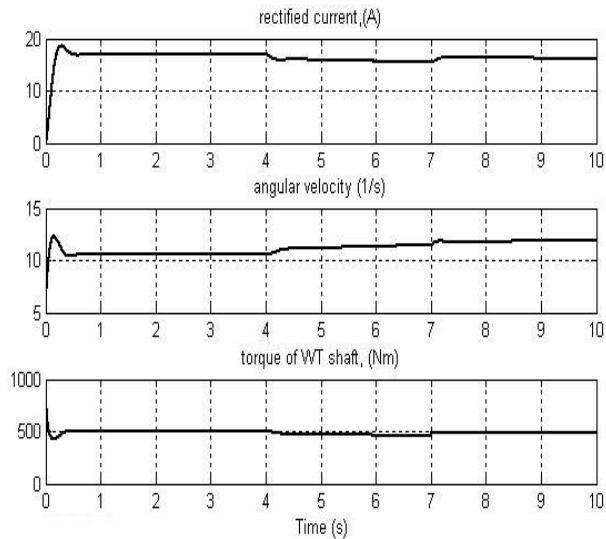


Fig. 8. Curves of the SG2 generator parameters at the following jumps of the action signals of generators: AG1- $\Delta v_{G1}=10 \div 14$ m/s, at $t_1=5$ s; $\Delta U_{G1}=3 \div 1$ V, at $t_2=4$ s, SG2 - $\Delta v_{G2}=9 \div 12$ m/s, at $t_1=7$ s; $\Delta U_{G2}=3.0$ V, at $t_2=0$ s

As it can be seen on Fig. 8, the change of the more powerful wind turbine's (AG1) operation mode has impact into the operation of the smaller wind turbine (SG2). However, this impact is not considerable (it does not exceed 10 %) and it can be easily compensated by the adjusting of control signal U_{k2} in the circuitry of the generator's SG2 current control.

5. Conclusions

1. The proposed conversion system for power supply from the park of wind turbines into electric grid allows using only the one mutual grid-connected inverter.
2. The described power conversion system with one mutual inverter is friendly to various types and

capacities of wind turbines' generators – any types of wind turbines can be included into the system.

3. Voltage of the wind turbines' generators in the proposed scheme can adjust to the voltage of electric grid automatically.
4. Capacity of the power storing capacitor has a significant inverse impact into the amplitude of electromagnetic pulsations of the voltage on the inverter's terminals and of the inverted current.
5. As it was researched, the impact of one generator into the operation of other generators can be neglected.
6. The main advantage of the proposed scheme for power supply from the wind park is cost-effectiveness of the power conversion system.
7. The made up mathematical model allows to research effectively the multi-generational systems of power supply from park of WTs into EG over the one inverter in order to find the ways for the improvement of such systems.

6. References

1. AWEA Small Wind Turbine Global Market Study 2008. Published by the American Wind Energy Association, June 2008. – 26 p.
2. <http://www.allsmallwindturbines.com> (called on 07.02.2009).
3. Murray D. Big Opportunities for the Small Wind Industry. Go Green Energy, LLC. 2008. – p.5. (<http://www.gogreenenergyllc.com> – called on 03.04.2008).
4. Kepalas V., Ramonas Č., Adomavičius V. Connection of the RES-based Power Plants into the Electric Grid // *Electronics and Electrical Engineering*, 2007. – Nr. 8(80). – P.67-72.
5. Adomavičius V., Ramonas Č., Kepalas V. Control of wind turbine's load in order to maximize the energy output // *Electronics and Electrical Engineering*, 2008. – Nr. 8(88). – P.71-76.
6. Adomavičius V., Ramonas Č. Power supply from the park of wind turbines over the one grid-tied inverter // *Proceedings of the International Conference "Biosystems Engineering and Processes in Agriculture"*. - No. 13, 2008. – P.77-80.
7. Paulauskas M., Kepalas V., Ramonas Č. Platuminio asinchroninio ventilinio kaskado dinamika // *ISSN 1392 - 1215 Elektronika ir elektrotechnika*, 1996. – Nr. 4(8). – P. 56-58.

COMPARISON OF SMALL SCALE WIND TURBINES' PROPERTIES

Vytautas ADOMAVIČIUS*, Thomas WATKOWSKI**, Edmundas ŽILINSKAS***, Alfonsas ADOMAVIČIUS****

* The Centre for Renewable Energy Technologies at Kaunas University of Technology, Lithuania

**Lithuanian-German joint venture UAB TOMETA, Germany

***Joint Stock Company UAB SAULES ENERGIJA, Lithuania

****Kaunas Business Machines Company, Lithuania

Abstract: Manufacturers from all over the world produce many types of small scale wind turbines, which parameters are measured under different conditions. Therefore comparison and choosing of the small wind turbine are not very simple tasks. The method used for comparison of small wind turbines by means of comparative indexes is presented in this paper and applied for the evaluation of 45 small wind turbines of horizontal axes and 14 small wind turbines of vertical axes. Calculations of the comparative indexes of the selected small scale wind turbines were carried out on basis of data from internet. The rating of small wind turbines from both classes according to the comparative indexes was carried out and the corresponding results presented in the paper. A distinct general superiority of small horizontal axis wind turbines against the vertical axis wind turbines is showed by means of columnar diagrams.

Keywords: wind energy, small scale wind turbines, efficiency, cost-effectiveness, comparison.

1. Introduction

Wind turbines (WT) of capacity up to 100 kW are classed to the small scale. Presently small scale wind turbines are the fastest growing of any renewable energy technology. Over 120 manufacturers produce over 300 small wind turbines of various designs and capacities in all over the world [1-3]. Two varieties of wind turbines exist: horizontal axis wind turbines (HAWT) and vertical axis wind turbines (VAWT). Currently the HAWT prevails – number of their types makes up about 85 % from the whole number of the small WT types of both varieties. Superiority of HAWT is even greater if the cumulative installed capacity of both varieties is compared.

Demand of small scale wind electric power systems is growing rapidly because they are one of the most cost-effective home-based renewable energy systems. They can be applied for various purposes: for feeding of electrical appliances, production of domestic hot water

or space heating [4, 5]. Attractiveness of these systems is also nonpolluting and power production without any fuel.

As it is foresighted, business of small wind turbines in future will keep growing rapidly [6, 7]. This trend will be actuated due to the decreasing price of small WT. The target price 1000 € for 1 kW (or 1€ for 1W) of installed capacity can be achieved rather soon. The best small WT already are close to it.

2. Peculiarities of the small scale wind turbines' estimation

Various manufacturers of small WT test them at different conditions. Rated speed of various WT is very different as well – from 8 m/s up to 17 m/s. Standard testing conditions for small WT are not established yet. Some manufacturers are not giving the power curves for their WT. Sometimes the manufacturer are claiming that their WT can put out a certain quantity of energy per month while productivity of WT will mostly depend on the local wind energy resources in the site of WT's installation. Therefore choosing of wind turbine is rather responsible task, which is related with possibility to suffer considerable financial losses, especially when the necessary capacity of WT or their number is high. In the meantime unambiguous standard testing conditions (STC) are established for measurement of the photovoltaic cells or modules nominal output power. They are following:

- the irradiance level is 1 000 W/m² (or one sun) ,
- the reference air mass (AM) 1,5 solar spectral irradiance distribution,
- temperature of PV cell or module junction is 25°C.

The air mass index AM 1.5 correspond the solar zenith angle equal to 48.19°.

Similar unambiguous standard testing conditions could be established as well for the small WT designed for operating at low, moderate and high wind speeds. The independent testing laboratories should perform the testing and certification of newly designed WT.

3. Methods used for comparison of WT's parameters

Comparison of both horizontal axis wind turbines and vertical axis wind turbines properties can be performed by means of the comparative indexes. Index of comparative price of the WT, which evaluates its cost-effectiveness, can be used as one of the main indexes. It can be calculated by dividing the price of WT C (without price of tower and VAT) by the WT's capacity at the wind speed 10 m/s P_{10} :

$$K_{ew} = \frac{C}{P_{10}}; \text{€}/\text{W} \quad (1)$$

Another comparative index can be used for evaluating the relative power of wind turbine relational with one kilogram of its weight. It will allow comparing very different wind turbines as well. It can be calculated by dividing the WT's capacity at the wind speed 10 m/s P_{10} by the turbine's weight (without tower):

$$K_{wk} = \frac{P_{10}}{m}; \text{W}/\text{kg} \quad (2)$$

Index of comparative power K_{wm} reflects the technical efficiency of wind turbine. It shows what power the

wind turbine develops at the wind speed 10 m/s per 1 m² of the swept area S and can be determined as follows:

$$K_{wm} = \frac{P_{10}}{S}; \text{W}/\text{m}^2 \quad (3)$$

We suggest the combined comparative index evaluating the wind turbine's technical efficiency and cost-effectiveness. Calculation of this index is not complicated as well:

$$K_{te} = \frac{K_{wm}}{K_{ew}} = \frac{P_{10}^2}{S \cdot C}; \text{W}^2/\text{m}^2\text{€} \quad (4)$$

Further on, calculations of the comparative indexes of all selected small wind turbines according the formulas (1) – (4) were carried out on basis of data from internet [1] and other sources [2, 3].

4. Comparison of HAWT's parameters

The presented above comparative indexes were calculated for every WT of the group comprising of 45 small scale HAWTs having different design and capacity – from 108 W up to 45 kW. 5 best and 3 worst results for every comparative index were selected for the presentation below in Fig. 1 – Fig. 4.

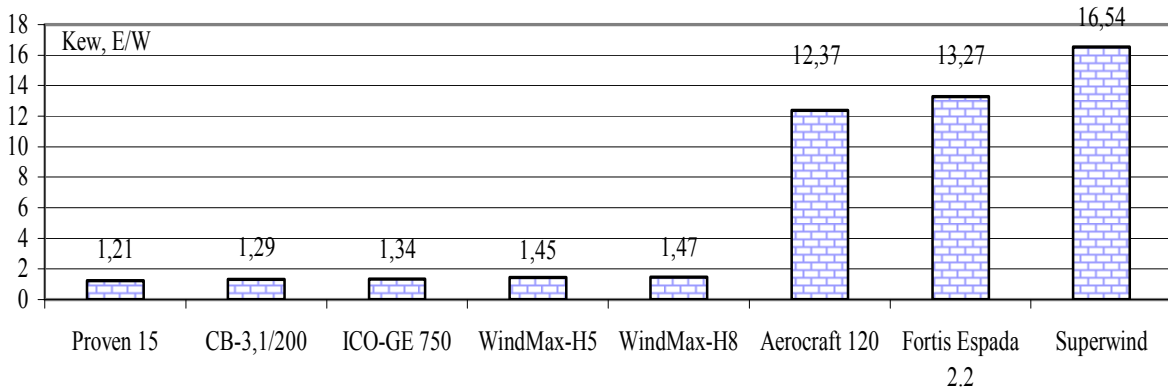


Fig. 1. The 5 lowest and the 3 highest prices of small HAWTs for 1 watt

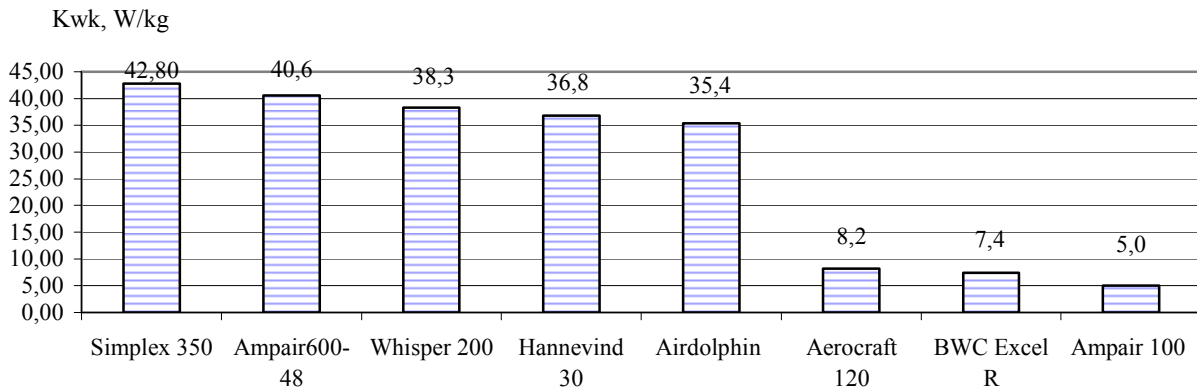


Fig.2. The 5 highest and the 3 lowest capacities of small HAWT per 1 kg of their weight (without tower)

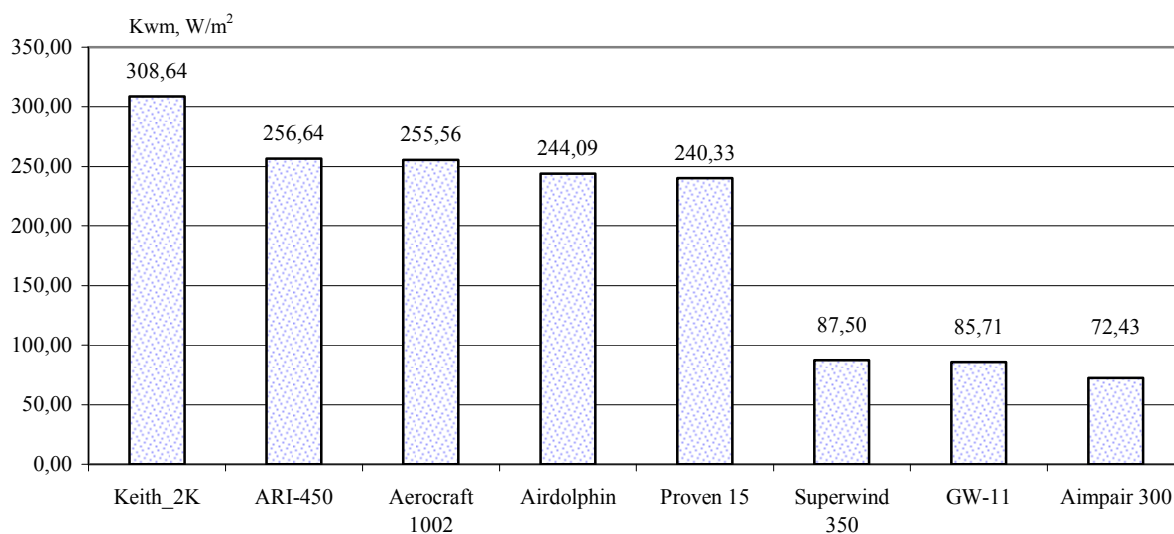


Fig. 3. The 5 highest and the 3 lowest capacities of small HAWT per 1 m² of their swept area

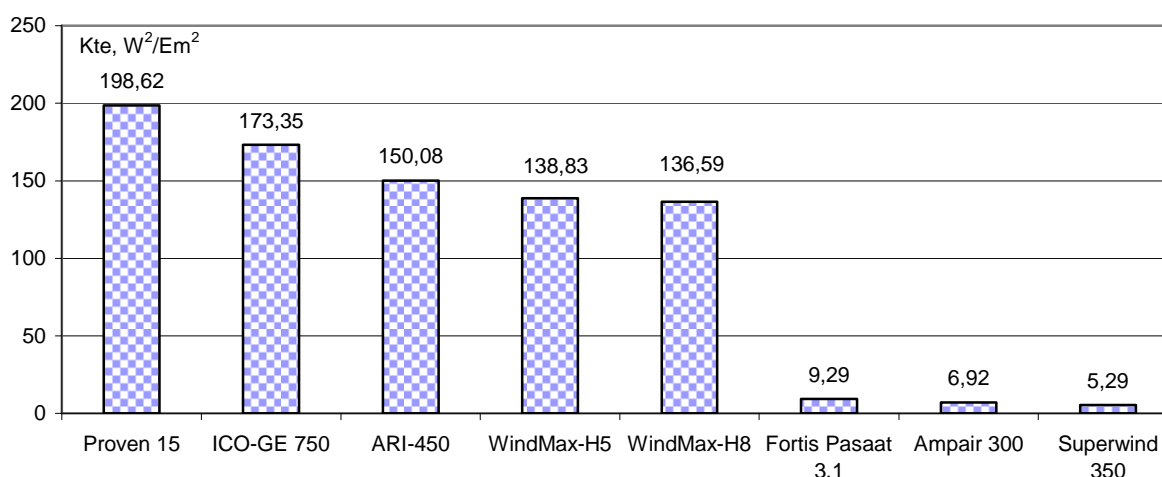


Fig. 4. The 5 highest and the 3 lowest technical-economical efficiencies of the 45 researched small HAWT

A power of all wind turbines at the same wind speed 10 m/s was used for calculations of the comparative indexes instead of the rated values of power because in contrary the comparison would be baseless. The rated power values of various WT are determined at the very different values of wind speed. This value of wind speed (10 m/s) was chosen because the overwhelming part of EU territory is covered by areas of low and moderate wind speeds. E.g., winds of high speed in range 15-17 m/s in Kaunas region are blowing approximately only few hours per year at the best case.

Analysis of the calculated comparative indexes for the small HAWTs disclosed very considerable differences between the best and the worst values. This proves the necessity of serious research before the selection of the proper wind turbine in order to avoid possible financial losses. Only the most efficient and cost-effective wind turbines can be successfully used for home-based renewable energy systems.

The main parameters of the 5 best small HAWTs of 45 researched are given in Table 1. The rating was performed on basis of the calculated comparative index of technical-economical efficiency (Fig. 4). According to the results of research, the best rating has small HAWT Proven 15.

Table 1. Parameters of the 5 best small HAWTs of 45 rated by the index of technical-economical efficiency

Name of HAWT	Name of parameter			
	Rated power, W	Rated wind speed, m/s	Swept area, m ²	Price, €
Proven 15	15 000	9,8	63,58	18 511
ICO-GE 750	750	12	2,54	789
ARI-450	450	11,8	1,54	495
WindMax-H5	485	13	1,54	450
WindMax-H8	775	12,5	2,54	750

5. Comparison of VAWT's parameters

Comparison of VAWTs was carried out in a similar way as it was performed for the mentioned above group of HAWTs: the comparative indexes were calculated for every WT of the group comprising of 14 small scale

VAWTs of different types. The swept area of VAWTs was considered as the axial section of the cylinder swept by the wind rotor of turbine. 5 best and 3 worst results for every comparative index were selected for the presentation below in Fig. 5 – Fig. 8.

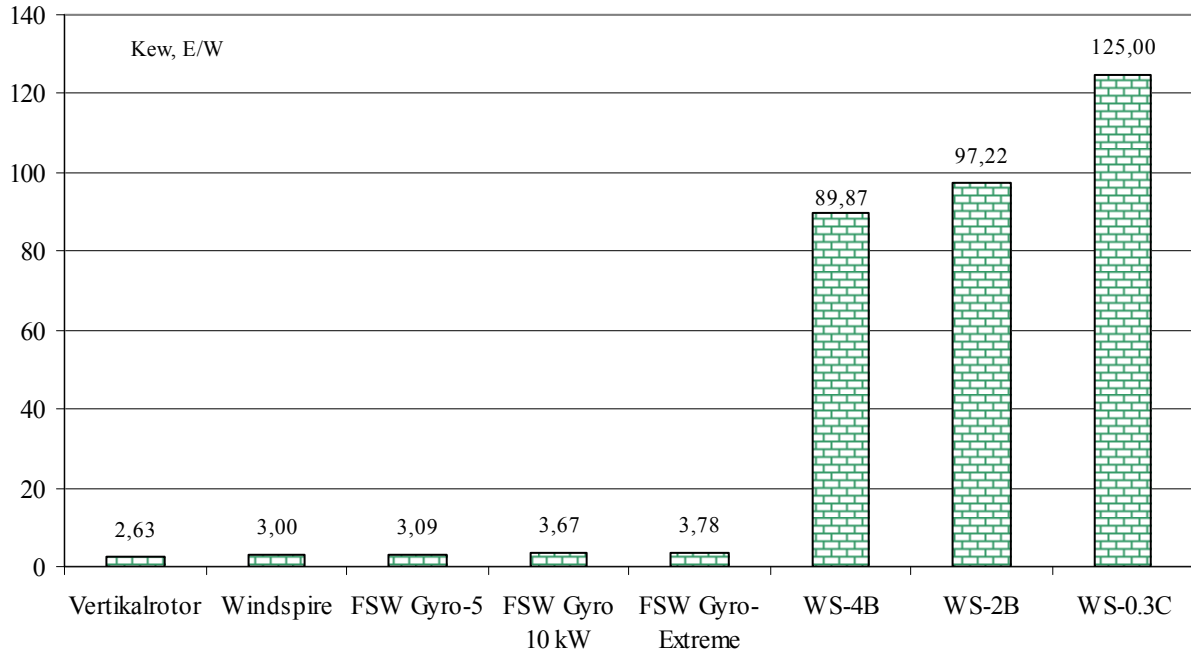


Fig. 5. The 5 lowest and the 3 highest prices of small VAWTs for 1 watt

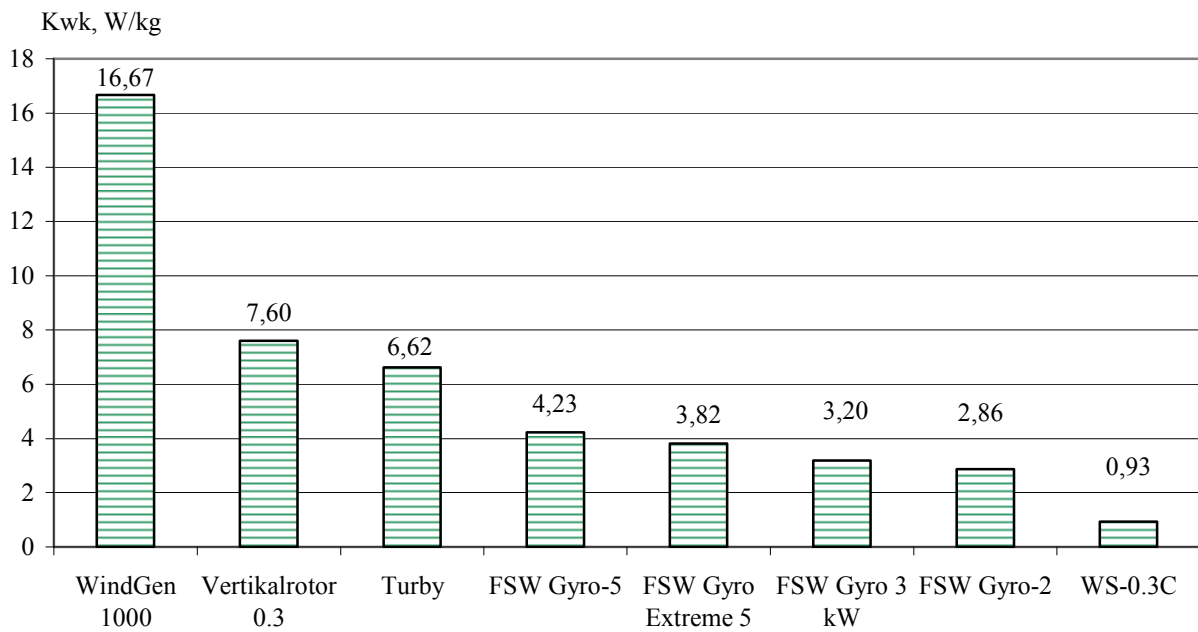


Fig. 6. The 5 highest and the 3 lowest capacities of small VAWT per 1 kg of their weight (without tower)

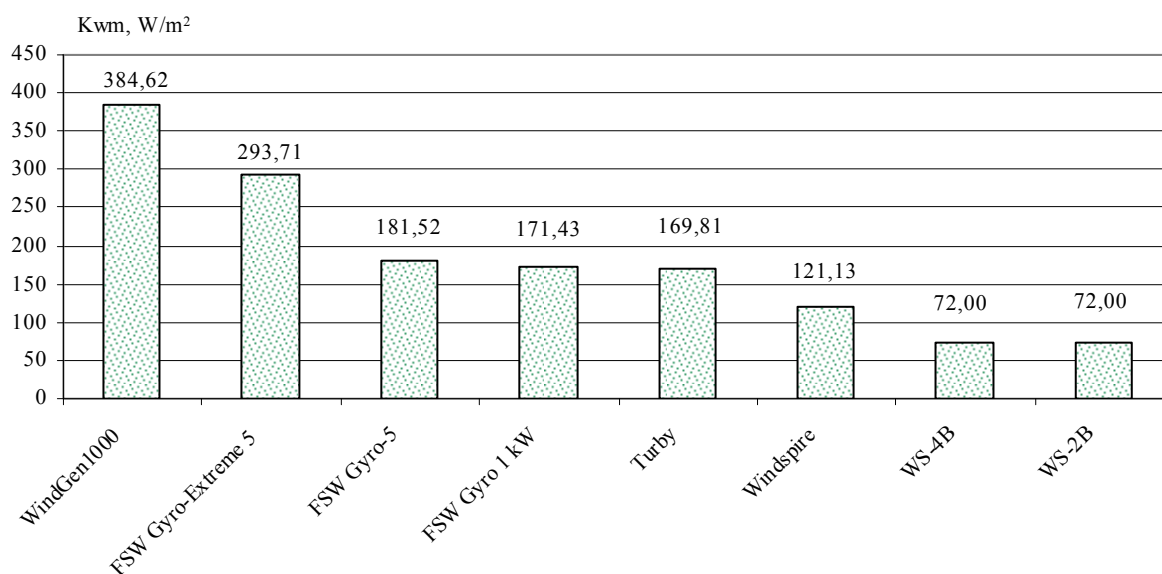


Fig.7. The 5 highest and the 3 lowest capacities of small VAWT per 1 m² of their swept area

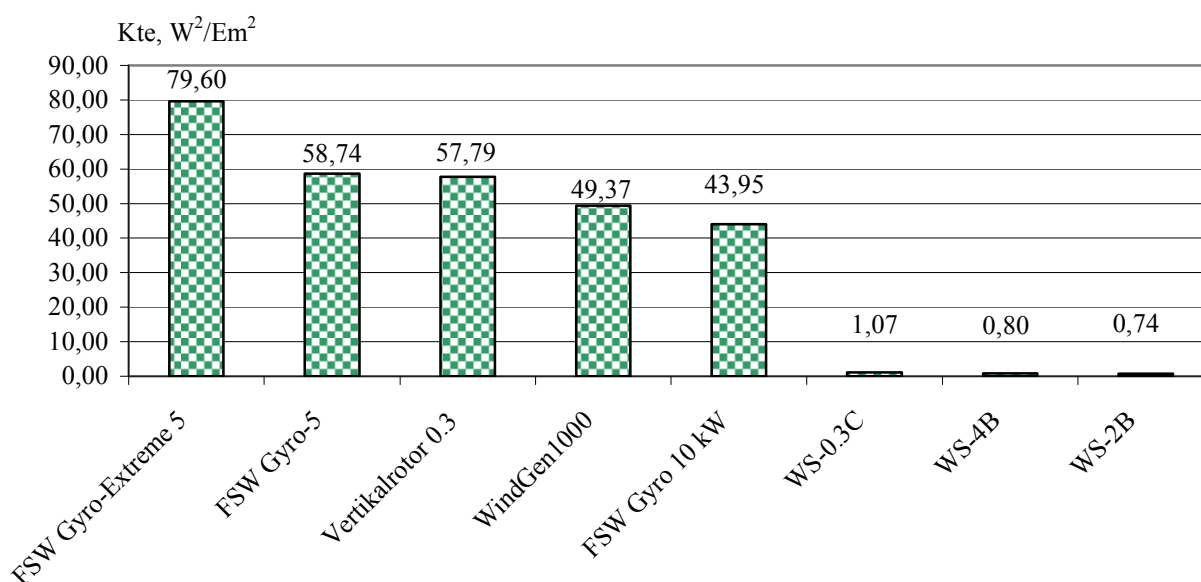


Fig. 8. The 5 highest and the 3 lowest technical-economical efficiencies of the 14 researched small VAWT

Analysis of the calculated comparative indexes for the small VAWTs disclosed vast differences between the best and the worst values again as in case of HAWTs. The extreme values of comparative indexes differ approximately from 5 (see Fig. 7) to 100 times (see Fig. 8) what is a signal urging to perform a serious examination of the wind turbine's properties before the doing decision to specify or/and purchase one or another WT. The problem of the WT's selection is topical as well regarding the choice between the HAWT and VAWT.

The main parameters of the 5 best small VAWTs of 14 researched are given in Table 2. Number of the examined VAWTs is smaller than HAWTs because the number of produced and available in the internet small WT of vertical axis is overwhelmingly smaller as well.

Table 2. Parameters of the 5 best small VAWTs of 14 rated by the index of technical-economical efficiency

Name of VAWT	Name of parameter			
	Rated power, W	Rated wind speed, m/s	Swept area, m ²	Price, €
FSW Gyro-Extreme 5	500	12,5	1,43	1 550
FSW Gyro-5	500	10,72	3,03	1 700
Verticalrotor 0.3	300	12,5	2,5	998
WindGen1000	1 000	12,5	1,56	4 675
FSW Gyro-10	10 000	11,62	37,2	22 000

The power curves of WTs and their acoustic noise should be evaluated as well for the more comprehensive

research [8]. The power curve gives important information on the WT's operation in the range of high wind speeds what can have more or less positive or negative impact into the total energy output. The acoustic noise levels may be very important when the WT is installed in noise-sensitive surroundings.

6. Comparison of HAWTs against VAWTs

Comparison of the average indexes of 5 best HAWTs against 5 best VAWTs is presented in Fig. 9 and Fig 10. As it is shown in the columnar diagrams, the lowest average prices for 1 watt and the highest average capacities per 1 kg of the 5 best small HAWTs

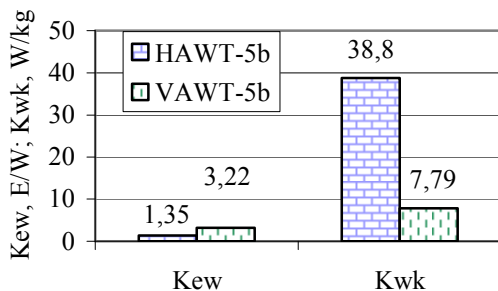


Fig. 9. Comparison of the lowest average prices for 1 watt and the highest average capacities per 1 kg of the 5 best small HAWTs against the 5 best VAWTs

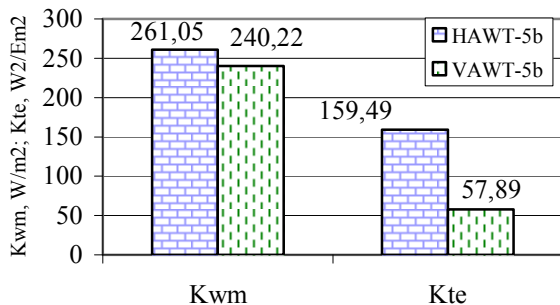


Fig. 10. Comparison of the highest average capacities per 1 m² of swept area and the highest average technical-economical efficiencies of the 5 best small HAWTs against the 5 best VAWTs

A distinct general superiority of small horizontal axis wind turbines against the vertical axis wind turbines can be seen in Fig. 9 and Fig. 10. The average price for 1 watt of the 5 best small HAWTs is over 2 times lower in comparison with the 5 best VAWTs. The highest average capacity per 1 kg of the 5 best small HAWTs is about 5 times higher if compared against 5 best VAWTs. Only capacities of small VAWT per 1 m² of their swept area are almost equal for both varieties. This index for the best of VAWTs (384.62 W/m²) is even better than for the best of HAWT's (308.64 W/m²). However, the highest average technical-economical efficiency of the 5 best small HAWTs compared against the 5 best VAWTs is about 3 times better.

7. Conclusions

1. Demand of small scale wind electric power systems in the world market is growing rapidly because they are one of the most cost-effective home-based renewable energy systems.
2. The comparative indexes were used for the evaluation of small wind turbines comprising two groups: 45 small wind turbines of horizontal axes and 14 small wind turbines of vertical axes.
3. Analysis of comparative indexes 45 small wind turbines of horizontal axes showed very considerable differences between the best and the worst values.
4. Analysis of comparative indexes 14 small wind turbines of vertical axes showed the same trends as in case small wind turbines of horizontal axes.
5. A distinct general superiority of small horizontal axis wind turbines against the vertical axis wind turbines is showed by means of columnar diagrams.

8. References

1. <http://www.allsmallwindturbines.com> (called on 03.02.2009).
2. Small Wind Turbine Global Market Study 2008. Published by the American Wind Energy Association. AWEA, June 2008. – 26 p.
3. Christensen K. Catalogue of Small Windmills from 5 W to 50 kW, 2006. Nordic Folkecenter for Renewable Energy. – 105 p.
4. Adomavičius V. Sizing of wind-based energy system for homestead's power and heat. Proceedings of International conference Electrical and Control Technologies – 2007. KTU, Kaunas, 2007. – pp. 157-162.
5. Adomavičius V. The concept of wind energy consumption for heat and power in the dwelling houses. Proceedings of the 12th International conference Technical and Technological Progress in Agriculture. Raudondvaris: IAE at LUA, 20-21 September, 2007. – pp. 226-230.
6. Martinez F., Herrero L.C., Santiago P. G. and Gonzales J. M. Analysis of the efficiency improvement in small wind turbines when speed is controlled. 1-4244-0755-9/07/\$20.00©2007 IEEE.
7. Murray D. Big Opportunities for the Small Wind Industry. Go Green Energy, LLC. 2008. – 5 p. (<http://www.gogreenenergyllc.com> – called on 02.16.2009).
8. Migliore P., van Dam J. and Huskey A. Acoustic tests of small wind turbines. AIAA-2004-1185. – pp. 14.

PECULIARITIES OF WIND POWER PLANTS' WORK IN THE SMALL POWER SYSTEM

Tomas DEVEIKIS*, Enrikas NEVARDAUSKAS*, Renata STANIONIENĖ**

*Kaunas University of Technology, Lithuania

**The Centre of Renewable Energy Technologies at KTU, Lithuania

Abstract: The small power system usually is formed when large power system is destroyed after some emergencies. Capabilities of small power system with wind power plants to work as autonomous system are investigated. The model of small isolated power system and calculations are proposed according to the real data. Wind power plant parks are analyzed for reactive power and voltage control in the small power system.

Keywords: wind station, reactive power, voltage control, small power system.

1. Introduction

Currently, the number of distributed generators connected into the electricity system is increasing in Europe. Small generators may work in a fault mode generating electricity to small system when fault occurs in the electricity network.

Small system concept is the system including one or more generators and consumers which might be disconnected from centralized system and to work autonomously.

Local system simulation is performed based by actual network data with existing distributed generators working in the network system. Also, the possible operation of wind power station in local system is given. The potential of voltage controlling through reactive power generation or consumption in the latest wind power station is analyzed. Dynamic stability of local system is analyzed when local system is disconnected due to fault in the network system.

2. Main principles of small system

Small system is described as one or more power generators (PG) supplying electricity to certain consumers' group and managing to operate independently certain period, while fault is being solved in the network system.

During fault period part of the network is disconnected from the network. The disconnection is possible in the part of the network as also in the line with one generator.

Generator or group of generators should work and maintain nominal voltage and frequency supplying electric to connected network part during disconnection and when system is disconnected. Sectional breaker is disconnected remotely. Small system scheme in the network is given in fig. 1.

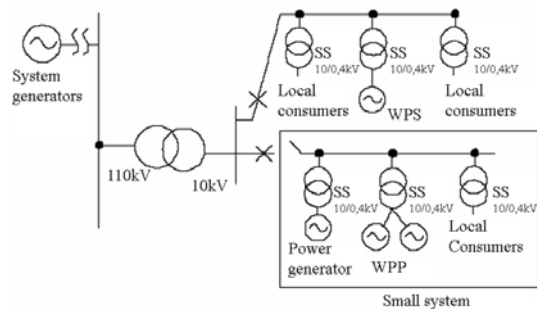


Fig. 1. Small system in network system

Lithuania's electricity system splitting to the A, B, C, D regions with disconnection points is given. Each region is connected to one or more disconnection points. The regional disconnection points of electricity network are given in fig. 2.

The main object in local system is power balance between load and generation in real time. The balance must be maintained by the lead generator controller. This imply to limited penetration of distributed generators into the network system concerning load extent. Traditional network can not create a local system without the connected distributed generators.

Small system mode requires estimation of reactive and active power balance.

Significant factor to the small system is created power loss (reactive power) in the network airlines.

Power line or transformer would disconnect of the electricity network during disturbance in balanced system.

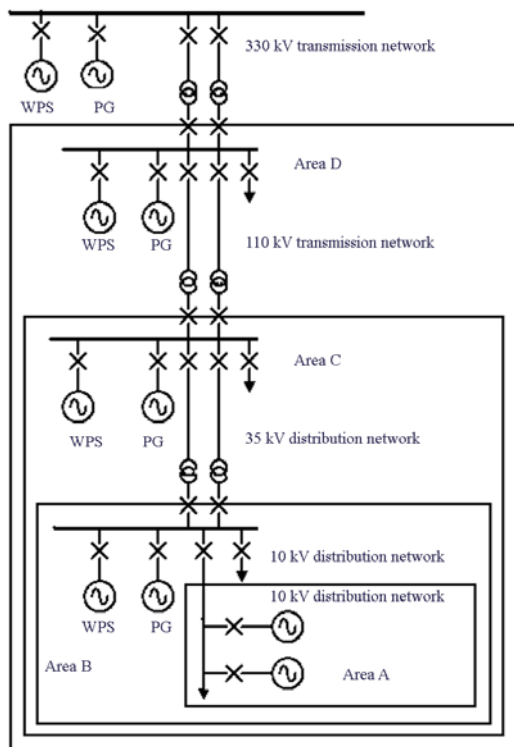


Fig. 2. Regional network disconnection points

During disconnection from large system generator or generators of small system is set to control voltage and frequency. Generators must provide lacking reactive and active power in the small network systems. Active energy power lack can be covered with additional facilities as diesel generators, gas turbines, kinetic energy storages, which are connected to small system or certain regions. Reactive power lack can be covered with use of wind power station (WPS) with induction and synchronous generators connected to small system. The high power imbalance forms immediately after network disconnection. In addition, the generator's automatic voltage regulator is required to respond and control reactive power demand of electricity system. During this period of balancing the voltage and frequency is unstable and may deviate from the limits. Short-term transient process depends on the generator control system regulator functioning.

The control system's effectiveness depends on the scheme and its settings, which are variable among the producers.

Synchronous generator and the control unit connected to a small system have to control active power and the power factor and to respond to the changing speed and voltage resulting in disconnected system.

If the generator power range and the excitation are sufficient, the small electrical system can achieve and balance power, frequency and maintain a stable no less than nominal voltage.

Small system active power balance basis:

Power increment or decrement is achieved by changing turbine generator's speed;

Turbine speed regulator sustains the required frequency, which is directly related to the generator's revolutions.

Small system reactive power balancing:

Voltage reduction or increment is possible with shunt reactors or capacitors;

Wind power plants with reactive power capacity regulation;

Main factors are power generation and load balancing. Other factors such as electricity network disconnection, generator controlling and responsiveness, protection determination is a technical solutions.

Summer minimum and winter maximum regimes have to be evaluated during small system potential operation analysis.

Small system operation is no possible, when the load is greater than the maximum generated power. This is a basic rule of a small system.

If a small system can not disconnect and work during disconnection, generators should be able to start independently and to generate full rated power from zero regulating voltage and frequency.

3. Reactive power control of wind power plants in electricity network

The generating wind power depends on the wind speed. Wind power stations have certain characteristics which are different to induction and synchronous generators.

There are wind power stations with double fed induction generator (DFIG). Generator stator windings are connected to the electricity network and the rotor windings are connected through the electronic power converters with current control circuits mainly used for direct / alternating voltage conversion. In this case, the electrical and mechanical rotor frequencies are separated while electronic power converter compensates the difference between the mechanical and electrical frequency with additional current and frequency control. The variable speed control has become possible by DFIG. This means that the mechanical rotor speed can be controlled according to certain function, resulting maximum amount production of energy.

Wind power with DFIG can control reactive power charging current to the rotor. In this case, there is no relation between the ratio of reactive power and the other factors as the rotor speed and active power generation.

Instead of that, a certain rotor speed and the active power consumption enable generation or consumption of reactive power. The generator torque and the generation of the reactive power directly depends from the current, which is maintained from the electronic power converter feeding from the rotor.

Voltage regulation by consuming and generating reactive power with wind power stations consisting DFIG enables to control reactive power in certain range. Reactive power control limit is $\pm 0.2 Q/P_n$ at nominal power and active power control limit is $\pm 0.5 Q/P_n$ at above 0.5 nominal active power.

Wind power station V80 can generate or consume 1 Mvar reactive power at the maximum.

Generated reactive power may vary depending on DFIG type. Vestas manufacturer PQ-type wind power station characteristic is presented in fig. 3.

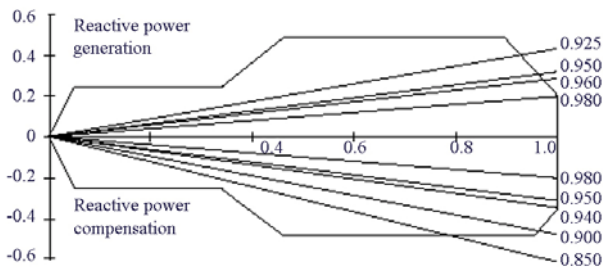


Fig. 3. Vestas PQ-type wind power station characteristic

Wind power stations with wind vane directly connected to the generator is expressed as wind power plants with direct gear. Generator may have a synchronous generator with phase rotor or permanent magnets. Stator is not directly connected to the network, though through the digital power converter. Wind power plant with an electronic transmitter has the option to control generated power, electrical energy and voltage.

The generator torque and reactive power generation directly depends on the current, which is maintained from electronic power converter feeding rotor.

Current necessary to create the necessary torque sets converter possibility of reactive power generation or consumption. This means that the generator power factor and electrical load factor in network side can be controlled by the converter independently of each other.

Wind power station with a voltage control unit can control the point voltage by changing the amount of reactive power generation or consumption. The control action is performed as follows: the voltage is measured at a certain point, and the signal is transmitted to the voltage controller. The controller determines the amount of reactive power, which might be consumed or generated according to controller transfer function.

This is the easiest way to enable wind power station to control only the terminal voltage on the stepping generator terminals, however the voltage is not controlled by the network points if reactive power is uncontrolled. However, this may be not sufficient. Though, wind power station which can control reactive power capacity, can support point voltage close to local consumers nominal voltage. When the measured voltage is too low reactive power generation is increased, and vice versa, when the voltage is too high, reactive power generation is reduced.

Enercon E-82 and E70 maintain power factor $\cos \varphi = 1$, and also does not require and do not produce reactive power when active power is changing in range from 0 kW to 2000 kW. It also can support power factor uneven zero. This allows wind power stations to promote reactive power control and to maintain voltage in the network. Reactive power range depends on the wind power station model and configuration. Enercon E-70 PQ characteristic is presented in fig. 4.

Enercon E-70 reactive power control limit is between $\pm 0.5 Q / P_n$ at the nominal power. Wind power station E S-70 specifications are $S=2050$ kVA, $P=2000$ kW, and $Q=1000$ kvar. By choosing additional STATOM system might be eliminated active power 0.2 (p.u.) load limit of generation and reactive power consumption or generation point starts at 0 in wind power park.

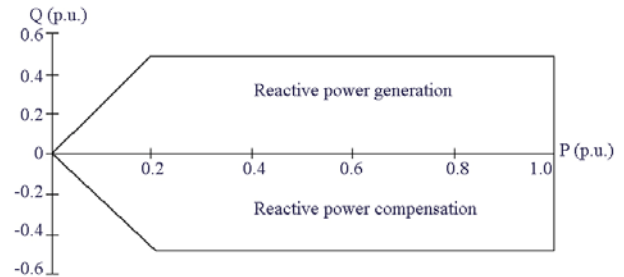


Fig. 4. Enercon PQ wind power station characteristic with synchronous generator and phase rotor

Enercon wind power stations are variable modifications depending on generating power or reactive power consumption. In particular case active power generation depends on reactive power consumption. The voltage must be measured in two or more points to balance power transformer with tap is used.

4. Model of small electrical system with the wind power stations

Small system consists of Mažeikių power station with two generators and three wind power parks, which are connected to the 110 kV network (fig. 5).

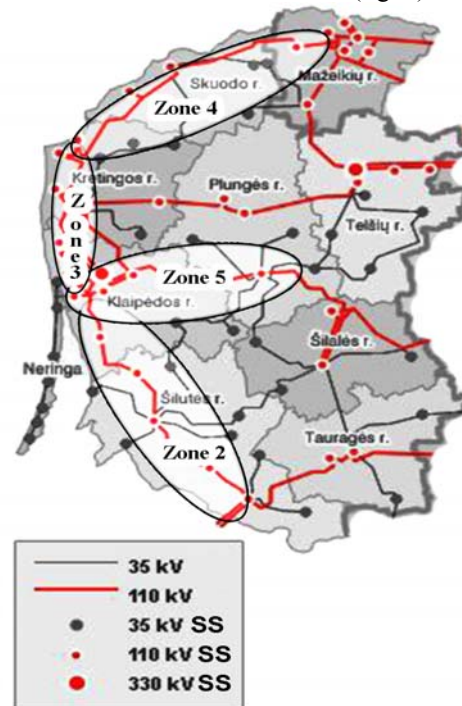


Fig. 5. The possible operation of the small system in Zones 3 and 4

Mažeikių power station consists of two 100 MW generators. However, generators are limited to 80 MW by turbine.

The wind power park of 30 MW total power consisting of 15 Enercon E-70 type 2 MW rated power wind power stations is connected to Zone 3 Palanga-Šventoji 110 kV transmission network. Substation power rating is 32 MVA. The wind power park 16.5 MW total power consisting of 6 Vestas V-100 type 2.75 MW rated power wind power stations is connected to Zone 4 Šventoji-

Židikai 110 kV transmission network. Substation power rating is 32 MVA.

Zone 4 to the 110 kV transmission network segment of the Holy-Židikai, Benaičiuose connected to the village of 6 wind power park Vestas V-100, a power of 2.75 MW each and 20/110 kV transformer substation. 14 MW of wind power is generated additionally by Enercon E-82 type wind power stations in Zone 4.

Total capacity of wind power parks is 60 MW. "Mustang" program is used for simulation. Situation is simulated in 110kV power line. It is also disconnected the line from Klaipėda Židikų substations. Switchover is performed in line sections Mažeikių power station-Varduva and Juodeikiai, Židikai – Klaipėda substation. In this line section is essential consumers such as Mažeikių nafta, Klaipėda port, Būtingė oil terminal and villages (Židikai, Skuodas, Lenkimai, Šventoji, Palanga, Tauraukis).

The main generator is Mažeikių power plant maintaining frequency, voltage, active and reactive power balance. Voltage must not exceed $\pm 10\%$ of the nominal voltage. Different regimes of minimum, average and maximum in summer and winter mode of wind power generation is performed.

Main consumer is Mažeikių nafta consuming 55 MW of active power and 3.5 Mvar of reactive power. Mažeikių power plant one generator instantaneous change is 7% of 80MW power. Minimal power generation of one generator is 2% of 80 MW power. Reactive power generation limits is from 20 Mvar to 85 Mvar at 80 MW power generation.

Generator voltage range is from 10 kV to 11.5 kV. Voltage change while wind power parks generate nominal power and generator voltage on generator terminals is 10.5 kV is given in figure 6. Voltage change is 10% range. Reactive power varies from 9 to 13 Mvar in different modes. The wind power park is connected in point 5 also maintains voltage in point 6.

During fault in network system small system is disconnected. Small system voltage fluctuation is simulated in Mažeikių power plant and Varduva line during short circuit fault nearby Mažeikių power plant substation. Generator power fluctuates during short circuit but after 10-15 seconds stabilize.

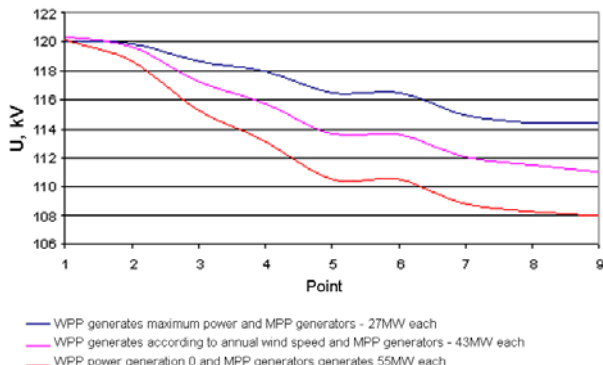


Fig. 6. Voltage change in small system at different wind power park generation

After disconnection Mažeikių power plant power change in small system is given in fig. 7.

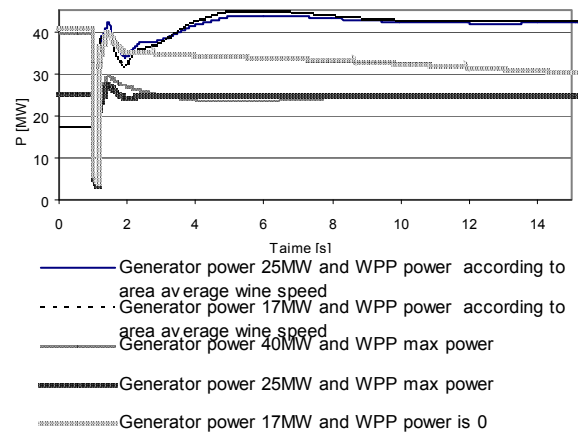


Fig. 7. Mažeikių power plant power change in small system after disconnection

After disconnection small system frequency change is given in fig. 8.

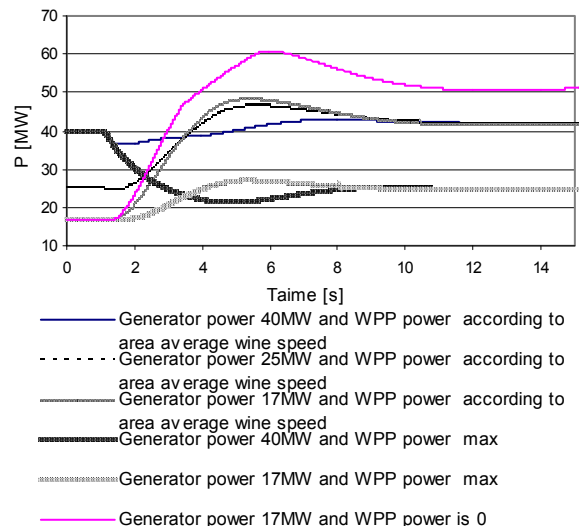


Fig. 8. Small system frequency change after disconnection

Mažeikių power plant one generator operation change at different regimes is given in fig. 9. Second generator power change is identical.

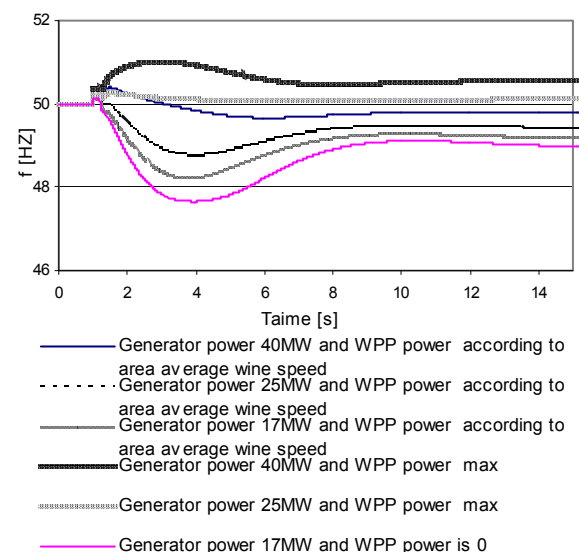


Fig. 9. Generator power change at different regimes in small system where short circuit location is Mažeikių power plant – Varduva line

Voltage change during disconnection while system generator generates 40 MW and wind power park power generation is at maximum is given fig. 10.

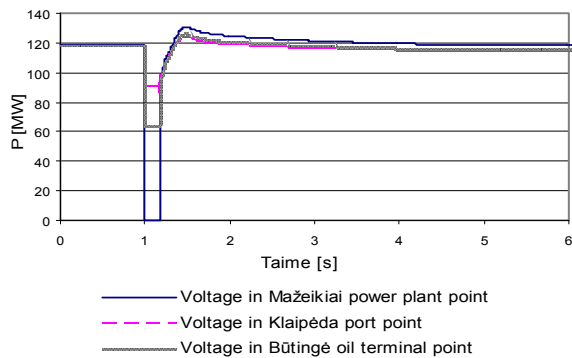


Fig. 10. Voltage change during disconnection while system generates 40 MW and wind power park power generation is at maximum

Voltage change during disconnection while system generator generates 40 MW and wind power park power generation is according to area average wind speed fig. 11.

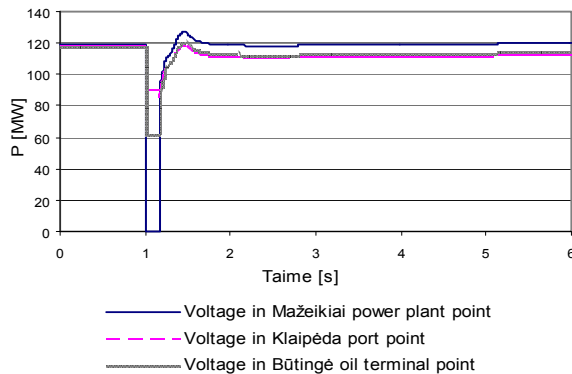


Fig. 11. Voltage change during disconnection while system generates 40 MW and wind power park power generation is according to area average wind

Voltage change during disconnection while system generator generates 17 MW and wind power park power generation is according to area average wind speed fig. 12.

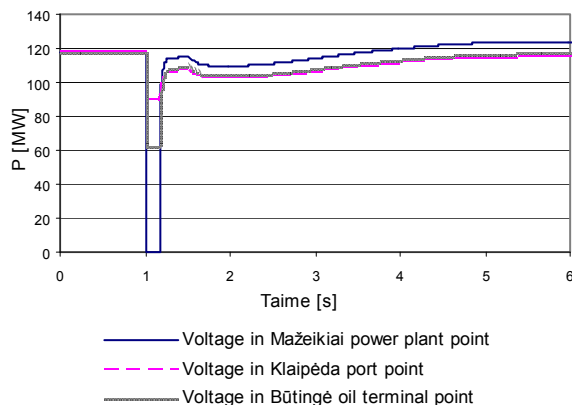


Fig. 12. Voltage change during disconnection while system generates 17 MW and wind power park power generation is according to area average wind

System power fluctuates during disconnection but after short period stabilizes. Active power and reactive power change in 14 MW wind power park point during disconnection from network system while Mažeikių power plant generators generates 40 MW power each is given in fig. 13.

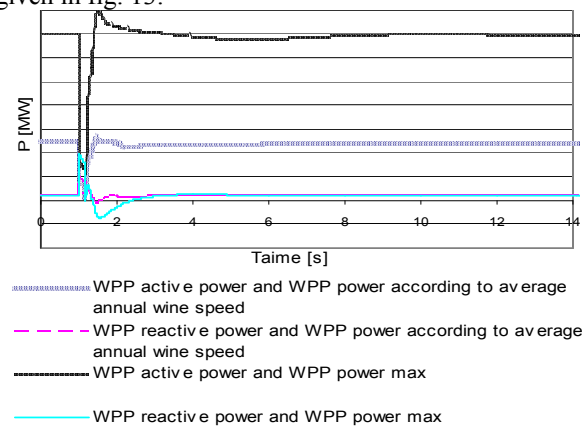


Fig. 13. Active and reactive power change 14 MW wind power park point during disconnection from network system while Mažeikių power plant generators generates 40 MW power each

Wind power parks generated power is given in fig. 14 when measurements were performed every 2 minutes in real time.

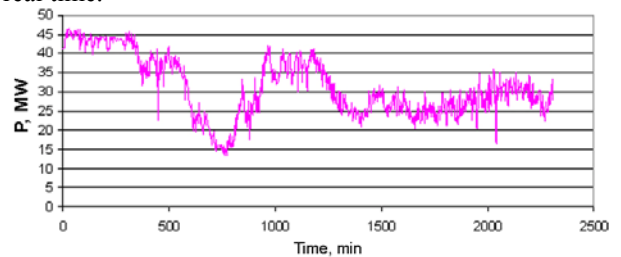


Fig. 14. Wind power parks generated power in time

Peak power fluctuations is after 2182 minute which reaches 6 MW value. This is most complicated operation moment in 2500 minute cycle.

Wind power park power generation fluctuation up to 6 MW is presented in fig. 15.

Mažeikių power plant generator manages to change power generation up to 1.6 MW per minute, then both generators may change power generation up to 6.4 MW per 2 minutes. Mažeikių power plant may balance wind power park power generation fluctuation.

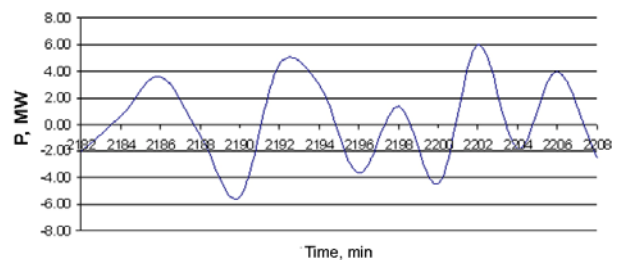


Fig. 15. Wind power park generated power during the period

Load forecast model must be applied for this region after disconnection. Mažeikių power plant generators are loaded based on load forecast model.

5. The future concept of small power grid

At present, wind power plants connected to the electrical network causes balancing problems.

The suggested model allows to use renewable sources more effectively and to supply heat to certain districts as well as electrical power by using the electrical and thermal energy supplied by fuel cells.

The power grid with wind power plants, fuel cells and energy storage system (shown in fig. 5) could operate in island conditions. Also, such system could operate connected to the external power grid and be isolated in case of accident until the external power system is restored.

The presented system covers fuel cells, energy storage, electrolyzers, hydrogen storage, wind power plants and consumers. Conventional generating units can be connected as well.

The effectiveness of fuel cells is better comparing to the conventional power sources and can reach 40-60% for power generation and up to 90% for power and heat generation.

The hydrogen could be stored in stationary tank and used instead of diesel fuel. The hydrogen is produced from water by electrolysis. The electrical energy would be supplied by wind power plants in real time or by electrical storage system. Also, regenerative fuel cells can generate hydrogen as well. This system operates in closed cycle to produce hydrogen from water.

The following types of fuel cells are suitable to use in the power system: SOFC, PAFC and MCFC. The electrical capacity of such fuel cells could be 50-3000 kW. For quick startup and load following, PEMFC and DMFC could be used. The startup time of PEMFC varies from 1 s to couple seconds. The loading could vary from 10 to 100%.

The energy storage system – vanadium redox battery (VRB) is suggested to be installed in the power grid (fig. 16). The accumulated energy can reach few hundreds MWh. The large VRB energy storage system can operate jointly with wind power parks and to supply power during peak loads. For smoothing the load diagram, capacity of VRB system must be high enough (few MW). At present, large VRB systems are used for industrial objects and energy supply systems and their capacity is of range 25 kW – 10 MW.

Stationary power plants based on fuel cells like DFC300, DFC1500 and DFC3000 could be connected in the power grid. To increase the power, these power plants can be connected to work in parallel. For hydrogen production, the hydrogen plant like DFC300MA could be used.

At present, the price of renewable energy generation is very high (the relative price is 2500\$/kW for a fuel cell and 2000 \$/kW for wind power plant). The capital price of fuel cells could drop significantly if such systems were installed in the decentralized power grid to work at basis load. According to World Alliance for Decentralized Energy reports, decentralized power plants would significantly decrease investments required

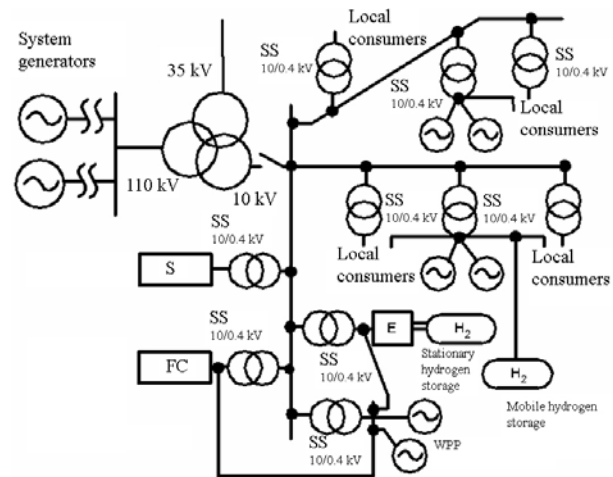


Fig. 16. The concept of power grid with wind power plants, fuel cells and energy storage system

for power grid development. The distributed generation would give not only economical benefit but also ensure the real concurrence between different energy suppliers. At market conditions, the energy sector would be developed more intensively and efficiently because the priority is given to the most effective solutions in the market.

6. Conclusions

The power system should be flexible and be able to separate into islands after large disturbances and emergency conditions.

Small power system or part of large one can work in island conditions without power supply interruptions.

Operation conditions of a part of the power system which is intended to be disconnected during emergency conditions must be analyzed. For disconnection without large disturbances and without significant frequency variation, the generating units should be balanced according to the total load in this area.

In order to avoid system collapse in islanded network after disconnection of pilot generating unit, the back-up generator should be installed for system restoration.

The analysis of dynamic stability shows that the small power system can be successfully disconnected from the main power grid and sustain the stable operation.

7. References

1. Deveikis, Tomas, Nevardauskas, Enrikas Stanioniene Renata. Investigation of electromagnetic compatibility of wind power station and electrical network user // EMD 2008 : proceedings of the XVIII International Conference on Electromagnetic Disturbances, September 25-26 2008, Vilnius, Lithuania. - ISSN 1822-3249. - Vilnius. - 2008, p. 155-160
2. Assessment of Islanded Operation of Distribution Networks and Measures for Protection. ETSU Report ETSU K/EL/00235/REP. 2001.
3. www.enercon.de
4. www.vestas.com